

2

AGARD-R-711

AGARD-R-711

AGARD

ADVISORY GROUP FOR AEROSPACE RESEARCH & DEVELOPMENT

7 RUE ANCELLE 92200 NEUILLY SUR SEINE FRANCE

AGARD REPORT No. 711

Special Course on Aerodynamic Characteristics of Controls

DTIC
OCT 20 1983

NORTH ATLANTIC TREATY ORGANIZATION



DISTRIBUTION AND AVAILABILITY
ON BACK COVER

83 10 20 067

10-A133950

FILE COPY

10-A133950

AGARD-R-711

NORTH ATLANTIC TREATY ORGANIZATION
ADVISORY GROUP FOR AEROSPACE RESEARCH AND DEVELOPMENT
(ORGANISATION DU TRAITE DE L'ATLANTIQUE NORD)

AGARD Report No.711
SPECIAL COURSE ON AERODYNAMIC CHARACTERISTICS OF CONTROLS

Accession For	
NTIS	X
DTIC	
Univ	
Govt	
Date	
By	
Remarks	
A	

LIBRARY
MARCH 1983

The material assembled in this book was prepared under the combined sponsorship of the Fluid Dynamics Panel, the von Kármán Institute and the Consultant and Exchange Program of AGARD and was presented as an AGARD Special Course at the von Kármán Institute, Rhode-St-Genèse, Belgium 21-25 March 1983.

THE MISSION OF AGARD

The mission of AGARD is to bring together the leading personalities of the NATO nations in the fields of science and technology relating to aerospace for the following purposes:

- Exchanging of scientific and technical information;
- Continuously stimulating advances in the aerospace sciences relevant to strengthening the common defence posture;
- Improving the co-operation among member nations in aerospace research and development;
- Providing scientific and technical advice and assistance to the North Atlantic Military Committee in the field of aerospace research and development;
- Rendering scientific and technical assistance, as requested, to other NATO bodies and to member nations in connection with research and development problems in the aerospace field;
- Providing assistance to member nations for the purpose of increasing their scientific and technical potential;
- Recommending effective ways for the member nations to use their research and development capabilities for the common benefit of the NATO community.

The highest authority within AGARD is the National Delegates Board consisting of officially appointed senior representatives from each member nation. The mission of AGARD is carried out through the Panels which are composed of experts appointed by the National Delegates, the Consultant and Exchange Programme and the Aerospace Applications Studies Programme. The results of AGARD work are reported to the member nations and the NATO Authorities through the AGARD series of publications of which this is one.

Participation in AGARD activities is by invitation only and is normally limited to citizens of the NATO nations.

The content of this publication has been reproduced
directly from material supplied by AGARD or the authors.

Published July 1983

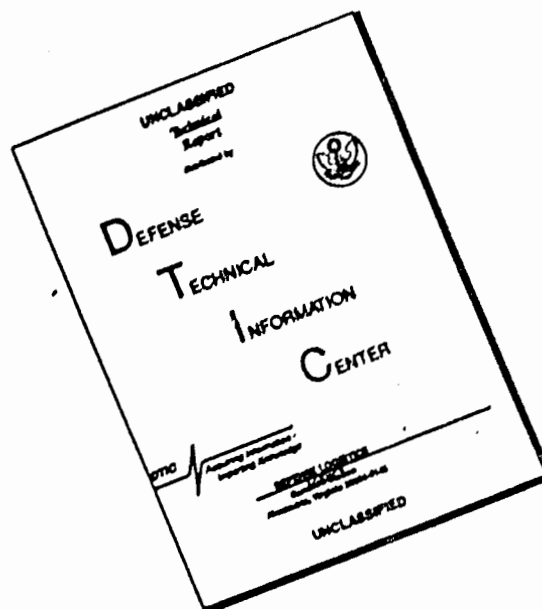
Copyright © AGARD 1983
All Rights Reserved

ISBN 92-835-1457-2



Printed by Specialised Printing Services Limited
40 Chigwell Lane, Loughton, Essex IG10 3TZ

DISCLAIMER NOTICE



THIS DOCUMENT IS BEST QUALITY AVAILABLE. THE COPY FURNISHED TO DTIC CONTAINED A SIGNIFICANT NUMBER OF PAGES WHICH DO NOT REPRODUCE LEGIBLY.

PREFACE

The use of electronic aids for aircraft guidance and control has increased the importance of the aerodynamic characteristics of the various forms of aircraft control and the need to improve our understanding of them. There has also been increasing interest in Direct Force Controls where the immediate response due to the force changes produced by the control is exploited rather than the slowly developing response of the resulting moment. The performance advantages of reducing the size of stabilising surfaces by achieving artificial stability through the use of the control surfaces coupled to electronic stabilising systems are now well appreciated. Such developments also have promise for gust alleviation and flutter control. They have brought to the fore the need to understand the aerodynamic behaviour of non-steady or oscillatory controls.

A symposium on this subject was sponsored by the Fluid Dynamics Panel of AGARD in May 1979. The Course aimed to provide a review of the main points of interest from that symposium and to present expert surveys of the state of the art.

The material assembled in this book was prepared under the combined sponsorship of the Fluid Dynamics Panel, the von Kármán Institute and the Consultant and Exchange Program of AGARD and was presented as an AGARD Special Course at the von Kármán Institute, Rhode-St-Genèse, Belgium on 21-25 March 1983.

SPECIAL COURSE: STAFF

SPECIAL COURSE DIRECTOR: Professor A.D.Young
Queen Mary College, Aeronautics Dept.
Mile End Road
London E1 4N6
UK

LECTURERS

Mr H.H.B.M.Thomas
Consultant-Aerodynamics Dept.
Royal Aircraft Establishment
Farnborough
Hants GU14 6TD
UK

Prof. Dr Ing. H.Körner
Director
Institut für Entwurfsaerodynamik
DFVLR
Postfach 3267
3300 Braunschweig – Flughafen
Germany

Professor G.J.Hancock
Dept. of Aeronautical Engineering
Queen Mary College
Mile End Road
London E1 4NS
UK

Mr D.G.Mabey
Structures Dept.
Royal Aircraft Establishment
Bedford MK41 6AE
UK

Mr A.M.Skow
Manager, F-5 Aerosciences
Northrop Corporation, Aircraft Group
3901 West Broadway
Hawthorne
California 90250
USA

Prof. Dr Ing. G.Sachs
Hochschule der Bundeswehr München
Flugmechanik und Flugführung
Fliergerhost
8014 Neubiberg
Germany

Dr M.E.Eshelby
College of Aeronautics
Cranfield Institute of Technology
Cranfield
Bedford MK43 0AL
UK

Dr J.N.Nielsen
Nielsen Engineering & Research Inc.
510 Clyde Avenue
Mountain View
California 94043
USA

LOCAL COORDINATOR

Professor J.Sandford
von Kármán Institute
72 Chaussée de Waterloo
1640 Rhode-St-Genèse
Belgium

AGARD REPRESENTATIVE

Mr R.H.Rollins II
AGARD
7 rue Ancelle
92200 Neuilly-sur Seine
France

CONTENTS

	Page
PREFACE	iii
SPECIAL COURSE STAFF	iv
	Reference
INTRODUCTORY REMARKS AND REVIEW OF 1979 SYMPOSIUM by A.D.Young	1
THE AERODYNAMICS OF AIRCRAFT CONTROL; by H.H.B.M.Thomas	2
MATHEMATICAL MODELLING AND THEORETICAL METHODS FOR THE AERODYNAMIC BEHAVIOUR OF CONTROL DEVICES; by H.Körner	3
DYNAMIC EFFECTS OF CONTROLS; by G.J.Hancock	4
EXPERIMENTAL METHODS TO DETERMINE CONTROL EFFECTIVENESS IN WIND TUNNELS; by D.G.Mabey	5
CONTROL OF THE FOREBODY VORTEX ORIENTATION BY ASYMMETRIC AIR INJECTION; by A.M.Skow and D.J.Peake	6
CONTROL OF ADVANCED FIGHTER AIRCRAFT; by A.M.Skow	7
DIRECT FORCE CONTROL; by G.Sachs	8
EXPERIMENTAL METHODS IN FLIGHT FOR THE MEASUREMENT OF CONTROL CHARACTERISTICS; and by M.E.Eshelby	9
AERODYNAMICS CHARACTERISTICS OF MISSILE CONTROLS; by J.N.Nielsen	10

INTRODUCTORY REMARKS AND REVIEW OF 1979 SYMPOSIUM

by

Prof. A.D. Young,
Dept. of Aeronautical Engineering,
Queen Mary College,
Mile End Road, London, E1 4NS, England.

1. INTRODUCTION

My aim in this introductory talk is to give a brief historical review of aircraft controls and their development, and thereby to introduce the major topics which the experts who follow me will consider in some detail.

It is not unusual for a Lecture Series to have an AGARD Symposium as a precursor and this series is no exception. There was an AGARD Symposium on the subject of 'Aerodynamic Characteristics of Controls' in May 1979¹. However, a Symposium is primarily a gathering of experts presenting for mutual benefit the results of their recent research, whereas the prime aim of a Lecture Series is educational, namely to start with fundamentals and then bring the young worker to the point where he can readily understand the aims, priorities and techniques of current developments. But, of course, there is always much material of educational value in the presentations at a Symposium, and the 1979 Symposium was particularly rich in such material. Therefore, I have thought it illuminating to refer to a few of the major lessons to be learned from the Symposium and I have found it helpful for my purpose to summarise briefly one of the papers presented which was particularly instructive.

2. BRIEF HISTORICAL REVIEW OF TRADITIONAL CONTROLS

Since the early days of flight, the standard controls of fixed wing aircraft have been ailerons, elevator and rudder, primarily controlling motion in roll, pitch and yaw, respectively (see Fig. 1). They operate by providing moments about the appropriate axis; the resulting rotary motion then leads to incidence changes of the lifting surfaces, i.e. wings, tail plane and fin, which in turn result in forces which contribute to the overall aircraft response to the initial control movement.

The process of achieving a required response is, however, by no means simple. For example, to start to climb from level flight the elevator is rotated by some negative angle, i.e. upwards (see Fig. 2 for the sign conventions) thus increasing the download on the tail plane. This download will at first reduce the height of the aircraft, but it also produces a nose-up (positive) pitching moment on the aircraft and as the nose rotates the incidence of the aircraft increases and hence so do the lift and drag as well as the weight component of the aircraft along the flight path. The increased lift helps to initiate the climb, but unless the engine thrust is increased the speed will fall. The aircraft can be trimmed in a steady climb when the changes in pitching moment associated with its changed incidence and speed balance that due to the elevator movement and the forces along and normal to the flight path, including the engine thrust, also balance.

Again, a negative deflection of the ailerons, i.e. a downward movement of the port aileron and an upward movement of the starboard aileron, will result in a clockwise (positive) rolling moment. The resulting rolling motion will only achieve a steady rate when the associated incidence changes of the wings due to the rate of roll (positive for the starboard wing and negative for the port wing) result in a negative rolling moment which balances that due to the initial aileron movement. However, we have also to take account of a possible yawing moment that results from the asymmetric drag changes associated with the aileron movements, and this will require some rudder movement to balance it out. Here we see an example of a coupling effect where a control movement may induce moments about more than one axis.

It is as well to remind oneself that even a relatively simple manoeuvre like a change of heading without sideslip in horizontal flight requires a sequence of movements of all three controls. It requires an initial rudder movement to provide a yawing moment, aileron movements to initiate and then hold the angle of bank needed to provide an inward component of the lift to balance the centrifugal force on the aircraft in the turn, and some upward elevator movement to balance out the nose-down pitching moment that would otherwise be evident because the banked aircraft is turning in a horizontal plane about a vertical axis and not an axis normal to the plane of its wings. All these control movements will then be reversed and finally nulled as the required heading is attained and the wings are returned to the horizontal. Coupling effects add to the complexity of the manoeuvre, and if the aeroplane has sideslip then additional forces and moments result which will play a part.

As aircraft performance improved and wing loadings rapidly increased during the thirties and subsequently it became necessary to increase the lifting ability of the wings during landing and take-off and high lift trailing edge flaps, as well as leading edge slats, were developed. The flaps soon began to compete with the ailerons for spanwise room along the wing trailing edge, and as a result interest developed in the use of spoilers to augment or even replace the ailerons as rolling controls. These are upward moving surfaces on the upper surface of the wings (see Fig. 1) which when operated decrease the lift of the wing to which they are attached.

For aircraft that are not very large and do not fly very fast, it is possible for the pilot to make the required control movements by means of direct mechanical linkages between his control stick (or rudder bar) and the control surfaces. Some reduction of the stick forces needed can be achieved by aerodynamic balancing of the control surfaces (e.g. by the use of set-back hinges or small auxiliary controls, called balance tabs, which are on the trailing edge of the control surface and move in an opposite sense). However, with increase of size and speed, it becomes necessary to use hydraulic or electric motors to drive the controls. The use of powered controls does not reduce the need to know what the control hinge moments

are, since the system must be designed to cope with them, or the need to strive to reduce them because the weight and size of the motors must be kept to a minimum. It then becomes necessary to shape the stick forces, by means of a system of artificial 'feel', to preserve the characteristics that experience has taught are desirable.

From the foregoing, it will be clear why we seek to represent the main aerodynamic characteristics of controls by parameters that in some way relate the resulting moments and forces that act on the aircraft as well as the hinge moments of the controls to the control movements generating them. On the assumption that the controls are linear in action, convenient and useful parameters are the rates of change of the moments or forces with control deflection or with rate of change of control deflection. These parameters are referred to as control derivatives. For example $L_{\dot{\delta}}$ ($=\partial L/\partial \dot{\delta}$) is the rolling moment due to aileron deflection derivative. Similarly, $L_{\dot{\xi}}$ is the rolling moment due to rate of aileron deflection and it is an example of a dynamic derivative.

The assumption of linearity is reasonable for conventional controls at small deflections (i.e. less than about 15°) and small angles of incidence (i.e. less than about 10°). However, control behaviour can become markedly non-linear at large control settings or large angles of incidence or yaw. This is usually because of the onset or growth of flow separation when major changes in pressure distribution can be caused by small changes in geometry. Again, if the control is blanketed by extensive wakes from forward surfaces we can expect the control to become relatively ineffective. Non-linearities may also readily arise at transonic speeds when large shock movements with associated dramatic changes in pressure distribution can result from small changes in control settings, incidence or yaw angle. Flow separation caused by a shock wave is not uncommon and adds further complexity to the overall picture.

It will be clear that for any control there will be a setting for which the force or moment that it generates is a maximum and that maximum is also a parameter of major importance since it determines the limits within which the control can be expected to be effective.

3. THE IMPACT OF RECENT TECHNOLOGICAL DEVELOPMENT

The above remarks describe briefly the aerodynamics of traditional forms of controls of aircraft and set the scene up to a couple of decades ago. More recently, there have been dramatic if evolutionary developments, by no means yet complete, spurred on by the inexorable pressures for improved economy and performance for all types of aircraft and for improved manoeuvrability at the expanding limits of the flight envelopes of military aircraft. These developments were made possible by rapid progress in the growing related technologies of servo-systems, electronics and computers, themselves much stimulated by the demands of the burgeoning guided weapons industry. The particular aerodynamic problems of control systems for missiles will be dealt with by Dr. Nielsen, and I shall not touch on them further except to remark that the growing requirement for military aircraft to operate at large angles of pitch and yaw has in recent years brought some convergence in the aerodynamics of missiles and military aircraft.

The first of these developments followed the use of powered controls because they enabled the use of servo-systems which improved the stability of the aircraft under flight conditions where it would be otherwise inadequate. These servo-systems were coupled to the controls so as to provide additional damping where needed in the longitudinal and lateral modes of the aircraft. It was a logical step then to proceed to a so-called manoeuvre demand system where the pilot can specify a particular manoeuvre or flight pattern by appropriate settings of his instruments and the response of the aircraft is duly shaped through the controls to meet his requirement. Such a system is also referred to as 'fly-by-wire' (FBW), since the traditional mechanical linkage between the pilot and the controls is here replaced by some form of electrical signalling.

The next major development stage which is still in progress then readily follows. One development is to design an aircraft ab initio so as to exploit as fully as possible the performance advantages of reduced natural stability using the tools of digital signalling and on-board computers. Thus, we aim to reduce the size of the stabilising surfaces (e.g. tailplane and fin) and so reduce drag and weight, and the required stability is automatically achieved through the control surfaces governed by appropriate laws in response to suitable sensors. Likewise, we can exploit the possibility of alleviating high stress concentrations in the aircraft structure by modifications of the load distributions through the control system, and hence we can gain some reduction in structure weight and extension of fatigue life. We can also adapt such systems to reduce peak accelerations at crew stations and so improve the ride quality of the aircraft. Yet another application is to change the critical flutter conditions to advantage by suitable de-coupling of oscillatory modes of the aircraft. These developments are often referred to as Active Control Technology (ACT) and the vehicles designed to involve this technology are sometimes called Control Configured Vehicles (CCV).

Another development of note is growing pressure for so-called Direct Force Controls (DFC). The manoeuvring requirements of fighter aircraft point to the advantages of being able to generate directly substantial lift and side forces and so loosen the normal tight coupling between translatory and rotary motions. For very large aircraft, the initial adverse response as an elevator is deflected can present problems which a control producing direct lift could obviate. We shall hear in much more detail about these recent technological advances from Dr. Thomas and Dr. Skow whilst D.F.C. is also the subject of Prof. Sachs' lectures.

4. NOVEL CONTROLS

These developments highlight the need for new forms of control additional to the traditional ones, particularly when demands are made for flight conditions where the traditional controls become ineffective. At the Symposium of 1979¹ reference was made to a variety of types of control that have attracted attention in recent years. Fig. 3 provides illustrations of some of these. They include:-

- a) Rotatable foreplanes or canards, both vertical and horizontal. These provide initial forces in the same sense as the required manoeuvre (unlike elevators), are usually free from the blanketing

effects of upstream wakes at high angles of attack or yaw and are promising as direct force controls.

- b) Rotatable strakes. These operate much like close-coupled horizontal canards and they generate at incidence well defined leading edge vortices that interact with downstream lifting surfaces in a way which can readily be exploited.
- c) Elevons. These are elevator surfaces that can be operated differentially to produce rolling as well as pitching moments and so can be used to augment or replace ailerons.
- d) Tipperons. These are moving surfaces at the wing tips which can also be used to augment or replace ailerons. They can generally remain effective at high angles of wing incidence unlike conventional ailerons, since their incidence is not tied to that of the wing.
- e) Flaperons. These are flaps which can be operated differentially as ailerons. They can be effective at high speeds but the interactions involved with neighbouring surfaces can be very complex.
- f) Pylon Split flaps. These can be used to augment the rudder as a yawing control under conditions (e.g. high incidences) when the latter becomes ineffective.

In addition to the above, leading edge flaps in combination with trailing edge flaps can be adapted to act as controls. Their effectiveness for small movements shows up to advantage at transonic speeds. Spoilers generally show flat regions of poor response for small movements, venting usually helps to reduce such regions, but a more ambitious scheme involves segmenting the spoilers, with the segments operated in a sequence determined by a control system designed to achieve a near linear response over the whole deflection range.

Blown flaps can be used as a powerful control for landing a STOL aircraft at speeds below the minimum drag speed with a control system that schedules the stick force and throttle to conform to the pilot's normal experience at speeds above the minimum drag speed. Spanwise blowing can be used to modify the development and trajectory of leading edge vortices and hence the forces and moments which they induce over rearward lying surfaces. At high angles of attack, the vortex formation over the forebody of a fuselage can become asymmetric with consequent large side forces. These forces can be considerably modified and controlled by blowing from suitably positioned orifices on the surface. We shall hear more of these developments from Dr. Skow. It must be emphasised that these novel forms of control can be no less complex in their effects and interactions than conventional controls. An example of this is illustrated in Fig. 4 showing the strong side forces that can be produced by the differential action of horizontal canards. It will be clear that to develop efficient shaping laws for a control system it is essential to know the aerodynamic characteristics of the control surfaces involved in detail and these must include all interference and coupling effects.

It must also be emphasised that for ACT applications such as relaxed stability or flutter control, the controls must be effective at the frequencies of interest. This makes it necessary to examine their dynamic characteristics at such frequencies. At high frequencies, we may expect significant phase differences between the control movements and the consequent aerodynamic response, and there is some evidence to suggest that for spoilers there can be large reductions in effectiveness at high frequency (see Ref. 3). Dynamic effects are the subject of the lectures to be given by Professor G.J. Hancock.

5. STATUS OF PREDICTIVE THEORIES AND EXPERIMENTAL TECHNIQUES

Current lifting surface theories usually start with the assumption of inviscid flow. With a defined trailing edge, the Kutta condition enables such solutions to be unique and they can be regarded as representing the flow with attached boundary layers and infinite Reynolds number. They can be made to approximate more closely to the flow at a finite Reynolds number by including an allowance for the presence of the boundary layer. As long as the flow is attached, the latter acts as equivalent to a small displacement of the surface normal to itself as far as the external inviscid flow is concerned. It must be noted, however, that there is as yet no completely reliable method of modelling turbulent boundary layers in three dimensions. Further, if the flow is extensively separated then the available modelling processes become less than adequate. Transonic flows also present special problems associated with the presence of shock waves and their interactions with the boundary layers. Unsteadiness adds further problems to the modelling of turbulent boundary layers.

Such methods can be extended to apply to lifting surfaces with controls, but since the controls are often situated towards the rear of the surfaces where the boundary layers are thickest viscous effects become particularly important and must be closely modelled if the control characteristics are to be reliably predicted. Progress is being made and we shall hear something of this during the course of the Lectures by Professor Körner and Dr. Thomas, but we shall not be surprised to learn that the major problems lie in dealing with separated flows, three dimensional flows, non-steady flows and transonic flow.

Experimental methods also have their problems. To minimise scale effects and to achieve as high a Reynolds number as possible wind tunnel models are often made as large as possible in relation to the tunnel dimensions. However, the large model supports needed can then introduce significant effects which are not easy to correct for, whilst the constraints due to the tunnel walls can be difficult to determine with adequate accuracy at transonic Mach numbers. Aeroelastic effects can also present special difficulties both in flight and in wind tunnels as can the measurement of the dynamic characteristics of controls. We shall learn much more of the techniques and problems of experimental methods in the Lectures of Dr. Mabey and Dr. Eshelby.

6. AN INTERESTING SEQUENCE OF RESEARCH PROJECTS ²

In the foregoing, I have touched on some of the major lessons that were evident from the 1979 Symposium. One of the papers presented at the Symposium was particularly graphic and comprehensive and I thought it would be helpful to briefly summarise this paper for you as it offers illuminating illustrations of these lessons as well as of others.

The paper was by Johannes and Whitmoyer and entitled 'AFFDL Experience in Active Control Technology' ². It describes a series of research programs that started in 1966 and which are still in progress. The initial program (1966-68), called the Load Alleviation and Mode Stabilisation Program (LAMS), was aimed to explore on a B52 how far the existing controls combined with an array of rate gyros as sensors could be adapted to alleviate gust loads and control the natural modes of this large flexible aircraft. The controls were ailerons, rudder, elevator and spoilers with inner and outer panels, the outer being used symmetrically. The results were encouraging and showed a substantial reduction in basic fatigue damage rates but also showed the importance of taking account of lag effects in the response to spoiler movements. The next program, called the CCV-B52 Program (1971-74) was a logical extension of the first and was aimed to explore what could be achieved by introducing new control surfaces to provide flutter mode control, manoeuvre load control, ride control, fatigue reduction and augmented stability. The new controls included vertical and horizontal canards, flaperons and outboard ailerons. The design goals set were a reduction of turbulence induced oscillation at the pilot's station of 30%, a reduction of wing root bending moments by 10% during a specified 1g pull up manoeuvre, adequate flying qualities with the C.G. at the aft neutral point position, and flutter free operation 10 knots above the unaugmented flutter speed. We were told that all these goals were achieved.

Simultaneously, there was a related programme of work concerned with the application of ACT to fighter aircraft. This was called the Survivable Flight Control System Program (1969-73) and for this an F4 aircraft with a fly-by-wire system with no mechanical links was used. This quadruplexed, manoeuvre demand system used analogue signalling. The aircraft was reported to have much improved response and damping characteristics and better tracking ability as compared with the basic F4 aircraft, but the roll rate response was judged too fast for conventional flight. This pointed to the need for a multi-mode system capable of being tailored during a flight to suit each task and for this a digital system was clearly needed. The next stage was called the Precision Aircraft Control Technology/CCV F4 Program (1971-77) for which close coupled horizontal canard surfaces were added as well as fixed leading edge slats. These canards permitted flight at a negative static margin of -7.5% and they were effective in providing direct lift control, not so much because of their own lift which was largely balanced by the download on the wings behind due to the downwash induced by the canards, but because of the load on the tailplane and elevator in trimming out the pitching moments produced by the canards. Indeed, in the same way, trimming out the yawing moment produced by a vertical canard by means of the rudder can be used to generate a direct side force. However, these tests showed, as already noted, that horizontal canards if operated differentially can also produce substantial side forces, particularly at high angles of attack, and this was borne out by subsequent wind tunnel tests on a YF16 model (see Fig. 4). It is of interest to note that in an early program of this series on a NT33A aircraft in 1971 side forces were generated by trimming out the yawing moments generated by asymmetric operation of drag petals on the wing tip tanks. These gave valuable experience in the use of side force control in the execution of flat turns and lateral translation in dive bombing attacks, but the amount of side force generated by such means was relatively small.

The next major stage was the CCV-YF16 Program (1973-77). This was designed to explore more fully the tactical advantages of direct force control and to examine the effects on manoeuvrability of a relaxed stability system on the YF16 aircraft. Here, vertical canards were used for direct side force and direct lift was obtained by coordinated deflection of the wing trailing edge flap and the horizontal tail. It was not expedient to use horizontal canards mainly because of difficulties of installation on this aircraft. A number of manually commanded unconventional flight modes were investigated ranging from vertical path control at constant angle of attack to directional attitude control at constant flight path angle (see Fig. 5) and these were deemed to offer significant tactical advantages in combat. However, they also brought out the importance of a prior thorough knowledge of the aerodynamic interactions associated with the controls. For example, at high angles of attack the blanketing of the tail plane by the trailing edge flaps when operated negatively (up) may make trim impossible for lack of control power, the incidence can then increase uncontrollably until a new but undesirable stable state is reached. The authors state - 'Although the closed loop flight control system was generally effective in masking undesirable aerodynamic characteristics there are definite limits to this ability' and they stress 'the importance of a thorough and accurate definition of bare airframe aerodynamics'.

As already noted, these investigations exposed the need for a digital control system that tailors the control laws to suit individual tasks. A further program was therefore mounted on an A-7D aircraft called the AD-7D Digital Multi-mode Flight Control System Program (1973-76). Although the control surfaces used were the conventional ones, the system showed significant improvements in air-to-air and air-to-ground tracking and strafing tasks.

The last completed program was the Integrated Flight and Fire Control Program (IFFC) (1978-81). As its name implies it combines flight control, fire control and weapon systems in such a way that the pilot can play an optimum part in their use, particularly in evasive manoeuvres and air-to-air tracking.

Finally, and still in progress, is the Advanced Fighter Technology Integration Program (AFFI-16) in which most of the advances of the previous fighter programs are to be incorporated in a F16 aircraft.

CONCLUDING REMARKS

The 1979 Symposium pointed to a number of important problem areas for future research. Since these areas were at the frontiers of our knowledge at the time I believe it will help you if I recapitulate what they were, and in the light of what you will hear during the course of the Lecture Series you should be able to judge how far we have progressed during these last four years and where effort should be directed in the future.

The Executive Summary of the Symposium noted:-

- 1) The need for a better data base. The major organised sources of design aids are the ESDU data sheets and DATCOM. They are very valuable but they are based on data which are at least 20 years old. More modern data needs to be collected and analysed. We also need supplementary research programs of a fundamental nature to meet gaps in the data base.
- 2) Our knowledge of dynamic effects on control characteristics is very inadequate particularly at transonic speeds.
- 3) Theoretical methods for predicting aerodynamic characteristics of controls are inadequate in accounting for viscous effects and flow separation and are not reliable enough for transonic speeds.
- 4) Interference and cross-coupling effects are very important but not well understood.
- 5) We lack adequate information to distinguish which are the important derivatives for ACT and we lack reliable methods for their determination.

REFERENCES

1. Aerodynamic Characteristics of Controls. AGARD Conference Proceedings No. 262, May 1979.
2. R.P. Johannes & R.A. Whitmoyer AFFDL Experience in Active Control Technology. Paper No. 10 of Ref. 1.
3. R. Destuynder Problemes d'Aerodynamique Instationnaire Poses Par l'Utilisation des Gouvernes dans le Control Actif. Paper No. 18 of Ref. 1.

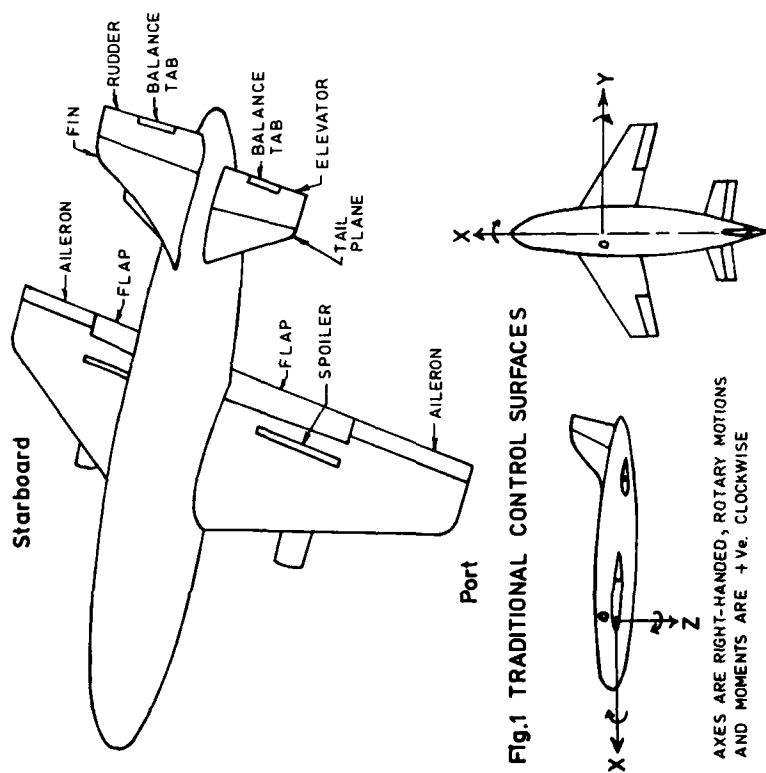


Fig.1 TRADITIONAL CONTROL SURFACES

VELOCITY COMPONENTS	OX	OY	OZ
ANGULAR VELOCITY COMPONENTS	U	V	W
CONTROL MOVEMENTS	p	q	r
	y	z	y
+ ve. CONTROL MOVEMENTS	AILERONS ELEVATOR RUDDER		
	ST. (DOWN) DOWN TO PORT		
	PORT UP		

Fig.2 SIGN CONVENTIONS

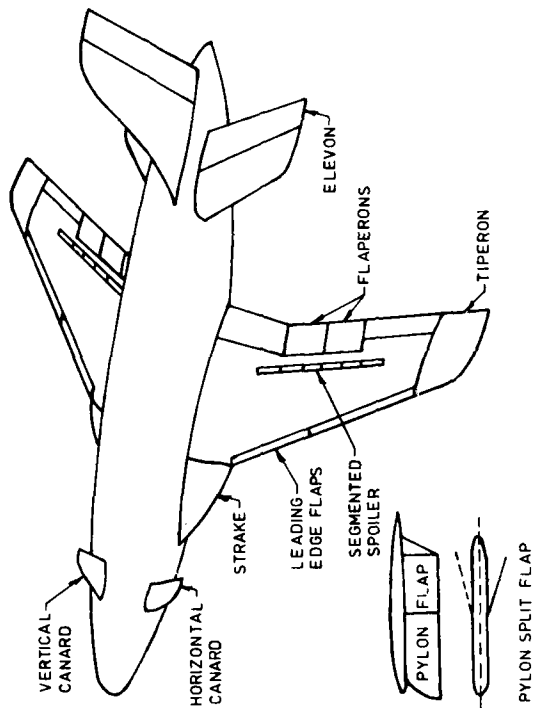


Fig 3 SOME NOVEL CONTROLS

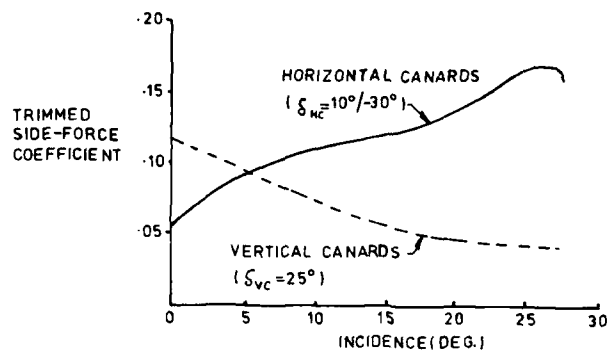


Fig. 4 SIDE FORCE COEFFICIENTS DUE TO HORIZONTAL AND VERTICAL CANARDS ON CCV VF-16 (REF.2)

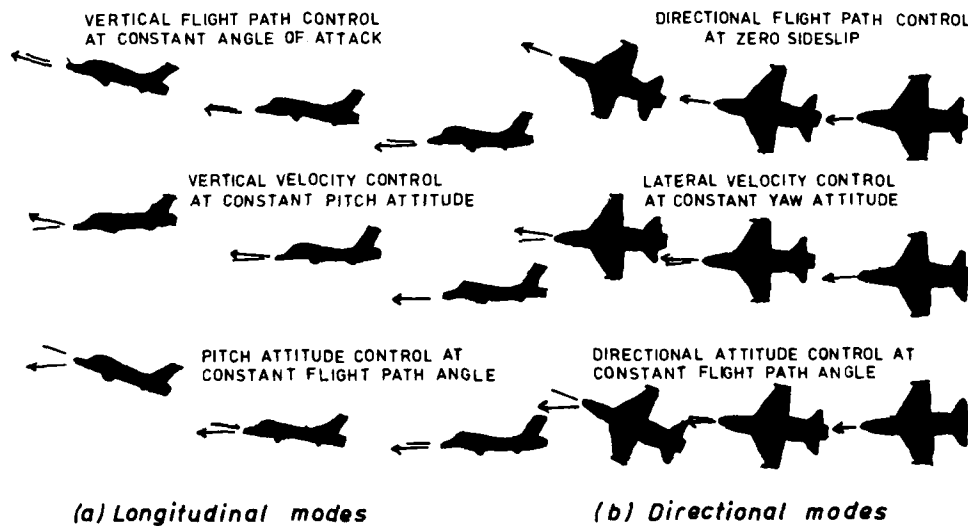


Fig. 5 UNCONVENTIONAL CONTROL MODES TESTED ON CCV YF-16 AIRCRAFT (Ref. 2)

THE AERODYNAMICS OF AIRCRAFT CONTROL

A general survey in the context of active control technology

H.H.B.M. Thomas*

3 Avenue Road, Farnborough, Hampshire, GU14 7BW, UK

SUMMARY

The Introduction of Active Control Technology into the design of aircraft has been accompanied by the use of additional control devices or motivators and an expansion in the uses to which existing motivators are put, either individually or in combination with each other or one of the novel forms of control.

A general survey is attempted of the different properties such as maximum control powers, effectiveness generally and to some extent the actuating moments as is an assessment of their relative importance in different contexts. The present data base available to the aircraft designer from different sources is examined in some detail with particular attention to identifying the direct and indirect effects. Particular emphasis is placed on the efficiency of the motivator at extreme flight conditions, characterised by high angle of attack and high subsonic speeds.

Symbols

- (i) Deflections of motivators,
- | | |
|-------------------------------------|----------|
| producing primarily pitching moment | η |
| producing primarily rolling moment | ξ |
| producing primarily yawing moment | ζ |
| producing primarily forces | δ |
- (ii) Suffices which identify the motivator type
- | | |
|---------------------|-----|
| Aileron | A |
| Canard | C |
| Horizontal Canard | HC |
| Vertical Canard | VC |
| Elevator | e |
| Eleven | E |
| Flap | F |
| Leading edge flap | LEF |
| Trailing edge flap | TEF |
| Pylon mounted flap | PF |
| Nozzle flap | N |
| Rudder | R |
| Spoiler | S |
| Tail }
Tiperon } | T |

For example, a spoiler which intended for use as a roll motivator has deflection ξ_S whilst one designed to generate lift changes as the direct or primary function has deflection δ_S .

1 INTRODUCTION

When the late S.B. Gates, who had a happy knack with words, spoke of aircraft stability and control being "the two sides of the same coin" he had clearly glimpsed the truth of a much broader proposition that the dynamics of the aircraft generally and its control are closely linked. The full implication and potential of this close relationship could only be realised with the advent of Advanced Control Technology (ACT). In fact, the merger of the two aspects of design become increasingly more complete with the passage of time and aircraft design proceeded down its evolutionary path. The important stages in this process are identified by the graphic representation of Fig 1.

On the left is the simple unaugmented aeroplane with a direct mechanical link between the pilot and each motivator (control surface) thereby enabling the pilot to manoeuvre his aeroplane at will by manipulation of the motivators. It was the task of the pilot to coordinate his control inputs to obtain the desired response. An adequate level of stability of the different modes of motion had to be provided by fixed aerodynamic surfaces.

* Consultant.

The stage represented by the central diagram refers to the aircraft design in which the motivators are used to augment or modify both stability and response. The first of these took the form of effectively increasing the damping of an oscillatory mode of motion of the aircraft, for example, the Dutch Roll or lateral oscillation. In the second instance the response to the motivators was shaped as in a manoeuvre-demand system. This stage was rendered possible by the introduction of power operation of the motivator and servo-systems into the design. The importance of the control characteristics has now increased relative to the other aerodynamic characteristics.

On the right is the aircraft of current interest. Here the abandoning of the mechanical link in favour of a fly-by-wire system and the use of an on-board computer permit development in many directions. By use of not only the usual motivators but also others, more highly specialised in their function, it is possible to embark on a relaxation of the stability of the bare airframe, de-coupling of degrees of freedom, load alleviation and/or limitation in gusts or manoeuvres etc. The resulting aircraft is often referred to as a "control-configured vehicle (CCV)". The significance of the motivator characteristics has increased further in relation to other aerodynamic characteristics, but it is necessary to guard against interpreting this as meaning that knowledge and understanding of the latter characteristics can be more relaxed. It may not be too rash to say that, some basic lift/drag properties apart, they may come to dominate the aerodynamic side of aircraft design. If this be so then it is clear that it is necessary to be sure that knowledge and understanding of the aerodynamic action of motivators is adequate in all respects, that is, not only in respect of established motivators, but also in respect of what factors make for a good motivator.

With these thoughts in mind the bulk of this paper is concerned with a broad, overall review of the present data base, that is, the collection of empirical and theoretical data that may be used as a basis for design. The results from a considerable number of recent wind-tunnel and flight tests are examined under headings which correspond to different aspects of motivators. These headings are (i) the direct effect or the intended primary function (ii) the indirect effect which is the force or moment produced concurrently and as a result of the motivator deflection only. These are further subdivided accordingly as the effect is a moment or a force. In addition some attention is given to the actuating moments, to the interaction between a motivator and other components of the aircraft, to the difficulty of ensuring accuracy in the acquisition of the empirical data and the prospects as regards the development of theoretical methods.

A tentative attempt is made at assessing the degree of dependence of various active control systems on motivator characteristics. In the light of this assessment maximum control power comes in for special scrutiny, especially at the extreme flight conditions of large angle of attack and high subsonic speeds, since this is a probable critical design case. The increasing importance of interference and cross-coupling terms generally is noted.

2 AERODYNAMIC FACTORS AFFECTING THE EFFECTIVENESS OF A MOTIVATOR

It is possible and useful to set down a number of basic factors which, in part at any rate, determine the effectiveness of a particular motivator. These are as follows:

- (1) Its magnitude - if a surface this is its area, if a jet then its momentum.
- (2) Arm if the intention is to produce a moment about the cg. This may not be immediately discernible in some cases, for example, for aileron control, but is evidently related to (4).
- (3) The intrinsic design and characteristics of the motivator.
In other words that which determines how the motivator functions when it is separated from the aircraft along with any necessary adjoining structure. For example, an elevator as part of the tailplane in isolation.
- (4) The location of the motivator.
This is its disposition in relation to other aircraft components which can interact with the flow over the motivator, *in situ*. The flow environment within which the motivator operates may be affected in three ways:
 - (a) the direction of flow is changed,
 - (b) the general level of kinetic pressure in the incident flow is lowered compared with its free-stream value,
 - (c) the non-homogeneous nature of the local stream.

The examples of the subsequent sections serve to illustrate the effect of each of the above factors.

3 DIRECT EFFECTIVENESS

3.1 Pitch motivators

For the aft-tail arrangement the contribution of the tailplane to static stability is proportional to its effective angle of attack. Thus it is seen that, in accord with the trends indicated in Table 1, the contribution of the close-coupled tailplane to stability is much reduced relative to that of its long-arm counterpart. Thus for preser

day combat aeroplanes the tailplane tends to become mainly a contributor to the damping-in-pitch of the bare airframe. The need for increased control power for trim and manoeuvring as the aircraft speeds moved into the supersonic regime saw the all-moving tailplane, with or without elevator, replace the traditional elevator as the primary pitch motivator. The short tail arm removed the need for an extended aft-body with its disadvantages of extra weight, drag and complexity.

Thus the present-day combat aircraft takes on the typical shape shown in Fig 2.

The usual motivator characteristics associated with the tailplane of such a layout employing closely coupled, low tailplane are well demonstrated by wind-tunnel measurements of the pitching moments on a representative fighter concept⁶ at different tail settings for a range of lift coefficients and Mach number. The cambered sweptback wings and cambered fuselage of this model are chosen for optimum cruise and manoeuvre performance at a Mach number of 1.4. For the indicated reference centre of moments, the configuration is just stable at subsonic speeds and shows the usual increase of stability as the Mach number passes through unity and beyond (see Fig 3). The control effectiveness ($\partial C_m / \partial \eta_T$) increases at transonic speeds but drops to almost half its value at subsonic speeds as the Mach number approaches 2.0. The low tailplane position ensures that the effectiveness is maintained throughout the lift-coefficient range. Some loss of effectiveness is noticeable at the extreme up elevator angles tested.

These results may be contrasted with those for a configuration with a high tailplane. From among the number of tests of transport aircraft models with high tails, the one chosen⁷ to highlight the differences was tested with both tailplane and elevator deflections. The first point to note is that the negative slope of the pitching moment coefficient with respect to angle of attack at small values give place to a reversed slope somewhere between 20° and 30° angle of attack, see Fig 4. Thus, whereas the contribution of the tailplane to the static stability of the aircraft is large near zero angle of attack, it becomes progressively smaller as the angle of attack is increased beyond a certain value. These trends in the pitching moments contributed by the tailplane are accounted for by the much reduced kinetic pressure of the local flow field and increased downwash as at some angle of attack the tail moves towards the wing wake and becomes immersed in it.

The same factors affect the pitching moments due to the tailplane deflection and the elevator deflection. Because the downwash at the tail at low angles of attack is small and the kinetic pressure almost at its free stream value, the tailplane and elevator, singly or together, behave much as they would for the isolated tailplane. Accordingly the two motivators remain effective up to the stalling angle of the tailplane. Naturally, an earlier and more dramatic loss of effectiveness occurs when the elevator is deflected in the same sense as the tailplane, although it is interesting to note that just below the stalling angle (for $\eta_e = 10^\circ$) the curve is more linear.

At an angle of attack of 20° stalling conditions are reached considerably earlier around tailplane deflections of about 7.5° to 8° . This implies that for this order of tailplane angle the effective angle of attack of the tailplane must be in the neighbourhood of 18° or that the downwash angle is about 10° . The tail is now much nearer the wing wake. However the negligible change in the tailplane effectiveness at small deflections shows that the kinetic pressure changes in the incident flow are small.

Different conditions pertain at the angle of attack of 30° because the tail is now immersed in a strong wing wake. The retention of effectiveness up to tailplane angles of 20° indicates that even at this setting the large downwash ensures that the tailplane is unstalled. The loss of effectiveness at tailplane angles less than 8° indicate a loss of kinetic pressure at the tail location.

The effectiveness of the tailplane for the F-4E aircraft⁸ has been derived from flight test data in the form of the derivative, $\partial C_m / \partial \eta_T$. Wind-tunnel test data are available for the same aeroplane. The results from these two sources make an interesting comparison (Fig 5). The flight test records were taken in separate flights covering the two ranges of angle of attack of 5° to 20° and 20° to 40° . Within the lower range of angles the value of $\partial C_m / \partial \eta_T$, deduced from the flight test data, shows the derivative falling off with increase in the angle of attack. In contrast, the derivative deduced for the range 20° to 40° remains virtually unchanged. Results are also available from two separate tunnel tests and are compared with the $\partial C_m / \partial \eta_T$ values obtained from the flight tests. It is interesting that the flight data for the lower angles of attack agree with one wind-tunnel test data whilst those for the large angles of attack agree more closely with the other tunnel test data. The problem of large trim drag on an aeroplane designed to operate at supersonic speeds has on occasion resulted in the adoption of a tailless design. The pitch motivator in this case is usually an elevon (a flap type control fitted to the wing trailing-edge). It is found that these have reasonably well-behaved characteristics. However, on slender wings operating at very high angles of attack a breakdown of the vortex flow occurs, which results in the vortex bursting and moving across the span. Under these conditions some deterioration of effectiveness is to be expected.

In the example shown in Fig 6, which refers to a supersonic cruise fighter concept designed for optimum performance at a Mach number of 1.8, the manner in which the derivative $\partial C_m / \partial \eta_T$ varies with increase of Mach number indicates a slight increase of effectiveness as transonic conditions are approached from below followed by the characteristic drop as the Mach number increases supersonically.

Elevon type motivators in the shape of an inboard flap incorporating a two-dimensional nozzle and an outboard plain flap have been tested¹⁵ at low speed for three combinations. These are a wing-body configuration, a wind-body with canard and lastly the last configuration with a strake added to the canard. The effect of three levels of thrust coefficient where tested, zero, 0.2 and 0.3. In Fig 7 only the results for the first and last of these are displayed. In the absence of thrust augmentation the addition of a fixed canard has a large beneficial effect on the pitching moments due to flap deflection to the limit of increased maximum lift coefficient. Both the wind-body combination generally and the wing-body-canard configuration for zero flap setting only exhibit pitch-down tendency near the maximum lift condition. Introduction of flap deflection on the wing-body-canard converts the pitch-down of the configuration without canard and of the unflapped wing-body-canard configuration into a pitch-up tendency. This implies a significant adverse interference between the wing, flaps and canard which must result in an appreciable forward shift of the additional loading due to flap deflection. It may also be seen that the strake, which has little effect over most of the lift coefficient range, aggravates this pitch-up trend.

The tests with thrust were undertaken later to see if its introduction would eliminate the pitch-up trend. Some alleviation of the pitch-up tendencies does occur but they still persist for the canard with strake. Addition of the thrust has increased appreciably the effectiveness of the flaps away from the stall. It is of interest that the same order of increase is already present at a thrust coefficient of 0.2 suggesting that augmentation up to boundary-layer control has by then been reached and no further improvement follows increase of the thrust coefficient to 0.3.

Canard surfaces may be used as pitch motivators and at this stage it is proposed to examine their characteristics only in this role. In the earlier more general discussion of the aerodynamic factors affecting their effectiveness in the role of pitch motivators, the point has already been made that, in contrast to the aft tail, they are subject to upwash (in place of downwash). Accordingly, if attached to the fuselage and in the neutral position ($\eta_c = 0$) their effective angle of attack will, if anything, exceed somewhat that of the aircraft. Moreover the conditions in the incident flow are never far removed from those in the free stream ahead of the aircraft.

The first of these effects implies that the total effective angle of attack of a canard, when used to produce nose-up pitching moments, is of the order of the angle of attack of the aircraft plus the canard deflection if not somewhat in excess of this angle. Accordingly the canard can reach its stalling angle at quite modest deflections when used in the sense just mentioned. In a recovery attempt from a high angle of attack condition, deflection of the canard in the nose-down pitch sense tends to unstall it.

The influence of a canard on pitching moments has been examined in wind-tunnel tests of a number of closely-coupled canard configurations. The results of some of these tests are now considered.

For the aircraft configuration¹³ of Fig 8, it can be seen that the pitching moment increment due to a 10° deflection of the canard soon drops off as the angle of attack or the lift coefficient of the aeroplane is increased and over a small range of lift coefficient actually reverses. The very small effect spanwise blowing over the wing has on these trends demonstrated conclusively that the loss in effectiveness is attributable to stalling of the canard. This is further confirmed by the retention of effectiveness up to the highest lift coefficient used in the test (1.3), when spanwise blowing over the canard surfaces is introduced. Another test¹⁴ refers to a wing-canard combination of higher sweep and the same trends may be seen, see Fig 9. Tests also exist of the same wing, but now fitted with trailing-edge flaps and in combination with a flapped canard of increased size. Here the canard flap is set at 30° whilst the wing flap deflection is varied for two settings of the canard surfaces, with the results shown in Fig 10. The pitching moment coefficients with the canard deflected $+5^\circ$ show a pitch-up tendency at lift coefficients between unity and the stall. With the canard deflected through -5° the pitch-up trend is delayed to higher lift coefficients (>1.8). With the constant canard flap angle of $+30^\circ$ it is inconceivable that the canard is other than in upload throughout. If anything an early stall would be expected with a canard deflection of $+5^\circ$ and high angle of attack. The deflection of the canard in the other direction through -5° would be expected to delay the onset of stalled condition by some 10° in the angle of attack. In fact, the angles of attack quoted for pitch-up onset in the two cases are 15° and 24° , a separation of 9° . Therefore the cause of the pitch-up trend is almost certainly a wing-canard interference effect. It is of interest to note that the wing flap as a pitch motivator remains effective at all lift coefficients and that some improvement occurs for the case with canard deflected through -5° .

The influence of Mach number on canard effectiveness¹⁴ as a pitch motivator is illustrated by the test results shown in Fig 11. Here the same surfaces are employed as a canard and an aft-tail. Appropriate adjustments were made in the centre of gravity location. It is seen that both devices maintain effectiveness (at small deflection at any rate) throughout the Mach number range. The pitching moment derivative, $\partial C_m / \partial \eta$, displays similar variation with Mach number, but the aft-tail is more effective than the canard, the amount being much more than can be explained by arm length.

3.2 Roll motivators

The conventional motivator for generating rolling moments is the aileron. Because of the loss of effectiveness exhibited by ailerons at high angles of attack, other forms

of roll motivators have been brought into use either to replace the ailerons or to supplement them. The characteristics of the various types that have been tested are now discussed.

The deterioration in aileron effectiveness just referred to stems from the separation of the wing flow, which for a sweptback wing occurs towards the wing tip. This has been in the past the usual position for the aileron to take advantage of the long moment arm. In an attempt to offset the loss, the ailerons have been in some cases relocated at mid-span. Tests of such an arrangement shows that the move is only partially successful. As the unpublished results presented in Fig 12 show the loss of effectiveness is still present at subsonic speeds even for the small aileron deflection (± 7.5), although this loss becomes less marked at transonic speeds and beyond. Large aileron deflections aggravate the loss at subsonic speeds.

Although the expected drop in effectiveness occur for small angles of attack and supersonic speeds, this level of effectiveness is more nearly maintained as the angle of attack and aileron deflection increase.

Some improvement in the behaviour of ailerons can be discerned in the results shown in Fig 13 which shows the effect of adding a slat²⁰ to the leading edge of the outer wing. The main effect of the slat is to delay the onset of the breakdown of the flow. Thus at a Mach number of 0.6 the rolling moments due to an aileron angle of 30° drops abruptly at an angle of attack of 12° on the unslatted wing. A similar, but not so severe, drop occurs at the later angle of attack of around 16° in the case of the wing with slat. The slat has little effect at the highest angle of attack tested. At the Mach number of 0.9 there is again a rapid fall off of rolling moment at much the same angle of attack followed by a rapid recovery beyond an angle of attack of 16° . Shock-induced separation is almost certainly present and must affect the behaviour. A second series of tests refer to ailerons in combination with spoiler control and discussion of these results is deferred till later.

Such losses are not the only one to occur at high subsonic speeds. The effects of aeroelasticity can cause an appreciable loss of effectiveness at all high speed conditions as the results for the Concorde²¹ and Viggen²² aircraft, see Fig 14, show. In the case of the Viggen both rigid and elastic models were tested in the tunnel so that the results for the elastic model may be compared with estimates based on correction of the rigid model results. Good agreement is obtained for the elastic/rigid factor. Equally good agreement was obtained when the rolling moment derivative, $\partial C_l / \partial \xi$, obtained by correction of the rigid WT-model for full-scale elasticity when compared with values deduced from flight tests. Use of the mid-span or inboard position for ailerons can reduce the aeroelastic loss, but there is not always an overall gain.

As an example of what can happen the results of tests of one-piece flaperons on a model of the YF-17 aeroplane¹⁻⁹ are now examined. The configuration is shown in Fig 15 and the effect on the rolling moment generated by a differential aileron deflection of 20° (total angle) of relocating the inboard end of a flaperon extending to 0.75 semispan is also shown. If account is taken of aeroelastic effects the adverse effect of interference with the elastic tailplane and the more serious loss due to the wing elasticity, the resultant rolling moment is reduced and becomes reversed for a Mach number of 1.1. Moving the inboard end of the flaperon outward reduces the adverse interference with the tailplane, but at the same time reduces the rigid rolling power of the flaperon without significant improvement in the overall roll effectiveness. In an attempt to overcome these problems segmented flaperons were tested, that is, the one-piece flaperon was subdivided into two separate flaps, which may when used actively be moved in an antisymmetric manner with respect to the aircraft and symmetrically with respect to the deflection of the two segments on each wing, or in an asymmetrical manner as regards the segments on the port or starboard wing. With equal and opposite deflections of the flap segments the interference effect on the tailplane becomes favourable. This leads after account is taken of the aeroelastic effects to the results shown in Fig 16.

Of late there has been little development in the technology of spoiler type motivators. Nothing has emerged that radically alters the general summary given in DATCOM³, which somewhat abbreviated reads "At subsonic and transonic speeds, spoilers do not, in general, provide linear variation of effectiveness with spoiler projection, particularly at small deflections. This deficiency can be corrected by use of a slot or slot deflector behind the spoiler. For thin wings at high angles of attack spoilers are ineffective. This ineffectiveness can be partially overcome by the use of a slot behind the spoiler and by the use of leading-edge devices ... In order to achieve maximum effectiveness, spoilers should be located towards the rear portion of the wing, for the following reasons (i) the ineffectiveness of spoilers at small deflections increases with distance from the trailing edge (ii) the lag time at low speeds becomes excessively long for forward-mounted spoilers. The optimum spanwise extent and position of spoilers are determined primarily by wing sweep. The higher the sweep angle, the farther inboard the spoilers should be placed." The loss of spoiler effectiveness at high angle of attack cannot be²³ estimated by any known method and has to be determined by experiment. A typical example of the drop in effectiveness and the improvement that can be effected by use of a slot deflector is given in Fig 17. By deflecting the slot flap through half the deflection of the spoiler a 40% increase in the rolling moment increments is obtained at the lower angles of attack. Moreover the effectiveness at large angles of attack and Mach number 0.6 is also improved except at the small spoiler deflections. Similar trends are shown by the curves for the high subsonic Mach number of 0.9.

Results from tests of a plain spoiler tested in conjunction with an aileron on a model of the F-4 aircraft have already featured in Fig 13. These tests examine the effect of a wing leading-edge slat on the rolling moments produced by the combination of motivators. At the lower Mach number of 0.6 neither the addition of spoiler or the slat increased effectiveness at around an angle of attack of 20° . For the aileron plus spoiler (unslatted wing) negligible improvement is noticeable over the aileron about at an angle of attack of 15° and a Mach number of 0.9. The addition of the slat improves matter for angles of attack close to 15° for the higher Mach number and over a more extended angle of attack range at the lower Mach number.

Spoilers have also been tested (and used) on a number of transport-type aircraft. The lift increments due to a spoiler on a model of the outboard portion of the wing of an aircraft (aspect ratio 7.0 and 30° sweepback of the quarter chord line) shown in Figs 18 and 19 are for spoilers mounted on the shroud of a high lift flap and occupying the spanwise position between 40 per cent and 80 per cent of the wing semi-span. A slat is fitted to the wing leading edge. In the first of the two figures just referred to can be seen the effect of opening up a gap between the wing surface and the leading edge of the flap spoiler. Increased effectiveness throughout angle-of-attack range up to the stall accompanies the opening up of a gap of 3 per cent chord. However, doubling the gap size brings the lift coefficient increments beyond an angle of attack of 10° to the level of those for the no gap. The spoiler chord was kept constant at 12 per cent wing chord throughout, so that the height of the spoiler trailing edge changes with the gap size. It is difficult to speculate as to the influence of the two effects (a) gap at constant spoiler height and (b) spoiler height.

The improved effectiveness at small deflections to be seen in Fig 18b is probably a gap effect as such. Again there is no merit in increasing the gap above a certain size.

The benefits of a slot or slot-deflector behind the spoiler have already been noted. It, therefore, comes as no surprise to learn that venting through the flap shroud results in improved effectiveness. In all eight variants where tested covering not only the size of the vent, but also its position chordwise. Only three are selected for presentation in Figs 19a and b. These test results are for a plain spoiler with a 3 per cent gap and with the flaps deflected 40° .

It is interesting to compare the effectiveness of the spoiler arrangements just described with another type¹⁻⁴. Here the spoiler consists of part of the trailing edge portion of the flap shroud, see Fig 20. The characteristics of the spoiler, even with no gap, are more linear, whilst opening of a gap, as before, results in increased effectiveness. Some increase is obtained in changing from a 3 per cent gap to a 6 per cent gap, but the increase is not proportional. Of further interest is the fact that the spanwise centre for the incremental load due to the spoiler is close to the position of the centre of area of the spoiler. It is, furthermore, little affected by the parameter changes considered previously.

Another means of overcoming the nonlinearity and dead zone characteristics of spoilers at small deflections is the use of digitally controlled segment spoilers, which provide only three discrete deflections. Some wind-tunnel tests and ground simulator studies¹⁻⁷ demonstrates that satisfactory roll control can be obtained apart from the usual deterioration at high angles of attack, beyond the stall. It is proposed to flight test a fully-developed system of segmented spoilers.

In as much as they delay the onset of flow breakdown leading-edge devices (slat and flaps) are expected to extend the range in angle of attack for which spoilers are effective. It is, however, doubtful whether they will play a role as the primary roll motivator.

Differentially deflected tail panels have been used to supplement different aileron arrangements to provide better overall roll control. In the absence of any ailerons and possibly with outboard ailerons in use, the flow environment, in which the tail panels of a close-coupled aeroplane operate, is such that the effective angle of attack about which differential deflection takes place is small. The rolling moment produced by the differential tail is almost independent of the angle of attack. However, the magnitude of the moment is small, since for a fuselage mounted tail the moment arm is small.

Wind-tunnel tests on the F-15 aeroplane bear out these statements, since it was found that the sum of separate contributions of the aileron and the differential tail equals the measured combined rolling moment. This last never falls below 60 per cent of its low angle of attack value throughout the range in angle of attack of 0° to 40° , for both the wind-tunnel results and the flight results, as Fig 21 shows.

In the YF-16 aeroplane^{24,25} differential tail was used in conjunction with a flaperon (inboard aileron of appreciable span), see Fig 22. Once again on its own the differential tail contributes an almost constant rolling moment (not more than 20 per cent reduction) throughout. The combined roll motivator shows a drop off in the rolling moment produced by an aileron deflection of -20° and tail deflection of -5° . This is basically the deterioration in the aileron effectiveness, but may also contain some interference effect on the tail.

In isolation from the fuselage (that is, if the fuselage position occupied by the canard were replaced by a fixed aerofoil surface) a differentially deflected canard would be expected to behave in much the same way as its tail counterpart, except that it would

be subject to adverse effects at large angles of attack. At a sufficiently large angle of attack and a modest differential angle, it would be possible for both surfaces to be stalled. However, when the canard panels are mounted on a forebody the action of the differentially deflected panels on the flow around the body results in large interference effects so that most significant force produced is a sideforce. More is said of these effects under following separate headings.

All-moving wing tips (tipperons) do not seem to have found favour with aeroplane designers. Their use has been considered for missiles. However, this attitude may be changed when the benefits of introducing some differential into the deflections of each tip so that up-going tip (i.e. trailing-edge up) moves through a greater angle than the down-going tip are appreciated. This differential in the angles is determined by the aircraft angle of attacks.

Some tests¹⁻⁶ made of tipperons mounted on a model of a fighter type configuration with an aspect ratio 4.0 wing of 35° sweepback, see Fig 23. Two tipperon planforms were tested, one trapezoidal and the other, of slightly larger aspect ratio, triangular. The latter is a somewhat more effective roll motivator at low angles of attack, but there is little to choose between them at high angles of attack. The rolling moment increments produced by each of the following, tipperon, aileron and flaperon, are compared in Fig 23. It is interesting to note that the up-going tipperon (~70°) retains effectiveness well up the angle of attack range, but requires a moderately large angle of attack to reach its peak effectiveness. In Fig 24 the rolling moment increments have been examined in terms of the effective geometric angle of attack of the tipperon ($\alpha + \zeta_{TA}$). As is clear the influence of the wing angle of attack as such on the moment generated is not large, but equally it is evident that some interaction between the tipperon and the wing occurs. The use of tipperons as roll motivators denies the aircraft designer the facility of mounting missiles on the wing tips.

Another and more specialised roll motivator is a tip motivator, which changes the wing span asymmetrically. This device could take the form of a rotating surface similar to the arrangement by which wing sweep is varied. Its effect amounts to a sideways shift in the wing load distribution, so that the rolling moment generated is roughly proportional to the lift coefficient. Accordingly, this motivator serves only as a means of augmenting other devices. Its effectiveness decreases beyond the angle of attack for which the flow breaks down over the outer wing.

Two other schemes which also only yield rolling moment at high angle of attack are illustrated in Fig 25. These are an asymmetric strake and one-sided spanwise blowing.

A basic and potentially powerful means of generating rolling moments is differential sweep of the port and starboard wings of a variable-sweep aeroplane. Its use is limited by the difficulty of deflecting the panels sufficiently rapidly.

3.3 Yaw motivators

The traditional yaw motivator is the aft-mounted rudder. There has been little incentive to departure from its use since rudder deflection usually produces an almost constant moment throughout the operational angle-of-attack range, even beyond the wing stall. Furthermore, it maintains its effectiveness as Mach number is increased subsonically, but suffers the usual and expected drop at supersonic speeds.

All-moving fins should be more efficient yaw motivators on purely aerodynamic grounds, but when elastic deformation under load is taken into account they may not show the same superiority.

As an example of how the effectiveness of a motivator is affected by the flow field within which it operates the effect of changes in certain parameters has upon the rudder yawing moment coefficient, on a high-wing transport aircraft with external flow jet flaps and a high tailplane²⁶, is worthy of consideration. As may be seen from Fig 26 the yawing moment due to 20° of rudder, with the wing flaps at 60° and no blow, is maintained well beyond the wing stalling angle (tests show this to be 10°) but finally dropping slightly at the extreme angles of attack. When, however, the rudder angle is increased to 40° the variation of the yawing moment with angle of attack shows a dramatic drop beyond 20° with reversal present around 30°. These losses in effectiveness are more severe than that which can be ascribed to the flow separation of the rudder at the larger deflection angle. Confirmation of this comes from the results of tests with blowing applied over the rudder, but still more over the wing trailing-edge flaps. This increases the effectiveness of the rudder, at both 20° and 40° deflection, over the angle-of-attack range 0° to 26°, in the case of 20° of rudder and 0° to 15° for 40° of rudder. Around an angle of attack of 30° the yawing moments due to each deflection drops to a near zero level. It is important to note that the yawing moment produced by the 40° deflection is larger with blow than without blow throughout the range of angle of attack tested. This is an indication of the beneficial influence blowing has on the breakdown of flow associated with large rudder deflection. It is evident that some other effect, which is adversely affected by blowing, must be present. It is not possible to ascertain what this interference effect is on the basis of the information given²⁶.

The tests with engine power ($C_u = 3.74$), which as might be expected has a powerful effect on the aerodynamics of the wing and flap as shown by the results for the maximum lift coefficients, with and without engine jet, 8.5 at an angle of attack of 25° and 2.5 at an angle of attack of 10° respectively, shed little light on the matter. Delay in any deterioration arising from the effects of wing-flap wake would be expected at the higher

angle of attack of 25° and this seems to be present in the results for both blown and unblown rudder. The injection into the wake of such a powerful jet might have been expected to speed up the flow of the fin and rudder, but at angles of attack of less than 20° there is no evidence of this, which presumably implies that the flapped-wing wake is too low to directly affect the rudder. The effectiveness of the rudder at 40° deflection is, however, materially improved. That a number of conflicting influences are at work here is demonstrated by the loss of effectiveness suffered by the rudder at 20° deflection between the angles of attack of 25° and 30° .

With blowing present over both the wing flap and the rudder there is all-round improvement.

Engine thrust per se has a direct effect on the yawing moments produced by a rudder. The derivative $\partial C_n / \partial \delta_R$ measured on two model arrangements of the B-1 aircraft serve to illustrate this effect. In Fig 27 the variation of the rate of change of yawing moment coefficient with rudder angle with Mach number is shown. One set of results refer to an unpowered sting-mounted model and the other to a strut-mounted model with simulated engine thrust effects. The difference between them cannot be entirely ascribed to the beneficial effect the jet plumes of the body-mounted engines has on the rudder, since some small changes in shape of the aft fuselage have to be made to accommodate the sting.

For combat aircraft, in which the engines are often embedded in the fuselage and exhaust at the base of the fuselage, aft of the fin and rudder, the effect, just discussed, would be expected to be less. In this context the results of tests made on the F-15 aircraft²⁸ and a 3/8-scale, unpowered model are worthy of examination. During the full-scale tests three levels of engine mass flow were used and it was found that there was no detectable consistent trend with engine mass-flow change. This seems to support the above proposition. However, the tests of the unpowered model show levels of the rate of change of yawing moment coefficient with rudder deflection some 20 per cent less than those derived from the full-scale tests. The underlying cause of this discrepancy is not immediately clear. Ref 28 suggests that it is attributable to scale effects. Against this it may be argued that the sideforce coefficient for the fin and rudder, $(\partial C_y / \partial \delta)_{fin}$, would be also subject to the same scale effects, which would affect the values of N_y and N_r . The agreement, model and full-scale, is good for these two derivatives, which suggests that the values of $(\partial C_y / \partial \delta)_{fin}$ in the two cases must be close. It may be, therefore, necessary to look elsewhere for the explanation of the discrepancy. One possibility is some difference in gap or rudder geometry.

The influence of the flow environment within which the fin and rudder operate may be directly assessed from the results of wind-tunnel described in Ref 1-12. A model of a fighter type aircraft incorporating a wing leading-edge flap set at 15° and an uncambered strake, see Fig 28, was the subject of these tests. They include measurements of the kinetic pressures in the region of the fin and of the yawing moment derivative $(\partial C_n / \partial \delta_R)$ for deflection of a part-chord rudder and an all-moving fin. The pressure survey was made in the absence of the fin and indicates very little loss of kinetic pressure at angles of attack 0 and 20° . However, at an angle of attack of 35° , the kinetic pressures (see Fig 28) over the lower portions of the fin and extending further upwards to half-way up the rudder at the rear of the fin chord compared with the regions near the leading edge are down to less than half its free-stream value. The pattern of the wake will, of course, be altered somewhat by the introduction of the fin with a deflected rudder (even at zero sideslip) due to the action of the flow field of the fin and rudder itself. Nevertheless the results just quoted give a clear indication of the rudder yawing moments to be expected. The measured forces and moments due to the rudder shown in Fig 29 are in accord with this statement. These show that by an angle of attack of 52° the rudder and all-moving-fin have become totally ineffective.

As is to be expected an all-moving fin produces greater yawing moments than the part-chord rudder, but the original paper suggests that design and structural problems may be such as may cause the all-moving fin to be deflected through only 15° as compared with the 30° assumed for the rudder. Thus when maximum rudder power is a dominant factor the scales may be tipped in favour of the rudder, which may also show a weight advantage.

Reduction of rudder control power due to aeroelastic effects on both fin and fuselage can be appreciable. Here the results for two aeroplanes, previously discussed, serve to illustrate the point. In the case of the Concorde²¹, the estimated values of the rate of change of the yawing coefficient with rudder deflection is reduced to about half their values when aeroelasticity is accounted for, see Fig 30, and when thus corrected are in fair agreement with values derived from flight test results. The aeroelastic effects are, of course, proportional to the square of the equivalent airspeed and, therefore, their magnitude is altitude dependent as may be seen in the Viggen²² results also shown in Fig 30.

When rudder design is considered within the context of active control systems, some of these, for example relaxed lateral stability, will result in smaller fin sizes, whereas in others increased effectiveness is at a premium. Accordingly means of increasing the rudder powers within a given fin and rudder size must be sought. The use of slotted rudders²⁹ is one possibility and the more direct approach of increasing rudder to fin size is another. The latter needs to be done in such a way as to avoid the worst of the structural problems of the all-moving fin.

Other forms of aerodynamic devices seem likely to be associated with the simultaneous generation of larger rolling moments than the rudder. The tiperon (already examined as a roll motivator) is such a device. However, if means of scheduling the deflections on the

port and starboard sides with angle of attack are forthcoming, the results of the tests, previously considered¹⁻⁶, indicate that yawing moment control can be achieved up to angles of attack of 40° or more. It is, of course, necessary to have an alternative roll motivator to generate the cancelling rolling moments to make a de-coupled yaw motivator of the tipperons, see Fig 31.

There are certain specialised means of producing yawing moments over a limited range of angle of attack. Those, which yield yawing moments at high angles of attack only, are almost sure to find a use in supplementing the conventional rudder control as its effectiveness drops off, but discussion of this aspect of control is deferred till later.

Fins or fins and rudders mounted on the fore-body of an aeroplane produce yawing moments which are smaller than those of a conventional rudder as the wind-tunnel and flight tests¹⁸ of the CCV YF-16, Fig 32, indicate. There are, however, interference effects to be considered as well as non-linearity of the yawing moment with deflection of the canard.

3.4 Force motivators

Means exist whereby the forces acting on an aeroplane may be changed. To date little use has been made of such force motivators apart from some limited application of direct lift control in exercising control over the approach path to land.

Longitudinal force motivators

One component of the aircraft is there primarily to provide longitudinal force and that is the engine. The slow response characteristics of engine thrust has restricted its use as a motivator within a control system. Energy management is an area where active control of engine thrust will in future play an important role. These considerations are outside the scope of this paper.

Equally air brakes are not in the present sense used as motivators.

The most immediate way of changing speed quickly as might be needed in combat manoeuvres of the rapid deceleration type is to enable the aeroplane to manoeuvre quickly and safely into a high angle-of-attack and high-g condition.

Direct lift motivators

Means of changing the lift acting on the wings have been part of the aeroplane scene for a long time. To improve the aircraft's take-off and landing characteristics a variety of trailing-edge flaps, some of sophisticated design, have been in use. Just as in the case of the engine setting these have been used, almost exclusively in the past, in a selective rather than a motivator sense. There now emerge other tasks to which these devices, or more strictly something like them, may be harnessed. To the augmentation of lift in the positive (upward) sense for the phases of flight mentioned previously there has been added the need to enhance the lift capability of an aircraft in manoeuvring conditions. Where the lift generation for the purpose of attaining and sustaining increased g-levels is achieved by selecting settings of manoeuvre flaps, slats etc, it does not strictly speaking come into the field of active control. If, however, these devices are operated automatically and in a scheduled manner with both angle of attack and Mach number, they assume a more active role. The whole subject of how to maximise lift and minimise drag and the related handling problems, which get in the way of achieving the lift levels possible, is too wide a topic to be treated adequately within a section of a paper like the present one. It is, it must be stressed, important in relation to active control technology and aircraft design, if only because it defines the aerodynamic environment in which other flight control systems are expected to function.

Attention is now directed to lift generating motivators, which are part of such control systems as those which aim to alleviate manoeuvre loads, gust loads or improve ride quality, according as to which of these last two objectives is judged the more important. Such motivators are required to adjust lift (in both the positive and negative sense) with rapid response.

The large trailing-edge flaps used in the take-off and landing of aeroplanes have highly specialised geometry to meet the ever more acute needs of transport aircraft, in particular, during these phases of flight. From the lift viewpoint these needs centre around the achievements of high lift coefficients at some fixed setting. They are, therefore, inappropriate for use in the control system just referred to previously. This is on two counts namely, that the rate of deflection is unlikely to be sufficiently rapid and that their section shapes are ill-suited to work efficiently for upward deflection. It is possible that a part-span, part-chord portion of the landing flap could be used for the purpose. Here it is worth bearing in mind that a small chord flap or double flap operated through larger than usual angles may have something to offer.

An alternative is to seek rapid adjustment of the lift by the combined use of the usual trailing-edge flaps and spoilers operating about a non-zero deflection. Such a scheme is described in two of the papers appearing at the AGARD symposium proceeding, Ref 1 (1-4 and 1-16). In such an application³¹ the spoiler has to be mounted far back on the wing chord otherwise there is a change of lift slope as well as lift, see Fig 33. During the tests on the 9% thick aerofoil shown there, the spoiler was represented by a small fence normal to the aerofoil surface. The use of a device to vary slot width at the leading-edge of the flap (see Fig 33) is encouraging in that little change in lift curve slope occurs, but the lift changes progressively as the slot width is increased.

Engine thrust may form the basis of lift motivators using devices which leave the thrust unchanged but deflect or alter its action. These are vectoring of the thrust, deflection of jet flaps or even the adjustment of jet efflux over the blown flap by flow restriction. Some tunnel tests of the Buccaneer aircraft³², wind-body model, give results for the lift due to plain trailing-edge flaps. The same tests show the augmentation of lift that attends blowing at the leading-edges of the wing and the flap. In the results displayed in Fig 34 the aileron of the half-wing model is also deflected downwards through 30° . For the unblown flap, the increments in lift coefficient decreases somewhat as the angle of attack is increased. With flaps deflected through 45° the lift coefficients are smaller than those for the flap at 30° , indicating a breakdown in the flow over the flap. Relatively low values of C_{μ} (the blowing momentum coefficient) are sufficient to double the lift increments due to flap. Additional blowing at the wing leading-edge (at 1.5 per cent chord) delays the stall and gives a higher maximum lift coefficient.

Some further information on the favourable effects of spanwise blowing near the leading-edge of wings and in combination with leading and trailing-edge flaps may be obtained from Ref 13.

Sideforce motivators

The possible advantages accruing from the provision of a sideforce motivator, or force motivators in general, has only come to the fore in recent years. Not surprisingly there is evidence to suggest that direct force control (decoupled from any moment) can result in unconventional motions potentially beneficial to the pilot. Thus direct lift control may be used in an automatic mode to increase precision in tracking accuracy, whilst lateral translational modes have a place in air-to-ground operations.

The difficulty from the aircraft designer's point of view is that motivators intended to supply sideforce as the direct effect almost all generate other forces and moments. They are, furthermore, not particularly effective, whilst the indirect effects such as yawing, rolling and pitching moments are large relative to the direct effects. The required moment cancellation to decouple sideforce may entail an appreciable drag penalty.

Both single and twin canard surfaces mounted below the nose region of the aeroplane exhibit such shortcomings. Furthermore, the sideforce produced drops throughout the angle-of-attack range. This is illustrated in Fig 35, which refers to twin so-called vertical canards, where it may be seen that at an angle of attack of 30° the arrangement generates only a third of the sideforce it does at zero angle of attack.

Similar, but more erratic, variation with angle of attack is present in the test results presented in Fig 36¹⁻¹⁷. Both single and twin motivators were tested and the twin canards were also tested at an under-wing position. The under-wing canards retain effectiveness a little better than the forward mounted surfaces as the angle of attack is increased, but these also are ineffective for angles of attack in excess of 25° . As is to be expected, as a result of reducing the moment arm, the indirect yawing moments due to the underwing vertical canards are smaller than those of the forward mounted surfaces. Around an angle of attack of about 25° the yawing moments are more equal, see Fig 36b.

When considering application to a design it is necessary to bear in mind that in a trimmed or compensated state the aft-mounted yaw motivator produces a sideforce as well as the cancelling yawing moment, so the combination of motivators yields augmented sideforces. To increase the sideforce generated beyond those observed in the tests mentioned previously would probably result in so large a size of vertical canard as to give rise to problems with ground clearance and/or compatibility with carriage of stores.

In contrast to the force characteristics just discussed, the sideforce (an indirect effect) produced by differentially deflected horizontal canards (Fig 35b) shows an increasing trend with increase in the angle of attack. Appreciable augmentation of these sideforces occurs when the yawing moment produced are cancelled by rudder deflection. Other favourable properties are brought out in Figs 35c and 35d. At a given angle of attack the sideforce is approximately linear with the total deflection angle and there is but little variation in the motivator characteristics throughout the Mach number range 0.2 to 1.2. When it is remembered that the sideforce arises out of interference effects on the adjoining parts of the aircraft these trends are surprising. A number of other test results^{16,19,21} bears out these findings and serve to make the differentially deflected horizontal canards one of the more attractive sideforce motivators. It is, however, still necessary to be fully aware of the extent to which these surfaces, particularly when operated about different mean positions, can affect other aerodynamic characteristics of the aircraft through interference.

The two types of sideforce motivators previously discussed are compared in Fig 37 with another type¹⁻¹⁴ in respect of their relative effectiveness and variation of the sideforce produced as the angle of attack is increased. This third type consists of split flaps fitted to the under-wing pylons, which are designed to carry external stores. The wind-tunnel model of the Alpha Jet aircraft¹⁻¹⁴ was fitted with two such pylons on the port and starboard wings. Six component measurements (that is, contributions to C_x , C_y , C_z and C_l , C_m , C_n) were made for each flap acting singly and in combination for deflections between 0° and 60° in the port and starboard sense.

Due to the complicated manner in which the interference effects with other aircraft components vary, the sideforce contribution of each individual flap differs from flap to flap, when each flap is deflected through the same angle and in the same sense. For instance, of the inner two flaps, the one deflected towards the fuselage is the more

effective, whilst of the outer two flaps, that deflected away from the fuselage is marginally the better. The matter is made more complicated by the fact that the outer flap deflected towards the fuselage retains its effectiveness at large deflections better than the outer flap deflected away from the fuselage.

What matters in application are the combined effects. These are displayed in Fig 38 which also shows that the individual effects cannot be superimposed. The sideforce increases linearly with deflection to begin with, but falls off at the larger angles ($>30^\circ$).

It was found, in the course of these tests, that without the store in position the split flap was only half as effective a sideforce generator as shown by the curves of Fig 39. Extending the depth of the pylon restored the sideforce nearly to the level of that with stores present, thus suggesting that the presence of the store effectively increases the aspect ratio of the pylon. However, an end-plate of length equal to the pylon chord, but of width only of the order of the pylon depth failed to produce a similar effect, resulting in only a small partial restoration of the sideforce.

Equal deflections by no means represents an optimum arrangement and the original paper suggests a control law, which it is hoped to use in flight tests, and which reduces indirect moment effects.

One further means of generating sideforce has been investigated and this consists of differential spanwise blowing¹³ over the wings. As the trends illustrated in Fig 40 this device has the following merits. The sideforce produced is almost constant for angles of attack from 0° to 16° and even increases somewhat beyond this. As the value of the jet momentum coefficient is increased the sideforce also increases, more than linearly.

4 INDIRECT AND INTERFERENCE EFFECTS

There is usually a discernible force or moment, which a motivator is intended to generate. This is designated here as the direct effect and is for the most part the most significant effect. The rudder, for example, is intended primarily to provide yawing moments. In doing so it also produces a sideforce and a rolling moment. These then are the indirect effects even though the sideforce on the fin and rudder is an essential part of the yawing moment. Both direct and indirect motivator effects arise from the changes in the forces acting over the motivator and its immediate adjoining components of the aircraft, but in the case of moments they also depend on the location *per se* within the airframe. Thus, for instance, deflection of an elevator changes the pressure distribution over the elevator, the fixed tailplane and the rear of the fuselage. The sum of the pressure differences (upper and lower surfaces) yields a change in tail lift (hence aircraft lift), whilst the accompanying moment depends on the tail arm.

In addition to those effects designated here as indirect, forces and/or moments resulting from application of the motivators can be modified by interference effects. These are the effects which arise from interaction between the motivator and other parts of the airframe not in its immediate vicinity. Examples of such effects are the reduction of the kinetic pressure in the wing wake affecting the elevator effectiveness and the yawing moment induced through the action of flow changes on the fin, which result from differential deflection of the tailplane panels. This latter effect is sufficient almost to mask the indirect yawing moment arising from the asymmetric deflection of the tail panels.

More generally, interference implies an aerodynamic interaction, often mutual, between the flows over two or more components of the aeroplane. It may, therefore, be present between two fixed, as well as movable components, of the aeroplane. Two motion variables of the aircraft or one motion variable and deflection of a motivator may be involved. The major effect the angle of attack has on the characteristics of a motivator is of the latter type. This is usually so strong at large angles of attack that it is rarely expressed in the form of a second-order derivative and on this account has already appeared throughout the text. In like manner the introduction of sideslip can affect aft-mounted motivators.

Indirect and/or interference effects may be coupling in nature. In this case the forces and/or moments relating to one axis (of a body axis-system) are affected by the presence of a parameter related basically to another axis. Examples are yawing moment due to aileron deflection and pitching moment due to sideslip. That these effects can be of growing importance in aircraft motions at high angle of attack is demonstrated by the studies of Ref 45.

It is not always possible to separate out indirect and interference effects and so, in what follows, they are considered together.

4.1 Pitching moments

If trailing-edge flaps are deflected symmetrical on the port and starboard wings they produce, in addition to the desired lift and drag changes, pitching moment contributions. These are of two kinds. First there is the indirect moment arising from the changes in pressure distribution over the wing. Second there is the interference effect on the tailplane due to changes within the wing wake.

In the case of the transport aircraft³⁴ of Fig 41, it is seen that, whereas the first type of pitching moment would be expected to be virtually the same for both the low-tail and the high tail configuration, the other is radically affected by the geometry of the tail.

To gain some insight into the nature of these differences it is necessary to consider the results shown in Fig 41 in some detail.

Firstly consider the pitching moments due to angle of attack for zero flap setting and either tailplane setting. The high tailplane exhibits the usual pitch-up trends, which indicate beyond an angle of attack of some 10° , the downwash at the tailplane has increased considerably and that the kinetic pressure is reduced giving smaller and smaller tailplane contributions to the pitching moments.

In contrast the low tailplane shows a reverse trend, that is, the tailplane contribution to the slope of the pitching moment with angle of attack increases, if anything, indicating that at zero flap setting the wing wake moves upward away from the tailplane as the angle of attack becomes large enough.

Changes in the kinetic pressures alone may be identified by examining the increments in the pitching moments due to tailplane deflection. For zero flap angle, the results for the high tailplane indicate kinetic pressure losses consistent with those mentioned earlier, whilst those for the low tailplane show a marginal increase in the tailplane effectiveness. This is again consistent with the previous argument.

For both high and low tailplanes the tailplane effectiveness ($\partial C_m / \partial \eta_T$), at a given flap setting, shows small losses of the same order of magnitude. Two effects are at work here, since deflection of the flap lowers the wing wake relative to the tailplane, but at the same time intensifies the wake. The nett effect is the outcome of the action of these two influences. As far as can be determined from the data this nett effect is some recovery of effectiveness for the high tailplane and a lowering of the effectiveness at all angles of attack for the low tailplane, when the flap deflections are $30^\circ/55^\circ$.

The effect of most immediate concern is the increment in pitching moment due to a given flap deflection.

At low angles of attack and the high tailplane the downwash is very small and the kinetic pressure near the free-stream value. For the low tailplane, under the same angle-of-attack conditions, the downwash and the kinetic pressure loss are both somewhat larger. These differences result in the somewhat lower pitching moment increments for the low tailplane configuration at all flap settings and for the two tailplane angles.

It is the variation of the pitching moments due to flap with angle of attack that is of real interest. Over the entire angle-of-attack range tested these suffer only a decrease of some 30 per cent for the high tailplane. For the low tailplane large changes are immediately obvious and these are such as to reverse the contribution for small flap angles in the case of tailplane angle 0° . Further increase in flap deflections produce small or nil nett contribution. Unlike the pitching moments due to tailplane deflection, which are mainly affected by kinetic pressures, the flap contributions arising from wing-tail interference depend upon both downwash and kinetic pressure changes. In the light of the trends shown by the tailplane effectiveness, it may be argued that the downwash changes dominate the differences for the pitching moments due to flap deflection in the two cases.

It is not possible to unravel further the nature of the interference effects on the tailplane for which tests of the wing-body combination at a range of tailplane angles for at least one flap setting would be required.

The upward deflection of trailing-edge flaps on the wing for direct lift control on the CCV YF-16¹⁸ gave rise to interference effects of the same character. As Fig 42a shows, large down-tailplane deflections are required to trim the pitching moments due to a flap deflection of -15° . This flight experience is explained by the wind-tunnel tests, the results of which are shown in Fig 42b. These indicate a falling tailplane effectiveness as the angle of attack is increased with a slight up-turn at the limit of test. Deflection of the lift flap through -10° reduces the contribution to pitching moment from 20° of tailplane deflection overall and some worsening of the trends with angle of attack. The fact that conditions at around 22° are such that the tailplane is almost on its limit necessitated the placing of a restriction on the use of the direct lift control at high angles of attack.

The results already given in Figs 9 and 10 show that deflected horizontal canards affect the pitching moment produced by the wing at an angle of attack or by flap deflection. The extent to which the latter effect is present may be gauged from the increments produced at a canard deflection of $+5^\circ$ and those produced by a canard deflection of -5° . The separation of the canard and wing in a direction normal to the wing plays an important part in defining the flow changes that will occur over the inboard portions of wing occupied by the trailing-edge flaps.

Differently deflected horizontal canard surfaces would be expected to give rise to an indirect pitching moment and also an interference effect. The magnitude of the first effect is governed by the effective angles of attack of the two panels, whilst the second arises from interference with the flow over the wing, the aircraft body and an aft-tailplane (if present).

If the moment due to the lift changes on the canard surfaces dominates it follows that for zero (and essentially for any small) angle of attack the two panels produce equal and opposite pitching moments so that there is a nett zero change in the pitching moment acting on the aeroplane. This seems to be the case for the canard configuration¹⁶ of Fig 43, at the two Mach numbers of 0.4 and 0.9. Otherwise it is necessary for all the interference

effects to be virtually self cancelling. By the same token the pitching moments for the $\pm 10^\circ$ canard deflections should be close to those for $\pm 0^\circ$. Such is the case here, apart from the values at high lift coefficients for Mach number 0.4, which may be accounted for by stalling of the panel deflected through $+10^\circ$ and/or interference effects.

The magnitude of the pitching moments due to asymmetric deflections of the canard can be appreciable as the tests for deflection of a single panel show. It is also recorded that no significant pitching moments were produced by anti-symmetric canard deflections on the CCV versions of the YF-16 and F-4 aircraft⁴.

Leading-edge flaps, strakes or slats can make a contribution to the overall pitching moments^{20,40}. This tends to become more pronounced with increase in the angle of attack so that the slope of the pitching moment with respect to angle of attack is reduced. Examples are shown in Fig 44 and Fig 45. These pitching moments are very configuration dependent.

Deflection of a spoiler (with or without a slot) alters the pressure distribution over the wing and so it is to be expected that some pitching moments are generated along with the intended rolling moment. The pitching moment contributions can be significant as the results shown in Fig 46 demonstrate. These refer to the spoiler arrangement of Fig 17.

Pitching moments associated with interference occur when pylon mounted flaps are operated to create sideforces, see under lift later.

4.2 Rolling moments

The most obvious example of a source of indirect rolling moment is that produced when a rudder is deflected. Even on fairly closely-coupled configurations the moment arm which produces the rolling moment is appreciably less than the fin arm, which is responsible for the yawing moment. A tailplane mounted on the top of the fin and rudder, as in Fig 26, causes the load distributions on the fin and rudder to increase towards its tip and so increases the ratio of the rolling moment to yawing moment. This can be as high as 0.5 in an extreme case, but a value of roughly half this is more typical^{27,44}, see, for example, Fig 47. As can be seen from these results the ratio is little affected by either variation in Mach number or angle of attack. This is quite usual.

Differentially deflected horizontal canards have already been discussed in the role as sideforce generators, although the effect is essentially one of interference. Divorced from the remainder of the aircraft the canards would be expected to produce rolling moment with some yawing moment. In this sense the rolling moment would be the direct effect, but the sideforce produced becomes the most significant effect when the horizontal canard is mounted on the aeroplane forebody. Thus in the context of the control of the aircraft it is more logical to regard the sideforce as the direct effect and the rolling moment as an indirect effect.

Asymmetric deflection of horizontal canard panels can produce sufficient asymmetry in the downwash field at the wing as to result in an induced rolling moment opposing that generated by the canard surfaces. The nett rolling moment acting on the aircraft may in this way be reduced. The magnitude of this effect might be expected to depend on the effective angle of attack of each panel and the differential between them. There is also present some small upwash due to the wing. The results of the tests on the canard configuration of Fig 43 which are presented in Fig 48 do not entirely support the notion that the rolling moments are determined by the geometric effective angle of each panel, since on the basis of that argument the moments, at a given angle of attack, for a zero port deflection and -10° deflection on the starboard side should equal those for $+10^\circ$ deflection on the port side and zero deflection on the starboard side at an angle of attack 10° greater. There is the possibility that the interference with the fins obscures the individual effects.

Twin fins mounted under the forebody at or forward of the wing position produce, in addition to sideforce and yawing moment (either may be regarded as the direct effect), some rolling moment. Ref 1-17 describe test results for both single and twin vertical canards. Those for the double fins exhibit a rather erratic behaviour with variation in the angle of attack, see Fig 49. This behaviour may not be wholly representative as the yawing moments of Fig 32 behave in a much more reasonable manner. It may be simply a question of accuracy as the incremental moments are obtained from differences of nearly equal numbers and so close to the limits of accuracy of the wind-tunnel balance.

Flaps fitted to underwing pylons¹⁻¹⁴, not unexpectedly, also produce some rolling moment along with the sideforce. Deflection of the short chord flaps in the same sense, to produce additive contributions to the sideforce, produce individual rolling moments not all in the same sense. The outer of the two flaps which are deflected towards the fuselage produces a rolling moment opposite in sign to each of the two flaps on the opposite side of the aircraft and which are deflected away from the fuselage. The inner of the two flaps deflected towards the fuselage produces very small rolling moments. When all the flaps are equally deflected and taken in combination they produce the rolling moments already displayed in Fig 38, along with the yawing moments.

4.3 Yawing moments

A well-known indirect yawing moment is that due to the differential deflection of the aileron (a roll motivator). It is usually adverse in sense and has been, of late, a source of trouble in the handling qualities of aeroplanes at moderate to high angles of

attack. In this case the yawing moment is produced by changes in the lift-dependent drag forces across the wing span resulting from the pressure distribution changes produced by deflection of the aileron. On this account it is a difficult quantity to estimate with any degree of accuracy.

The increments in yawing moment produced by a total aileron deflection of 30° on a model of the F-4 aeroplane²⁰, at Mach numbers of 0.6 and 0.9, are shown in Fig 50a, which also shows the effect wing leading-edge slats have on the sign and magnitude of the indirect yawing moments due to the aileron alone. In this instance the aileron deflection is such as to produce a positive rolling moment. The introduction of the slat has some effect on the small moments for angles of attack up to 10° , but beyond this angle of attack the effect is not significant. Deflection of a spoiler, Fig 50b, as an additional roll motivator causes the yawing moments to increase positively at the lower angles of attack, but again the yawing moments at the larger angles of attack are hardly affected. These findings are in accord with the results⁴³ for the rolling/yawing moment characteristics of a spoiler on an unflapped wing as the yawing moments shown in Fig 51 and the rolling moments of Fig 17 demonstrate. These results show that the two moments are of the same sign and become very small as the stalling angle of the wing is approached.

There is a slight indication that the yawing moment due to the spoiler will be maintained to larger angles of attack, as well as generally increased by the use of a slot deflector, especially at the larger spoiler projections.

At low angles of attack, the yawing moment produced as an indirect effect by the use of differentially deflected tailplane panels as a roll motivator is influenced by three factors. These are (a) the fact that the tailplane (in the neutral position as a roll motivator) carries a download, (b) the presence of the fin and rudder between the two panels and (c) the presence of tail anhedral. The three associated contributions to the yawing moment are all proverse with usually that linked to (b) being the dominant. At subsonic speeds the lift-dependent drag gives rise, on account of (a), to a proverse yawing moment at low angles of attack with a reversal to adverse characteristics at large angles of attack. At supersonic speeds, when the download on the tail is increased, the yawing moment is larger and proverse in sense.

Due to the differential in the tail panels and load changes they produce a sideforce induced on the fin in the direction towards the up-going tail surface. The resulting yawing moment contribution is proverse and roughly proportional to the sideforce derivative $(\partial C_Y / \partial \delta)_{fin}$. It, therefore, tends to exhibit the same sort of variation with Mach number. Because of wing-body interference with the flow over the fin the contribution due to the fin can decrease rapidly at very large angles of attack. It is possible for the total yawing moment under these extreme angle-of-attack conditions to become adverse, though small. Examples of the yawing moment increments due to differentially deflected tail panels are shown in Fig 29 and in Fig 52.

Spanwise blowing may reasonably be considered as primarily a sideforce motivator (see Fig 40), but it also gives rise to rolling and yawing moments. Because the sideforce is essentially acting close to the centre of gravity of the aeroplane at low to modest angles of attack these moments are small, see Fig 25a and Fig 25b, respectively. At large angles of attack, presumably because the moment arm increases (cf. Fig 40), the moments become appreciable and increasing with increase in the angle of attack.

When twin vertical canards, in combination with the rudder, are used to generate sideforce as on the CCV YF-16. The sideforce must be regarded as the direct effect and the yawing moments generated by the canards the indirect. These have already been displayed in Fig 32. It is possible, of course, to reverse the roles by cancelling sideforce by use of rudder.

Evidence has already been presented to show that differentially deflected horizontal canards, see Fig 35, may be regarded as sideforce generators primarily, particularly since the sideforce produced increases with increase in the angle of attack. In the light of these trends and the evidently almost constant moment arm the yawing moment associated with this particular motivator, it is hardly surprising that the yawing moments exhibit little variation with angle of attack, see Fig 53. Interference effects are present as well as the indirect effect of the moment due to the sideforce. Their presence are indicated by the fact that, whereas the sideforce varies almost linearly, with total deflection (angle between the two panels), the yawing moments does not (cf. $\pm 5^\circ$ deflection with 10° , 0° , also $\pm 5^\circ$ and $\pm 10^\circ$).

Pylon-mounted flaps designed to give a sideforce also produce a yawing moment. The short arm ensures that this is never appreciable. Evidence of the magnitude of the yawing moments resulting from equal deflection of four such flaps has been presented in Fig 38.

Some interesting effects are exposed in the tests leading to the development of the segmented flaperons, see Fig 16, on the YF-17 aeroplane. Tests of large span, one piece flaperons, with and without fins, demonstrate that almost all of the adverse yawing moment due to the flaperon arises from interference with the fins as shown by Fig 54. Segmented flaperons (see section 3.2) offer the possibility of adjusting the level of adverse yawing moments as has already been shown in Fig 16.

Although deflection of all-moving tips (tipperons) for roll control will, in general, also generate a yawing moment, the sense of this moment is not always the same for all combinations of port and starboard deflections. This may be seen from the limited results displayed in Fig 55. It follows that, if the deflections are carefully scheduled with

angle of attack and Mach number, it should be possible to produce any desired level and sign of the indirect yawing moment. If the chosen value be zero, an interesting fact emerges which shows that the angle of deflection of each tiperon for the largest rolling moment must be such that the geometric effective angles of attack are equal but opposite. For example, at 20° angle of attack, the yawing moment is zero for $\xi_{TS} = -55^\circ$, $\xi_{TP} = +15^\circ$ giving effective angles of attack of $-35^\circ/35^\circ$. The nature of the original data does not permit a more detailed analysis to be made.

4.4 Lift

All motivators designed to produce primarily a pitching moment must generate a lift force, since the moment itself (in all existing control systems) is the action of a lift force created on some part of the aircraft some distance from the centre of gravity. The lift, which in this context can be regarded as an indirect effect, is in many instances of little significance in relation to the response of the aircraft to control operation. However, the shorter moment arm associated with the use of elevons, as on a tailless aircraft and the close-coupling of tailplanes, the areas of which are a larger proportion of the wing area, tend to increase the significance of pitch motivator lift. Only the indirect effect has been mentioned thus far, but interference effects can also be present.

For transport aircraft, which have to a large extent retained the past conventional geometry of all types, the lift increments associated with the tailplane or elevator as the pitch motivator are small. The results of tests³⁴ to measure the contributions of trailing-edge flaps and tailplane deflection to the lift coefficient for a transport type aircraft, with a supercritical wing, shown in Fig 56 amply illustrate the validity of the above statement.

This finding may be contrasted with the effect of adding tail surfaces in close proximity to the wing has on the overall lift. Wind-tunnel test results for a large scale model of a closely-coupled advanced fixed-wing fighter³³ are shown in Fig 57. At zero tailplane angle the rate of change of lift increment with flap deflection is reduced by about 40 per cent, at zero angle of attack, by some 30 per cent at an angle of attack of 13° , but by 25° angle of attack there is little effect. Deflection of the tailplane through -20° (nose-down and thus giving a decrease in tail lift in isolation) restores the lift increment of the flap at the two lower angles of attack.

Some interesting results on the question of the generation of indirect lift emerge from the tests of the canard configuration¹⁵ of Fig 7. In this case the pitching moments are produced by the use of trailing-edge flaps, which take up the whole wing span. The outer portion consists of plain trailing-edge flaps whilst the inboard flaps incorporate a two-dimensional nozzle. Tests were made for model less canard as well, and the results in the first diagram of Fig 58 show the appreciable lift changes to be expected from such a powerful, short-arm pitch motivator. The main effect the addition of a canard has on the lift coefficient is to increase the maximum lift coefficient and delay appreciably the onset of stall. It may be recalled that at the same time the pitching moment contribution of the flaps also increased considerably as compared to its value for the wing-body configuration. If the flaps are viewed as suggested as pitch motivators it may be necessary to examine means of cancelling the significant indirect and interference lift. With the role reversed, which in view of the lift increments is acceptable, cancellation of the pitching moment increment must be considered. Either way it is hard to believe that either objective can be achieved without loss of effectiveness but such considerations could indicate a preference for one usage rather than the other.

Since most roll motivators depend upon the production of more or less equal amounts of force on the port and starboard wings, little or no indirect lift is generated in the process. This is certainly so in the case of ailerons or flaperons and it is to be expected to be so for tiperons (but no measurements are available). Equally differentially deflected tail panels produce negligible lift.

Spoilers, when used as roll motivators, create the rolling moment through generating a lift loss on a wing panel. Thus it is that the large spoiler featured in Fig 17 shows a loss of lift coefficient of the order of 0.2, which all but disappears (along, of course, with the direct rolling moment) at the stalling angle of the wing ($\approx 20^\circ$). As Fig 59 shows the losses are of the same order of magnitude for the two Mach numbers of the test. Again since the efficiency of the spoiler as a roll motivator is directly related to the lift change, the opening of a slot by the spoiler-slot-deflector arrangement, brings greater losses, which are retained to higher angles of attack. These results are typical of the spoilers and spoiler location in use at present^{1-4,1-7}.

If sideforce motivators are mounted under the wing surfaces or under the fuselage at the wing station, it is to be expected that lift and pitching moments will be generated at the same time due to interference effects. For example, the pylon-mounted flaps¹⁻¹⁴ previously examined in their role as sideforce generators yield the lift and pitching moment increments shown in Fig 60.

It is, of interest, to note that all four flaps contribute additively to the lift and drag increments, whilst the pitching moments increments do not. The inner flap, deflected towards the fuselage, yields a nose-up moment, whilst the other three contribute nose-down moments. The underlying cause must lie in the different interference effects. As the deflection of the odd one out will have a greater effect on the tailplane, it seems probable that the moment from this source of interference is in the nose-up sense and sufficient to overcome the expected nose-down contribution from the flap-wing interference.

Superposition of the individual increments fails to give the combined effects, shown in Fig 60, apart from drag. This indicates the presence of mutual interference.

On a conventional aircraft layout the rudder is the main contributor to indirect sideforce. This particular indirect effect has assumed greater significance for the close-coupled aeroplane, for which the fin arm is small and the sideforce, necessary to create the yawing moment, is correspondingly larger. Two motivators designed to function directly as roll motivators, but which in the process generate interference sideforce are the single-piece large span flap and differentially deflected tailplanes. They have already been discussed in the context of indirect and/or interference yawing moment of which the side-force under discussion is an essential part.

5 HINGE MOMENTS

Thus far only the forces and moments acting on the aeroplane as a result of actuation of each motivator have been considered. It is evident that, in general, effort is needed to actuate the motivator. In the case of rotating aerodynamic surfaces this takes the form of a moment about the hinge line. For the earliest types of aircraft the motivator was linked mechanically to a pilot input control (stick or wheel) and the required effort supplied by the pilot. Various factors such as physiological limitations, fatigue and ease of applying control rapidly forced the aeroplane designer to seek means by which the hinge moments could be appreciably reduced. Hence a variety of aerodynamic balance schemes came into being.

However, the vastly improved performance of the fighter type aeroplane and increases in the size and performance of transport aeroplanes pushed the hinge moments to many times their earlier values. This forced the designer to aim for very closely-balanced flap-type motivators. In turn, the even finer aerodynamic balance set tighter and tighter tolerances of the manufacture of the motivators. Furthermore, the means by which aerodynamic balance was achieved were unequally successful within the subsonic, transonic and supersonic speeds. The outcome was that power-operation was embraced with some enthusiasm by the aircraft designers, who saw it as a means of avoiding tedious development work extending into the initial flights and which had been so much part of each new project. This in turn meant that hinge moment characteristics had lost much of their old significance and, not surprisingly, there was a progressive fall-off in the degree to which they were studied experimentally. It is difficult to perform a proper judgement of the degree and extent of this fall-off in interest as it is not easy to account for *ad hoc* and, therefore, largely unpublished work. Hand in hand with the relaxed attitude towards hinge moments went a failure to develop the estimation methods set out in DATCOM³ and ESDU⁴ series.

Because of the paucity of experimental data relevant to current and future designs, it is not proposed to discuss in depth any individual set of results.

In general, active control applications are concerned with hinge moments in two flow regimes, namely the quasi-steady and the essentially non-steady. Results for some eight tests (wind-tunnel and flight) for each flow condition, covering the years 1960-78 are described in Ref 1, see 1-2. Apart from those just mentioned, only one set of quasi-steady hinge moment measurements feature in Ref 1, see 1-14. The sole set of measurements referred to are for under-wing pylon flaps of two chord ratios, 60 per cent and 30 per cent, approximately. Use of the smaller chord flap reduces the hinge moments for 40° flap deflection to something like a fifth of those for the larger chord flap.

Hinge moment coefficient derivatives, applicable with the linearised aerodynamic regime, have been calculated and measured for inboard elevons on the Concorde aeroplane⁴⁹. These cover the Mach number range 0 to 2.0. The experimental results, see Fig 61, indicate that the hinge moment characteristics are subject to considerably less variation in the transonic region than suggested by linearised theory.

In Ref 1-20 measured and calculated values of the lift, pitching moments and hinge moments, in oscillatory flow, for an aileron type control fitted to a sweptback wing of modest aspect ratio. Only the hinge moment results, see Fig 62, are quoted here. They refer to a flap oscillating at a fixed frequency and so the frequency parameter changes, as indicated, with change of Mach number.

6 UNSTEADY DYNAMIC EFFECTS

Thus far the emphasis, in the main, has been on the quasi-steady characteristics of motivators. Experience to date has suggested that, by and large, these are adequate for most aspects of the aircraft dynamics. There are, however, circumstances in which the quasi-steady characteristics are clearly inadequate or at best suspect.

In any problem, for which the dynamics of an oscillatory elastic mode is of primary significance, such as control systems aimed at postponement of flutter, the high frequency of these modes requires that aerodynamic derivatives appropriate to corresponding frequency parameter be used.

Other applications of motivators within an active control system and for which it may become necessary to account for the transient unsteady aerodynamic effects, associated with rapid application of the motivator, are in gust load and gust-response alleviation systems.

It is possible, of course, that the quest for ever more agile aeroplanes operating over wide limits will bring in its wake the need to broaden the areas of flight dynamics calling for the inclusion of unsteady effects. Is the significant difference noted in a

comparison of data derived respectively from wind-tunnel tests and from flight tests present in Ref 1-3 an early indication of this trend as indeed the authors of the paper suggest? In as much as moderate, rather than small, tailplane deflections are required on the aeroplane in question to give meaningful test data for analysis, it is to be expected that subsonically the acceleration in pitch that result is large and, in consequence, the rate of change in the angle of attack high. The trend shown by variation with Mach number of the discrepancy between $\partial C_m / \partial \eta_T$ as measured in the wind-tunnel and as deduced from the flight test data, see Fig 63, supports the above plausible explanation. It is interesting to note that pitching moment derivatives with respect to tailplane deflection is alone in showing such discrepancy. All other direct and indirect motivator derivatives show good agreement.

7 NOVEL MOTIVATORS FOR USE IN EXTREME FLIGHT CONDITIONS

Mention has already been made of devices that only come into their own at high angles of attack. Examples of such devices and their effects on the forces and moments acting on the aeroplane are presented in Figs 25a, 25b and 49. These devices may have a motivator role in violent manoeuvres bordering on departure flight conditions and in subsequent entry into quasi-steady equilibrium states such as the superstall or spin. Many of the usual motivators become ineffective at extremes in the angle of attack and so recovery to the normal flight conditions becomes difficult or impossible.

To the devices already discussed must now be added the control of the asymmetric body vortices that arise when a body with a long pointed nose is set at a high angle of attack. It has been demonstrated in Ref 1-24 that blowing tangentially in the downstream direction near the nose can so modify the vortex system as to generate usable yawing moments. The amount of yawing moment produced increases with increase in the jet momentum coefficient, but, as can be seen from Fig 64, quite modest values of C_u yield appreciable yawing moment contributions. If the forebody-vortex control is used in conjunction with 30° of rudder deflection the combined yawing moment suffers a dip of only about 30 per cent at most of the rudder yawing moment at zero angle of attack in the angle of attack range 20° to about 32° and beyond this angle a large increase occurs.

It is anticipated that such motivators will find application in spin prevention and spin recovery systems. The particular choice of motivators depends upon the nature of the spin modes of motion to be guarded against. For flat, fast spins, the emphasis will rest on generation of yawing moments, but in steep spins control of rolling moments may be required as well.

Mention of these highly non-linear dynamic problem areas leads naturally to the next topic.

8 NON-LINEAR AND COUPLING EFFECTS

Non-linearities which derive from high angles of attack and/or large motivator deflections have to a large extent already appeared in the preceding sections. In like manner sideslip, at the larger angles, can also introduce nonlinearities into various forces and moments. Additional non-linearities occur which are coupling in character. Coupling is taken to imply that the forces and moments relating to one axis (of a body-axis system) are affected by a parameter basically related to another axis. A number of the indirect and interference effects previously discussed are of this kind, for example, the yawing moment due to aileron deflection. As this example illustrates coupling terms are not necessarily non-linear, but here the emphasis is on this aspect.

In particular those forces and moments arising under the combined action of motivator deflection and some motion variable are of interest. It may eventually be necessary to proceed to a completely non-linear functional treatment of certain effects within a mathematical model of the airframe aerodynamics. A number of effects may continue to be adequately represented by a derivative albeit a higher order derivative. Ref 45 gives an indication of the importance of some of these effects in the spin motion of a particular aircraft configuration.

Published experimental data relevant to present-day designs are sparse. However, it seems reasonably safe to speculate that forces and moments which are highly dependent on the angles of incidence (α and β) for zero motivator deflections will also exhibit a high degree of dependence on these parameters when the motivators are deflected.

9 THE MOTIVATOR AS PART OF AN ACTIVE CONTROL SYSTEM

Up to now the discussion has centred mainly around the purely aerodynamic aspects of the various motivators taken one at a time. Within the design of an actively controlled aeroplane the number of tasks to be catered for have increased considerably. The motivators, singly or often in combination, must provide the necessary forces and moments required by control systems designed to meet the different functions listed in Fig 65, which also speculates as to the relative importance of various aspects of motivator design. The classification was prepared for Ref 1-2 and nothing has yet emerged that would cause it to be modified.

Some of the papers contained in the symposium proceedings, Ref 1, examine the potential of some active control technology systems. The excellent review (Ref 1-10) of the use of some active systems engineered into existing aircraft designs gives ample

proof of the benefits accrued. It must be borne in mind, however, that these demonstrations of what ACT can do suffer somewhat from the constraints imposed by the need to integrate into an existing configuration. Other papers presented studies related to specific tasks such as the papers on canard and tail designs for relaxed stability. The one by Kehrer¹⁻⁵ and the other by Nguen, Gilbert and Sue Grafton¹⁻¹¹. The application of direct lift control was examined in flight on two different types of aircraft, the YC-14 transport aircraft¹⁻⁸ and the DFVLR HPB 320, in-flight simulator aircraft¹⁻¹⁶. On the first aircraft the lift increments came from blown flaps, whilst on the second they were provided by spoilers operating from non-zero deflection in combination with trailing-edge flaps.

Again a number of the functions listed in Fig 65 are considered by Moynes and Nelson¹⁻⁹. These are alleviation of gust response or ride smoothing, as it is sometimes called, manoeuvre enhancement and the following decoupled modes of control:

- (a) Vertical flight path control - in which the pitch attitude of the aircraft changes but not the angle of attack;
- (b) Vertical translation mode - in which the angle of attack changes but not the attitude;
- (c) Longitudinal pointing mode - in which both angle of attack and attitude change but not the flight path, thus permitting the fuselage to be pointed in a desired direction;

Similar lateral modes can be envisaged and were to some extent demonstrated in the tests of Ref 1-10. These are,

- (a) Directional flight path control - in which the aircraft is yawed but the sideslip angle remains zero;
- (b) Lateral translation mode - in which a lateral velocity is imparted to the aeroplane, but the attitude-in-yaw or azimuth angle remains constant;
- (c) Directional pointing mode - in which the sideslip angle changes, but the flight path directional angle remains constant. This implies a change in the direction in which the fuselage is pointing.

In the past, each motivator was viewed in the context of one primary task, but as already noted this one-to-one relationship between task and motivator no longer holds good. It is probable that greater freedom of choice in the design of a control system emerges if more than one motivator contributes to the force or moment required for control.

The different control functions expected from a fully active flight control system set different demands upon the motivator characteristics. For the essentially open-loop functions it is the amount of control that matters, but for the closed-loop functions fast actuation rates matter rather more. It may be advantageous to consider supplying extra motivators to cater for the separate needs on future aeroplanes, designed from their inception to be CCVs.

This discussion would not be complete without some mention of the use to which certain types of motivators may be put on an intermittent basis to improve basic aircraft performance and safety during manoeuvring flight. The motivators currently in use, leading-edge flaps, trailing-edge flaps and the more recent proposal to use variation of wing sweep (F-14 aircraft) are described a little more fully in Ref 1-2.

10 ALTERNATIVE MOTIVATOR CONCEPTS

The foregoing discussion suggests that there is a number of ways in which improved basic motivator characteristics would aid the design of active control systems. It seems unlikely that such improvements will come from a totally new and revolutionary motivator concept. Rather it is necessary to look for improvements from the better use of existing concepts.

It seems difficult to imagine that, provided the level of response is reasonable, pilots will not derive much advantage from the decoupled modes associated with the integration of force motivators into the aeroplane design. A factor in the ready acceptance of these extra modes of control will be whether they can be accommodated without additional cockpit controls.

In the search for optimum motivator design another question arises and it is the following. Is there an inherent advantage to be gained by allocating different motivator functions to different parts of the aircraft? Thus the tasks of gust alleviation, load alleviation and manoeuvre enhancement along with the provision of desired lift/drag characteristics for take-off and landing may be better allocated primarily to wing motivators. This implies that, apart from perhaps the generating of lift, all other forces and moments would come from motivators outside the wing. Indirect and interference effects have to be accounted for and measures taken to cancel unwanted action and/or response.

These thoughts lead to the following suggestions for layouts which may be worth investigating experimentally.

The addition of canards fixed to the forebody has been used in the first place as a means of relaxing stability of the unaugmented aircraft and in conjunction with deflection

of the aft tailplane to provide significant lift control. Their usefulness as pitch motivators in the pull-up sense is restricted by stalling of the canard surface. Likewise it is necessary to rotate the canard surfaces through large angles in the nose-down sense at the high angles of attack. If the engineering of the scheme can be accomplished without significant weight penalty and the canard allowed to float free except when in use as a motivator, the canard essentially operates at a zero effective angle of attack at all times. Its effectiveness as a pitch motivator would then be independent of the angle of attack of the aeroplane. The effect of canard on the aeroplane aerodynamic centre is now nil.

This, in turn, leads on to the observation that the question, the answer of which was sought in Ref 1-5 and 1-11 as to whether aft tail is superior to canard or not, in the context of relaxed static stability, was perhaps not the one that should have been posed. Rather the two surfaces should perhaps appear on the same aeroplane and suitably sized canard and aft-tailplane fitted in such a manner that at subsonic speeds the canard floats freely and at supersonic speeds the aft tailplane floats freely. In this way a more equitably degree of static instability may be achieved at all speeds. Tests would be needed to clear up the question of what should happen over a narrow transonic band of speeds.

Some more fundamental changes may be needed to put into effect if the notion of separating certain motivator functions is pursued. If the wing surface is reserved for those devices intended to optimise aircraft performance and the other active control tasks which it was indicated earlier would be best fulfilled by wing-mounted motivators, the other motivators have to be located off the wings. A possible layout meeting these requirements is shown in Fig 66. It is a matter for pure speculation as to whether such a layout would be successful.

There is on the face of it ample scope for control. For example, the port and starboard surfaces, fore and aft, may be deflected antisymmetrical as a roll motivator. Symmetrically they function conventionally as pitch motivator or alternatively as a lift motivator.

The investigation described in Ref 1 do not advance any concrete evidence that there is a need to increase the effectiveness of particular motivators. This may or may not be a true reflection of affairs as regards the moment motivators, but the amount of force control that can be usefully deployed can hardly be said to be fully tested. If increased effectiveness of the aerodynamic surface which forms a particular motivator is needed it may be worth turning to the use of some engine power to augment the effectiveness. As has been shown the concept can be engineered in a number of ways ranging from pure jets with no flap surface through blown flaps with a jet efflux at the leading-edge of the flap to the "two-dimensional" nozzle deflected as a flap. Perhaps too it is time to revive the idea of using small chord double flaps operated through large angles for some of the active control functions using wing-mounted motivators.

11 SPECIALISATION TO MISSILES

Of the aerodynamic problems relating to their control missiles and aeroplanes share some but not others. The operational envelope of the missile differs from that of the aeroplane in a number of important essentials. At worst the missile is launched at high acceleration to soon reach high subsonic speeds. Its entire speed range may then extend some way into the supersonic regime.

The configuration of most missiles falls into one of two categories, cruciform wings mounted on a long cylindrical body with a pointed nose with either a set of aft cruciform surface or a set of canard cruciform surfaces.

Missiles share common ground with present-day aeroplanes in being required to manoeuvre through large angles of incidence. The essential difference here is that for the aeroplane the large angle of incidence is confined to the pitch plane, that is, it is an angle of attack. In contrast, the missile is expected to achieve high angles of incidence in any plane, that is, in the usual aeroplane terms large angles of attack and large angles of sideslip. The usual angles of incidence used in missile aerodynamics are the incidence magnitude angle (the angle between the x-axis and the velocity vector, sometime represented by α) and the incidence plane angle (the angle between the incidence plane, xV , and the zx plane; that is, the out-of-symmetry plane angle, often designated roll angle).

The motivators can consist of either all-moving surfaces, trailing-edge flaps or all-moving wing tips. The large number of interacting components ensure that the problems of interference and non-linearities are at least as daunting as they are for the aeroplane and have been around longer.

Even in the steady-state condition of constant angles of incidence, a complicated system of vortices is generated, as indicated in Fig 67. The body nose sheds a pair of vortices, the leading aerofoil surfaces shed vortex sheets which become two vortex pairs as the flow proceeds downstream, whilst that part of the body connecting the two sets of cruciform surfaces results in yet another pair. All these vortices interact as they are convected downstream and when they reach the aft cruciform surface they interfere with the individual surfaces as well as being themselves influenced by the flow field for the surface. Their pattern in relation to the surfaces is thus complicated and is the underlying cause of many of less amenable to interpretation interference effects, mostly non-linear in character.

Although much has been done over the years in development of estimation methods for missile aerodynamics generally, little attention has been concentrated upon the non-linear control terms.

Some recent papers^{46,47,48&1-25} partially make good the gap. It is not proposed to examine here in any detail experimental results pertaining to the aerodynamics of missile controls.

Non-linear and interference aerodynamic forces and moments have been part of the missile scene almost from the outset as the cruciform type missile manoeuvres to high angles of incidence to create a large lift force, to which the body makes a substantial contribution. In as much as there has been in the meantime, a constant striving to extend the operational angles of attack of the aeroplane, the two types of vehicles come closer together in some aspects of their aerodynamics. The adoption of bank-to-turn techniques for certain classes of missiles may serve to bring the two fields even closer together.

12 METHODS OF ESTIMATING THE MOTIVATOR FORCES AND MOMENTS

12.1 Semi-empirical methods and experimental methods

"An aeroplane of conventional configuration" was a meaningful phrase up to about a couple of decades ago. Now, as must be clear from the preceding text, such a phrase is virtually meaningless. However, the methods for estimating the forces and moments due to motivators in current use rest mainly upon empirical or semi-empirical analysis of data then available, for instance the methods to be found in DATCOM³ and ESDU⁴ publications. These have strictly limited applicability for present-day designs and probably even less for some future aeroplanes.

It is important in deciding how best to remedy the shortcomings of what exists to examine the degree of significance to be attached to each aspect of the motivator characteristics. This has already been done in Fig 65.

Given the almost endless variety of aeroplane layout and the fact that there seem to be no grounds for supposing that a "conventional" shape of the next decade will emerge, it is unlikely that broadly based systematic testing is possible. Nevertheless, the data base must be broadened. It may in time be possible to identify a few of the more promising layouts for exploiting active control technology. If this be so, then some systematic testing of these layouts will help in developing new methods or up-dating the old.

12.2 Theoretical methods

A review of progress¹⁻¹ in the *ab initio* calculation of aerodynamic characteristics, in general, and motivator characteristics, in particular, shows steady progress over the last few years. However, much remains to be achieved. It is impossible in the course of a review of a general nature like the present to go into the question of the development of theoretical methods in any detail. For further information the reader should refer to papers dealing specifically with the topic^{1-1,1-18,60}.

An attempt has been made here to indicate in tabular form, see Table 2, the degree of progress made in calculating the characteristics of flaps fitted to aerofoil surfaces. Certain areas do not feature at all in this table. These represent areas in which there has been very little or no progress. The calculation of a three-dimensional flow with separation is, for instance, such an area, although there has been some progress in the treatment of highly swept with leading-edge vortex flow where there is a more orderly separation.

Accounting for viscosity, the presence of the boundary layer and its interaction with shockwaves remain as difficult and relatively unexplored areas. The ability to account for finite thickness by itself is, as remarked by Körner¹⁻¹, of questionable value, when, as happens at subsonic speeds, this effect and the effect of viscosity tend to cancel.

The capability to deal with the aerodynamics of an airframe in an integrated fashion is inherently embodied in the so-called panel methods. The difficulties lie in the development of mathematical models for the interacting flows like wakes, especially in some asymmetric conditions.

Perhaps development along present lines may not in the shorter term be the best means by which the aerodynamicist can help the designer. Development is slow and hard won, so perhaps some thought might be given to the development of simpler and cruder theories for calculating interference effects.

13 FACTORS AFFECTING THE ACCURACY AND APPLICATION OF EXPERIMENTAL DATA

Even when there exist no doubt about the relevance of aerodynamic data from any source to the design of a specific aeroplane, there are some factors that need to be considered carefully. Important ones are scale effects or Reynolds number effect, model/model support interference, wind-tunnel constraint effects and the aeroelasticity of the model on the one hand and the full-scale aircraft on the other. These factors have repercussions on the ease of acquisition and/or the accuracy of experimental data.

13.1 Scale and tunnel constraint effects

The extrapolation from model to full-scale conditions has been a problem as long as there have been aircraft. There are very few tunnels in operation that are large enough to produce realistic Reynolds numbers and so offer a straight-forward way out of trouble. Even given that sufficiently large tunnels were more freely available, the making of large models with operative motivators and capable of withstanding the high aerodynamic load incurred in tests at high speed and large angles of attack is bound to prove a costly undertaking. An alternative approach, which has been in use for some time, is to aim to simulate on the wind-tunnel model boundary layer conditions appropriate to full-scale. The difficulty here lies in saying what constitutes the most representative. Recent investigations by Mabey *et al*¹⁻²⁰ are intended to shed some light on how best to choose the scale and transition fixing. Some preliminary conclusions are drawn from the work already done and reported in the paper quoted.

To illustrate the degree of uncertainty that can surround a given set of wind-tunnel test results two examples are given. The first of these relates to the oscillatory hinge-moment characteristics of a trailing-edge flap on low aspect ratio wing¹⁻¹, see Fig 68. Hinge-moments are particularly sensitive to scale effects if they refer to a trailing-edge flap, which occupies the rear portion of the aerofoil chord.

The second illustration concerns the influence of the test Reynolds number on the total lift and the lift increment due to a spoiler on a part-span wing model¹⁻⁴ based on a transport aircraft with wings of aspect ratio 7 and sweep 30°. Fig 69 shows the variation in total lift and difference are present for zero spoiler deflection. In fact, the differences for the three speeds actually decrease as the spoiler angle is increased. Hence to assess properly the trends shown by the incremental lift, Fig 70, is difficult.

It may be argued that the availability of test results from full-scale flight or from large-scale models, in free or remotely controlled flight, should help to resolve some of the problems of scale by providing what might be considered the correct values of the various aerodynamic characteristics. Unfortunately it is often difficult or not possible to isolate the scale effects from other effects which may contribute to discrepancies between model and full-scale. These are aeroelastic effects, differences in detail geometry and in the case of static wind-tunnel tests unsuspected dynamic or unsteady flow effects.

If a model that is large in relation to the wind-tunnel cross section dimensions is used, the tunnel constraint correction may be so large as to be prejudicial to the overall accuracy of the test results. Part-span or half models bring in a degree of unrepresentativeness near the root of the wing.

13.2 Aeroelastic effects

Attention has been drawn from time to time throughout the paper to the fact that ailerons and rudders are particularly sensitive to aeroelastic effects. It could be argued that, as both models and the full-scale structures are subject to these effects, a possible way out is to test models correctly scaled aeroelastically as well as geometrically. This is a difficult undertaking and rarely entered into.

One technique to circumvent the problem is to employ as rigid as possible a model and to apply corrections based on measured aerodynamic and the known structural properties of the aircraft to obtain good approximations to the actual characteristics of the motivators.

An alternative technique is to test models of distorted shape based on the shape the aircraft is expected to acquire in flight. Different flight conditions call for different models. Furthermore only the effect of the steady loads at the mean flight condition can be introduced.

Another aspect of aeroelasticity which does not relate directly to experiments enters into the design of active control systems. In those systems such as one aimed at postponement of flutter and load alleviation it becomes increasingly necessary to construct a fully-representative mathematical model of the aircraft embracing both aerodynamic and structural aspects as well as the 'rigid-body' modes of motion and the elastic modes. The need to reconcile in a rational manner data from semi-empirical or empirical sources on the one hand with data only available from theory on the other hand may prove a real stumbling block.

14 CONCLUDING REMARKS

In a technical evaluation² of the AGARD symposium on "Aerodynamic characteristics of controls" the present author drew a number of conclusions and on the basis of these made certain recommendations as to the direction future research should take. Insufficient information has become available to make a new assessment.

For better or for worse the aircraft designer continues and it would seem will continue to rely heavily upon empirical data. The data base is at present inadequate to allow development of semi-empirical estimation methods as in the past. It is necessary to give urgent consideration to the broadening of the data-base so that it can be both representative and comprehensive.

In this context it is necessary to bear in mind that, in the applications so far described in the literature, active control systems have been introduced into aircraft, the

basic shapes of which were dictated by other considerations. To exploit to the utmost the potential of ACT it is essential to consider the needs of the active control systems at a very early stage in design, as further and more radical changes in aircraft shape make their appearance. The configuration-dependent nature of many of the important aerodynamic characteristics can then make the provision of a broad data base difficult.

At present theory cannot help resolve some of these difficulties since development seems to be most lacking in the areas of perhaps greatest need and importance. The stress laid throughout on interference effects is an instance of this in that the mathematical modelling of the flow both on and off the aerofoil in a truly representative way seems a distant prospect.

Again increasing importance attaches to knowledge of high angle of attack effects, transonic speed effects and effect of flow unsteadiness.

Knowledge and understanding of interference and cross-coupling effects associated with motivators are incomplete, nor is their significance within active control systems appreciated.

There is the question of whether more attention should be given to engine-airframe integration in relation to motivators, that is, using the engine thrust in various ways to enhance motivator efficiency.

Finally there is a need to identify more precisely the relative importance of different motivator characteristics in a particular application and to assess the extent to which the unsteady aerodynamic characteristics will be needed for systems other than the obvious ones, such as a flutter postponement system.

Table 1
TAILPLANE LOCATION AND ITS RELATIONSHIP TO THE EFFICIENCY OF THE
TAILPLANE AS A STABILISER AND AS A MOTIVATOR

Tailplane location	Angle of attack, α	Flow environment changes			Tailplane efficiency	
		Local kinetic pressure	Downwash	α_{Teff}	As a stabiliser	As a motivator
Far aft, low	Low	Near to free-stream	Small	$+\alpha$	Good	Good
	High	Near to free-stream	Small	$+\alpha$	Reasonably good up to tail stall	Good
Far aft, high	Low	Near to free-stream	Very small	$\approx \alpha$	Good	Good
	High	Marked decrease	Large	$< \alpha$	Poor	Poor
Closely-coupled, low	Low	Somewhat less than free-stream	Moderately large	$< \alpha$	Fair	Good
	High	Somewhat less than free-stream	Moderate	$< \alpha$	Fair	Good
Closely-coupled, high	Low	Near free-stream	Small to moderate	$< \alpha$	Reasonable	Good
	High	Decreases as α become large	Moderately large	$< \alpha$	Fair to poor	Fair to poor

Table 2
CHART OF PROGRESS IN DEVELOPMENT OF THEORETICAL METHODS FOR CALCULATING THE
CHARACTERISTICS OF FLAP-TYPE MOTIVATORS ON WINGS OF FINITE ASPECT RATIO

Speed regime	Type of flow		Thickness	Rating
Subsonic	Attached inviscid	Steady	Zero	****
		Unsteady	Zero	****
	Attached with boundary layer effects	Steady	Finite	***
		Unsteady	Finite	***
Transonic	Attached inviscid	Steady	Zero	**
			Finite	**
		Unsteady	Zero	*
			Finite	*
Supersonic	Attached inviscid	Steady	Zero	***
			Finite	
	Attached inviscid	Unsteady	Zero	***
			Finite	

REFERENCES

- 1 Aerodynamic characteristics of control. AGARD Conference Proceedings No.262, Sept 1979. Individual papers within these proceedings are referred to in the text by 1- followed by the number of the paper, e.g. Ref 1-4 refers to the fourth paper
- 2 H.H.B.M. Thomas, Technical Evaluation Report on the Fluid Dynamics Panel Symposium on Aerodynamics of Controls. AGARD Advisory Report No.157, March 1980
- 3 Stability and Control Handbook of the United States Air Force
- 4 Aerodynamics Sub-series, Engineering Sciences Data. Engineering Sciences Data Unit, London
- 5 Joy C. Donaldson, Bibliography of Control Characteristics of Aircraft. RAE Lib. Bib.377, March 1980

- 6 S.M. Dollyhigh, Subsonic and supersonic longitudinal stability and control characteristics of an aft-tail fighter configuration with cambered and uncambered wings and cambered fuselage. NASA TN D-8472, September (1977)
- 7 K. Aoyagi and W.H. Tolhurst, Large-scale wind tunnel tests of a subsonic transport with aft engine nacelles and high tail. NASA TN D-3797, January (1967)
- 8 B.J. Eulrich and E.G. Rynaski, Identification of nonlinear aerodynamic stability and control parameters at high angle of attack. Paper 2 of AGARD CP 172 (1974)
- 9 W.T. Suit and J.L. Williams, Longitudinal aerodynamic parameters of the Kestrel aircraft (XV-6A) extracted from flight data. NASA TN D-7296 (1973)
- 10 R.J. Margason, R.D. Vogler and M.M. Winston, Wind-tunnel investigation at low speeds of a model of the Kestrel (XV-6A) vectored thrust V/STOL airplane. NASA TN D-6826 (1972)
- 11 B.L. Shrout, Aerodynamic characteristics at Mach numbers from 0.7 to 2.16 of a supersonic cruise fighter configuration with a design Mach number of 1.8. NASA TM X-3559 (1977)
- 12 A. Jean Ross, Determination of Aerodynamic derivatives from transient responses in manoeuvring flight. Paper 14 of AGARD CP 172 (1974)
- 13 G.E. Erickson and J.F. Campbell, Improvement of manoeuvre aerodynamics by spanwise blowing. NASA TP 1065 (1977)
- 14 R.B. Eberle, R.T. Stancil and W.C. Fowler, A critical review of canard relative to aft horizontal tail based on low- and high-speed tunnel tests of a fighter/attack configuration. AIAA 71-8 (1971)
- 15 L.P. Yip and J.W. Paulson, Effects of deflected thrust on the longitudinal aerodynamic characteristics of a close-coupled wing-canard configuration. NASA TP 1090 (1977)
- 16 R.J. Re and F.J. Capone, An investigation of a close-coupled canard as a direct side-force generator on a fighter model at Mach numbers from 0.4 to 0.9. NASA TN D-8510 (1977)
- 17 S.C. Stumpfl and R.A. Whitmoyer, Horizontal canards for two-axis CCV fighter control. Paper 6 of AGARD CP 157 (1974)
- 18 R.A. Whitmoyer, Aerodynamic interactions on the fighter CCV test aircraft. Paper 16 of AGARD CP 235 (1978)
- 19 D.H. Bennett, F4/CCV - Flight tests of advanced technology. SAE 740861 (1974)
- 20 E.J. Ray and E.G. Hollingsworth, Subsonic characteristics of a twin-jet swept-wing fighter model with manoeuvring devices. NASA TN D-6921 (1973)
- 21 Ph. Poisson-Quinton, Slender wings for civil and military aircraft. Israel Annual Conference on Aviation and Astronautics (1978)
- 22 J. Kloos and L. Elmeland, Static aeroelastic effects on the aerodynamics of the SAAB 37 Viggen aircraft, a comparison between calculations, windtunnel tests and flight tests. ICAS 74-55 (1974)
- 23 A.D. Hammond, Aerodynamic characteristics of a spoiler-slot-deflector control on a 45° sweptback-wing-fuselage model at high subsonic speeds. NASA TN D-2037 (1963)
- 24 W.P. Gilbert, L.T. Nguyen and R.W. van Gunst, Simulator study of the effectiveness of an automatic control system designed to improve the high-angle-of-attack characteristics of a fighter airplane. NASA TN D-8176 (1976)
- 25 J.P. Lamers, Design for departure prevention in the YF-16. AIAA 74-794 (1974)
- 26 L.P. Parlett, H.D. Greer and R.L. Henderson, Wind-tunnel investigation of an external-flow jet-flap transport configuration having full-span triple-slotted flaps. NASA TN D-6391 (1971)
- 27 H. August, B-1 airplane model support and jet plume effects on aerodynamic characteristics. AIAA 73-153 (1973)
- 28 K. Iliffe, Estimation of aerodynamic characteristics from dynamic flight test data. Paper 15 of AGARD CP 235 (1978)
- 29 R.F. Osborn, Investigation of a double slotted rudder for application on advanced tactical support aircraft. AFFDL-TR-75-94 (1975)
- 30 Manoeuvre limitations of combat aircraft. AGARD AR to be published
- 31 J.W. Stickle and R.C. Henry, Wind-tunnel study to explore the use of slot spoilers to modulate the flap-induced lift of a wing. NASA TN D-4664 (1968)

- 32 S.F.J. Butler, Low-speed wind-tunnel tests on a sweptback wing model (Buccaneer Mark 1) with blowing at the wing leading edge and over the flaps and drooped ailerons. ARC R & M 3655 (1967)
- 33 D.J. Giulianetto and R.L. Maki, Low speed aerodynamic characteristics of a large-scale model with a thin, highly swept, 2.67 aspect ratio wing having a cranked leading edge. NASA TN D-6919 (1972)
- 34 P. Fournier, Low-speed aerodynamic characteristics of a transport model having 42.33° swept low wing with supercritical airfoil, double-slotted flaps, and T-tail or low tail. NASA TM X-3276 (1975)
- 35 R.F. Stewart and R.E. Whitehead, Analysis of advanced variable camber concepts. Paper 14 of AGARD CP 241 (1977)
- 36 The effects of buffeting and other transonic phenomena on manoeuvring combat aircraft. AGARD AR 82 (1975)
- 37 E.J. Ray, L.W. McKinney and J.G. Carmichael, Manoeuver and buffet characteristics of fighter aircraft. Paper 24 of AGARD CP 102 (1972)
- 38 W.R. Burns and J.T. Lawrence, Aerodynamic design and flight test of US Navy aircraft at high angles of attack. Paper 25 of AGARD CP 102 (1972)
- 39 C.L. Bore, Post/stall aerodynamics of the Harrier GR1. Paper 19 of AGARD CP 102 (1972)
- 40 J.K. Buckner, P.W. Hill and D. Benepe, Aerodynamic design evolution of the YF-16. AIAA 74-935 (1974)
- 41 J.P. Lamers, YF-16 high angle of attack flight test experience. Paper 25 of AGARD CP 199 (1975)
- 42 E.F. Carlson, Direct sideforce control for improved weapon delivery accuracy. AIAA 74-70 (1974)
- 43 H. Wunnenberg and W.J. Kubbatt, Advanced control concepts for future fighter aircraft. Paper 8 of AGARD CP 241 (1977)
- 44 P.W. Kirsten, A comparison and evaluation of two methods of extracting stability derivatives from flight data. Paper 18 of AGARD CP 172 (1974)
- 45 H.H.B.M. Thomas and G.F. Edwards, Mathematical models of aircraft dynamics for extreme flight conditions (theory and experiment). Paper 27 of AGARD CP 235 (1978)
- 46 C.A. Smith, J.N. Nielsen and M.J. Hensch, Prediction of aerodynamic characteristics of cruciform missiles to high angles of attack. AIAA Paper 79-0024 (1979)
- 47 J.E. Fidler and M.B. Bateman, Aerodynamic methods for high incidence missile design. AIAA Journal, Spacecraft & Rockets, Vol.12, No.3, pp.162-8 (1975)
- 48 J.N. Nielsen, M.J. Hensch and C.A. Smith, A preliminary method for calculating the aerodynamic characteristics of cruciform missiles to high angles of attack including effects of roll angle and control deflections. Office of Naval Research Rpt. ONR-CR215-226-4F (1977)
- 49 VKI Lecture Series 99, Aerodynamic inputs for problems in aircraft dynamics (1977)

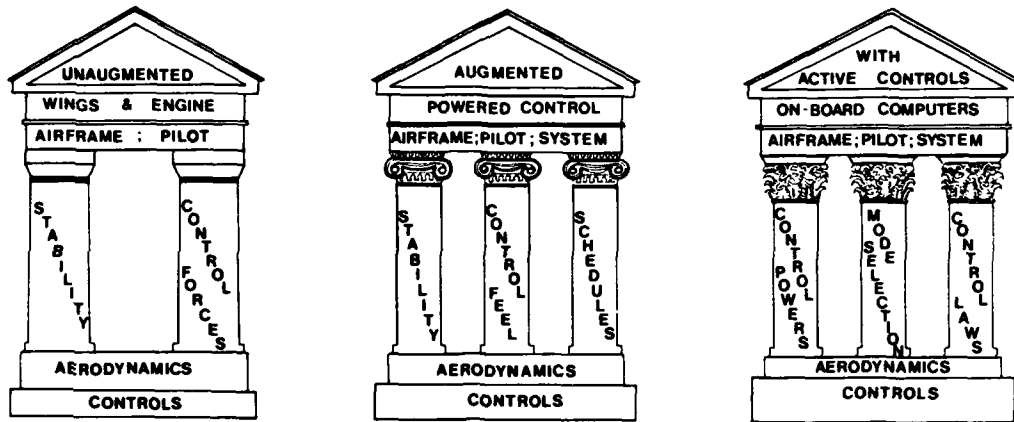


Fig 1 Relative importance of motivator aerodynamics and airframe aerodynamics within an aircraft design

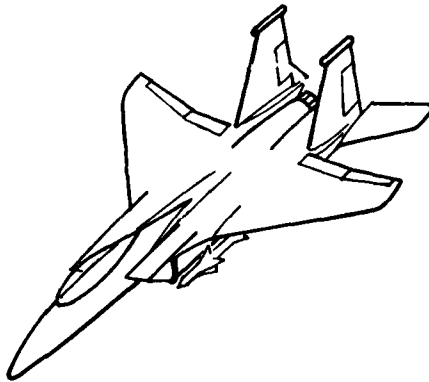


Fig 2 Typical close-coupled aircraft

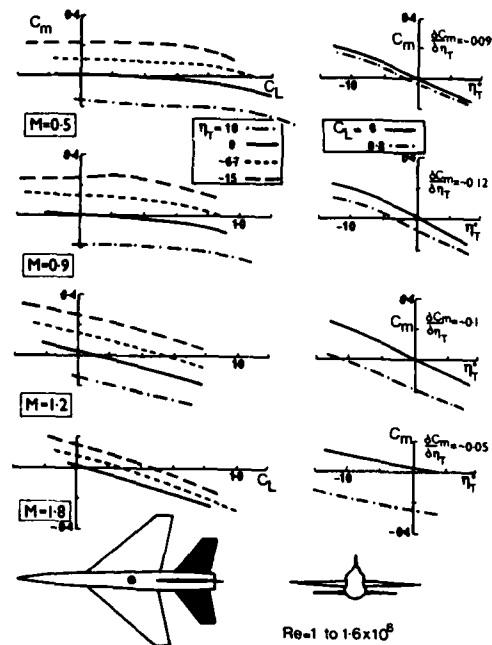


Fig 3 Effect of Mach number and lift coefficient on pitching moment due to tailplane deflection for a subsonic fighter configuration

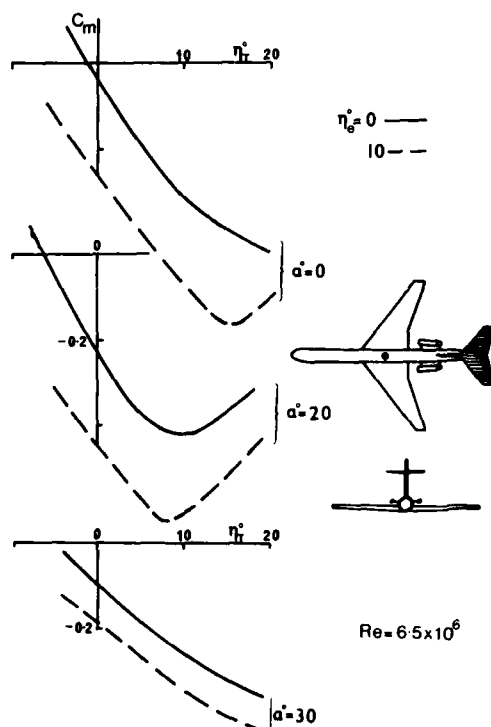


Fig 4 Effect of angle of attack on pitching moment due to tailplane deflection and elevator setting for a high-tailed transport concept

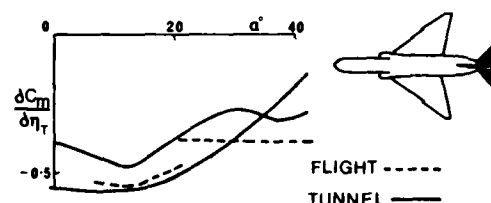


Fig 5 Variation with angle of attack of pitching moment derivative due to tailplane deflection

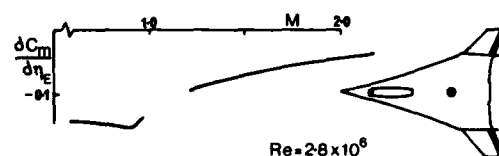


Fig 6 Variation with Mach number of pitching moment derivative due to elevons for a supersonic fighter concept

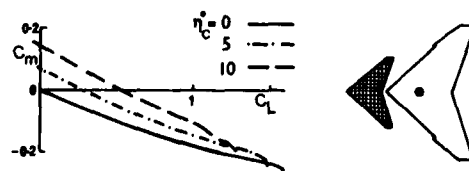


Fig 9 Variation with angle of attack of pitching moment due to a deflected canard for a swept-wing-canard configuration

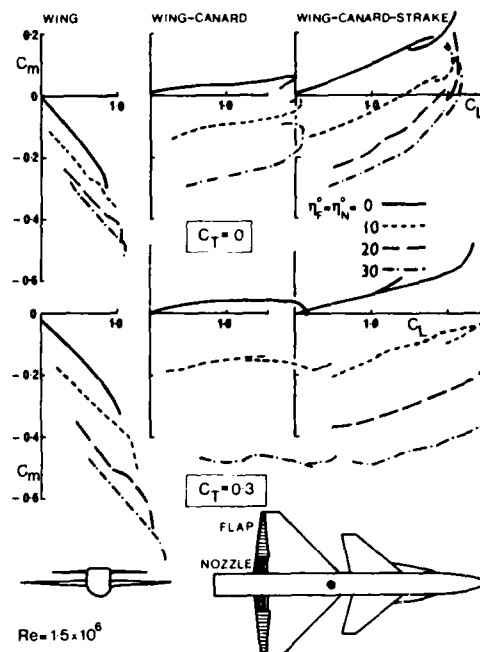


Fig 7 Effect of thrust on variation with angle of attack of pitching moment due to trailing-edge and nozzle flaps for wing-canard-strake configurations

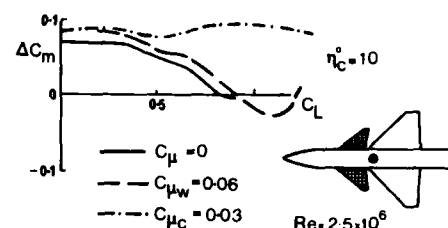


Fig 8 Effect of spanwise blowing on incremental pitching moment due to canard deflection and its variation with angle of attack for a research canard model

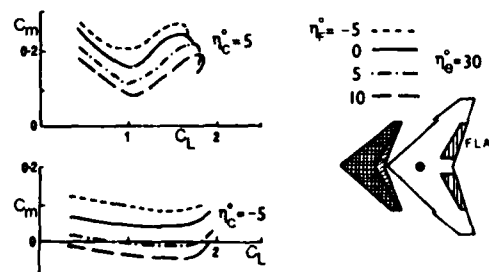


Fig 10 Effect of canard and elevator setting on pitching moment due to wing trailing-edge flaps and its variation with angle of attack for a swept-wing-canard configuration

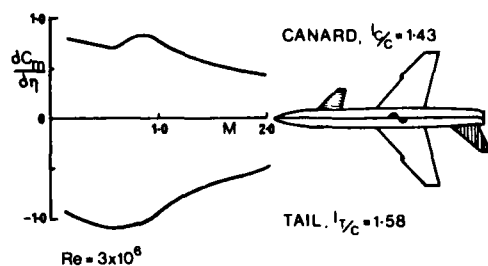


Fig 11 Comparison of the pitching moment due to a canard and a tailplane, $M = 0$ to 2.0 , for a research configuration

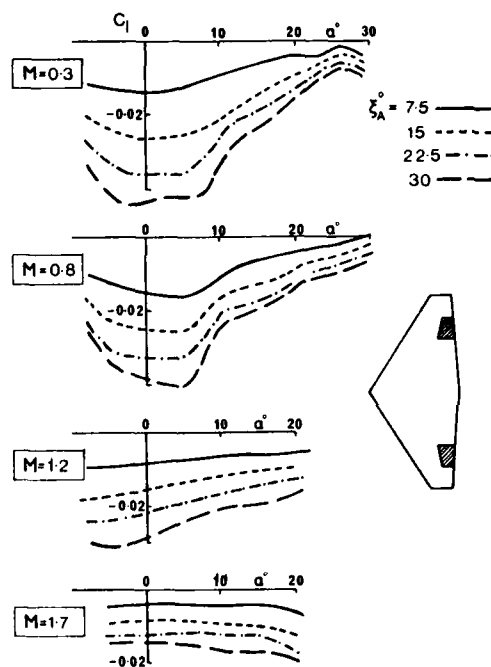


Fig 12 Variation with angle of attack and Mach number of the rolling moment due to mid-span ailerons, for a combat aircraft

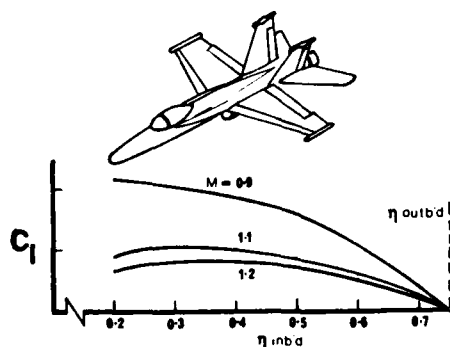


Fig 15 Variation with inboard edge location of the rolling moment due to a flap at a total aileron angle of 20° , outboard edge fixed at 0.75 semispan

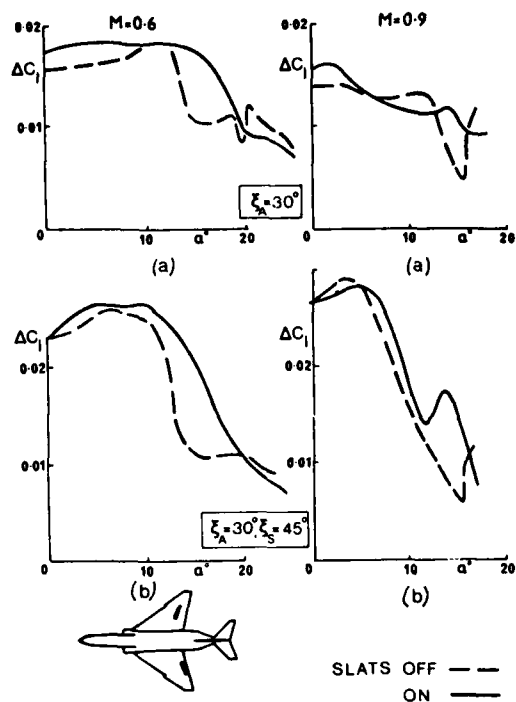


Fig 13 Effect of leading-edge slats on the rolling moment due to aileron and spoiler at different angles of attack for the F-4 aeroplane.
(a) aileron alone; (b) aileron and spoiler

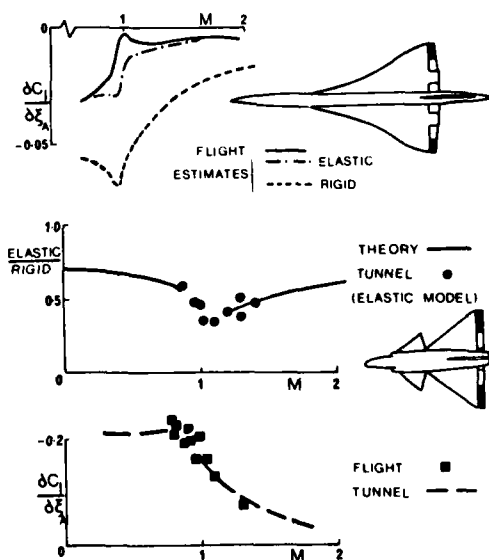


Fig 14 Effect of aeroelasticity on the variation with Mach number of the rolling moment due to ailerons.
(a) Concorde; (b) Viggen

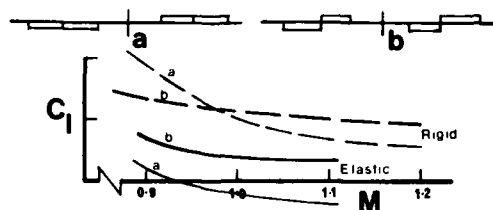


Fig 16 Comparison of rolling moment coefficients for single-piece flaperon and opposed segmented flaps, showing the effect of aeroelasticity

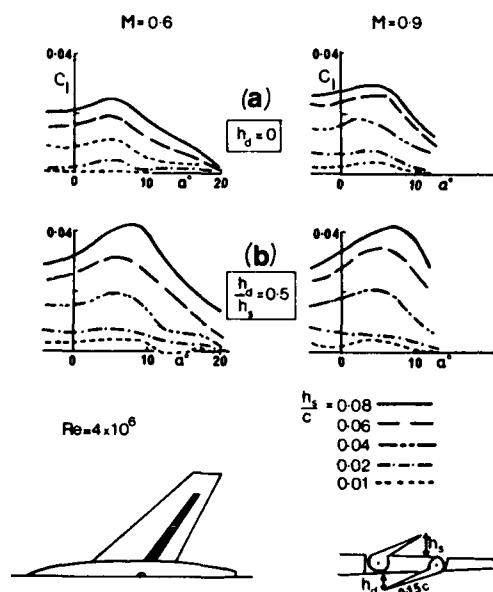


Fig 17 Effect of Mach number on the variation with angle of attack of the rolling moment due to a spoiler and a spoiler-slat-deflector (research wing). (a) spoiler; (b) spoiler-slat-deflector

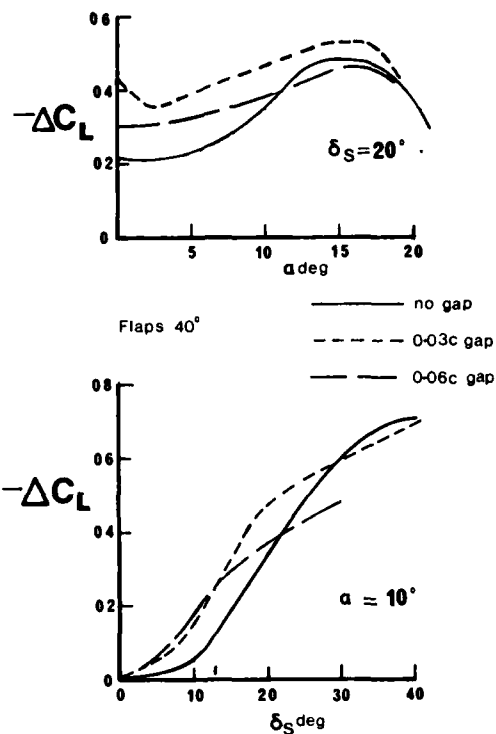


Fig 18 Effect of a gap on the incremental lift due to a plain spoiler of constant chord

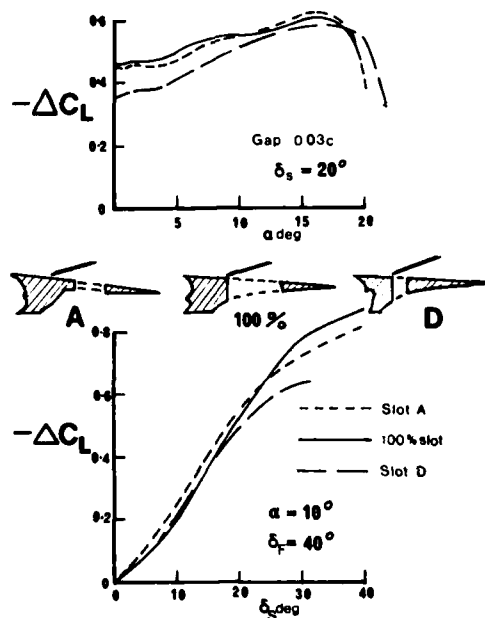


Fig 19 Effect of slot geometry on the lift increment due to a spoiler

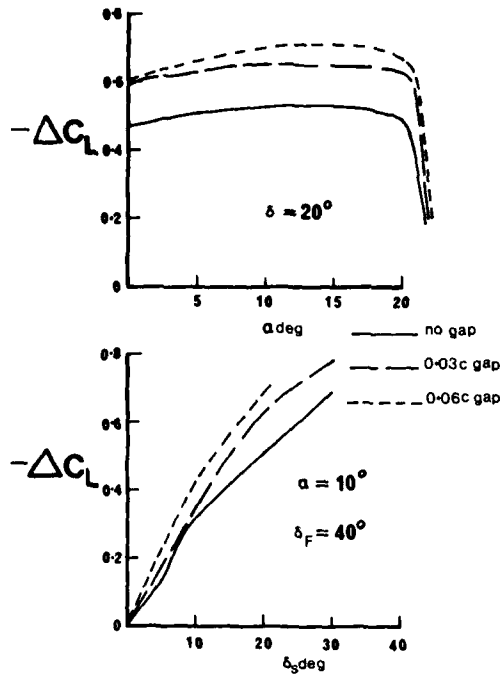


Fig 20 Incremental lift due to a moving shroud type spoiler

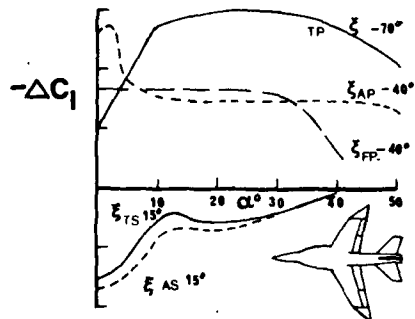


Fig 23 Comparison of the effectiveness as roll motivators of tiperons, ailerons and flaperons

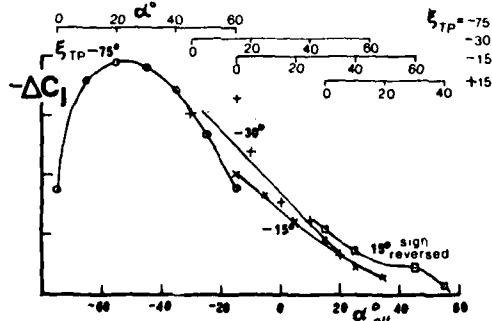


Fig 24 Dependence on the geometric effective angle of attack of the rolling moments produced by a tiperon

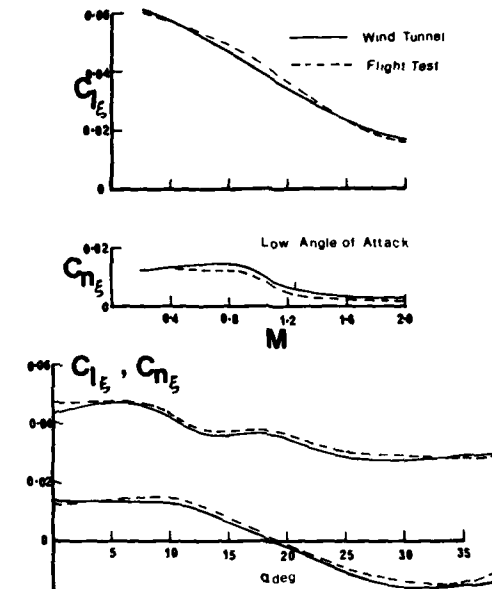


Fig 21 Effect of Mach number at low angle of attack and of angle of attack at $M = 0.9$ on rolling and yawing moment derivatives for the ailerons of F-15 aeroplane

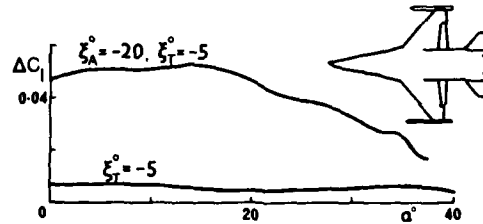


Fig 22 Variation with angle of attack of rolling moment due to an aileron and differential tail, YF-16 aeroplane

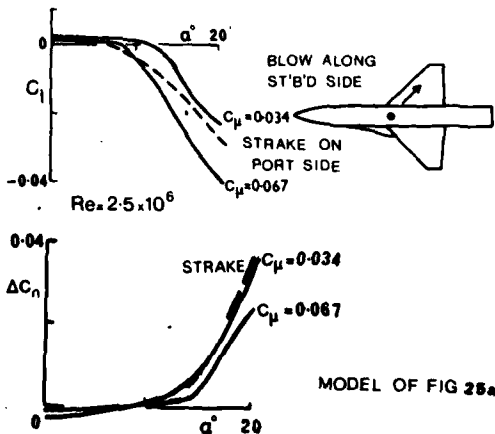
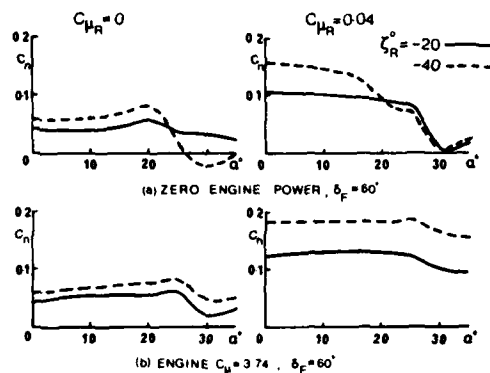


Fig 25 Rolling and yawing moments due to differential strake projection or differential spanwise blowing. Effect of angle of attack. (a) rolling moments; (b) yawing moments



$Re = 0.35 \times 10^6$

Fig 26 Effects of jet momentum coefficients on the yawing moments due to rudder at various angles of attack for a high-tail transport configuration with jet-flap

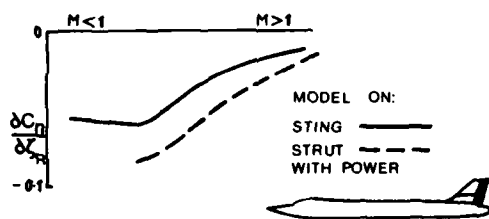


Fig 27 Interference and power effects on the variation with Mach number of the yawing moment derivative due to rudder, B-1 aeroplane

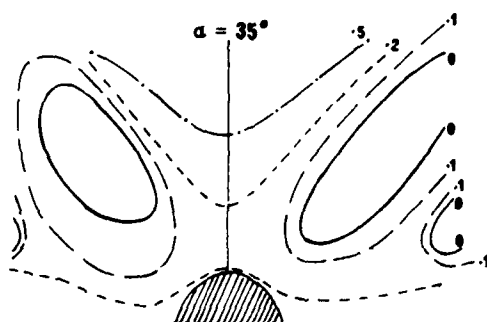


Fig 28 Survey of kinetic pressures in the plane immediately behind the fin location

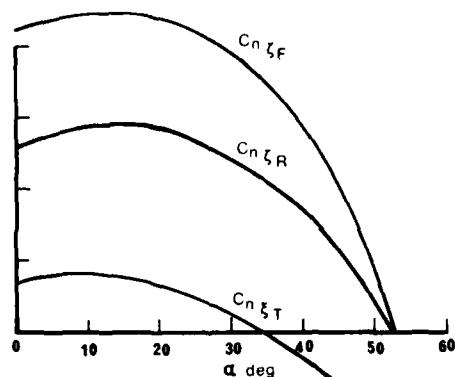


Fig 29 Comparison of yawing moment derivatives due to all-moving fin, rudder and differentially deflected tailplanes

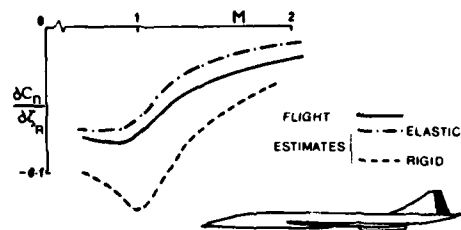


Fig 30 Effect of aeroelasticity on the variation with Mach number of the yawing moment derivative due to a rudder. (a) Concorde; (b) Viggen

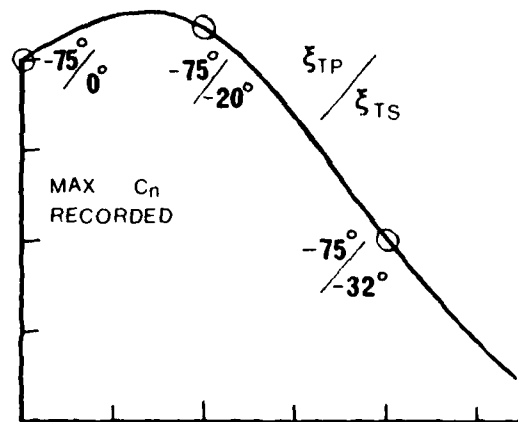


Fig 31 The tiperon as a possible yaw motivator and the indirect rolling moments produced

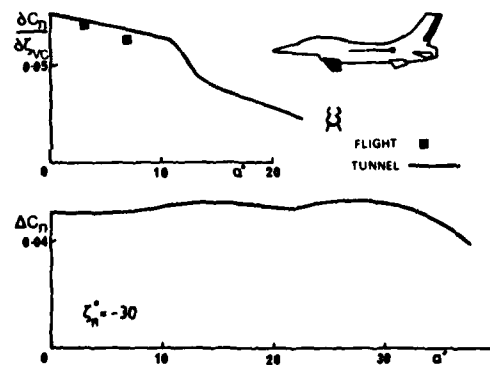


Fig 32 Variation with angle of attack of the yawing moment derivative due to vertical canards and the incremental yawing moment due to a rudder angle of -30° for the CCV, YF-16 aeroplane

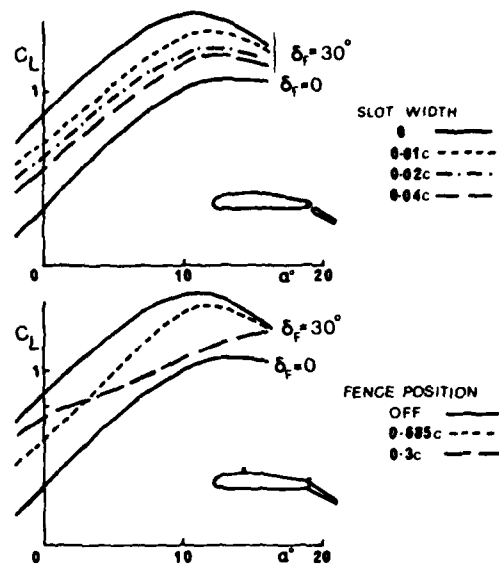


Fig 33 Effect of slot width and fence (spoiler) position on the variation with angle of attack of the lift due to a trailing-edge flap, 9% aerofoil

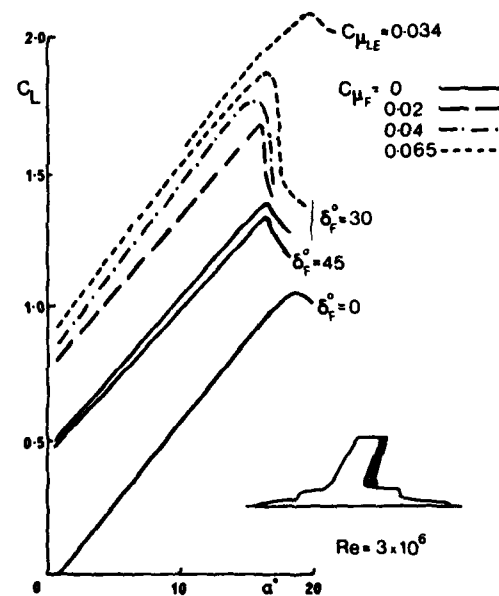


Fig 34 Effect of blowing on the lift due to a trailing-edge flap

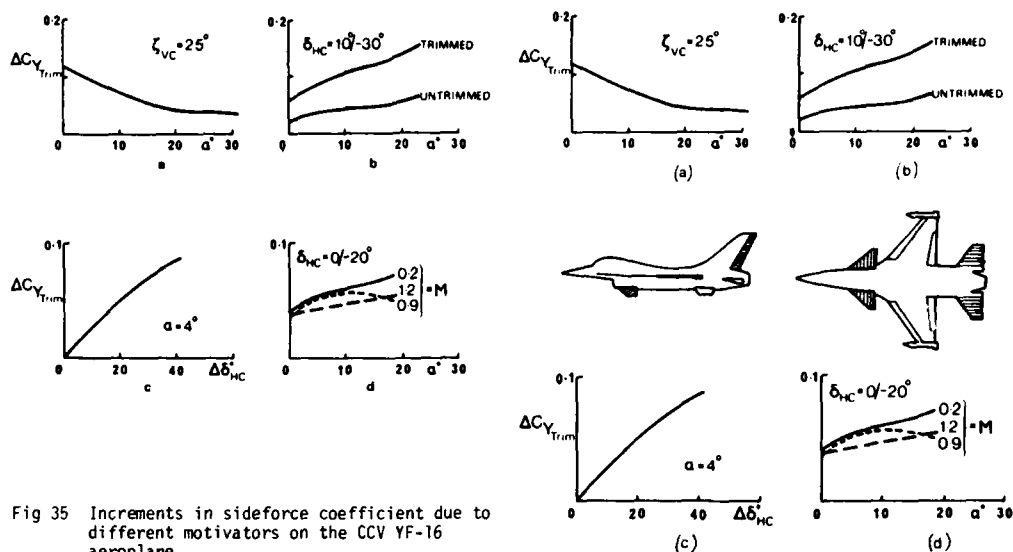


Fig 35 Increments in sideforce coefficient due to different motivators on the CCV YF-16 aeroplane.
(a) vertical canards; (b) horizontal canards; (c) variation with total deflection of horizontal canards; (d) variation with α and Mach number

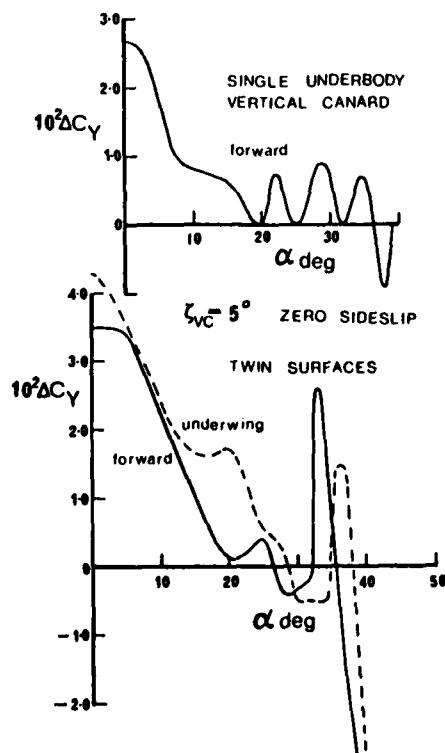


Fig 36a Increments in sideforce coefficients for single and twin vertical surfaces in different positions

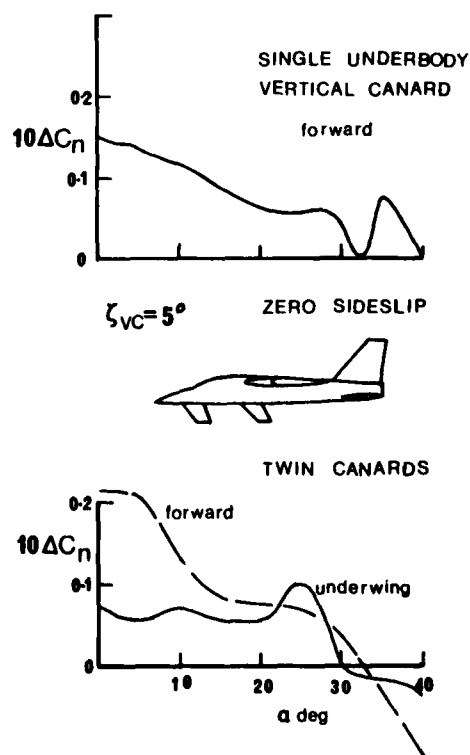


Fig 36b The yawing moment increments associated with the single and twin vertical surfaces

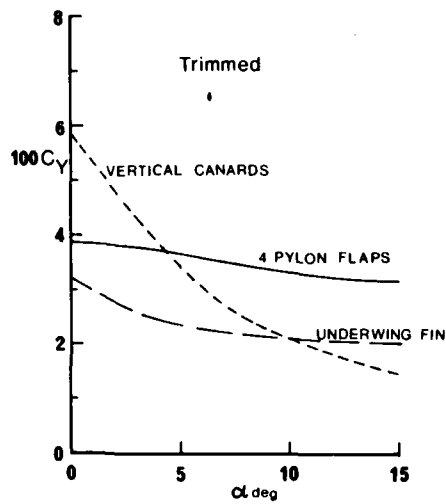


Fig 37 Comparative effectiveness of some sideforce motivators

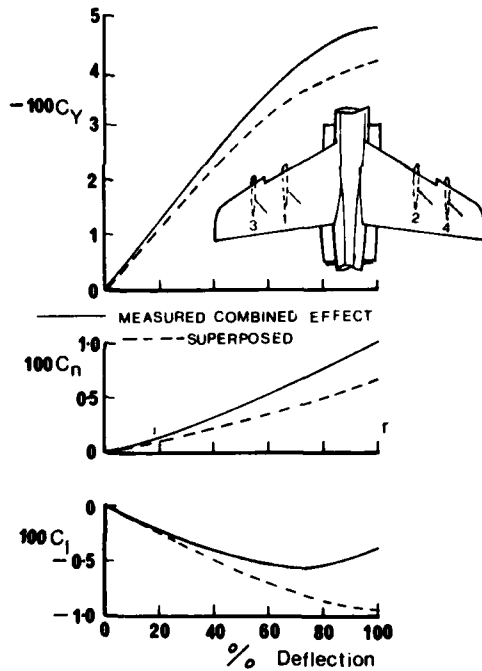


Fig 38 Sideforce, yawing moment and rolling moment due to four pylon-mounted split flaps

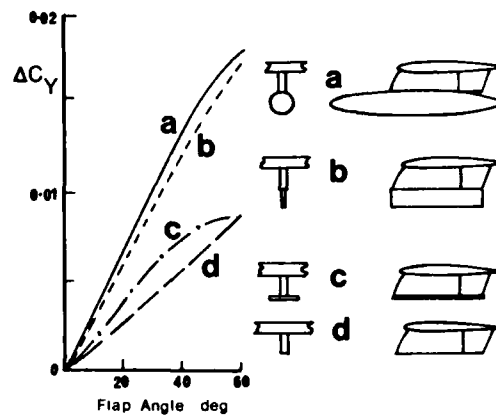


Fig 39 Effect of geometry on sideforce increment due to flap 1 of Fig 38

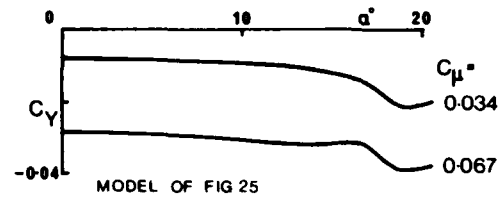


Fig 40 Variation (with angle of attack) of sideforce due to asymmetric blowing on the wing of a research canard model

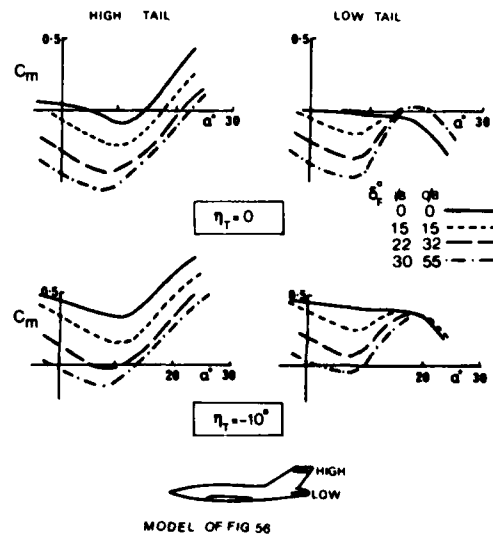


Fig 41 Effect of tailplane position and setting on the pitching moment due to trailing-edge flap and angle of attack; supercritical-wing transport aircraft

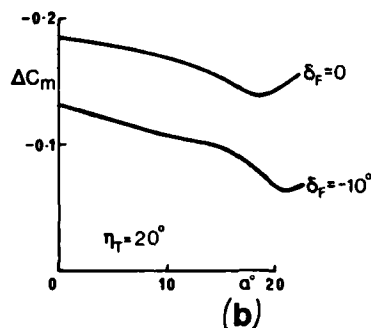
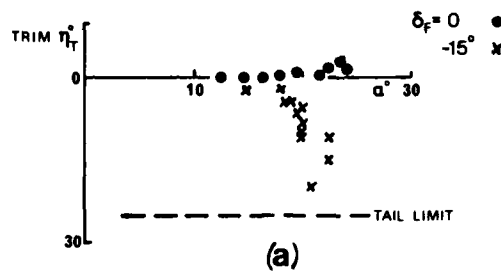


Fig 42 Effect of up-deflection of trailing-edge flap on tailplane power, CCV YF-16 aeroplane.
(a) flight results for tailplane angle to trim; (b) tunnel results for pitching-moment increment due to tailplane deflection

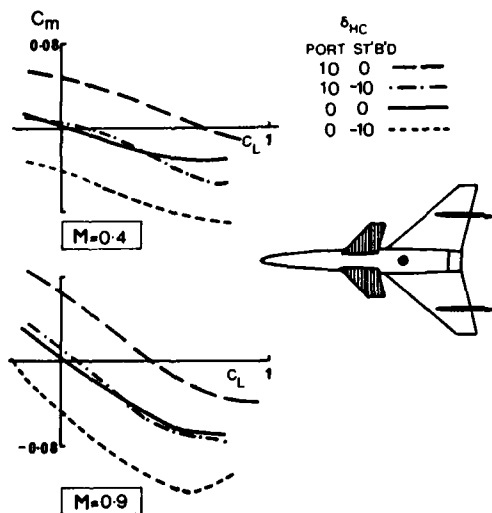


Fig 43 Effect of differential canard deflection on pitching moment due to angle of attack for a research canard concept

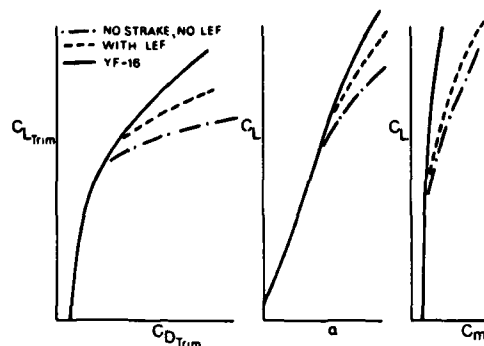


Fig 44 Effect of strake and leading-edge flap on trim for YF-16 aeroplane

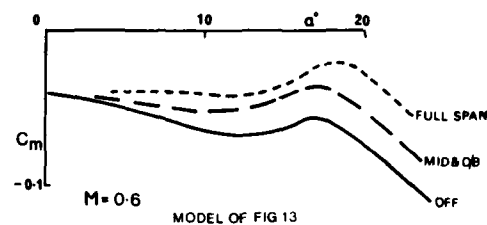


Fig 45 Effect of leading-edge slats on pitching moment at angle of attack; F-4

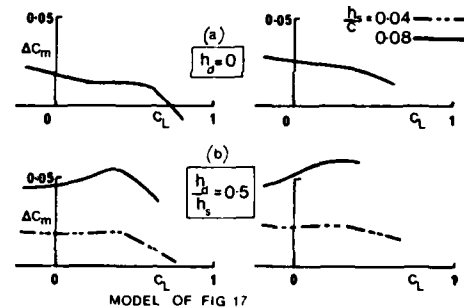


Fig 46 Variation with lift coefficient of the incremental pitching moments due to a spoiler and spoiler-slot-deflector; research wing model

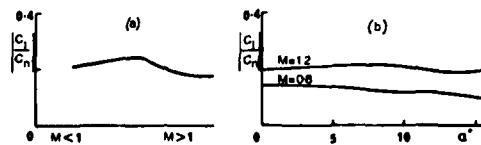


Fig 47 Ratio of rolling moment to yawing moment due to rudder.
(a) variation with Mach number; B-1
(b) variation with angle of attack; F-1-11E

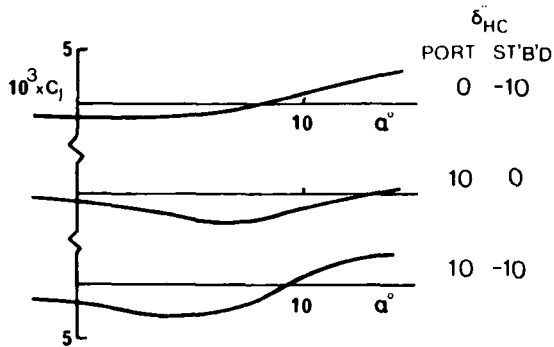


Fig 48 Variation with angle of attack of rolling moment due to differential horizontal canard deflection; research canard concept

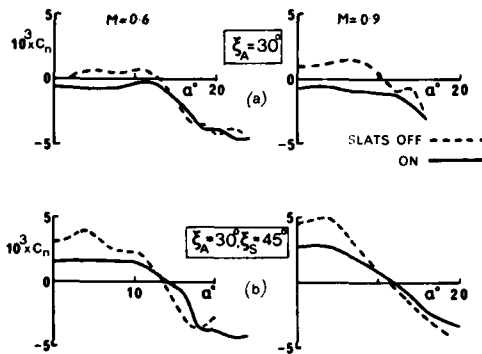


Fig 50 Effect of slats on yawing moment due to aileron and spoiler for F-4 aeroplane. (a) aileron alone; (b) aileron and spoiler

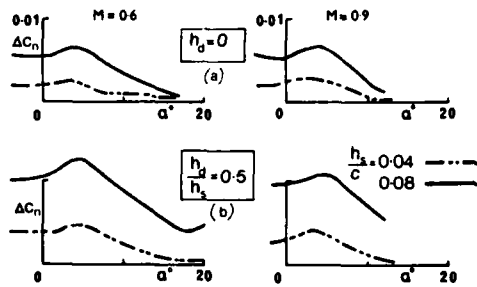


Fig 51 Effect of Mach number on yawing moment due to spoiler and spoiler-slot-deflector at angle of attack. (a) spoiler; (b) spoiler-slot-deflector

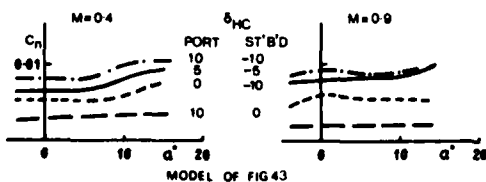


Fig 53 Variation with angle of attack of yawing moment due to differential horizontal canard; research canard concept

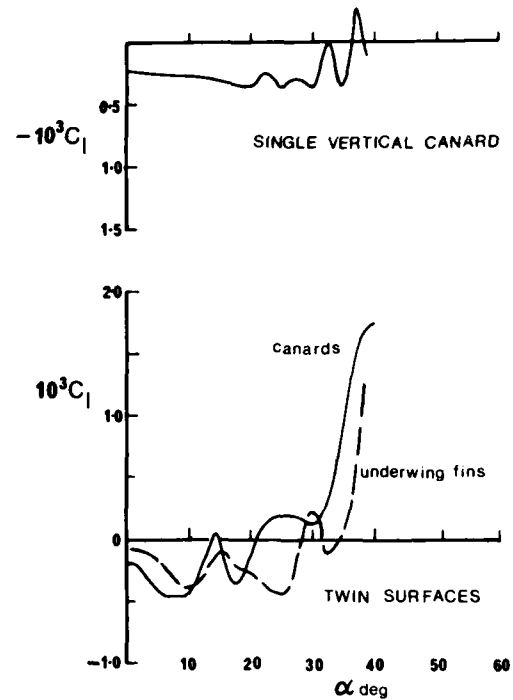


Fig 49 Rolling moment coefficient increments due to deflection of single and twin vertical surfaces

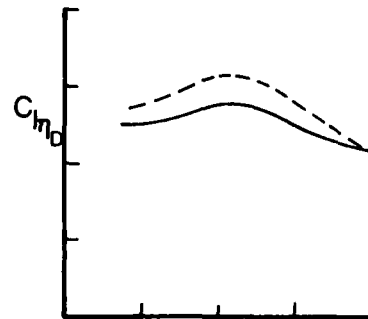


Fig 52 Rolling and yawing moment derivatives due to differentially deflected tailplane surfaces. Variation with Mach number

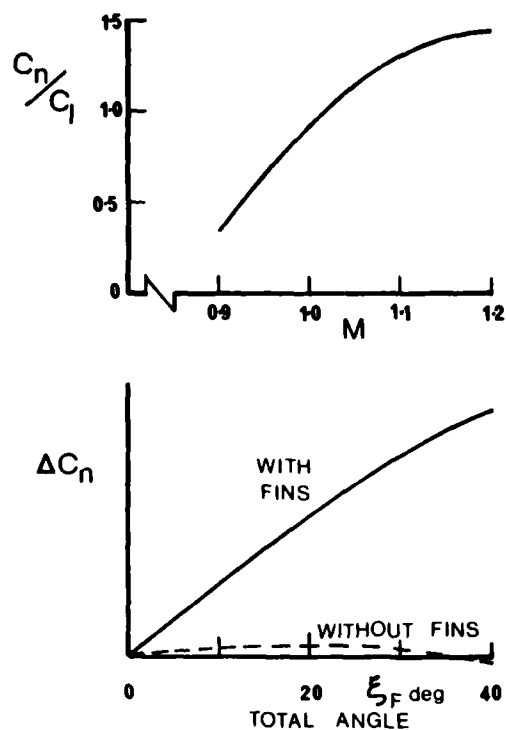


Fig 54 Ratio of rolling to yawing moment for 75 per cent semispan flaperon and comparison of yawing moments with and without fins

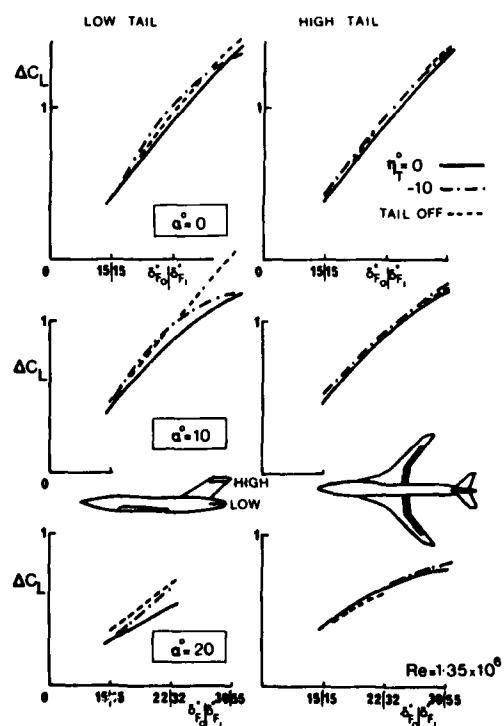


Fig 56 Effect of angle of attack and tail position on the incremental lift due to trailing-edge flaps; supercritical-wing transport concept

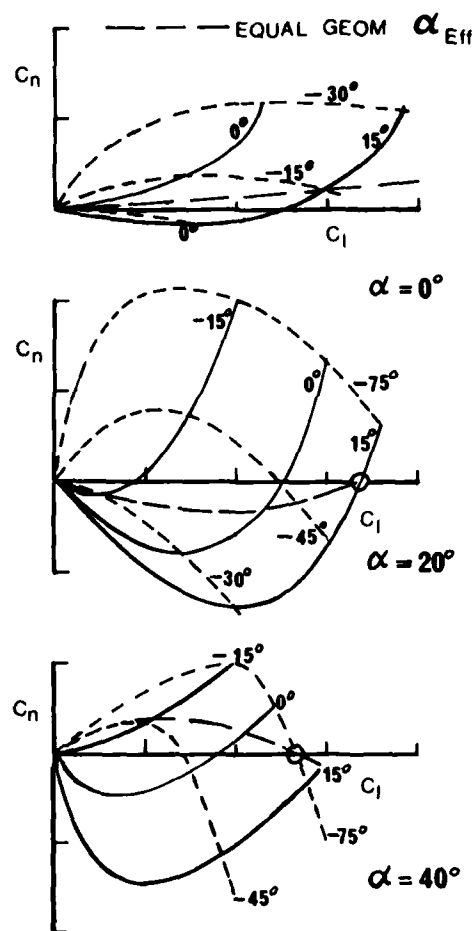


Fig 55 Increments in yawing and rolling moment coefficients for a range of tiperon deflections at three values of the angle of attack

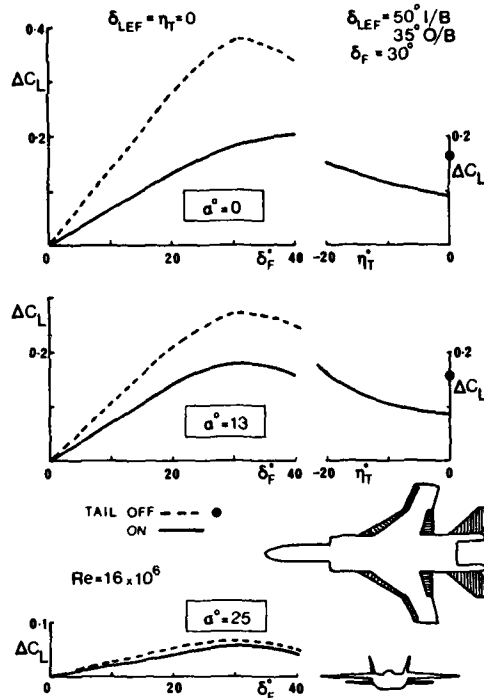
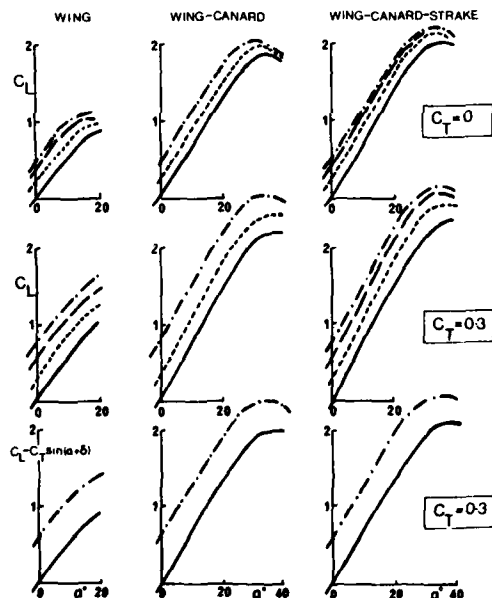


Fig 57 Effect of the angle of attack and tail setting on the variation with flap deflection for different deflections of a high lift system



MODEL SHOWN IN FIG 7

Fig 58 Effect of thrust coefficient on lift due to trailing-edge flaps and nozzle flaps for wing-canard-strake configurations

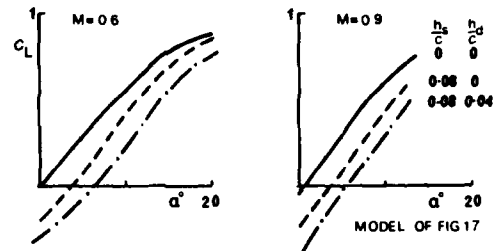


Fig 59 Variation of lift due to spoiler and spoiler-slot-deflector with angle of attack; research wing

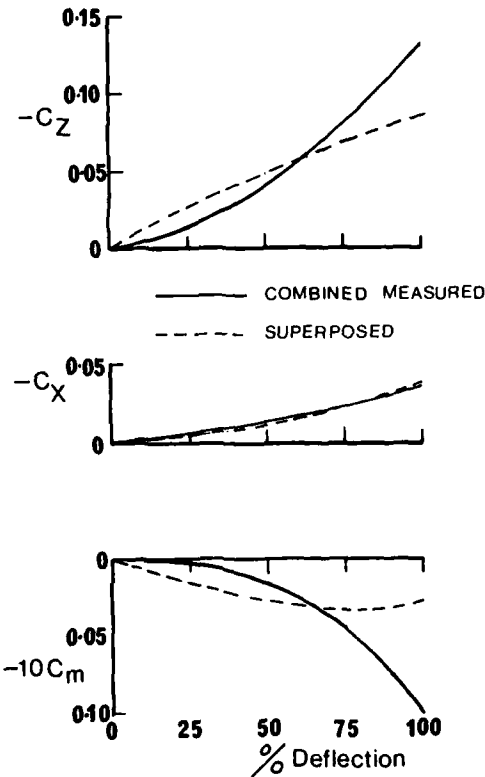


Fig 60 Increments in the Z-force, X-force and pitching moment coefficients due to four pylon flaps

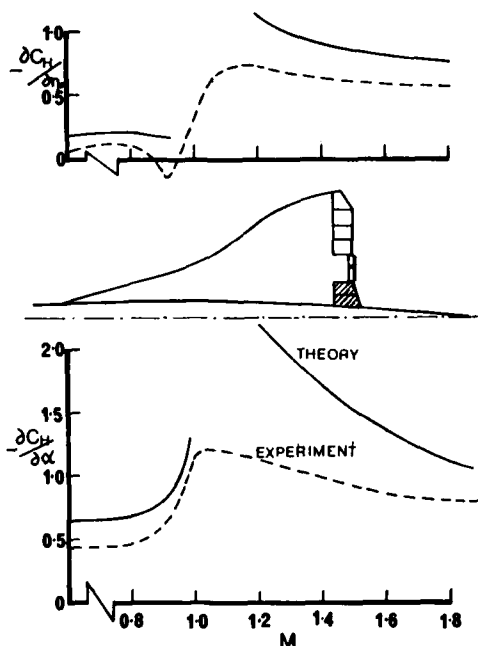


Fig 61 Hinge moment coefficient derivatives for an inboard Concorde elevator

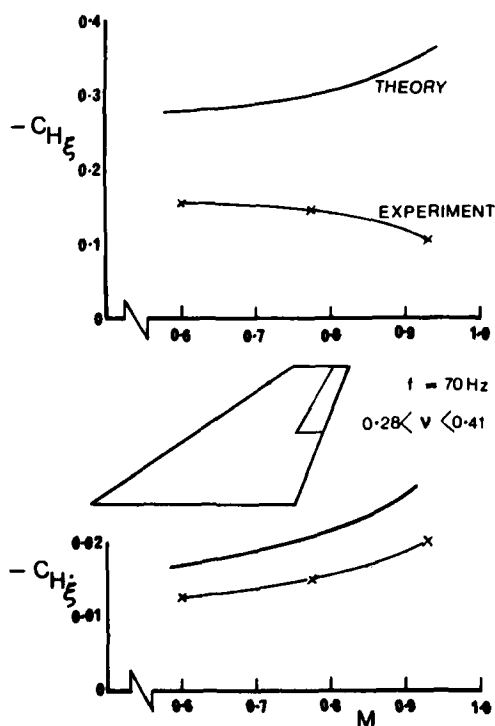


Fig 62 Hinge moment coefficient derivatives for flap-type motivators

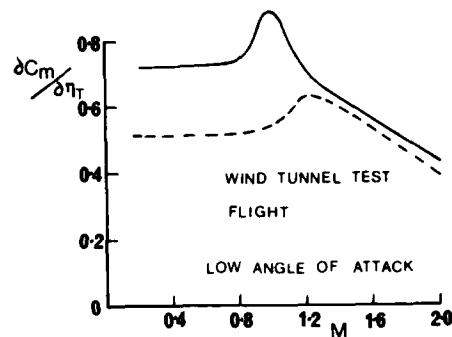


Fig 63 Variation with Mach number of elevator effectiveness for F-15 aeroplane

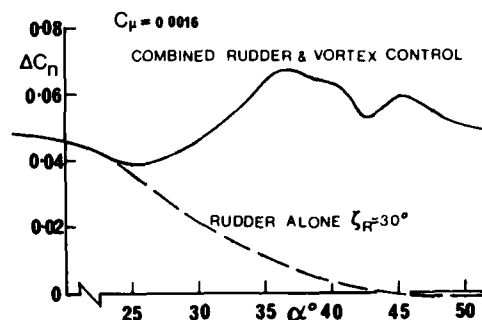


Fig 64 Increments in yawing moment coefficient due to rudder and rudder plus vortex blowing control

	ACTUATION FORCE OR MOMENT	CONTROL DERIVATIVES	MAXIMUM POWER
STABILITY AUGMENTATION			
DEPARTURE & SPIN PREVENTION			
RELAXED STABILITY			
MANOEUVRE ENHANCEMENT			
GUST, LOAD, FLUTTER ALLEVIATION			
MANOEUVRE DEMAND			
DECOUPLED RESPONSE			
ADAPTIVE OR INSENSITIVE			

Fig 65 Degrees of dependence of various control systems on control characteristics

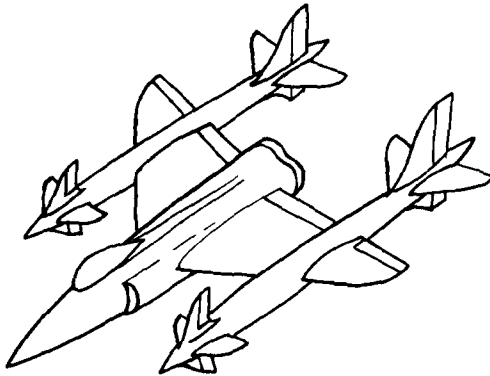


Fig 66 A possible concept for an ACT aeroplane with twin canard and tail units

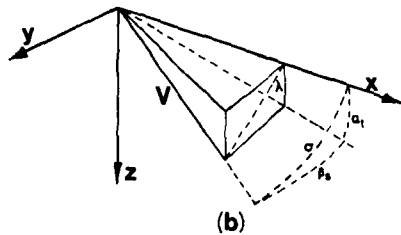
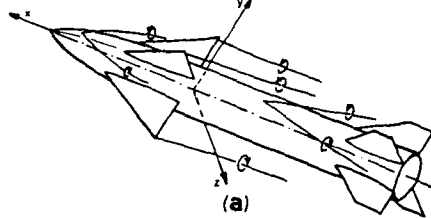


Fig 67 (a) Vortex systems for a typical cruciform missile configuration;
(b) Incidence angles

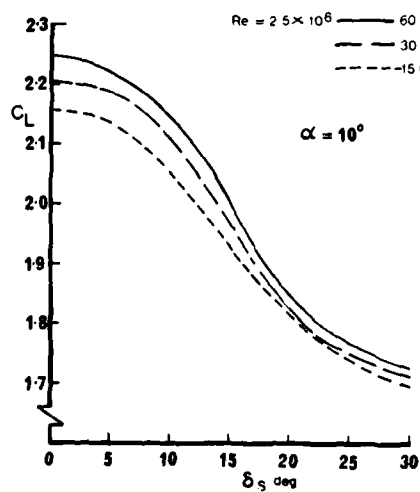


Fig 69 Scale effect on the total lift due to flaps at 40° for various spoiler deflections

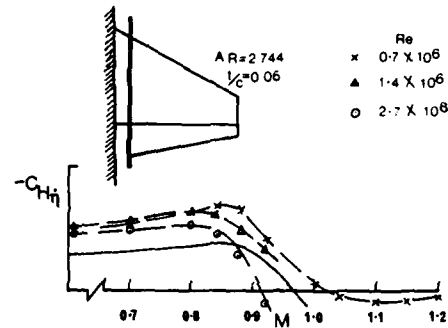
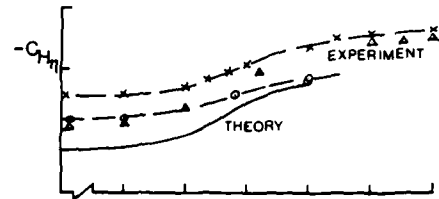


Fig 68 Effect of Reynolds number on the hinge moment characteristics of an oscillating flap

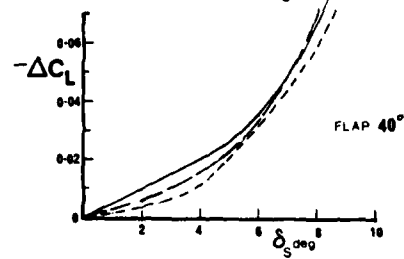
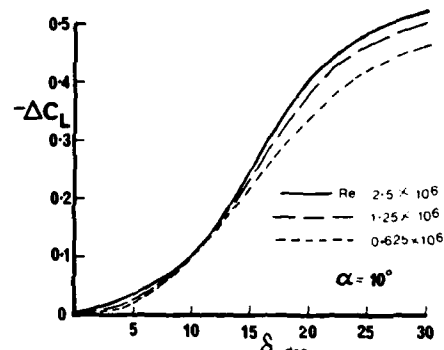


Fig 70 Effect of Reynolds number on the lift increment due to a perforated spoiler

MATHEMATICAL MODELLING AND THEORETICAL METHODS
FOR THE AERODYNAMIC BEHAVIOUR OF CONTROL DEVICES

Horst Körner *)

Institut für Entwurfsaerodynamik der DFVLR, Braunschweig, Germany

SUMMARY

A survey of the theoretical aerodynamic aspects of control devices is given. This is done for subsonic, transonic and supersonic attached flow; some comments on separated flow are given, too. The basic flow equations are introduced. Various calculation methods based on these equations are reviewed. This is followed by a comparison between theoretical and experimental results.

NOTATIONS

x, y, z	coordinate system	ϕ, ψ	potential functions
t	time	ψ	phase shift of the unsteady values
c	chordlength	a	spanwise loading function
\bar{c}	mean aerodynamic chord	h	chordwise loading function
s	halfspan	c_p	pressure coefficient
l	characteristic length ($l = c/2$ for airfoil) ($l = s$ or \bar{c} for wings)	Δc_p	load coefficient
α	angle of attack	c_p', c_p''	real resp. imaginary part of the unsteady pressure distribution (eqn. 4)
δ	flap deflection		
S	surface	$c_L, c_{L\delta}, c_{L\dot{\delta}}$	lift coefficient resp. derivative due to flap deflection
V	volume		
R	gas constant	c_D	drag coefficient
T	temperature	$c_m, c_{m\delta}, c_{m\dot{\delta}}$	pitching moment resp. derivative due to flap deflection
p	pressure		
ϵ	internal energy	$c_h, c_{h\delta}, c_{h\dot{\delta}}$	hinge moment resp. derivative due to flap deflection
s	entropy		
κ	isentropic exponent		
U	undisturbed flow velocity	SUBSCRIPTS	
$\vec{v} = \begin{bmatrix} u \\ v \\ w \end{bmatrix}$	velocity vector	S	steady
a	speed of sound	K	kink
$M = \frac{U}{a}$	Mach number	m	medium
M^*	critical Mach number	i	amplitude
$Re = \frac{U \cdot \bar{c}}{\nu}$	Reynolds number	FF	far field
$k = \frac{\omega \cdot l}{U}$	reduced frequency		
$\omega = 2\pi f$	circular frequency		
f	frequency		
K	transonic similarity parameter		

*) Dr.-Ing.
Director of Institute for Design-Aerodynamics, DFVLR

1. INTRODUCTION

Figure 1 shows control devices on an airplane, some of them typical for a fighter type aircraft, others for a subsonic transport aircraft. There is a subdivision between longitudinal and lateral controls. This is not at all stringent since longitudinal devices may also be used for lateral control as spoilers and differential tail for roll control and vice versa.

As can be seen the main aerodynamic problems that have to be treated are

- wings with control devices and
- mutual interference of wings.

The problem of the aerodynamicist is, to give good prediction for the effectiveness of control devices for steady and unsteady deflection. This is a task which can be solved by theoretical and experimental means.

The most straight-forward way providing data for control-surfaces, is the theoretical approach. Figure 2 gives a classification of the methods available or in development. First there has to be done a subdivision into

- attached flow and
- separated flow.

For attached steady and unsteady flow powerful methods have been developed on the basis of the potential theory with some allowance for viscous effects by boundary layer which give reasonable results for subsonic and supersonic flow. In the transonic case there are still severe deficiencies which are connected with the strong nonlinearity of the governing equations. Recent approaches in the transonic and supersonic region concentrate on the solution of the Euler equations plus consideration of viscous effects.

For separated flow a distinction must be made between those flow types where there exists a well-formed primary structure, e.g. the shedding of a free vortex sheet rolling up, and those where no primary structure can be observed, e.g. the flow behind bluff bodies. For the separated flow with certain primary structures, singularity models of the separated region may be constructed, in order to achieve an approximate solution. This leads to good results. When there is obviously no primary structure the singularity models are somewhat doubtful and the full solution of the Navier-Stokes-equations would be appropriate. This way is indeed the most comprehensive but also the most laborious one, and only a few solutions for practical purposes have been given up to now.

Another subdivision of methods resp. problems, which may be used, is the classification between steady and unsteady deflection of the control devices. The following states may be distinguished:

- Fixed control device.
This is the case of steady flow. There exist special classes of methods.
- Slowly oscillating movement of the device ($k \leq 0.05$).
For this case the steady methods can be used for a quasi-steady evaluation, since the aerodynamic forces and moments are in phase with the movement.
- Fast oscillating movement of the device ($k \geq 0.05$).
Methods for attached flow have been developed for this case. The aerodynamic forces and moments are no longer in phase with the movement.
- Suddenly deflected control device.
This case can be treated by the oscillatory methods by a Fourier analysis of the step-function. For some cases exact solutions exist which can be used for inspection of approximate methods.

General literature on theoretical methods is available. [1] and [2] among others give the basis, [3] and [4] concentrate on practical prediction methods and applications for the steady case, whereas [5], [6] and [7] deal with the unsteady case. [8], [9] and [10] give short resumes of prediction-methods for the unsteady case. The recent development of prediction-methods is given in [11], [12] and [13]. This paper is an extended version of a survey paper on theoretical methods for active control devices [14].

2. SUBSONIC ATTACHED FLOW

2.1 Basic equations

The basic equation of linearized subsonic potential flow is

$$(1 - M) \phi_{xx} + \phi_{yy} + \phi_{zz} = 0 \quad (1)$$

where M is the free stream Mach number and ϕ is the velocity potential. This equation can

be transferred by Goethert rule to the Laplace-equation

$$\phi_{xx} + \phi_{yy} + \phi_{zz} = 0 \quad (2)$$

or

$$\nabla^2 \phi = 0.$$

The linearized potential equation for the unsteady case is

$$\nabla^2 \phi - \frac{1}{a^2} \left[\frac{\partial}{\partial t} + U \frac{\partial}{\partial x} \right] \phi = 0 \quad (3)$$

where a is the speed of sound and U the flight speed. Basic boundary condition is the requirement of tangential flow on the surface.

2.2 Outline of the methods

Since the solution procedure for steady and unsteady flow is similar, a unique treatment of both cases will be given. Two main classes of methods have to be distinguished, the

- conformal mapping methods
- singularity methods.

The conformal mapping technique has been worked out by THEORDORSON [15] to a comprehensive theory for steady and unsteady twodimensional flow. Nevertheless the singularity-methods have become much more important since these methods could be extended without major difficulties to the 3D case.

Due to the linearity of the subsonic potential equation the principle of superposition of solutions can be applied. So basic solutions of the equations as sources, vortices and doublets may be combined in an arbitrary way to find the flow field required. This singularity technique has been used for the development of a large number of subsonic theories and will be described subsequently for the 3D case, which includes the 2D one. For the development of these methods both the velocity and the acceleration potential have been used successfully.

The subsonic singularity method can be divided into two classes:

- loading function methods
- discrete loading methods.

The loading function method, also called lifting surface method, is a thin wing resp. thin airfoil theory. The basic steady approach has been developed by MULTHOPP [16] and TRUCKENBRODT [17], the extension to the unsteady case has been given by LASCHKA [18], [19] and DAVIES [20].

Thin wing theory means that thickness effects are neglected because they are of minor importance compared with the lift effects. Since lift effect can be simulated by vortices and doublets, these singularities are the basis of thin wing theory. The problem to be solved may then be formulated as an integral-equation for the downwash of the wing. This equation can also be derived by Green's theorem.

The solution of this integral equation is found by introducing loading functions with unknown scale factors in chordwise and spanwise direction to approximate the load of the wing. Figure 3 shows typical loading functions for the subsonic lifting surface theory. The choice of the loading functions must be consistent with the singular behaviour of the leading edge of the wing (h_0 , h_1 , h_2 , h_K), the hinge line (h_K) and the wing tip (a_0 , a_1). The load must also satisfy the Kutta condition at the trailing edge. After introduction of these loading functions the integral-equation is reduced to a system of linear equations where the scale factors of the loading-functions have to be evaluated. This can be done after having introduced a number of control-points on the wing where flow tangency has to be satisfied.

The loading functions used in chordwise direction are derived from 2D thin airfoil theory. Thus the loading function h_0 is the load distribution of a flat plate at incidence, the so-called first Birnbaum-distribution. The loading function h_1 is a combination of the first Birnbaum-distribution and the second one, which gives the 2D result of a 2D plate with parabolic camber at zero lift. The loading function h_K is a combination of the first Birnbaum-distribution and the distribution of a 2D flat plate with a kink at zero lift. This kinked plate distribution has two singular points, first the leading edge which is the well-known square root singularity of the plate and a kink singularity which has logarithmic character.

The spanwise loading function a_0 is an ellipse, the well-known elliptic circulation distribution of a wing with minimum induced drag at given lift coefficient and aspect ratio.

Part-span flaps, the discontinuity of the trailing edge brings some diffi-

culty. This has been overcome within the loading-function procedure by taking into account the flap discontinuity which has been derived by MULTHOPP [21], [22].

The other type of methods which will be discussed here are discrete loading methods. Here it is useful to subdivide into

- vortex/doublet lattice methods and
- panel methods.

While vortex/doublet lattice methods only treat the thin wing, panel methods enable a general solution of thick lifting bodies.

The vortex-lattice method for steady flow has been developed by FALKNER [23] and RUBBERT [24], extensions of this method have been given among others in [25] and [26]. The unsteady case has been treated by HEDMAN [27] and ABANO and RODDEN [28].

Basis of this method again is the downwash-equation of lifting surface theory. The idea of this method is, to discretize the load of the wing in small elements. Thus the wing has to be subdivided in a large number of small trapezoidal elementary wings - called panels - arranged in strips parallel to the free stream and with leading edge, trailing edge and hinge-line coinciding with edges of the panels (see figure 4). It has been shown that the lift of a panel can be concentrated on the quarter chord line of the panel with trailing vortices at the tips. This horseshoe-vortex whose strength has to be determined represents the steady effect of the panel. By a line of doublets on the quarter chord line the oscillatory effect can be taken into account. The downwash boundary condition then is satisfied at a pivot-point which is located at $3/4$ chord along the center line of each panel. The basic integral equation of lifting surface theory is thus reduced to a set of linear equations, which has to be solved for the unknown load.

The advantage of this method is its rather simple handling in comparison to the lifting surface method since it can be used without difficulties for complex nonplanar lifting systems [29]. When using the loading function method complications arise since the characteristic singular behaviour of the solution must be known a priori and must be incorporated in the method in form of appropriate loading functions. This is not the case with the vortex/doublet-lattice method, where singular points are distant from pivot points a priori.

In order to get good accuracy for the vortex/doublet-lattice method, 100 panels for a half-wing are necessary to get an appropriate load distribution in span- and chordwise direction. A still higher number is needed for a wing with control devices. Even with this high number of panels the accuracy of this method is not as high as of the loading function method. Since it seems not worthwhile to achieve a higher accuracy than $\pm 3\%$ because thickness and viscous effects have not been taken into account, also the vortex/doublet-lattice method can be seen as a powerful method.

A somewhat different approach to the thin wing discrete methods has recently been given by GEISLER [30]. Instead of a doublet-line Geißler uses a doublet-field on the panel.

The most recent and most comprehensive approach to subsonic lifting bodies is the panel method. For steady flow the basics of this method have been derived by HESS and SMITH [31] and RUBBERT and SAARIS [32]. Amplifications of this method have been given in [33] to [36]. The unsteady approach has been treated in [37], [38] and [39]. A survey on panel methods as well as vortex-lattice methods is given in [40].

The basic idea of the panel method is similar to the vortex-lattice method. The surface of the body is subdivided into a large number of trapezoidal panels as shown in figure 5. The solution of the governing Laplace equation for steady flow is constructed by arranging a distribution of basic singularities on body and wake surface. The effect of these discrete singularity distributions on each panel produces disturbance velocities at other points of the surface. At these pivot-points - each panel has one on its centre - the velocities are evaluated as an integral, employing Green's theorem. This integral expresses the induced velocity at a body pivot-point in terms of the known body geometry and the unknown perturbation singularity strength. Satisfying the condition of flow tangency at the pivot-points yields determining the singularity strength. This procedure is quite similar to the vortex-lattice method.

The version most widely used in practice for steady flow has source singularities on the surface to get the thickness effect and vortex singularities in the body mean surface and the wake for representation of the lift effect. Unsteady effects can be treated by placing doublets on the mean surface or on the surface itself. For steady flow this powerful method is already extensively used. For unsteady flow first results have been achieved.

The methods described so far, suffer from the deficiency that viscous effects are not included. In the 2D case standard-methods have been developed which take into account the boundary-layer effect. Based on the pressure distribution of the inviscid code, a boundary-layer calculation is performed and its effect in return amplifies the boundary condition at the contour. This leads to an iteration procedure in which outer flow and boundary layer are calculated alternatively until both are matched in a convenient way. As to the change of the boundary condition on the contour two approaches have to be distinguished

- adding the displacement-thickness to the contour

- prescribing an outflow on the surface which is equivalent to the growth of the displacement of the boundary layer.

Both methods are used and have their special merits.

Whereas for 2D cases this procedure is usual, in 3D only some first results for steady flow condition without controls have been published.

2.3 Discussion of results

To prove the validity of the methods described, some typical theoretical results will be presented, which have been verified experimentally by wind-tunnel investigations. In order to have a consistent nomenclature within this paper, a few denominations of the original contributions have been changed. Unchanged remain different presentations of unsteady pressure and derivatives, which can be given either divided in real and imaginary part or in magnitude and phase shift.

$$c_{\text{unsteady}} = c' + ic'' = |c| \cdot e^{i\varphi} \quad (4)$$

Both nomenclatures have been used here.

Figure 6 shows results for a twodimensional airfoil with oscillating flap [41]. The real and imaginary part of the pressure distribution are given for a reduced frequency between 0 and 1. The singular behaviour of the flap-kink can be seen quite clearly. It can also be seen that the flap-singularity acts in phase with the movement of the flap. The figure shows furthermore that good agreement between theory and experiment can be achieved. It must however be noted that with rising frequency the discrepancies in c_p'' are growing.

The data at least important for control effectiveness are the derivatives. Fig. 7 shows results for a 16% thick airfoil with a trailing edge flap [42]. Results are given for lift, pitching moment and hinge moment over the reduced frequency. The experiments are compared with linearized theory (flat plate with kink), with a singularity-method where the singularities are placed on the contour, and with a method where this singularity-method is coupled with a boundary-layer calculation. The comparison shows that with boundary layer the best agreement can be achieved, although still some discrepancies remain. This may be due to a certain slot-flow, which is not taken into account.

Let us now have a look on the 3D case. Figure 8 shows results for an untapered swept wing with two flaps acting in antiphase. Theoretical results achieved with the discrete loading method by GEISSLER [30] are compared with wind-tunnel results [43]. Results are given for two sections. The agreement between theory and experiment is quite good. Some small discrepancies can be observed at the leading edge of the control surface. This is obviously due to a small gap in the experimental case.

Results for a swept wing with oscillating flap at a high subsonic Mach number are given in figure 9. The results achieved with a loading function method after [44] compare quite well with the experimental data.

Most of the results presented up to now have been achieved with airfoil resp. thin wing theories. One major deficiency of these theories is the neglect of thickness effects. This can be overcome by the use of panel-methods. Figure 10 compares results from thin wing theory [30] and panel-method [39] for the wing discussed in figure 8. The thickness effect alters the pressure distribution significantly. Compared with the experiment, it is difficult to decide, whether the incorporation of the thickness effect brings an improvement or not. Obviously thickness effects and viscous effects are partially cancelling each other as known from the steady case. This may explain the rather good agreement which is usually found when comparing pressure distributions received from inviscid thin-wing theories and experiments.

The second main problem of control aerodynamics is the interference between main wing and tail or canard. Figure 11 shows theoretical results from loading function method [19] for a wing with variable sweep followed by a tail-unit. Results are given for the unsteady pressure distribution in a specified section of the tailplane due to wing pitch oscillation compared with experiments [45]. For the moderate sweep cases the agreement between theory and experiment is quite good. In the case of 70° sweep larger discrepancies occur since now the tailplane is strongly influenced by the boundary layer of the wing, the deformation of the vortex-sheet and before all by the tip-vortex. All these viscous effects are not covered by theory.

Figure 12 shows results for the reverse problem: interference of a pitching tail in the main wing. As can be seen this influence is rather small. The theoretical prediction agrees fairly well with the experimental data.

3. TRANSONIC ATTACHED FLOW

3.1 Basic equations

The conservation laws of mass, momentum and energy for inviscid flow can be written in the form

$$\text{Mass:} \quad \int_V \frac{\partial \rho}{\partial t} dV + \int_S \rho \vec{v} \cdot d\vec{S} = 0 \quad (5)$$

$$\text{Momentum:} \quad \int_V \frac{\partial (\rho \vec{v})}{\partial t} dV + \int_S \rho \vec{v} \cdot \vec{v} d\vec{S} = - \int_S p d\vec{S} \quad (6)$$

$$\text{Energy:} \quad \int_V \frac{\partial \left[\rho \left(\epsilon + \frac{1}{2} \vec{v}^2 \right) \right]}{\partial t} dV + \int_S \rho \left(\epsilon + \frac{1}{2} \vec{v}^2 \right) \vec{v} \cdot d\vec{S} = - \int_S p \vec{v} \cdot d\vec{S} + L_M + L_W \quad (7)$$

with L_M as term of the inertial forces and L_W as term of the heat conduction. Together with the gas law

$$\frac{p}{\rho} = RT \quad (8)$$

these are four equations for the four unknown \vec{v} , p , ρ and $\epsilon(T)$. This integral form of the equation for mass, momentum and energy can be derived in an elementary way and is the most comprehensive formulation of the basic equations of inviscid flow.

For the evaluation of transonic flow inertial forces and heat conduction are neglected and the isentropic gas law is introduced. These are the basic equations used within the "Finite Volume Method" in transonic flow, the most comprehensive approach available at this time.

Now most of the methods used in transonic flow have the differential form of the conservation-laws as basis. The integral form can be transferred to the differential form by using the Gauss theorem

$$\int_V \nabla \cdot \vec{a} dV = \int_S \vec{a} \cdot d\vec{S} \quad (9)$$

This leads to the conservation-laws in differential form

$$\text{Mass:} \quad \frac{\partial \rho}{\partial t} + \nabla \cdot (\rho \vec{v}) = 0 \quad (10)$$

$$\text{Momentum:} \quad \frac{\partial \vec{v}}{\partial t} + (\vec{v} \cdot \nabla) \vec{v} = - \frac{1}{\rho} \nabla p \quad (11)$$

(Euler)

$$\text{Energy:} \quad \frac{D \left(\epsilon + \frac{1}{2} \vec{v}^2 \right)}{Dt} + \frac{1}{\rho} \frac{Dp}{Dt} = 0 \quad \left(\frac{Ds}{Dt} = 0 \right) \quad (12)$$

$$\text{Gas-Law:} \quad \frac{p}{\rho^\kappa} = \text{const.} \quad (13)$$

Equation (12) says that the total differentiation of the entropy versus time is zero. This is consistent with isentropic flow and irrotationally or conservation of rotation generated at a singular line or point.

An important point of the Gauss theorem is, that it is only valid for steady functions within the field. Since shocks occur their appropriate representation in a method based on these equations has to be proven. This is not the case, when using the equations in integral form.

When irrotationality is given, a potential function

$$\phi = \frac{\partial u}{\partial x} \quad (14)$$

can be introduced. Introducing furthermore the speed of sound

$$a^2 = \frac{dp}{d\rho} \quad (15)$$

the set of equations can be reduced to the potential equation and the Bernoulli's equation

$$\begin{aligned}
& (a^2 - \phi_x^2) \phi_{xx} + (a^2 - \phi_y^2) \phi_{yy} + (a^2 - \phi_z^2) \phi_{zz} - 2\phi_x \phi_y \phi_{xy} - 2\phi_x \phi_z \phi_{xz} - 2\phi_y \phi_z \phi_{yz} + \\
& + 2\phi_x \phi_{xt} + 2\phi_y \phi_{yt} + 2\phi_z \phi_{zt} - \phi_{tt} = 0
\end{aligned} \tag{16}$$

$$a_0^2 - a^2 = (\kappa - 1) \left[\frac{1}{2} (\phi_x^2 + \phi_y^2 + \phi_z^2) - \phi_t \right]. \tag{17}$$

This is for the unsteady case, the formulation for the steady case is as follows:

$$(a^2 - \phi_x^2) \phi_{xx} + (a^2 - \phi_y^2) \phi_{yy} + (a^2 - \phi_z^2) \phi_{zz} - 2\phi_x \phi_y \phi_{xy} - 2\phi_x \phi_z \phi_{xz} - 2\phi_y \phi_z \phi_{yz} = 0 \tag{18}$$

$$a_0^2 - a^2 = \frac{\kappa - 1}{2} [\phi_x^2 + \phi_y^2 + \phi_z^2]. \tag{19}$$

These equations are the basis for a number theoretical methods. For various other methods still more simplified equations have been used as the transonic small perturbation equation, where only the dominant nonlinear part of the full potential equation is left. Introducing a perturbation potential

$$\phi = U x + \varphi \tag{20}$$

the steady state form of the transonic potential equation (TSP) is

$$\left(K - (\kappa + 1) \phi_x \right) \phi_{xx} + \phi_{yy} + \phi_{zz} = 0. \tag{21}$$

This form together with Bernoulli's equation has often been used for steady transonic methods. A further local linearization leads to a special form of the TSP, valid for Mach numbers near 1

$$\phi_{yy} = c(\kappa + 1) \phi_x \tag{22}$$

the so-called parabolic equation.

For all sets of equations there is the same boundary condition as posed by the problem: no flow through the contours of body, resp. bodies.

In contrast to the subsonic case these equations are nonlinear and the well-known techniques used in subsonic flow as superposition of solutions cannot be used.

Another difficulty that arises in the transonic flow regime is due to the occurrence of subsonic and supersonic flow fields around the wing at the same time. This means for the steady case, that the governing equation changes its type from elliptic (subsonic) to hyperbolic (supersonic) within the flow field. This difficulty has been overcome by the introduction of different regions of influence for the subsonic and the supersonic case [46]. In the unsteady case this brings no difficulties since these equations are uniformly hyperbolic. Therefore time-dependent methods also have been used to find the steady state solution ($t \rightarrow \infty$).

Another difficulty arises from the occurrence of shock-waves, which does not allow a priori the assumption of isentropic flow. Since the existence of potential flow suggests isentropic, this is a crucial point. It has been shown that for weak shocks, potential theory is still appropriate, but if stronger shock or multiple shocks occur the conservation-equations (Euler) have to be used. Furthermore Jameson has shown [47] that using the full potential equation it may occur that different solutions can be got which is due to the non-uniqueness of the continuum problem.

A comment has to be given to the fulfilment of the boundary conditions on wing and body. This depends to a substantial part on the fitting of the network to the contour. The simplest network is the cartesian approach in which the boundary conditions can only be fulfilled in a linearized way. Refinements as grid-embedding [48] lead to an appropriate representation of complex configurations.

In general the favorite way to get better fulfilment of the boundary conditions is to transform the flow field into a rectangle. This leads to networks of O or C form, given in fig. 13. A somewhat different approach is the use of streamline coordinates. All methods have their special merits. Fig. 14 shows a C type grid which moves with the flap deflection of the airfoil [49].

The transformations become more complex for the 3D case. One alternative here is to go back to the cartesian approach with grid embedding, the other is to use a sophisticated block-structured grid system [50].

3.2 Outline of the methods

A great number of theoretical methods has been developed on the basis of the different equations given in chapter 3.1.

Hodograph method: Basis of this method is the linear hodograph equation which has to be evaluated in the hodograph-plane. This method has its special merits for twodimensional airfoil design.

Local linearization: Due to the relative simplicity of the parabolic equation used for this approach, this method has been exploited to a large extent. Nevertheless the method of local linearization did not achieve major importance since it has several shortcomings which restrict its applicability. So this method is only applicable to M-numbers near 1. Furthermore shock-waves, and round leading edges cannot be treated. Results of this method are known for the steady and unsteady case [51] - [53].

Integral equation: Basis of this method is an integral equation which can be derived from the potential equation using Green's theorem. The method due to Oswatitsch allows substantial savings in computation efforts since it provides a reduction of dimensions by one when an appropriate assumption for the decay of the velocity transverse to the streamwise direction is made. The integral equation gives good results for subcritical flow but exhibits some critical features, when the flow becomes supercritical. Nevertheless also these difficulties can be overcome. Steady methods of this type have been developed by [54] and [55], unsteady methods by [56] and [57].

Finite difference: This type of method has been pushed forward in the last years to such an extent, that effective prediction methods for steady and with some restrictions for unsteady flow are available. Two different types of methods have to be distinguished

- relaxation methods
- time progressing methods.

The relaxation technique is at the moment the most widely used prediction method for steady and unsteady flow. Therefore this technique will be described a bit more in detail for the steady 3D case [58], [59], [60].

Basic equations for this technique may be the widely used TSP equation (21) together with equation (19). These equations are transferred into finite difference equations for which the solution has to be evaluated throughout the flow field near the wing-body configuration (see figure 15). At a certain distance from the configuration the far field solution is connected with the finite difference solution. For the finite difference procedure within the network different types of operators are used

- centered finite difference molecules for subsonic (elliptic) points
- backward oriented finite difference molecules for supersonic (hyperbolic) points and
- a mixture of both for points aft of the boundary supersonic-subsonic flow.

The boundary condition on the configuration is satisfied by yielding flow tangency at mesh-points, which border on the body.

The solution for the potential within the finite difference network is found by successive line relaxation following the direction of the flow. This so-called sweeping through the flow field has to be repeated until a converged solution has been achieved. Since the number of field points for a 3D wing is approximately 50,000 to 200,000 and up to 200 iterations in the finest grid are needed to achieve an acceptable accuracy, the computer time is rather high. It takes up to 1 hour on an IBM 3081.

The method described here is with certain modifications, e.g.

- use of full potential equation [61]
- use of mapping technique to get a more appropriate computation field [61], [62]
- conservative or non-conservative formulation

the at this time standard method for 3D transonic flow computations with shocks. These methods can be used without difficulties for flap deflections as far as no separation effects occur.

For the relaxation methods a rather simple extension to the unsteady oscillatory flow is possible, when only small deflections are assumed [63 - 65]. The other promising type of finite difference method is the time progressing method which first has been developed for the steady case using the solution $t + \Delta t$ as the steady solution. This method which has been developed on the basis of the Euler equation by YOSHIHARA [66], [67] and others [68 - 69] is especially appropriate for the suddenly deflected control device. Results for

oscillatory flow achieved with this most accurate method may also be used as reference for the much faster relaxation methods which only give approximate result. An alternative approach to this method is the Alternating-Direction Implicit (ADI) method proposed by BALLHAUS [70], [71], [72] which uses an implicit discretization of the governing equation. Due to this technique the computation time needed can be speeded up considerably.

Finite element: A further alternative approach to the transonic problem is the finite element method. This method which is widely used in the calculation of static structures, has not been adopted in fluid mechanics to a large extent. Methods for 2D and 3D steady flow have been developed by [73] and [74], unsteady approaches have been given by [75] and [76]. As in the relaxation technique, special care has to be taken for the supercritical case.

Finite volume: The perhaps most effective approach to the steady and unsteady flow problem in transonic flow is the finite-volume approach [77]. Methods based on the full potential equation in conservative formulation have been developed by [78] and [79]. The most comprehensive approach is the application of the finite-volume approach on the Euler-equations [80].

Although a number of methods for transonic flow are given here - these are only a selection of much more publications on this topic - a comprehensive method for 3D wings with oscillating flaps has not been presented up to now. Nevertheless some special problems have been tackled as the mutual interference of two airfoils [81] and the airfoil with flaps and slats [82], [83]. As to viscous corrections a number of methods has been extended to incorporate boundary-layer effects. The procedure is the same as indicated for subsonic flow.

3.3 Discussion of results

For the transonic case some selected results will be presented which show the special features and the state of the art of methods in transonic flow. These results are compared with experiments from wind-tunnel.

Fig. 16 shows a comparison of theory and experiment for two cases. The theories used are subsonic thin airfoil theory and the TSP method after EHLERS [63]. For the lower Mach number the magnitude of Δc_p is given very badly by the transonic theory; on the other hand at $M = 0.85$ the specific feature of the moving shock is predicted qualitatively quite well, but the absolute value is overestimated. Also in phase shift there are remarkable discrepancies.

Results which show the influence of the boundary layer are given in fig. 17. Experimental results are compared with TSP results after [85]. It can be seen quite clearly that the viscous correction brings a considerable improvement towards a better agreement between theory and experiment. Nevertheless the shock itself is not yet represented well.

Let us turn over to overall results. Fig. 18 gives experimental results in comparison with linear theory, TSP method without and with viscous correction. As in fig. 17 the results with viscous correction compare best with experimental results.

One of the key problems of transonic flow is the proper representation of the shock. Fig. 19 shows the difference in shock location using TSP method and Euler method. Certain discrepancies can be seen which have an influence on the lift coefficient given in the lower diagram.

A comparison with experiment is given in fig. 20. Although a powerful method (time marching method on the basis of the Euler equation) is used, the agreement between theory and experiment is not acceptable. The results show that for transonic flow the methods used are still far from giving quantitatively good results. This may be partially due to local separation effects which are not incorporated in these theories.

4. SUPERSONIC ATTACHED FLOW

4.1 Basic equations

As in the subsonic case the pure supersonic flow can be treated by linearized theory. This allows all the simplifications implicated with a linearized treatment as discussed for subsonic flow. The basic equation for steady flow is

$$(M^2 - 1)\phi_{xx} - \phi_{yy} - \phi_{zz} = 0. \quad (23)$$

The linearized potential equation for the unsteady case is identical to subsonic case

$$\nabla^2 \phi - \frac{1}{a^2} \left[\frac{\partial}{\partial t} + U \frac{\partial}{\partial x} \right]^2 \phi = 0. \quad (24)$$

When the Mach number comes near 1 or exceeds 3 nonlinear terms of the full potential equation have to be taken into account. Linear theory also fails in areas, where shock-waves impinge with the surface.

4.2 Outline of the methods

According to the type of equation to be solved two different types of methods must be distinguished (figure 21)

- singularity-methods for the solution of the linear potential equation
- field-methods for the solution of the potential-equation with nonlinear terms or the Euler equations.

Singularity-methods: As in subsonic flow, the potential-equation can be transferred into an integral-equation which is the basis of all supersonic theories. Special features of supersonic theory are

- range of dependence: only the area of the Mach-cone in front of the pivot-point has an influence on the flow condition in the pivot point
- subdivision between sub- and supersonic edges: subsonic edges have a singular behaviour different from the supersonic case. When there is a supersonic edge, there is no mutual dependence of upper and lower side of the wing around this edge.

There exist several different formulations to treat the supersonic problem. Among others the most important are

- integration of the downwash [86], [87]
- integration of the velocity potential [88], [89]
- acceleration potential [90].

All three formulations have their special merits. There are also several ways integrating the range of influence. The most important are given in figure 25, covering

- square boxes [91]
- Mach boxes [88], [90], [92]
- characteristic boxes [86], [87]
- boxes adjusted to wing geometry [93], [94].

No best choice can be given, since this depends often from geometry and range of Mach number. All these techniques give appropriate results if the evaluation for each box is done in a proper way.

Field-methods: For a more refined analysis of the supersonic flow of complex configurations methods must be used which base on a potential equation with the most important nonlinear terms, the full potential equation or even the Euler equations abandoning the concept of isentropic flow. Such methods - at this time in the status of development - are finite difference [95] and finite volume techniques [96]. Up to now none of these methods has been used for the prediction of control effectiveness. This is especially due to the high amount of computation effort needed for these techniques compared with singularity-methods.

4.3 Discussion of results

For steady flow figure 22 shows results evaluated with the flexstab-programm [97], a program-set developed by BOEING and NASA, which contains elements of the theories described in [32] and [94] for subsonic and supersonic flow. The results show quite good agreement in the subsonic part, except at the hinge-line where some deviations occur. The supersonic case exhibits good accuracy on the main wing but rather large discrepancies for the load on the flap, although the tendency is given in the right manner.

An unsteady result is given in figure 23 for a swept wing with an oscillating flap at a low supersonic Mach number [98]. Here results of theory and experiment are compared in four spanwise sections. The theories used are lifting surface theory after SADLER and ALLEN [88] (BAC method) and an extension of STARK's theory [87] (MBB method). As can be seen the calculated load distribution on the rear part of the wing agrees quite well with the measurements.

For the same wing figure 24 shows the lift coefficient and the hinge moment due to flap oscillation over the reduced frequency. Although the discrepancies in the real part of the coefficients go up 25%, fair agreement between the two theories, which give nearly identical results, and experiment is obvious.

5. LEADING EDGE VORTEX FLOW

Among separated flows leading edge vortex flow as it occurs on

- slender delta wings and on
- strakes

is a phenomenon that can be used in flight since this flow exhibits favorable nonlinear lift effects. Comprehensive information on this type of flow is given in [99].

Methods based on potential theory have been established to solve the vortex flow field above slender wings. Four different approaches have been developed

- leading edge suction analogy [100], [101]
- vortex-lattice method [102], [103], [104], [105]
- free vortex sheet method [106]
- Euler approach [107].

The first method only gives overall forces and moments, the vortex-lattice some information on the load distribution of the wing, while the free vortex sheet method, which is a higher order panel method gives detailed results of the pressure distribution. These three methods can be used for subsonic flow. A method which can also be used for the transonic and the supersonic case is the solution of the Euler equation. This method is still in the stadium of being developed.

Figure 25 shows the discretization after the vortex-lattice method for a rectangular wing of small aspect ratio. As in linear flow case the wing itself is subdivided into a number panels with appropriate horseshoe-vortices and pivot-points. While the trailing vortices in general leave the wing at the trailing edge, those vortices which originate from the wing tip, roll up. The figure shows quite clearly this rolling-up process of the different trailing vortices originating from the tip.

Steady results for a highly swept wing with trailing edge flap achieved with the vortex-sheet method are given in figure 26 [108]. The comparison with experimental data shown for two sections exhibits fair agreement between theory and experiment. Nevertheless it can be seen that there remain discrepancies at the leading edge due to separation and at the kink station.

6. SEPARATED FLOW WITHOUT PRIMARY STRUCTURES

Attached flow can be tackled by potential theory or by the solution of the Euler equations as has been shown in the chapters 2 to 4. Even separated flow with free vortex shedding can be treated by these theories (chapter 5). In contrast to this the generally separated flow exhibits more difficulties since the solution of the full Navier-Stokes-equations has to be executed, if a comprehensive solution is required.

Now fully separated flow in flight should in general be avoided - except post-stall operations of fighters. Nevertheless there is urgent need in the knowledge of occurrence of separation and its development after its beginning, since this effects the loss of control effectiveness. Therefore these solutions are of special importance, but unfortunately only few methods with restricted applicability have been developed so far. The theoretical methods can be subdivided into two classes

- hybrid methods using inviscid- and boundary-layer theory
- methods solving Navier-Stokes equations.

Whereas the first class of methods in general uses potential theory combined with boundary-layer calculations and some empirical modelling of the dead air region, the second approach is the most comprehensive but also the most laborious one with respect to computer time.

Hybrid methods: Some methods - up to now only steady approaches - have been developed to evaluate the maximum lift of single airfoils and airfoils with flap [109] - [113]. Figure 27 shows the theoretical model for the flow past an airfoil with flap after JACOB [114]. In this theory a vortex distribution is located along the contour of the airfoil and the flaps to simulate the potential flow. This potential flow calculation is followed by a boundary-layer calculation for each part of the airfoil. If the boundary-layer calculation indicates separation, beginning from the point of separation, a dead air model on the rest of the surface is constructed by a source distribution located on the separated part of the contour. Claiming the same pressure value for S, T and U gives a boundary condition for the rate of outflow. The separation point depends on the pressure distribution. Since this pressure distribution itself is not known a priori but has to be evaluated, an iteration-process has to be started which has a good chance to converge as JACOB has shown [109]. Figure 27 shows results of this theory compared with experiments after [115]. As can be seen quite good agreement is achieved not only for the slope of the lift curve but also for the lift maximum.

Using the 2D characteristics of an airfoil respectively airfoil plus flaps the high lift performance of a 3D wing of moderate and large aspect ratio can be evaluated after the method of WELTE [116].

Solution of the Navier-Stokes equations: At least the solution of the Navier-Stokes equation provides results for partly and fully separated flow. A survey of solutions of the Navier-Stokes equations is given in [117]. But this is no well established technique for general cases. There arise difficulties in the solution especially of those cases relevant for practical application. The following statements can be given:

- most of the solutions provided up to now deal with laminar flow
- the calculation in the turbulent flow regime requires models for turbulence. Only some very crude models are available up to now
- the computer time for the solution of the Navier-Stokes equations for practical cases is extremely high.

Therefore calculations of practical interest as on airfoils at high Reynolds numbers are scarce. Calculation of the viscous flow past airfoils has been done by DEIWERT [118] and McCORMACK [119]. STEGER and BAILEY [120] have extended this method to unsteady flap deflection and give pilot results for transonic aileron buzz which compare fairly well with experiments.

7. CONCLUSIONS

For the prediction of control-effectiveness theoretical methods are available for all speed ranges. The applicability of those methods is generally restricted to attached subsonic and supersonic flow. At transonic flow condition there are still strong discrepancies between theory and experiment. Separated flow can only be treated for some very specific cases.

8. LITERATURE

Text books and survey papers

- [1] LAMB, H. Hydrodynamics. Cambridge University Press, New York, 1963.
- [2] MILNE-THOMPSON, M.L. Theoretical Hydrodynamics. McMillan Comp., London, 1955.
- [3] SCHLICHTING, H. Aerodynamics of the airplane. McGraw-Hill, New York, 1979.
- TRUCKENBRODT, E.
- [4] THWAITES, B., ed. Incompressible Aerodynamics. Oxford University Press, 1960.
- [5] MAZET, R., ed. AGARD Manual of Aeroelasticity, Vol. II., London, 1961.
- [6] BISPLINGHOFF, R.L. Aeroelasticity. Addison-Wesley Publ. Comp. Inc., Reading, Mass., 1957.
- ASHLEY, H.
- HALFMAN, R.L.
- [7] FÖRSCHING, H.W. Grundlagen der Aeroelastik. Springer Verlag, Berlin/Heidelberg/New York, 1974.
- [8] LASCHKA, B. Unsteady aerodynamic prediction methods applied to aero-elasticity. AGARD-R-645, p. 1-1 to 1-31 (1975).
- [9] ASHLEY, H. Unsteady subsonic and supersonic inviscid flow. AGARD-CP-227, p. 1-1 to 1-32 (1977).
- [10] FÖRSCHING, H.W. Prediction of unsteady airloads on oscillating lifting systems and bodies for aeroelastic analyses. Prog. Aerosp. Sci. 1978, Vol. 18, p. 211 to 269, Pergamon Press, Oxford.
- [11] - Subsonic/transonic configuration aerodynamics. AGARD-CP-285 (1980).
- [12] - Computation of viscous-inviscid interactions. AGARD-CP-291 (1980).
- [13] - Special course on unsteady aerodynamics. AGARD Rep. No. 679.
- [14] KÖRNER, H. Theoretical aerodynamic methods for active control devices. AGARD-CP-262, p. 1-1 to 1-31 (1978).

Subsonic attached flow

- [15] THEODORSEN, T. General theory of aerodynamic instability and the mechanism of flutter. NACA Rep. 496 (1935).
- [16] MÜLTHOPP, H. Methods for calculating the lift distribution of wings. ARC R+M 2884 (1955).
- [17] TRUCKENBRODT, E. Tragflächentheorie bei inkompressibler Strömung. Jb. 1953 WGL, p. 40 to 65 (1953).

- [18] LASCHKA, B. Zur Theorie der harmonisch schwingenden tragenden Fläche bei Unterschallströmung. Z. Flugwiss. Vol. 11 (1963), p. 265 to 292.
- [19] LASCHKA, B. Interfering lifting surfaces in subsonic flow. Z. Flugwiss. 18 (1970), p. 359 to 368.
- [20] DAVIES, D.E. Calculation of unsteady generalized airforces on a wing oscillating harmonically in subsonic flow. ARC R+M 3409 (1965).
- [21] MÜLTHOPP, H. Berechnung der Auftriebsverteilung von Tragflügeln. Luftfahrtforschung 15 (1938), p. 153-169.
- [22] SCHWABE, M. Rechenschema zur Berechnung der Auftriebsverteilung von Tragflügeln. Luftfahrtforschung 15 (1938), p. 170-180.
- [23] FALKNER, V.M. The calculation of aerodynamic loading on surfaces of any shape. ARC R+M 1910 (1943).
- [24] RUBBERT, P.E. Theoretical characteristics of arbitrary wings by a non-planar-vortex lattice method. BOEING Comp. Rep. D6-9244 (1962).
- [25] GIESING, J.P. Lifting surface theory for wing-fuselage combination. McDonnell-Douglas Rep. DAC 67212, Vol. I (1968).
- [26] KÖRNER, H. Berechnung der potentialtheoretischen Strömung um Flügel-Rumpf-Kombinationen und Vergleich mit Messungen. Z. Flugwiss. Vol. 20 (1972), p. 351 to 368.
- [27] HEDMAN, S.G. Vortex lattice method for calculation of quasisteady state loadings on thin elastic wings. FFA Rep. 105 (1965).
- [28] ABANO, E.
RODDEN, W.P. A doublet-lattice method for calculating lift distribution on oscillating surfaces in subsonic flow. AIAA Vol. 7, p. 279 to 285 (1969).
- [29] RODDEN, W.P. A comparison of methods used in interfering lifting surface theory. AGARD Rep. 643 (1976).
- [30] GEISSLER, W. Calculation of the unsteady airloads on oscillating three-dimensional wings and bodies. AGARD-CP-227, p. 5-1 to 5-13 (1977).
- [31] HESS, J.L.
SMITH, A.M.O. Calculation of potential flow about arbitrary bodies. In: D. Küchemann et al: Progress in Aeronautical Sciences, Vol. 8, Pergamon Press, Oxford, 1967, p. 1 to 138.
- [32] RUBBERT, P.E.
SAARIS, G.R. A general three-dimensional potential flow method applied to V/STOL aerodynamics. SAE Air Transportation Meeting, New York 1968.
- [33] LABRUJERE, Th. E.
LOEVE, W.
SLOOFF, J.W. An approximate method for the calculation of the pressure distribution on wing-body combinations at subcritical speeds. AGARD-CP-71, p. 11-1 to 11-19 (1971).
- [34] KRAUS, W.
SACHER, P. Das MBB-Unterschall-Panelverfahren. MBB-Rep. UFE 672-70 (1970).
- [35] AHMED, S.R. Calculation of the inviscid flow field around three-dimensional lifting wings, fuselages and wing-fuselage combinations using panel method. ESA TT-210 (1975). In German: DLR-FB 73-102 (1973).
- [36] JOHNSON, F.T.
EHLERS, F.E.
RUBBERT, P.E. A higher order panel method for general analysis and design applications in subsonic flow. Lecture Notes in Physics, Vol. 59, p. 247 to 253 (1976).
- [37] HESS, J.L. The problem of three-dimensional lifting surface potential flow and its solution by means of surface singularity distribution. Computer Methods in Applied Mechanics and Engineering 4 (1974), p. 283 to 319.
- [38] MORINO, L.
TSENG, K. Steady, oscillatory and unsteady, subsonic and supersonic aerodynamics (SOUSSA) for complex aircraft configurations. AGARD-CP-227, p. 3-1 to 3-14 (1977).
- [39] GEISSLER, W. Nonlinear unsteady potential flow calculations for three-dimensional oscillating wings. AIAA Journ. 16, p. 1168 to 1174.
- [40] KÖRNER, H.
HIRSCHEL, E.H. The calculation of flow fields by panel methods: a report on Euromech 75. J. Fluid Mech. (1977), Vol. 79, part 1, p. 181 to 189.
- [41] BERGH, H.
TIJDEMAN, H. Binary flutter calculations with theoretical and empirical aerodynamic derivatives for a wing-control surface in two-dimensional incompressible flow. NLR-TR 68096U (1968).
- [42] DESOPPER, A.
GRENON, R. Couplage fluide parfait-fluide visqueux en écoulement instationnaire bidimensionnel incompressible et transsonique. AGARD-CP-291, p. 5-1 to 5-21 (1980).

- [43] FÖRSCHING, H.
TRIEBSTEIN, H.
WAGENER, J. Pressure measurements of a harmonically oscillating swept wing with two control surfaces in incompressible flow. DLR-FB 70-47 (1970).
- [44] MÜLLER, A.
SCHMID, H.
KINDLER, M. Berechnung der instationären Luftkräfte an Flügeln mit Rudern in Unterschallströmung. VFW-Fokker Rep. ZTL 4.05, Teil 2/1970.
- [45] BECKER, J. Interfering lifting surfaces in unsteady subsonic flow -- comparison between theory and experiment. AGARD Rep. 614 (1974).

Transonic attached flow

- [46] MURMAN, E.M.
COLE, J.D. Calculation of plane steady transonic flow. AIAA Journal 9, p. 114 to 121 (1971).
- [47] STEINHOFF, J.
JAMESON, A. Multiple solutions of the transonic potential flow equation. AIAA Paper 81-1019 (1981).
- [48] BOPPE, C.W.
AIDALA, P.V. Complex configuration analysis at transonic speeds. AGARD-CP-285, p. 26-1 to 26-13 (1980).
- [49] SCHIFF, L.B.
TOBAK, M. Some applications of aerodynamic formulations to problems in aircraft dynamics. AGARD-LS-114, p. 16-1 to 16-15 (1981).
- [50] LEE, K.D.
HUANG, M.
YU, N.J.
RUBBERT, P.E. Grid generation for general three-dimensional configurations. NASA-SP-2166, p. 355 to 366 (1980).
- [51] ZIEREP, J. Schallnahe Strömungen -- Beiträge zur parabolischen Methode. ZAMM Vol. 43, p. T182 to T187 (1963).
- [52] STAHARA, S.
SPREITER, J.R. Development of a nonlinear unsteady transonic flow theory. NASA-CR-2258 (1973).
- [53] ISOGAI, K. A method for predicting unsteady aerodynamic forces on oscillating wings with thickness in transonic flow near Mach number 1. NAL Rep. TR-368T (1974).
- [54] NÖRSTRUD, H. The transonic aerofoil problem with embedded shocks. The Aero. Quart. 24, 2 (1973), p. 129 to 138.
- [55] NIXON, D.
HANCOCK, G.J. Integral equation methods -- a reappraisal. Symposium Transsonicum II, Springer-Verlag Berlin/Heidelberg/New York, 1976, p. 174 to 182.
- [56] NIXON, D. A two-dimensional airfoil with a control surface oscillating at low frequency in high subsonic flow. The Aero. Quart 25, 3 (1974), p. 186 to 198.
- [57] ISOGAI, K. Approximate method for calculating aerodynamic loadings on an airfoil oscillating in high subsonic flow. NAL Rep. TR-455T (1976).
- [58] BALLHAUS, W.F.
BAILEY, F.R. Numerical calculation of transonic flow about swept wings. AIAA paper 72-677 (1972).
- [59] KLUNKER, E.B.
NEWMAN, P.A. Computation of transonic flow about lifting wing-cylinder combinations. J. Aircraft 11, (1974), p. 254 to 256.
- [60] SCHMIDT, W.
ROHLFS, S.
VANINO, R. Some results using relaxation methods for two- and three-dimensional transonic flows. Lecture Notes in Physics 35, Springer Verlag Berlin/Heidelberg/New York, p. 364 to 372, (1975).
- [61] JAMESON, A. Iterative solution of transonic flow over airfoils and wings, including flows at Mach 1. Comm. Pure Appl. Math. 27 (1974), p. 283 to 309.
- [62] ALBONE, C.M.
HALL, M.G.
JOYCE, G. Numerical solutions for transonic flows past wing-body combinations. Symposium Transsonicum II. Springer Verlag Berlin/Heidelberg/New York 1976, p. 541 to 548.
- [63] EHLERS, F.E. A finite difference method for the solution of the transonic flow around harmonically oscillating wings. NASA-CR-2257 (1973).
- [64] WEATHERILL, W.H.
SEBASTIAN, J.D.
EHLERS, F.E. Application of a finite difference method to the analysis of transonic flow over oscillating airfoils and wings. AGARD-CP-226, p. 17-1 to 17-13 (1977).
- [65] FRITZ, W. Transsonische Strömung um harmonisch schwingende Profile. DORNIER Rep. 78/16B (1978).
- [66] MAGNUS, R.J.
YOSHIHARA, H. Inviscid transonic flow over airfoils. AIAA paper No. 70-47 (1970).
- [67] MAGNUS, R.J.
YOSHIHARA, H. The transonic oscillating flap. AGARD-CP-226, p. 13-1 to 13-5 (1977).
- [68] BEAM, R.M.
WARMING, R.F. Numerical calculations of two-dimensional unsteady transonic flow with circulation. NASA TN-D 7605 (1974).

- [69] LERAT, A.
SIDES, J. Calcul numerique d'écoulement transsonique instationnaire. AGARD-CP-226, p. 15-1 to 15-10 (1977).
- [70] BALLHAUS, W.F.
LOMAX, H. The numerical simulation of low frequency unsteady transonic flow fields. Lecture Notes in Physics, Vol. 35, Springer-Verlag Berlin/Heidelberg/New York, 1975, p. 57 to 63.
- [71] COUSTON, M.
ANGELINI, J.J. Solution of nonsteady two-dimensional transonic small disturbance potential flow equation. ONERA TP 1978-69.
- [72] BALLHAUS, W.
GOORJIAN, P.
YOSHIHARA, H. Unsteady force and moment alleviation in transonic flow. AGARD-CP-227, p. 14-1 to 14-10, 1977.
- [73] BRISTEAU, M.O.
et al. Application of optimal control and finite element methods to the calculation of transonic flows and incompressible viscous flows. Numerical Methods in Applied Fluid Dynamic, Academic Press, London, p. 203-312 (1980).
- [74] EBERLE, A. Transonic potential flow computations by finite elements: airfoil and wing analysis, airfoil optimization. MBB-Rep. UF 1428 (1978).
- [75] CHAN, S.T.K.
BRASHEAR, M.R. Finite element analysis of unsteady transonic flow. AIAA Paper 75-875 (1975).
- [76] EBERLE, A. Computerprogrammtests des Finite-Element-Verfahrens zur Berechnung instationärer Profilströmungen. MBB-UF122-AERO-MT-396 (1979).
- [77] EVANS, M.W.
HARLOW, F.H. The particle-in-cell method for hydrodynamic calculations. Rep. LA-2139, 1957, Los Alamos Scientific Lab., Los Alamos, N. Mex.
- [78] JAMESON, A.
CAUGHEY, D.A. A finite-volume scheme for transonic potential flow calculations. AIAA Paper 77-635 (1977).
- [79] RIZZI, A.
BAILEY, H. Finite-volume solution of the Euler equations for steady three-dimensional transonic flow. Lecture Notes in Physics, Vol. 59 (1976), p. 347 to 352.
- [80] SCHMIDT, W.
JAMESON, A.
WHITFIELD, D. Finite volume solution for the Euler equation for transonic flow over airfoils and wings including viscous flow. AIAA Paper 81-1265 (1981).
- [81] SHANKAR, V.
MALMUTH, N.D.
COLE, J.D. Transonic flow calculations over two-dimensional canard-wing systems. J. Aircraft 18, p. 108-114 (1981).
- [82] GROSSMANN, G.
VOLPE, G. The viscous transonic flow over two-element airfoil systems. AIAA Paper 77-688 (1977).
- [83] ROSCH, H.
KLEVENHUSEN, K.-D. Flow computation around multi-element airfoils in viscous transonic flow. ICAS Proceedings 1980, p. 470-479.
- [84] TIJDEMAN, H. Investigations of the transonic flow around oscillating airfoils. NLR TR 77090U (1977).
- [85] GRENON, R.
DESOPPER, A.
SIDES, J. Effects instationnaires d'une gouverne en écoulement bidimensionnel subsonique et transsonique. AGARD-CP-262, p.19-1 to 19-14 (1978).

Supersonic attached flow

- [86] ETKIN, B. Numerical integration method for supersonic wings in steady and oscillating motion. UTIA Rep. 36 (1955).
- [87] STARK, V.J.E. Calculation of aerodynamic forces on two oscillating finite wings at low supersonic Mach numbers. SAAB TN 53, 1964.
- [88] ALLEN, D.J.
SADLER, D.S. Oscillatory aerodynamic forces in linearized supersonic flow for arbitrary frequencies, planforms and Mach numbers. ARC R+M 3415, 1963.
- [89] WOODCOCK, D.L.
YORK, E.J. A supersonic box collocation method for the calculation of unsteady airforces of tandem surfaces. AGARD Symposium on Unsteady Aerodynamics for Aeroelastic Analyses of Interfering Surfaces, Tonsberg, Norway, 1970.
- [90] MÜLLER, A. Berechnung der Druckverteilung an schwingenden Tragflügeln in Überschallströmung mittels eines Kollokationsverfahrens für die Küssnersche Integralgleichung. Dr.-Ing. Thesis, TU Munich, 1973.
- [91] PINES, S.
DUGUNDJI, J.
NEURINGER, J. Aerodynamic flutter derivatives for an oscillating finite thin wing in supersonic flow. JAS 23, p. 693, 1955.
- [92] TA LI Aerodynamic influence coefficients for an oscillating finite thin wing in supersonic flow. JAS 23, p. 613 to 622, 1955.
- [93] WOODWARD, F.A.
LARSON, J.W. A method of optimizing camber surfaces for wing-body combinations at supersonic speeds. BOEING Rep. D6-10741 (1965).

- [94] WOODWARD, F.A. Analysis and design of wing-body combinations at subsonic and supersonic speeds. J. Aircraft 5 (1968), p. 528 to 534.
- [95] WEILAND, C.
THIESS, H.J. Analysen berechneter dreidimensionaler reibungsfreier Strömungsfelder mit eingebetteten Verdichtungsstößen, Teil I. DFVLR-FB 78-09 (1978).
- [96] RIZZI, A.W.
KLAVINS, A.
McCORMACK, R.W. A generalized hyperbolic marching technique for three-dimensional supersonic flow with shocks. Lecture Notes in Physic, Vol. 35, Springer-Verlag Berlin/Heidelberg/New York, 1975, p. 341 to 346.
- [97] MANRO, M.E.
BOBBITT, P.J.
RODGERS, J.T. Comparison of theoretical and experimental pressure distributions on an arrow-wing configuration at subsonic, transonic and supersonic speeds. AGARD-CP-204, p. 11-1 to 11-14 (1976).
- [98] LODGE, C.G.
SCHMID, H. Unsteady pressure due to control surface rotation at low supersonic speeds. AGARD Rep. 647 (1976).

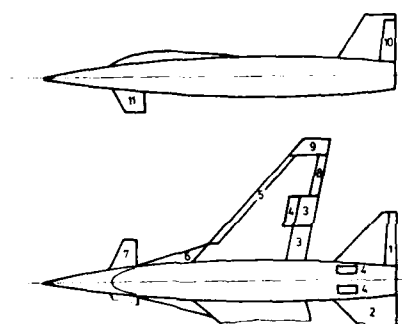
Leading edge vortex flow

- [99] - High Angle of Attack Aerodynamics. AGARD-CP-247 (1978).
- [100] POLHAMUS, E.C. A concept of the vortex lift of sharp-edge delta wings based on a leading-edge-suction analogy. NASA TN D-3767 (1966).
- [101] LAMAR, J.E. Extension of leading-edge-suction analogy to wings with separated flow around the side edges at subsonic speeds. NASA TR R-428 (1974).
- [102] BELOTSEKOVSKII, S.M. Calculation of the flow about wings of arbitrary planform at a wide range of angles of attack. RAE Lib. Transl. No. 1433 (1970).
- [103] REHBACH, C. Numerical investigation of vortex sheets issued along a separation line near the leading edge of wings. EUROMECH 41 Colloquium, Norwich (G.B.) (1973).
- [104] SCHRÖDER, W. Berechnung der nichtlinearen Beiwerte von Flügeln mit kleinem und mittlerem Seitenverhältnis nach dem Wirbelleitervorgang in inkompressibler Strömung. DFVLR-FB 78-26 (1978).
- [105] MASKEW, B.
RAO, B.M. Calculation of vortex flow on complex configurations. ICAS Proceedings 1982, p. 351a-3511.
- [106] BRUNE, G.W.
WEBER, J.A.
JOHNSON, F.T.
LU, P.
RUBBERT, P.E. A three-dimensional solution of flows over wings with leading-edge vortex separation. NASA-CR 2709 (1975).
- [107] HITZEL, S.
SCHMIDT, W. Slender wings with leading edge vortex separation. A challenge for panel methods and Euler codes. AIAA Paper 83-0562 (1983).
- [108] TINICO, E.N.
YOSHIMURA, H. Subcritical drag minimization for highly swept wings with leading edge vortices. AGARD-CP-247, p. 26-1 to 26-9 (1978).

Separated flow without primary structures

- [109] JACOB, K. Berechnung der abgelösten inkompressiblen Strömung um Tragflügelprofile und Bestimmung des maximalen Auftriebs. Z. Flugwiss. 17, July 1969.
- [110] STEVENS, W.A.
GORADIA, S.H.
BRADEN, J.A. Mathematical model for twodimensional multicomponent airfoils in viscous flow. NASA CR-1843 (1971).
- [111] GRASHOF, J. Berechnung der Druck- und Schubspannungsverteilung auf Körpern mit Totwasser in ebener inkompressibler Parallelströmung. Dr.-Ing. Thesis, TU Karlsruhe (1973).
- [112] DVORAK, F.A.
WOODWARD, F.A. A viscous/potential flow interaction analysis method for multi-element infinite swept wings. NASA CR-2476 (1974).
- [113] BRUNE, G.W.
MANKE, J.W. Upgraded viscous flow analysis of multi-element airfoils. AIAA Paper 78-1224 (1978).
- [114] JACOB, K.
STEINBACH, D. A method for prediction of lift for multi-element airfoil systems with separation. AGARD-CP-143, p. 12-1 to 12-16.
- [115] FORSTER, D.N.
IRWIN, H.P.A.H.
WILLIAMS, B.R. The two-dimensional flow around a slotted flap. RAE TR 70164 (1970).
- [116] PROKSCH, H.J.
WELTE, D. Theoretische Ermittlung des Überziehverhaltens und des Maximalauftriebs von Pfeilflügeln. ZTL Do 4.01/5 (1972).
- [117] BEAM, R.M.
WARMING, R.F. Implicit methods for the compressible Navier-Stokes and Euler equations. Von Karman Institute Lecture Series 1982-04 Computational Fluid Dynamics, March 29 - April 2, 1982.

- [118] DEIWERT, G.S. Recent computations of viscous effects in transonic flow. Lecture Notes in Physics, Vol. 59, p. 159 to 164 (1976).
- [119] MCCORMACK, R.W. A numerical method for solving the equations of compressible viscous flow. AIAA 81-110 (1981).
- [120] STEGER, J.L. Calculation of transonic aileron buzz. AIAA Paper 79-0134 (1979).
BAILEY, H.E.



LONGITUDINAL DEVICES

- 1 ELEVATOR
- 2 ALL MOVING TAIL
- 3 FLAP
- 4 SPOILER
- 5 LE FLAP
- 6 MOVABLE STRAKE
- 7 HORIZONTAL CANARD

LATERAL DEVICES

- 8 AILERON
- 9 ALL MOVING TIP
- 10 RUDDER
- 11 VERTICAL CANARD

Fig. 1: Control surfaces

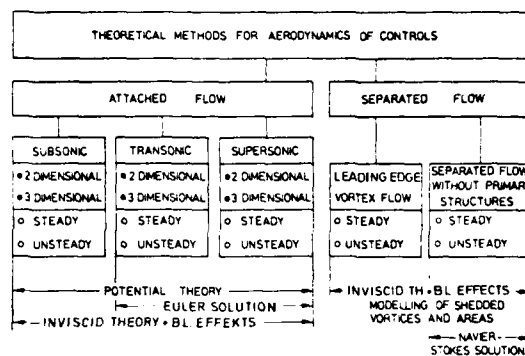


Fig. 2: Survey of theoretical methods

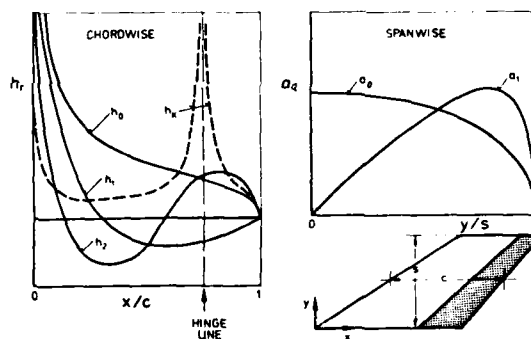


Fig. 3: Loading functions

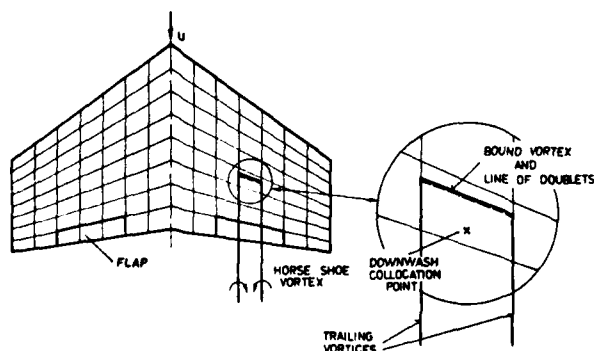


Fig. 4: Discretization of the wing for the vortex/doublet-lattice method

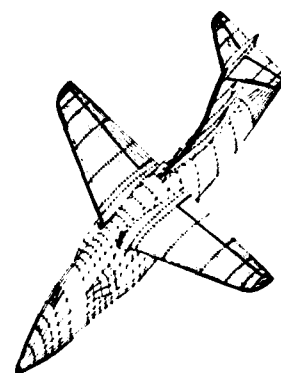


Fig. 5: Discretization of a fighter type aircraft for the panel method

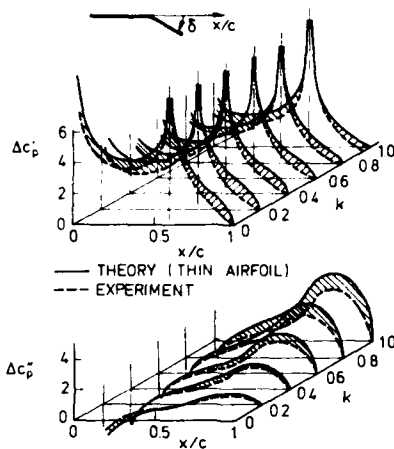
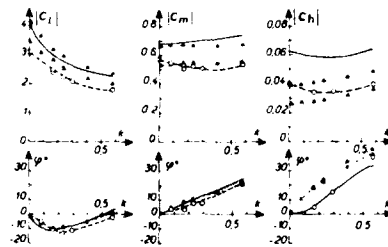


Fig. 6: Comparison theory - experiment for a two-dimensional airfoil with oscillating flap at various frequencies (adapted from [41])

$$M = 0.3 \quad \alpha = 0^\circ \quad \delta_m = 0^\circ \quad \delta_i = 1^\circ$$



—○— EXPERIMENT — LIN. THEORY
—▲— SING. METHOD
...▲... S.M. & B.L. METHOD

Fig. 7: Comparison theory - experiment for an airfoil with oscillating flap (adapted from [42])

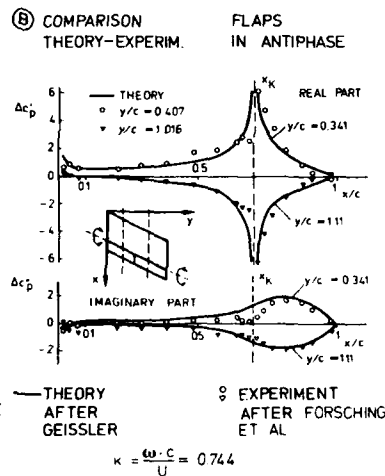
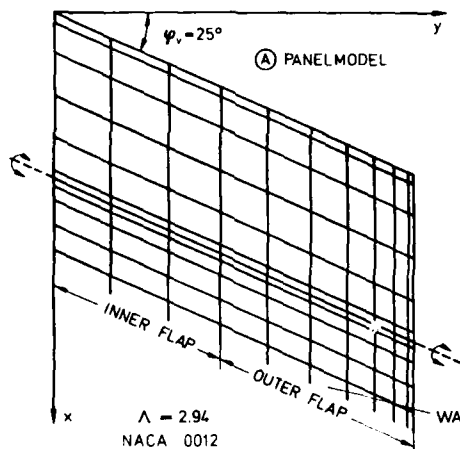


Fig. 8: Comparison theory - experiment for a swept wing with oscillating flap in incompressible flow (adapted from [43])

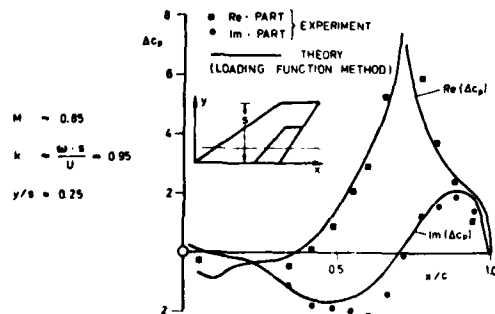


Fig. 9: Comparison theory - experiment for a swept wing with oscillating flap in incompressible flow (adapted from [43])

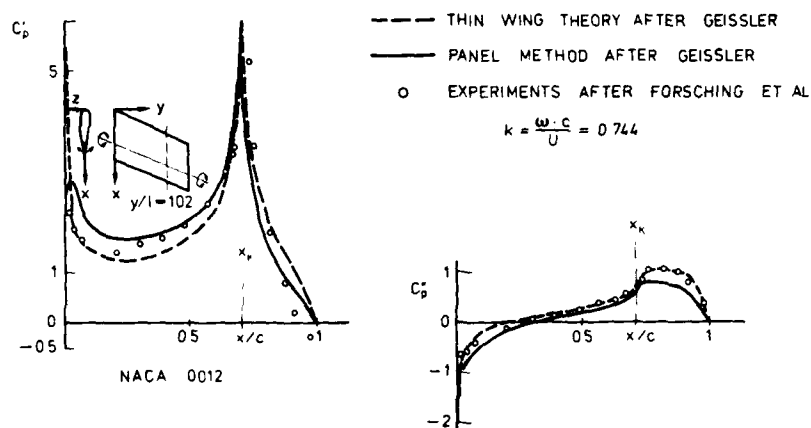


Fig. 10: Comparison theory - experiment for a swept wing with oscillating flap in incompressible flow (adapted from [39])

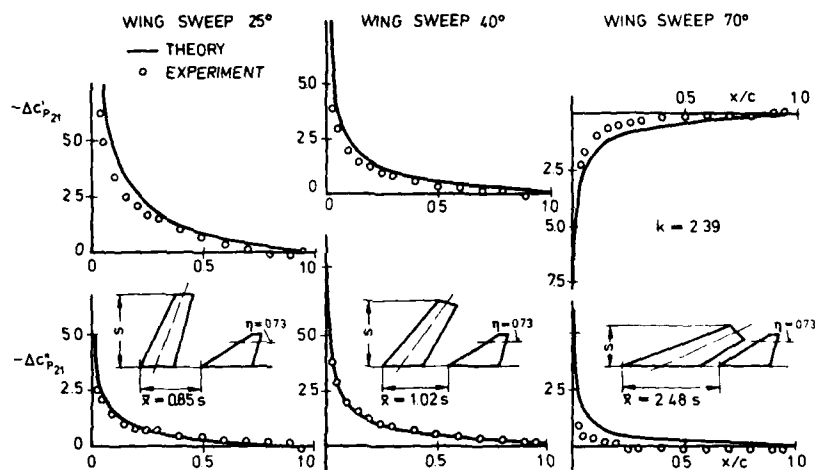


Fig. 11: Comparison theory - experiment for the pressure distribution on the tail due to wing pitch oscillation (adapted from [45])

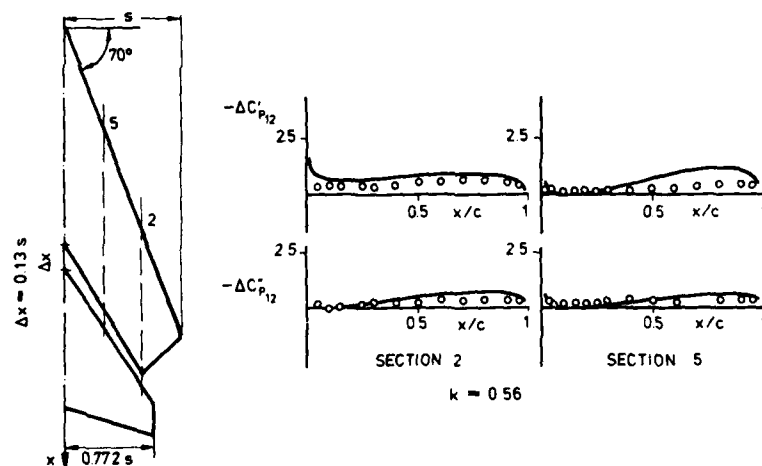
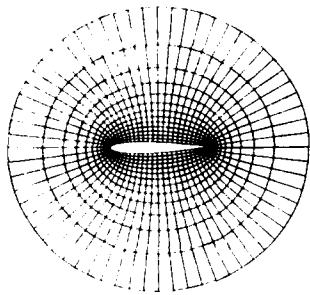
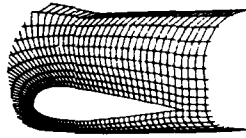
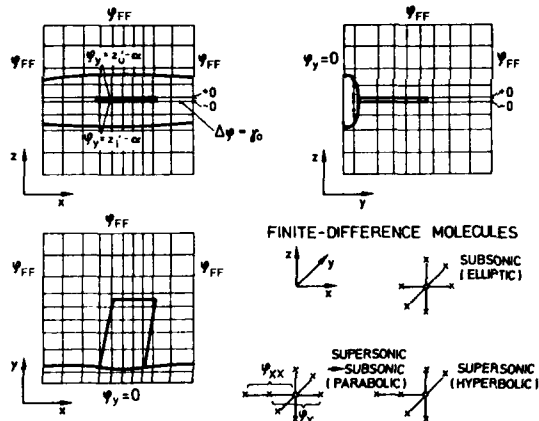
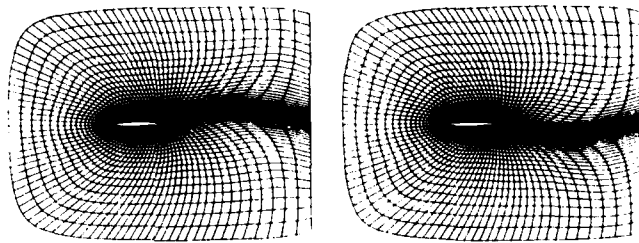


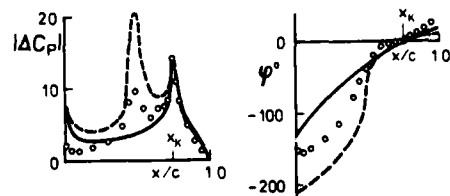
Fig. 12: Comparison theory - experiment for the pressure distribution on the swept wing due to tail pitch oscillation (adapted from [45])



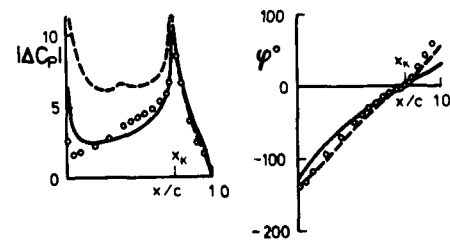
O-TYP GRID

C-TYP GRID APPLIED
TO A WING-BODY CONFIGURATIONFig. 13:
Grids for transonic methods
(adapted from [50])Fig. 14:
C-type grid deforming with
flap oscillation
(adapted from [49])Fig. 15:
3D-finite-difference mesh for solution of
the transonic-small-perturbation equationFig. 16:
Comparison theory - experi-
ment for an airfoil with
oscillating flap at trans-
sonic speed (adapted from
[84])

$M = 0.85$
 $k = 0.253$



$M = 0.8$
 $k = 0.179$



— THEORY, THIN AIRFOIL
--- THEORY, EHLERS
○ EXPERIMENT

NACA 64 A006

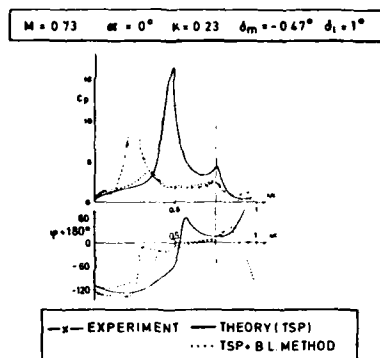


Fig. 17: Comparison theory - experiment for an airfoil with oscillating flap at transonic speed - upper side (adapted from [85])

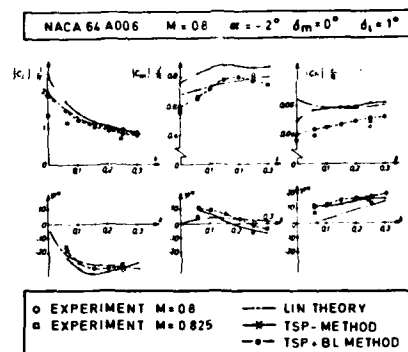


Fig. 18: Comparison theory - experiment for an airfoil with oscillating flap at transonic speed (adapted from [42])

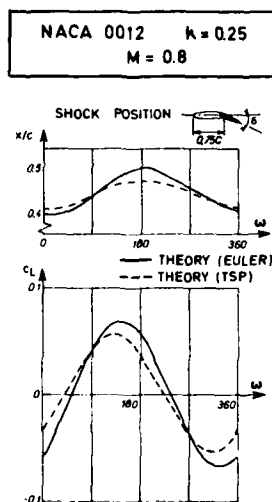


Fig. 19: Shock positioning and change of lift due to flap oscillation (adapted from [42])

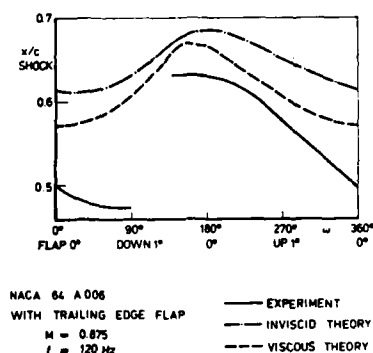


Fig. 20: Shock positioning on an airfoil due to an oscillating flap (adapted from [67])

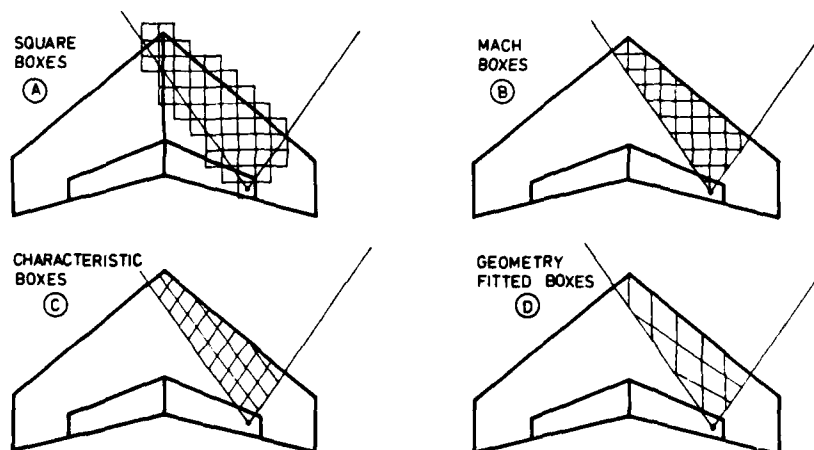
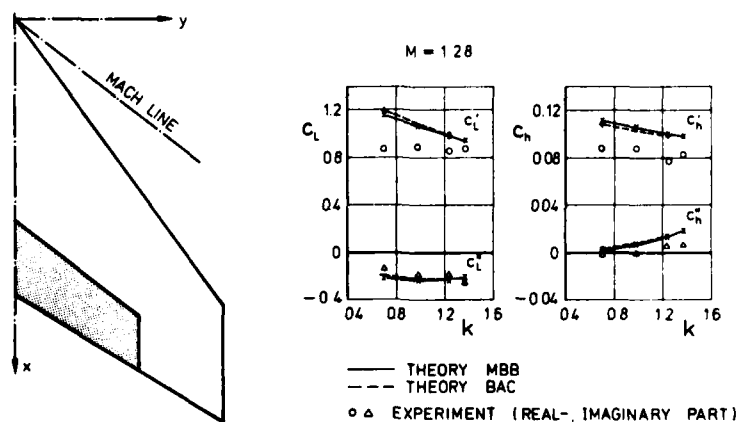
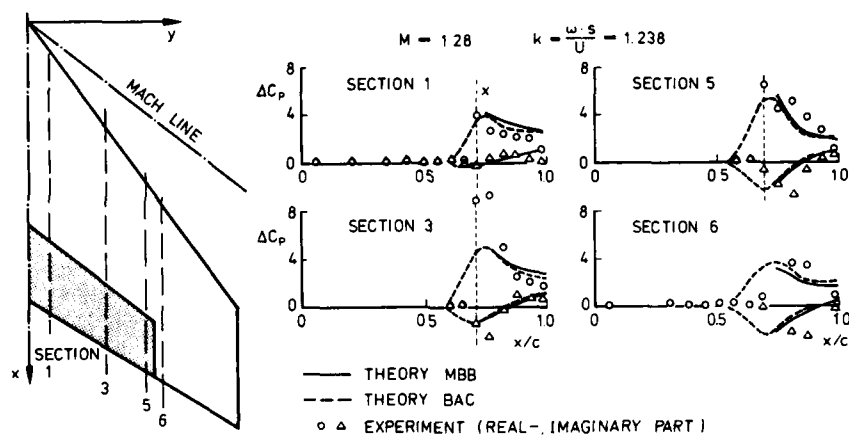
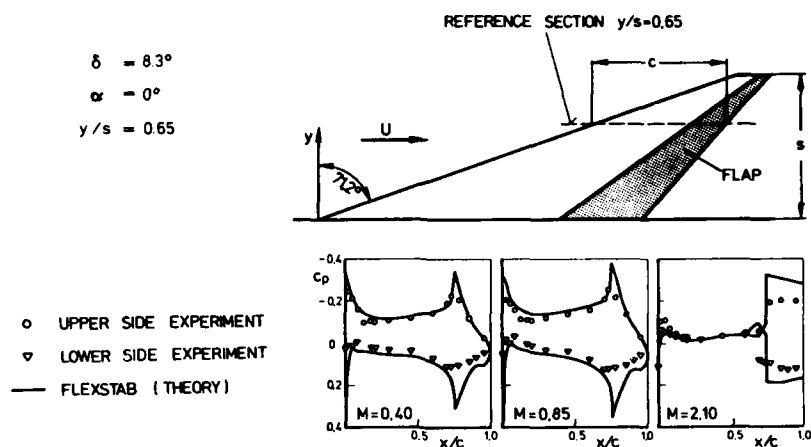


Fig. 21: Subdivision of the wing area inside the Mach-cone for different evaluation techniques



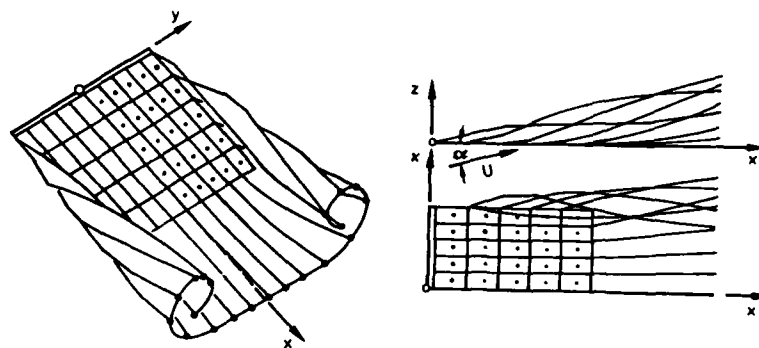


Fig. 25: Slender-wing vortex flow

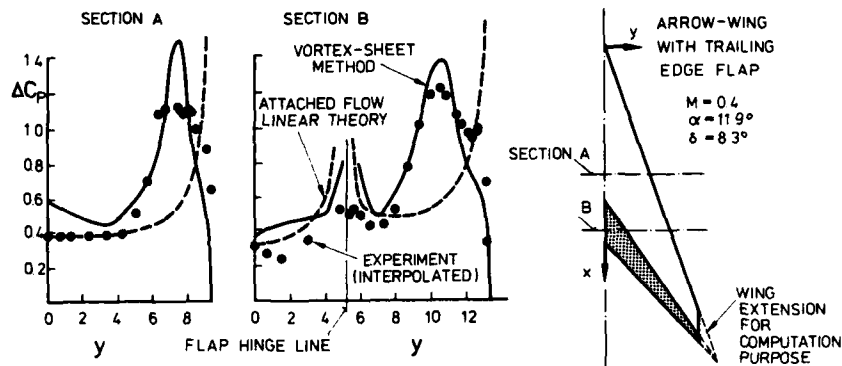


Fig. 26: Comparison theory - experiment for an arrow-wing with flap deflection (adapted from [108])

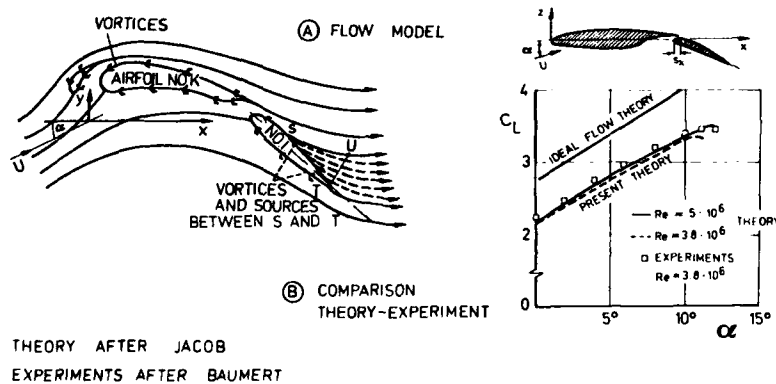


Fig. 27: Comparison theory - experiment for the maximum lift of a multi-element airfoil (adapted from [114])

DYNAMIC EFFECTS OF CONTROLS

by

G.J. Hancock,
Department of Aeronautical Engineering,
Queen Mary College, (University of London).

1. INTRODUCTION

Aerodynamics of controls are concerned with the understanding, both in qualitative and quantitative terms, of the aerodynamic loading induced on the surface of an aircraft configuration following the deployment of a control surface. It is necessary to know the overall forces and moments on the aircraft configuration in order to calculate aircraft response and to ensure structural integrity; it is necessary to know the loads on the control in order to design the actuation system.

When dynamic effects are introduced, there are three aspects:

- i) the qualitative understanding, and quantitative determination, of the unsteady aerodynamic loading on an aircraft configuration when a deflection of a control surface follows a specified time-dependent input, typical of a pilot (either human or automatic) control input;
- ii) the determination of the aircraft response as a consequence of (i);
- iii) the determination of the dynamic motion of an aircraft, including both the overall rigid body modes and the structural response modes, when there is an active feedback system (e.g. stability augmentation, active control technology); in this case the time-dependent input to a control deflection is not known *a priori*, there is an interdependence between the control motion, the unsteady aerodynamic loads induced, and the aircraft dynamic motion.

Aspect (i) which is concerned with the quantitative prediction of unsteady aerodynamic loads based on theory and/or wind tunnel measurements following a specified control input is a purely aerodynamic problem. Aspect (ii), given the aerodynamic input from (i), is a purely dynamic problem. But to apply the unsteady aerodynamic information from aspect (i) in the calculation of the aircraft response, as required in aspect (ii), it is necessary for the unsteady aerodynamic information to be expressed in a mathematical form which is compatible with the method of solution of the dynamic equations of motion. Conventionally, aircraft dynamics are calculated through the use of aerodynamic derivatives. Alternatively, if the unsteady loads are given as specified time dependent functions, the equations of motion can be integrated directly in successive time intervals. It is when contemporary aspect (iii) is considered that the question of the mathematical representation of unsteady aerodynamic loading for compatibility not only with the mathematical solution of the dynamic equations of motion, but also, and more significantly, with modern control design theory, becomes acute.

It is the aim of this lecture to outline some of the background concepts and methods underlying the interface of aerodynamics and dynamics.

The topics to be described in this lecture follow the sequence:

- i) qualitative descriptions of the unsteady aerodynamic characteristics associated with the movement of control surfaces (trailing edge controls, leading edge controls, spoilers) at various Mach numbers;
- ii) a summary of the methods of prediction of unsteady control surface aerodynamics;
- iii) a preliminary indication of comparisons between results from theory and experiment;
- iv) the concept of aerodynamic derivatives;
- v) the interface between aerodynamics and dynamics.

2. QUALITATIVE DESCRIPTIONS OF UNSTEADY AERODYNAMICS2.1 Trailing Edge Control on Two Dimensional Aerofoil2.1.1 Low speed

Consider first the changes in flow about a symmetric two dimensional aerofoil with a trailing edge control in a low speed stream when the control angle is changed rapidly, as shown in Fig. 1. Before the control surface is deflected (i.e. for time $t < 0$) it is assumed, for convenience, that the aerofoil with its control surface, is at zero lift. Then starting at $t = 0$ let the control surface angle move rapidly from zero to a finite angle (say between 5° - 10°) and then remain fixed at that angle. The phrase 'rapidly' at this stage means that the control has moved from its initial position to its final position in the time it takes the free stream air to travel a distance less than half a chord. It is assumed that the control does not move through such a large angle that the flow separates.

As shown in Fig. 2, for small time t , a starting vortex is created in the neighbourhood of the trailing edge of the control, and this shed vortex is convected downstream with virtually the free stream velocity. Wake vorticity is shed continuously as the circulation about the aerofoil builds up with time, but the major part of the wake vorticity is concentrated in the starting vortex. From the condition of conservation of overall circulation, the total circulation about the aerofoil and wake must be zero,

assuming that there was no circulation to start with for $t=0$; thus the circulation about the aerofoil and its control is equal and opposite to the total circulation around the wake. The shed vortex and wake vorticity induce a downwash in the neighbourhood of the aerofoil, thus decreasing the effective incidence of the aerofoil; this downwash about the aerofoil decreases as time increases as the shed vortex moves further downstream from the aerofoil. So the circulation Γ about the aerofoil and control will increase with time t , tending to an asymptotic value associated with the final steady state of the aerofoil with its steady deflected control.

The build-up of lift on an aerofoil with a 30% trailing edge control when the control angle is changed rapidly is shown in Fig. 3; the lift response $L(t)$, relative to its final steady value L_s , is plotted against t/\hat{t} , where $\hat{t} (= c/V)$ is the time it takes the free stream to travel a distance of one chord. The behaviour of the lift for small time t is not shown, large transient effects can occur depending on exactly how the control is moved. It is seen that, at a low free stream Mach number, the lift reaches 2/3 of its final steady state very quickly, in about $1\hat{t}$, and reaches 90% of its final steady state value in about $7\hat{t}$.

Now crudely, the downwash induced about the aerofoil by the wake vorticity is inversely proportional to the distance of starting vortex downstream of aerofoil. So, assuming that the starting vortex convects downstream with the free stream velocity, the circulation about the aerofoil builds up to its asymptotic steady state as $1/t$. This rate of build up to the asymptotic state is relatively slow. As shown in Fig. 3, $L(t)$ attains 95% of its final steady value in about $13\hat{t}$, but to attain 99% of its steady value requires a time of about $70\hat{t}$.

Fig. 4 shows the chordwise load distributions for $t/\hat{t} = 3$ and in the final steady state; it is seen that the overall lag effect in the lift is due to the slower rate of build up of the load over the forward part of the aerofoil compared with the aft part of the aerofoil, including the control.

In the discussion so far it has been assumed that the trailing edge control moves 'rapidly' from zero to an angle in time $t/\hat{t} < 1$. But this rate of 'rapidity' is an ideal, which cannot be achieved either in full scale aircraft or in wind tunnel experiments, because of practical mechanical limitations. Current gust alleviation studies indicate that typical rates of control movement, which are necessary and thought to be realistic with modern actuator technology, involve control movements from one angle to another in about $4-5\hat{t}$ (i.e. in the time the free stream moves a distance of 4-5 aerofoil chords). For a practical case, of an aerofoil (plus control) chord of 2m in a low speed stream of 100 m/s this rate is equivalent to a control angle rotation of say ($0^\circ \rightarrow 10^\circ$) in about 0.1s. Fig. 5 shows the build of lift corresponding to ramp rise times of control angle of $4\hat{t}$, and $20\hat{t}$.

The rise time of $4\hat{t}$ (i.e. of the order 0.1s) would correspond to an active control application while a rise time of $20\hat{t}$ (i.e. of the order of 0.5s) is more typical of an input from a pilot or stability augmentation system. It is seen that the time dependent lifts follow the control inputs but with lag effects and the approach to the final steady state is still associated with the asymptotic behaviour. The lag effects decrease as the rise time of control movement becomes longer.

For a slow rate of application of the control angle, the time dependent lift follows the time dependent control angle and the lift at any instant of time is virtually equal to the steady state lift associated with the instantaneous value of the control angle. This situation is referred to as quasi-steady. But it should be realised and understood that quasi-steady does not imply an instantaneous relationship. Quasi-steady behaviour occurs when the rates of change of the control input are slow compared with the rate at which the unsteady wake effects are convected downstream so that the local flow about the aerofoil has sufficient time to build up to a local steady state at each instant of time. In broad terms, on the argument that the lift is within 5% of its steady value at any time, then a ramp rate extending over at least $30\hat{t}$ would appear to be quasi-steady.

Unsteady characteristics are usually presented in terms of the in-phase and out-of-phase force components relative to an oscillatory motion of the control surface. The in-phase and out-of-phase lift components for a 30% trailing edge control surface oscillating with frequency ω are shown in Fig. 6, plotted against the non-dimensional frequency parameter $\nu (= \omega c/V)$. It is noted that

$$\nu = \frac{\omega c}{V} = 2\pi \frac{c}{V\lambda/\omega} = 2\pi \frac{\text{chord}}{\text{spatial wavelength}}$$

Quasi-steady can be regarded as the range of ν where the effects of ν on the lift are small. From Fig. 6, it would appear that quasi-steady conditions occur if $\nu < 0.05$, this order of magnitude suggests

$$\frac{\text{wavelength}}{\text{chord}} > 120.$$

A $\frac{1}{2}$ (wavelength) would correspond to a ramp rise time which indicates a rise time of $30\hat{t}$ for quasi-steady conditions; this number ties in the value given in the previous paragraph.

The trends described above all relate to a two dimensional aerofoil in an infinite air stream. But to obtain quantitative data wind tunnels are used. So the question arises of wind tunnel wall interference effects. Since, at this stage, the discussion is restricted to two dimensional characteristics, only wind tunnel floor and ceiling effects need be considered. Now the floor and ceiling extend under and over both the aerofoil and its control, and the entirety of the shed wake. By inspection, thinking in terms of images of the wake in the tunnel floor and ceiling, it can be appreciated that the aerofoil lift in the tunnel approaches its asymptotic limit as $1/t^2$, which is an order faster than the aerofoil in an infinite stream. Typical results for the build up of lift following rapid ramp changes in control angle are shown in Fig. 7. It is seen that even for relatively small models (e.g. $c/h = 1/6$) that there are significant wall effects. There are additional effects associated with a downstream diffuser; in a diffuser the free stream velocity decreases so the wake is not convected away as rapidly as in unconfined air stream, causing a relative lag in the build up of the lift because slightly higher downwash velocities

are induced about the aerofoil.

In all of the above flows, it is assumed that the flows remain attached. Once separation occurs, the subsequent behaviour differs significantly from that described above. Separated flows are not discussed further here, but separated flows figure prominently later in the section on spoiler characteristics.

2.1.2 Sub-critical flow

The development of the flow field following rapid changes in the angle of a trailing edge control as described for the low speed case in the previous section, namely the formation of a starting vortex and its convection downstream, are essentially the same when the Mach number of the free stream is increased. The differences are more quantitative than qualitative associated with the time taken for disturbances to propagate their effect through the field. When the Mach number of the free stream is low, disturbances are propagated through the flow field relatively quickly so that the effect of a disturbance is felt throughout the field almost instantaneously and simultaneously. But a disturbance is propagated at the speed of sound relative to the local velocity. Thus the upstream propagation of information takes longer as the free stream Mach number increases. It follows therefore that there are increasing lag effects in the downwash at the aerofoil induced by the shed wake vorticity, as free stream Mach number increases, thus delaying the asymptotic approach to the final steady state. To illustrate these effects, Fig. 8 shows the type of build up of lift following a rapid control surface deflection for free stream Mach numbers 0.5 and 0.8, assuming for now that a free stream Mach number of 0.8 can still be regarded as subcritical. The effects of Mach number on the build up of lift are clearly significant. In addition, there are differences in the behaviour at small t ; this is due to the effects of free stream Mach number on the generation of disturbances at the aerofoil surface.

Thus, it can be deduced that while at a low free stream Mach number (e.g. $M_\infty = 0.2$) a ramp rise time of 30ϵ would give a quasi-steady response, at a free stream Mach number of 0.5 a ramp rise time of about 60ϵ would be necessary for a quasi-steady response. But remembering that ϵ is inversely proportional to V , that is, to Mach number, the ramp rise time in real time for quasi-steady responses at the two Mach numbers are about the same.

2.1.3 High subsonic flows with shock waves

Supercritical flows become more complicated because disturbances cannot be propagated upstream in the local embedded supersonic regions.

First consider a symmetric aerofoil with an undeflected trailing edge control at zero incidence in a supercritical shock free condition and then rotate the trailing edge control rapidly through a positive angle (i.e. trailing edge downwards). If the rotation is rapid enough, the upper and lower control surfaces act locally like pistons so that expansion waves are generated and radiated outwards from the upper control surface while compression waves are generated and radiated outwards from the lower control surface, and again a starting vortex region is formed aft of the trailing edge. As the disturbances propagate and interact with the initial flow, the upper surface expansion region will be extended rapidly towards the control trailing edge but the lower surface compression and downstream subsonic conditions will terminate the growing expansion region on the upper surface with the formation of a shock wave. The shock wave will start in the neighbourhood of the trailing edge of the control and move forwards over the upper surface possibly ahead of the control hinge line as the new steady state becomes established, the shock strength will increase as the shock moves forward. The contraction of the supercritical region initially on the aerofoil lower surface by the compressions from the lower surface of the control will be orderly (i.e. isentropic) without the formation of shock waves. The build up of lift to its final asymptotic steady state will be extremely slow because of the time taken for the wake effects to be transmitted upstream and around the embedded supersonic region. It is possible that the shock will move slowly aft to the final steady state. The above sequence is shown diagrammatically in Fig. 9(i).

If in the initial state, with the symmetric aerofoil and its control surface at zero angle of incidence, (symmetric) shock waves are present then following a rapid change in control angle) similar processes to those described above still occur but now there are the additional complications associated with the interaction of the upper surface shock with the upper control surface expansion and the lower surface shock reinforced by the lower control surface compressions. So to start with the upper surface shock will move aft rapidly but then move forward as the lower surface compressions make themselves felt. This sequence is shown in Fig. 9(ii).

The supercritical Mach number regime is non-linear in the sense that it is not possible to read across from one response to another, as demonstrated in the classic experiments reported by Tidjeman on a NACA 64A006 aerofoil with a trailing edge control surface, oscillating harmonically with an amplitude of 1° . Three types of flows were identified:

- Type 'A' A sinusoidal shock wave motion where the shock moves nearly sinusoidally but with a phase shift relative to the control surface motion. There also exists a phase shift between the shock motion and its strength, the maximum shock strength is not encountered when the shock reaches its maximum downstream location but at a later time during its upstream motion.
- Type 'B' Is similar to type 'A' except that now as the shock moves aft in each cycle, the strength of the shock becomes sufficiently weak that the shock disappears.
- Type 'C' In slightly supercritical conditions shock waves are formed periodically but just propagate upstream and disappear as the embedded supersonic region vanishes during each cycle.

2.1.4 Supersonic speeds

At supersonic speeds, all flow effects are local to the control surface. There are no upstream effects

ahead of the control hinge while the developing vorticity patterns in the wake do not influence what is happening on the control surface. The time dependent variation of the lift when a trailing edge control is moved rapidly is shown in Fig. 10, for a free stream Mach number of 1.4; it is seen that at small values of t the lift reaches 75% of its final steady state value and that the asymptotic steady state is reached in the order of 3ℓ .

2.2 Leading Edge Control on a Two-Dimensional Aerofoil

A leading edge control might be used in conjunction with a trailing edge control for manoeuvrability purposes or for some active control technology applications (e.g. flutter suppression) where it is necessary to control both the lift and pitching moment characteristics. When a leading edge control is rotated nose downward it decreases the effective incidence but introduces positive camber, thus there are two opposing effects contributing to the lift, in fact the overall lift change is quite small. Nevertheless the overall build up of lift to its steady (small) value following a ramp change in leading edge control angle depends on the overall change of circulation, will be similar to that described in the earlier sections, because it is associated with the influence of the shed wake vorticity.

Fig. 11 shows the load distributions along the chord of the leading edge control/aerofoil combination, following a rapid change in control angle, at $t/\ell = 3.0$ and in the final steady state as $t/\ell \rightarrow \infty$; the point of interest is that although the two distributions are virtually identical in fact the total lift at $t/\ell = 3.0$ is 80% of the final steady state lift. It can be deduced that the overall moment responses are much more sluggish with a trailing edge control compared with a leading edge control.

2.3 Two-Dimensional Spoilers

Upper surface spoilers are currently used as lift dumpers or as roll controls. Spoilers have advantages as controls when conventional controls are ineffective (e.g. outboard ailerons at high subsonic speeds) or when high lift systems extend over most of a wing span. Investigations are in progress to assess whether or not spoilers can be used in gust alleviation systems where it is necessary to lose lift quickly.

A deployed spoiler at a steady angle as shown in Fig. 12 causes the flow to separate forming a closed wake region aft of the aerofoil. Lift on the aerofoil is lost through a compression ahead of the spoiler, which reduces the upper surface suction especially in the leading edge region while the suction in the separated flow region aft of the spoiler, through the trailing edge Kutta condition, reduces the pressures on the lower surface. In steady conditions, the change in lift with spoiler angle is not linear; at small spoiler angles the flow over the spoiler reattaches to the aerofoil surface ahead of the trailing edge with little change in overall lift. Only when the separated flow region extends beyond the trailing edge is there a significant loss in lift. One important difference between the spoiler and trailing edge control is the large drag resulting from the flow separation aft of the spoiler while, at least for moderate angles, the flow over a trailing edge control remains attached. An example of the change in steady lift with spoiler angle is shown in Fig. 13, but these variations can differ depending on spoiler location, on the spoiler chord and on aerofoil incidence.

There is often a gap between the foot of the spoiler and the aerofoil surface essentially to reduce buffet loads. It has been found that in practice there is little effect of this gap on the aerodynamic characteristics.

For unsteady spoiler motions, that is, for rapid ramp changes of spoiler angle, there are two phases. The first concerns the rate of development of the local separation flow about the spoiler, the second concerns the rate of overall change in lift.

When a spoiler is opened rapidly a vortex motion is formed just aft of the spoiler trailing edge, as shown in Fig. 14. This vortex motion takes a short time to develop before the vortex moves downstream. Because the vortex is in the vicinity of solid aerofoil surface the effective image of the shed vortex in the aerofoil surface essentially induces a velocity in the opposite direction to the free stream direction thus the convection velocity downstream of the spoiler vortex is less than the free stream velocity, this convection velocity is approximately $1/8$ of the free stream velocity. As the vortex convects downstream it loses its strength, leaving behind the vorticity associated with the steady state shear flow between the outer flow and the inner flow in the dead air region. In this period of formation of the separation region before the shed vortex from the spoiler reaches the aerofoil trailing edge, the suction inside the developing separation region are higher than in the later steady state; if these suction is sufficiently larger than the compression ahead of the spoiler then a temporary overall increase in lift is possible. These early transient effects can be Mach number dependent because the upstream compressions depend on the upstream propagation of spoiler disturbances. Once the spoiler vortex and the separation region extends beyond the trailing edge, there is a rapid loss in lift as the lower surface pressures respond to the new trailing edge Kutta condition. The subsequent loss of lift to the asymptotic steady state depends on the downstream convection of the shed vorticity from the spoiler tip and the aerofoil trailing edge. When there is a separation region enclosing a dead air region shed vorticity is convected along the upper and lower shear regions with about $1/2$ of the free stream velocity, this effect reduces the rate of loss of lift. Exactly what happens to the convection velocities of the shed vorticities on the upper and lower shear regions when they combine into the thick wake region downstream is not clear.

The delay times for the developing separation region to reach the trailing edge to commence the process of lift loss are acceptable for a spoiler located towards the aft end of the aerofoil at say more than 70% aerofoil chord from aerofoil leading edge, when the spoiler is used as a roll control; whether the delay is acceptable in a gust alleviation application remains to be seen. But when a spoiler is located forward at, say, 25% aerofoil chord from the aerofoil leading edge the combination of spoiler vortex formation and slow convection over the aerofoil upper surface gives appreciable lag times; such a sluggish response means that a forward spoiler is completely unacceptable even when used as a roll control. This fact has been well known since the 1930's from test flight experience at that time using spoilers as roll controls.

The flow characteristics described above follow the opening of a spoiler, leading to a loss in lift. When a spoiler is closed rapidly the local separated flow region is swept away virtually with the free stream velocity, as shown in Fig. 16. Thus, there are virtually no local flow lag effects when a spoiler is closed, this differs fundamentally from the opening case. There is still, of course, the same overall rate of change of circulation associated with the convection of the wake vorticity with the free stream velocity behind the aerofoil, but this build up will follow broadly the same trend as the build up of lift with a trailing edge control. This major difference in aerodynamic behaviour in the opening and closing of spoilers with its pronounced hysteresis effect creates considerable difficulties in a feedback control system design.

In the next Lecture in this Series, Mabey quantifies these various spoiler characteristics.

2.4 Finite Span Controls

The same aerodynamic processes described for two dimensional configurations apply to controls on finite wings, wake vorticity is generated which is convected downstream causing lag effects. However, the span of the wake vorticity is now finite, thus following a rapid ramp change in control angle and assuming that the flow remains attached, the approach to the asymptotic steady state is now much faster, of the order of $(1/c^2)$; with the magnitude dependent on Mach number. This asymptotic behaviour is one of the most important results in unsteady aerodynamics; it turns up later when the concept of aerodynamic derivatives is discussed.

Low aspect ratio controls, possibly all moving controls, will most probably induce separations along their leading edges. But the separated flows in this case will be well ordered with the separations taking the form of tightly rolled up vortices with their axes aligned at small angles relative to the free stream. Although formation of vorticity takes longer than dissolution of vorticity the separated flow field will be formed or destroyed virtually in the time the free stream passes over the root chord of the control. The subsequent build up or loss time will depend more on the span than on the chord. An important feature is the interaction of the transient spanwise vortices with downstream surfaces, e.g. a forward canard inducing separated vortices which interact with wing and tailplane, and in lateral motions with the fuselage and fin.

3. RANGE OF PREDICTION METHODS

The aim of this section is to give a summary of the current state-of-the-art of the methods of prediction of the loads on aircraft configurations arising from the unsteady motion of controls. There will be no attempt to describe details of the theoretical methods, such an undertaking requires a full lecture series on its own (e.g. ref. 1). Ashley⁽²⁾ has given an excellent review and bibliography. But much of the mathematical language and modelling resembles the steady case which is discussed in this Lecture Series by Körner.

3.1 Two-Dimensional Aerofoils with Trailing or Leading Edge Controls

3.1.1 Low speeds

Inviscid linearised theory neglects viscous effects and neglects the effect of aerofoil thickness and assumes that all of the vorticities which represent the aerofoil, control surface wake are placed on a planar sheet. Numerical solutions for the case of a harmonically oscillating control can be found by:-

- i) superposition of number of continuous loading functions over the aerofoil and control surface which have the correct form of mathematical singularities at the aerofoil leading and trailing edges and at the control hinge line; the so-called Kernel function methods based on the work of Multhopp, Garner, Davies, Stark, Landhal, Cunningham (see ref. 2);
- ii) representation of the planar vorticities on the aerofoil, control surface and wake as piecewise linear over small elements, (the Queen Mary College programs are based on this approach);
- iii) representation of that part of the planar vorticity on the aerofoil and control surface which contributes to the load as discrete vortices while the wake vorticity aft of and associated with each discrete vortex is either continuous (vortex doublet) based on the work of Rodden (see ref. 2) or discrete (unsteady vortex lattice), again in-house at Queen Mary College.

All of the pertinent literature is listed in reference 2.

The Kernel function and vortex doublet methods are restricted to the case of a harmonically oscillating control surface, but method (ii) and the unsteady vortex lattice method can be generalised to calculate the loadings following a specified arbitrary motion of a control surface. These latter two methods can also be used for non-planar wakes.

More exact numerical inviscid solutions are available based on the so-called surface singularity methods^(3,4) or internal singularity methods⁽⁵⁾ which solve the inviscid potential flow about a thick aerofoil profile and a thin non planar vortex wake, for both arbitrary and harmonically time varying control surface motions.

Although there has been considerable effort and progress on the understanding and prediction of unsteady boundary layers, see ref.(1), the incorporation of unsteady boundary layers into the unsteady loading calculations is in its infancy. A general problem when boundary layers are introduced concerns the form of the unsteady Kutta condition in the neighbourhood just aft of the trailing edge. One particular difficulty when there is a deflected control surface concerns the prediction of the boundary layer flow characteristic around the discontinuity in aerofoil profile at the control hinge on both the upper and lower surfaces.

Unsteady transition on both the upper and lower surfaces is known to play an important role, at least at the Reynolds numbers in wind tunnel experiments, but such effects are not calculable at present.

3.1.2 Subcritical flows

In steady two-dimensional flows the inviscid linearised subsonic equations can be solved by simple transformation into a low speed form so that all of the techniques available for incompressible flows can be applied. But for unsteady flows such a transformation is not possible. The basic form of the equations differ when free stream Mach number is taken into account because at a finite subsonic Mach number disturbances radiate outwards at a finite velocity relative to the free stream whereas in incompressible flows disturbances radiate outwards infinitely quickly (mathematically speaking) relative to the free stream.

All of the methods summarised in section 3.1.1 can be applied to solve the inviscid linearised subsonic equations for the oscillatory motion of a control surface. The methods cannot in general be used to generate solutions for an arbitrary time dependent motion of a control surface. There are analytic solutions to determine the transient loading following a step change in aerofoil incidence or pitch, but not, as far as known, for a step change in control surface angle.

However, in principle if:

$\tilde{L}(\omega)e^{i\omega t}$ = oscillatory lift acting on an aerofoil when the control surface is oscillating with unit amplitude at frequency ω where, as already defined,

ν = frequency parameter = $\omega c/V$,

so $\tilde{L}(\omega)$ is complex with in-phase and out-of-phase components. And if

$L_H(\xi)$ = lift response acting on the aerofoil and control when the control undergoes a step change, i.e.

$\begin{cases} \text{control angle} = 0 & \text{for } \xi < 0 \\ \text{control angle} = \text{unit angle} & \text{for } \xi > 0 \end{cases}$

then $L_H(\xi)$ is zero for $\xi < 0$, and $L_H(\xi)$ builds up to the asymptotic steady state associated with the unit control angle. It is known that

$$L_H(\xi) = \frac{1}{2\pi} \int_{-\infty}^{\infty} \frac{\tilde{L}(\nu)}{i\nu} e^{i\nu\xi} d\nu \quad (1)$$

Eqn.(1) is a standard result which relates a step response to an oscillating response for a linear system.

In principle if $\tilde{L}(\nu)$ can be calculated for subsonic Mach numbers then the step response $L_H(\xi)$ can be determined by numerical integration. But the integral in eqn.(1) covers all frequencies. Essentially, the low frequency behaviour of $\tilde{L}(\nu)$ determines the behaviour of $L_H(\xi)$ at large time whereas the high frequency behaviour of $\tilde{L}(\nu)$ determines the behaviour of $L_H(\xi)$ at small times. But there are numerical limitations to the range of frequency parameters for which the oscillatory subsonic equations can be solved, usually the methods are limited to $0 < \nu < 2$. Fortunately, for flutter calculations, this range of frequency parameter covers the practical range of structural mode frequencies. It is commonly agreed that in the limit of $\nu \rightarrow \infty$ the loading at each point on the aerofoil surface is given by one dimensional compressible flow piston theory. The behaviour of $\tilde{L}(\nu)$ is then interpolated between $\nu = 2$ to $\nu \rightarrow \infty$. In contemporary applications this interpolation is regarded as satisfactory.

For an arbitrary control surface motion $\eta(\tau)$, $t > 0$, then the lift response $L(\xi)$ is given by the standard convolution integral, assuming linear aerodynamics,

$$L(\xi) = \int_0^\xi L_H(\xi - \tau) d\eta(\tau) \quad (2)$$

The non-dimensionalisation with respect to \hat{L} has been omitted for convenience. Eqn.(2) is discussed in more detail later. The calculation of $L(\xi)$ in the frequency domain is done by substituting eqn.(1) into eqn.(2).

3.1.3 Supercritical speeds

For the non-linear equations relevant to the transonic speed range finite difference numerical techniques provide the basis of a wide range of techniques. The literature is vast and the frontiers are fast expanding, as indicated by the annual AGARD Lecture Series.

Two-dimensional steady problems can be solved by:

- i) the isentropic irrotational transonic small perturbation equation in non-conservative or conservative form, satisfying either the planar boundary conditions or the curvilinear boundary conditions on an aerofoil surface;
- ii) the isentropic irrotational full potential equation in conservative form;
- iii) the isentropic equations in their conservative form;
- iv) the Euler equations.

The effects of attached boundary layers have been incorporated using integral equation type boundary layer methods.

For the time dependent problem, field equations can be solved, in principle, at successive time intervals so there is no restriction to simple harmonic motions. At the present time, programs in general usage are based on the potential equations, usually the small perturbation potential equation, with the limitation that the unsteady motions are relatively slow; oscillatory motions for example would be limited to low values of frequency parameters, say $\nu < 0.3$. Investigations into the extension of the methodology to higher rates of change and higher frequency parameters is a major area of current research, substantial progress is claimed in the U.S.A.

Because the basic equations, even in their most simplified form, are non-linear, solutions cannot be superimposed. The calculation of a step response and its subsequent use in a convolution-type integral to estimate the response to an arbitrary time dependent input is not altogether valid, even though attempts are being made to apply such an approach at transonic speeds.

3.1.4 Supersonic speeds

Linearised supersonic aerofoil theory is well established, as given in standard text books; it is not discussed further here.

3.2 Spoilers

Steady spoiler prediction methods as developed in the U.S.A.⁽⁶⁾ and U.K.⁽⁷⁾ are for low free stream Mach numbers, assuming inviscid flow models and solving the problem by surface singularity panel methods. An upper surface separation streamline from the spoiler tip and a lower separation streamline from the trailing edge enclose a 'dead air' region, the two separation streamlines are assumed to come together some distance aft of the trailing edge to form a closed dead region. This closure is essential in order to bring the predicted static pressure in the dead air region close to the experimental value. Either vorticity, or source, singularities can be placed on the aerofoil surface, vorticity singularities can be placed on the spoiler and on the upper and lower separation streamlines. The strengths of these singularities are determined by satisfying the conditions of tangency of flow on the whole of aerofoil surface, the spoiler surface and on the separation streamlines. In addition, it is either necessary to ensure that there is no static pressure discontinuity across the separation streamlines, or alternatively, it can be assumed that the static pressure is uniform along the separation streamlines, implying that the static pressure is uniform within the wake. The only empirical factor required is the length of the wake before wake closure, usually a wake length of about 0.2 chord gives reasonable results. Some progress has been made in the U.S.A. to incorporate wake mixing effects into the theoretical model⁽⁸⁾.

Methods are becoming available to predict the oscillatory loads when the spoiler is oscillating in simple harmonic motion with a relatively small amplitude, based on extensions to the above inviscid model⁽⁹⁾. Investigations are currently in progress to estimate the unsteady loading associated with a time dependent spoiler motion.

All of the theoretical work so far is for low Mach numbers, there is a need to develop models to deal with higher subsonic Mach numbers. Furthermore, there is a need to incorporate wake mixing effects into the models to eliminate the need for any empiricism.

3.3 Finite Wings with Edge Controls

Linearised subsonic theory is well developed and standardised to calculate oscillatory loads associated with simple harmonic inputs. The main methods are the Kernel function method (superposition of known loading functions which satisfy the edge singularity conditions at the leading edge, trailing edge, wing tip, control hingeline, etc.), and the vortex-doublet method (discretisation of the loading distribution).

Linearised subsonic theory has also been extended to the oscillatory interaction between two surfaces, for example, a wing and a downstream tailplane, and also for tail type configurations. These planar lifting surface models have been combined with fuselage surface singularity distributions to predict wing-body interference effects on oscillatory loads. In addition, planar surface theory has been combined with thin pylon and thin nacelle configuration to determine oscillatory pylon-nacelle-wing interference loads; it is usually assumed that there is unrestricted flow through the nacelle, (i.e. that there is no engine present); this assumption is not unreasonable in cruise conditions where the mass flow through an engine is not too far off from a through-flow condition.

All of the subsonic linearised methods are restricted to the calculation of oscillatory loads, prediction methods are not available for arbitrary control motions. To obtain the step response characteristics, it is necessary to use Fourier transform as indicated by eqn.(1).

Unsteady, non-linear, transonic theory for finite wings is relatively under-developed primarily because there are still areas concerning the two-dimensional case which need to be clarified.

Oscillatory linearised supersonic theory for finite wings is standard. The main area of uncertainty concerns the non-linear region in the supersonic/transonic Mach number range.

4. SOME COMPARISONS BETWEEN THEORY AND EXPERIMENT

It is thought to be worthwhile to introduce into this lecture some indications of the agreement, or rather lack of it, between theoretical prediction and wind tunnel measurements. So comparisons for a two-dimensional aerofoil with trailing edge control at low speed are presented.

The results presented in Table 1 taken from ref.(10) compare recent water tunnel experimental measurements for oscillatory control surface motions with exact inviscid theories which include aerofoil thickness; the results are given for unit control angle amplitude. The Reynolds number was 4.6×10^5 , tunnel wall corrections are included and transition was fixed.

		LIFT		MOMENT		HINGE MOMENT	
		In-phase	Out-of-phase	In-phase	Out-of-phase	In-phase	Cut-of-phase
$V = 0.50$	(Experiment)	0.89	-0.034	0.31	0.102	0.052	0.028
	(Theory)	1.14	-0.11	0.38	0.11	0.077	0.028
$V = 1.0$	(Experiment)	0.78	0.16	0.29	0.22	0.044	0.063
	(Theory)	0.95	0.14	0.35	0.24	0.066	0.070
$V = 2.0$	(Experiment)	0.66	0.511	0.23	0.43	0.018	0.13
	(Theory)	0.78	0.591	0.27	0.50	0.041	0.15

Table 1

It is seen from Table 1 that there are considerable differences between theory and experiment for overall lift, overall moment and hinge moment; the differences appear to be more pronounced for the in-phase than for the out-of-phase. The in-phase lift and moment theory overpredicts measurement by 20-25%, while in-phase hinge moment theory overpredicts measurement by 50%. To give credibility to the measurements it should be stated that for an aerofoil oscillating in either pitch or heave comparison of theory and experiment for lift and moment are within 10%, and so the lack of agreement is particular to control aerodynamics.

Because the theoretical results are determined from numerically exact thick aerofoil theory, the differences are attributed to viscous effects, but it is by no means obvious why viscous effects should be so much pronounced for an oscillatory control surface than for an oscillatory aerofoil. However, at the hinge line, the boundary layer experiences a high local expansion and compression every cycle. Large variations in boundary layer characteristics might be introduced and hence affect the overall circulation through the Kutta conditions. Another effect could be associated with small gaps between the leading edge of the trailing edge control and the main aerofoil, even the smallest gap can connect the upper and lower surface pressures and affect the boundary layer characteristics.

Mabey presents in the following lecture more comparisons between theory and measurement for finite wings, and their controls, at higher subsonic Mach numbers.

5. ON CONCEPT OF AERODYNAMIC DERIVATIVES

The treatment of aircraft dynamics using aerodynamic derivatives is well entrenched in the aeronautical literature. But there is an increasing awareness that the mathematical basis for such aerodynamic derivatives is imprecise and that there is a need to comprehend more fully the meaning and limitation of derivatives in this era of fast acting controls, especially when non-linear effects are important.

To start with, consider a three-dimensional wing at zero incidence, in a free stream at a subcritical Mach number. At a datum time $t = 0$, a trailing edge control (e.g. an elevator) is deflected suddenly through a unit angle. Then the lift response following this step control angle deflection

$$\begin{aligned} &= 0 \quad \text{for } t < 0 \\ &= L_H(t) \quad \text{for } t > 0 \end{aligned} \quad (3)$$

It is implied that $L_H(t)$ is identically zero for $t < 0$. At time $t = 0$, there will be an impulse in $L_H(t)$ proportional to the Dirac delta function $\delta(t)$, associated with the fact each element of the surface moves like a one-dimensional piston generating a local one-dimensional wave field. For large time, $t \rightarrow \infty$, then

$$L_H(t) \rightarrow L_H(\infty) = L_S, \quad (4)$$

where L_S is the steady lift associated with the unit control angle. As already explained for a finite wing, $L_H(t)$ approaches its final steady state as $(1/t^2)$.

Consider now the lift induced by a time dependent control angle motion $\gamma(t)$ for $t > 0$. Assuming that the problem is a linear one then the lift build up is given by the standard convolution integral

$$L(t) = \int_{0-}^{t+} L_H(t-\tau) \frac{d\gamma(\tau)}{d\tau} d\tau. \quad (5)$$

Eqn.(5) states that $L(t)$ is the cumulative effect of a sequence of small step inputs of magnitude $d\gamma$ at time τ . It is necessary for mathematical reasons to be precise on the limits; the limit $t = 0-$ implies the time just prior to $\tau = 0$ and the limit $t+$ refers to the time τ just after $\tau = t$. Eqn.(5) can be re-expressed in the form

$$L(t) = L_H(\infty) \gamma(t) + \int_{0-}^{t+} (L_H(t-\tau) - L_H(\infty)) \frac{d\gamma(\tau)}{d\tau} d\tau. \quad (6)$$

Note that $L_H(\infty)$ is the asymptotic steady state for a unit control angle so $L_H(\infty)$ is a constant independent of time. Hence $L_H(\infty)$ is identified with the normal steady state derivative

$$L_H(\infty) = \frac{\partial L}{\partial \gamma} \Big|_{\text{steady}} = L_{\gamma}. \quad (7)$$

Now introduce

$$\begin{aligned} f(t, t-\tau) &= \int_{0-}^{t+} (L_H(t-\tau') - L_H(\infty)) d\tau' \\ &= \int_{t-\tau}^t (L_H(\tau') - L_H(\infty)) d\tau' \end{aligned} \quad (8)$$

Since $L_H(r)$ is $O(1/r)^2$ for large r , then the integrand in eqn.(8) is integrable; furthermore, $J(t,0)$ is $O(1/t)$ for large t .

Integrating eqn.(6) by parts gives

$$L(t) = L_H \dot{\gamma}(t) + J(t,0) \frac{d\gamma(t)}{dt} - \int_0^t J(t,t-r) \frac{d^2\gamma}{dr^2} dr, \quad (9)$$

where

$$J(t,0) = \int_0^t (L_H(r) - L_H(\infty)) dr. \quad (10)$$

In eqn.(10), $J(t,0)$ can be interpreted simply as the indefinite integral of the step function response function. From eqn.(9), $J(t,0)$ can be regarded as the aerodynamic derivative associated with $\dot{\gamma} (= d\gamma/dt)$, i.e.

$$J(t,0) \equiv L_{\dot{\gamma}}. \quad (11)$$

It is noted that $L_{\dot{\gamma}}$ is time dependent at least for small (real) time; but for $t > 100 \hat{t}$ (about 2 secs from the beginning of the manoeuvre) then $L_{\dot{\gamma}}$ is virtually constant, independent of time.

It might be thought that the process developed above in eqns.(6 to 10) to generate $J(t,0)$ could be applied once again to eqn.(9) and so generate a $\ddot{\gamma}$ derivative. But the above procedure cannot be taken any further because the integral of $J(t,0)$ over a long time period tends to infinity as $\ln t$. So eqn.(9) is the end of the line. Two constant derivatives $L_{\dot{\gamma}}$ and $L_{\ddot{\gamma}}$ can be identified but there is a third integral term which cannot be resolved further. Eqn.(9) should be interpreted with care, it is incorrect to think of the first term, which is proportional to $\dot{\gamma}$ as first order, the second term, which is proportional to $\ddot{\gamma}$ as second order and the integral as a higher order term; the integral itself can be the same order of magnitude as $\dot{\gamma}$ term. Nevertheless, it is true that if $\dot{\gamma}$ is constant, then $L(t)$ is given by the first two terms in eqn.(9).

The next question refers to the respective contributions of each of the three terms in eqn.(9) to the instantaneous lift $L(t)$. Garner⁽¹¹⁾ has recently made an extremely significant calculation by estimating these three components for a trailing edge control motion, representative of a control motion to alleviate a gust loading, at $M_\infty = 0.8$ on a finite wing of aspect ratio 8, leading edge sweep 23° , with a 23° trailing edge control span situated at wing tip. One of Garner's results is shown in Fig. 15. For a rapid continuous control input, rotating the control to an angle and retracting it in time (20 \hat{t}), say 0.15 s, the contributions for $L_{\dot{\gamma}} \dot{\gamma}(t)$, $L_{\ddot{\gamma}} \ddot{\gamma}(t)$ and the integral term (the third term of eqn.(9)) are shown. The curve $L_{\dot{\gamma}} \dot{\gamma}(t)$ indicates incidentally the form of $\dot{\gamma}(t)$, the control input. It is seen that the contribution of $L_{\ddot{\gamma}} \ddot{\gamma}(t)$ and the integral term are about the same order of magnitude. The response cannot be expressed in terms of derivatives ($L_{\dot{\gamma}} \dot{\gamma} + L_{\ddot{\gamma}} \ddot{\gamma}$) alone, the integral term cannot be neglected. In fact, the first term $L_{\dot{\gamma}} \dot{\gamma}$ by itself is a better approximation than ($L_{\dot{\gamma}} \dot{\gamma} + L_{\ddot{\gamma}} \ddot{\gamma}$). However, for slower rates of control angle change, then the two terms involving the ($L_{\dot{\gamma}} \dot{\gamma} + L_{\ddot{\gamma}} \ddot{\gamma}$) derivatives would then probably become sufficiently accurate.

When non-linearities occur, associated with flow separation and reattachment, it may be possible to superimpose basic flow responses. For example, if a ramp rate response function $L_R(t)$, for $t > 0$, is defined as the lift response on a wing at an initial incidence α , with the control angle initially at γ , and then the control is moved at time $t = 0$ at a constant rate $\dot{\gamma}$ for time $\Delta\tau$, after which the control angle remains constant at $(\gamma + \dot{\gamma}\Delta\tau)$. Thus in non-linear flows $L_R(t)$ is a function also of $\alpha, \gamma, \dot{\gamma}$ and $\Delta\tau$; thus $L_R(\alpha, \gamma, \dot{\gamma}, \Delta\tau, t)$. If $L_S(\alpha, \gamma)$ refers to the steady lift at incidence α and control angle γ then

$$L_S(\alpha, \gamma + \dot{\gamma}\Delta\tau) = L_R(\alpha, \gamma, \dot{\gamma}, \Delta\tau, \infty). \quad (12)$$

A range of experiments would have to be carried out for different $\alpha, \gamma, \dot{\gamma}$, and $\Delta\tau$ to give $L_R(\alpha, \gamma, \dot{\gamma}, \Delta\tau, t)$, and incidentally $L_S(\alpha, \gamma)$. Once such a comprehensive range of experimental information was known then it may be possible to write down a relationship for the lift response $L(t)$ for an arbitrary input $\dot{\gamma}(t)$, namely, assuming α constant,

$$L(t) = \int_0^t L_R(\alpha, \gamma(r), \dot{\gamma}(r), dr, t-r). \quad (13)$$

Eqn.(13) presumes that responses can be superimposed, history effects are associated with wake effects, which are being convected downstream; if the sequence of wake effects do not interact then the assumption is not unreasonable. Shed effects from attached flows however travel faster than shed effects from separated flows so there could be complications. Another question concerns the fact that $L_R(t)$ itself is based on the premise that the flow is steady before the control angle starts moving, but it is implied in eqn.(13) that when the increment of control angle is applied at time τ that the 'initial' flow prior to τ is in a transient state.

To estimate the integral in eqn.(13), it would be necessary to divide the time interval $(0, t)$ into elements dr , taking $\dot{\gamma}(r)$ as uniform in those time elements, and equal to $\{\dot{\gamma}(r)dr - \dot{\gamma}(r-1)\}/dr$.

Representing an input $\dot{\gamma}(t)$ by piecewise linear functions,

$$L(t_n) = \sum_{i=1}^n L_R(\alpha, \gamma_i, \frac{\dot{\gamma}_{i+1} - \dot{\gamma}_i}{t_{i+1} - t_i}, t_{i+1} - t_i, t_n - t_i). \quad (14)$$

To simplify eqn.(14), it is assumed that the rate of change of $\dot{\gamma}(t)$ is sufficiently slow that the unsteady effects are associated with the last time interval $(t_n - t_{n-1})$, then it is possible to write

$$L(t_n) \approx L_S(\alpha, \gamma_{n-1}) + L_R(\alpha, \gamma_{n-1}, \dot{\gamma}_{n-1}, t_n - t_{n-1}, t_n - t_{n-1})$$

$$\approx L_s(\alpha, \gamma) - \frac{\partial L_s(\alpha, \gamma)}{\partial \gamma} \dot{\gamma}_n (t_n - t_{n-1}) + L_R'(\alpha, \gamma_{n-1}, \dot{\gamma}_{n-1}, t_n - t_{n-1}). \quad (15)$$

The function $L_R'(\alpha, \gamma, \dot{\gamma}, t)$ now denotes the lift response starting at $t = 0$ with initial incidence α , initial control angle γ , and then the control moves at a constant rate $\dot{\gamma}$. It may be thought that $L_R(\alpha, \gamma, \dot{\gamma}, t)$ would be a linear function of γ and $\dot{\gamma}$, for when both $\dot{\gamma}$ and t are zero, L_R is zero. Thus eqn.(15) becomes, assuming α does not change with time,

$$\begin{aligned} L(t) &\approx L_s(\alpha, \gamma(t)) + \left[\left(-\frac{\partial L_s(\alpha, \gamma)}{\partial \gamma} \right) + \frac{\partial^2 L_R(\alpha, \gamma, \dot{\gamma}, t)}{\partial \dot{\gamma} \partial t} (t_n - t_{n-1}) \right] \dot{\gamma}(t) \\ &\approx L_s(\alpha, \gamma(t)) + L_{\dot{\gamma}}(\alpha, \gamma(t)) \dot{\gamma}(t). \end{aligned} \quad (16)$$

where $L_{\dot{\gamma}}$ denotes a function which depends on $(\alpha, \gamma(t))$ and which can be regarded as the 'coefficient' of $\dot{\gamma}$. Such a function might be obtained experimentally. The validity of eqn.(16) is difficult to assess and requires much further investigation both theoretically and experimentally at a fundamental level.

6. UNSTEADY AERODYNAMICS FOR ACTIVE CONTROL APPLICATIONS

Active control applications are broadly in two areas. Relaxed stability, manoeuvre demand, spin prevention, manoeuvre load control are concerned with overall aircraft dynamic motions where, because the overall motion of the aircraft is involved, the rates of response are relatively slow in aerodynamic time, so the aerodynamics can be expressed in terms of derivatives, hopefully in terms of non-linear ones in the non-linear ranges of flight as indicated in eqn.(16). However, for those active control applications such as gust response, ride quality, flutter suppression, which involve much more rapid responses, it has been demonstrated that normal derivatives are inadequate. But the division is blurred; any system designed for, say, relaxed stability needs to be stable when inputs from structural responses are introduced.

There are a variety of complementary methods used to design control systems, some utilise the frequency domain (e.g. Nyquist), some utilise the s-plane (e.g. root locus), others use the time domain (e.g. for transient behaviour).

Oscillatory loads can be estimated from a combination of theory and experiment for the range of frequencies which cover most of the practical structural modes. It is possible to interpolate from this practical range of frequencies ($\gamma < 2.0$) to $\gamma = \infty$, without significant errors being introduced. It is therefore possible to study the design of control systems in the frequency plane.

But in the time domain the key function is the step response function $L_H(t)$. But $L_H(t)$ can only be calculated in numerical form. It is therefore necessary to express $L_H(t)$ in an empirical analytic form, which gives a straightforward Laplace transform (i.e. it can be expressed as a transfer function) and then used in s-plane synthesis calculations.

In one of the earliest type of approximation, it was assumed that

$$L_f(t) = \frac{dL_H(t)}{dt} \approx k \delta(t) + e^{-P_1 t} \sum_{r=0}^{m-1} c_r t^r \quad c_r > 0, \quad (17)$$

where P_r, c_r are constants to give a 'good' fit to the known accurate $L_H(t)$ function. There is a delta function at time t equal to zero to represent the piston theory loading. A more generalised form is

$$L_f(t) = \frac{dL_H(t)}{dt} \approx k \delta(t) + \sum_{r=1}^m e^{-P_r t} \sum_{s=r}^n c_{rs} t^s, \quad (18)$$

where the P_r can be in complex conjugate pairs. Both eqns.(17, 18) are in a suitable form to give a reasonable Laplace transform. It will be noted that neither of eqns.(17, 18) satisfy the correct limiting behaviour as $t \rightarrow \infty$; the exponential functions all decay more rapidly than $1/t^2$. A consequence of this defect is that when either eqn.(17) or eqn.(18) is used in a control system design analysis spurious stability roots arise in the mathematics. Often it is clear which are the spurious roots so that they can be ignored. But their existence is a nuisance and can lead, sometimes, to doubts.

To avoid spurious roots (or in modern parlance, undesirable augmented states) Edwards et al⁽¹²⁾ have been developing an alternative approach. A basic problem is to understand the stability problem.

$$M \frac{d^2 q}{dt^2} + D \frac{dq}{dt} + K q = \int_{-\infty}^{\infty} L_{\delta q}(t-r) q(r) dr + \int_{-\infty}^{\infty} L_{\dot{\gamma}}(t-r) \dot{\gamma}(r) dr, \quad (19)$$

where

$$\dot{\gamma}(t) = R \frac{dq}{dt} + T q,$$

and

q is a response variable,

M, D, K , represent inertial, structural damping and structural stiffness terms,

$\dot{\gamma}(t)$ is a control surface angle,

R, T represent rate and direct feedback,

$L_{\delta q}(t)$ is the generalised load due to a unit impulse change in q ,
 $L_{\delta \eta}(t)$ is the generalised load due to a unit impulse change in η . } an impulse function $L_s(t) = \frac{d}{dt} L_u(t)$

Transforming eqn.(19) to the s-plane by taking the Laplace transform

$$(Ms^2 + Ds + K - \bar{L}_q(s)) \bar{q}(s) = \bar{L}_\eta(s)(Rs + T) \bar{\eta}(s). \quad (20)$$

Now the oscillatory aerodynamic derivatives $\tilde{L}_q(v)$ and $\tilde{L}_\eta(v)$ can be calculated, where v is the non-dimensional frequency parameter. It is now assumed that $s = i v$, as in a frequency analysis, so

$$\bar{L}_q(s) \equiv \tilde{L}_q(is). \quad (21)$$

The implications of this assumption are obscure, at least to the lecturer, and need to be clarified.

Thus, substituting eqn.(21) into the left hand side of eqn.(20), eigenvalues can be found from

$$(Ms^2 + Ds + K - \tilde{L}_q(is)) = 0. \quad (22)$$

These eigenvalues, which are effectively the flutter eigenvalues, are then taken to the eigenvalues for $\bar{L}_\eta(s)$ on the right hand side of eqn.(20). This procedure implies that the eigenvalues of the left hand side of eqn.(20) represents the eigenvalues for the complete system when the terms on the right hand side of eqn.(20) are included, since the eigenvalues of both sides of this equation would be the same. The eigenvalues thus determined for $\tilde{L}_\eta(s)$ can be identified with the values of the exponential powers P_r in the empirical expansion for $L_u(t)$ as defined in eqn.(18). In this way, $L_u(t)$ is approximated in terms of the system characteristics being designed, providing a basis of mathematical compatibility and consistency in the synthesis process. It is unfortunate however that the eigenvalues are the incorrect ones for the complete system because from eqn.(20) the full system eigenvalues are given to the same order of approximation, by

$$(Ms^2 + Ds + K - \tilde{L}_q(is) - \tilde{L}_\eta(is)(Rs + T)) = 0. \quad (23)$$

Perhaps an alternative, but more cumbersome approach, would be to write

$$Ms^2 + Ds + K - \tilde{L}_q(is) = K_1 \prod_{j=1}^N (s - a_j), \quad (24)$$

where a_j are the N eigenvalues of the left hand side of eqn.(24); and

$$Ms^2 + Ds + K - \tilde{L}_q(is) - \tilde{L}_\eta(is)(Rs + T) = K_2 \prod_{j=1}^M (s - b_j), \quad (25)$$

where b_j are the M eigenvalues of the left hand side of eqn.(25), then the 'eigenvalues' of $\bar{L}_\eta(s)$ could be obtained from

$$K_2 \prod_{j=1}^M (s - b_j) - K_1 \prod_{j=1}^N (s - a_j) = 0. \quad (26)$$

Eigenvalues from eqn.(26) could then be used as the exponential powers P_r in eqn.(18). This last paragraph is purely speculative and requires much more consideration. It is hoped that some of the ideas have been illustrated.

7. CONCLUDING REMARKS

The aim of this lecture has been to introduce some of the underlying concepts regarding unsteady aerodynamics and their incorporation into dynamic studies, with some indication of current research.

But there are some main areas of importance which the unsteady aerodynamicist has yet to confront. One example concerns the time dependent aerodynamics associated with canard movements and the transient loads induced downstream on fuselage, main wing, tailplane, fin, etc. Another example concerns the unsteady aerodynamics related to the use of vectored thrust in flight. So there are plenty of problems to engage the contemporary unsteady aerodynamicist.

REFERENCES

1. Special Course on Unsteady Aerodynamics. AGARD Report No. 679, 1980.
2. H. Ashley Unsteady Subsonic and Supersonic Flow. AGARD Conference Proceedings 227, 1977.
3. J.P. Giesing Non-linear Two-Dimensional Unsteady Potential Flow with Lift. Jour. Aircraft 5(2), 1968.
4. B.C. Basu, G.J. Hancock. Unsteady Motion of a Two-Dimensional Aerofoil in Incompressible Inviscid Flow. Jour. Fluid Mech., Vol. 81, Part 1, 1978.
5. B.C. Basu Mean Camberline Singularity Method for Two-Dimensional Steady and Oscillatory Aerofoils and Control Surfaces in Inviscid Incompressible Flow. ARC Current Paper 1391, 1978.
6. W.H. Wentz, C. Ostowalc, H.C. Seetharam. Effects of Design Variables on Spoiler Control Effectiveness, Hinge Moments and Wake Turbulence. AIAA 19th Aerospace Sciences Meeting, January 1981.
7. H.B. Tou, G.J. Hancock. To be published.

8. N.J. Pfeiffer, G.W. Zumult. A Computational Model for Low Speed Flows past Aerofoils with Spoilers. AIAA-81-0253, 1981.
9. H.B. Tou, G.J. Hancock. To be published.
10. V.J.E. Stark Measurement of Derivatives for an Oscillating Aerofoil with Flap. Journal of Aircraft, Vol, 18, May 1981.
11. H.C. Garner The application of subsonic theoretical aerodynamics to active controls. Royal Aircraft Establishment TR 81060, May 1981.
12. J.W. Edwards Application of Laplace transform methods to aerofoil motion and stability calculations. AIAA Paper 79-0772, 1979.

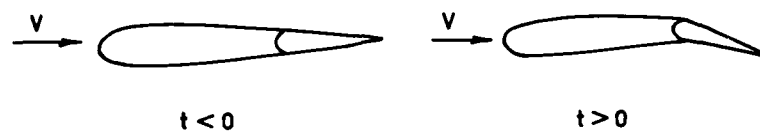


Fig.1 Rapid change in trailing edge control angle

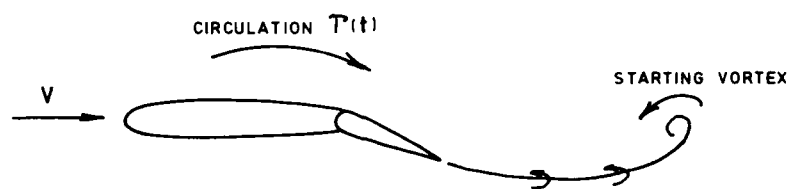


Fig.2 Developing flow field

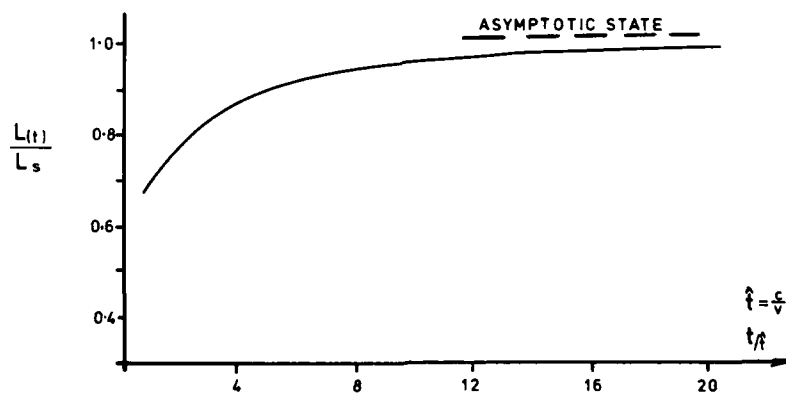


Fig.3 Transient lift following rapid change of trailing edge control angle.

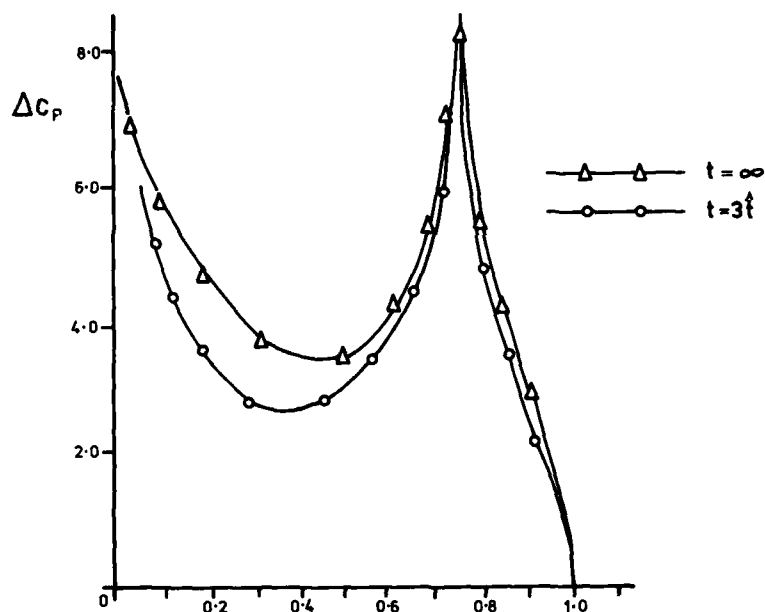


Fig. 4 Chordwise loading of transient lift following rapid change of trailing edge control.

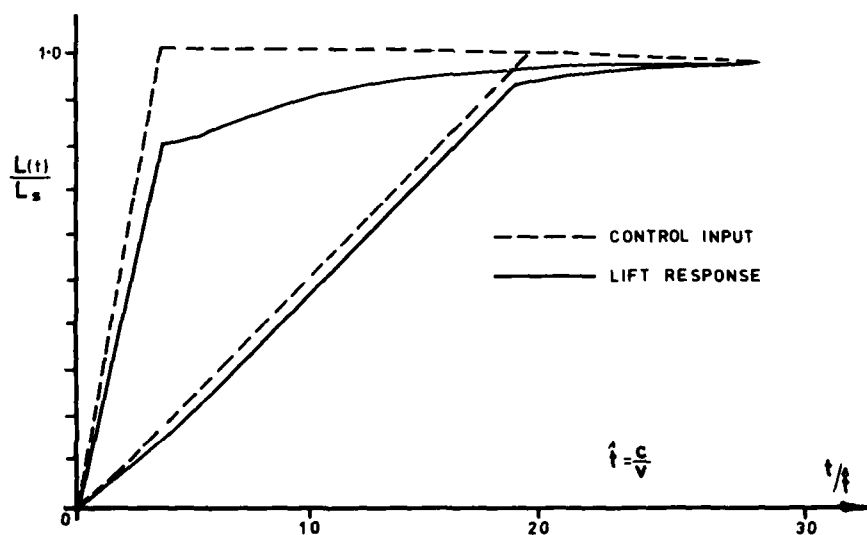


Fig. 5 Lift response for slower changes in trailing edge control.

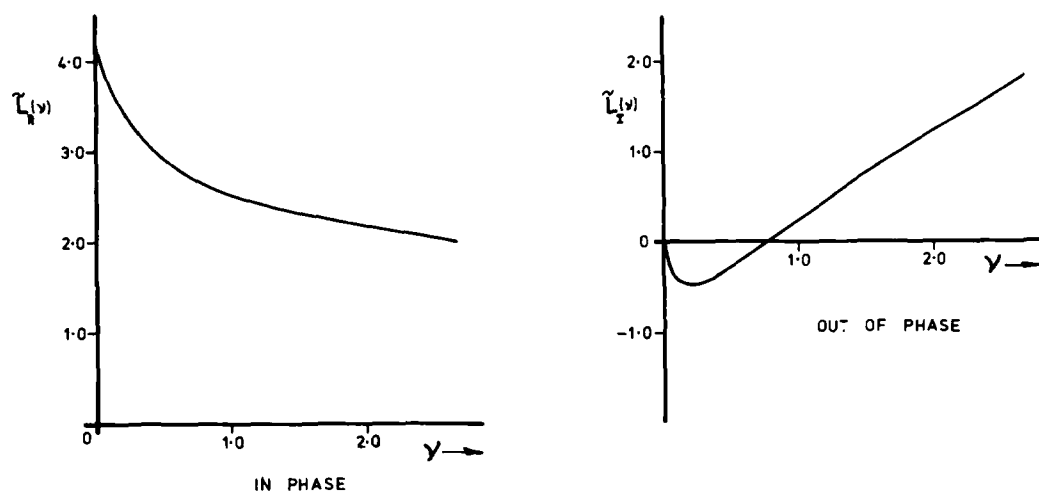


Fig. 6 Oscillatory forces for trailing edge control in simple harmonic motion.

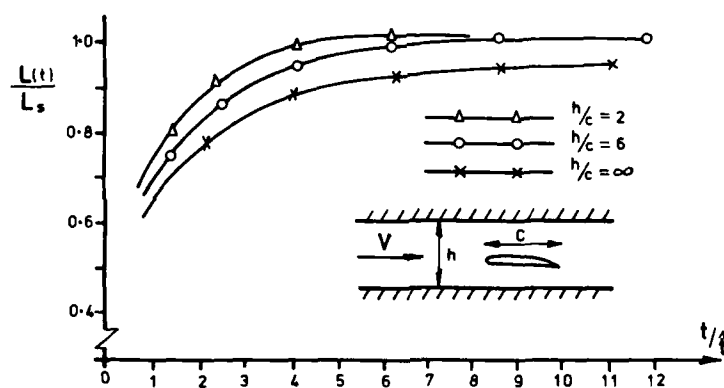


Fig. 7 Effect of tunnel wall interference.

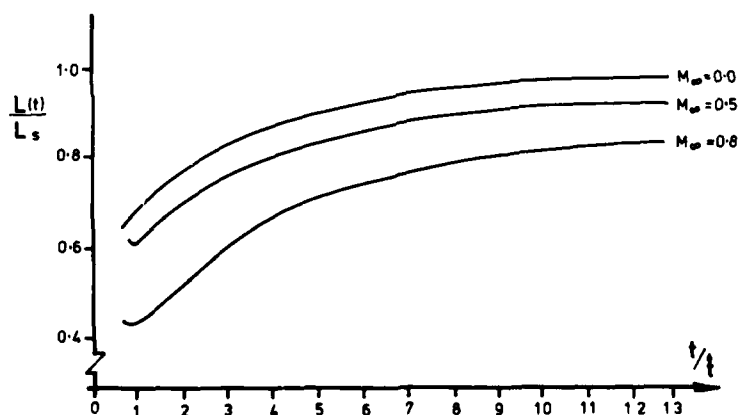


Fig. 8 Effect of free stream Mach No. on transient lift.

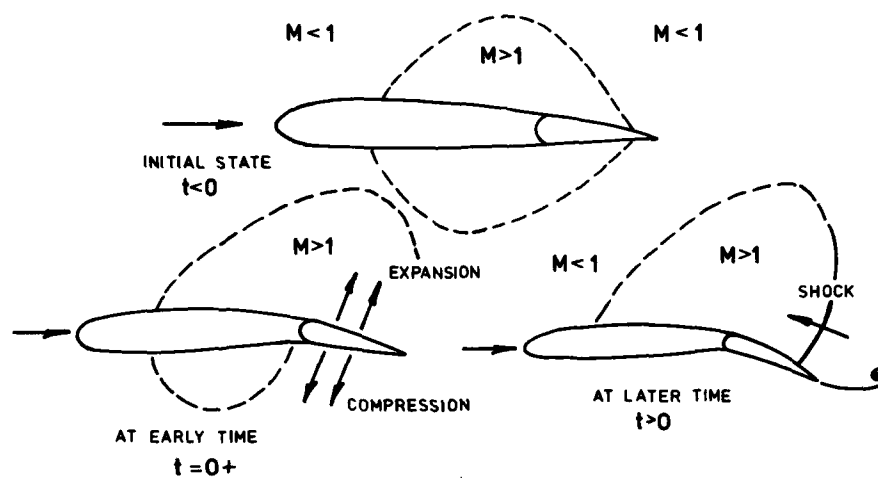


Fig. 9(i)

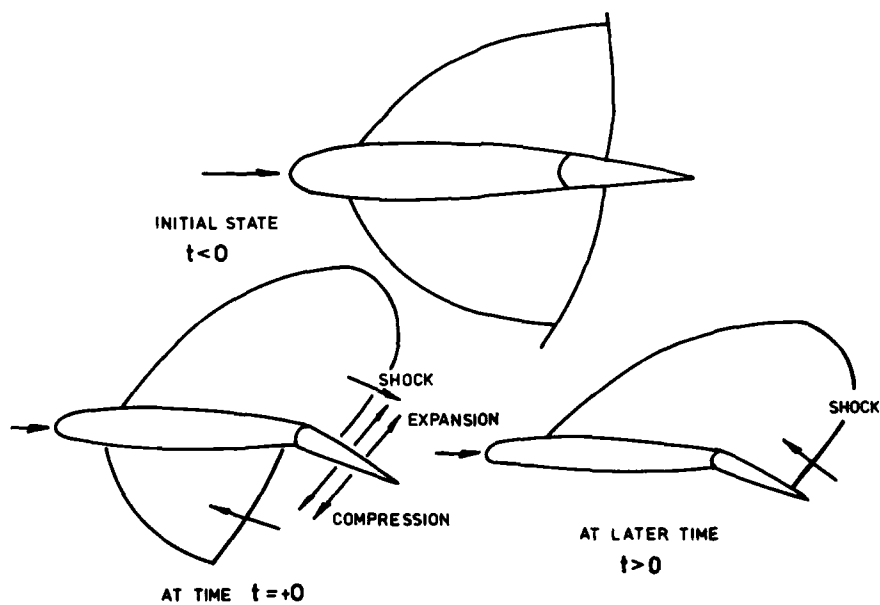


Fig. 9(ii)

Fig. 9 Application of rapid trailing edge control at transonic speeds.

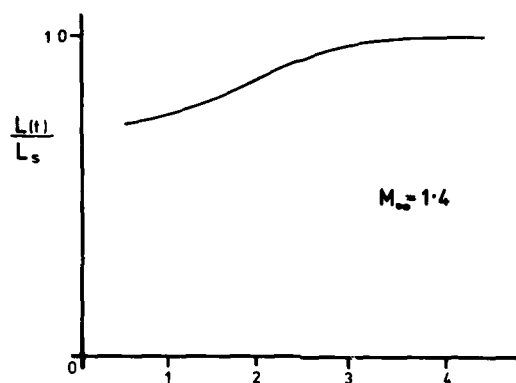


Fig. 10 Transient lift for rapid trailing edge control motion at supersonic speed.

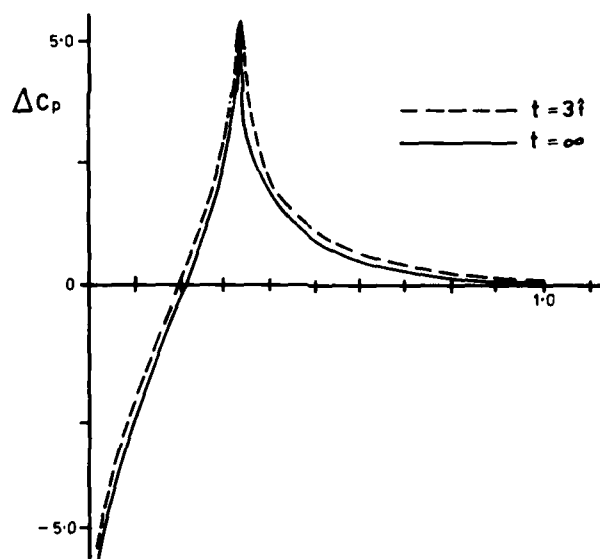


Fig. 11 Chordwise loading following rapid change of leading edge control ($M_\infty \ll 1$)

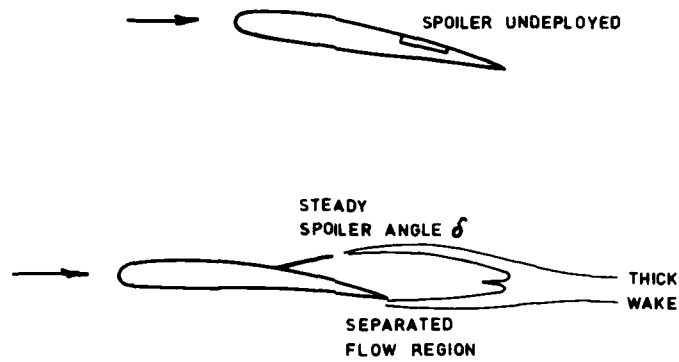


Fig. 12 Flow past aerotail/spoiler.

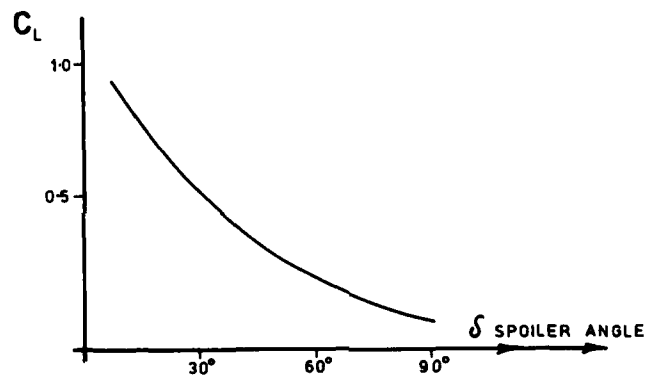


Fig. 13 Steady spoiler characteristics.

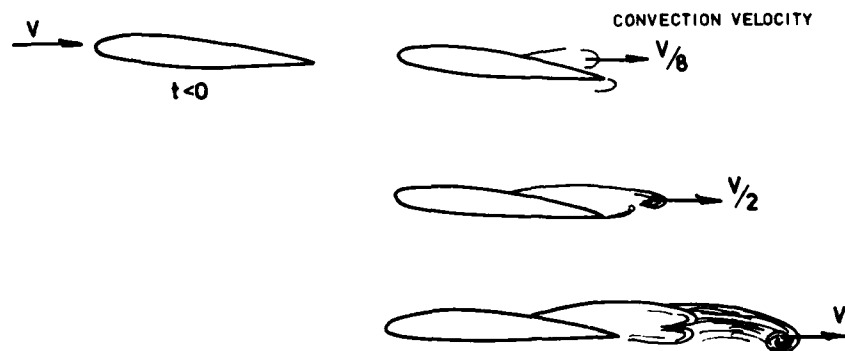


Fig. 14 Flow characteristics following spoiler opening.

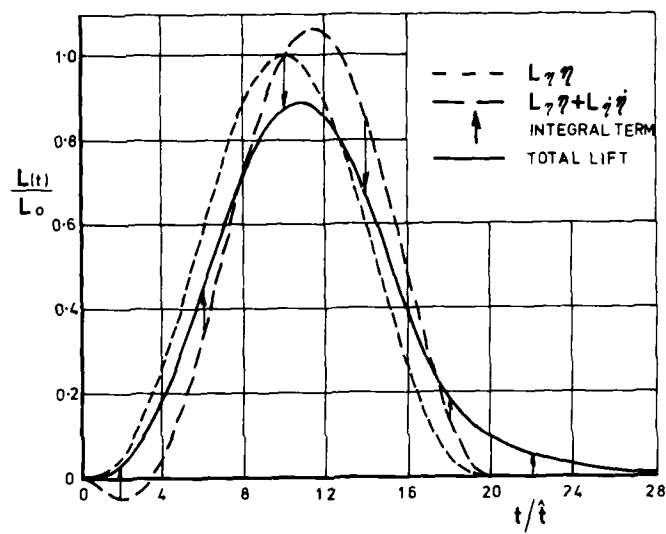


Fig. 15 Contributions to lift from trailing edge control.

EXPERIMENTAL METHODS TO DETERMINE CONTROL EFFECTIVENESS IN WIND TUNNELS

by

D. G. Mabey
Aerodynamics Department
Royal Aircraft Establishment
Bedford, UK

SUMMARY

The methods used to determine control effectiveness in wind tunnels are reviewed, using illustrative examples. Major experimental difficulties are enumerated.

The controls discussed include tailplanes, ailerons, airbrakes and spoilers. Both steady and unsteady measurements are considered, although the emphasis is on unsteady measurements and transonic speeds.

As an illustration of the current interest in Active Control Technology, the paper includes some results from an experiment in which a trailing-edge flap is driven 'closed loop' to reduce the response of a model wing to flow unsteadiness.

This paper was prepared for the AGARD lecture series on 'Aerodynamic Characteristics of Controls' to be given on 22 March 1983 in Brussels.

NOTATION

E	tunnel width	R	unit Reynolds number
C_p	pressure coefficient	s	semi span
$R(C_p)$, $I(C_p)$	real and imaginary defined in Ref 27	S	wing area
C_p/δ	modulus defined in Ref 27	t	time
c	local chord	T	time to operate spoiler
\bar{c}	average chord	U	free-stream velocity
C_L	lift coefficient	Subscripts a	adverse lift
C_m	pitching moment coefficient	f	final lift
C_l	rolling moment coefficient	α	wing-incidence
f	frequency	δ	control deflection
H	tunnel height	η	y/s - fraction of semi span
h	hinge moment coefficient	η_T	tail angle
I	control inertia	ϕ	phase angle
M	Mach number	ν	frequency parameter fc/U
P_t	tunnel total pressure	ζ	total damping (% critical)
		ρ	free-stream density

1 INTRODUCTION

The provision of adequate control effectiveness has been a prime objective of aerodynamic research since the Wright Brothers developed their successful flying machine with the help of model tests in a wind tunnel. They realised that the problems of stability and control were more important than mere performance in the design of a successful flying machine^{1,2}.

The literature on the measurement of control effectiveness is virtually open-ended and the tiny selection given here is illustrative, rather than comprehensive. A comprehensive review³ of the aerodynamics of controls given by Ross and Thomas includes 54 references and a bibliography of another 197 references.

Aerodynamic surface control surfaces develop the necessary forces to enable the aircraft to fly in steady attitudes and to manoeuvre. Typical controls are illustrated in Fig 1, which includes also the definitions of positive forces and moments. On a conventional aircraft the forces and moments developed by the tailplane and the foreplane (or canard) normally control the longitudinal stability of the aircraft. The rudder, the fin and the ailerons normally control the lateral stability of the aircraft. The airbrakes can modulate the aircraft drag, whereas the flow spoilers in the wing can simultaneously modulate both the aircraft drag and the wing lift. Often there are quite strong interactions between the different aerodynamic controls. These interactions may be unfavourable, eg deflection of an airbrake may cause an excessive change in the tailplane angle required

to trim. A major factor in determining the position of controls is the need to minimize these interactions.

Measurements of control effectiveness in wind tunnels pose many problems we must discuss.

2 MAJOR EXPERIMENTAL PROBLEMS

A well known problem is that of scale effects. A Reynolds number on the average chord of a large model might be as high as 10×10^6 (compared to a full scale Reynolds number of 50×10^6). However, the corresponding Reynolds number on the wing tip or the tailplane of the model may be only 2×10^6 , with all the local difficulties this may imply in achieving the best compromise on turbulent boundary layer thickness⁴.

For most wind tunnel experiments the importance of fixing transition to ensure fully turbulent boundary layers is accepted. However there is careful discussion about the best compromise (roughness, height and position) needed to provide the most representative boundary layer thickness to cover a range of conditions. The measurements of control hinge moment given here (Figs 14, 15 and 17) suggest that transition should always be fixed for control measurements at subsonic speeds. Unless the flow is fully laminar, increasing Reynolds number with free transition gives a thicker boundary layer at a trailing-edge control, caused by the forward movement of transition, rather than a thinner boundary layer as implied in Ref 5. In the author's view the advice given in Ref 5 to test with free transition is not well founded, and could produce errors.

A less widely appreciated problem is the correct representation at model scale of the gaps invariably found at full scale⁶; gap effects can be appreciably larger than those due to the inadequacies in the correct simulation of Reynolds number.

Tunnel interference often presents serious problems for control measurements, particularly at subsonic and transonic speeds. While wall corrections for a single aerofoil can be estimated to sufficient accuracy by Glauert's theory⁷, this theory breaks down for large flap deflections⁸.

Another problem is the assessment of the effects of static and aeroelastic distortion, both at model and full scale. These effects are particularly important for swept forward, composite wings⁹.

Modern military aircraft and missiles cover a wide flight envelope, including separated flows and transonic speeds. If control measurements are to be understood, extensive flow visualisation may be needed.

Despite these difficulties, aerodynamicists have been generally successful in predicting the static performance of aircraft controls, but rather less successful in predicting the dynamic performance. Here the emphasis is on unsteady measurements due to control surfaces, because these are more difficult and because of the author's personal interest.

Ideally force and pressure measurements should be regarded as complementary. However, there are serious difficulties in measuring forces at anything other than quasi-steady conditions. In contrast, recent advances¹⁰ allow the measurement of steady and unsteady pressures simultaneously, and this could offer many advantages for experiments with control surfaces.

The experimental techniques used to measure control forces are now discussed in conjunction with typical measurements.

3 CONTROL STEADY FORCES

3.1 Six component balance measurements

Force measurements with six component balances are essential to establish the basic longitudinal and lateral stability of an aircraft project. In principle these measurements also can give much useful information about control forces.

A good review of strain gauge balances is included in Ref 11. A description of more recent practice in the design and calibration of sting type balances is given by Dubois¹². Such balances are usually mounted inside the aircraft or missile model being tested. Careful design and precise machining allows the separation of model force and moment components, which are then measured using strain gauges. The paper discusses the use of finite element structural analysis to improve mechanical design and describes the need and means for minimizing thermal effects. The balances must be carefully calibrated to determine coefficients for the low level interactions between components. These may result from unavoidable imperfections in fabrication or strain gauge misalignment.

As an illustration of the value of control forces derived from internal strain gauge balance measurements, some control forces¹³ measured on a small model (1/48 scale) of a typical strike aircraft (Fig 2), at a Reynolds number of about $Re = 1.3 \times 10^6$ are discussed. Fig 2 shows the model/tunnel size ratios adopted to minimise the tunnel interference.

Fig 3 shows the rear fuselage of model and the aircraft, and the serious distortion necessary to accommodate the supporting sting. For this model the jet tube area was

carefully blended into the rear fuselage lines of the aircraft to produce a circular exit hole from the balance, but other compromises are often essential. Rear fuselage distortion is a serious problem when attempting to represent a twin jet aircraft like the present one. With large transport aircraft, which often have the jet engines mounted on the wings, precise measurements of tailplane effectiveness may demand the use of a special model eg a twin-boom support. This complication was not considered justified for the present configuration. The model was so small that different tailplane angles were provided by changing the tailplane inserts.

Fig 4 shows some measurements used to establish the basic longitudinal stability of the aircraft. Fig 4a shows typical curves of pitching moment coefficient v lift coefficient for the model without the tailplane and for the three tailplane inserts. From curves like these the tail-angles to trim for level flight at different altitudes and centre of gravity positions can be obtained (Fig 4b). In the present example the flight measurements of the tail angle to trim at sea level are in fair agreement with the estimates from the tunnel tests in the Mach number range from 0.70 to 0.85, suggesting that the effects of rear fuselage distortion were equivalent to a change in downwash angle of about 0.5° . These measurements were made with a model with 0.5% blockage in a slotted working section and were judged interference free up to a Mach number of about 0.99. However, the measurements at Mach numbers from $M = 1.02$ to 1.20 are certainly subject to some interference¹⁴, and are therefore shown dotted in Fig 4b. In general tunnel interference at transonic speeds is likely to be most serious at the tailplane position, when shocks from the nose of the model are reflected from the tunnel walls. Recent experience with the space shuttle suggests that more attention should be given to tunnel interference at transonic speeds¹⁵.

Fig 5 shows that the change in the tail angle to trim due to the extension of a pair of airbrakes fitted with strakes is about 2° , both in the tunnel and in flight. Hopefully an incremental comparison of this type should not be significantly affected by rear fuselage distortion or tunnel interference. If a smaller change in tail angle is required, this can be achieved readily by appropriate modification to the forward facing strakes. This was not attempted during the tunnel tests, because the strakes could be rapidly altered during the flight trials.

Fig 6 shows how the aileron effectiveness was established. On this small model a gap was provided at the inboard edge of the aileron and grooves were machined along the hinge line on both upper and lower surfaces of the steel wings (Fig 6a). For the initial measurements of longitudinal and lateral stability these grooves were filled with araldite. For tests of aileron effectiveness the araldite was removed and the ailerons were bent about the hinge line, using a special clamp. (This method can be used only once or twice, but does solve the problem of sealing the aileron hinge line.) Aileron rolling power was found to be proportional to the aileron deflection (Fig 6b), although at transonic speeds and high lift coefficients the aileron power was reduced by flow separations (Fig 6a). The rolling power measured in the wind tunnel is about 30% greater than that measured in flight. Differences of this magnitude or larger are often found in tunnel/flight comparisons³ and are consistent with estimated effect of static aeroelastic distortion on the aircraft.

3.2 Component balance measurements

On larger wind tunnel models it is often possible to incorporate component balances to measure static control forces or moments directly. This is particularly important for missiles, where there are often large mutual interactions between aerodynamic surfaces and where control hinge moments may be limited. Fig 7 shows some typical measurements at a Mach number of 2.8 the control normal force on a missile (Fig 7a) with four small rectangular controls immediately downstream of four slender wings¹⁶. The effect of the wing wake as it passes over the controls near zero incidence gives a sharp drop in effectiveness particularly for large control deflections (Fig 7b). Winter and Mills attempt to interpret the aerodynamics of this control and relate it to the flow field (Fig 7c). However the large number of combinations of missile attitude and control surface deflection inevitably generate an enormous volume of data, which is often presented without analysis. Ref 17 gives a more recent example of some of the problems encountered.

3.3 Pressure measurements

Steady pressure measurements are used, as a matter of routine, to provide loading information for aircraft designers and to verify theories. Steady pressure measurements can also give valuable detailed information about the static effectiveness of controls. A recent report by Manro indicates some of the typical problems, encountered when testing an arrow wing with leading and trailing-edge controls¹⁸.

One serious problem is maintaining an adequate seal along the hinge line. On this model a foam seal was fixed in the small gap between the flap brackets, whereas the flap brackets themselves locally sealed the hinge line (Fig 8a).

On this highly swept wing ($\Lambda = 71^\circ$) increasing the incidence provides a radical change in the type of flow, from being fully attached (at say $\alpha = 2^\circ$) to being dominated by a highly swept vortex (at $\alpha = 16^\circ$), as indicated by the contours of C_p (Fig 8b). These radical changes in pressure distribution can only be defined by providing large numbers of pressure orifices. On this model about 30 orifices were provided on seven spanwise stations, a total of 210 orifices. For trailing-edge controls it is desirable, but often difficult, to provide a pressure orifice at the trailing-edge. For the present

model at $\alpha = 16^\circ$ (Fig 8c) the trailing-edge pressure at $\eta = 0.50$ where the flow is still attached on the upper surface, can be inferred by extrapolation of the pressures measured on the upper and lower surfaces. However for $\eta = 0.65$, under the vortex where the flow is separated on the upper surface, the trailing-edge pressure cannot be defined in this way, and there is some uncertainty in the local load distribution, which would make a significant error in the estimation of the local hinge moment on the control. Ideally pressure orifices should always be closely spaced near the control hinge line, because of the singularity there in the potential flow.

3.4 Control measurements during spinning tests

Control effectiveness during spinning tests at high angles of incidence may be measured either by drop-model flight tests¹⁹ or by a model tested on a rotary balance in a wind tunnel.

A rotary balance measures the forces and moments acting on a model while it is subjected to steady rotational flow conditions. The historical background for this apparatus is discussed in Ref 20. A sketch of the apparatus²¹ in the Langley Spinning Tunnel, suitable for testing 1/5 scale models, is shown in Fig 9. Some details of the apparatus and some typical measurements on a model of the F-15 aircraft, covering an angle of incidence range from 8° to 90° , are given in Ref 22. Ref 23 gives some analysis of the measurements, which includes the effects of control deflections. Barnhart's description of the method used to establish the tare corrections with this apparatus is particularly interesting²².

The rotary balance at the NASA Langley Full Scale Tunnel can test even larger models, which can also be used for flight tests involving drop model techniques²⁴. Thus the aerodynamic data can be measured with the rotary balance at the same Reynolds number as in flight and the data used, together with conventional static force data involving control movements as inputs to theoretical spin prediction programmes for correlation with results of flight tests.

4 CONTROL UNSTEADY FORCES

Control unsteady forces are becoming of increasing importance, because many advanced aircraft designs involve some form of Active Control Technology (ACT). Typical applications of ACT include flight with 'relaxed' static stability margins (appropriate to low frequency rigid body modes of aircraft) or improvements in ride comfort (reduced responses at the higher frequency, structural modes of aircraft). This is the application illustrated in section 4.4.

4.1 Dynamic force balances and model requirements

Dynamic force balances are used to measure the total forces on rigid models when driven at low frequencies appropriate to aircraft rigid body modes. Controls are not normally represented on these models, apart from a control (either a tailplane or foreplane), which may be required to establish the longitudinal static trim of the model. Orlik-Ruckemann has given a comprehensive review²⁵ of the techniques used to determine dynamic stability parameters in wind tunnels, based on either forced or decaying oscillations. As Lambourne remarked²⁶ "when the model itself is moving, the force being measured will include contributions from the model inertia which are usually much larger than the aerodynamic force whose magnitude is to be determined. The aerodynamic force is thus obtained as the difference of two measurements, one wind-on and the other wind-off. For the difference to represent accurately the aerodynamic force it is necessary for the motion of model, including any elastic distortion, to be the same for the two measurements; if not additional inertial force will appear as a spurious aerodynamic force. Such changes in the mode of motion can be caused by the oscillatory aerodynamic force if the model is less than rigid under dynamic conditions. Hence while the measurement of unsteady aerodynamic forces may be possible at low frequencies, it becomes much more difficult at high frequencies".

It follows from these remarks that for unsteady force measurements at high frequencies, stiff, light models are required. Recent experience²⁷ suggests that stiff, light wind tunnel models can be made in carbon fibre. Carbon fibre provides a three-fold increase in the ratio of E/ρ as compared to steel. Hence a carbon fibre model, geometrically identical with a steel model, has modal frequencies about 1.7 times that of the steel model. Thus potentially carbon fibre models offer reduced dynamic aero-elastic distortion, which has many advantages, even when the unsteady aerodynamic forces are being determined by the integration of unsteady pressures (section 4.3).

4.2 Dynamic component force balances

Dynamic component force balances may be driven either by inexorable excitation or by a resonant system powered by a small exciter. An advantage of applying inexorable motion is the ability to control an unstable, or negatively damped, model. Also the model can be oscillated in a chosen motion and at any frequency and it is probably easier to detect and measure forces that are nonlinear. The principal disadvantage is the large excitation force that is needed and the massive construction that accompanies it. Both techniques have to solve the problem of separating the aerodynamic forces from the large inertial forces and resolving the aerodynamic forces into the various component derivatives but the methods of doing this are different.

A balance to measure the principal wing forces due to control surface motion is shown in Figs 10 and 11 and fully described in Ref 28. It supports a half-model at the wall of a tunnel, and an oscillatory motion can be imposed on the control surface by a vibrator connected to it through a push rod and shaft. The frame to which the model is attached is supported at three locations by strain gauge elements which measure the unsteady reactions. These, together with the measured excitation force, when operated upon by a set of dynamic calibration factors yield the oscillatory inphase and inquadrate components of lift, pitching moment and rolling moment. Hinge moment components are determined by a torque-measuring unit incorporated in the shaft driving the control surface (Fig 11).

The balance is suitable for tests in tunnels with working section areas up to about 1 m². It has operated satisfactorily at frequencies up to about 100 Hz using low aspect ratio models of rigid construction. Attempts to use this balance with a model of aspect ratio 6 clearly showed the difficulty of measuring unsteady forces on a model not having sufficient rigidity. The high aspect ratio model, shown later in Fig 22, is an example where the advantage lies with unsteady pressure, rather than force, measurements.

Fig 12 shows some measurements²⁹ of the total dynamic lift induced by an oscillating flap on the low aspect ratio wing. The lift derivative in phase with the motion (z_β) is only about 60% of that predicted by the linear theory of Ref 30 over the Mach number range from $M = 0.6$ to 0.9 . The measured lift in quadrature with the motion (z_β') does not even have the trend with Mach number predicted by the theory. Fig 13 shows similar evidence for the pitching moment. The position with regard to the flap hinge moment is even more unsatisfactory. Fig 14 shows that the hinge moment in phase with the motion ($-h_\beta$) decreases with Mach number, whereas the theory predicts an increase. In contrast, the hinge moment in quadrature with the motion ($-h_\beta'$) shows the correct trend against Mach number, but is only about 60% of that predicted. These anomalies on a simple configuration of 5% thickness/chord ratio were tentatively explained in Ref 29 in terms of a semi-empirical correction for aerofoil section and boundary layer effects together with a correction for wall interference. However both corrections were restricted to low frequency and to subcritical flow and would not be applicable to other configurations. Similar anomalies have been cited previously on a number of aerofoils, the measured forces being about 70% of those predicted³¹. For aerofoils the anomalies discussed are often attributed to the omission of wing and boundary layer thickness from the calculations and when these thicknesses are included some improvement is achieved³¹. Direct experimental evidence for boundary layer effects on wings with oscillating controls has recently become available (see section 4.3.2).

Fig 14 includes some interesting effects of the state of the boundary layer on the control hinge moments. These effects were observed in preliminary tests in a small wind tunnel²⁹. Considering first the stiffness derivative, with free transition this is appreciably higher at $p_t = 1.0$ bar than in the datum experiments (measurements in a larger tunnel with fixed transition). Then an increase in total pressure to $p_t = 1.8$ bar lowers the stiffness derivative because of the thicker boundary layer caused by the forward movement of transition. In contrast, with fixed transition the stiffness derivative is independent of total pressure, and a little lower than in the datum experiments. Considering the damping derivative, with free transition this is somewhat higher at $p_t = 1.0$ bar than in the datum experiment. An increase in total pressure to $p_t = 1.8$ bar produces a further increase. For this derivative the important factor is the change in phase angle caused by the variation in thickness of the time-dependent turbulent boundary layer. (See section 4.3.2 and Ref 27.) In contrast, with fixed transition the damping derivative is independent of total pressure, and in excellent agreement with the datum experiments. Hence a much more consistent set of measurements was achieved with fixed transition.

The discrepancies between theory and experiment shown in Fig 14 are so large that recently renewed efforts have been made in the United Kingdom to improve the methods of measuring dynamic hinge moments. Gaukroger *et al* showed³² that for a flap mounted on a spring of stiffness k_0 ,

$$-h_\beta = (\nu^2 - \nu_0^2)(I/\rho S \bar{c}^4) \quad , \quad (1)$$

and

$$-h_\beta' = 2(\nu\mu - \nu_0\mu_0)(I/\rho S \bar{c}^4) \quad , \quad (2)$$

where I = moment of inertia about flap hinge axis,

ρ = free-stream density,

S = flap area,

\bar{c} = flap chord,

ν and ν_0 = wind-on and wind-off frequency parameters, based on free stream velocity

and μ and μ_0 = wind-on and wind-off damping-% critical.

If the flap is free mounted on a bearing, the spring stiffness is zero and the total damping is small, so that equations (1) and (2) become

$$-h_\beta = \nu^2(I/\rho S \bar{c}^4) \quad (3)$$

and

$$-h_g = 2\nu u(I/\rho S \bar{C}^4) \quad (4)$$

Miles *et al* used this simple method³³ to determine the hinge moment coefficients at low speeds in a low turbulence wind tunnel on a flap fitted to a rectangular half model, mounted vertically (Fig 15). For lightness the control surface was manufactured from an aluminium tube around which spanwise unidirectional carbon fibre reinforced plastic (CFRP) strips were attached to provide bending stiffness. The trailing-edge was made of balsawood. Light alloy fittings were fixed into each end of the control so that it could rotate in close-tolerance ball races. The root end fitting was extended so that a small torque motor could be attached to oscillate the flap, if the turbulence level in the tunnel was insufficient to excite significant response. An accelerometer was glued at the root of the control to measure the response. The rotational inertia of the flap could be changed by altering the mass balances (Fig 15a).

Fig 15b shows that the stiffness derivative, h_g , falls rapidly as the Reynolds number increases from $Re = 0.25 \times 10^6$ to 0.50×10^6 , and then remains in good agreement with the theoretical value. The initial decrease may be attributed to the thickening of the turbulent boundary layer close to the control caused by the forward movement of transition, for transition was not fixed on this model. Fig 15c shows that the smaller damping derivative is also in good agreement with the theory. The agreement between the measured and estimated values of both derivatives is remarkable, because there was no seal between the wing and the control, whereas the theory assumes a perfect seal. This favourable result is in marked contrast to the measurements shown in Figs 14 and 17 and highlights the uncertainties in the estimation of hinge moments.

Although this method is simple, it does not allow the mean angle of the flap, or its amplitude, to be adjusted to particular values. These features are essential for measurements at transonic speeds, where nonlinearities occur frequently. Recently Jones has demonstrated a new method³⁴ which allows these parameters to be varied. The method used to oscillate the flap utilizes the end rotation of a propped-cantilever beam (Fig 16). The beam acts as the major stiffness component of the system and can be changed easily to alter the system frequency. A thin flexible tube is fitted as a seal between the control and the wing.

The control rod is attached rigidly to the simply-supported end of the beam. The flap oscillates when the beam is driven in its fundamental mode of vibration by an electromagnetic shaker connected to the root of the beam. The outer end of the control rod is supported by a spring steel cruciform strip, which provides vertical and horizontal rigidity, while being torsionally weak. This system uses steel flexures for bearings and thus should not produce variations in damping with applied load, as conventional bearings do.

Jones used an advanced 'frequency sweep' technique to determine the control frequency and dampings in 'wind-off' and 'wind-on' conditions according to equations (1) and (2). For this control both the stiffness and the damping derivatives were only about half the estimated value (Fig 17). Roughness sizes to fix transition at about $p_t = 0.5$ bar was applied close to the leading-edge of the model. This roughness would have been inadequate at the lower Mach numbers for $p_t = 0.23$, and this may explain the somewhat higher values of the stiffness derivative measured there, shown linked with a dotted line in Fig 17a. This is exactly the same trend shown in the low speed experiments with free transition (of Fig 15b above), and as observed in the review of Moore.

4.3 Unsteady pressure measurements

Unsteady pressure measurements can provide much detailed information about the dynamic effectiveness of controls, but they require special techniques for recording and analysis. Only a brief introduction can be given here; more details are given elsewhere^{26,35,36,37}.

4.3.1 Experimental techniques

The preferred method of making unsteady pressure measurements is with small transducers connected to surface orifices by the shortest possible passage (Fig 18). This method allows pressures to be measured simultaneously, so that integrations for lift and pitching moment, and the measurement of cross correlations are possible. (Use of specially designed amplifiers allows the steady and unsteady pressures to be recorded together¹⁰.) This method also allows pressure-time variations which are not sinusoidal (eg see section 4.3.3). Fig 18 shows several methods of installing a transducer within a model and connecting it to an orifice at the surface. In all cases a coating of silicone rubber or other slightly resilient substance is used to seal the body of the transducer in a hole only slightly larger than its diameter. It is obviously preferable for the orifice plugs, but not the transducers to be inserted into the model before finally machining the surface. The main requirements for good installation are:

the block into which the transducer is inserted should protect it from mechanical stress;

the volume of air at the face of the transducer and the length of the connecting passage between transducer and orifice should be as small as possible.

It is usually difficult to keep the connecting passage short when the orifice is near a trailing edge. When an arrangement, such as that shown in Fig 18d is used, it is important to test for unwanted transmission features. The disadvantage of this method is the cost of the required number of transducers and the complication of having to install them in a manner that allows their eventual recovery.

An alternative, cheaper method, essentially limited to sinusoidal pressure variations, uses small-bore tubing to transmit the aerodynamic pressures to a location, usually just outside the working section where they are measured. In this method it is economical to use one transducer and a pressure switch (a Scanivalve) to measure a number of pressures sequentially. The length of tubing means that the unsteady pressure measured by the transducer is not the same as the unsteady pressure acting at the orifice. The transfer function of such a typical system with a tube length of about 1 m is shown in Fig 19. There is usually good agreement between the transfer function calculated by theory³⁸ and that measured in a laboratory bench test. Unfortunately, as shown in Fig 20 the transmission characteristics change when there is a flow across the orifice and the effect increases with local Mach number. It is possible to make allowance for this effect but it requires at least one transducer to be installed in the model to allow calibration to be made under the flow conditions. Use of a tube system allows a stiff and relatively simple construction for the model. This method has been pioneered by the NLR, and used with great success by Tijdeman³⁹ for his classic measurements of control effectiveness on two-dimensional aerofoils at transonic speeds.

Calibration of both types of pressure measuring system is important because the final results and any comparisons with theory ultimately depend on it. The calibration should include the whole system as installed in the model, and, as far as possible, should be done under similar conditions to those obtaining during the actual measurements. Although it is possible for calibration to be based only on steady pressures it is preferable to make use of a device for generating oscillatory pressures. A hand-held instrument that can be moved across the model from orifice to orifice is shown in Fig 21. A rubber tube at the outlet allows the oscillatory pressure to be applied to the orifice of the transducer under test. Either a displacement transducer or a reference pressure depends on the thermodynamic behaviour of the enclosed air; this generally remains unknown so that the device cannot be regarded as an absolute standard. In practice the pressure generator itself is calibrated against an established reference transducer over a range of frequency. The reference transducer chosen for this task is judged to have a dynamic sensitivity identical to its static sensitivity which is measured against a pressure standard.

4.3.2 Pressures generated by an oscillating trailing-edge flap

The typical swept wing (RAE Wing A) shown in Fig 22 was used for an extensive series of oscillatory pressure measurements at subsonic and transonic speeds^{27,40,41}, using small transducers. Two main problems were encountered during these experiments²⁷. The first was the provision of an effective seal along the hinge line of the flap. The second problem was caused by the flexibility of the steel wing. Although for the improved model the light, stiff carbon fibre flap could be driven at frequencies as high as 300 Hz, the wing motion effectively still restricted the measurements to quasi-steady frequencies (1 Hz) and to an anti-resonance frequency between the first and second bending frequencies, at about 60 Hz and 200 Hz respectively. Making the model in carbon fibre would have raised these frequencies to about 102 Hz and 340 Hz. The anti-resonance frequency would then have been about 240 Hz.

Figs 23 and 24 illustrate the important influence of the boundary layer on the oscillatory pressures measured across the chord of a typical spanwise section $\eta = 0.60$ (section 3 of Fig 22). The measurements show both the modulus and the phase of the oscillatory pressures relative to the flap motion. In general, with the thin turbulent boundary layer at the hinge line allowed by free transition, the flap lift curve slope is significantly increased relative to the value with the thick turbulent boundary layer formed with fixed transition. Thus at $M = 0.80$ (Fig 23) the increase in flap lift curve slope produces a significant increase in the magnitude of the oscillatory pressures measured over the whole section. A similar increase was expected and observed in the quasi-steady measurements. However in addition with the thinner boundary layer there is a significant increase (about 60°) in the phase lag of the oscillatory pressures over the forward portion of the section, whereas over the central portion this increase is only about 30° . This change in phase angle was unexpected and is probably due to the displacement effect of the time-dependent turbulent boundary layer²⁷. Fig 22 also includes the predictions according to linearised theory⁴². Generally the magnitude of the vector is well predicted. Although upstream of $x/c = 0.60$ the predictions are in better agreement with the measurements made with transition fixed rather than with transition free, this should be considered fortuitous, because the theory takes no account of wing or boundary layer thickness. Close to the hinge line the predictions are, in fact, in better agreement with the measurements made transition free. It is important to recall that at $x/c = 0.30$ the local Mach number is 0.96, so that such good agreement is really surprising. As regards phase angles the theory predicts an oscillatory pressure at $x/c = 0.05$ which lags by about 50° . The pressure observed lags by about 60° . Similar discrepancies in phase angle are observed right across the section and must be attributed to the higher local velocities caused by the wing thickness.

When the wing flow is transonic, the pressures produced by oscillation of the flap are dominated by the type of shock wave/boundary layer interaction (Fig 24). Thus at $M = 0.90$, when transition is free, we have seen that the shock wave/boundary layer interaction is laminar and extends over a long portion of the chord (say from $x/c = 0.3$ to 0.6). The interaction causes large oscillatory pressures in this region in addition to the large

oscillatory pressures which would be expected in the subsonic portion of the flow field close to the hinge line. In marked contrast, with fixed transition the oscillatory pressures associated with the shock are somewhat smaller and concentrated about the mean shock position at $x/c = 0.3$. Downstream of the turbulent shock wave/boundary layer interaction the oscillatory pressures first fall rapidly and then increase towards the hinge line. The magnitude of this increase is quite small until the hinge line is approached, and its character resembles that observed in the same region at $M = 0.8$ (cf Fig 23). The measurements suggest that the flap lift curve slope is still appreciably higher with the thin turbulent boundary layer produced by free transition. In addition we notice that there is once again a significant change in phase angle, for upstream of $x/c = 0.5$ the transition free measurements lag behind those with transition fixed by about 10° to 20° . This lag is in the same sense as that observed at subsonic speeds (Fig 23). This again suggests that the lag is not primarily caused by a changed mean flow, but by a dynamic phenomenon associated with the significant change in the boundary layer thickness. The lack of agreement of these measurements made with transition fixed and free suggests that for transonic speeds transition should always be fixed a safe distance upstream of the maximum forward excursion of the oscillatory shock wave, rather than close to the leading edge, in an attempt to obtain aerodynamic characteristics appropriate to higher Reynolds number.

Boundary-layer thickness is likely to have a much greater influence on the characteristics of a trailing-edge flap on a thick supercritical wing, particularly when this operates close to separation. Hence, when testing supercritical wings with oscillating trailing-edge flaps, some boundary layer thickness variation should always be included as an aid to the assessment of full scale performance.

4.3.3 Pressures generated by a rapidly moving spoiler

A recent experiment, fully described in Ref 43, is now briefly discussed. This relates to rapidly operating a spoiler to 'dump' the lift developed when a wing encounters a severe 'design' gust. If successful this application of Active Control would improve the safety of an aircraft.

Project studies suggest that for effective gust alleviation spoiler deflections of 40° are required in 0.1 second (a spoiler rate of $400^\circ/\text{s}$). Higher rates of rotation are required on scale models, because aerodynamic delay times are directly related with the distance travelled by the wing, eg for extension of a spoiler $t_1 = n_1 c/u$, where n_1 is a dimensionless constant appropriate to the particular time delay t_1 . Hence for similarity on a 1/10 scale model, 40° spoiler movement will be required in 0.01 second (a spoiler rate of $4000^\circ/\text{s}$). This extreme requirement was met by the development of special hydraulic equipment⁴⁴.

Fig 25 shows some typical measurements at subsonic speeds of the lift developed on this model as a function of the spoiler deflection, δ , for both static and dynamic conditions. For static deflections, the lift is unaltered for the range of δ from 0 to 5° . This region corresponds with the formation of a local bubble downstream of the spoiler, with reattachment upstream of the trailing-edge. From the range from $\delta = 5^\circ$ to 30° the lift decreases linearly. This characteristic is typical of most spoiler configurations. For rapid extensions of the spoiler the results are completely different. The spoiler lift first *increases*, owing to the continued reattachment of the flow downstream of the spoiler and the development of a strong vortex. This is an 'adverse lift' effect, which would increase the load due to a gust. In fact the lift does not return to its original value until about $\delta = 17^\circ$, and then decreases gradually as the flow separates and a long bubble develops. For rapid retraction of the spoiler the differences from the static curve are much less dramatic. We may visualise lift increasing steadily as the bubble is swept away downstream. The transient measurements in Fig 25 form a 'hysteresis' loop about the static measurements, recalling the type of hysteresis loop often observed on aerofoil sections.

Inevitably Fig 25 gives an incomplete view of the transient aerodynamics of the spoiler, for it does not include any variation of spoiler rate or freestream velocity. For subsonic speeds, dimensional analysis⁴³ suggests that the measured aerodynamic time delays should be expressed in terms of the time taken to move the spoiler, and should be functions of the aerodynamic times UT/c . For spoiler extension an excellent correlation of the measured time delays for the adverse and final lift is obtained using this parameter for Mach numbers from $M = 0.25$ to 0.70 at both spoiler rates used in the tests (Fig 26a). The magnitude of the adverse lift coefficient is also correlated by this parameter. Plainly the adverse lift effect will be significant at full scale spoiler rates of $400^\circ/\text{s}$, which corresponds roughly with $UT/c = 5$. For spoiler retraction a good correlation of the much smaller time delays is also obtained (Fig 26b). Fig 27 compares two subsonic time histories for spoiler extension and retraction, chosen to have the same value of $UT/c = 5$ by appropriate choice of U and T . Good agreement is obtained, particularly for the extension of the spoiler, despite the differences in Mach number, Reynolds number and shape of the spoiler time history.

Although the present measurements are restricted to zero wing incidence there is evidence (reviewed in Ref 43) to suggest that the time delays would not be greatly affected by the wing lift coefficient. In particular, Hoerner's measurements in a water tunnel at a $C_L = 1.0$ are in good agreement with the present tests (Fig 26a). Although static deflection of the spoiler creates local high frequency pressure fluctuations (on the upper surface downstream of the hinge line), there is no significant response (buffeting) at the first wing bending frequency.

4.4 Reduction of response to turbulence by active control

The flexibility of the steel model of RAE Wing A allows it to respond, not only to the harmonic pressures produced by the oscillation of the trailing-edge flap, but also to the random flow unsteadiness in the wind tunnel (section 4.3.2). The main response due to the flow unsteadiness was at the fundamental and overtone bending frequencies, which were well separated at 60 and 208 Hz respectively. The trailing-edge flap could be driven at frequencies up to 300 Hz and hence it was considered possible to reduce the responses in both modes by the choice of appropriate control laws. In a successful preliminary experiment⁴⁵ only the response in the first mode was considered, but this was decreased by approximately 90% without any significant variation in the response of the other modes.

The principle of the Active Control System adopted is illustrated in Fig 28. First the 'open loop' transfer function between the flap and the wing motion is determined over a narrow range of frequencies around the fundamental frequency. The model drive and the Transfer Function Analyser are both computer controlled to reduce tunnel running time. This measurement must be made for every combination of Mach number, M , and kinetic pressure, q , of interest. The 'open loop' transfer function provides a reliable initial guide to the choice of an appropriate phase angle to give viscous (velocity) damping in the 'feed back' control circuit. The model accelerations produced by flow unsteadiness are integrated, passed through a narrow band-pass filter (set at the fundamental bending frequency) and a variable gain control. The gain is cautiously increased until minimum response is achieved. Further increases in gain produce rapid increases in model response, probably because the feed-back circuit then operates on low level, harmonic electronic noise, rather than on the small random aeroelastic response of the model.

Fig 29 illustrates some typical results for $M = 0.80$ with the Active Control circuit 'off' and 'on'. Fig 29a shows a large reduction in response close to the wing tip at the fundamental frequency, together with a small reduction in the over-tone bending mode. Fig 29b shows the corresponding reduction in pressures measured at one point. The pressure spectra are virtually identical, except at the wing bending frequency, where there is a marked reduction with active control, due to the reduced wing response.

The reductions obtained at transonic speeds are particularly noteworthy, because here the phase angle between the wing tip accelerometer and the flap force suddenly changes by nearly 180° compared to the measurements at subsonic speeds ($M = 0.45$ to 0.97) and at $M = 1.25$ (Fig 30). The phase angle between the flap displacement and the flap force only varies a little, so that control reversal does not occur. Hence the reversal in phase angle observed was attributed to a change in the sign of the aerodynamic damping in the first bending mode, probably caused by a separation at the wing tip in this speed range. The sudden change in phase angle shown in Fig 30 implies that at higher total pressures there would be a danger of single degree of freedom flutter in this mode, just above a free-stream Mach number of 1.

This simple method of reducing the response to turbulence has many advantages. The open loop characteristic is directly measured with the actual boundary layer thicknesses on the model, and any gap effects which are present. In principle the same method could be applied in flight although different transfer functions would be inevitable because of differences in boundary layer thickness, gap effects aero-elastic distortion and the wing frequency parameter. The main restrictions of the method are that both the structure and the aerodynamics must be linear and that the modes must be well separated. The principle of superposition was shown to be valid (at least for flap amplitudes of about 1°) in a previous experiment⁴⁰. Hence with the feed-back circuit in operation, the flap can be driven at the required frequency, and the wing pressures at that frequency can be measured (cf the examples cited in Ref 45).

Preliminary studies using the rms tip accelerations suggest that a maximum flap amplitude of about 5° would be required in a heavy buffeting condition produced by local flow separations on the wing, assuming that the control effectiveness remains close to the zero lift value. This amplitude is well within the capability of the present electro-magnetic drive system, for the model first bending frequency. However, a much stiffer model would be required to carry the load. Other recent examples of the use of ACT in wind tunnel experiments were given by Destuynder⁴⁶.

5 CONCLUSIONS

This review of experimental methods to assess control effectiveness in wind tunnels has suggested five main conclusions:

- (1) Boundary layer transition should be fixed, and some variation of Reynolds number achieved.
- (2) Gaps in control surfaces should be carefully represented.
- (3) Tunnel and sting interference must be minimised.
- (4) Effects of aeroelastic distortion should be considered, both at model and full scale.
- (5) Flow visualisation should be used to help explain variations in control effectiveness, particularly for separated flows.

The effects of controls on aircraft buffeting have not been discussed in this paper. In the author's view much more effort should be applied to this question, particularly when developing high lift systems for low speeds.

6 Acknowledgments

The author wishes to thank his colleagues in RAE for providing unpublished data for this paper^{33,34}. He wishes also to thank Mr N.C. Lambourne for permission to quote from Ref 26.

REFERENCES

1. P.E. Garber, "The Wright Brothers contribution to airplane design", Ed J.D. Pinson, In Diamond Jubilee of Powered Flight, 1978
2. F.J. Hooven, The Wright Brothers flight-control system canard configuration, Scientific American, Vol 239, November 1978, pp 166-168, 170-178
3. A.J. Ross and H.H.B.M. Thomas, A Survey of experimental data on the aerodynamics of controls, in the light of future needs, Paper 2 of AGARD CP 262, May 1979
4. A.B. Haines, Possibilities for scale effect on swept wings at high subsonic speeds, Paper 14 of AGARD CP 83, April 1971
5. A.W. Moore, Scale effects on oscillatory control surface derivatives, ARC CP 1151 (1969)
6. H. Försching, Some remarks on the unsteady airloads on oscillating control surfaces in subsonic flow, Paper 10 of AGARD CP 296, September 1980
7. H. Glauert, Wind tunnel interference on wing bodies and airscrews, R&M 1566, September 1933
8. O de Vries and G.J.L. Schipholt, Two dimensional tunnel wall interference for multi-element aerofoils in compressible flow, Paper 20, AGARD CP 174, October 1975
9. T.J. Hertz, M.H. Shirk and R.H. Ricketts, On the track of practical forward-swept wings, Astronautics and aeronautics, January 1982, pp 40-52
10. B.L. Welsh and C.R. Pyne, A method to improve the temperature stability of semiconductor strain gauge pressure transducers, RAE Technical Report 77155 (1977)
11. A. Pope and K.L. Goin, High-speed wind tunnel testing, Chapter 7 - Force and moment measuring devices, pp 242-283, John Wiley 1965
12. M. Dubois, Six component strain gauge balances for large wind tunnels, Experimental Mechanics 21/11, pp 401-407, November 1981
13. D.G. Mabey and G.P. Illot, RAE Unpublished.
14. F. O'Hara, L.C. Squire and A.B. Haines, An investigation of interference effects on similar models of different size in various transonic tunnels in the UK, RAE Technical Note Aero 2606, February 1959
15. J.M. Underwood and D.R. Cooke, A preliminary correlation of the orbiter stability and control characteristics from the first two space shuttle flights (STS 1 and 2) with pre flight predictions, AIAA 82-0564, March 1982
16. K.G. Winter and S.M. Mills, Characteristics of aft mounted all moving rectangular control surfaces on a slender cruciform model at Mach numbers from 0.6 to 2.8, ARC CP 1011, 1968
17. W.D. Washington and D.J. Spring, An experimental investigation of wing-tail interference on a typical supersonic missile, AIAA 82-1339, August 1982
18. M.E. Manro, Transonic pressure measurements and comparisons of theory to experiment on three arrow wing configurations, NASA CR 3434, February 1982
19. J.R. Chambers and K.W. Iliff, Estimation of dynamic stability parameters from drop model tests, Paper 11, AGARD LS 114, March 1981
20. W. Bihrlé and V.S. Bowman, The influence of wing, fuselage and tail design on rotational flow, J. Aircraft, Vol 18, November 1981
21. W. Bihrlé, R.S. Hultberg and W. Mulcay, Rotary balance data for a typical single-engine low wing general aviation design for an angle of attack range of 30° to 90°, NASA CR 2972, 1978
22. B. Barnhart, F-15 rotary balance data for an angle of attack range of 8° to 90°, NASA CR 3478, May 1982
23. B. Barnhart, Analysis of rotary balance data for the F-15 aircraft, including the effect of conformal fuel tanks, NASA CR 3479, 1982

24. J.R. Chambers and J.S. Bowman, Stall/spin techniques used by NASA, AGARD CP 199, Paper 13 1975
25. K. Orlik-Rückemann, Review of techniques for determination of dynamic stability in wind tunnels, Paper 3, AGARD LS 114, May 1981
26. N.C. Lambourne, Experimental techniques in unsteady aerodynamics, Paper 10, AGARD R679, May 1980
27. D.G. Mabey, B.L. Welsh and B.E. Cripps, Further aerodynamic characteristics of moving trailing-edge controls at subsonic and transonic speeds, RAE Technical Report 80134 (1980)
28. K.C. Wight and N.C. Lambourne, A control-surface oscillatory derivative rig for use with half models in high-speed wind tunnels ARC CP 1353 (1976)
29. N.C. Lambourne, K.C. Wight and B.L. Welsh, Measurement of control surface oscillatory derivatives on a sweptback, tapered model wing in two transonic tunnels, R&M 3806, 1976
30. D.E. Davies, Calculation of unsteady generalised airforces on a wing oscillating harmonically in subsonic flow, R&M 3409, 1963
31. H. Tijdeman, High subsonic and transonic effects in unsteady aerodynamics, NLR TR 75-079U, May 1975
32. D.R. Gaukroger, D.A. Drane and R. Gray, A technique for measuring oscillatory aerodynamic hinge moments from forced response characteristics, ARC CP 1253 (1973)
33. C.J.W. Miles, D.A. Drane and S.A. Canham, On the Wind tunnel measurement of oscillatory control hinge moment derivatives, RAE Unpublished, April 1981
34. R.T. Jones, An experimental determination of transonic hinge moment derivatives, RAE Technical Report to be issued
35. J.J. Horsten, Recent developments in the unsteady pressure measuring technique at NLR, NLR MP 81055U, October 1981
36. J.W.G. van Nunen, Notes concerning testing time requirements in steady and unsteady measurements, Paper 2 AGARD R615, June 1974
37. B.L. Welsh and D.M. McOwat, Presto - a system for the measurement and analysis of time dependent signals, RAE Technical Report 79135 (1979)
38. H. Bergh and H. Tijdeman, On the influence of the main flow on the transfer function of tube transducer systems used for unsteady pressure measurements, NLR MP 72023U (1972)
39. H. Tijdeman, Investigations of the transonic flow around oscillating airfoils, NLR TR 77-090U
40. D.G. Mabey, D.M. McOwat and B.L. Welsh, Aerodynamic characteristics of moving trailing-edge controls at subsonic and transonic speeds, Paper 20, AGARD CP 262, May 1979
41. D.M. McOwat, B.L. Welsh and B. Cripps, Time-dependent pressure measurements on a swept wing with an oscillating trailing-edge flap, RAE Technical Report 81033 (1981)
42. W.R. Marchbank, Evaluation of pressure distributions on thin wings with distorted control surfaces oscillating harmonically in linearised compressible subsonic flow, R&M 3783, 1978
43. D.G. Mabey, B.L. Welsh, G. Stott and B.E. Cripps, The dynamic characteristics of rapidly moving spoilers at subsonic and transonic speeds, RAE Technical Report 82109 (1982)
44. G. Stott and C.R. Pyne, RAE Technical Report in preparation
45. B.L. Welsh and B.E. Cripps, The reduction by active control, of the turbulence response of a swept wing model at subsonic and transonic speeds, RAE Technical Report 81136, (1981)
46. R. Destuynder, Problèmes d'aérodynamique instationnaire posés par l'utilisation des gouvernes dans le control actif, Paper 18, AGARD CP 262, May 1979

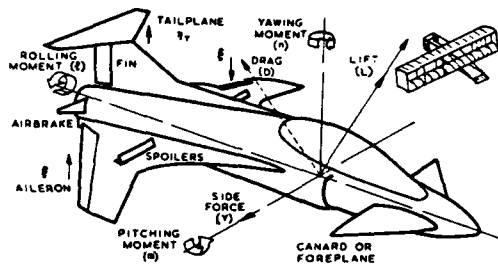
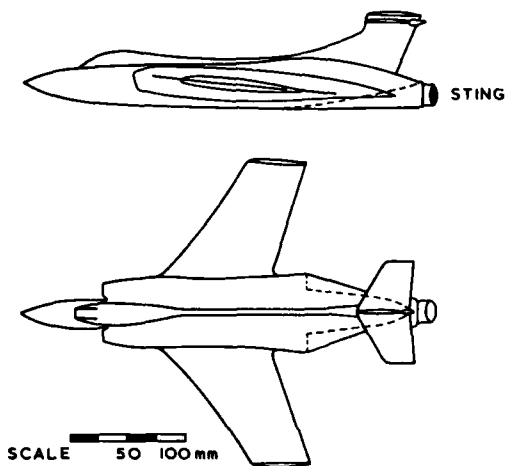
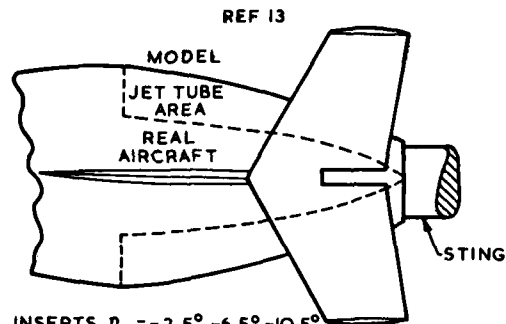


Fig 1 Definitions of positive forces and moments



TUNNEL INTERFERENCE		
CRITERIA	MODEL	RECOMMENDED
$2s/b$	0.30	≤ 0.4
$2s\bar{c}/bH$	0.024	≤ 0.15
BLOCKAGE	0.005	≤ 0.01

Fig 2 Typical wind tunnel model



INSERTS $\eta_T = -2.5^\circ, -6.5^\circ, -10.5^\circ$
 INSERT $\eta_T = -2.5^\circ$ SHOWN

0 10 20 30
mm

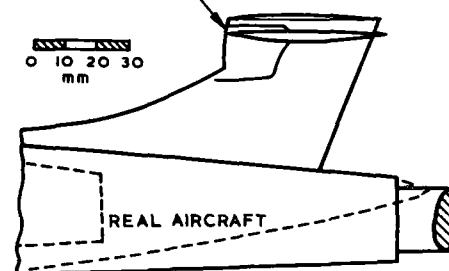
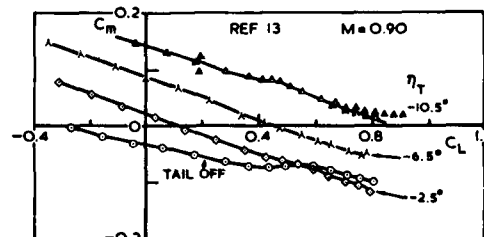
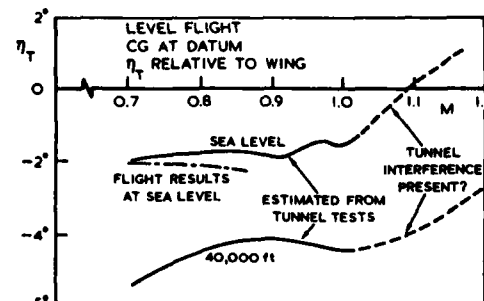


Fig 3 Rear fuselage distortion with internal 6 component strain gauge balance



(a) PITCHING MOMENTS v LIFT COEFFICIENT



(b) TAIL ANGLE TO TRIM v MACH NUMBER

Fig 4 Longitudinal static stability and transonic tunnel interference

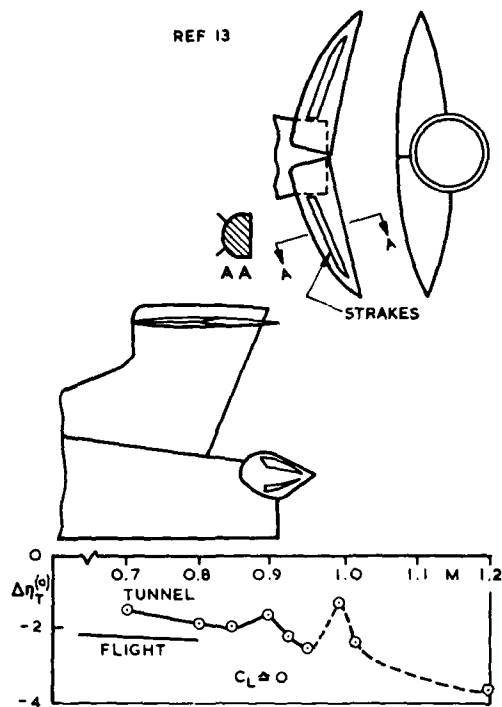
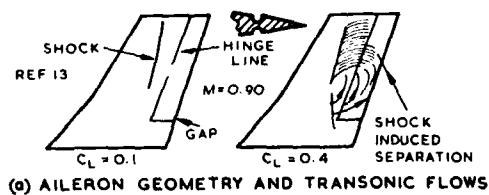


Fig 5 Change in tail angle to trim due to airbrakes



(a) AILERON GEOMETRY AND TRANSONIC FLOWS

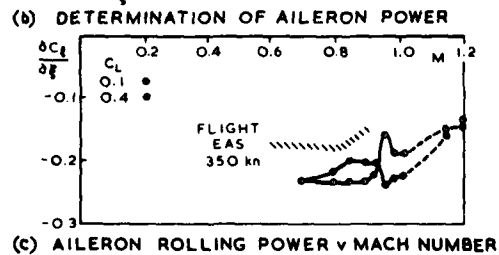
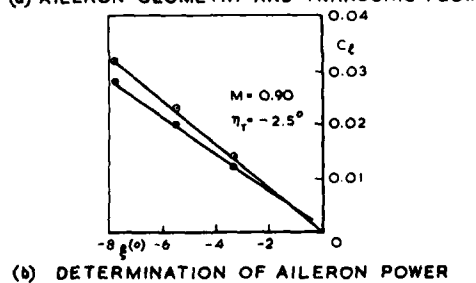
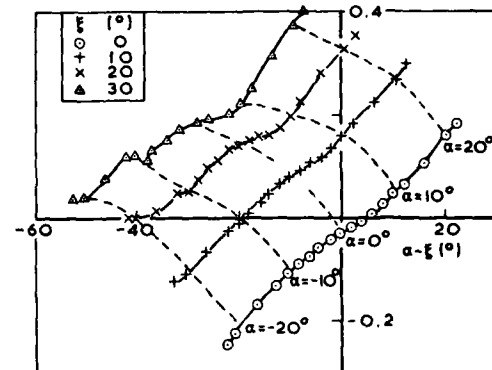


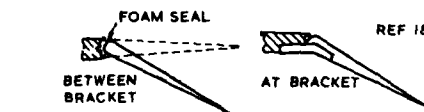
Fig 6 Aileron effectiveness



(a) MISSILE



(b) CONTROL PANEL NORMAL FORCE (ZERO ROLL)

(c) FLOW DIRECTIONS AT CONTROL (ZERO ROLL $\alpha = 20^\circ$)Fig 7 Problems of missile controls ($M = 2.8$)

(a) FULL SPAN TRAILING EDGE FLAP

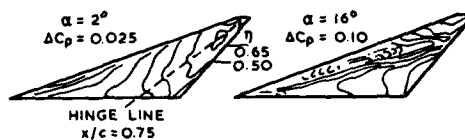
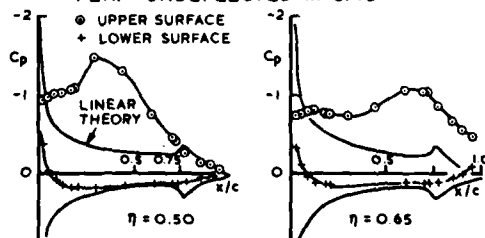
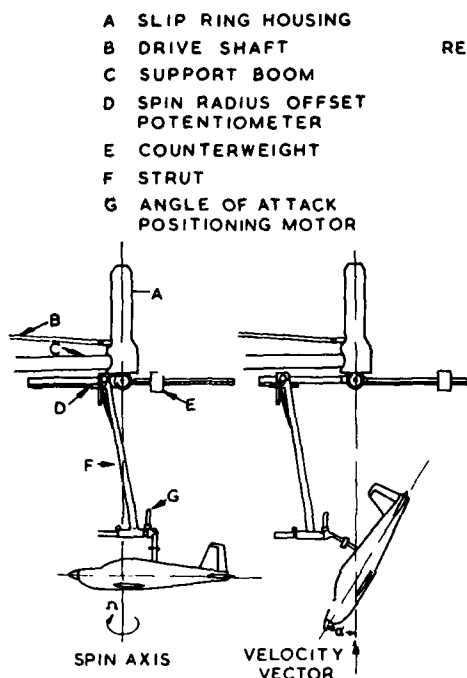
(b) UPPER SURFACE PRESSURES FLAP UNDEFLECTED $M=0.40$ (c) TYPICAL SPANWISE PRESSURE DISTRIBUTIONS $M=0.40$, $\alpha = 16^\circ$ FLAP DEFLECTED 8°

Fig 8 Pressure plotting to determine static control effectiveness



(a) SIDE VIEW OF MODEL

Fig 9 Sketch of rotary balance apparatus

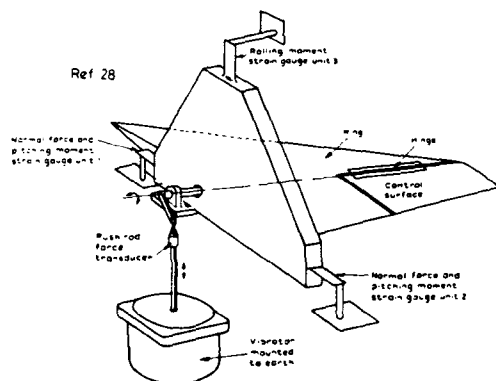


Fig 10 Force measuring system (schematic)

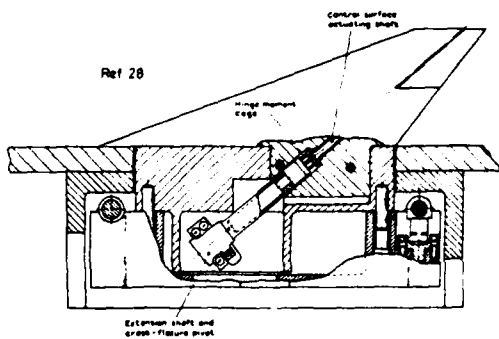
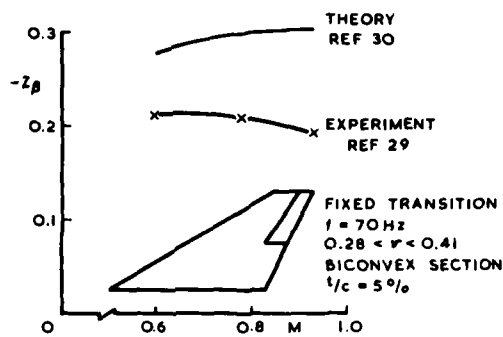
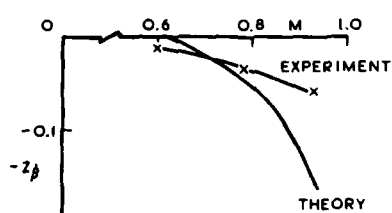


Fig 11 Details of wing mounting and control surface drive

REF 21

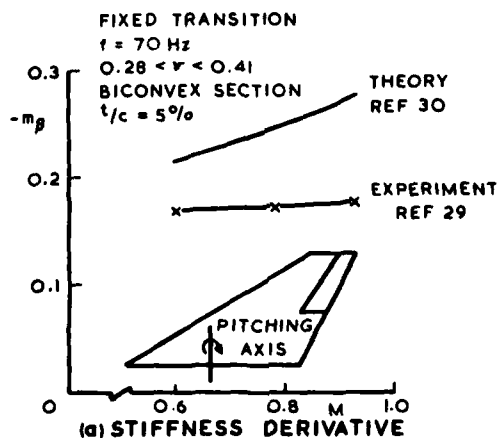


(a) STIFFNESS DERIVATIVE

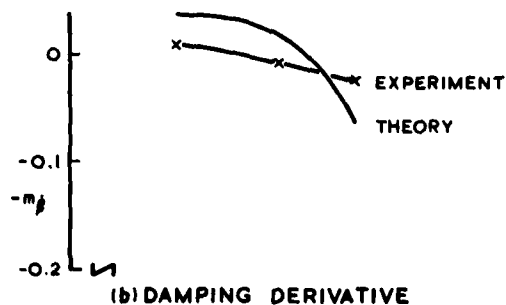


(b) DAMPING DERIVATIVE

Fig 12 Lift due to oscillating flap v Mach number



(a) STIFFNESS DERIVATIVE



(b) DAMPING DERIVATIVE

Fig 13 Pitching moment due to oscillating flap v Mach number

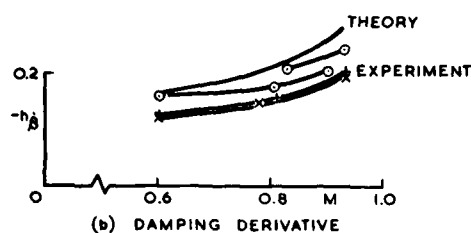
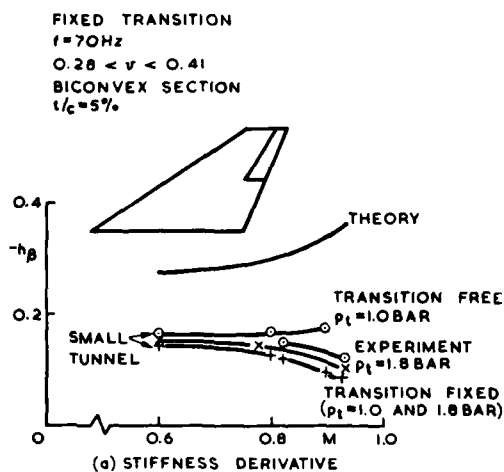


Fig 14 Hinge moment due to oscillating flap v Mach number

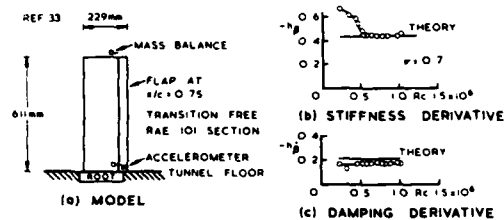


Fig 15 Simple method of measuring oscillatory control hinge moments

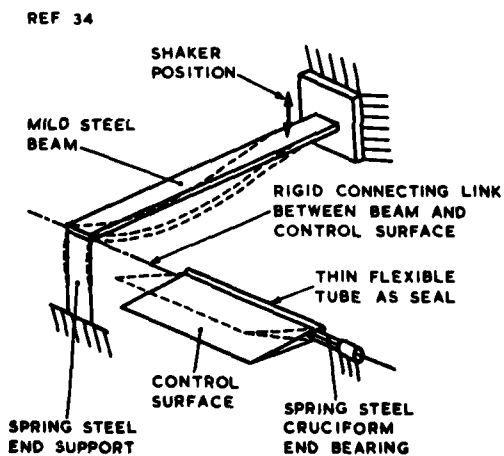


Fig 16 System for oscillating the control surface

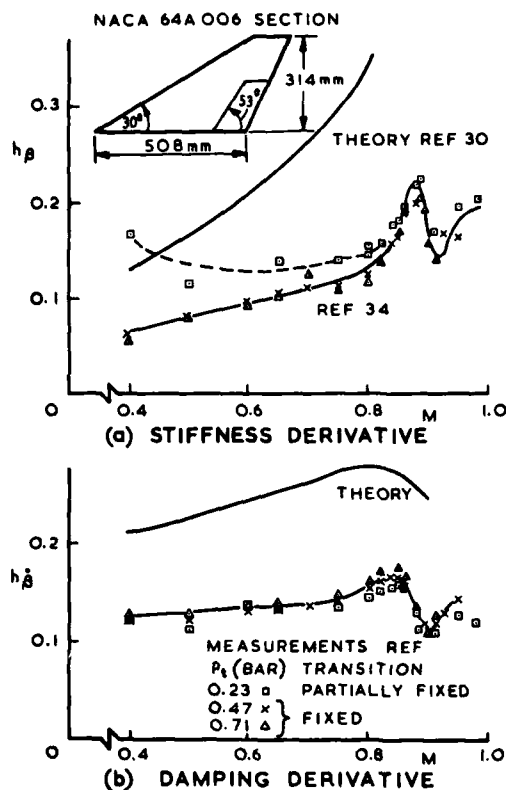


Fig 17 New measurements of oscillatory control hinge moments

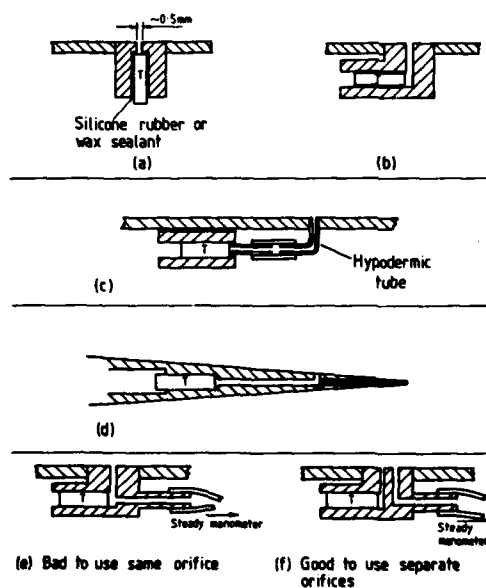
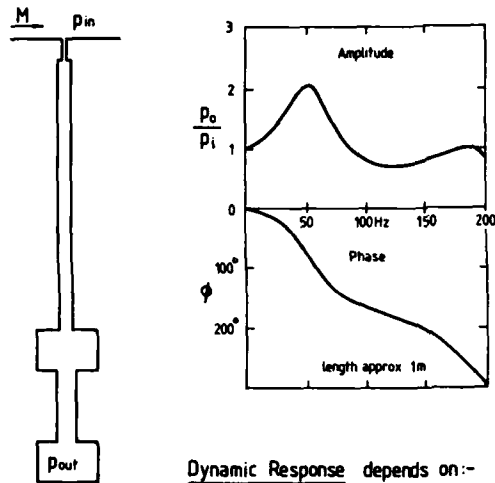
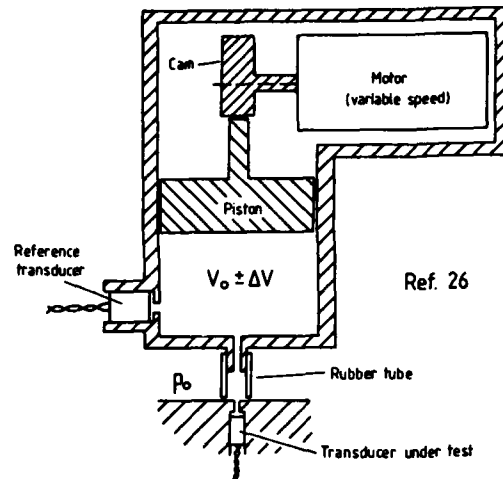


Fig 18 Installation of pressure transducers (Ref 26)



Dynamic Response depends on:-
 Tube length, diameter, volumes.
 Air density, temperature.
 Tangential flow Mach number.

Fig 19 Dynamic response of a long tube for small amplitudes



Oscillatory pressure $\approx \Delta p \sin \omega t$

$$\Delta p \approx \frac{P_o \Delta V}{V_o} \times \begin{matrix} 1.0 \text{ for isothermal} \\ 1.4 \text{ for adiabatic} \end{matrix}$$

Fig 21 Oscillatory pressure generation

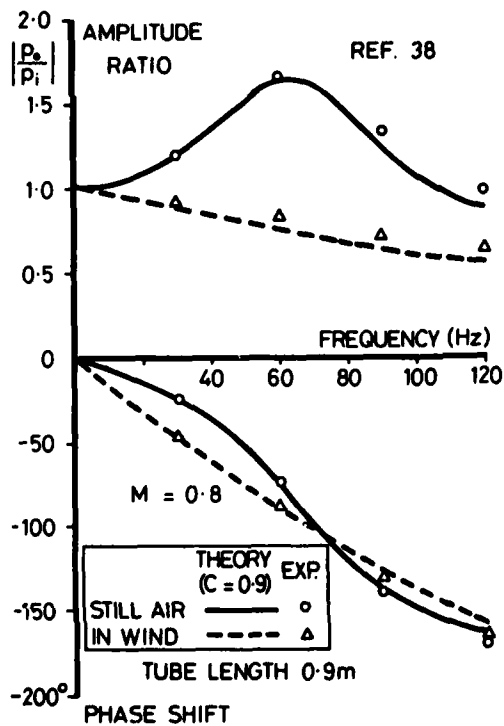


Fig 20 Effect of flow on transfer function of tube

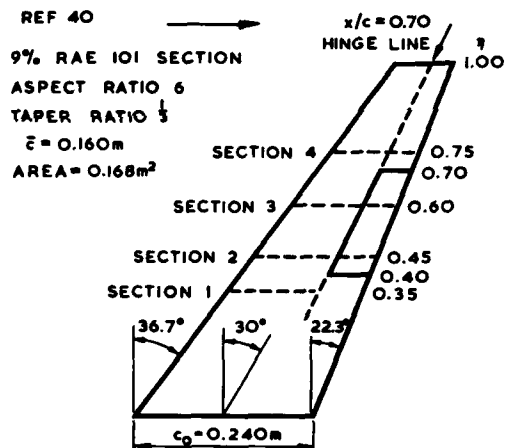


Fig 22 RAE Wing A. Pressure distributions at sections 1 to 4 measured with oscillating trailing-edge flap

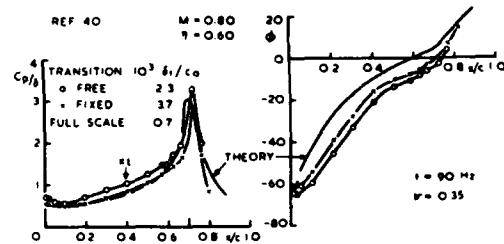


Fig 23 Magnitude and phase of subsonic pressure distribution

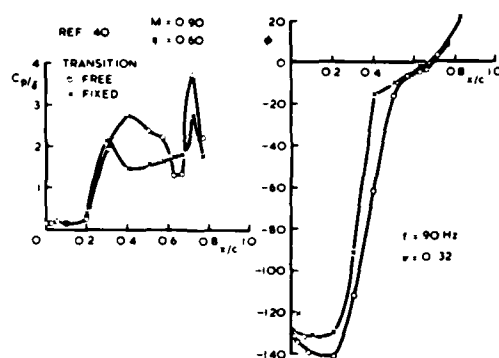


Fig 24 Magnitude and phase of transonic pressure distribution

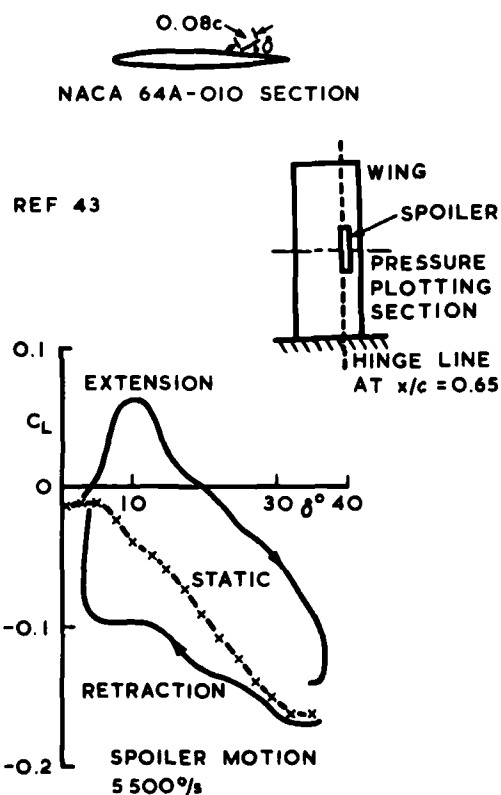
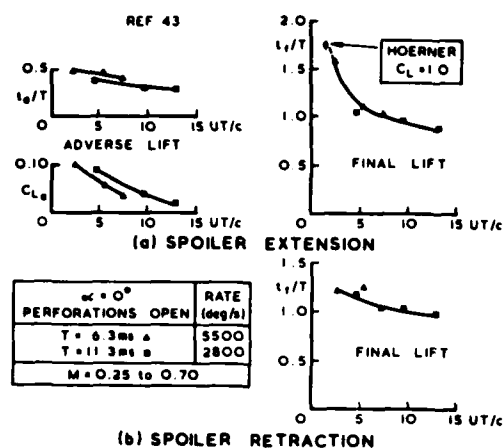
Fig 25 Lift v spoiler deflection for static and dynamic motion
 $M = 0.50, \alpha = 0^\circ$ 

Fig 26 Correlation of aerodynamic delays for spoiler movement

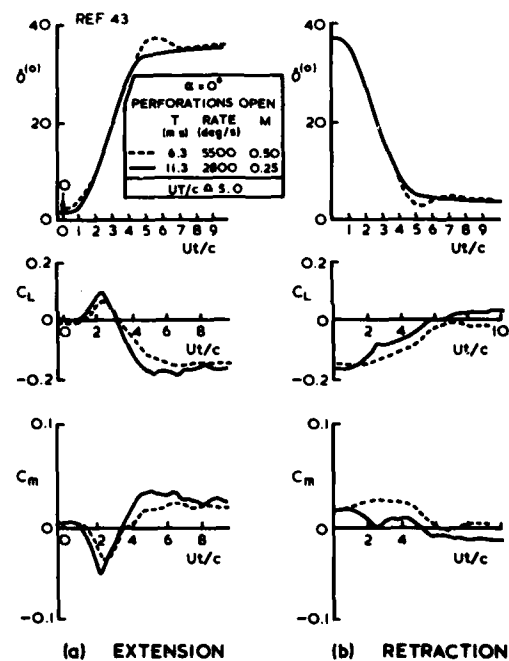


Fig 27 Correlation of subsonic time histories

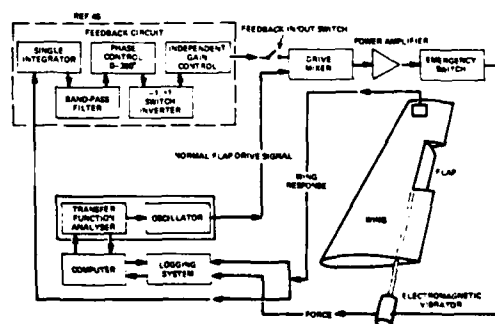


Fig 28 Principle of active control drive system

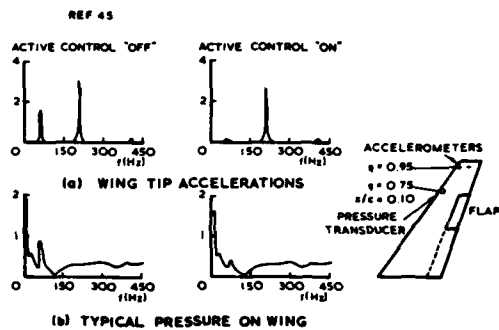


Fig 29 Typical effectiveness of active control
($M = 0.80$, $p_t = 0.94$ bar)

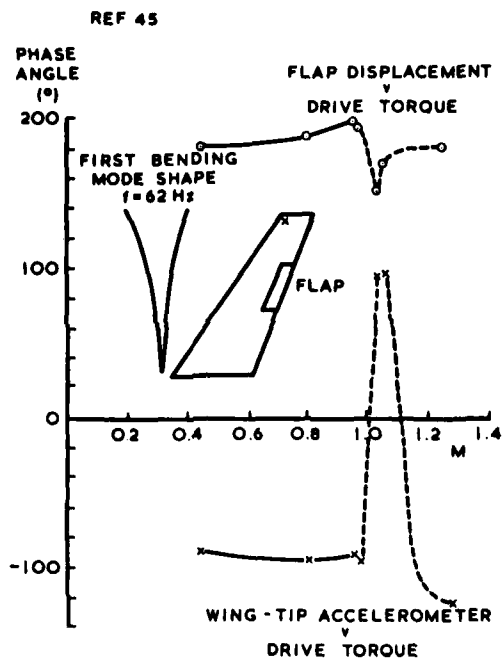


Fig 30 Phase angles of open loop transfer function at wing first bending frequency

**CONTROL OF THE FOREBODY VORTEX ORIENTATION BY ASYMMETRIC AIR
INJECTION: (PART A) APPLICATION TO ENHANCE DEPARTURE/SPIN
RECOVERY OF FIGHTER AIRCRAFT AND (PART B) DETAILS
OF THE FLOW STRUCTURE**

by

A.M. Skow, Manager, F-5 Aerosciences
Northrop Corporation, Aircraft Division
One Northrop Avenue, Hawthorne, California 90250

D.J. Peake, Senior Research Scientist
NASA Ames Research Center
Moffet Field, California 94035

CONTENTS

A.	Application to Enhance Departure/Spin Recovery of Fighter Aircraft	A.5	Preliminary Assessment of Design Feasibility
A.1	Introduction	A.6	Conclusions and Recommendations
A.2	Background	B.	Details of Flow Structure
	A.2.1 Forebody Flowfields at High Angles of Attack	B.1	Introduction
	A.2.2 Asymmetric Vortex Control		B.1.1 Asymmetric Vortex Wake About Forebody at Incidence
	A.2.3 Previous Research		B.1.2 Control of Asymmetric Vortices
	A.2.4 Present Studies	B.2	Experimental Results and Discussion
A.3	Experimental Apparatus and Test Program		B.2.1 Structure of Asymmetric Vortex Wake
	A.3.1 Water Tunnel Tests		B.2.2 Control by Blowing of Asymmetry in the Leeward Flow
	A.3.2 Wind Tunnel Tests	B.3	Conclusions
A.4	Discussion of Results	C.	Reference
	A.4.1 Water Tunnel Tests		
	A.4.2 Wind Tunnel Tests		
	A.4.3 Six-Degree-of-Freedom Simulation		

SUMMARY

This paper describes a novel concept which has been developed to provide powerful directional control effectiveness for a fighter aircraft at high angles of attack, where more traditional controls have very limited capability. The concept utilizes the energy concentrated in the strong forebody vortices (which form on slender bodies at high relative incidence) by controlling the lateral orientation of the vortices with respect to the body.

A large volume of research which has been performed in recent years to attenuate the magnitude of the asymmetric forces and moments on slender bodies such as those on missiles and some fighter aircraft. This body of work showed that the forebody vortices on these configurations are very sensitive to small disturbances in the flow, such as would be caused by asymmetric surface imperfections on a body, especially near the apex of the nose.

The present concept grew out of this more general body of work and seeks to utilize the inherent sensitivity of the vortex positioning and its bi-stable nature to an advantage allowing control of the forces which are developed. As it turns out, the direction or sense of the asymmetric vortex pair is much easier to control than to attenuate.

Part A of this paper describes the work which was done to develop the concept for application to an aircraft and, as such, is directed toward the effects of the concept on aircraft forces and moments and on the flight mechanics of the aircraft during maneuvering at high angles of attack.

The objective of this part of the study was to utilize the side force associated with asymmetric vortices, in a controlled manner, to enhance the ability of the fighter to recover from a departure from controlled flight. The results from these water tunnel and wind tunnel experiments show that a small amount of tangential blowing along the forebody near the apex can effectively alter the forebody vortex system and generate large restoring yawing moments. Six-degree-of-freedom digital simulation results show that this concept can substantially enhance departure recovery characteristics of fighter aircraft with long, slender forebodies.

Part B of the paper describes the results of experiments which were conducted on a cone model, where the principal test objective was to develop an understanding of the fluid mechanics involved in the process of vortex control. Knowledge gained in these more generic tests should allow the concept to be applied to a wider range of configurations.

NOMENCLATURE

A1	primary attachment line	S1	primary separation line
A2	secondary attachment line	S2	secondary separation line
$C_p = \frac{P - P_\infty}{q_\infty}$	static pressure coefficient	\tilde{x}	longitudinal position (from apex)
C_{YB}	side force coefficient from balance	Y_d	nozzle lateral offset
C_{YP}	side force coefficient from integrated surface pressures at $\tilde{x}/l = 0.87$	α	angle of attack, angle of incidence
C_μ	blowing moment coefficient	$\tilde{\alpha} = \alpha/\alpha_c$	relative incidence
d	base diameter of forebody	α_T	threshold angle of attack
i	axial length of forebody	β	sideslip angle
l/d	forebody fineness ratio	θ_c	semi-angle at apex of forebody
M_∞	free-stream Mach number	θ_n	nose semi-apex angle
q_∞	free-stream dynamic pressure	ϕ	circumferential angle around cone surface, measured from windward generator: negative on port side
Re	Reynolds number	ϕ_j	jet position
r_n/d	nose bluntness	ϕ_R	forebody roll angle (with roll degree of freedom)

A. APPLICATION TO ENHANCE DEPARTURE/SPIN RECOVERY OF FIGHTER AIRCRAFT

A.1 INTRODUCTION

For fighter aircraft that operate in the air combat maneuvering (ACM) arena, flight at high angles of attack (AOA), near the limits of controllability, is an inherent part of both offensive and defensive maneuvering. Reluctance to operate in this regime because of possible departure from controlled flight limits the capability of the man-machine combination to deliver its maximum performance. Pilot confidence is the key to effectively operating close to control boundaries, and pilot confidence is a function either of the aircraft system's natural resistance to departure or of the pilot's ability to easily recover from the occasional out-of-control condition associated with high-AOA maneuvering. Unfortunately, many aircraft in the inventories of the free world's air forces exhibit a high degree of susceptibility to departure and spin entry. Such aircraft have a departure threshold that is generally beyond maximum lift but well within the ACM gross maneuver envelope. Many of these aircraft also have poor departure recovery characteristics, and generally require the pilot to act quickly in order to regain control of his aircraft. Since most pilots spend relatively little time near control limits in training or in normal operational flying, they are often unprepared for their first departure. The standard out-of-control reaction is frequently one of panic, followed by ejection.

In an attempt to improve this situation, military training commands have instituted programs to better prepare the pilot for the disorientation he will experience in a departure and to give him a better chance of taking positive recovery action in a timely manner.

Engineers and scientists are also tackling the problem. One engineering approach has been to use motion and attitude sensors in conjunction with the aircraft's control system to "automatically" recover the aircraft from the departure. State-of-the-art sensors can determine whether the aircraft has departed from controlled flight and can determine the direction of motion much more quickly than the average pilot. Relatively simple control laws can be programmed into a control system to enable it to respond to these sensor inputs and place the control surfaces in position to optimize the chances of recovery. Such a control system would be much more reliable than the average pilot; the only drawback to concepts developed using this approach is that, for most aircraft, control effectiveness in the departure AOA region is severely degraded when compared to control effectiveness at lower AOA. This sometimes forces the designer to lower the threshold AOA for the automatic recovery system into a region in which it could be activated unnecessarily. If more effective control devices could be developed, however, this general approach could be used to design a system with the potential to dramatically reduce the loss of life and equipment resulting from out-of-control flight accidents.

Part A of this paper describes an analytical and experimental study undertaken to develop a novel control concept that is highly effective in the AOA region above stall, and could be mechanized in the manner outlined above. The vortex blowing control concepts tested in this study were designed to alter the asymmetric orientation of the forebody vortex system, taking advantage of the large aerodynamic forces produced by this asymmetry. The effects of these blowing concepts on the overall stability and control characteristics of an aircraft at AOA are reported in Part A of this paper and in Reference 1. Companion papers by Peake, Owen, and Johnson (References 2 and 3) discuss the fluid mechanics and topology associated with forebody blowing about a slender cone model.

A.2 BACKGROUND

A.2.1 Forebody Flowfields at High Angles of Attack

It is well known that an asymmetric vortex system forms on the leeward side of aircraft and missile forebodies at high AOA (References 4 through 9). The degree of asymmetry and the strength of the vortices depend on several parameters, the primary ones being AOA, fineness ratio (l/d), nose semi-apex angle (θ_n), and nose bluntness (r_n/d).

At incidences generally greater than twice the nose semi-apex angle, these asymmetric vortices become strong enough to produce values of side force and yawing moment large enough to influence the departure resistance of an aircraft (References 10 through 15). These asymmetric side forces may not only generate a departure from controlled flight but, once the departure has occurred, they may aggravate the tendency of an aircraft to enter a flat spin mode. In addition, since these vortices have been observed to remain in an asymmetric orientation even under coning conditions, they can oppose recovery from a spin (References 16 and 17).

These vortices have been observed to behave in a bistable manner, and are usually oriented in one of two mirror-image states (References 18 through 20); the mirror-image orientation assumed by a vortex is influenced by minute geometric imperfections, especially near the apex of the nose.

A.2.2 Asymmetric Vortex Control

The overall objective of the present study was to harness the power of this vortex system and use the side force generated by its asymmetric nature as a control device. Such a device would be effective in the AOA region beyond stall and could be used, with proper system design and following appropriate control laws, to greatly enhance the capability of an aircraft to recover from a departure from controlled flight.

A.2.3 Previous Research

The basic concept of controlling the yawing moments generated by long, slender forebodies to aid spin recovery was first proposed by Nelhouse et al. in 1960 (Reference 10). These investigators pursued three means of controlling the yawing moments: strakes or spoiler strips placed along the inboard side of the nose (right side in a right spin), induced circulation about the forebody produced by rotating a conical nose section, and flap-type surfaces placed either on both sides or only on the inboard side of an aircraft nose. Each of these concepts proved effective in promoting rapid recovery from various types of spins on different models. Similar experiments using asymmetric nose strakes, reported by Chambers et al. in 1970 (Reference 21), showed equally promising results on a different aircraft configuration. Kruse conducted experiments on the effect of spinning an axisymmetric body about its longitudinal axis, and noted that the peak-to-peak variation of side force decreases with increased spin rate. His data also showed that the time-averaged side force is reduced as the body is spun (Reference 22). Cornish and Jenkins conducted experiments with symmetric tangential blowing near the nose of an aircraft but were unsuccessful in affecting the spin recovery characteristics of their particular configuration (Reference 23).

A.2.4 Present Studies

The present work concentrated on the experimental evaluation of concepts to control the forebody side force through asymmetric tangential blowing near the apex of the nose. The concept of augmenting the spin recovery capability of a fighter aircraft by controlling, through blowing, the side force produced by the nose was first proposed by Skow in 1977 (Reference 24).

Several practical considerations were taken into account in order to screen out devices that would not be applicable to fighter aircraft regardless of their effectiveness. The screening criteria used were:

1. The tangential blowing concepts must be sufficiently effective to not require abnormally large quantities of air or unattainable mass flow rates.
2. The blowing nozzles must be located in a region aft of the radar antenna so radar performance would not be affected adversely.

A.3 EXPERIMENTAL APPARATUS AND TEST PROGRAM

A.3.1 Water Tunnel Tests

Preliminary tests of various forebody vortex blowing control concepts were conducted in early 1978 in the Northrop 16- by 24-inch diagnostic water tunnel on a 0.025-scale model of an F-5F aircraft. The Northrop water tunnel is a single-return, low turbulence facility and is operated at a test section velocity of 0.1 meter per second (0.35 foot per second), which corresponds to a Reynolds number of approximately 1×10^5 per meter (3×10^4 per foot). The F-5F model was equipped with two parallel rows of dye injection orifices located on the lower surface of the fuselage forebody. Visualization of the forebody flowfield is achieved when the dye flows out of these orifices and is entrained into the separated shear layer or layers, which in turn roll up into well defined vortices.

The water tunnel tests were conducted to screen a large number of potentially useful blowing schemes by comparing, in a qualitative manner, the relative capability of each concept to control the forebody vortex orientation. The blowing concepts tested consisted of small nozzles located on the surface of the forebody at various locations. The angle of the blowing jet relative to the free stream was also varied. Water was supplied to the blowing nozzle through a small tube running down the centerline of the model. Accurate mass flow rates were set by using a water flow meter in the supply line, external to the tunnel. Additional water tunnel tests were conducted on two tangent ogive-cylinder bodies to determine the effect of vortex

blowing control on more generic shapes. The tangent ogive forebodies had fineness ratios (L/d) of 3.5 and 5.0. Each was tested with a common circular-cylinder afterbody ($L/d = 4.5$). Tangential blowing in a downstream direction was tested for a matrix of positions on the surface of both bodies.

The experiments were performed over an AOA range of 0 to 60 degrees. All water tunnel tests were performed at zero sideslip angle. Vertical and lateral positions of the vortex cores were determined at a fixed longitudinal station for the matrix of nozzle geometries at various blowing rates. In this manner the relative effectiveness of each concept was evaluated and optimum nozzle locations were determined.

A.3.2 Wind Tunnel Tests

Based on the results of the water tunnel tests, the most promising nozzle geometries were selected for proof-of-concept testing in the wind tunnel.

Testing was conducted in the Northrop low-speed wind tunnel. This tunnel is a horizontal, atmospheric, single-return facility capable of test section Reynolds numbers up to 7.9×10^6 per meter (2.4×10^6 per foot) and dynamic pressures up to 9580 Newtons per square meter (200 pounds per square foot). The test section is 10 feet wide, 7 feet high, and 20 feet long. The tunnel has a contraction ratio of 12:1, which gives a streamwise turbulence level of less than 0.1 percent in the test section.

Tests were conducted using a 0.1-scale F-5F model equipped for asymmetric blowing at two fuselage stations on the upper surface of the forebody. A plenum chamber for the blowing system was located in the nose of the model. This plenum chamber was pressurized from an external source through an air supply line routed from a support near the back of the sting, forward along the top of the model, and buried just aft of the canopy. Care was taken to ensure that the supply line was nonmetric. Figure 1 shows the model installation in the tunnel and illustrates the blowing apparatus.



FIGURE 1. WIND TUNNEL TEST MODEL

The blowing nozzles were designed to provide choked flow at the nozzle exit plane. A nozzle calibration was performed to determine actual discharge coefficients. Plenum total pressure and temperature and nozzle mass flow rate were measured and used to compute nozzle jet velocity and, hence, the blowing momentum coefficient (C_{μ}).

Wind tunnel tests were performed at a dynamic pressure of 2494 Newtons per square meter (50 pounds per square foot), corresponding to a Reynolds number of 4.3×10^6 per meter (1.3×10^6 per foot). Plenum pressures for the blowing system ranged from 1.1 to 4.2×10^6 Newtons per square meter (165 to 615 pounds per square inch), yielding blowing momentum coefficients (C_{μ}) based on wing area of between 0.008 and 0.032. Data were taken over an AOA (α) range of 0 to 90 degrees in 2-degree increments and over a sideslip (β) range of ± 25 degrees in 5-degree increments.

A.4 DISCUSSION OF RESULTS

A.4.1 Water Tunnel Tests

A.4.1.1 Asymmetric Tangential Blowing Concepts

Water tunnel experiments performed with the 3.5/ d tangent-ogive forebody indicated that, for the range of longitudinal positions tested (approximately 1.0 to 2.0 body diameters aft of the apex of the nose), the most effective tangential blowing arrangement was with the nozzle directed aft and on the same side of the body as the higher primary vortex. (This would be on the side opposite to the direction of a departure or spin, since the driving side force is produced by the vortex in the closest proximity to the surface.) The topology of the asymmetric vortex development is discussed by Peake et al. in References 2 and 3.

As shown in Figure 2, with the model at zero sideslip angle, when a sufficient quantity of mass flow is directed in a concentrated jet beneath the high primary vortex, the asymmetric primary vortex system can be induced to form in its mirror-image state. The blowing coefficients shown are referenced to the

model base diameter. The blowing momentum required to induce a complete reversal of the vortex core positions (i.e., mirror-image state) was found to be a function of the longitudinal position of the nozzle relative to the apex of the nose, the radial position of the nozzle relative to the windward generator, and the model AOA. As seen in Figure 3, significant reductions in required momentum coefficient are noted as the nozzle is moved toward the apex of the nose at a constant nozzle lateral offset (Y/d). The approximate location of a typical radar antenna is shown for reference. Note that significantly higher values of jet momentum are required to produce reversal at higher AOA.

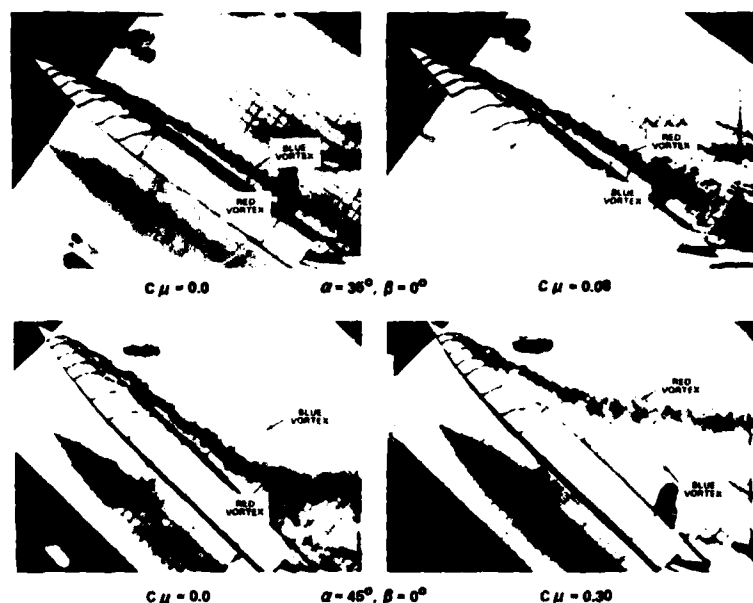


FIGURE 2. DEMONSTRATION OF VORTEX CONTROL ON A 3.5 CALIBER TANGENT-OGIVE MODEL

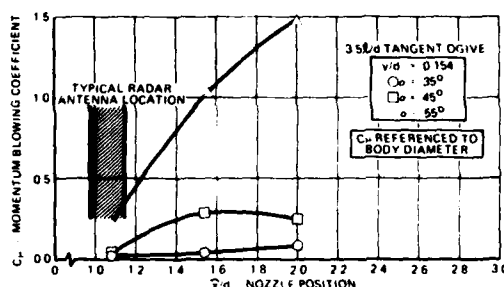


FIGURE 3. VARIATION IN BLOWING REQUIREMENTS WITH LONGITUDINAL POSITION OF NOZZLE

Figure 4 illustrates the effect of nozzle radial position on blowing control effectiveness. As the nozzle is displaced angularly away from the leeward generator at a constant longitudinal position, an increase in blowing effectiveness is noted. The optimum radial position appears to correspond to a lateral position slightly outboard of the center of the higher vortex core.

Water tunnel experiments performed on the F-5F model using the tangential, aft-blowing concept yielded the results shown in Figure 5. These results are consistent with those obtained with the tangent-ogive models and illustrate that, at zero sideslip angle, it is possible to induce the vortices to reverse orientation (i.e., mirror-image state) with sufficient quantities of blowing on a realistic fighter aircraft configuration.

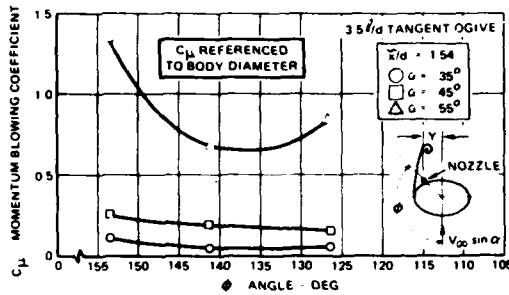


FIGURE 4. VARIATION IN BLOWING REQUIREMENTS WITH RADIAL POSITION OF NOZZLE

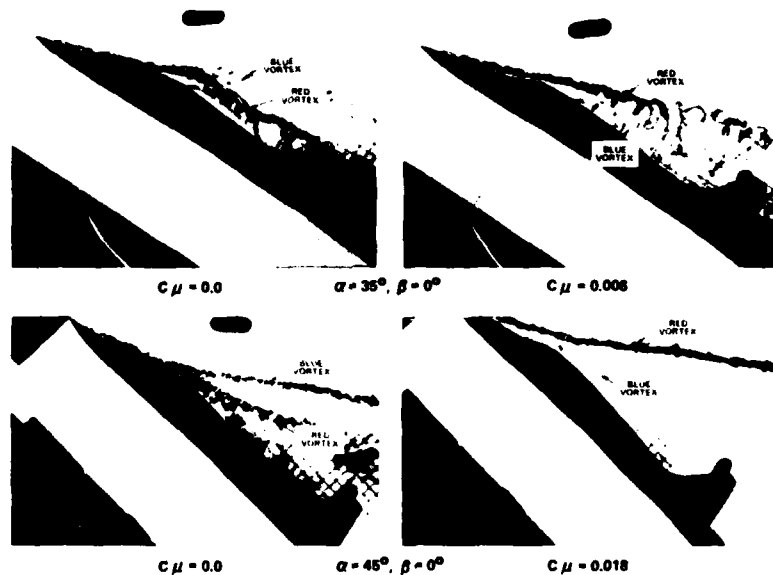


FIGURE 5. DEMONSTRATION OF VORTEX CONTROL ON A FIGHTER MODEL

A.4.2 Wind Tunnel Tests

From the results of the water tunnel tests previously discussed, the most promising vortex control schemes were chosen for proof-of-concept testing in the low-speed wind tunnel. Two blowing nozzle locations were selected.

A.4.2.1 Vortex Blowing Control Concepts

Figure 6 presents the measured effect of aft tangential blowing on yawing moment at zero and ± 5 degrees of sideslip for the F-5F aircraft. With blowing off, an asymmetry in the yawing moment at zero sideslip begins to develop at an AOA of approximately 32 degrees ($\alpha/\theta_n = 2.0$). With blowing on, even at the lowest jet momentum coefficient tested ($C_{\mu} = 0.008$), the asymmetry begins to develop slightly earlier, at an AOA of 24 degrees ($\alpha/\theta_n = 1.5$) and, at zero sideslip, forms in the opposite sense to the blowing-off case. The asymmetry in the side force or yawing moment is very easy to see at zero sideslip, but the asymmetric nature of the primary forebody vortex system applies a strong bias to the forces and moments at nonzero sideslip as well. Inspection of the data in Figure 6 at $\beta = \pm 5$ degrees indicates that the vortex blowing concept reverses the sense of the bias at AOA up to approximately 50 degrees.

At AOA beyond 24 degrees, the largest incremental change in yawing moment is obtained at the lowest momentum coefficient tested. The increment then increases approximately linearly as the jet momentum coefficient is increased, up to the maximum mass flow rate tested.

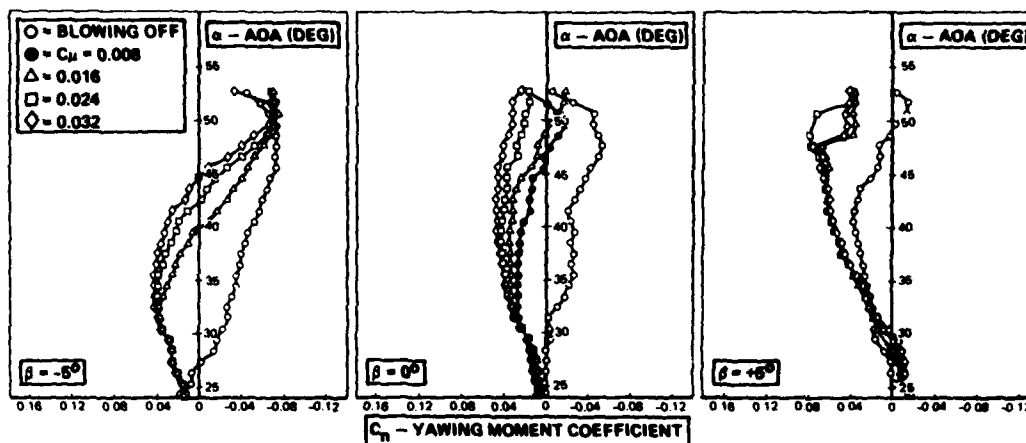


FIGURE 6. VORTEX BLOWING CONTROL EFFECTIVENESS

Figure 7 presents the incremental yawing moment generated by the vortex control system as a function of AOA. These data are compared with the incremental yawing moment produced by full deflection of the conventional rudder of the F-5F. Note that even the lowest jet momentum coefficient tested provides yawing moments in the AOA range from 35 to 55 degrees that are comparable to those produced by the rudder at very low incidences. Also, it is interesting to note that the vortex control effectiveness begins to increase in the same AOA region in which rudder effectiveness is declining rapidly. This leads to a rather interesting conclusion: at low AOA, directional stability and control are best provided by aerodynamic surfaces located behind the aircraft center of gravity, e.g., a vertical tail and a rudder, and at high post-stall AOA, directional control as well as stability can best be provided by an aerodynamic device located ahead of the center of gravity, near the apex of the nose.

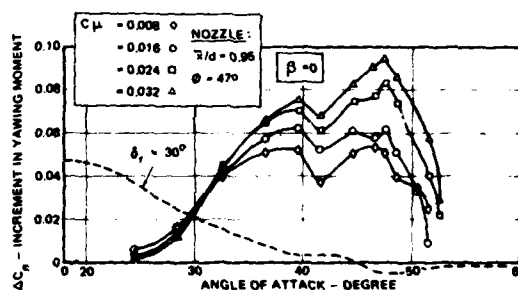


FIGURE 7. VORTEX BLOWING CONTROL EFFECTIVENESS

Figure 8 illustrates the effectiveness of the vortex blowing control device as a function of sideslip at a constant angle of attack ($\alpha = 47$ degrees). These data indicate that over a very wide range of sideslip angles, the vortex blowing control device produces a significant incremental yawing moment (in this case a yawing moment to the left in opposition to the yawing moment produced by the blowing-off vortex asymmetry). The reversal in incremental yawing moment at a sideslip angle of 6 degrees caused some concern, but the impact of this phenomenon on the effectiveness of the device could not be assessed by inspection of the wind tunnel data only; simulation of the overall effectiveness was required.

A.4.3 Six-Degree-of-Freedom Simulation

The capability of the blowing concepts to augment the departure and spin recovery capability of an F-5F fighter aircraft was evaluated by means of a digital six-degree-of-freedom (6DOF) computer simulation. The baseline aerodynamic model used in this simulation has been validated by comparison of calculated and flight test trajectories of many coupled, high-AOA maneuvers flown during spin tests of this aircraft. An algorithm was developed to model the incremental forces and moments generated by the blowing devices, as determined from the low-speed wind tunnel experiments.

Maneuvers were simulated by specifying grossly aggravated control inputs, which were found during spin susceptibility testing to produce departures and spin entries. The departures and spins generated were found to be difficult to recover from using traditional recovery control inputs both in flight and in the simulation.

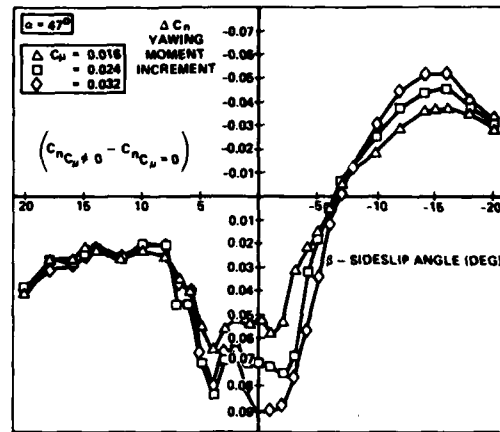


FIGURE 8. EFFECT OF SIDESLIP ON VORTEX BLOWING CONTROL POWER

The threshold AOA and yaw rate at which the device was activated were varied in the simulations, as was the blowing mass flow rate. The optimum yaw rate/AOA threshold and the general effect of blowing momentum were determined in this manner. Figure 9 presents a typical series of time histories at a given mass flow rate in which the threshold AOA was varied. Recoveries are seen to be significantly improved when the blowing device is activated early in the departure but severely degraded when the device is activated after the departure has been allowed to progress toward spin entry.

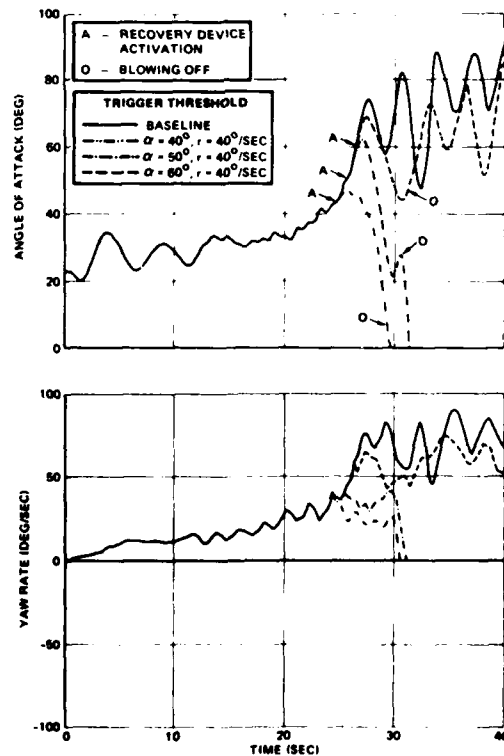


FIGURE 9. SAMPLE TIME HISTORY OF DEPARTURE RECOVERY AUGMENTED BY VORTEX BLOWING

A blowing threshold angle of attack, α_T , of 40 degrees provides good recovery augmentation and is well beyond the AOA for maximum lift coefficient, and thus has no impact on the maneuvering capability of the F-5F aircraft. For each simulation a yaw rate deadband of ± 40 degrees per second at an AOA of 40 degrees, decaying linearly to ± 20 degrees per second at an AOA of 60 degrees, was used. In this manner the blowing device is not activated until the yaw rate exceeds the deadband limit.

Figure 10 illustrates the final blowing control device schedule superimposed on the ACM gross maneuver boundary for the F-5F. A sample trajectory of a typical ACM is also shown. The maneuver simulated is a high-speed, high-g, maximum rate windup turn to the left with the aircraft at an AOA near the maximum lift coefficient ($C_{L_{max}}$). From this initial condition (indicated by ① on the figure), the pilot initiates a high-g turn reversal by applying full right rudder and aileron. Since most fighter aircraft are designed to roll about the flight path rather than the body axis, a large yaw rate develops in addition to the commanded roll rate (②). This yaw rate couples with the roll rate to produce a large nose-up pitch rate (③). The combination of yaw rate and high post-stall AOA produces a departure from controlled flight and a spin entry (④ and ⑤). At this point the pilot senses loss of control and initiates a conventional recovery, which is unsuccessful due to the reduced control effectiveness at high AOA; the aircraft enters a developed spin (⑥). For the case of a vortex blowing-assisted recovery, the blowing device is triggered when the maneuver trajectory crosses the activation threshold (A). The blowing device generates a strong side force on the nose in opposition to the direction of yaw, allowing an immediate recovery (B).

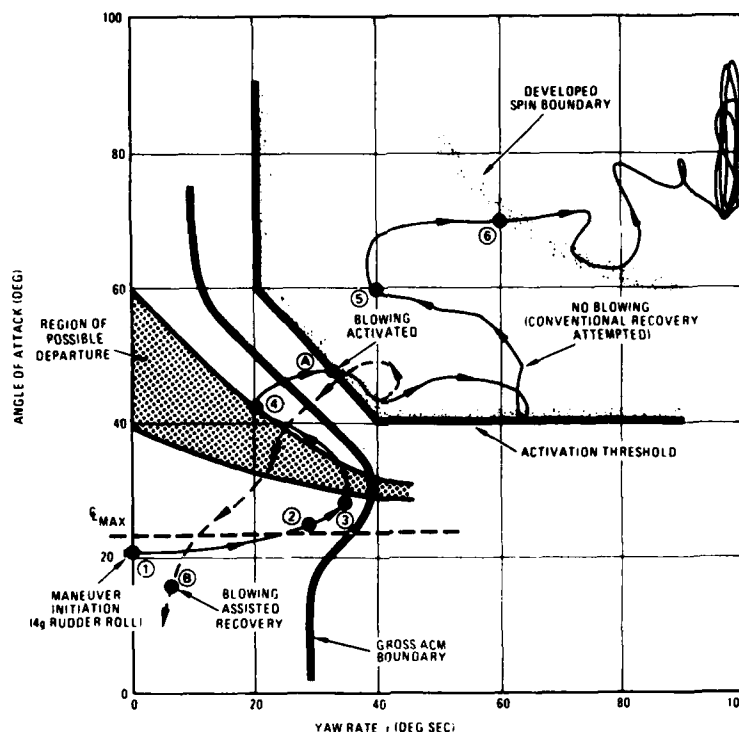


FIGURE 10. SAMPLE DEPARTURE TRAJECTORY

A.5 PRELIMINARY ASSESSMENT OF DESIGN FEASIBILITY

Using the results of the experiments and simulation discussed, some preliminary system design work was done to assess the feasibility of applying the blowing control concept to fighter or trainer aircraft. Factors considered in the feasibility study included effectiveness, reliability, complexity, impact on other systems, and suitability of the device for retrofit to in-service aircraft.

The wind tunnel experiments and 6-DOF simulation showed that an acceptable level of departure recovery enhancement could be achieved at blowing coefficients (C_{μ}) of 0.015 to 0.025. The required duration of blowing was found to be between 3 and 5 seconds. In order to maximize the reliability of the system, engine bleed air was not considered as a potential source for the blowing jet, inasmuch as engine flameouts at high AOA and yaw rate are to be expected. A solid propellant system was chosen as the most attractive source of blowing. Figure 11 shows a schematic diagram of the proposed blowing system.

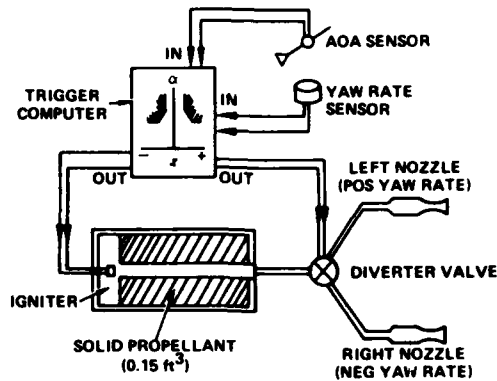


FIGURE 11. VORTEX BLOWING CONTROL SYSTEM SCHEMATIC

The solid propellant blowing system is estimated to require approximately 4.25×10^{-3} cubic meters of propellant. The total system weight is estimated to be less than 9.1 kilograms.

Figure 12 illustrates the region of the flight envelope over which the system is designed to produce the required blowing momentum coefficients. This region encompasses the low-speed transient area in order to provide maximum departure recovery enhancement, and is well outside of the primary ACM arena so that the maneuvering capability of the aircraft is not impacted adversely.

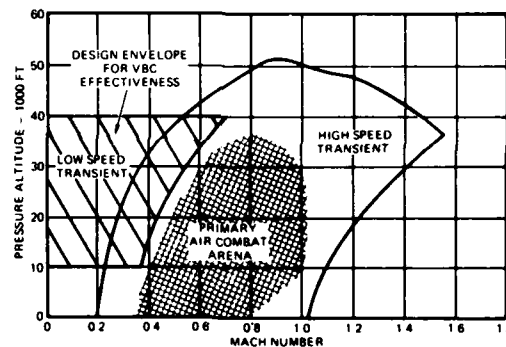


FIGURE 12. DESIGN ENVELOPE FOR VORTEX BLOWING CONTROL

A.6 CONCLUSIONS AND RECOMMENDATIONS

Based on small-scale water and wind tunnel experience, it has been shown that asymmetric tangential blowing along the surface of the forebody of an aircraft can be used to control the orientation of the lee-side vortex system at high AOA. Further, it has been shown that the forces and moments produced by these vortices can be used, in a controlled manner, to greatly enhance the predicted departure recovery characteristics of an existing fighter aircraft configuration. Blowing rates required to produce these forces and moments were shown to be small owing to the fluid amplification afforded by vortex growth. Volume requirements are reasonable, and indicate that such a concept could be applied to a new aircraft or retrofitted to an existing aircraft with minimum impact on other aircraft systems.

Further experiments must be conducted on a large-scale free-flight model to substantiate the predictions. Further analysis should be done to determine whether this concept could be used not only as a departure recovery enhancement device but also as a departure inhibitor.

B. DETAILS OF THE FLOW STRUCTURE

B.1 INTRODUCTION

B.1.1 Asymmetric Vortex Wake About a Forebody at Incidence

Asymmetric vortices on the leeward of flight vehicles at high angles of incidence (References 8, 14, and 25 through 27) can cause severe stability and control problems. The asymmetric flow induces side forces on the forebody and consequent yawing moments that may overwhelm the counteractions available from control surface deflections. Analogous with the flow about most aircraft and missile forebodies at incidence, where crossflow effects dominate, is the flow about a slender cone. Having already established the structure of the symmetric separated flow about a circular cone at moderate incidence (References 3, 28, and 29), where free shear layers spring from primary and secondary separation lines to form well-organized, spirally coiled vortex motions, we may use the cone as a convenient vehicle to investigate the asymmetric flow complexities at elevated attitudes. Rather than destroying the asymmetric vortices to alleviate the induced side loads, our aim has been to retain the power of the vortices by controlling their orientation (References 1, 2, 3, and 24). The emphasis has been to acquire not only overall forces, pressures, and separation line locations on the cone, but to accompany these with laser vapor screens of the asymmetric vortex wake to produce a conceptual framework of the flow. The 1.4-meter (54-inch) long, 5-degree semiangle cone was sting-mounted on a roll gear in the Ames 1.8- by 1.8-meter (6- by 6-foot) closed-circuit wind tunnel. Two spherically tipped, interchangeable frusta were manufactured to fit the front of the model. One frustum was smooth, and the second had provision for blowing ports, as shown in Figure 13. The apparatus is described fully in References 2, 3, and 28.

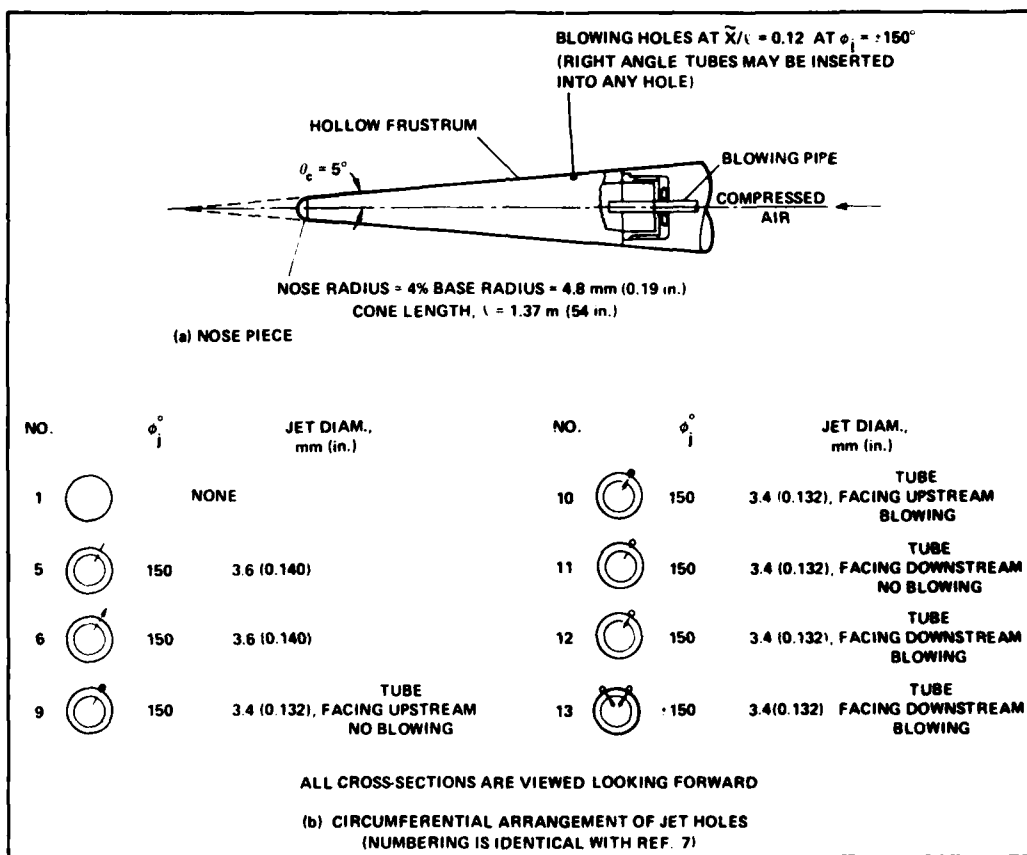


FIGURE 13. SCHEMATIC OF WIND TUNNEL MODEL AND BLOWING NOZZLE LOCATIONS

The onset of asymmetry for a forebody alone typically occurs when the forebody angle of incidence, α , exceeds twice the nose semiangle, θ_c . The ratio, α/θ_c , is called the relative incidence, $\bar{\alpha}$, an important parameter when comparing slender nose shapes of different θ_c . In wind tunnels it has been found that the onset phenomenon (References 8, 25, and 28) and the initial direction of the side force are responsive to small changes in geometry at the nose, Reynolds number, and free-stream Mach number. This sensitivity is detected up to relative incidences at which there are transonic conditions with embedded shock waves in the leeward crossflow, whereupon the side forces disappear (References 2, 25, 26, and 28).

A candidate mechanism for consideration to explain the initial development of asymmetry in the subsonic vortex flow is related to the known susceptibility to instability (Reference 30) of inflexional velocity profiles. Such profiles exist in the vicinity of the primary vortices and the saddle-type singular point that encloses the flow above the vortices in the crossflow plane (References 2 and 31). Some recent research is helpful in illuminating this instability mechanism. Nishioka and Sato (Reference 32) experimentally showed that the initially steady symmetric laminar flow about a two-dimensional circular cylinder becomes unstable beyond a certain (low) Reynolds number. The new flow produced is time-dependent and periodic, and develops into the Karman vortex street. A theoretical study accompanying the experiment suggests that the steady flow becomes unstable to anti-symmetric disturbances in the vicinity of the enclosing saddle point. Imagine the consequence of this result for impulsive flow development past the same two-dimensional cylinder. For Reynolds numbers less than this low value, the transient flow approaches a steady state as time approaches infinity and this steady state is symmetric, but for larger Reynolds numbers the transient flow is symmetric only at small values of t . As time approaches infinity, the steady state to which this flow is tending becomes unstable, with the result that antisymmetric disturbances can grow sufficiently large to once again promote the beginning of the Karman vortex street.

If we now invoke the impulsive-flow analogy and imagine a fixed plane through which a slender, circular cross-sectional, three-dimensional body passes with a downward velocity, one expects to see in this plane a flow development with time (i.e., the structure and mechanisms) similar to that of the impulsively started cylinder. Since the particular Reynolds number is low when the vortex street begins, we may postulate that all three-dimensional bodies tested would evidence the instability if they were sufficiently long. Its manifestation depends on the rapidity with which the velocity profile that becomes unstable is approached, as well as on the size or amplitude of the initial asymmetric disturbance. So far, then, we note that the candidate mechanism has been developed in accordance with observations of the laminar wake. References 7 and 33, however, illustrate that the structure of both the laminar and turbulent asymmetric wakes about slender bodies at incidence appear similar.

We therefore propose to extend the range of applicability of the candidate mechanism to also explain the asymmetry phenomenon in fully developed turbulent flow. Furthermore, on the basis of this candidate mechanism, we may predict that when leeward shock waves form in the crossflow about a three-dimensional body, the effects of vortex asymmetries in the wake will tend to disappear. Such an event is likely because there can be no direct transfer of the effects of amplified disturbances in the saddle-point region to the body and vice-versa.

About the cone, the local asymmetric flow perturbations developing about extremely small roughnesses at the nose may not only amplify downstream in the wake but may also govern the initial direction of the asymmetry. Near-mirror images of the side force/incidence performance of a slender cone, for example, are obtained at body roll angles of ± 90 degrees (Reference 2). The small surface irregularities may also lead to asymmetric transition (Reference 27). In the range of transitional Reynolds numbers, therefore, we may postulate an additional candidate mechanism in the existence of a steady asymmetric mean flow (Reference 34). In the practical flow case of a slender body at incidence, we shall frequently be dealing with laminar, transitional, and turbulent flows, where both candidate mechanisms will be possibilities. Nevertheless, for our cone, laminar and transitional flows are restricted to the region close to the nose, so that we anticipate the character of the flow at the enclosing saddle point to dominate the wake development.

B.1.2 Control of the Asymmetric Vortices

Because the direction of the leeward asymmetry is sensitive to small irregularities in the surface at the nose, it is conceivable that the degree of asymmetry may be controlled by a single small strake to counter the vorticity imparted by the geometrical imperfection; or by spinning the nose, to remove altogether the sensitivity to nose perturbations (Reference 10). On the other hand, to perturb the flow in a controllable and repeatable manner without a "parasite" configuration penalty, we should like to make small but measurable changes to the effective forebody geometry near the nose by novel active means to potentially alter the asymmetric leeward flow structure. Some recent results of Sharir et al (Reference 35) have demonstrated the potential for control by air injection normal to the surface. They advised that blowing symmetrically from jets on the windward side of the nose of a missile configuration was effective in diminishing the side force. We propose that blowing from the leeward side, in the vicinity of the separation lines, should produce an even greater effect on the asymmetric flow development. For comparison with various jet configurations employed in our experiments, the usefulness of passive devices such as an asymmetrically positioned strake and roughness elements has also been investigated (Reference 3).

B.2 EXPERIMENTAL RESULTS AND DISCUSSION

B.2.1 Structure of Asymmetric Vortex Wake

Up to relative incidences of more than 2 for our cone model, the leeward vortices remain symmetrically disposed about the pitch plane, stemming from symmetric primary and secondary separation lines, S1 and S2, on the cone surface. At relative incidence slightly greater than 2.5, however, the leeward vortices take on an asymmetric pattern. Figures 14(a) to 14(e) illustrate the sequence of asymmetric flow field developments up to $\alpha = 3.6$ at $M_\infty = 0.6$, obtained in the wind tunnel using a vapor screen illuminated by an expanded laser line set normal to the cone surface. The view is towards the apex of the cone from the base of the body; the roll orientation of the cone was fixed. Figures 15(a) to 15(e) are corresponding interpretations of the leeside vortex wake, as projections of the three-dimensional stream surfaces in the experimental external flow onto crossflow planes normal to the cone surface. These projections provide the continuous patterns of crossflow streamlines in association with a limited number of singular points (i.e., zero velocity points in the crossflow plane) that yield a conceptual framework of the fluid mechanics. Notice, in Figure 15(a), the following characteristic features: The primary vortices result from the separation of the windward boundary layers at S1, and the induced boundary layer growth from the attachment line A1 near the leeward ray is eventually caused to depart from S2 as secondary vortices of opposite sign to, and tucked beneath, the primary vortices. Additional attachment

lines, A2, are found between the separation lines, S1 and S2. The characteristic convergence of skin-friction lines towards a separation line, and divergence away from an attachment line, are displayed in Figures 16(a) and 16(b).

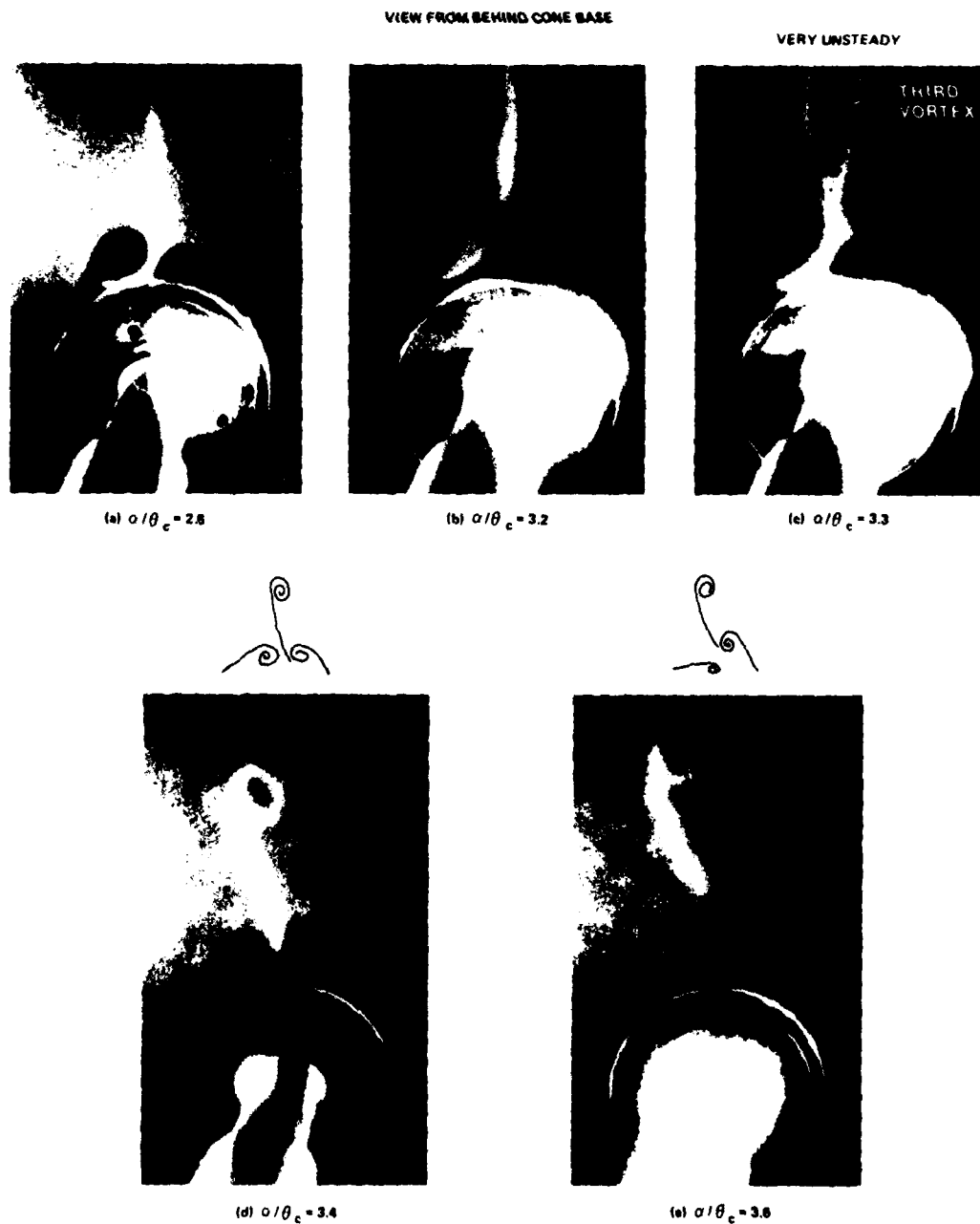


FIGURE 14. LASER VAPOR SCREEN - DEVELOPMENT OF VORTEX ASYMMETRY

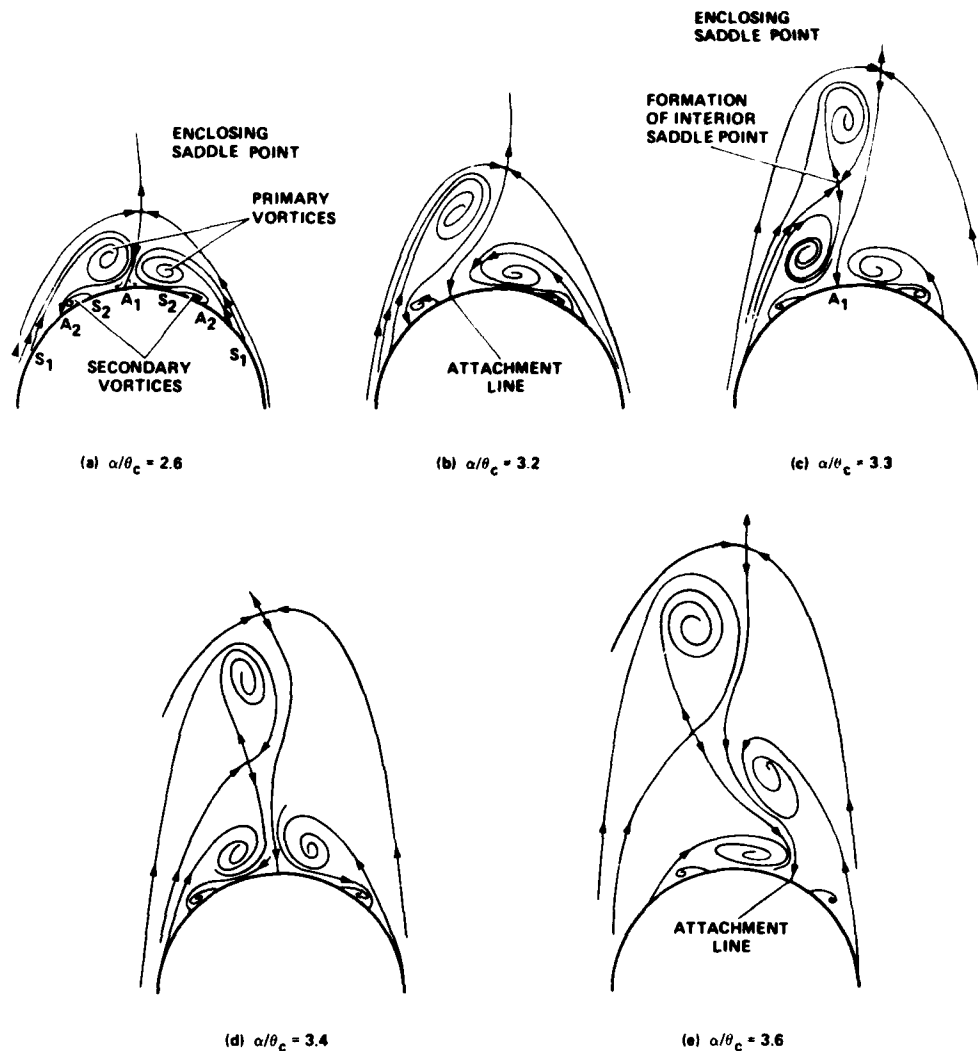


FIGURE 15. LEESIDE VORTEX WAKE STRUCTURE

Let us assume an asymmetric disturbance to originate at the nose, of the same rotation, say, as the port side primary vortex. If this disturbance amplifies in the vicinity of the enclosing saddle point as a consequence of instability of the inflexional velocity profiles, there will be an effective increase in the vorticity of the port side primary vortex. This vortex will enlarge slightly and move away from the surface as shown in Figures 14(a) and 15(a). As the relative incidence increases up to 3.2, the feeding shear layer continues to stretch, as shown in Figures 14(b) and 15(b). At a relative incidence of 3.3, in conjunction with the appearance of gross unsteadiness of the secondary vortices, the elongated shear layer itself passes through a shedding stage, as shown in Figure 14(c), until at a relative incidence of 3.4 there is definitive evidence of a third spiral vortex motion, as shown in Figure 14(d). In order that the two vortices of the same rotational direction be able to coexist in tandem on the left-hand side, the rules of topology (Reference 9) instruct us that a new saddle point must be inserted between them, as shown in Figure 15(c). As the relative incidence increases still further, the starboard-side primary vortex begins to grow, as shown in Figures 14(d) and (e) and 15(d) and (e), resulting eventually in the repetition of the shedding process for the opposite side; these incidences at which shedding occurs correspond with the maximum induced side loads. Note that the one crossflow streamline emanating from the enclosing saddle point to the body at A1 as shown, for example, in Figure 15(e), always partitions the left- and right-hand sides of the wake. Except during the shedding process, each flow field is constituted of well organized spiral vortex motions. In addition, scanning the plane of the laser vapor screen from the nose to the base of the forebody demonstrated virtually identical structure of the crossflow along the entire length of the cone.

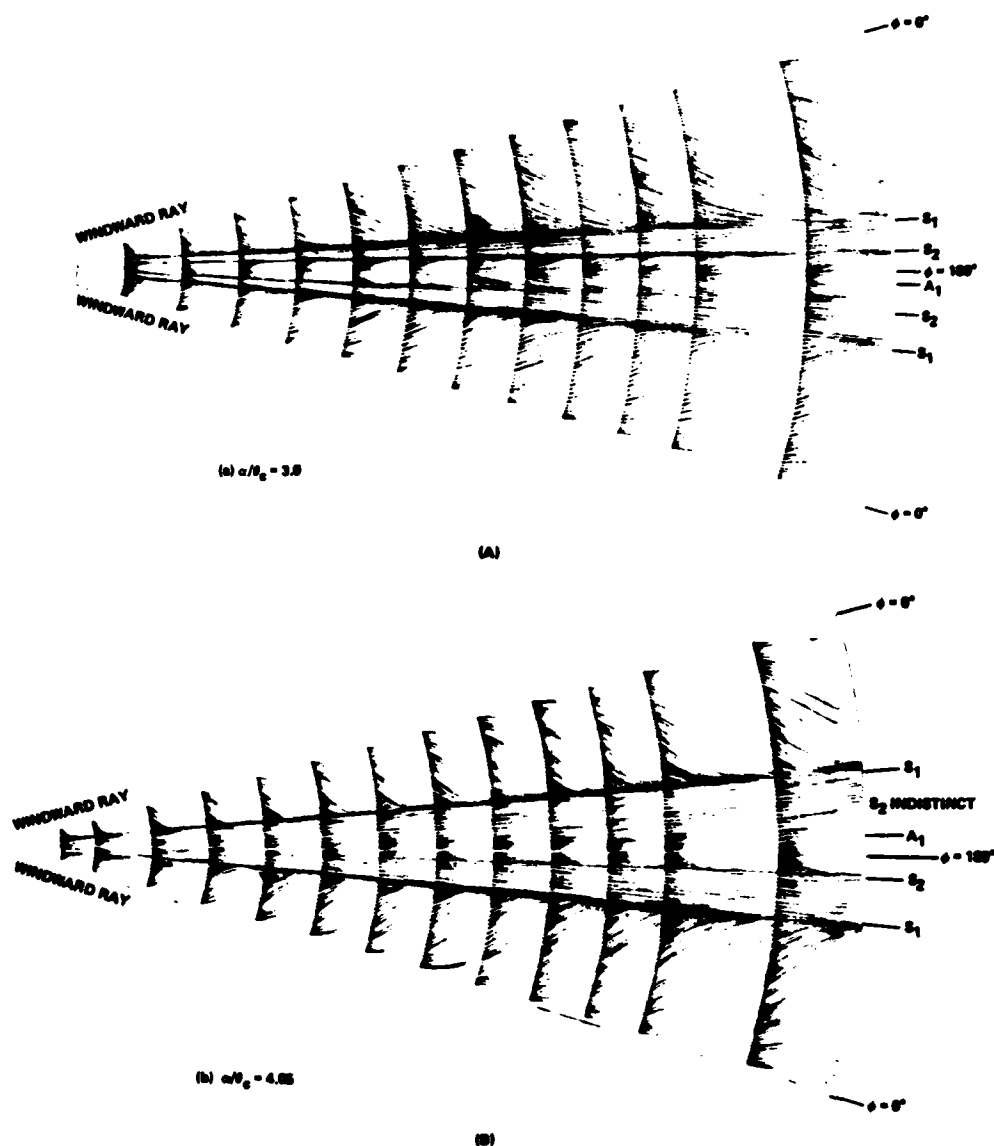


FIGURE 16. SURFACE SKIN FRICTION LINES

Figure 16(a) displays the unwrapped asymmetric skin-friction line pattern at a relative incidence of 3.0, corresponding with an external vortex pattern between Figures 14(a) and (b). We see, in Figure 16(a), that, as in the case of symmetric separation (Reference 3), the primary and secondary separation lines S1 and S2 remain coincident with certain conical rays, but now the entire surface pattern is skewed to the port side. The circumferential pressure gradient turns adverse closer to the windward ray on the port side than on the starboard side, causing substantial changes in the respective rates of skewing in the skin-friction line development. At a relative incidence of 4, on the other hand, the skin-friction line pattern is skewed to the right, as shown in Figure 16(b), consistent with the external flow photograph shown in Figure 14(e). Note that although we are not able to detect any circumferential movement of the windward attachment line at $\phi \sim 0$ degrees, the primary attachment line A1 does shift with respect to the leeward meridian, following the excursion of the overall flow structure towards, first, the port side and, second, the starboard side.

B.2.2 Control by Blowing of Asymmetry in the Leeward Flow

B.2.2.1 Flow Structure

Since the flow visualization results, allied with topological notions, have allowed us to develop a conceptual framework of the asymmetric flow, the next step is to ask how the flow orientation might best be controlled by active means. We have suggested that an amplified disturbance can be disruptive in the vicinity of the enclosing saddle point (again, see Figure 15). Let us now introduce a small but measured amount of

air, blowing as a controlled disturbance, into the stream near the nose but on the leeside. Let us also locate the jet between the primary and secondary separation lines S1 and S2 on one side of the leeward meridian, its disposition chosen to be situated beneath the primary vortex that initially lifts off the surface (Reference 1). Figure 17 illustrates a proposed model of the flow in terms of the crossflow streamlines in a plane near the base of the cone looking towards the apex. In the figure, the jet issuing normal to the surface is situated to the right of the leeward meridian. The ensuing interaction between the free-stream and the jet plume penetrating downstream produces a new pair of skewed contrarotating vortices above the forebody vortices. In Figure 17, the median line of the jet efflux is depicted as a crossflow streamline commencing at the cone surface and terminating at the saddle point that interconnects the jet vortices. It is seen that the skewed orientation of the jet vortices must occur to attain a balance of forces on the four vortex cores. The model also shows that introducing the jet vortices into the crossflow plane moves the enclosing saddle point further into the free-stream, thereby reducing its influence at the surface. In addition, the reorganized interactive flow structure may prevent altogether the development of the shedding process that results in the formation of the third vortex.

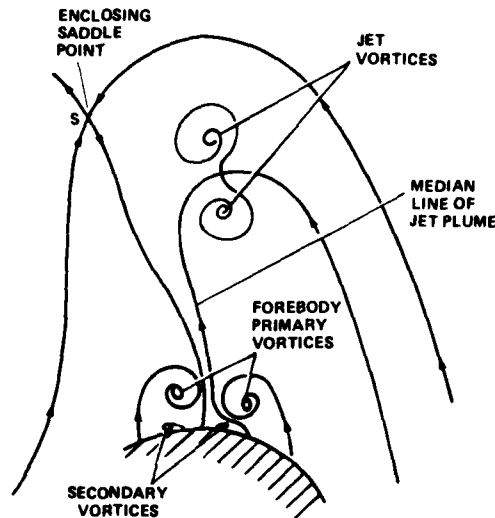


FIGURE 17. LEESIDE VORTEX WAKE STRUCTURE WITH BLOWING JET

The candidate flow model of Figure 17 appears to be validated in the three laser vapor screen pictures shown in Figures 18(a) through 18(c) with normal blowing. The planes of illumination are at $\bar{x}/l = 0.87$, with the views looking forward, and where 200 static pressure ports were situated around the surface. Although the two nose frusta in Figure 13(b) were manufactured to tight tolerances, we might still expect that the initial direction of the asymmetry for each nose would be unpredictable. Thus, for the particular nose frustum used in obtaining the results of Figure 18 (No. 6 in Figure 13), it so happens that, in the absence of blowing, the starboard vortex lifted off first (this is the mirror image, of course, of the flow development illustrated in Figures 14 and 15). Then holding the cone relative incidence constant at 3.3, slightly higher than the value at which shedding (production of the third vortex) was observed in Figure 14, the change in orientation of the forebody vortices as the blowing rate C_μ is increased, is shown in Figure 18(a), (b), and (c). The jet orifice diameter is 3.6 millimeters (0.140 inch) and is located at $\phi_j = 150$ degrees beneath the (initially) higher vortex. The forebody vortices are the bright oval blobs close to the cone, while the jet vortices in the kidney-shaped bright zone are skewed at almost 90 degrees from the horizontal. At a blowing rate, C_μ , of 0.0014, Figure 18(b) shows that the initial asymmetric orientation is the same as that with no plowing. The low port-side vortex enhances the section pressures on that side, providing a side force to the left. As C_μ increases to 0.003, as shown in Figure 18(b), the surface pressure distributions about each side of the meridian plane are almost coincident and there is no overall side force. With further addition of jet momentum flux, as shown in Figure 18(c), the orientation of the forebody vortices is the mirror state of Figure 18(a), and the side force is now to the right. Note that throughout this range of C_μ , at this given relative incidence of 3.3, the skewness of the jet vortices changes little. As their strength increases with the increasing C_μ , their effect is reflected in the revised orientation of the forebody vortices, producing a stable flow configuration. The jet vortices alter the relative amounts of free-stream entrained into the forebody vortices, ultimately favoring the side opposite the blowing point. Finally, Figures 18(a) through 18(c) appear to demonstrate that the shedding mechanism and the production of the third vortex so evident in Figure 14(c) has been prevented. The picture appears much the same for all directions of blowing, but with the tangential modes the structure is less well defined.

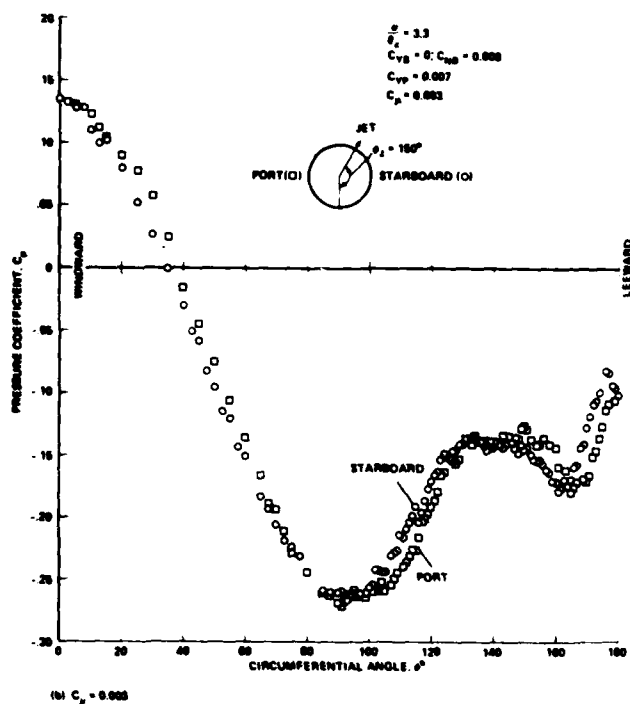
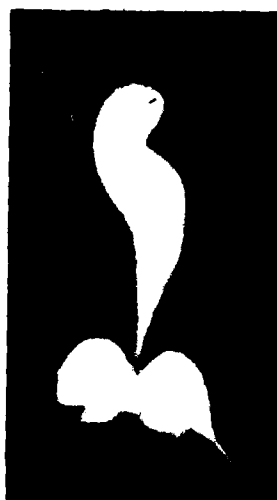
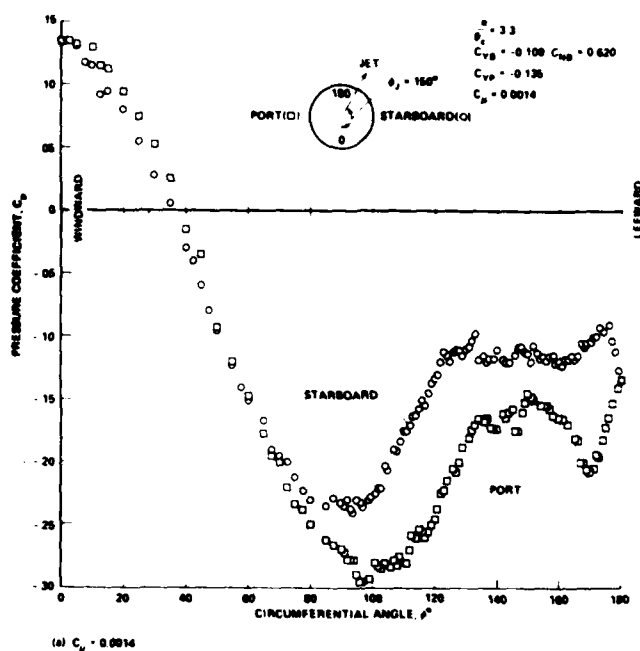
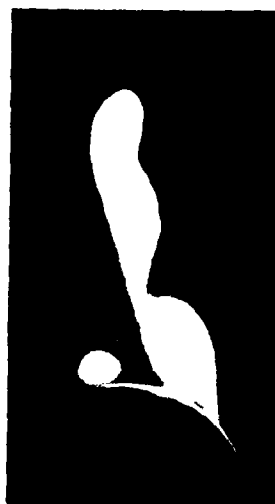


FIGURE 18. LASER VAPOR SCREEN AND CIRCUMFERENTIAL PRESSURES FOR $C_\mu = 0.0014, 0.0030, 0.0062$

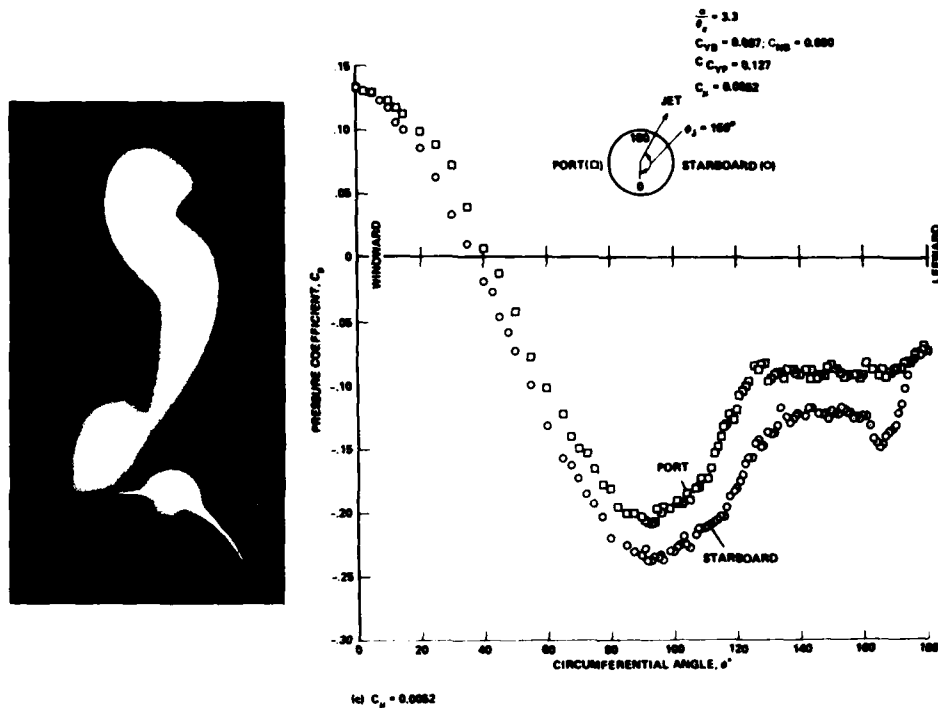


FIGURE 18. LASER VAPOR SCREEN AND CIRCUMFERENTIAL PRESSURES FOR $C_\mu = 0.0014, 0.0030, 0.0062$ (Continued)

B.2.2.2 Effectiveness of Blowing in Changing Side Force Magnitude and Direction

The change in overall side force coefficient (C_{YB} , measured with the balance) as the rate of air injection C_μ grows, is depicted in Figure 19. The cone is at a constant relative incidence of 3.2, slightly less than the setting at which the vapor screen pictures of Figure 18 were taken and close to that at which shedding to form the third vortex was seen in Figure 14. Figure 19 provides force polars not only for air injected normal to the surface (Configuration 6 in Figure 13), but also for tangential blowing both upstream and downstream along a conical ray (Configurations 10 and 12 respectively).

Remembering that the objective of the blowing is to exert positive control over the orientation of the forebody vortices, we see how this might be achieved (Figure 19) for, first, yielding $C_{YB} \sim 0$ for a minimum blowing rate and, second, providing a range of side force that might be used for maneuvering (the different offsets at $C_\mu = 0$ are caused by the three different asymmetric blowing port arrangements). With regard to the former, the upstream pointed jet is the optimum arrangement at this particular relative incidence ($\bar{\alpha} = 3.2$), but the downstream injection provides $C_{YB} \sim 0$ over an extensive range of C_μ ($0.0025 < C_\mu < 0.0055$). With regard to the latter, both normal and tangential injection perform creditably, but normal injection is preferred. Injection also suppressed the substantial fluctuations in side force (Reference 3).

Corresponding with blowing rates greater than 0.005 (see the right-hand side of Figure 19), Figure 20 presents the effect on the side force at constant C_μ as α is increased to 4. The effectiveness of upstream and downstream tangential blowing in delaying the onset of asymmetry and also in reversing the side force development relative to the no-blowing case is presented in Figure 20. Note also the degradation in controlling the direction of the side force when a pair of jets symmetrically disposed at $\phi_j + 150$ degrees about the leeward meridian is used, although the onset of asymmetry is usefully delayed. This offset in C_{YB} at low relative incidence occurred for all configurations. Whether this was due to angularity in the free-stream or model misalignment is speculative; in either event the offset has no bearing on the trends of the results.

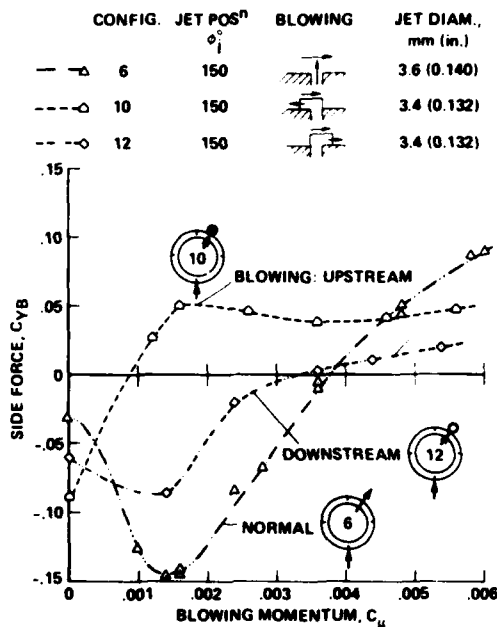


FIGURE 19. SIDE FORCE POLARS

Finally, a test was performed at a relative incidence of 3.2 to investigate the effect of rolling the model with the downstream-pointed jet off (Configuration 11 of Figure 13) and then with the blowing rate at 0.0054 (Configuration 12). The circumferential positions of the blowing tube during the roll excursion are shown at the bottom of Figure 21, the view again looking forward from the base of the cone. The datum setting in roll angle of the body, $\phi_R = 0$ degrees, is when the jet is located 150 degrees from the windward ray, as shown in the bottom left-hand side of Figure 21. The side force continues to be measured in the wind axis system of coordinates. Rolling in an anticlockwise sense, we see, in the forebody roll angle range of 0 to 30 degrees, that the jet is able to reverse the direction of the side force in comparison with the no-blowing case; this is the control exerted by blowing beneath the higher of the two primary vortices. Once past $\phi_R \sim 30$ degrees, however, the ability of the jet to reverse the side force is lost. In the body roll angle range of 30 degrees $< \phi_R < 55$ degrees, the jet issues beneath the low vortex and exaggerates the side force magnitude, but effects no control over side force direction. In the remainder of the body rolling sequence (30 degrees $< \phi_R < 180$ degrees) with the jet now positioned on the windward side, the blowing changes neither the side force amplitude nor its direction to any significant extent. Thus, Figure 21 shows that the single air jet can only effect reversal of the side force when blowing beneath the high vortex (0 degrees $< \phi_R < 30$ degrees) and can only modulate the amplitude when blowing on the leeside (0 degrees $< \phi_R < 70$ degrees). When blowing from the windward side, the jet's behavior is analogous to that of a solid roughness element.

B.3 CONCLUSIONS

Small quantities of air injected from a single orifice near the nose prevent shedding (i.e., formation of additional vortices) in the asymmetric vortex wake about a slender conical forebody. Injecting air also permits control of the magnitude of the induced side force at angles of incidence up to (at least) four times the semi-nose angle. The blowing location was inboard of the primary separation line on one side of the leeward meridian at 150 degrees from the windward ray.

When the jet is situated beneath the higher of the two asymmetrically disposed primary vortices, the control is additionally effective in reversing the direction of the side force.

The thrust coefficient, C_μ , based on the maximum cross-sectional area of the forebody, is no greater than 0.006.

Asymmetric injection from the windward side of the cone proved ineffective in controlling either the magnitude or the direction of the side force.

The choice between blowing either normal to the surface or tangentially upstream or downstream is open. It would depend on the C_μ available and whether the objective was to provide either a nominally zero side force or a finite side force and prescribed direction for lateral control purposes, in the design range of incidence.

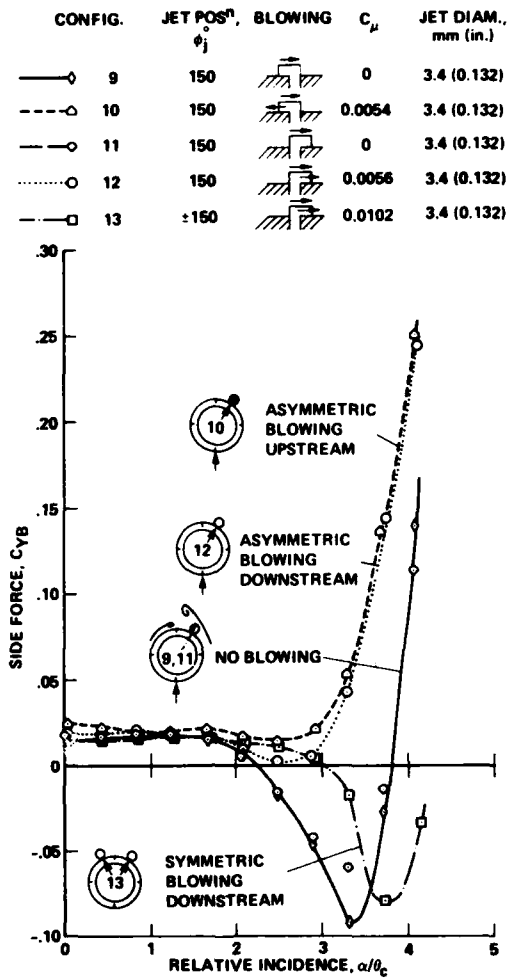


FIGURE 20. INCIDENCE - FORCE PERFORMANCE WITH TANGENTIAL BLOWING

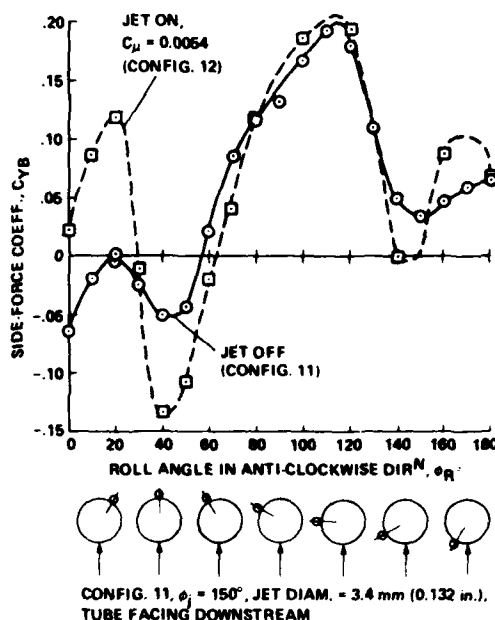


FIGURE 21. CIRCUMFERENTIAL PRESSURE DISTRIBUTIONS

C. REFERENCE

1. Skow, A.M., Moore, W.A., and Lorincz, D.J., "Forebody Vortex Blowing - A Novel Control Concept to Enhance Departure/Spin Recovery Characteristics of Fighter and Trainer Aircraft," AGARD-CP262-24, May 1979.
2. Peake, D.J., and Owen, F.K., "Control of Forebody Three-Dimensional Flow Separation," AGARD-CP262-15, May 1979.
3. Peake, D.J., Owen, F.K., and Johnson, D.A., "Control of Forebody Vortex Orientation to Alleviate Side Forces," AIAA-80-0183, January 1980.
4. Nielsen, J.N., "Non-Linearities in Missile Aerodynamics," AIAA-78-20, January 1978.
5. Allen, H.J., and Perkins, E.W., "Characteristics of Flow Over Inclined Bodies of Revolution," NACA-RM-A50L07, 1951.
6. Clark, W.H., Peoples, J.R., and Briggs, N.M., "Occurrence and Inhibition of Large Yawing Moments During High Incidence Flight of Slender Missile Configurations," AIAA-72-968, 1972.
7. Coe, P.L., Jr., Chambers, J.R., and Letko, W., "Asymmetric Lateral-Directional Characteristics of Pointed Bodies of Revolution at High Angles of Attack," NASA-TN-D-7095, November 1972.
8. Keener, E.R., and Chapman, G.T., "Onset of Aerodynamic Side Forces at Zero Sideslip on Symmetric Forebodies at High Angles of Attack," AIAA-74-770, August 1974.
9. Peake, D.J., and Tobak, M., "Three-Dimensional Interactions and Vortical Flows with Emphasis on High Speeds," NASA-TM-81169, March 1980.
10. Nelhouse, A.I., Klínar, W.J., and Scher, S.H., "Status of Spin Research for Recent Airplane Designs," NASA-TR-R-57, 1960.
11. Greer, H.D., "Summary of Directional Divergence Characteristics of Several High-Performance Aircraft Configurations," NASA-TN-D-6993, 1972.
12. Anderson, C.A., "Stall/Post-Stall Characteristics of the F-111 Aircraft," AGARD-CP102-18, April 1972.
13. Skow, A.M., and Titiriga, A., Jr., "A Survey of Analytical and Experimental Techniques to Predict Aircraft Dynamic Characteristics at High Angles of Attack," AGARD-CP235-19, May 1978.
14. Skow, A.M., Titiriga, A., Jr., and Moore, W.A., "Forebody/Wing Vortex Interactions and Their Influence on Departure and Spin Resistance," AGARD-CP247-6, October 1978.
15. Edwards, O.R., "Northrop F-5F Shark Nose Development," NASA-CR-158936, October 1978.

16. Tobak, M., Schiff, L.B., and Peterson, V.L., "Aerodynamics of Bodies of Revolution in Coning Motion," AIAA Journal, Vol. 7, No. 1, January 1969.
17. Schiff, L.B., and Tobak, M., "Results from a New Wind-Tunnel Apparatus for Studying Coning and Spinning Motions of Bodies of Revolution," AIAA Journal, Vol. 8, No. 11, November 1979, pp 1953-1958.
18. Lamont, P.J., and Hunt, B.L., "Pressure and Force Distributions on a Sharp-Nosed Circular Cylinder at Large Angles of Inclination to a Uniform Subsonic Stream," J. Fluid Mech., Vol. 76, Part 3, 1976, pp 519-559.
19. Lamont, P.J., and Hunt, B.L., "Prediction of Aerodynamic Out-of-Plane Forces on Ogive-Nosed Circular Cylinders," J. Spacecraft, Vol. 14, No. 1, January 1977, pp 38-44.
20. Hunt, B.L., and Dexter, P.C., "Pressures on a Slender Body at High Angle of Attack in a Very Low Turbulence Level Air Stream," AGARD-CP247-17, October 1978.
21. Chambers, J.R., Anglin, E.L., and Bowman, J.S., Jr., "Effects of Pointed Nose on Spin Characteristics of a Fighter Airplane Model Including Correlation with Theoretical Calculations," NASA-TN-D-5921, September 1970.
22. Kruse, R.L., "Influence of Spin Rate on Side Force of an Axisymmetric Body," AIAA Journal, Vol. 16, No. 4, April 1978, pp 415-416.
23. Cornish, J.J. III, and Jenkins, M.W.M., "The Application of Spanwise Blowing to High Angles of Attack Spin Recovery," AGARD-CP247-9, October 1978.
24. Moore, W.A., Skow, A.M., and Lorincz, D.J., "Enhanced Departure/Spin Recovery of Fighter Aircraft Through Control of the Forebody Vortex Orientation," AIAA-80-0173, January 1980.
25. Peake, D.J., Rainbird, W.J., and Atraghji, E.G., "Three-Dimensional Flow Separations on Aircraft and Missiles," AIAA Journal, Vol. 10, No. 5, May 1972, pp 567-580.
26. Keener, E.R., Chapman, G.T., and Kruse, R.L., "Effects of Mach Number and Afterbody Length on Onset of Asymmetric Forces on Bodies at Zero Sideslip and High Angles of Attack," AIAA-76-66, January 1976.
27. Ericsson, L.E., and Reding, J.P., "Vortex-Induced Asymmetric Loads in 2-D and 3-D Flows," AIAA-80-0181, January 1980.
28. Peake, D.J., Owen, F.K., and Higuchi, H., "Symmetrical and Asymmetrical Separations about a Yawed Cone," AGARD-CP-247, October 1978.
29. Peake, D.J., Fisher, D.F., McRae, D.S., "Flight Experiments with a Slender Cone at Angle of Attack," AIAA-81-0337, January 1981.
30. Stuart, J.T., "Hydrodynamic Instability," in Laminar Boundary Layers, Ed., L. Rosenhead, Clarendon Press, 1963, pp 492-579.
31. Tobak, M., and Peake, D.J., "Topology of Two-Dimensional and Three-Dimensional Separated Flows," AIAA-79-1480, July 1979.
32. Nishioka, M., and Sato, H., "Mechanism of Determination of the Shedding Frequency of Vortices Behind a Cylinder at Low Reynolds Numbers," J. Fluid Mechanics, Vol. 89, Part 1, 1978, pp 49-60.
33. Werlé, H., "Tourbillons de corps fuselés aux incidences élevées," L'Aéronautique et l'Astronautique, Vol. 6, 1979, pp 3-22.
34. Kamiya, N., Suzuki, S., and Nishi, T., "On the Aerodynamic Force Acting on a Circular Cylinder in the Critical Range of the Reynolds Number," AIAA-79-1475, July 1979.
35. Sharir, D., Portnoy, H., and Rom, J., "A Study of the Effects of Jets from a Slender Body of Revolution on the Side Forces Acting on It at Large Angles of Attack in Low Speeds," TAE-337, Technion, Israel Institute of Technology, May 1978.

CONTROL OF ADVANCED FIGHTER AIRCRAFT

by

A.M. Skow
Manager, F-5 Aerosciences
Northrop Corporation Aircraft Division
One Northrop Avenue
Hawthorne, CA 90250
USA

CONTROL OF FIGHTER AIRCRAFT

PRESENTATION OUTLINE

- INTRODUCTION
- BASIC AERODYNAMIC EFFECTIVENESS
- CONTROL CRITERIA
- CONTROL CONTROVERSIES
 - TAIL LOCATION
 - ANGLE OF ATTACK LIMITING
- FUTURE DIRECTIONS
 - THRUST VECTORING - PANACEA?
 - CONTROL IMPLICATIONS OF NEW ACM TACTICS
 - ULTRA-FAST ACTUATORS
 - NOVEL CONTROLS

- INTRODUCTION**
- CONTROL OF FIGHTER AIRCRAFT IS THE MOST CHALLENGING PROBLEM IN AIRCRAFT DESIGN
 - INTEGRATION REQUIREMENTS
 - AERODYNAMICS
 - STABILITY
 - CONTROLABILITY
 - PERFORMANCE
 - ACCELERATION
 - MANEUVER
 - AIR DATA
 - REDUNDANCY/REGRITS
 - ELECTRONICS
 - SOFTWARE
 - INTERFACE REQTS
 - HARDWARE
 - ULTRA-FAST ACTUATORS
 - SYSTEM PERFORMANCE
 - COMPLEXITY
 - PROPULSION
 - WEAPON DELIVERY
 - CCIP/CCIP
 - IFPC
 - STRUCTURE
 - FLUTTER SUPPRESSION
 - CONTROLS/DISPLAYS

BASIC AERODYNAMIC EFFECTIVENESS

- AERODYNAMIC EFFECTIVENESS VARIES WITH:
 - ANGLE OF ATTACK
 - ANGLE OF SIDESLIP
 - MACH NUMBER
 - DYNAMIC PRESSURE (AEROELASTIC EFFECTS)
 - WING PLANFORM
 - FOREBODY GEOMETRY
 - INTERACTIONS/COUPLING

BASIC AERODYNAMIC EFFECTIVENESS

AERODYNAMIC EFFECTIVENESS VARIES WITH:

• ANGLE OF ATTACK

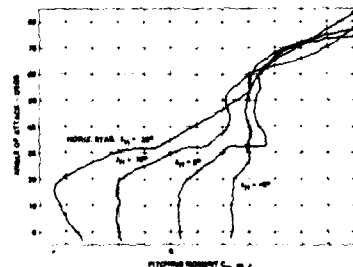
- ANGLE OF SIDESLIP
- MACH NUMBER
- DYNAMIC PRESSURE (AEROELASTIC EFFECTS)
- WING PLANFORM
- FOREBODY GEOMETRY
- INTERACTIONS/COUPLING

ANGLE OF ATTACK EFFECTS

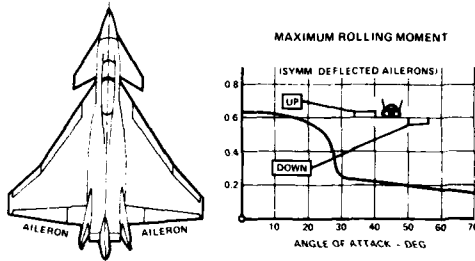
- PITCH, ROLL AND YAW CONTROL EFFECTIVENESS DEGRADES AS AOA IS INCREASED
- WHY?
 - PITCH AND YAW CONTROL SURFACES BECOME IMMERSED IN WING/BODY WAKES
 - ROLL CONTROL SURFACES, TYPICALLY PLACED AT OUTBOARD WING LOCATION BECOME ENVELOPED IN LOW ENERGY AIR FROM WING TIP STALL
 - INTERACTION OF FOREBODY AND WING VORTICES CREATE ADVERSE PRESSURE FIELDS IN THE VICINITY OF THE EMPENNAGE
- CONTROL REQUIREMENTS TYPICALLY SET BY HIGH AOA EFFECTIVENESS

EFFECT OF ANGLE OF ATTACK ON PITCH CONTROL POWER

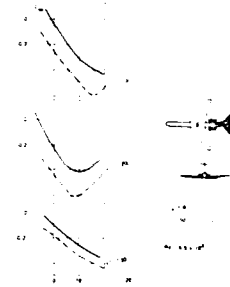
- LOW MOUNTED, AFT TAIL F-20



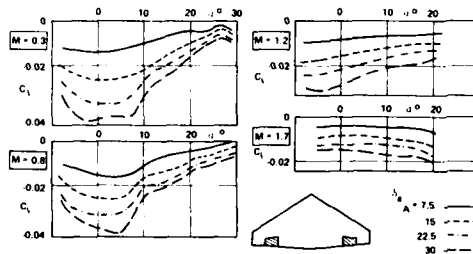
EFFECT OF ANGLE OF ATTACK ON ROLL CONTROL POWER ELEVONS



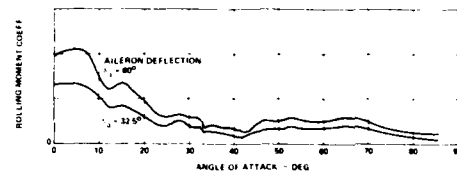
EFFECT OF ANGLE OF ATTACK ON PITCH CONTROL POWER HIGH MOUNTED, AFT TAIL TRANSPORT AIRCRAFT



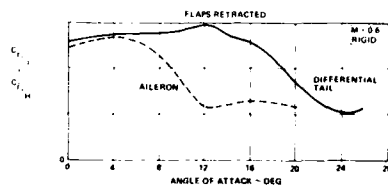
EFFECT OF ANGLE OF ATTACK ON ROLL CONTROL POWER - AILERONS



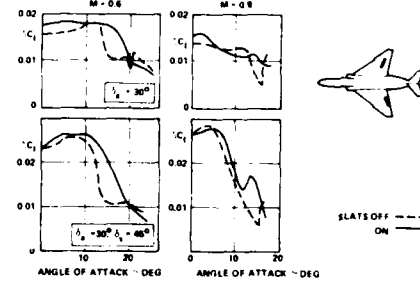
EFFECT OF ANGLE OF ATTACK ON ROLL CONTROL POWER - AILERONS, LOW SPEED F-20



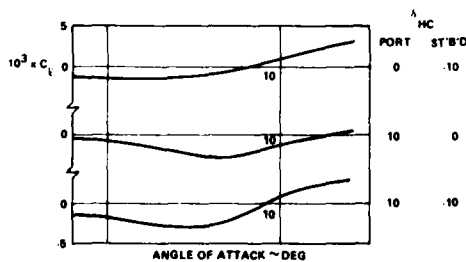
EFFECT OF ANGLE OF ATTACK ON ROLL CONTROL POWER - AILERONS VS DIFFERENTIAL TAIL YF-17 DATA



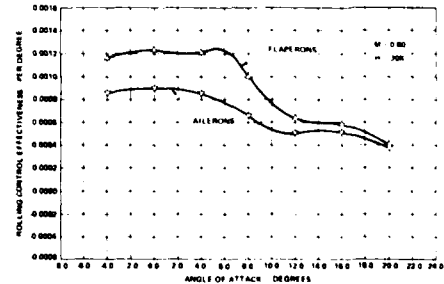
EFFECT OF SLATS ON ROLL CONTROL POWER WITH ANGLE OF ATTACK - AILERONS, AILERONS/SPOILERS



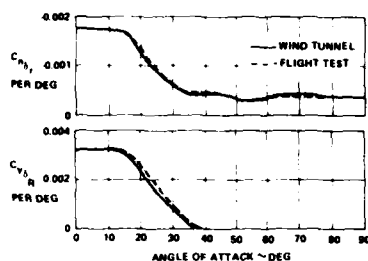
EFFECT OF ANGLE OF ATTACK ON ROLL CONTROL POWER - DIFFERENTIAL CANARD



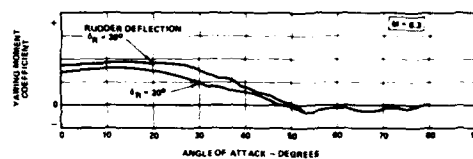
EFFECT OF ANGLE OF ATTACK ON ROLL CONTROL POWER F-18L DATA AILERONS VS FLAPERONS



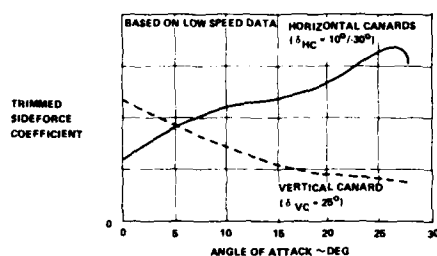
EFFECT OF ANGLE OF ATTACK ON DIRECTIONAL CONTROL POWER F-15 RUDDER EFFECTIVENESS LOW SPEED



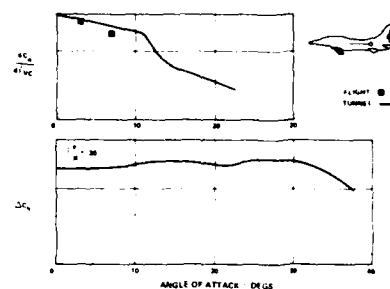
EFFECT OF ANGLE OF ATTACK ON DIRECTIONAL CONTROL POWER — RUDDER (SINGLE VERTICAL) F-20 DATA



EFFECT OF ANGLE OF ATTACK ON SIDE-FORCE CONTROL POWER HORIZONTAL VS VERTICAL CANARDS CCV-YF-16



EFFECT OF ANGLE OF ATTACK ON YAW CONTROL POWER — VERTICAL CANARD CCV YF 16 DATA



BASIC AERODYNAMIC EFFECTIVENESS

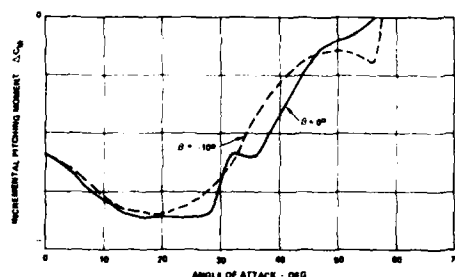
AERODYNAMIC EFFECTIVENESS VARIES WITH:

- ANGLE OF ATTACK
- ANGLE OF SIDESLIP
- MACH NUMBER
- DYNAMIC PRESSURE (AEROELASTIC EFFECTS)
- WING PLANFORM
- FOREBODY GEOMETRY
- INTERACTIONS/COUPLING

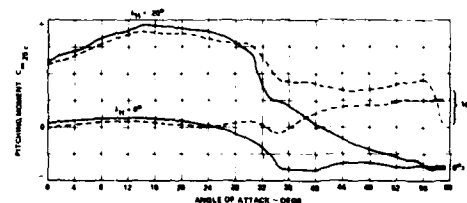
ANGLE OF SIDESLIP EFFECTS

- CONTROL EFFECTIVENESS DEGRADES AS SIDESLIP IS INCREASED
- WHY?
 - SYMMETRIC PITCH AND ROLL CONTROL SURFACES BECOME ASYMMETRIC WITH SIDESLIP THEREBY CREATING REDUCED FORCES AND MOMENTS
 - SIDESLIP CREATES SIDEWASH WHICH CAN AFFECT PITCH, ROLL AND YAW FORCES, BUT IN PARTICULAR YAW
 - AS SIDESLIP INCREASES AIRCRAFT BECOMES LESS AND LESS STREAMLINED AND MORE AND MORE LIKE A FLAT PLATE

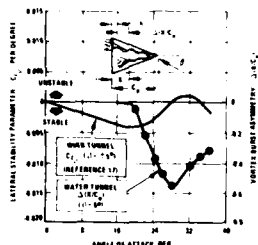
EFFECT OF SIDESLIP ON INCREMENTAL PITCHING MOMENT DUE TO HORIZONTAL TAIL DEFLECTION ($\delta_H = -20^\circ$) F-20 DATA



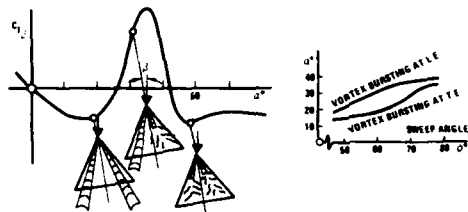
F-20 HORIZONTAL TAIL EFFECTIVENESS IN THE PRESENCE OF SIDESLIP



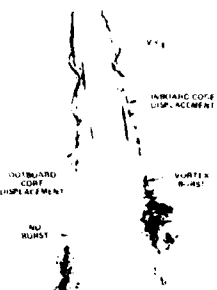
COMPARISON OF WATER TUNNEL VORTEX BURST ASYMMETRY AND WIND TUNNEL LATERAL STABILITY CHARACTERISTICS (70-DEGREE DELTA WING)



ROLL STABILITY VERSUS ANGLE OF ATTACK FOR A PURE DELTA WING



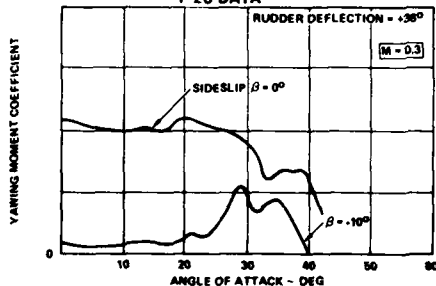
ASYMMETRIC LEX VORTEX BREAKDOWN IN SIDESLIP



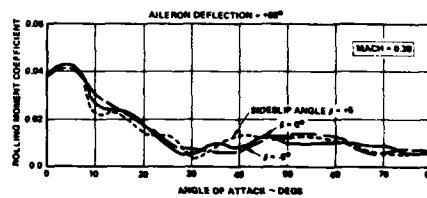
EFFECT OF SIDESLIP ON 70-DEGREE DELTA WING VORTEX CORE STABILITY: $\alpha = 25$ DEGREES



RUDDER EFFECTIVENESS IN THE PRESENCE OF SIDESLIP F-20 DATA



AILERON EFFECTIVENESS IN THE PRESENCE OF SIDESLIP F-5E DATA



BASIC AERODYNAMIC EFFECTIVENESS

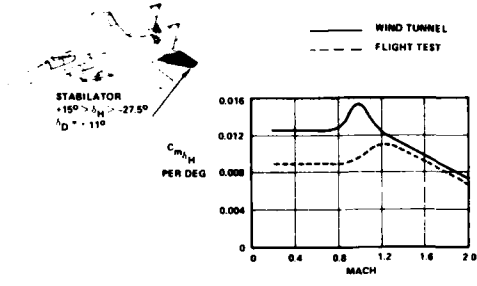
AERODYNAMIC EFFECTIVENESS VARIES WITH:

- ANGLE OF ATTACK
- ANGLE OF SIDESLIP
- MACH NUMBER
- DYNAMIC PRESSURE (AEROELASTIC EFFECTS)
- WING PLANFORM
- FOREBODY GEOMETRY
- INTERACTIONS/COUPLING

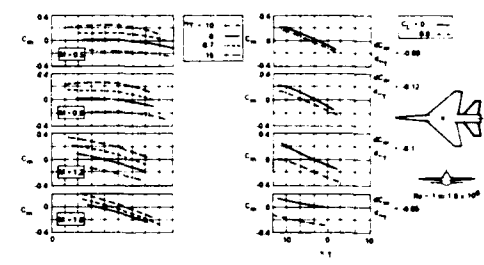
MACH EFFECTS

- PITCH, ROLL AND YAW CONTROL EFFECTIVENESS DEGRADES AS MACH NUMBER INCREASES
- WHY?
 - ON ANY LIFTING SURFACE THE LIFT CURVE SLOPE DECREASES WITH MACH NUMBER
 - AT SUBSONIC SPEEDS DEFLECTION OF CONTROL SURFACE CHANGES CIRCULATION IN REGION OF SURFACE
 - AT SUPERSONIC SPEEDS DEFLECTION OF CONTROL SURFACE HAS ONLY AN EFFECT ON CONTROL SURFACE ITSELF
- CONTROL REQUIREMENTS TYPICALLY SET BY HIGH TRANSONIC, SUPERSONIC EFFECTIVENESS

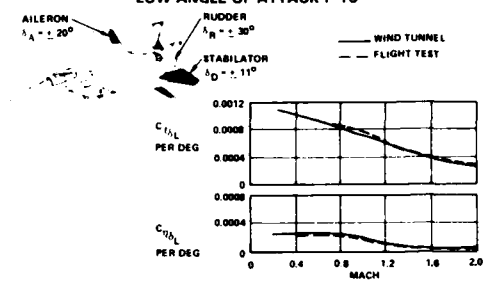
EFFECT OF MACH NUMBER ON
PITCH CONTROL POWER
LOW ANGLE OF ATTACK F-15 DATA



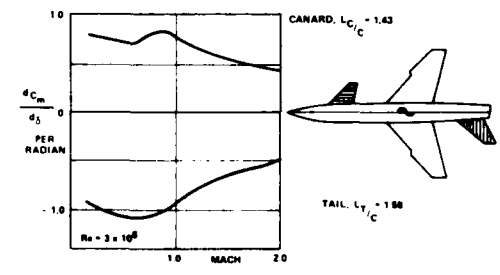
EFFECT OF MACH NO ON PITCH CONTROL POWER
- AFT TAIL



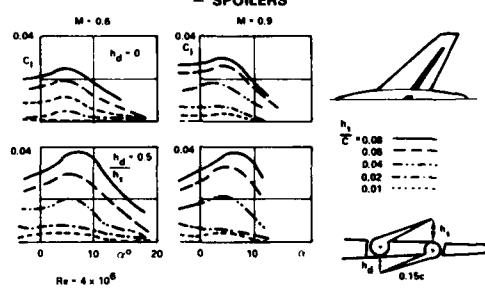
EFFECT OF MACH NUMBER ON ROLL
CONTROL POWER
LOW ANGLE OF ATTACK F-15



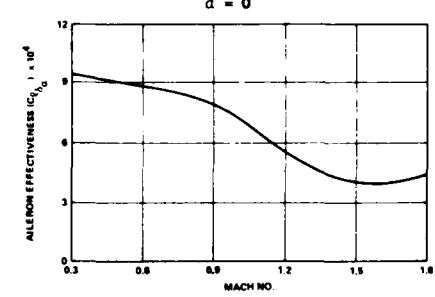
EFFECT OF MACH NO ON PITCH
CONTROL POWER
- CANARD



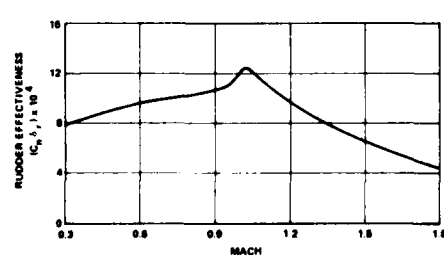
EFFECT OF MACH NO ON ROLL
CONTROL POWER
- SPOILERS



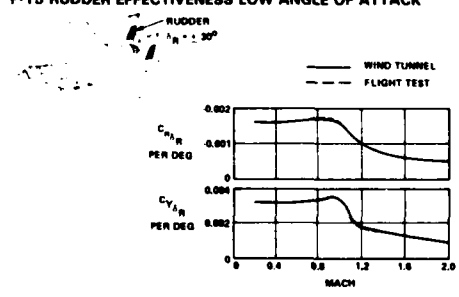
EFFECT ON MACH NO ON ROLL CONTROL
POWER - AILERON



EFFECT OF MACH NO ON DIRECTIONAL
CONTROL POWER
- RUDDER



EFFECT OF MACH NUMBER ON
DIRECTIONAL CONTROL POWER
F-15 RUDDER EFFECTIVENESS LOW ANGLE OF ATTACK

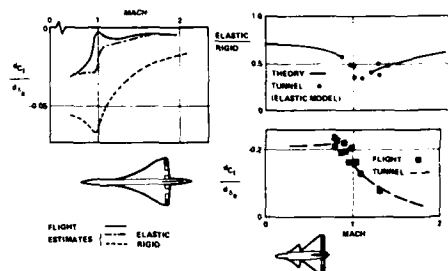


BASIC AERODYNAMIC EFFECTIVENESS

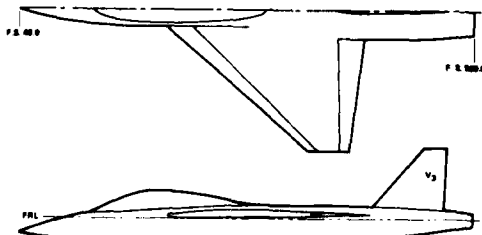
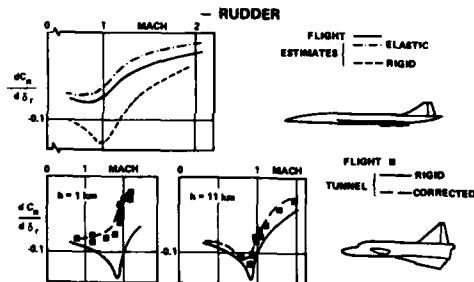
AERODYNAMIC EFFECTIVENESS VARIES WITH:

- ANGLE OF ATTACK
- ANGLE OF SIDESLIP
- MACH NUMBER
- DYNAMIC PRESSURE (AEROELASTIC EFFECTS)
- WING PLANFORM
- FOREBODY GEOMETRY
- INTERACTIONS/COUPLING

EFFECT OF AEROELASTICITY ON ROLL CONTROL POWER
— AILERON



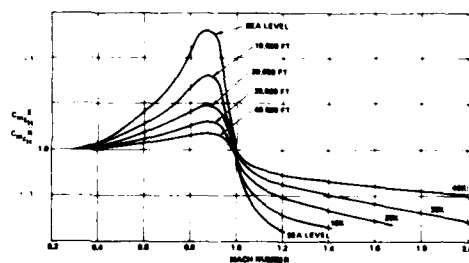
EFFECT OF AEROELASTICITY ON YAW CONTROL POWER
— RUDDER



DYNAMIC PRESSURE/AEROELASTIC EFFECTS

- AIRFRAME FLEXIBILITY IS A SIGNIFICANT FACTOR IN DETERMINING CONTROL EFFECTIVENESS
- AILERON EFFECTIVENESS IS NORMALLY REDUCED DUE TO WING TORSION/BENDING
- RUDDER EFFECTIVENESS REDUCED DUE TO FUSELAGE BENDING/TORSION. DIRECTIONAL STABILITY IS SIMILARLY REDUCED
- VARIED INFLUENCE ON HORIZONTAL TAIL EFFECTIVENESS DEPENDING ON HINGE POSITION AND MACH NUMBER

EFFECT OF AEROELASTICITY ON PITCH CONTROL POWER
— AFT TAIL F-20 DATA

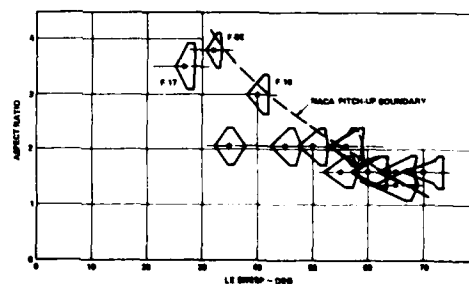


BASIC AERODYNAMIC EFFECTIVENESS

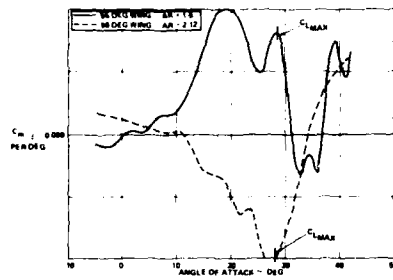
AERODYNAMIC EFFECTIVENESS VARIES WITH:

- ANGLE OF ATTACK
- ANGLE OF SIDESLIP
- MACH NUMBER
- DYNAMIC PRESSURE (AEROELASTIC EFFECTS)
- WING PLANFORM
- FOREBODY GEOMETRY
- INTERACTIONS/COUPLING

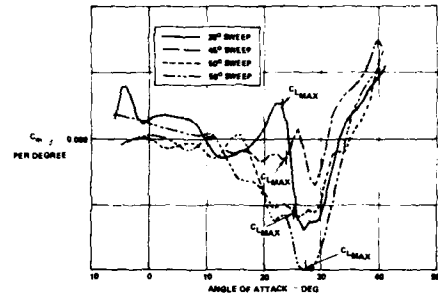
WING PLANFORM TESTING



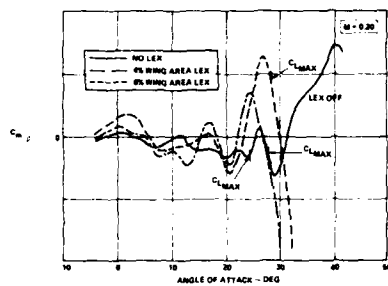
EFFECT OF ASPECT RATIO ON C_m/β



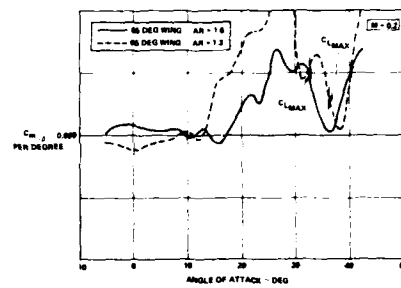
EFFECT OF L.E. SWEEP ON C_m/β



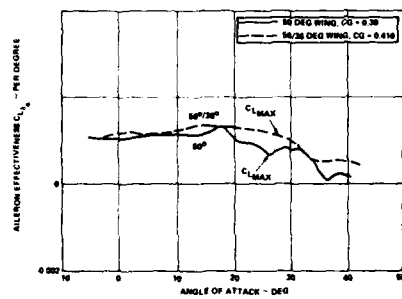
EFFECT OF LEX ON C_m/β
45° WING



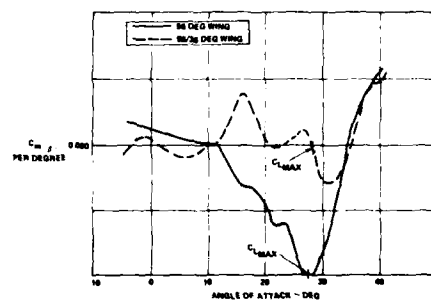
EFFECT OF ASPECT RATIO ON C_m/β



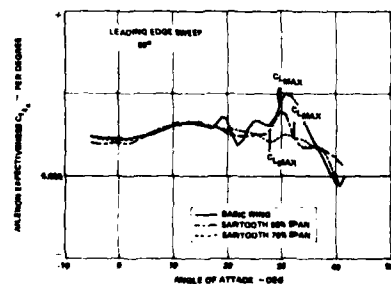
EFFECT OF LEADING EDGE CRANK ON ROLL
CONTROL POWER



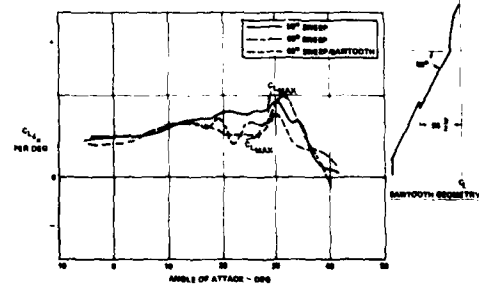
EFFECT OF LEADING EDGE CRANK ON C_m/β

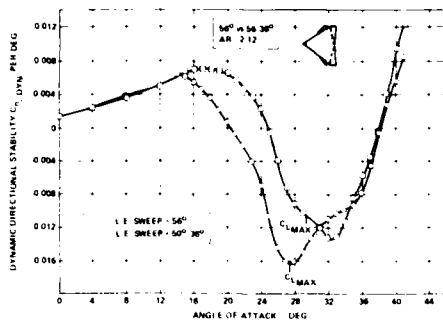


EFFECT OF SAWTOOTH ON ROLL
CONTROL POWER

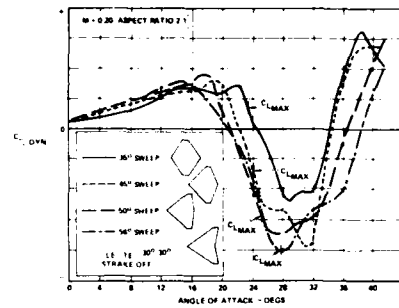


EFFECT OF SWEEP AND SAWTOOTH ON ROLL
CONTROL POWER

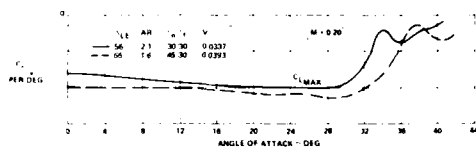
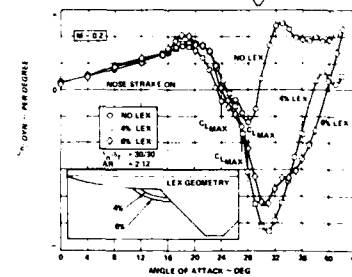


EFFECT OF LEADING EDGE CRANK ON $C_{n\beta}$ DYN

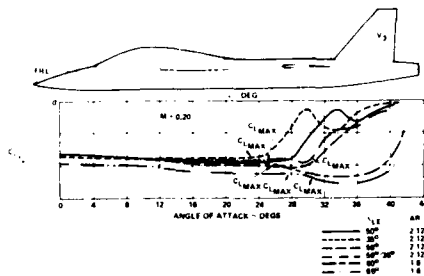
EFFECT OF WING LEADING EDGE SWEEP



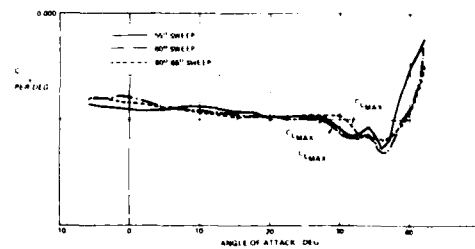
EFFECT OF ASPECT RATIO ON VERTICAL STABILIZER (V3) CONTROL POWER

EFFECT OF LEX ON $C_{n\beta}$ DYN
45° WING

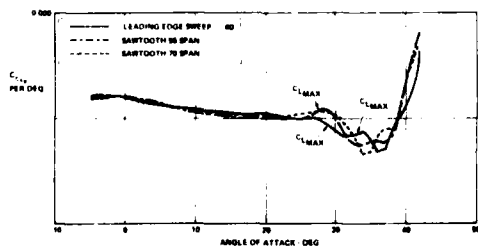
VERTICAL STABILIZER (V3) CONTROL POWER WITH VARIOUS WING PLANFORM L.E. SWEEPS



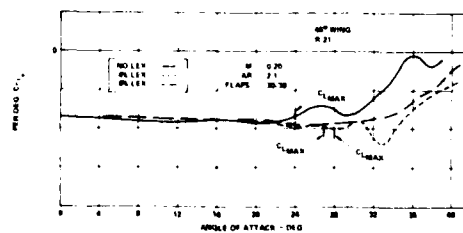
EFFECT OF SWEEP AND SAWTOOTH ON VERTICAL TAIL CONTROL POWER



EFFECT OF SAWTOOTH ON VERTICAL TAIL CONTROL POWER



EFFECT OF LEX ON VERTICAL STABILIZER (V3) CONTROL POWER



BASIC AERODYNAMIC EFFECTIVENESS

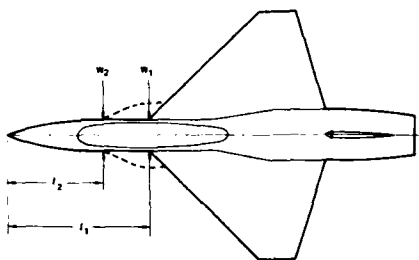
AERODYNAMIC EFFECTIVENESS VARIES WITH:

- ANGLE OF ATTACK
- ANGLE OF SIDESLIP
- MACH NUMBER
- DYNAMIC PRESSURE (AEROELASTIC EFFECTS)
- WING PLANFORM
- FOREBODY GEOMETRY
- INTERACTIONS/COUPLING

FOREBODY GEOMETRY

- AERODYNAMIC EFFECTIVENESS VARIES WITH FOREBODY GEOMETRY
- WHY?
 - WITH A SHORT FOREBODY, THE FOREBODY VORTEX IS AFFECTED BY LEX GEOMETRY
 - WITH A LONGER FOREBODY THERE IS LESS INTERACTION BETWEEN THE FOREBODY AND LEX VORTICES
 - FOREBODY SHAPE HAS POWERFUL EFFECT ON ZERO SIDESLIP AERODYNAMIC FORCES AND MOMENTS
 - AT HIGH ANGLE OF ATTACK FOREBODY CAN BE THE SOLE SOURCE OF AIRPLANES DIRECTIONAL STABILITY

FOREBODY LENGTH EFFECT



VORTEX INTERFERENCE

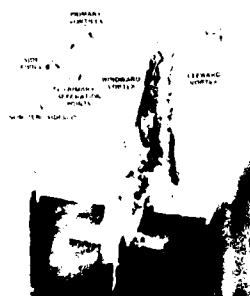
• SHORT FUSELAGE FOREBODY VORTEX AFFECTED BY LEX VORTEX



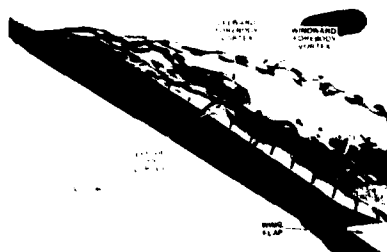
• LONG FUSELAGE FOREBODY VORTEX LESS AFFECTED BY LEX VORTEX



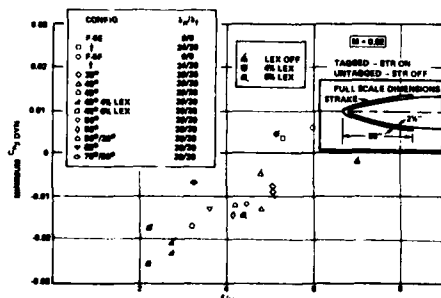
F-5F FOREBODY VORTEX ORIENTATION IN SIDESLIP (NORTHROP WATER TUNNEL)



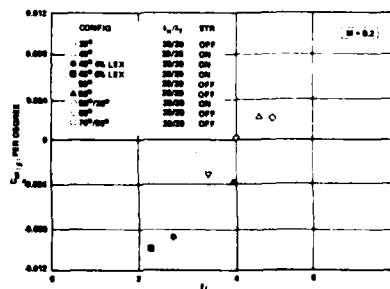
NORTHROP WATER TUNNEL FLOW VISUALIZATION OF THE STRONG COUPLING BETWEEN THE FOREBODY AND WING-LEX VORTEX FLOW FIELDS AT SMALL ANGLE OF SIDESLIP

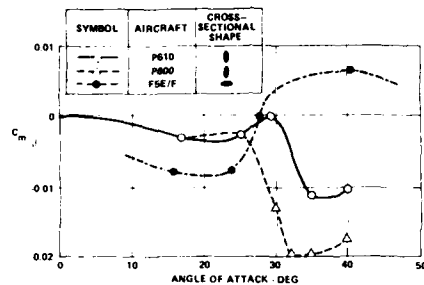
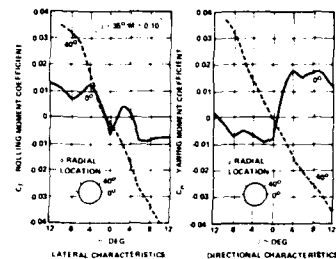


EFFECT OF FOREBODY FINENESS RATIO ON MINIMUM $C_{n\beta}$ DYN

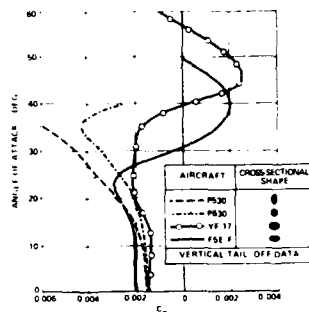
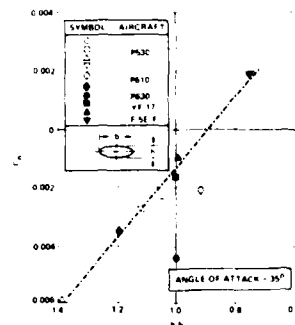


EFFECT OF FOREBODY FINENESS RATIO ON $C_{m\beta}$ AT MINIMUM $C_{n\beta}$ DYN



EFFECT OF FOREBODY SHAPE ON $C_{m\beta}$ EFFECT OF NOSE STRAKE RADIAL LOCATION ON LATERAL DIRECTIONAL CHARACTERISTICS
F-18 DATA

EFFECT OF NOSE SHAPE ON STABILITY

EFFECT OF NOSE ELLIPTICITY ON $C_{n\beta}$ 

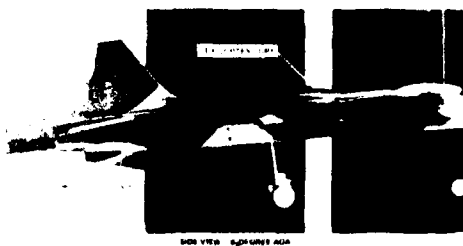
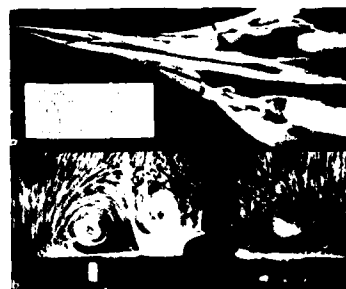
BASIC AERODYNAMIC EFFECTIVENESS

AERODYNAMIC EFFECTIVENESS VARIES WITH

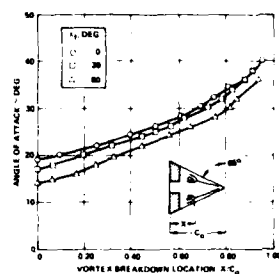
- ANGLE OF ATTACK
- ANGLE OF SIDESLIP
- MACH NUMBER
- DYNAMIC PRESSURE (AEROELASTIC EFFECTS)
- WING PLANFORM
- FOREBODY GEOMETRY
- INTERACTIONS/COUPLING

INTERACTIONS/COUPLING

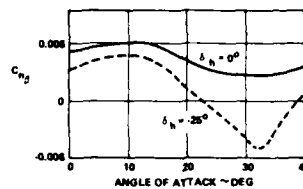
- VORTEX FLOW INTERACTIONS
- YAW/ROLL MOMENTS DUE TO $\alpha \neq 0, \beta \neq 0$
- LATERAL-DIRECTIONAL STABILITY EFFECTS DUE TO PITCH CONTROL DEFLECTION
- PITCH MOMENTS DUE TO RUDDER TOE-IN (F-18)
- ADVERSE SIDEWASH AT VERTICAL TAIL DUE TO FLAPERON DEFLECTION
- ADVERSE YAW DUE TO ROLL CONTROL DEFLECTION
 - AILERONS
 - DIFFERENTIAL AFT TAIL
 - DIFFERENTIAL CANARD

NORTHROP WIND TUNNEL SMOKE FLOW
VISUALIZATION OF A LEX VORTEX CORE AT
LOW AOA (FROM REFERENCE 20)VORTEX FLOW DEVELOPMENT
ON A CONCORDE SST MODEL

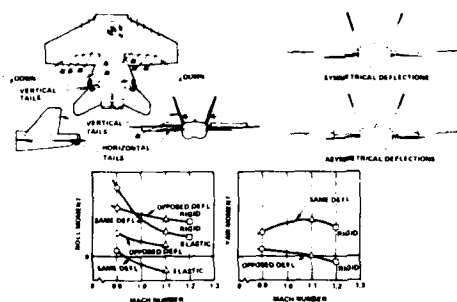
EFFECT OF DEFLECTED TRAILING-EDGE FLAP ON VORTEX BREAKDOWN CHARACTERISTICS OF 65-DEGREE DELTA WING



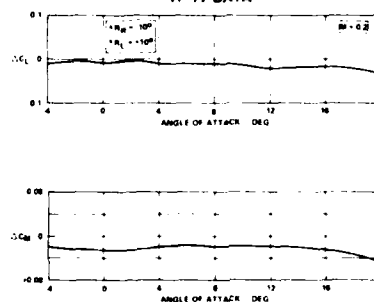
EFFECT OF HORIZONTAL TAIL DEFLECTION ON DIRECTIONAL STABILITY



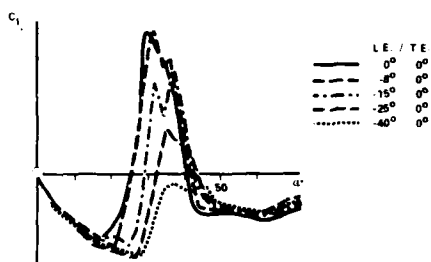
SEGMENTED FLAPERON PERFORMANCE



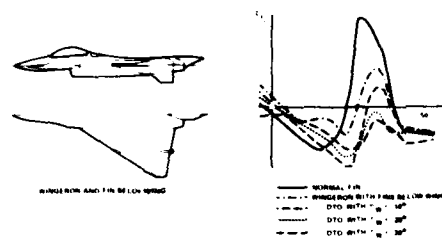
INCREMENTAL LIFT AND PITCHING MOMENT DUE TO RUDDER TOE IN VF-17 DATA



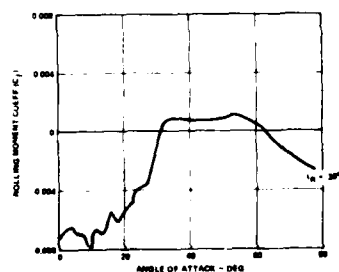
ROLL STABILITY DUE TO LEADING EDGE FLAPS



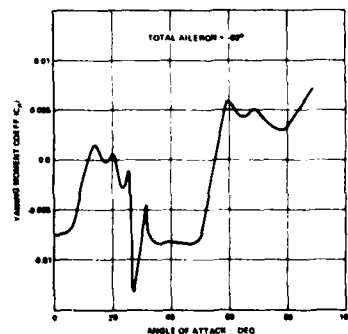
ROLL STABILITY DUE TO WINGERONS



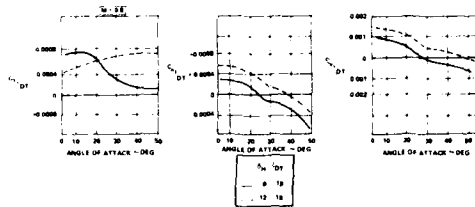
ROLLING MOMENT DUE TO RUDDER DEFLECTION



YAWING MOMENT DUE TO AILERON DEFLECTION



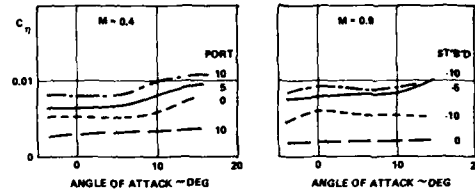
EFFECT OF DIFFERENTIAL TAIL ON YAWING MOMENT AND SIDEFORCE



CONTROL CRITERIA

- PITCH -
- ROLL -
- YAW -
- FAILURE TRANSIENTS -

VARIATION OF YAWING MOMENT DUE TO DIFFERENTIAL HORIZONTAL CANARD



PITCH CRITERIA

- NWLO WITHOUT OVER-ROTATION
- FLIGHT ENVELOPE
 - LOAD FACTOR
 - SPEED
 - ALPHA
- DIVE RECOVERY

DOMINANT

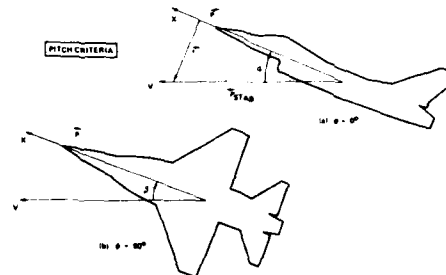
- RECOVERY FROM HIGH ATTITUDE MANEUVERS
 - STATIC
 - KINEMATIC COUPLING
 - INERTIAL COUPLING
- AVOIDANCE OF CONTROL SYSTEM COMPLEXITY
 - TIME TO DOUBLE AMPLITUDE WITH NEGATIVE RSS

RECOVERY FROM HIGH ATTITUDE MANEUVERS

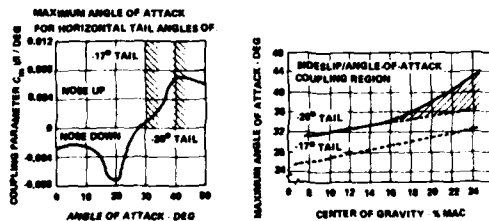
PITCH CRITERIA

- STATIC - RECOVERY FROM HIGH ALTITUDE, LOW ALPHA ZOOM
- KINEMATIC COUPLING (WING ROCK)
 - INCREASES MAXIMUM ALPHA
 - REQUIRES ADDITIONAL PITCH CONTROL
- INERTIAL COUPLING (PITCHING MOMENT DUE TO YAW AND ROLL RATES)
 - INCREASES MAXIMUM ALPHA
 - REQUIRES ADDITIONAL PITCH CONTROL

KINEMATIC COUPLING



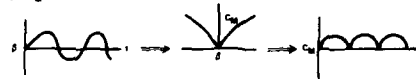
EFFECT OF PITCHING MOMENT DUE TO SIDESLIP ON KINEMATIC COUPLING ($\alpha - \beta$)



KINEMATICS

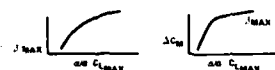
PITCH CRITERIA

- WING ROCK CAUSES OSCILLATORY SIDESLIP ANGLES
- ΔC_{y1} DUE TO β



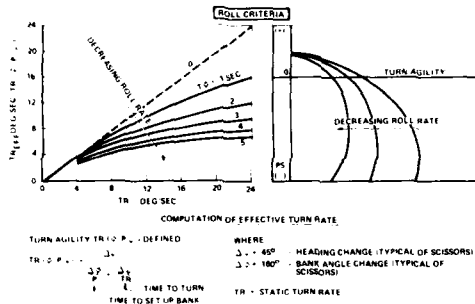
- PSEUDO STEADY STATE ASSUMPTION

APPLY ΔC_{y1} TO WIND TUNNEL DATA FOR FLIGHT DATA CORRELATION

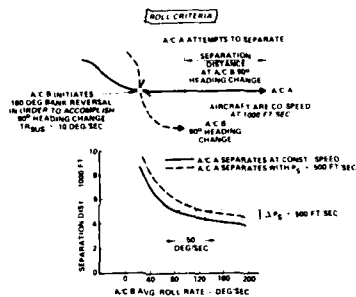


$$\Delta C_{y1} = 0.04 \Delta C_{y1}^{MAX} \quad (\text{ONE WAVE AREA AVG})$$

COMBAT MANEUVERING EFFECTIVE TURN RATE



SEPARATION DISTANCE AS A FUNCTION OF TARGET ROLL RESPONSE



ROLL COORDINATION (LCDP)

ROLL CRITERIA

$$LCDP = C_{n3} - \left(\frac{C_{n\delta_a} + K C_{n\delta_r}}{C_{l\delta_a} + K C_{l\delta_r}} \right) C_{l\beta}$$

K = AILERON - RUDDER RATIO

- ADVERSE YAW DUE TO AILERON ($-C_{n\delta_a}$) PRODUCES SIDESLIP THAT OPPOSES ROLLING MOMENT FROM AILERONS IN PRESENCE OF POSITIVE DIEDRAL EFFECT ($-C_{l\beta}$)
- RUDDER CAN COUNTER THIS EFFECT THROUGH ARI
- EFFECT ON DEPARTURE CRITERIA

YAW CRITERIA

- MAINTAIN STRAIGHT FLIGHT PATH
- ASYMMETRIC MANEUVERING
- ASYMMETRIC EXTERNAL STORES
- ASYMMETRIC THRUST
- CROSS-WIND LANDING
- INERTIAL COUPLING
- FLIGHT CONTROL SYSTEM CONSIDERATIONS

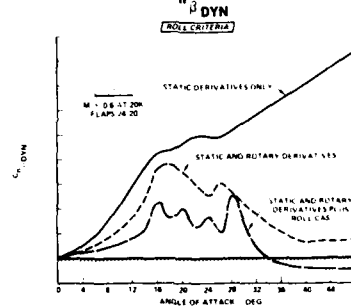
COMBAT MANEUVERING SIGNIFICANCE OF ROLL RESPONSE

ROLL CRITERIA

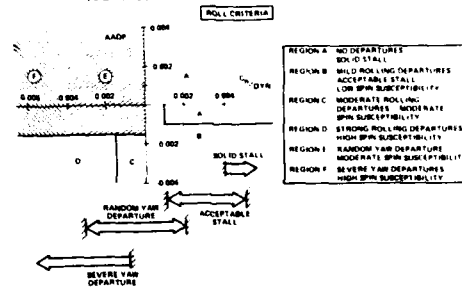
THE VALUE OF ROLL RATE CAN BE EQUATED TO SPECIFIC EXCESS POWER P_s IN THE FOLLOWING SCENARIO

- ATTACKER BREAKS OFF GUN ATTACK AND CROSSES TARGET FLIGHT PATH
- TARGET EXECUTES A REVERSE BANK AND TURNS TOWARD ESCAPING ATTACKER AT AN AVERAGE OF 10 DEG/SEC TURN RATE
- SEPARATION DISTANCE BETWEEN ESCAPING ATTACKER AND TURNING TARGET IS COMPUTED AS A FUNCTION OF TARGET AVERAGE ROLL RATE DURING THE REVERSE BANK FOR TWO CASES
 - ESCAPING ATTACKER AT CONSTANT SPEED
 - ESCAPING ATTACKER ACCELERATING ($\Delta P_s = 500$ FT/SEC)
- IN MID-RANGE OF AVERAGE ROLL RATES, A VALUE OF 50 DEG/SEC FOR THE TARGET IS EQUIVALENT TO 500 FT/SEC P_s FOR THE ESCAPING ATTACKER

FLIGHT CONTROL SYSTEM CONSIDERATIONS DEGRADATION IN $C_{n\beta}$ DYN WITH ROLL CAS



COMPARISON OF WEISSMAN AND NORTHROP DEPARTURE CRITERIA



FLIGHT CONTROL SYSTEM CONSIDERATIONS

YAW CRITERIA

- YAW CAS IMPROVES DEPARTURE RESISTANCE $C_{n\beta}$ DYN
- YAW CONTROL EFFECTIVENESS
- POSITIVE DIEDRAL

FAILURE TRANSIENTS

- IF SINGLE FAILURE EXCEEDS AIRCRAFT LIMITS FAIL-OP CAPABILITY REQUIRES FBW
- IF SINGLE FAILURE IS CONTROLLABLE WITHIN LIMITS FAIL-OP CAPABILITY CAN BE ACHIEVED WITH BACK-UP CONTROL SYSTEM
 - CONTROL LAW RECONFIGURATION FOR SINGLE FAILURE
 - REQUIRES SIMULATION TO DETERMINE EFFECTS
- CONTROLLABILITY LIMITS MUST BE SPECIFIED
- EFFECTS ON THREE-AXES CONTROLLABILITY WITH SINGLE AXIS FAILURE

CONTROL CONTROVERSIES

- WHERE DO YOU PUT THE TAIL?
 - AFT-TAIL?
 - CANARD?
 - TAILLESS?
- ANGLE OF ATTACK/LOAD FACTOR LIMITING
 - GOOD, BAD OR UGLY?
- FLYING QUALITIES ENGINEERS OF THE 80'S
 - AERONAUTICS VS ELECTRONICS

WHERE DO YOU PUT THE TAIL?

- AFT TAIL?
- CANARD?
- TAILLESS?

OBJECTIVES

- COMPARE TAILLESS, CANARD & AFT TAIL CONFIGURATIONS USING AERODYNAMIC CONTROL ONLY
- EVALUATION
 - STABILITY & CONTROL CHARACTERISTICS
 - DRAG-DUE-TO-LIFT CHARACTERISTICS
- UNDERSTAND BASIC PRINCIPLES OF CONFIGURATIONS
- USE APPROXIMATIONS IN ORDER TO SIMPLIFY THE PRESENTATION AND UNDERSTANDING

WING PLANFORM

- SAME BASIC PLANFORM USED ON ALL CONFIGURATIONS
 - LOW ASPECT RATIO
 - HIGH LEADING EDGE SWEEP
 - LOW TAPER RATIO
- RATIONALE
 - TREND IS IN THIS DIRECTION FOR FUTURE FIGHTERS
 - TAILLESS REQUIRES LOW ASPECT RATIO
 - ONLY PLANFORM THAT CAN BE USED ON ALL THREE CONFIGURATIONS
 - THE COMPARISON OF AFT-TAIL AND CANARD CONFIGURATIONS IS ESSENTIALLY INDEPENDENT OF WING PLANFORM

AERODYNAMIC PERFORMANCE CRITERIA

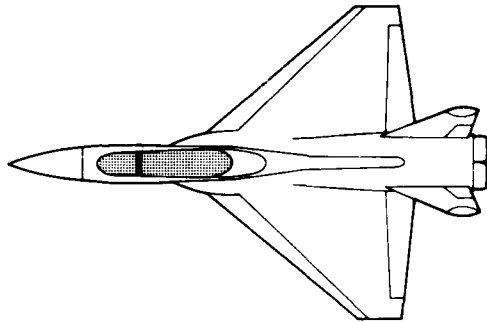
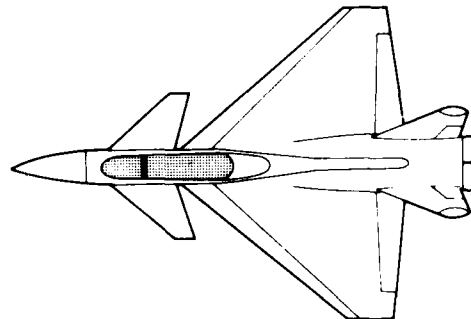
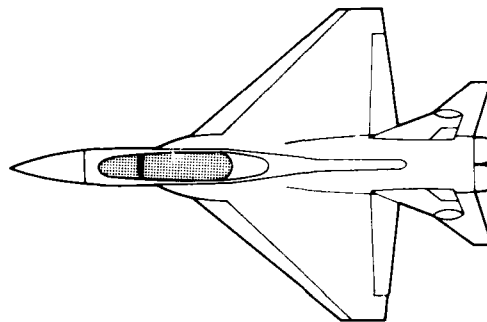
- ANGLE OF ATTACK - 0° TO 15°
 - MINIMIZE DRAG FOR PRIMARY COMBAT PERFORMANCE REGION
- ANGLE OF ATTACK - 15° TO $30^\circ/40^\circ$
 - MAXIMIZE LIFT FOR INSTANTANEOUS TURNS

STABILITY & CONTROL CRITERIA

- ANGLE OF ATTACK - 0° TO $30^\circ/40^\circ$
 - PROVIDE PITCH TRIM CAPABILITY
 - PROVIDE POSITIVE DYNAMIC STABILITY WITH FAST CONTROL RESPONSE ABOUT ALL AXES
- ANGLE OF ATTACK - $30^\circ/40^\circ$ TO 60°
 - PROVIDE STABILITY DURING PITCH TRANSIENTS RESULTING FROM INTENTIONAL MANEUVERS AT LOW SPEED
 - EVALUATE CAPABILITY FOR TRIMMED POST STALL OPERATION AS AN OPTIONAL CONSIDERATION
- ANGLE OF ATTACK - 60° TO 90°
 - PROVIDE POSITIVE AERODYNAMIC STABILITY TO PRECLUDE DEPARTURES DURING INADVERTENT PITCH EXCURSIONS AT LOW SPEED

AERODYNAMIC CONFIGURATION ASSUMPTIONS

- ACTIVE CONTROLS - SCHEDULED WITH ANGLE OF ATTACK OR COMMANDED BY AUTOMATIC CONTROL SYSTEM & PILOT
- VARIABLE CAMBER (LEADING EDGE & TRAILING EDGE FLAPS)
- PRIMARY CONTROL BY ELEVON, CANARD OR AFT TAIL (WITHOUT THRUST DEFLECTION)
- NEGATIVE STATIC STABILITY LEVEL (FLAPS & CONTROLS FIXED) SELECTED FOR EACH CONFIGURATION TO OPTIMIZE PERFORMANCE WHILE SATISFYING STABILITY & CONTROL CRITERIA

TAILLESS CONFIGURATION**CANARD CONFIGURATION****AFT-TAIL CONFIGURATION****EVALUATION PROCEDURE**

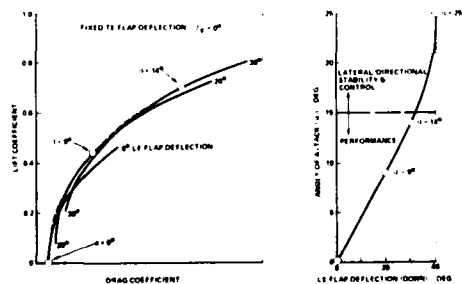
- IN REALITY, AN ITERATIVE PROCESS IS USED TO SELECT THE DEFLECTIONS OF THE LEADING EDGE & TRAILING EDGE FLAPS
- HOWEVER, TO SIMPLIFY THE PRESENTATION WE WILL
 - FIRST, DETERMINE THE OPTIMUM LEADING EDGE & TRAILING EDGE FLAP DEFLECTION SCHEDULES TO MINIMIZE DRAG AT ANGLES OF ATTACK FROM 0 TO 15°
 - SECOND, ABOVE 15° ANGLE OF ATTACK, SELECT FLAP DEFLECTIONS FROM STABILITY & TRIM CONSIDERATIONS
 - THIRD, DETERMINE THE WING/FUSELAGE PITCHING MOMENTS WITH THESE FLAP SCHEDULES
 - FOURTH, EVALUATE THE STABILITY & CONTROL OF THE THREE COMPLETE CONFIGURATIONS, USING EITHER ELEVON CONTROL, CANARD CONTROL OR AFT-TAIL CONTROL

WING PROFILE DRAG EFFECT OF LEADING EDGE & TRAILING EDGE FLAPS

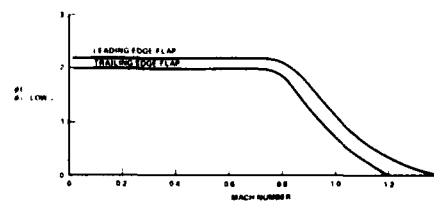
- SUBSONIC SPEEDS
 - LEADING EDGE & TRAILING EDGE FLAPS PROVIDE A SIGNIFICANT REDUCTION IN DRAG AS A FUNCTION OF ANGLE OF ATTACK
 - FLAPS CAN BE SCHEDULED WITH ANGLE OF ATTACK TO PROVIDE MINIMUM DRAG AT PERFORMANCE CONDITIONS
- SUPERSONIC SPEEDS (> 1.2)
 - TRAILING EDGE FLAPS DO NOT REDUCE DRAG
 - LEADING EDGE FLAPS AT VERY LOW DEFLECTIONS MAY PROVIDE SOME BENEFIT, DEPENDING ON LEADING EDGE SWEEP

WING PROFILE DRAG AT LIFT

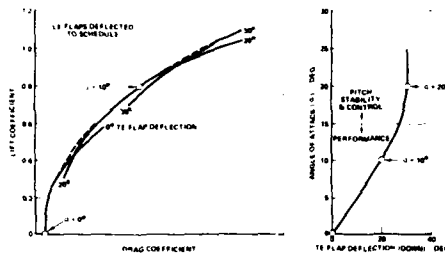
SELECTION OF LEADING EDGE FLAP SCHEDULE—SUBSONIC WING/FUSELAGE DRAG



LEADING AND TRAILING EDGE FLAP SCHEDULES FOR MINIMUM PROFILE DRAG VARIATION WITH MACH NUMBER

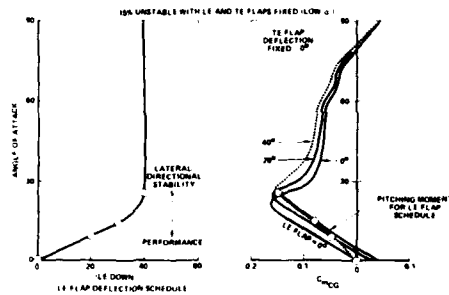


SELECTION OF TRAILING EDGE FLAP SCHEDULE—SUBSONIC WING/FUSELAGE DRAG

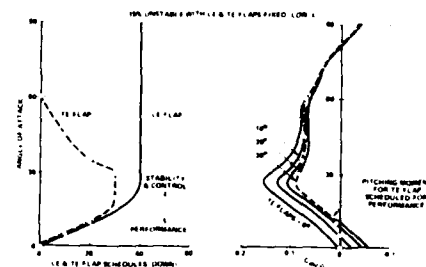


WING/FUSELAGE PITCHING MOMENT WITH SCHEDULED DEFLECTIONS OF LEADING EDGE & TRAILING EDGE FLAPS

VARIABLE LEADING EDGE FLAPS WING/FUSELAGE PITCHING MOMENT



VARIABLE TRAILING EDGE FLAPS WING/FUSELAGE PITCHING MOMENT LE FLAP SCHEDULED FOR OPTIMUM PERFORMANCE AND STABILITY



TRIM DRAG DETERMINATION

TRIM DRAG AT LIFT

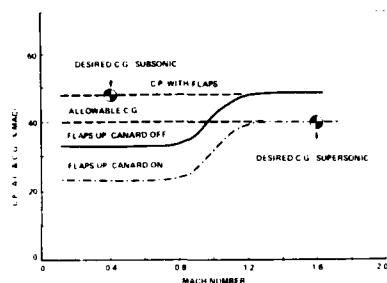
- THE TAIL-OFF PITCHING MOMENT DETERMINES THE SIZE & BASIC DIRECTION (UP OR DOWN) OF THE TAIL LOAD REQUIRED FOR TRIM
 - PRIMARY FACTOR IN TRIM DRAG
- THE TAIL-ON PITCHING MOMENT CHARACTERISTICS ARE ONLY USED TO DETERMINE THE LOCAL FIELD DIRECTION & TAIL DEFLECTION NEEDED TO ACHIEVE THE REQUIRED TRIM LOAD
 - SECONDARY FACTORS IN TRIM DRAG

SUBSONIC TRIM DRAG

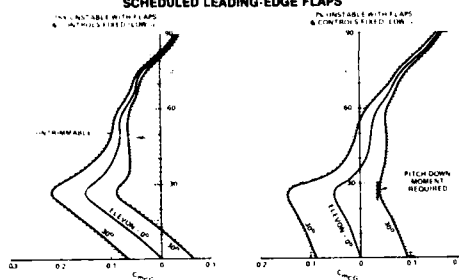
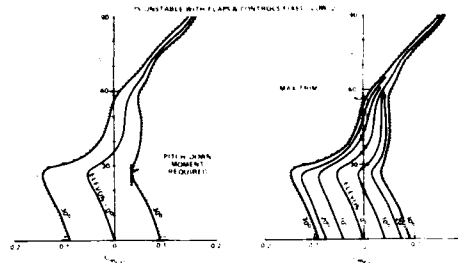
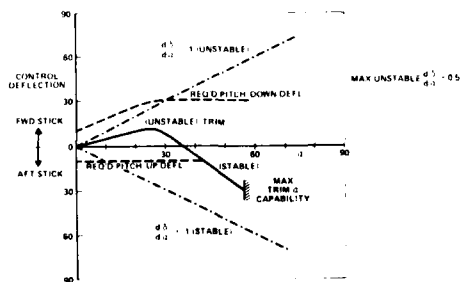
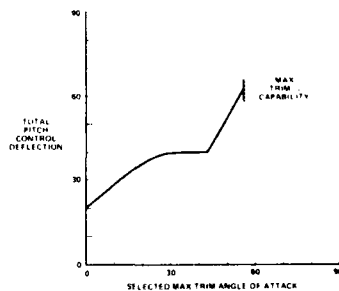
- OPTIMUM SUBSONIC TRIM DRAG OCCURS AT ZERO OR VERY LOW TAIL LOADS
 - DESIRABLE TO OPERATE AT THE TAIL-OFF CENTER OF PRESSURE WITH LEADING EDGE & TRAILING EDGE FLAPS SCHEDULED FOR MINIMUM PROFILE DRAG
 - LEADING EDGE & TRAILING EDGE FLAPS SCHEDULED FOR MINIMUM PROFILE DRAG PROVIDE 18% INCREASE IN STABILITY AT LOW ANGLE OF ATTACK
 - THEREFORE, OPTIMUM SUBSONIC TRIM DRAG IS ACHIEVED WITH THE AIRCRAFT 18% UNSTABLE WITH TAIL OFF & FIXED FLAPS (LOW ANGLE OF ATTACK)

SUPERSONIC TRIM DRAG

- OPTIMUM SUPERSONIC TRIM DRAG OCCURS AT ZERO OR SLIGHTLY POSITIVE TAIL LOAD
 - THEREFORE, OPTIMUM SUPERSONIC TRIM DRAG IS ACHIEVED WITH APPROXIMATELY NEUTRAL AIRCRAFT STABILITY WITH TAIL OFF AND FLAPS ZERO

CG AND TAIL-OFF CP POSITION AT LOW α (0° - 10°)

TAILLESS CONFIGURATION

TAILLESS CONFIGURATION
EFFECT OF CG ON PITCH CONTROL
LIMITS WITH ELEVONS
SCHEDULED LEADING-EDGE FLAPSTAILLESS CONFIGURATION
PITCH CONTROL WITH ELEVONS
SCHEDULED LEADING-EDGE FLAPSTAILLESS CONFIGURATION
ELEVON DEFLECTIONTAILLESS CONFIGURATION
TOTAL PITCH CONTROL DEFLECTIONTAILLESS CONFIGURATION
SUMMARY

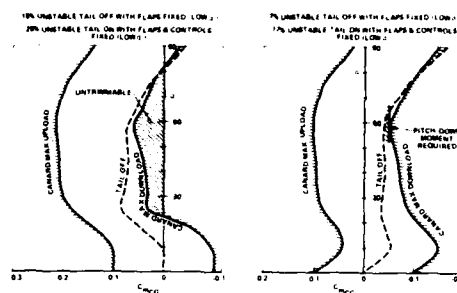
- FOR TRIM & PITCH-DOWN CONTROL AT MEDIUM ANGLE OF ATTACK, MUST MOVE CENTER OF GRAVITY 8% FORWARD OF THE OPTIMUM CENTER OF GRAVITY FOR MINIMUM TRIM DRAG
- WITH FIXED FLAPS & CONTROLS, THE TAILLESS CONFIGURATION IS 7% UNSTABLE (LOW ANGLE OF ATTACK)
- TAILLESS CONFIGURATION BECOMES STABLE ABOVE 25° ANGLE OF ATTACK
- TRIMMED POST-STALL OPERATION CAN BE ACHIEVED AT 50° - 80° ANGLE OF ATTACK, DEPENDING UPON THE SHAPE OF THE PITCHING MOMENT CURVE & ELEVON EFFECTIVENESS
- PITCH-DOWN RESPONSE CAN BE ACHIEVED WITH $\pm 30^\circ$ ELEVON DEFLECTION

TAILLESS CONFIGURATION
SUMMARY (Continued)

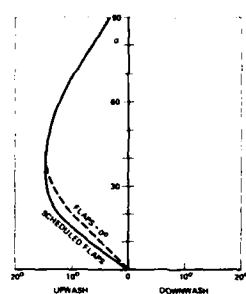
- ELEVON HINGE MOMENTS ARE VERY HIGH
- DO NOT HAVE ENOUGH CONTROL VARIABLES TO ACHIEVE DIRECT LIFT/FUSELAGE POINTING MODES

CANARD CONFIGURATION

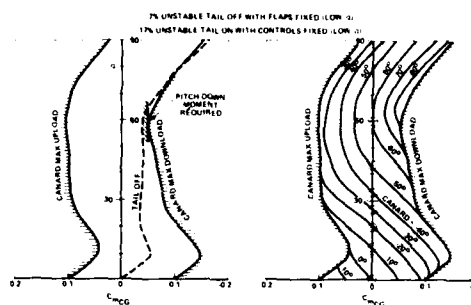
CANARD CONFIGURATION PITCH CONTROL LIMITS SCHEDULED LE AND TE FLAPS



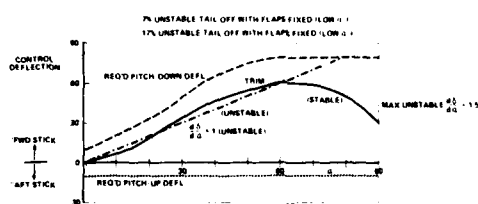
CANARD CONFIGURATION FLOW FIELD AT CANARD



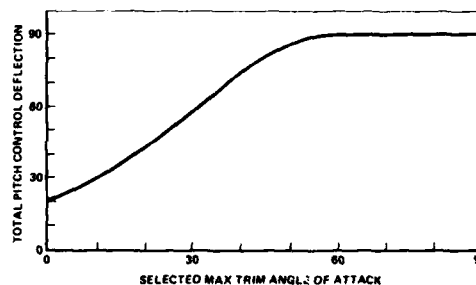
CANARD CONFIGURATION PITCH CONTROL SCHEDULED LE AND TE FLAPS



CANARD CONTROL DEFLECTION



CANARD CONFIGURATION TOTAL PITCH CONTROL DEFLECTION



CANARD CONFIGURATION SUMMARY

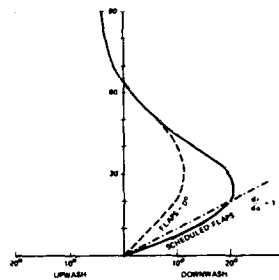
- FOR TRIM & PITCH-DOWN CONTROL AT HIGH ANGLE OF ATTACK, MUST MOVE THE CENTER OF GRAVITY 8% FORWARD OF THE OPTIMUM CENTER OF GRAVITY FOR MINIMUM TRIM DRAG
- WITH FIXED FLAPS & CONTROLS, THE CANARD CONFIGURATION IS 7% UNSTABLE TAIL OFF AND 17% UNSTABLE TAIL ON (LOW ANGLE OF ATTACK)
- CANARD CONFIGURATION BECOMES AERODYNAMICALLY MORE UNSTABLE ABOVE 18° ANGLE OF ATTACK & ONLY BECOMES STABLE ABOVE 60° ANGLE OF ATTACK
- TRIMMED POST-STALL OPERATION AT 60° ANGLE OF ATTACK REQUIRES 40° OF CANARD DEFLECTION
- AT 60° ANGLE OF ATTACK, 20° ADDITIONAL CANARD DEFLECTION IS REQUIRED FOR PITCH DOWN CONTROL (TOTAL = 60°)

CANARD CONFIGURATION SUMMARY (Continued)

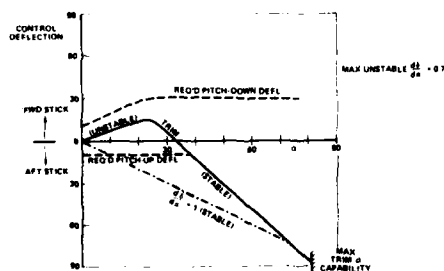
- CANARD CONTROL RATES FOR TRIM & DYNAMIC STABILITY ARE VERY HIGH
- DIRECT LIFT CAN BE OBTAINED WITH TRAILING EDGE FLAPS
- CAN BE USED IN CONJUNCTION WITH ANGLE OF ATTACK FOR POSITIONING, TRACKING OR PROVIDING POSITIVE INITIAL LIFT RESPONSE IN PITCH TRANSIENTS
- CANARD PROVIDES ADDITIONAL POSITIVE INITIAL LIFT IN PITCH TRANSIENTS

AFT-TAIL CONFIGURATION

AFT-TAIL CONFIGURATION
FLOW FIELD AT TAIL



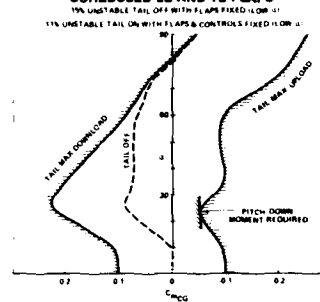
AFT TAIL CONTROL DEFLECTION



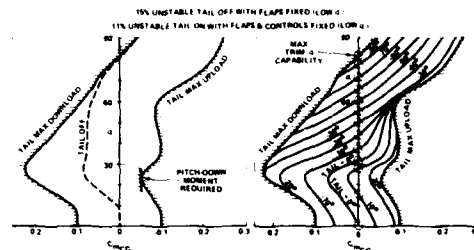
AFT-TAIL CONFIGURATION SUMMARY

- THE AFT-TAIL AIRCRAFT CAN USE THE CENTER OF GRAVITY FOR OPTIMUM PERFORMANCE
- WITH FIXED FLAPS & CONTROLS, AFT-TAIL AIRCRAFT IS 18% UNSTABLE TAIL OFF & 11% UNSTABLE TAIL ON (LOW ANGLE OF ATTACK)
- AFT-TAIL CONFIGURATION BECOMES STABLE ABOVE 25° ANGLE OF ATTACK
- TRIMMED POST-STALL OPERATION AT 80° ANGLE OF ATTACK CAN BE ACHIEVED WITH -40° OF TAIL DEFLECTION
- PITCH DOWN RESPONSE CAN BE ACHIEVED WITH +30° DEFLECTION

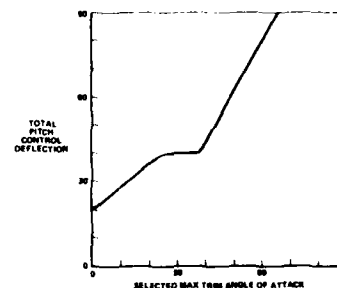
AFT TAIL CONFIGURATION
PITCH CONTROL LIMITS
SCHEDULED LE AND TE FLAPS



AFT TAIL CONFIGURATION
PITCH CONTROL
SCHEDULED LE & TE FLAPS



AFT-TAIL CONFIGURATION
TOTAL PITCH CONTROL DEFLECTION

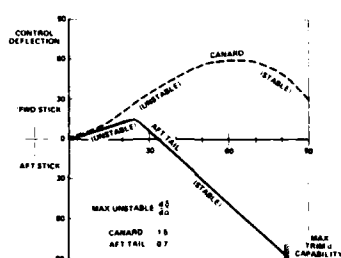


AFT-TAIL CONFIGURATION SUMMARY (Continued)

- TAIL CONTROL RATES FOR TRIM & DYNAMIC STABILITY ARE ATTAINABLE
- TAIL HINGE MOMENTS ARE LOW, RESULTING IN REASONABLE POWER REQUIREMENTS
- DIRECT LIFT CAN BE OBTAINED WITH TRAILING EDGE FLAPS, TRIMMED WITH THE AFT-TAIL
- CAN BE USED IN CONJUNCTION WITH ANGLE OF ATTACK FOR POSITIONING, TRACKING OR PROVIDING POSITIVE INITIAL LIFT RESPONSE IN PITCH TRANSIENTS

COMPARISON AFT-TAIL VS CANARD

AFT TAIL VS CANARD TRIM CONTROL DEFLECTIONS



AFT-TAIL VS CANARD PERFORMANCE

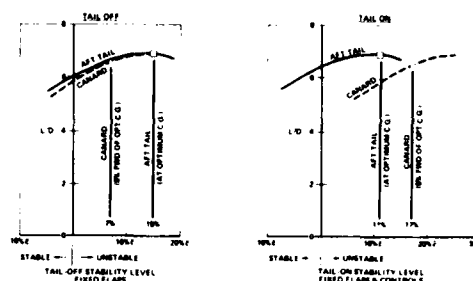
PERFORMANCE COMPARISONS ARE MADE USING CONFIGURATIONS THAT ARE UNRESTRICTED IN ANGLE OF ATTACK DURING MANEUVERING TRANSIENTS

- TRIM DRAG IS ESSENTIALLY EQUAL AT THE CENTER OF GRAVITY FOR OPTIMUM PERFORMANCE
- AFT-TAIL AIRCRAFT CAN FLY AT THE CENTER OF GRAVITY FOR MINIMUM TRIM DRAG
- CANARD AIRCRAFT TRIM DRAG IS PENALIZED BY THE FORWARD CENTER OF GRAVITY MOVEMENT REQUIRED FOR PITCH-DOWN CONTROL

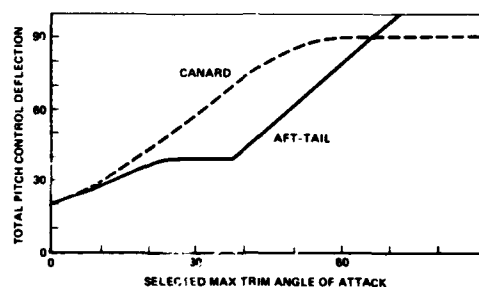
AFT-TAIL VS CANARD STABILITY & CONTROL

- STABILITY LEVEL AT LOW ANGLE OF ATTACK
 - BOTH AIRCRAFT CAN FLY UNSTABLE
 - AFT-TAIL AIRCRAFT IS MORE UNSTABLE TAIL OFF (DESIRED FOR PERFORMANCE)
 - CANARD AIRCRAFT IS MORE UNSTABLE TAIL ON (UNDESIRABLE FROM CONTROL SYSTEM CONSIDERATIONS)
- STABILITY AT HIGH ANGLE OF ATTACK
 - AFT-TAIL AIRCRAFT BECOMES AERODYNAMICALLY STABLE ABOVE 25° ANGLE OF ATTACK (DESIRABLE)
 - CANARD AIRCRAFT REMAINS AERODYNAMICALLY UNSTABLE TO 60° ANGLE OF ATTACK (UNDESIRABLE)
- CONTROL SYSTEM
 - CANARD CONTROL SURFACE DEFLECTION RATES ARE HIGHER - TOUGHER CONTROL SYSTEM DESIGN & GREATER RISK

AFT TAIL VS CANARD SUBSONIC L/D ($C_L = 0.7$)



AFT-TAIL VS CANARD TOTAL PITCH CONTROL DEFLECTION



AFT-TAIL VS CANARD MANEUVER MODES

- POST-STALL OPERATION
 - BOTH AIRCRAFT CAN PROVIDE POST-STALL OPERATION BY TRIMMING TO VERY HIGH ANGLE OF ATTACK ($> 80^\circ$), DEPENDING UPON THE SELECTED HORIZONTAL TAIL DEFLECTION ANGLE
- DIRECT LIFT
 - BOTH AIRCRAFT PROVIDE DIRECT LIFT CAPABILITY USING TRAILING EDGE FLAPS
 - POSITIVE INITIAL LIFT RESPONSE IS PROVIDED BY THE TRAILING EDGE FLAPS, WITH THE CANARD PROVIDING SOME ADDITIONAL POSITIVE INITIAL LIFT IN TRANSIENTS

AFT-TAIL VS CANARD CONFIGURATION INTEGRATION

- THE CANARD AIRCRAFT CONFIGURATION HAS OPERATIONAL & DESIGN PROBLEMS FROM THE STANDPOINT OF:
 - VISIBILITY
 - ACCESS TO COCKPIT
 - EQUIPMENT ACCESS IN COCKPIT AREA
 - INLET FLOW
 - WING DESIGN OPTIMIZATION
- CANARD AIRCRAFT HAS BETTER ENGINE ACCESS

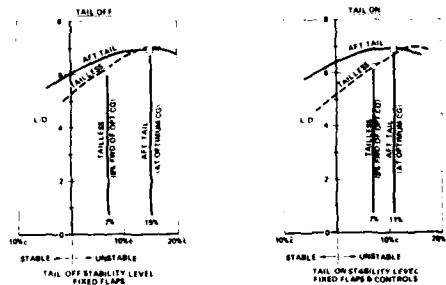
AFT-TAIL VS CANARD CONCLUSIONS

- WITH ACTIVE CONTROLS, THE COMBAT & MISSION PERFORMANCES ARE COMPARABLE
- THE CANARD CONFIGURATION DOES NOT HAVE ANY FUNDAMENTAL ADVANTAGES OVER THE AFT-TAIL AIRCRAFT
- THE AFT-TAIL AIRCRAFT HAS FEWER OPERATIONAL COMPROMISES, REDUCED DESIGN COMPLEXITY AND LOWER RISK

THEREFORE

- THE AFT-TAIL AIRCRAFT IS PREFERRED OVER THE CANARD AIRCRAFT

AFT-TAIL VS TAILLESS SUBSONIC L/D ($C_L \sim 0.7$)



AFT-TAIL VS TAILLESS PERFORMANCE

PERFORMANCE COMPARISONS ARE MADE USING CONFIGURATIONS THAT ARE UNRESTRICTED IN ANGLE OF ATTACK DURING MANEUVERING TRANSIENTS

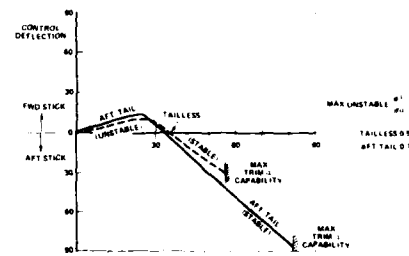
- AFT-TAIL AIRCRAFT CAN FLY AT CENTER OF GRAVITY FOR MINIMUM TRIM DRAG
- TAILLESS AIRCRAFT HAS HIGHER LIFT/DRAG RATIO AT OPTIMUM CENTER OF GRAVITY, BUT IS PENALIZED BY FORWARD CENTER OF GRAVITY MOVEMENT REQUIRED FOR PITCH DOWN CONTROL
- RESULTING LIFT/DRAG RATIOS AT SUBSONIC SPEEDS INDICATE SUPERIORITY FOR THE AFT-TAIL AIRCRAFT

AFT-TAIL VS TAILLESS STABILITY & CONTROL

- STABILITY LEVEL AT LOW ANGLE OF ATTACK
 - THE AFT-TAIL AIRCRAFT IS MORE UNSTABLE THAN THE TAILLESS AIRCRAFT (DESIRABLE FOR PERFORMANCE)
 - HOWEVER, CONTROL SYSTEM DESIGN IS WITHIN PRACTICAL LIMITS AND REASONABLE RISK
- STABILITY AT HIGH ANGLE OF ATTACK
 - BOTH AIRCRAFT BECOME STABLE ABOVE 25° ANGLE OF ATTACK
- CONTROL SYSTEM POWER
 - TAILLESS AIRCRAFT HAS SLIGHTLY LOWER PITCH CONTROL SURFACE RATES
 - HOWEVER, TAILLESS AIRCRAFT HAS SIGNIFICANTLY HIGHER HINGE MOMENTS
 - RESULT IS THAT TAILLESS AIRCRAFT HAS SIGNIFICANTLY HIGHER PITCH CONTROL POWER REQUIREMENTS

COMPARISON AFT-TAIL VS TAILLESS

AFT-TAIL VS TAILLESS TRIM CONTROL DEFLECTIONS



AFT-TAIL VS TAILLESS MANEUVER MODES

- POST-STALL OPERATION
 - BOTH AIRCRAFT CAN PROVIDE POST-STALL OPERATION BY TRIMMING TO VERY HIGH ANGLE OF ATTACK
 - THE AFT-TAIL AIRCRAFT CAN ACHIEVE >80° ANGLE OF ATTACK, DEPENDING UPON THE SELECTED HORIZONTAL TAIL DEFLECTION ANGLE
 - THE TAILLESS AIRCRAFT CAN ACHIEVE 60° - 80° ANGLE OF ATTACK, DEPENDING UPON THE SHAPE OF THE PITCHING MOMENT CURVE AND ELEVON EFFECTIVENESS
- DIRECT LIFT
 - THE AFT-TAIL AIRCRAFT PROVIDES DIRECT LIFT CAPABILITY USING TRAILING EDGE FLAP, TRIMMED WITH THE HORIZONTAL TAIL PITCH CONTROL
 - THE TAILLESS AIRCRAFT CAN NOT PROVIDE DIRECT LIFT AS THE TRAILING EDGE FLAPS ARE THE PITCH CONTROL

AFT-TAIL VS TAILLESS CONFIGURATION INTEGRATION

- AFT-TAIL AIRCRAFT
 - STABILITY & CONTROL CONTRIBUTION OF HORIZONTAL TAIL, ESPECIALLY AT HIGH ANGLE OF ATTACK, ALLOWS MORE FLEXIBILITY IN SELECTION OF WING PLANFORM FROM AERODYNAMIC CONSIDERATIONS
- TAILLESS AIRCRAFT
 - ELIMINATION OF HORIZONTAL TAIL PROVIDES MORE FLEXIBILITY IN CONFIGURATION ARRANGEMENT IN TERMS OF WING PLANFORM AND LOCATION
 - TAILLESS AIRCRAFT HAS BETTER ENGINE ACCESS

AFT-TAIL VS TAILLESS

CONCLUSIONS

- IT IS DESIRED TO PROVIDE THE CAPABILITY FOR MAXIMUM MANEUVERS WITHOUT LIMITING THE ANGLE OF ATTACK DURING PITCH TRANSIENTS
 - RESULTING CONFIGURATION AND LIFT/DRAG RATIO FAVORS THE AFT-TAIL AIRCRAFT
- IT IS DESIRED TO PROVIDE DIRECT LIFT MODES
 - USING AERODYNAMIC CONTROL, THIS CAN NOT BE ACHIEVED WITH THE TAILLESS AIRCRAFT

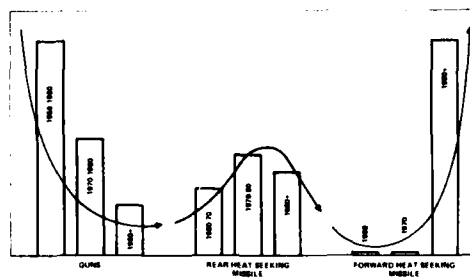
THEREFORE

- THE AFT-TAIL AIRCRAFT IS PREFERRED OVER THE TAILLESS AIRCRAFT

ANGLE OF ATTACK/LOAD FACTOR LIMITING
- GOOD, BAD OR UGLY

- HISTORICAL TRENDS
- WHY α/η LIMITING?
- WHY NOT α/η LIMITING?
- HOW HIGH?
- HOW HARD?
- CONCLUSIONS

HISTORICAL WEAPON USAGE TREND IN AIR COMBAT



HISTORICAL TRANSFER

- ALL FIGHTER AIRCRAFT HAVE 8 LIMITERS
- T.386/F-4A-4 LIMITED CONTROL POWER-LARGE POSITIVE STABILITY
 - F.106/F-111 STICK SHAKER/LUTHER
 - F-18 LAT-OAR AUTHORITY REDUCED AS H_{12}
 - F-18 ACTIVE α LIMITING, ROLL RATE LIMITING, RUDDER FADE OUT, AUTOMATIC SPIN RECOVERY
MANUAL PITCH OVERRIDE
 - F-18 NO 8 LIMITER, LAT-OAR AUTHORITY REDUCED AS H_{12}
 - M-20B: ELASTIC α LIMITER
 - F-35 NO 8 LIMIT, BLENDING PITCH RATE/LOAD FACTOR COMMAND

ELEMENTS OF AGILITY

LONGITUDINAL

- * ACCELERATION HIGH USABLE THRUST & LOW DRAG FAST ENGINE RESPONSE IS ALSO IMPORTANT BUT IS NOT CONSIDERED IN THE COMPARISONS
- * DECELERATION
 - AT HIGH AOA FLAT PLATE AREA OF AIRCRAFT
 - AT LOW AOA SPEED BRAKES IDLE THRUST

●ITCH

- | | |
|---|---|
| * TURN RATE | HIGH USEABLE LIFT (NO AOA LIMITING) |
| * PITCH RESPONSE FOR TURN AND NOSE POINTING | GOOD HORIZONTAL TAIL EFFECTIVENESS WITH NO CONTROL SURFACE POSITION/RATE LIMITING |

LATERAL

- NOTE UNLOADING TO ROLL AT LOW AOA LIMITS PILOT CONTROL OF POSITIONING AND COMPROMISE YAW/T RACRAFT SURVEILLANCE

ANYONE THIC

4. TRANSIENT MANEUVERING TO RAPIDLY SWEEP MANEUVER PLANE
REQUIRES HIGH DEPARTURE SPIN RESISTANCE

ENERGY RESERVE FLABILITY

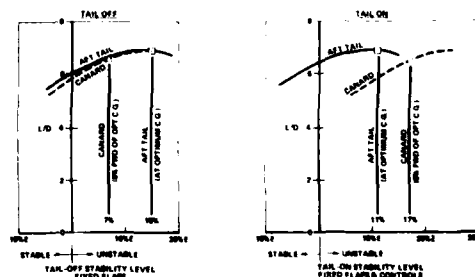
NEW ACM GROUND RULES

- THE ALL ASPECT IR MISSILE HAS SIGNIFICANTLY ALTERED AIR-TO-AIR TACTICS
- THE A/C THAT CAN POINT FIRST CAN SHOOT FIRST
- E/M COMPARISONS CAN BE MISLEADING (THIS HOLDS BOTH FOR "LOCAL" AND "GLOBAL" PRESENTATIONS)
- AN AIRCRAFT THAT DOES NOT HAVE HIGH AOA CAPABILITY IS AT A DISADVANTAGE AGAINST ONE THAT DOES. HIGH AOA MEANS HIGH RATE OF CHANGE OF NOSE POSITION
- USING THE ENERGY DEPLETING OPENING MANEUVER SHOULD ONLY BE ACCOMPLISHED IF ENERGY CAN BE READILY REGAINED - ESPECIALLY IN A MULTI-BOGEY ENVIRONMENT

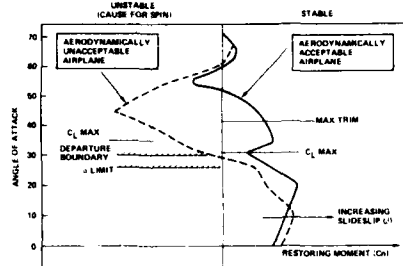
WHY a/a LIMITING

- "HEADS OUT OF THE COCKPIT" MANEUVERING - REDUCED WORKLOAD
- ALLOWS MANEUVER L/D ENHANCEMENT DUE TO MORE NEGATIVE STABILITY - ESPECIALLY CANARD/TAILESS
- POTENTIAL TO RELAX AERODYNAMIC DESIGN REQUIREMENTS AT POST-LIMIT AOA'S
- g-LIMITER PROVIDES STRUCTURAL PROTECTION
- g-LIMITER ALLOWS INITIAL ADVANTAGE IN ACM DUE TO RAPID BUILDUP TO M_1

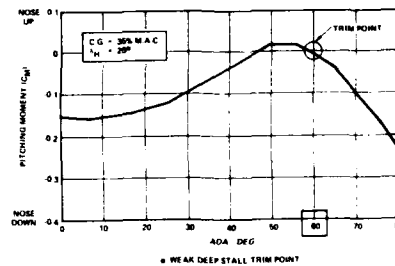
L/D ENHANCEMENT



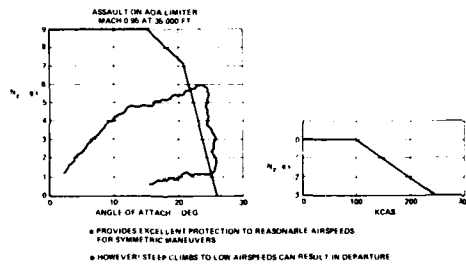
POTENTIAL TO RELAX AERODYNAMIC REQUIREMENTS DIRECTIONAL STABILITY



DEEP STALL



ANGLE-OF-ATTACK AND STRUCTURAL LIMITING



WHY NOT LIMITING

- AT LOW SPEEDS α LIMITER CAN BE DEFEATED MINIMUM AIRSPEED LIMIT IMPLIED
- AT HIGH ROLL RATES α LIMITER CAN BE DEFEATED DUE TO INERTIAL COUPLING ROLL RATE LIMITER IMPLIED
- DUE TO REDUCED PITCH CONTROL EFFECTIVENESS α_L MAY BE REQUIRED TO BE BELOW α_{MAX} LIFT
- α LIMITER REDUCES ACM EFFECTIVENESS BELOW THE CORNER SPEED
- α LIMITER MAY LEAD TO TENDENCY TO RELAX AERODYNAMIC REQUIREMENTS TOO MUCH AT POST LIMITER ANGLE OF ATTACK

HOW HIGH? $\alpha_L = ?$

FUNDAMENTALS

- FOR EVERY FIGHTER AIRCRAFT THERE IS AN AOA BEYOND WHICH MANEUVER CAPABILITY DEGRADES
- CONFIGURATION DEPENDENT
- MANEUVER DEPENDENT
- WEAPON DEPENDENT
- FOR MOST CONFIGURATIONS $\alpha_L = \alpha_{CLMAX}$
- REQUIRES GOOD AERODYNAMICS TO $\alpha_L = ?$
- WHERE α_L DEPENDS ON TYPE OF LIMITER (HARD VS SOFT)
- STRONG INTERACTION BETWEEN PITCH CONTROL, POWER AT α_L AND ALLOWABLE ROLL CONTROL
- HIGHER α_L MAY REQUIRE LOWER P_{MAX}
- HIGHER P_{MAX} MAY REQUIRE LOWER α_L
- FOR EVERY FIGHTER AIRCRAFT, THERE IS AN AOA AND YAW RATE WHERE DEPARTURE/SPIN WILL OCCUR
- IF A FIGHTER A/C CANNOT COMMAND AOA/YAW RATES CLOSE TO THESE VALUES THEN ITS CONTROL SURFACES ARE NOT LARGE ENOUGH
- α LIMITER CAN ALLOW AGGRESSIVE PITCH/YAW/ROLL RATES AND PROVIDE DEPARTURE/SPIN PROTECTION

HOW HIGH? (Continued)

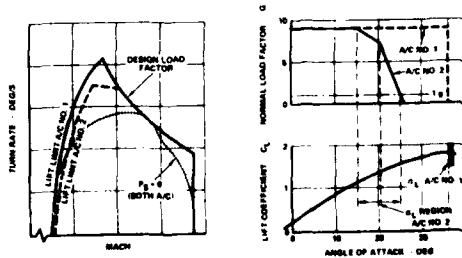
α_L MUST BE AT LEAST EQUAL TO α_{CLMAX}

ANALYSIS

- NEUTRAL HEAD-ON ENGAGEMENT
- A/C 1 VS A/C 2
- IDENTICAL PERFORMANCE
- IDENTICAL WEAPONS - ALL ASPECT MID RANGE IN MISSILE
- DIFFERENT α LIMITER SCHEDULES
- A/C 1 $\alpha_L = 30^\circ$ (C_{LMAX})
- A/C 2 $\alpha_L = 15$ (20° Htg)
- TWO ALTITUDES
- 8000 FT, 15000 FT
- TWO INITIAL MACH
- M = 0.8, M = 0.9
- TWO MANEUVER SCENARIOS
- HORIZONTAL PLANE
- VERTICAL PLANE

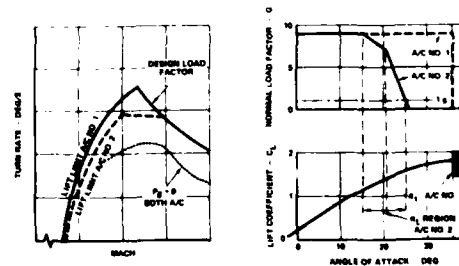
α LIMIT - ACM COMPARISON

h = 5,000 ft

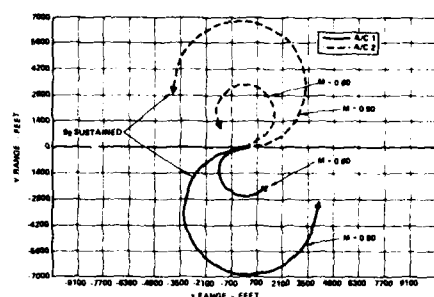


α LIMIT - ACM COMPARISON

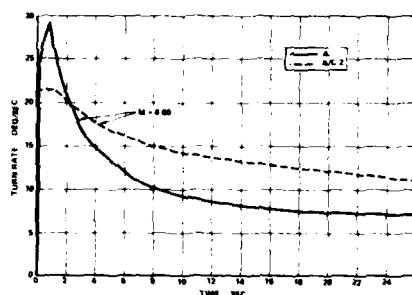
h = 15,000 ft



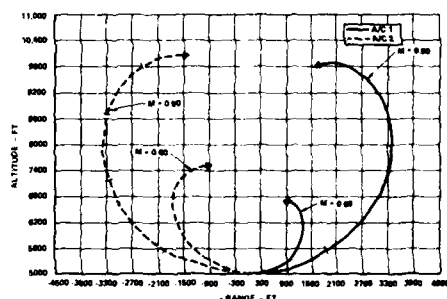
TURNING IN THE HORIZONTAL PLANE
ALTITUDE 5000 FT



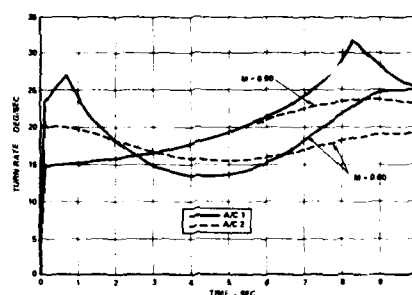
COMPARISON OF TURN RATE VERSUS TIME
AT 5000 FEET ALTITUDE



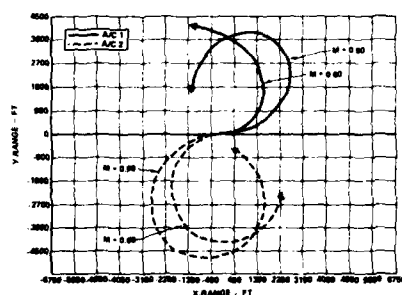
TURNING IN THE VERTICAL PLANE
INITIAL ALTITUDE 5000 FT



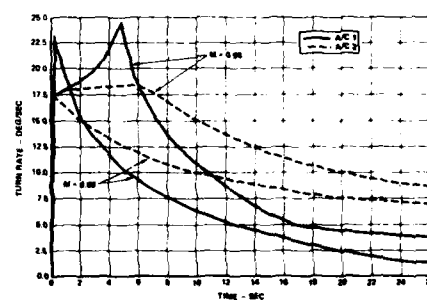
COMPARISON OF TURN RATE VERSUS TIME
TIME AT 5000 FT ALTITUDE



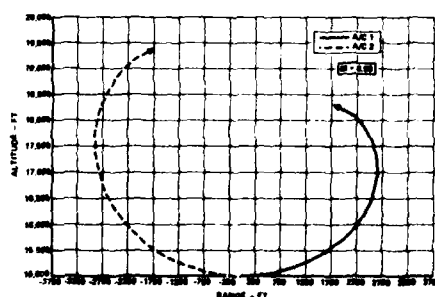
TURNING IN THE HORIZONTAL PLANE
ALTITUDE 15,000 FT



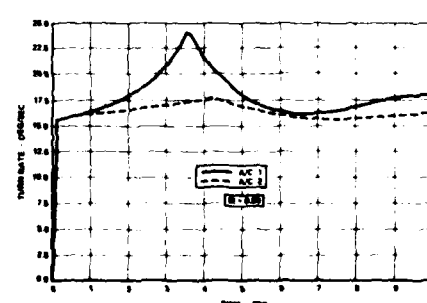
COMPARISON OF TURN RATE VERSUS TIME
AT 15,000 FT ALTITUDE



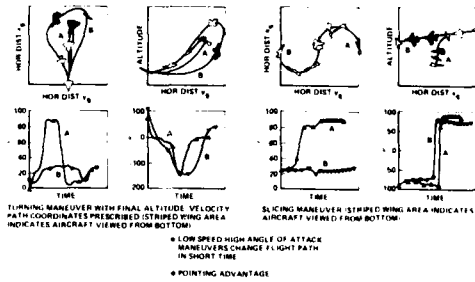
TURNING IN THE VERTICAL PLANE
INITIAL ALTITUDE 15,000 FT



COMPARISON OF TURN RATE VERSUS TIME
AT 15,000 FT ALTITUDE



ADVANTAGE OF POST-STALL MANEUVERING



HOW HIGH?

α_L MUST BE AT LEAST EQUAL TO α_{CLMAX}

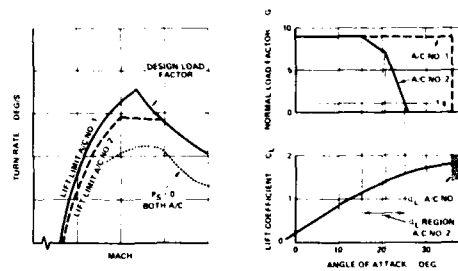
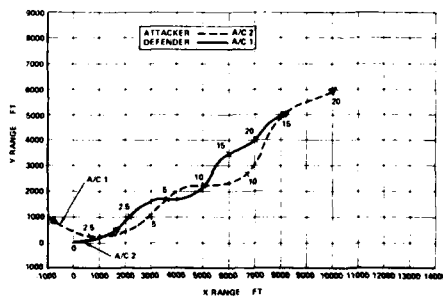
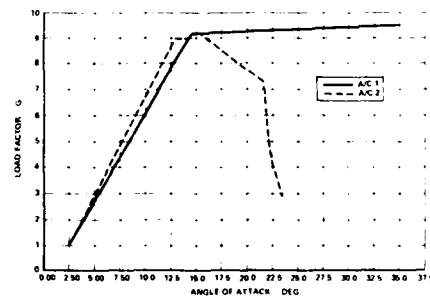
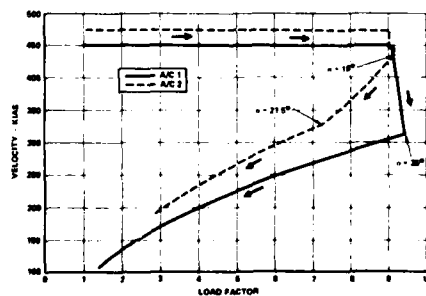
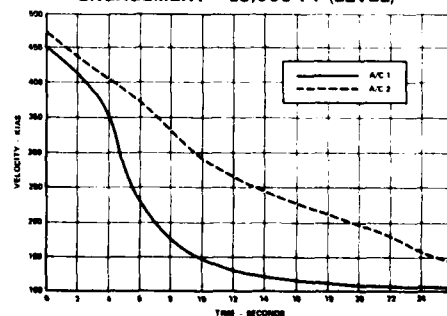
ANALYSIS: ACM EFFECTIVENESS

- A/C 1 IS DEFENSIVE @ $t = 0$
- A/C 1 VS A/C 2
- A/C 2 ABOUT TO COMPLETE STERN CONVERSION

HOW HIGH? (CONTD)

SUMMARY RESULTS: NEUTRAL ENGAGEMENT

- A/C 1 DEFEATS A/C 2 IF INITIAL ENERGY LEVEL IS HIGH
 - LOWER ALTITUDES
 - HIGHER MACH
- IF A/C 1 GOES TO α_L (35°) WHEN INITIAL ENERGY IS LOW
A/C 2 WINS
- A/C 1 HAS GREATER FLEXIBILITY TO MANAGE
TURN RATE/ENERGY STATE

 α LIMIT - ACM COMPARISON
h = 15,000 ft
FORCED OVERTHOOT TO SCISSORS
ENGAGEMENT 15,000 FT (LEVEL)FORCED OVERTHOOT TO SCISSORS
ENGAGEMENT — 15,000 FT (LEVEL)FORCED OVERTHOOT TO SCISSORS
ENGAGEMENT 15,000 FT (LEVEL)FORCED OVERTHOOT TO SCISSORS
ENGAGEMENT — 15,000 FT (LEVEL)

HOW HIGH

• SUMMARY RESULTS: DEFENSE ENGAGEMENT

— A/C 1 QUICKLY NEUTRALIZES A/C 2 BY CAUSING
OVERSHOOT ($t = 7.5$ SEC)

— ABILITY TO USE MAX LIFT IS KEY

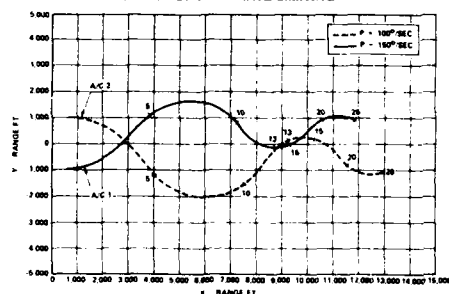
ROLL RATE LIMITER

ANALYSIS: ACM EFFECTIVENESS

- NEUTRAL - LINE ABREAST ENGAGEMENT
- 2,000 FT LATERAL OFFSET
- SCISSORS MANEUVERS TO GAIN ADVANTAGE
- A/C 1 $\rho_{MAX} = 150^\circ/\text{SEC}$
- A/C 2 $\rho_{MAX} = 100^\circ/\text{SEC}$

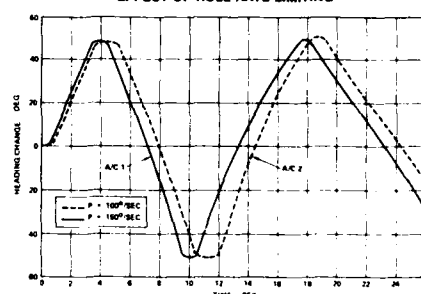
LEVEL TURN REVERSALS (SCISSORS)

15,000 FT STARTING MACH NO. = 0.9
EFFECT OF ROLL RATE LIMITING



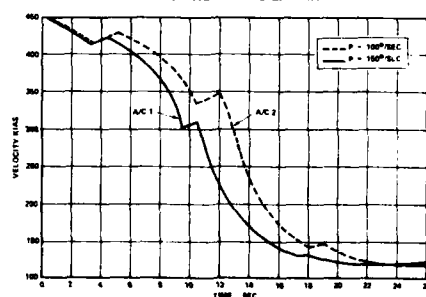
LEVEL TURN REVERSALS (SCISSORS)

15,000 FT START MACH NO. = 0.9
EFFECT OF ROLL RATE LIMITING



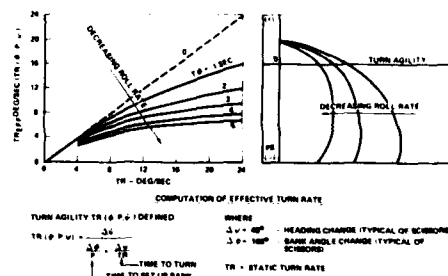
LEVEL TURN REVERSALS (SCISSORS)

15,000 FT START MACH NO. = 0.9
EFFECT OF ROLL RATE LIMITING



COMBAT MANEUVERING

EFFECTIVE TURN RATE

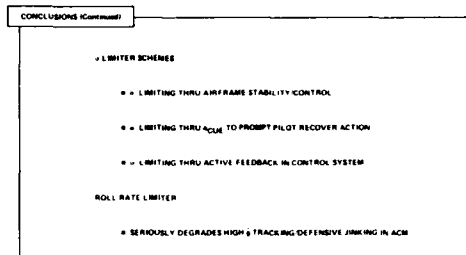
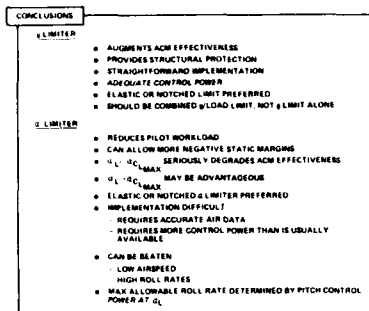


SUMMARY RESULTS

- A/C 1 ACHIEVES OFFENSIVE POSITION IN 12.5 SECS
- A/C 2 MUST START TURN APPROX 2 SECONDS EARLY TO BREAK EVEN
- BETTER ROLL RATE ESSENTIAL FOR WINNING

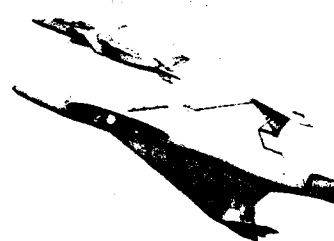
HOW HARD?

- POST-STALL STATIC PITCH STABILITY?
- DEEP-STALL PRESENT?
- NEAR/POST-STALL LATERAL DIRECTIONAL STABILITY, C_{NDYN} ?
- INERTIAL COUPLING?
- ZERO SIDESLIP ASYMMETRIES?
- KINEMATIC COUPLING?
- EXCESSIVE PITCH CONTROL POWER REDUCTION WITH α ?



FUTURE DIRECTIONS

- THRUST VECTORING/REVERSING - A PANACEA FOR ALL CONTROL PROBLEMS?



HISTORICAL OVERVIEW FLIGHT EXPERIENCE

THRUST REVERSERS

THERE HAVE BEEN FIVE AIRCRAFT APPLICATIONS (F-84C, F-100F, F-11A, VIGGEN, TORNADO) MAIN EFFORT HAS BEEN DIRECTED AT REDUCED LANDING ROLL, REVERSE THRUST APPLIED AFTER TOUCHDOWN

F-11A EXPERIMENTED WITH IN FLIGHT THRUST REVERSING FOR APPROACH CONTROL, LARGE TRIM AND STABILITY CHANGES DISCOURAGED THE INVESTIGATORS

THRUST VECTORING

THERE HAVE BEEN SEVERAL EXPERIMENTAL TYPES AND TWO PRODUCTION AIRCRAFT - HARRIER/AV8 AND YAK-36MP

RESEARCH HAS BEEN DIRECTED TOWARDS VTOL AND THE TRANSITION BETWEEN AERODYNAMIC LIFTING FORWARD FLIGHT AND THRUST LIFT. THE THRUST VECTOR HAS BEEN CONSTRAINED TO PASS THROUGH THE CENTER OF GRAVITY

HARRIER EXPERIENCE OF VECTORING IN FORWARD FLIGHT (VIFFING) HAS SHOWN INCREASE AIR COMBAT EFFECTIVENESS WITH VECTORING

HISTORICAL OVERVIEW

TECHNOLOGY STUDIES

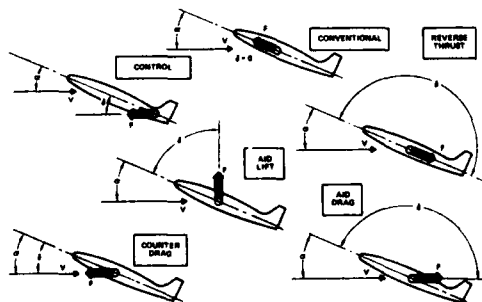
THRUST REVERSERS

- SIGNIFICANT UTILITY IN ACM
- WEIGHT PENALTY DOES NOT JUSTIFY USE FOR ACM ALONE
- FOR HIGH TRIM ADVANTAGE IN ACM INCREASES IMPORTANCE OF WEIGHT PENALTY DECREASES

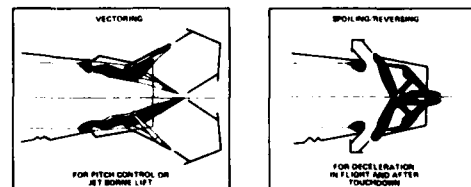
THRUST VECTORING

- MANEUVER ENHANCEMENT
 - LIFT AUGMENTATION (SUPER CIRCULATION)
 - CONVENTIONAL AIRCRAFT LAYOUT RESTRICTS BENEFIT
 - REQUIRES HIGH g IN NOZZLE IN CLOSE PROXIMITY TO WING
 - DIRECT LIFT $(L = L_0 + L_1)$
 - FOR CONVENTIONAL AIRCRAFT LAYOUT TRIM REQUIREMENTS ARE LARGE
- TRIM
 - USE VECTORING FOR TRIM, CANARD AFT TAIL, ELEVON FOR CONTROL
 - MAXIMIZES PERFORMANCE OF WING
 - MAXIMIZES TRIM DRAG
- CONTROL (TV²)
 - POTENTIAL IMPROVE CONTROL EFFECTIVENESS AT HIGH AOA/LOW g
 - CONTROL EFFORTS HAVE LESS POTENTIAL FOR COUPLING

THRUST VECTORING OPTIONS

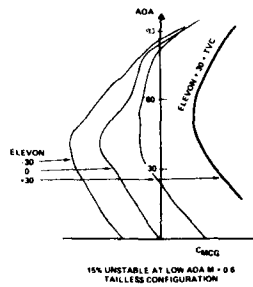


THRUST-VECTORING/THRUST-REVERSING NOZZLE CONCEPT

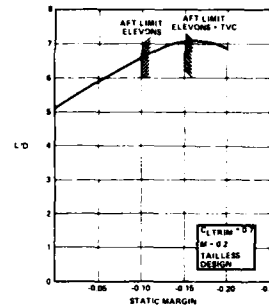


TECHNOLOGY PAYOFFS

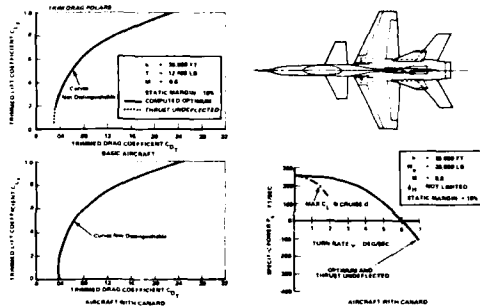
- 30-40% SHORTER TAKEOFF DISTANCE
- 70% SHORTER LANDING GROUND ROLLS (WT 40% DRY)
- 20% LOWER TAKEOFF AND 20% LOWER LANDING SPEEDS
- 10% HIGHER MAXIMUM CONTROLLABLE LIFT
- 2% LOWER SUPERIOR CRUISE DRAG

TVC ALLOWS USABLE α /MORE AFT CG

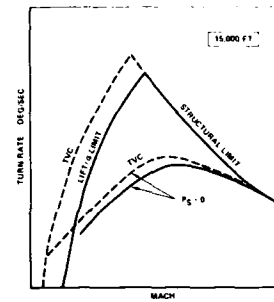
TVC ALLOWS IMPROVED MANEUVER L/D



EFFECT OF THRUST VECTORING ON L/D POLARS AND SPECIFIC POWER



TVC ALLOWS LOWER MINIMUM AIRSPEED/ IMPROVED TURN PERFORMANCE



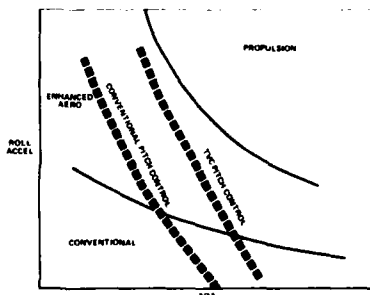
CONFIGURATION ARCHITECTURE FLEXIBILITY

- WIDER ALLOWABLE CG RANGE
- WING DESIGN (PLANFORM, SWEEP, AR) NOT NECESSARILY INFLUENCED BY CANARD OR AFT TAIL INTEGRATION
- IMPROVED AREA DISTRIBUTIONS AT ALL MACH
- MORE FLEXIBLE WEAPON INTEGRATION OPTIONS

BENEFITS OF TVC FOR ROLL CONTROL

- DIFFERENTIAL TVC IMPROVES HIGH α ROLL EFFECTIVENESS - ALLOWS HIGHER P_{MAX} TO BE GENERATED
- IMPROVES PITCH CONTROL POWER (SYM TVC) ALLOWS HIGHER P_{MAX} TO BE USED AT HIGH α
- DIFFERENTIAL VECTORING AT HIGH q ALLOWS HIGH LEVEL OF P_{MAX} TO BE GENERATED WITH LOWER WING STIFFNESS/WEIGHT PENALTY

LATERAL MANEUVER ENHANCEMENT



BENEFITS (Continued)

YAW

- DIFF TR ALLOWS HIGHER YAW RATES AT LOW q /HIGH α
- ALLOWS BETTER CONTROL BLENDING AT HIGH α (KEEP β UNDER CONTROL WHILE ROLLING)

DRAG

- DECOUPLED ENERGY MANAGEMENT
 - DECOUPLES DRAG CONTROL FROM FLIGHT PATH
 - MORE EFFECTIVE THAN SPEED BRAKE
- ESPECIALLY USEFUL FOR HIGH OVERTAKE SPEEDS (SLASHING ATTACK) TO INCREASE FIRING TIME WINDOW

CONCERNS

- ENGINE HAS TO STAY RUNNING
 - INCREASED AIRFRAME/ENGINE COMPATIBILITY REQUIREMENTS
- TR MAY COUPLE WITH SURFACE EFFECTIVENESS AND REDUCE $C_{n\dot{\beta}}, C_{n\dot{\delta}}, C_{m\dot{\delta}}$
- TVC WITH A/B?
 - A_g/A_g VARIATION WITH VECTORING?
- MULTI-FUNCTION NOZZLES FOR IFPC
 - FULL UTILITY REQUIRES HIGHLY COMPLEX CONTROL LAWS
 - MUCH MORE COMPLEX THAN FBW

FLIGHT TEST/WIND TUNNEL DATA

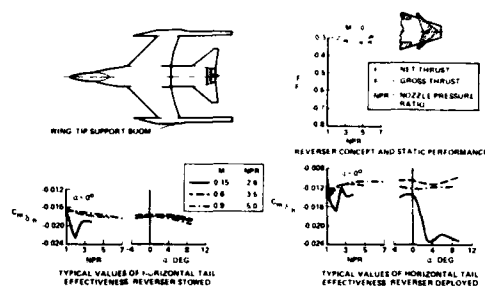
ALL FULL SCALE AIRCRAFT PREVIOUSLY TESTED WITH REVERSER HAVE EXPERIENCED STABILITY AND CONTROL PROBLEMS

AIRCRAFT ENGINE NUMBER	REVERSER	TEST	PROBLEM	CONDITION	PROBABLE CAUSE
F4U SINGLE	TARGET	FLIGHT	NOSE DOWN PITCHING MOMENT	APPROACH	INDUCED UPWASH ON HORIZONTAL TAIL
F800 SINGLE	TARGET	TUNNEL	SEVERE NOSE DOWN PITCHING MOMENT	LOW SPEED	INDUCED UPWASH ON HORIZONTAL TAIL
F100F SINGLE	CASCADE	TUNNEL	REDUCED LATERAL DIRECTIONAL STABILITY	LOW SPEED	REDUCED DYNAMIC PRESSURE ON VERTICAL STABILIZER
F100F SINGLE	CASCADE	FLIGHT	REDUCED LATERAL DIRECTIONAL STABILITY	APPROACH	REDUCED DYNAMIC PRESSURE ON VERTICAL STABILIZER
A37B TWIN	TARGET	TUNNEL	SEVERE LOSS OF LONGITUDINAL STABILITY	LOW SPEED	INTERFERENCE OF PLANE ON DOWNSTREAM HORIZONTAL TAIL
F11A SINGLE	BLOCKER DEFLECTOR	FLIGHT	UNACCEPTABLE PITCHING MOMENT	APPROACH	INTERFERENCE WITH HORIZONTAL TAIL
VIGGEN SINGLE	BLOCKER DEFLECTOR	GROUND	LOSS OF DIRECTIONAL STABILITY	LANDING	ASYMMETRIC PLANE TO FUSELAGE ATTACHMENT
TORNADO TWIN	TARGET	GROUND	LOSS OF DIRECTIONAL STABILITY	LANDING	INTERFERENCE WITH VERTICAL TAIL

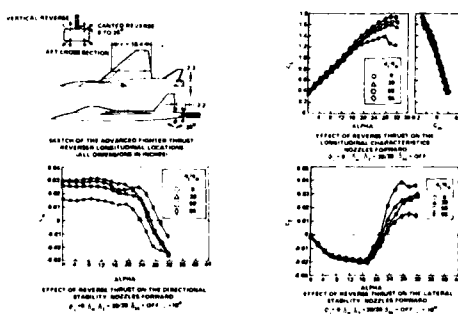
INFLIGHT USE OF VECTORING/REVERSERS

- DECELERATOR
 - REPLACE OR AUGMENT SPEED BRAKE
- POTENTIAL FOR USE IN AIR COMBAT
 - REDUCE PITCH MOTION ASSOCIATED WITH DECELERATION
 - FORCED OVERTHROTTLE
 - POINTING

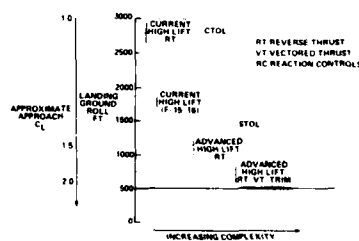
EFFECT OF THRUST REVERSING ON LONGITUDINAL POWER



REVERSER EFFECT ON STABILITY



INCREASED AIRCRAFT COMPLEXITY WITH REDUCED LANDING RUN CAPABILITY



CONCLUSIONS

- THRUST VECTORING IS A KEY TECHNOLOGY FOR FUTURE FIGHTERS
- THRUST REVERSING HAS UTILITY FOR STOL AND ENERGY MANAGEMENT IN ACM
- TECHNOLOGY INTEGRATION REQUIREMENTS ARE MAGNIFIED BY TVC
 - AERODYNAMICS
 - STABILITY AND CONTROL
 - PROPULSION INTEGRATION
 - ENGINE CONTROLS
 - AVIONICS
 - STRUCTURES
 - MECHANICAL
 - AIR DATA
- SIGNIFICANT POTENTIAL FOR ERROR
 - EARLY FLIGHT DEMONSTRATION REQUIRED

TOUGH TECHNOLOGY MANAGEMENT JOB

DIRECT FORCE CONTROL

by

Gottfried Sachs
 Professor of Flight Mechanics
 Hochschule der Bundeswehr München
 Neubiberg
 Germany

SUMMARY

Direct force control provides novel and unique motion capabilities of the aircraft due to independent control of flight path and attitude. In addition, flight path response characteristics can be speeded up. For direct lift control, it is shown how these novel capabilities may be utilized, with a discussion of possible deficiencies of conventional elevator control added for comparison. The aerodynamic characteristics of direct lift devices are described. This concerns not only lift but also drag characteristics which may be of significance for the long term response of the aircraft (flight path stability). For direct side force control, the novel motion capabilities possible are shown. This is followed by a description of the aerodynamic force characteristics of control surfaces applicable for direct side force control. In addition, coupling effects are discussed as well as effects on stability. In regard to direct drag control, some basic aspects concerning control surfaces and deceleration levels achievable are described.

NOMENCLATURE

$C_D = D/(\bar{q}S)$	Drag coefficient ($C_{D\delta} = \partial C_D / \partial \delta$)
$C_L = L/(\bar{q}S)$	Lift coefficient ($C_{L\alpha} = \partial C_L / \partial \alpha$, $C_{L\delta} = \partial C_L / \partial \delta$)
$C_l = L/(\bar{q}Ss)$	Rolling moment coefficient ($C_{lp} = \partial C_l / \partial (ps/V)$, $C_{lr} = \partial C_l / \partial (rs/V)$, $C_{l\beta} = \partial C_l / \partial \beta$)
$C_m = M/(\bar{q}S\bar{c})$	Pitching moment coefficient ($C_{m\delta} = \partial C_m / \partial \delta$)
$C_n = N/(\bar{q}Ss)$	Yawing moment coefficient ($C_{np} = \partial C_n / \partial (ps/V)$, $C_{nr} = \partial C_n / \partial (rs/V)$, $C_{n\beta} = \partial C_n / \partial \beta$, $C_{n\delta} = \partial C_n / \partial \delta$)
$C_Y = Y/(\bar{q}S)$	Side force coefficient ($C_{Y\beta} = \partial C_Y / \partial \beta$, $C_{Y\delta} = \partial C_Y / \partial \delta$)
D	Drag
g	Acceleration due to gravity
H	Altitude
k_x, k_y, k_z	inertia radius in roll, pitch and yaw
L	Lift, rolling moment
l_t	Tail arm
M	Mach number, pitching moment
m	Mass
N	Yawing moment
n	Load factor
n_v	Thrust dependence on speed, $T = T_0 (V/V_0)^{n_v}$
$n_x = (1/g) dV/dt$	nondimensional deceleration
n_y	nondimensional side acceleration
P	Roll rate
q	Pitch rate
$\bar{q} = (\rho/2) V^2$	Dynamic pressure
r	Yaw rate
S	Reference area
s	Half-span
T	Thrust
T_{DR}	Dutch-roll period
T_R	Rolling mode time constant
T_S	Spiral mode time constant
T_α	Period of the short-period mode
t	Time
V	Speed

Y	Side force
α	Angle of attack
β	Sideslip angle
γ	Flight path angle
Δ	Incremental value, e.g. ΔC_L
δ	Control surface angle
δ_e	Elevator angle
δ_f	Flap angle, flaperon angle
δ_H	Horizontal tail angle
δ_S	Spoiler angle
ζ	Rudder angle
ζ_{DR}	Dutch-roll damping ratio
θ	Pitch angle
$\mu = 2m/(\rho Ss)$	Relative density
ρ	Atmospheric density
ϕ	Roll angle
χ	Flight path heading
ψ	Yaw angle
ω_{nDR}	Dutch-roll undamped natural frequency

1. INTRODUCTION

Aircraft control with the use of conventional control surfaces such as elevators or ailerons can be considered a moment control technique which - via a change of the moment equilibrium - indirectly produces forces for controlling the motion of the aircraft. Furthermore, conventional aircraft control yields a coupling of attitude and flight path control. As a consequence, there are inherent limitations as far as separate control of attitude and flight path is concerned. The control techniques termed "Direct Force Control" provide a direct means for producing forces without influencing moment equilibrium. Such a capability removes the limitations caused by the coupling of attitude and flight path control and offers novel and unique modes of aircraft motion.

The translational motion of the aircraft may be characterized by

- Vertical translation / altitude
- Lateral translation / heading
- Speed.

Forces for controlling the translational motion are

- Lift forces
- Side forces
- Drag forces.

Therefore, the possible applications of direct force control are known as

- Direct lift control
- Direct side force control
- Direct drag control.

A direct force control capability not only provides independent control of attitude and flight path but also offers additional advantages which may be used for improving aircraft response characteristics. This is related to the time response after initiating the controls. Conventional control shows a response delay since the force necessary for controlling flight path does not exist before the moment equilibrium is changed. It is even possible that this effect is aggravated. Such a consequence occurs when a control surface deflection causes a force acting in the wrong sense which initially leads to a flight path change opposite to the intended response. Thus, a prolongation of the response delay considered may result. By contrast, a direct force control capability provides forces acting in the correct sense from the very beginning and no adverse time delay exists.

2. DIRECT LIFT CONTROL

2.1 CONVENTIONAL FLIGHT PATH CONTROL WITH THE ELEVATOR

Conventional flight path control with the elevator yields two effects which may be adverse. The first consists of the delay between initiation of the control and flight path response. As said before, this is due to the fact that a moment equilibrium change is necessary for producing a force. The second effect concerns aft tail and tailless configurations. For these configurations, the force produced at the tail due to an elevator deflection acts in a sense opposite to the flight path change commanded, Fig. 1. Consequently, the aircraft initially moves in the wrong sense. A further explanation is presented in Fig. 2. It is shown how the initial response in the wrong sense and rotational pitch dynamics

cause a delay in the buildup of lift. This in turn results in a delay of altitude buildup which is even more slowed down due to two integration steps between lift and altitude change, i.e. $\dot{H} \approx V\dot{\gamma} \approx (1/m)\int \Delta L dt$ and $\Delta H = \int \dot{H} dt$. From Fig. 2 it also follows that the time interval $t_{H=0}$ is an appropriate quantity for describing the adverse elevator lift effects considered. The quantity $t_{H=0}$ represents the time interval after which the altitude change commanded begins to build up in the right sense. An approximation for $t_{H=0}$ can be expressed as (Ref. 1):

$$t_{H=0} = 2\sqrt{3 \frac{C_L}{C_{L\alpha}} \frac{k_Y^2}{g l_t}} \quad (2.1)$$

This expression shows that the following effects contribute to an increase of $t_{H=0}$:

- Small tail arm l_t .
A small value of l_t may be particularly significant for tailless aircraft. In this case, it represents an effective value given by

$$l_t = -C_{m\delta}/C_{L\delta} \quad (2.2)$$

- Large values of k_Y^2/l_t .
This relation denotes an effect which especially concerns aircraft with high pitch inertia and sluggish response characteristics. It may be of particular interest for large aircraft or for further increase in the size of aircraft (Ref. 2, 3). For example, as k_Y and l_t increase in the same manner with the size of the aircraft, the time interval $t_{H=0}$ also increases.
- High lift coefficient C_L .
This may be of particular significance for STOL-aircraft operating at high lift coefficient.

The response delay due to adverse elevator lift is an inherent characteristic of aft tail or tailless configurations. This also concerns the possibilities of automatic control systems the aim of which is to augment rotational dynamics by speeding up pitch-attitude response, in particular with regard to short-coupled aircraft with high pitch inertia and sluggish response characteristics. An example is shown in Fig. 3. From this it follows that such an augmentation system improves response characteristics as far as pitch attitude is concerned. However, flight path delay is not reduced, but even increased. The reason for this is the fact that the additional elevator deflection commanded by the pitch response augmentation system causes an increase of the adverse elevator lift acting in the wrong sense. As a result, the moment dynamics are improved but the force characteristics show adverse effects.

2.2 CONTROL MODES WITH DIRECT LIFT CAPABILITY

Direct lift control can remove possible deficiencies of conventional control since the lift commanded is immediately effective. Furthermore, the decoupling of pitch attitude and flight path control attainable with direct lift capability offers novel aircraft motion characteristics. This is illustrated in Fig. 4 which shows different kinds of novel control modes described in the following:

- Flight path control with constant angle of attack,
Flight path angle and pitch attitude are changed, with angle of attack remaining constant,

$$\alpha = \theta - \gamma = \text{const}$$

Thus, this mode can be characterized by

$$\begin{aligned} \Delta\theta &= \Delta\gamma \\ \Delta\alpha &= 0 \end{aligned} \quad (2.3)$$

The direct lift commanded is fully used for changing flight path.

- Decoupled flight path control.
In this mode, the aircraft is able to change flight path angle without attitude change. From

$$\theta = \gamma + \alpha = \text{const}$$

it follows that

$$\begin{aligned} \Delta\theta &= 0 \\ \Delta\alpha &= -\Delta\gamma \end{aligned} \quad (2.4)$$

In this case, the direct lift commanded must exceed the opposite lift change due to $\Delta\alpha$ so that a net lift change remains for flight path control.

- Decoupled pitch attitude control.
In this mode, also called fuselage pointing, attitude can be controlled without changing flight path, i.e.

$$\gamma = \theta - \alpha = \text{const}$$

Thus

$$\begin{aligned} \Delta\gamma &= 0 \\ \Delta\alpha &= \Delta\theta \end{aligned} \quad (2.5)$$

The direct lift compensates for lift change due to $\Delta\alpha$.

Examples for the dynamics associated with the control modes described above are presented in Figs. 5, 6 and 7. They show the actuation of the control variables (flaperon deflection δ_F and horizontal tail deflection δ_H) and the response of aircraft motion variables.

2.3 CONTROL DEVICES FOR DIRECT LIFT

There are various types of devices applicable for direct lift control. For efficient use, they should have the following properties:

- A capability of providing lift changes up- and downward in order to control flight path deviations in both directions.
- A quick operation capability.
- No objectionable pitching moments. Otherwise, these moments must be trimmed out by an elevator deflection.

Fig. 8 gives an illustration of devices usable for providing direct lift:

- Flaps
- Spoilers
- Canards.

In addition to the devices shown, powered lift and vectored thrust may also be considered possibilities utilizable for direct lift control.

Flaps are a well-known high lift device. When conventionally used like in landing, flaps are operated in a slow manner. In regard to direct lift control application, a quick operation capability is necessary. Fig. 9 presents an example for the effectiveness of flaps used for direct lift control. The flap system shown consists of a main flap and a quickly operated auxiliary flap which is used for producing direct lift changes.

Spoilers can also be considered devices applicable for direct lift control. An example is shown in Fig. 10. An upward lift change is provided by reducing spoiler deflection, a downward lift change by an opposite deflection. They have to be operated about a datum deflection in order to provide a lift capability in both directions.

Horizontal canards also represent an effective means for providing direct lift. An example is shown in Fig. 11. In the case of canards, a deflection produces not only lift changes but also significant pitching moments. Despite the fact that this may contribute to a more complex control system, it is also advantageous since the elevator or horizontal tail deflection necessary for trim produces an augmenting lift component.

2.4 TRANSIENT RESPONSE CHARACTERISTICS OF DIRECT LIFT CONTROL

In the applications discussed so far, direct lift control can be considered a separate control technique without any elevator actuation or with elevator deflections only as a supporting means which may be necessary for pitching moment compensation or which may be used for changing pitching moment characteristics such that the motion modes with independent control of attitude and flight path can be performed. However, there may be also a control mode where direct lift control can be considered a means for supporting elevator control. This is discussed in the following.

For vertical flight path control, direct lift control provides the capability of producing lift instantaneously. This cannot be achieved by conventional elevator control since it shows a delay in lift buildup which results in an even greater delay of flight path response, in particular for aft tail and tailless configurations. Therefore, the response characteristics of elevator control may be improved by a combination with direct lift control. By using direct lift, the initial flight path response of the aircraft is speeded up. In the time following this initial phase, direct lift can be gradually reduced to zero since now the response characteristics of conventional elevator control are sufficient. This is illustrated in Fig. 12 which shows the response of a system employing direct lift control with transient characteristics and conventional elevator control. The gradual reduction of direct lift after the initial time phase requires a washout type system, the characteristics of which can be adjusted to the basic aircraft response in an appropriate manner. Fig. 13 shows a scheme of such a control system. An additional elevator deflection after the initial phase may become necessary for trim when there are pitching moments due to the washout of the direct lift. This may yield a control system scheme shown in Fig. 14.

It may be added that the combination described offers the repeated use of direct lift in the same sense, every time up to its maximum value. Such a utilization which is not otherwise possible may be of particular interest since the maximum lift capability of the direct lift device is generally limited.

2.5 DRAG CHARACTERISTICS AND FLIGHT PATH STABILITY

Not only are the lift characteristics of direct lift devices of interest but also their drag characteristics (Ref. 4,5). This is due to the fact that they contribute significantly to the long term response of the aircraft. It will be shown in the following that there are characteristic differences when considering different types of direct lift control devices.

For conventionally controlled aircraft, the long term response characteristics are of interest in regard to an effect which is known as flight path stability (Ref. 6,7,8). This refers to flying qualities associated with precise flight path control, in particular for the landing approach. The ratio of steady flight path angle to speed change following an elevator input can be used for describing flight path stability. For conventionally controlled aircraft, the following expression holds (with n_V characterizing thrust dependence on speed $T = T_0 (V/V_0)^{n_V}$ and subscript "0" denoting a reference state):

$$\frac{dy}{d(V/V_0)} = 2 \frac{\partial C_D}{\partial C_L} - (2 - n_V) \frac{C_D}{C_L} \quad (2.6)$$

This expression shows that drag/lift characteristics and thrust dependence on speed determine the steady response in flight path angle and speed. Two regions may be distinguished as follows:

- Region I: $dy/dV < 0$ or, from Eq. (2.6), $(1 - n_V/2)C_D/C_L > \partial C_D/\partial C_L$. This region is preferable from a flying qualities point of view.
- Region II: $dy/dV > 0$ or, from Eq. (2.6), $(1 - n_V/2)C_D/C_L < \partial C_D/\partial C_L$. This region shows adverse characteristics in regard to the flying qualities considered. The problems existing here degrade when dy/dV becomes more positive.

For flight path control with direct lift, the relation between flight path angle and speed can be expressed as (with angle of attack assumed to be constant):

$$\frac{dy}{d(V/V_0)} = 2 \frac{C_{D\delta}}{C_{L\delta}} - (2 - n_V) \frac{C_D}{C_L} \quad (2.7)$$

From this it follows that the drag characteristics of direct lift devices have a significant influence. Positive values of $C_{D\delta}/C_{L\delta}$ may be disadvantageous since they contribute to a positive gradient dy/dV . Contrary to this, negative values of $C_{D\delta}/C_{L\delta}$ have an opposite effect. A positive value of $C_{D\delta}/C_{L\delta}$ may be typical for flaps, as shown in Fig. 15. The other relationship (i.e. $C_{D\delta}/C_{L\delta} < 0$) is illustrated in Fig. 16 which shows characteristics of spoilers. Such a relationship implies that drag is reduced when lift is increased. For spoilers, this is due to the fact that an upward lift change requires a decrease in deflection which yields a reduction of drag.

3. DIRECT SIDE FORCE CONTROL

3.1 CONTROL MODES WITH DIRECT SIDE FORCE CAPABILITY

As described in the Introduction, a direct force capability removes limitations in regard to coupling of attitude and flight path changes and provides independent control of both. For direct side force control, this means that following modes illustrated in Fig. 17 are possible:

- Directional flight path control at zero sideslip and roll angle. This mode, which may also be termed wings level flat turn, can be used to change flight path angle in the horizontal plane without banking the aircraft. The application of a constant side force results in a constant yaw rate. Thus

$$\begin{aligned} \dot{\psi} &= \text{const} \\ \beta &= 0 \\ \phi &= 0 \end{aligned} \quad (3.1)$$

The direct side force commanded is fully used for changing flight path.

- Lateral translation at constant yaw attitude. With the use of this mode, a lateral translation is possible without changing yaw attitude. It may be characterized by

$$\begin{aligned} \psi &= \text{const} \\ \beta &= -\alpha \end{aligned} \quad (3.2)$$

The direct side force commanded must exceed the opposite side force due to sideslip so that a net side force remains for sideways translation.

- Decoupled yaw attitude control. Yaw attitude is provided without changing flight path, i.e.

$$\begin{aligned} \alpha &= \text{const}, \\ \psi &= -\beta. \end{aligned} \quad (3.3)$$

In this case, no resultant side force exists. Therefore, the direct side force applied compensates for the side force due to sideslip angle.

3.2 CONTROL DEVICES FOR DIRECT SIDE FORCE

Devices for providing a direct side force capability may be grouped as follows:

- Vertical control surfaces at the wing or at the fuselage midsection
- Canard type surfaces, mounted vertically or horizontally
- Rudder combined with asymmetric drag device.

Thrust vector deflection may also be considered a possibility for producing a side force.

An example for the aerodynamic effectiveness of direct side force devices mounted vertically at the wing is shown in Fig. 18. When properly located with regard to the center of gravity, this type of side force device may yield no adverse yawing moments. Another wing mounted device is shown in Fig. 19. Here, split flaps are used at four external store pylons already existing at the wing. This yields the advantage that it is not necessary to add separate control surfaces to the wing. Thus, drag and stability penalties can be avoided in the nonoperating position of the split flaps.

Whereas control surfaces at the wing or at the fuselage midsection may be mounted at a location where no yawing moments are produced, canard type devices inevitably introduce those coupling effects. This is illustrated in Fig. 20. For the canard configuration, a rudder deflection is necessary for trimming out the canard yawing moment. It also follows that the rudder deflection for trim produces an augmenting side force contribution.

An example for the direct side force capability of vertical canards is presented in Fig. 21. It may be noted that the effectiveness of vertical canards in this example significantly decreases with angle of attack. Other investigations show similar effects (Refs. 9-13).

As described earlier, horizontal canards provide a direct lift capability. In addition, this type of control device may also be used for direct side force control (Refs. 11,12,14). Differential deflection may yield a side force. This is illustrated in Fig. 22. The lower curve represents the untrimmed force contribution of the differentially deflected horizontal canards. For trimming out the yawing moments produced by the horizontal canards, a rudder deflection is necessary. This results in the upper curve of Fig. 22.

Another method for producing direct side forces is illustrated in Fig. 23. This method is based on a combined deflection of an asymmetric drag device and the rudder. The direct side force is produced by the rudder deflection which is necessary to compensate for the yawing moment of the asymmetric drag. The asymmetric drag device in the example shown in Fig. 23 employs wing tip tank petals. A similar method is to use split ailerons and the rudder (Ref. 12).

3.3 COUPLING EFFECTS

Control devices for direct side forces can cause considerable coupling effects concerning yaw, roll and even pitch axis. These effects can be considered adverse properties in regard to precision motion control and may contribute to a more complex control system, particularly when they show significant nonlinear characteristics. Coupling effects concerning the yaw axis - as already discussed - may be used to yield an advantage in so far as the rudder deflection necessary for trim results in an augmenting side force contribution. This presupposes $C_{n\delta}/C_{Y\delta} > 0$.

Examples of coupling effects in the roll axis are shown in Fig. 24 for a single control surface and a twin configuration. Fig. 25 illustrates pitching moment coupling effects for various types of canards.

Another kind of coupling and asymmetry concerns the differences which result when a control surface is deflected to the left or to the right. This is illustrated in Fig. 26. It shows the effects of 4 wing mounted flaps from which flaps 1 and 2 may be of particular interest. Although flaps 1 and 2 are almost of the same size, they show significant differences. This may be interpreted as an asymmetry in regard to a single control surface since a deflection of flap 2 as shown (i.e. to the right) is equivalent to a deflection of flap 1 to the left.

3.4 STABILITY EFFECTS

Direct side force devices mounted separately at the aircraft produce additional aerodynamic forces and moments when the aircraft is perturbed from trim. Thus, they have an effect on the stability characteristics of the aircraft. Depending on aircraft configuration and type of side force device used, these effects may be of smaller or greater significance. A characteristic feature is that considerable interference effects can exist. This complicates a prediction technique based on the characteristics of the isolated control surface. In the following, it is shown which effects on stability characteristics may result from side force devices.

A stability derivative of primary significance is the directional stability derivative $C_{n\beta}$. Fig. 27 shows which effect may be caused by vertical canards. The destabilization is more significant at low angles of attack whereas, for higher angles of attack, the stability level shows a smaller reduction due to a decrease in vertical canard effectiveness.

For the same canard configuration, the effect on dihedral effect is shown in Fig. 28. While the lowered directional stability level of the canard configuration presented in Fig. 27 was expected, the change of the dihedral effect was not anticipated. The result as shown in Fig. 28 was attributed to flow interference from the canards on the downstream wing.

Departure characteristics of the aircraft at high angles of attack are of great importance. A parameter commonly used to predict yaw departure tendencies is the dynamic directional stability derivative

$$(C_{n\beta})_{\text{dyn}} = C_{n\beta} \cos \alpha - \left(\frac{k_z}{k_x} \right)^2 C_{l\beta} \sin \alpha \quad (3.4)$$

From this expression it follows that both the dihedral effect $C_{l\beta}$ and the inertia ratio $(k_z/k_x)^2$ can yield a significant contribution. The effect of vertical canards on the dynamic directional stability derivative is shown in Fig. 29 for the same configuration as considered before. Comparison of the curves shows that for the high angle of attack range, the dynamic stability parameter is greater with canards installed than with them off. This results from the increase in the dihedral effect which is sufficiently large to offset the reduced directional stability.

The effect of canards on side force characteristics due to sideslip angle is illustrated in Fig. 30. The surfaces mounted below the body show their highest force levels at the lower end of the angle of attack range. This is followed by a reduction when the angle of attack is increased. The configuration with a single canard mounted above the body shows a rather low side force level for small angles of attack and a significant increase in the higher angle of attack range.

The examples presented so far show how lateral stability characteristics can be influenced by direct side force devices. However, it is possible that there are also effects concerning longitudinal stability. This is illustrated in Fig. 31 which shows pitching moment changes caused by various types of canards. From the examples presented it follows that significant effects may exist, the degree of which depends on the canard type considered.

As a consequence of the derivative changes, the dynamic stability of the aircraft is also influenced by direct side force devices. This concerns effects in regard to frequency, damping or time constants of the modes of motion of the aircraft. For lateral dynamics of the aircraft, the following modes of motion usually exist:

- Dutch-roll mode
- Rolling mode
- Spiral mode

Their characteristics as regards frequency, damping or time constants, respectively, can be described by the following approximative expressions:

- Dutch roll mode

$$\omega_{nDR} \doteq \frac{V^2}{\mu k_z^2} C_{n\beta} \quad (3.5)$$

$$L_{DR} \omega_{nDR} \doteq - \frac{V}{2\mu s} \left\{ C_{Y\beta} + \left(\frac{s}{k_x} \right)^2 C_{n_r} - \left(\frac{k_z}{k_x} \right)^2 \frac{C_{l\beta}}{C_{n\beta}} \left[C_{l_r} - \left(\frac{s}{k_z} \right)^2 C_{n_p} \right] \right\}$$

- Rolling mode

$$1/T_R \doteq - \frac{Vs}{\mu k_x^2} C_{l_p} \quad (3.6)$$

- Spiral mode

$$1/T_S \doteq \frac{g}{V} \left(\frac{C_{l_r}}{C_{l_p}} - \frac{C_{l\beta}}{C_{l_p}} \frac{C_{n_r}}{C_{n\beta}} \right) \quad (3.7)$$

Despite the fact that there are limitations in regard to the range of validity of the above approximations, a discussion of which is beyond the scope of this paper, they are nevertheless very useful to provide some basic insight into the effects of direct side force devices on dynamic stability. The expressions presented show that the dutch-roll mode may be of particular interest when changes in $C_{n\beta}$, $C_{l\beta}$ and $C_{Y\beta}$ exist as discussed before, since they all have an effect on this mode. In addition, effects due to a change in the yaw damping derivative C_{n_r} may also be of interest.

An example for the dynamic stability effects considered is presented in Fig. 32 which shows the influence of wing mounted control surfaces and canards on period and damping of the dutch-roll mode. The canard type devices yield greater effects, corresponding to their more pronounced influence on the stability derivatives as discussed in the examples before.

4. DIRECT DRAG CONTROL

Direct drag control is based on the ability to control forces parallel to the velocity vector of the aircraft or the flight path, respectively. Directly controlling drag which is already in practical use with airbrakes can provide a large deceleration capability in order to suddenly decrease level-flight speed. Furthermore, it can be used for glide path control and for controlling speed in dives. Control of forces parallel to the velocity vector can be achieved by aerodynamic control surfaces via drag modulation or by propulsive means.

In Fig. 33, it is shown how split flaps can be used for direct drag control. This type of control device provides the advantage of a twofold direct force control capability, i.e. direct drag control and direct side force control, as discussed before. Direct side force control is achieved by a deflection of one surface at each of the 4 pylons either to the left or to the right. A simultaneous deflection of both surfaces at each pylon produces drag forces which yield a resultant drag force in the plane of symmetry of the aircraft. An example for the drag force level attainable with such a configuration is given in Fig. 34. This shows that a considerable increase of drag coefficient can be achieved which is practically independent of Mach number. The deceleration attainable is illustrated in Fig. 35. From this it follows that the pylon split flap configuration considered shows great effectiveness and can provide high deceleration levels.

REFERENCES

- 1 Hafer, X., Sachs, G., Flugmechanik - Moderne Flugzeugentwurfs- und Steuerungskonzepte. Springer-Verlag, Berlin, Heidelberg, New York, 1980.
- 2 Hafer, X., Flugeigenschaftsprobleme zukünftiger Transportflugzeugentwicklungen. 13. Otto Lilienthal Lecture, Paris, 1972.
DGLR-Jahrbuch, pp. 27-50, 1972.
L'Aeronautique et l'Astronautique, No. 43, pp. 37-52 (in French).
- 3 Cleveland, F.A., Size effects in Conventional Aircraft Design. Journal of Aircraft, Vol. 7, pp. 483-512, 1970.
- 4 Hamel, P.G., Wilhelm, K.K., Hanke, D.H., Lange, H.-H., Steep Approach Flight Test Results of a Business-Type Aircraft with Direct Lift Control. AGARD-CP-160, pp. 21-1 - 21-10, 1975.
- 5 Hanke, D., Lange, H.-H., Fliegbarkheitsuntersuchungen zur Anwendung der direkten Kraftsteuerung in der Längsbewegung. DGLR-Symposium "CCV-Technologien", DGLR-Nr. 76-238, 1976.
- 6 MIL-F-8785C Military Specification - Flying Qualities of Piloted Airplanes, 1980.
- 7 Chalk, C.R., Neal, T.P., Harris, T.M., Pritchard, F.E., Background Information and User Guide for MIL-F-8785B(ASG). AFFDL TR 69-72, 1969.
- 8 Moorehouse, D.J., Woodcock, R.J., Background Information and User Guide for MIL-F-8785C. AFWAL-TR-81-3109, 1982.
- 9 Sonnleitner, W., Parametrische Untersuchungen zur Anwendbarkeit von Kinnrudern bei größeren Anstellwinkeln. DGLR/HOG Jahrestagung, DGLR-Nr. 78-112, 1978.
- 10 Sonnleitner, W., Windtunnel Investigations of Controls for DF on a Fighter-Type Configuration at Higher Angles of Attack. AGARD-CP-262, pp. 17-1 - 17-11, 1979.
- 11 Stumpf, S.C., Whitmoyer, R.A., Horizontal Canards for Two-Axis CCV Fighter Control. AGARD-CP-157, pp. 6-1 - 6-8, 1975.
- 12 Johannes, R.P., Whitmoyer, R.A., AFFDL Experience in Active Control Technology. AGARD-CP-262, pp. 10-1 - 10-20, 1979.
- 13 Whitmoyer, R.A., Aerodynamic Interactions on the Fighter CCV Test Aircraft. AGARD-CP-235, pp. 16-1 - 16-13, 1978.
- 14 Re, R.J., Capone, F.J., An Investigation of a Close-Coupled Canard as a Direct Side-Force Generator on a Fighter Model at Mach Numbers from 0.40 to 0.90. NASA-TN-D-8510, 1977.
- 15 Kehr, W.T., Longitudinal Stability and Control of Large Supersonic Aircraft at Low Speeds. AIAA Paper 64-586, 1964.
- 16 Moyens, J.F., Nelson, W.E., Jr., Flaperon Control - The Versatile Surface for Fighter Aircraft. AGARD-CP-262, pp. 9-1 - 9-18, 1979.
- 17 Rolls, L.S., Cook, A.M., Innis, R.C., Flight-Determined Aerodynamic Properties of a Jet-Augmented, Auxiliary-Flap, Direct-Lift-Control System Including Correlation with Wind-Tunnel Results. NASA-TN-D-5128, 1969.

- 18 Weise, K., Griem, H., Führungs- und Fliegarkeitsverbesserung im flughafennahen Bereich und bei der Landung. Statusseminar 1977 "Luftfahrtforschung und Luftfahrttechnologie", Bundesministerium für Forschung und Technologie, pp. 152 - 171, 1978.
- 19 Pinsker, W.J.G., Direct Lift Control. The Aeronautical Journal of the Royal Aeronautical Society, Vol. 74, pp. 817 - 825, 1970.
- 20 Wünnenberg, H., Sachs, G., Direkte Seitenkraftsteuerung - Möglichkeiten und Probleme einer Anwendung bei Kampfflugzeugen. DGLR-Symposium "CCV-Technologien", DGLR Nr. 76-239, 1976.
- 21 Hall, G.W., A Flight Test Investigation of Direct Side Force Control. The Society of Experimental Test Pilots, Technical Review, Vol. 11, pp. 74 - 89, 1972.
- 22 Esch, P., Wünnenberg, H., Direct Side Force and Drag Control with the Aid of Pylon Split Flaps. AGARD-CP-262, pp. 14-1 - 14-9, 1979.
- 23 Benner, W., Wünnenberg, H., Problematik und Realisierungsmöglichkeiten einer direkten Seitenkraftsteuerung bei Kampfflugzeugen. DGLR-Jahrestagung, DGLR-Nr. 74-84, 1974.
- 24 Moeken, B., Wünnenberg, H., Direkte Seitenkraft- und Widerstandssteuerung am Alpha Jet. Dornier Post 2/78, pp. 44 - 45, 1978.

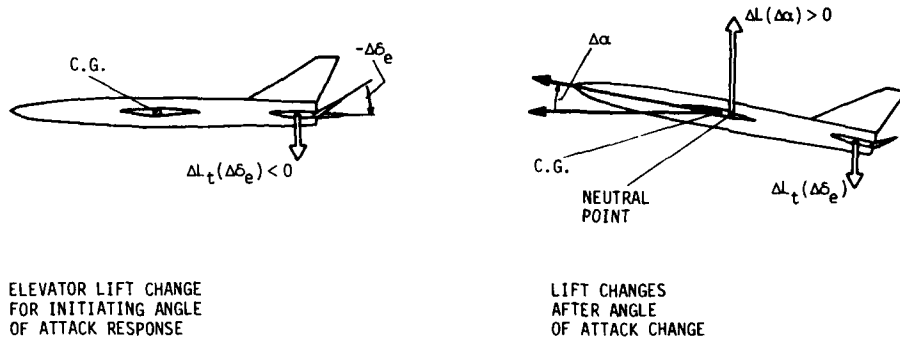


Fig. 1 Lift changes due to elevator and angle of attack change

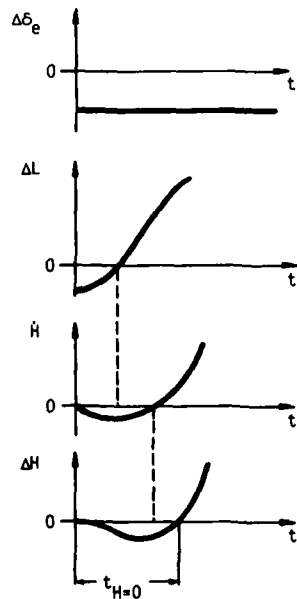


Fig. 2 Altitude response delay of conventional elevator control

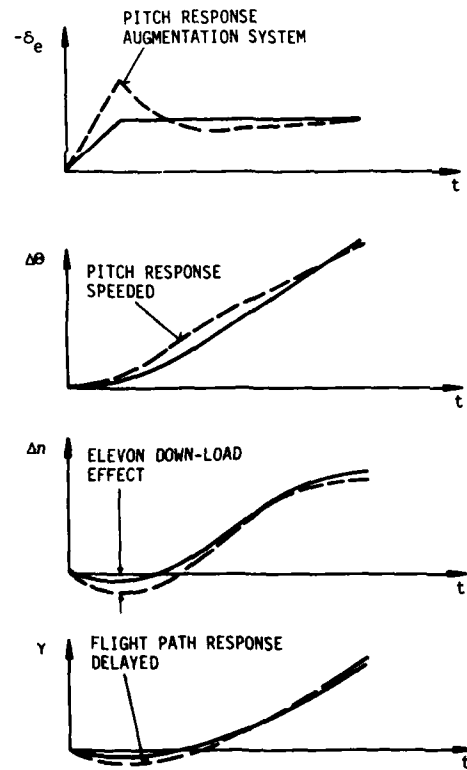


Fig. 3 Effect of pitch response augmentation on flight path response (from Ref. 15)

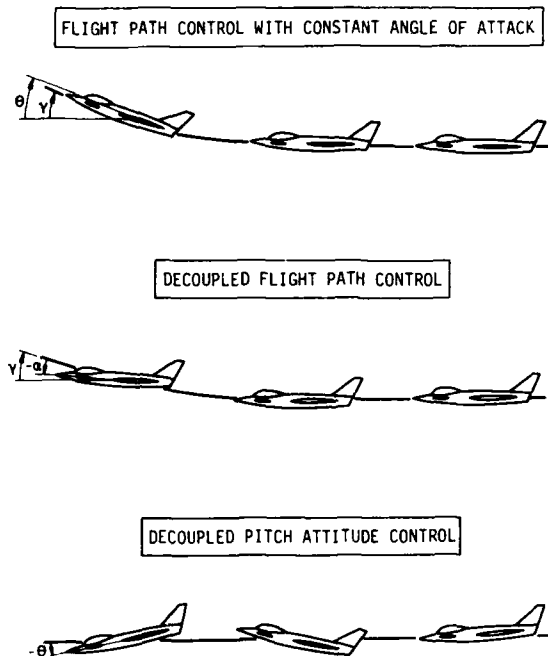


Fig. 4 Direct lift control modes (from Ref. 1)

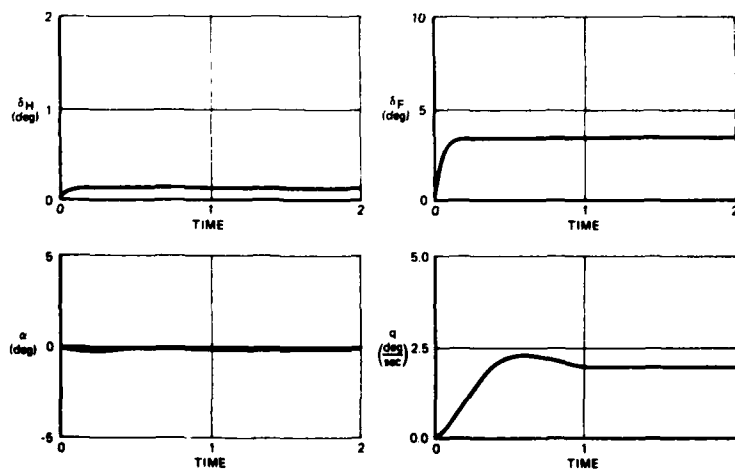


Fig. 5 Dynamics of vertical flight path control with constant angle of attack (from Ref. 16)

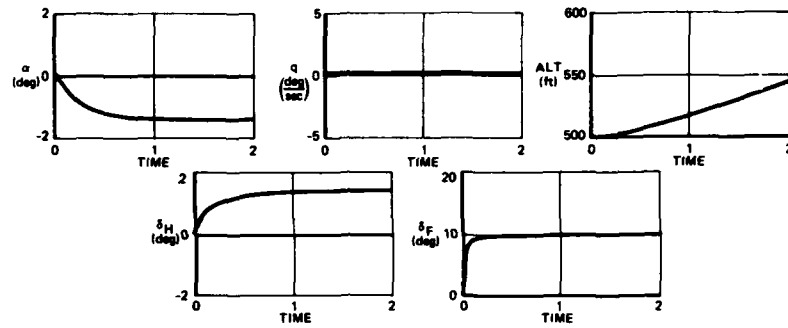


Fig. 6 Dynamics of decoupled flight path control (from Ref. 16)

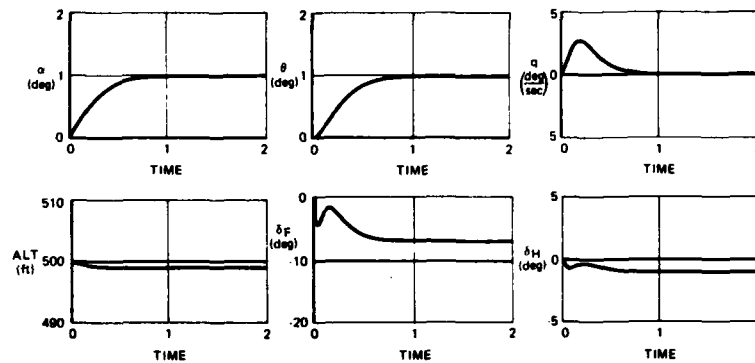


Fig. 7 Dynamics of decoupled pitch attitude control (from Ref. 16)

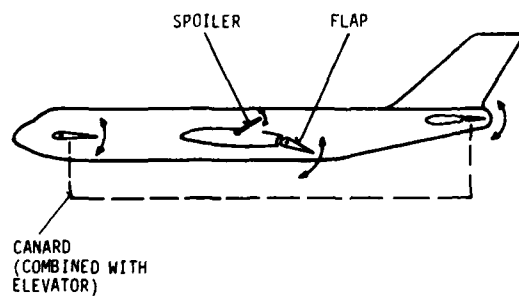


Fig. 8 Devices for direct lift

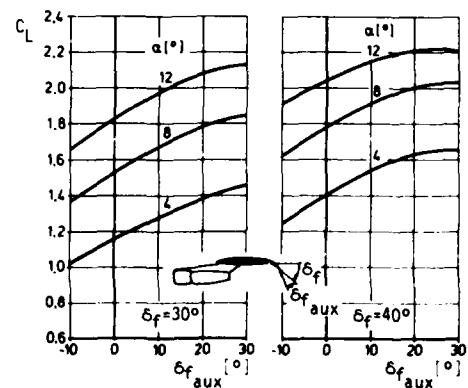


Fig. 9 Lift characteristics of flaps (from Ref. 17)

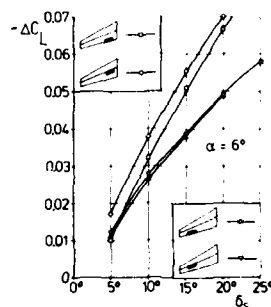


Fig. 10 Lift characteristics of spoilers (from Ref. 18)

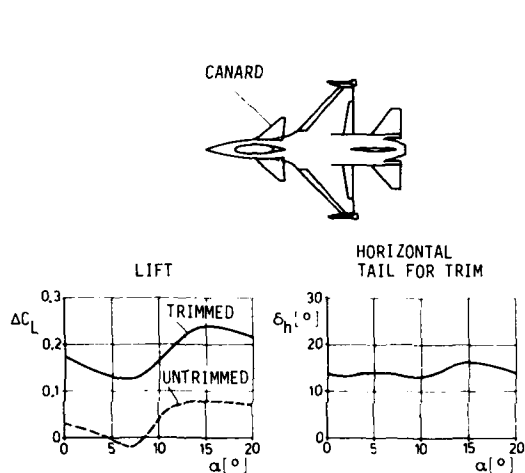


Fig. 11 Lift characteristics of canards for CCV YF-16 (from Ref. 11)

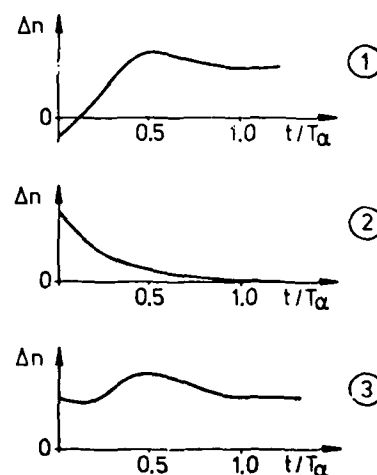


Fig. 12 Load factor response of direct lift control with transient characteristics (from Ref. 19)

- ① Elevator control alone
- ② Direct lift control alone
- ③ Total response

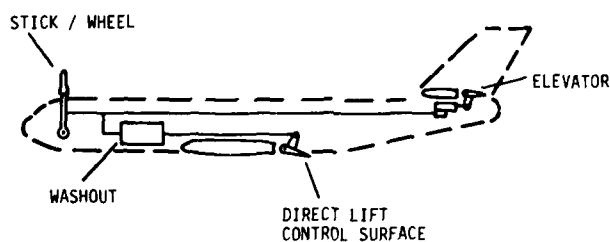


Fig. 13 Scheme of a system for transient operation of direct lift control

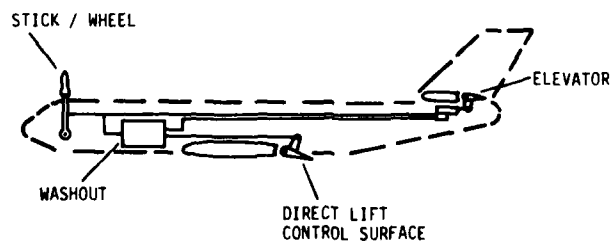


Fig. 14 Scheme of a system for transient operation of direct lift control with pitching moment compensation

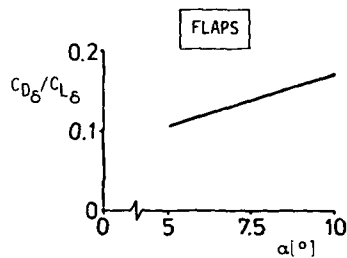


Fig. 15 Drag lift relationship of flaps (from Ref. 1)

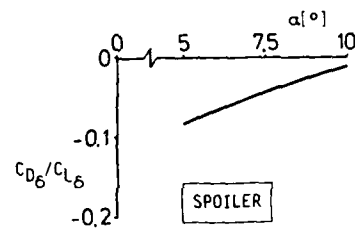


Fig. 16 Drag lift relationship of spoilers (from Ref. 1)

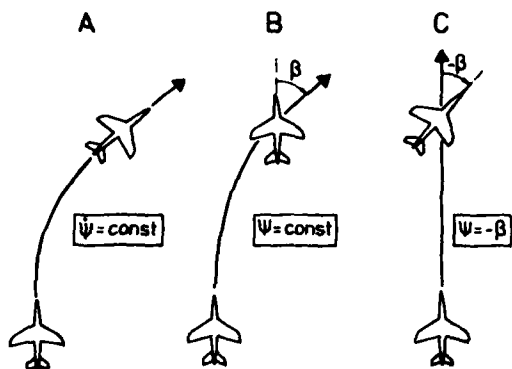


Fig. 17 Direct side force control modes (from Ref. 1)

A Direct flight path control at zero sideslip and roll angle
B Lateral translation at constant yaw attitude
C Decoupled yaw attitude control

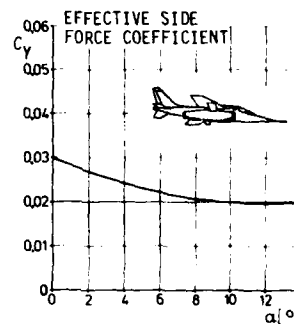


Fig. 18 Side force characteristics of control surfaces mounted at the wing (from Ref. 20)

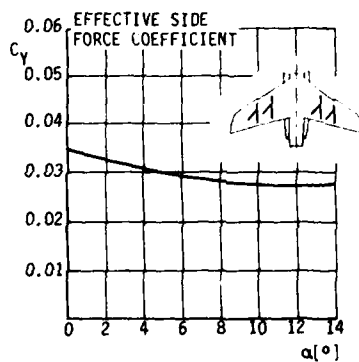


Fig. 19 Side force characteristics of pylon split flaps (from Ref. 20)

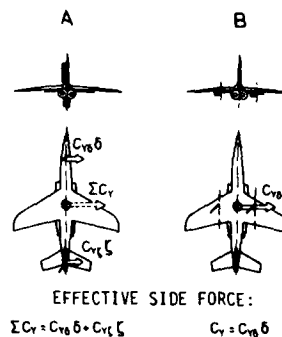


Fig. 20 Effective side forces (from Ref. 1)

A Vertical canard
B Control surfaces at the wing

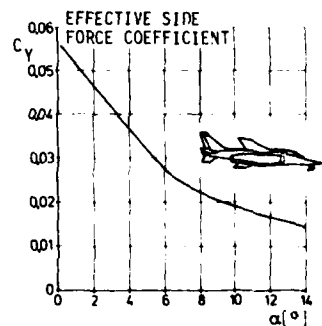


Fig. 21 Side force characteristics of canards (from Ref. 20)

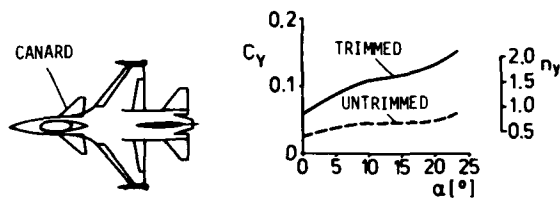


Fig. 22 Side force characteristics of horizontal canards (from Ref. 11)
 $M = 0.9$, $H = 3000$ m

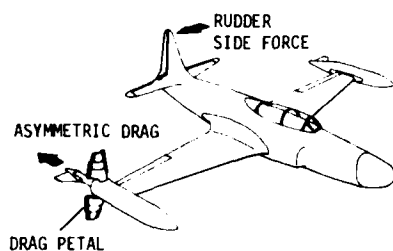


Fig. 23 Direct side force due to combined deflections of an asymmetric drag device and the rudder (from Ref. 21)

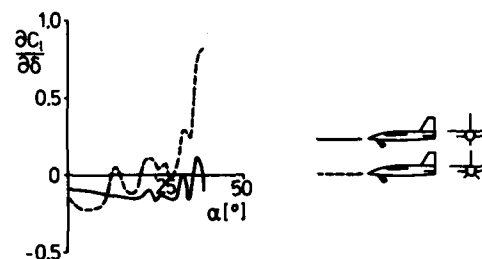


Fig. 24 Rolling moment coupling effects of canards (from Ref. 9)

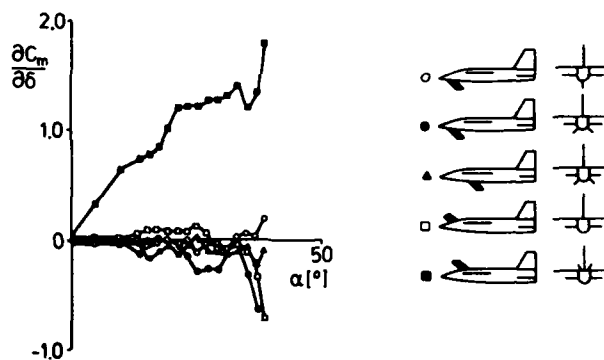


Fig. 25 Pitching moment coupling effects of canards (from Ref. 9)

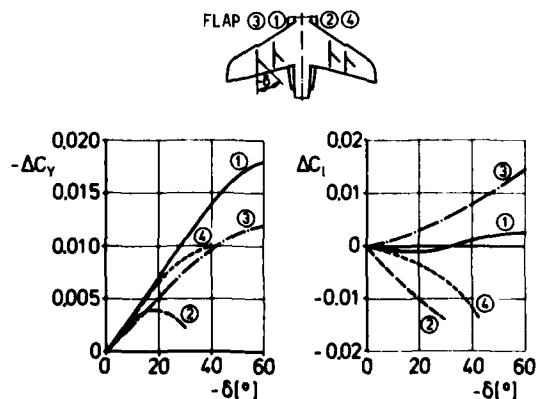


Fig. 26 Asymmetry and coupling effects of control surfaces at the wing (from Ref. 22)

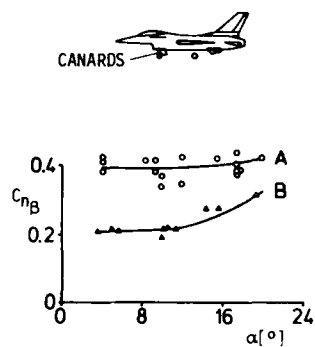


Fig. 27 Effect of vertical canards on directional stability $C_{n\beta}$ (from Ref. 13)
Flight test data, $M=0.6$ to 0.8
A Canards off
B Canards on

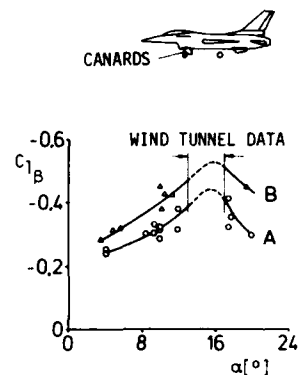


Fig. 28 Effect of vertical canards on dihedral effect (from Ref. 13)
Flight test data, $M=0.6$ to 0.8
A Canards off
B Canards on

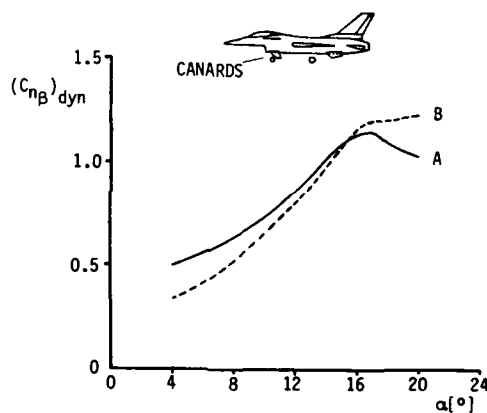


Fig. 29 Effect of vertical canards on $(C_{n\beta})_{dyn}$ (from Ref. 13)
Based on flight test data, $M=0.6$ to 0.8
A Canards off
B Canards on

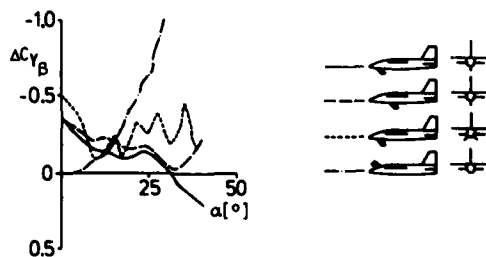


Fig. 30 Effect of canards on side force due to sideslip (from Ref. 9)

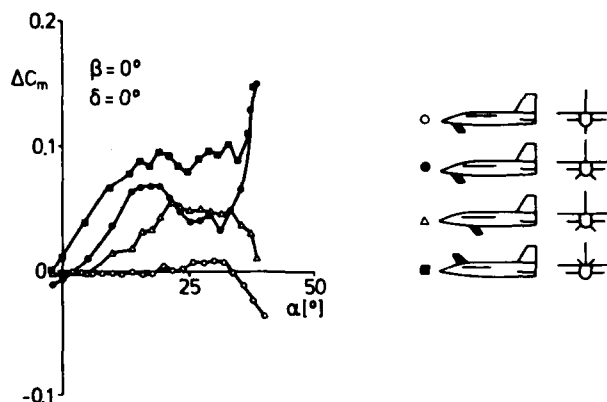


Fig. 31 Effect of canards on longitudinal stability (from Ref. 9)

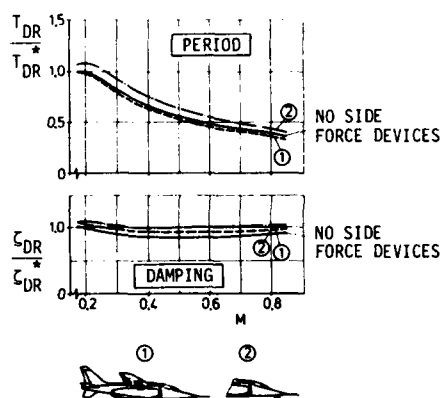


Fig. 32 Effect of direct side force devices on period and damping of the dutch-roll mode (from Ref. 23)
 T_{DR}^* , ζ_{DR}^* : Basic airplane without side force devices, $M = 0.2$

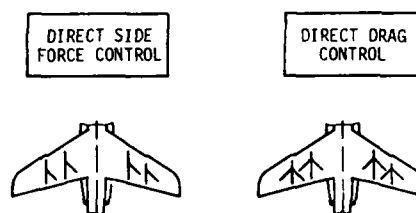


Fig. 33 Scheme for application of split flaps for direct side force and direct drag control (from Ref. 22)

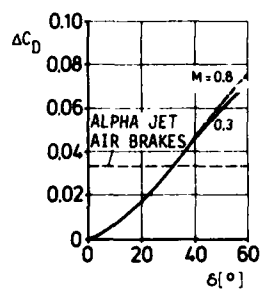


Fig. 34 Effect of pylon split flaps on drag (from Ref. 22)

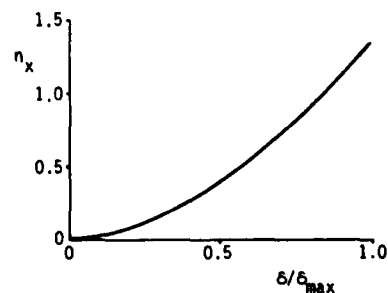


Fig. 35 Deceleration achievable with pylon split flaps (from Ref. 24)

EXPERIMENTAL METHODS IN FLIGHT FOR THE MEASUREMENT OF CONTROL CHARACTERISTICS

by
M. E. ESHELBY
College of Aeronautics
CRANFIELD INSTITUTE OF TECHNOLOGY
Cranfield
Bedford MK43 0AL
U.K.

SUMMARY

Although the measurement of control characteristics is relatively simple in the wind tunnel their flight measurement is not so straightforward. In general the control characteristics are implicit in the measurement of the handling qualities of the aircraft and do not appear as separately measured quantities. It is however possible to extract some data on control characteristics from the handling qualities trials and in this paper some methods of their assessment are considered. Principally the longitudinal control characteristics can be determined from static stability trials whereas the lateral directional control characteristics are derived from dynamic tests. Special trials in respect of aircraft flying beyond their normal limitations are discussed.

Methods of handling qualities assessment are also considered since these encompass the control characteristics of the aircraft.

NOTATION

a	Lift curve slope of wing.
a_0, a_1, a_2, a_3	Aerodynamic control lift parameters, eqn. 1.
b	Wing span.
b_0, b_1, b_2, b_3	Aerodynamic control hinge moment parameters, eqn. 2.
\bar{c}	Aerodynamic mean chord.
C_H	Coefficient of hinge moment.
C_L	Coefficient of lift.
C_M	Coefficient of pitching moment
g_0	Acceleration due to gravity.
h	Centre of gravity position, longitudinal.
h_0	Aerodynamic centre of aircraft less tail.
$\cdot H$	Hinge moment.
i_A, i_C, i_E	Dimensionless moments of inertia in roll, yaw and product of inertia.
L, l	Rolling moment, rolling moment derivative.
l_T	Tail arm.
m	Aircraft mass.
m_δ	Control tab gearing, eqn. 3.
m_δ	Control gearing, fig. 5.
M, m	Pitching moment, pitching moment derivative.
N, n	Yawing moment, yawing moment derivatives.
P	Control Force.
p	Rate of roll.
q	Rate of pitch.
r	Rate of yaw.
S	Gross wing area.
V	True airspeed.
\bar{V}	Tail volume coefficient = $S_T l_T / S \bar{c}$
x	Control column movement.
α	Angle of attack.
β	Angle of sideslip.
β_δ	Control tab angle.

δ	General aerodynamic control angle.
ϵ	Angle of downwash at the tail.
ζ	Rudder angle.
η	Elevator angle.
ξ	Aileron Angle.
μ_2	Aircraft lateral relative density parameter.
ρ	Air density.
ϕ	Roll attitude.
ψ	Yaw attitude.

SUBSCRIPT

δ, ξ, η, ζ	With respect to a control, general, aileron, elevator, rudder respectively.
p, r, v	With respect to roll, yaw, sideslip
o	Zero lift, datum.
T	Tail

1. INTRODUCTION

Flight trials have been a means of establishing the handling and control characteristics of aircraft ever since the first attempts were made to construct them. In the early days of aircraft development flight trials were often the first, and only, test performed to determine the adequacy of the control system, frequently with disastrous or fatal results. Such trials were often performed with no theoretical model or study to support them and, in many cases, without any structural analysis or test to ensure mechanical integrity.

As the design of aircraft developed from the construction of flying machines by private individuals into the embryo aircraft industry and the government establishments the need for prediction of flying and handling characteristics was seen and methods of estimation of the aerodynamic and structural qualities of the aircraft were developed. In parallel with the theoretical studies experimental methods of testing aircraft were also developed. These included static and dynamic structural tests and aerodynamic tests performed in artificial flight conditions in wind tunnels or similar devices. Such tests enabled much of the uncertainty to be eliminated from the design and resulted in an aircraft with predictable flying and handling qualities. Flight trials now take their proper place as the final test that the control characteristics are adequate for their purpose and enable the final small corrections to be made as necessary.

Experimental trials in wind tunnels are not however exact. There are many reasons why they do not fully simulate free flight conditions and these are contained in a previous paper, ref. 1. Briefly, wind tunnel tests are usually conducted on scale models of the aircraft or a part of the aircraft since it would be impracticable to provide a tunnel large enough to take a full sized aircraft at its design airspeed or Mach number. The combination of Reynolds number and Mach number for the flow will then be dissimilar in the tunnel test and flight test and correction to tunnel test results will be required to account for this. The detailed modelling of control gaps, slots, surface finish and minor detail can never be achieved adequately at scales of 1/10 or less compromising the similarity between the model and the full scale aircraft.

Wind tunnel tests may however have advantages over flight tests under some circumstances. Firstly, they can be used to investigate the basic flight envelope of the aircraft to check that the control authority is adequate over the normal flight regime, they can then be extended to explore the corners of the flight envelope in which flight trials will be difficult to perform and they can then be further extended to flight conditions outside the normal permitted flight envelope which would only be reached under extreme circumstances or an emergency. Possible inadequacies of control systems can be seen and corrected before any flight trials commence. Secondly, the model can be tested under simulated flight conditions in which it would be impossible to hold the aircraft in steady flight, at angles of attack above the stall for example. This would enable stall recovery techniques to be considered before flight.

Flow visualisation techniques can be used easily in a wind tunnel to search for separation or local flow distortions. The use of fluids and oils spread on the surface of the model, wool tufts and hot-wire, pitot or laser anemometers are all common methods of examination of airflow. In flight tests however such methods are rarely used because of the difficulty of observing the tests. Tufting to check the extent of flow separation is probably the most commonly attempted technique but this can only be applied to those parts of the aircraft which can be observed from the aircraft or from a chase aircraft. Any such tests are qualitative rather than quantitative.

The measurement of pressure distributions on wind tunnel models is another commonly employed technique which is rarely used in flight trials since the installation of static sources or pitot rakes on aircraft and the recording of the pressures is not normally possible in the numbers which would be required to survey the pressure distribution over a surface. Such techniques would only be used as a last resort in the investigation of a severe problem.

The isolation of control forces is also employed on tunnel models, particularly in dynamic cases, by the use of special hinges and supports for the control. Such measurements are not possible on aircraft since such control mountings would not be acceptable on the grounds of airworthiness. Generally the direct measurement of control forces other than those related to the hinge moment is not possible.

In flight trials it is normal practice to assess the overall handling qualities of the aircraft, in which the aerodynamic control characteristics are implicit, and not to look initially at the control characteristics as a separate entity. If problems are encountered then it may become necessary to check the control parameter in more detail. As a first step it is possible to extract the data from the handling trials results and to estimate the control parameters from this, the next phase would be to attempt to make some direct measurements to evaluate the control parameters so that corrective action can be taken.

2. AIRCRAFT CONTROLS

The aerodynamic flying control of an aircraft is usually in the form of a hinged portion of an aerofoil which alters its camber and thus the lift produced under any given airflow conditions, Fig. 1. An additional control, the tab, may also be fitted. This is similarly hinged to the main control surface and is used to reduce the hinge moment of the control to zero and thus allow the pilot to fly the aircraft with a zero control force as datum; this is known as flying with controls trimmed.

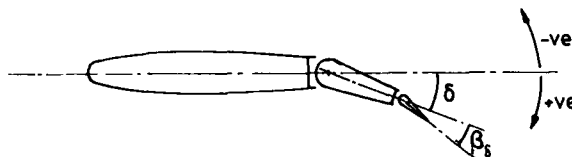


FIG 1. Control Notation, flap type control and tab.

Other forms of aerodynamic control may be used, for example, spoilers which reduce lift and increase drag, Fig. 2, but these are generally limited to lateral control, and are often used in conjunction with conventional flap type controls, and so will not be treated here in detail although all the principle comments made here will also apply in these cases.

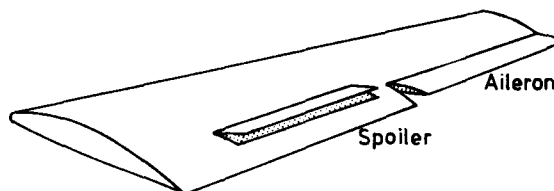


FIG 2. Conventional Aileron and Spoiler type controls.

The purpose of the flying control is to produce a moment about one axis of the aircraft so that the aircraft is held in its state of steady flight, $\Sigma M_{C.G.} \neq 0$, known as being in TRIM, or to produce an out of balance moment, $\Sigma M_{C.G.} = 0$, to cause the aircraft to rotate into a new attitude and to manoeuvre, Fig. 3.

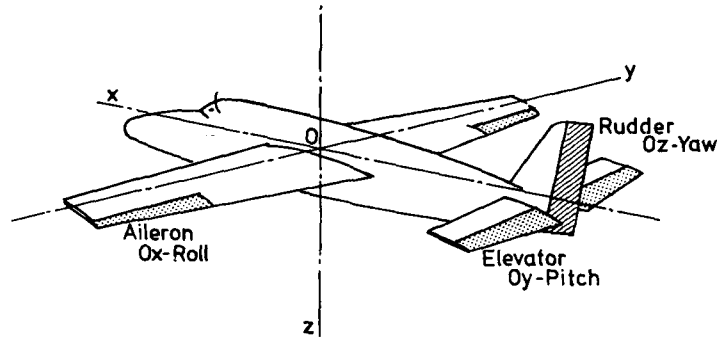


FIG 3. Flying Controls.

The moment produced by the control comes from the lift force acting at some distance from the appropriate axis of rotation. The lift force produced by the control can be described in coefficient terms as

$$C_{L_\delta} = a_0 + a_1\alpha_l + a_2\delta + a_3\beta_\delta \quad 1)$$

where

a_0 is a constant term which depends on the camber of the basic aerofoil section; for a symmetrical section $a_0 = 0$

$a_1 = \frac{dC_{L_\delta}}{d\alpha_l}$ is the lift curve slope of the basic airfoil. This will depend on the aspect ratio of the lifting surface and its section but will usually be of the order 4 to 6 per radian, 0.07 to 0.1 per degree.

$a_2 = \frac{dC_{L_\delta}}{d\delta}$ is the control effectiveness parameter and determines the rate of change of lift per unit change in control deflection. The value of a_2 depends on the control chord-width, for a control chord of 25% of the aerofoil chord $a_2 = \frac{1}{4}a_1$.

$a_3 = \frac{dC_{L_\delta}}{d\beta_\delta}$ is the tab lift parameter. This is usually small and the value of a_3 is generally about $0.1a_2$

Fig. 4 describes the control lift equation diagrammatically.

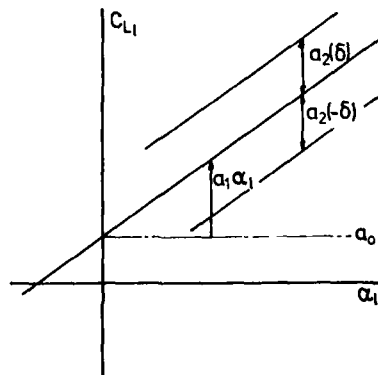


FIG 4. Control Lift Coefficient Equation.

The pressure loading on the control surface produces a moment at the control hinge which is reacted by the control system. This will be the pilots hand or foot in the case of a manual control system, or the actuator in a powered system, Fig. 5.

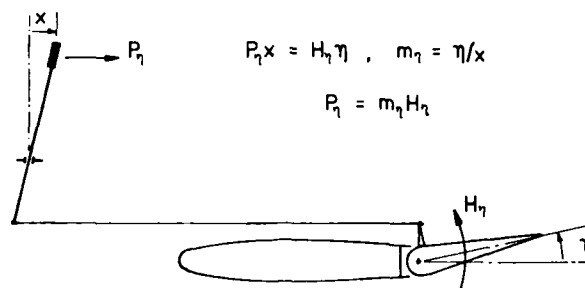


FIG 5. Control Force Convention, manual elevator control.

The hinge moment can be described in coefficient terms as

$$C_{H\delta} = b_0 + b_1 \alpha_i + b_2 \delta + b_3 \delta^2 \quad 2)$$

where

b_0 is a constant term which depends on the camber of the basic aerofoil section, for a symmetrical section, $b_0 = 0$.

$b_1 = \frac{dC_{H\delta}}{d\alpha_i}$ is the control float parameter. This may be +ve or -ve and determines the direction of movement of the free control with change of incidence of the aerofoil. If b_1 is +ve the control floats against the wind.

$b_2 = \frac{dC_{H\delta}}{d\delta}$ is the control heaviness parameter which determines the pilot applied force necessary to move the control through unit rotation. Under the normal convention b_2 must be negative, otherwise the control is overbalanced.

$b_3 = \frac{dC_{H\delta}}{d\delta^2}$ is the control tab heaviness parameter and is of similar magnitude to b_2 since the tab is used to reduce the overall hinge moment to zero; b_3 must also be negative.

Fig. 6 describes the control hinge moment equation diagrammatically.

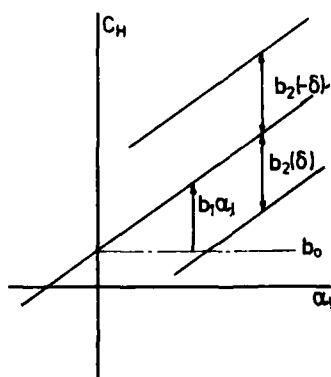


FIG 6. Control Hinge Moment Coefficient Equation.

In some cases the tab is geared to the control to modify the hinge moment characteristics. In a rigid gearing system the tab is moved in proportion to the movement of the parent control, Fig. 7, and the tab deflection becomes partly a geared function and partly a trimming function

$$\beta_{\delta} = \beta_0 + m_{\beta} \delta \quad 3)$$

where

β_0 is the trimming function set by the pilot through the trim wheel to reduce the overall hinge moment to zero and,,
 $m_{\beta} \delta$ is the geared deflection where m_{β} is the control to tab gearing.

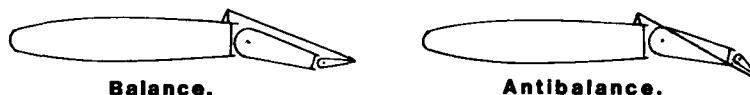


FIG 7. Control Geared Tab Systems.

Putting eqn. 3) into eqn. 1) and 2) respectively gives

$$C_{L_{\delta}} = a_0 + a_1 \alpha_L + (a_2 + a_3 m_{\beta}) \delta + a_3 \beta_0 \quad 1A)$$

and

$$C_{H_{\delta}} = b_0 + b_1 \alpha_L + (b_2 + b_3 m_{\beta}) \delta + b_3 \beta_0 \quad 2A)$$

which implies that the control effectiveness and control hinge moment parameters, a_2 and b_2 , are modified. Other forms of gearing, for example spring tabs and servo tabs, are used and similar expressions can be derived for the control lift and hinge moment coefficients. Also, alternative arrangements of controls can be made, such as all moving tailplanes, which will also modify the control parameters. Any system can however be reduced to the basic form of eqn. 1) and 2) although the parameters a_2 and b_2 may be complicated and contain a number of parameters including variables.

Methods are available of assessing the values of the control parameters a_2 , a_3 , b_2 , b_3 in flight for each aerodynamic control and these methods are employed to evaluate the control characteristics in cases when the adequacy of the control is in doubt.

3. FLIGHT MEASUREMENT TECHNIQUES

In flight it is not possible to measure any external forces or moments acting on the aircraft as it is in the wind tunnel by measuring the forces in the support system of the model. In flight it is only possible to measure forces or moments by considering their effect on the aircraft in terms of its motion or acceleration. Basically flight trials can be considered to be of two types; Static trials, in which the overall forces and moments on the aircraft are zero and the aircraft is in a steady state of flight known as being in Trim, or Dynamic trials, in which the aircraft is accelerating along or about its axis system.

In either case the aerodynamic controls are used to provide the appropriate forces and moments about the C.G. of the aircraft and so the control characteristics become implicit in the stability or handling characteristics of the aircraft. In assessing the aircraft for its stability and handling qualities for airworthiness purposes trials are performed to demonstrate the acceptability of the aircraft with respect to predetermined criteria. Trials on military combat aircraft will similarly contain the essential airworthiness tests but will also include trials concerned with the controllability of the aircraft in its combat manoeuvres. In all cases an overall acceptability is sought which implies that the aerodynamic controls are capable of producing the forces and moments on the aircraft necessary to achieve the required level of handling quality. If, as a result of the trials, it becomes necessary to examine the control characteristic in more detail then, in the first instance, it may be possible to extract from the handling qualities data some data relating to the control characteristics referred to in section 2, or it may be necessary to carry out additional special trials using special equipment to measure the control characteristics.

3.1. Static Stability Trials are a simple test to show that the aircraft will produce a natural aerodynamic moment which will tend to restore the aircraft to equilibrium following a small disturbance from its steady state of flight. It does not consider the long term equilibrium but only the initial reaction following the disturbance. It can be applied to both longitudinal (or symmetric) disturbances in angle of attack or lateral-directional (asymmetric) disturbances in sideslip. Whilst these trials are far from a complete assessment of the aircraft handling qualities they are simple to perform and produce easily interpreted data from which some information relating to the control characteristics can be deduced.

3.1.1. Longitudinal Static Stability. The longitudinal static stability is based on the pitching moment equation of the aircraft. Since the theory is well known (refs. 2, 3) it will not be quoted here except in summary.

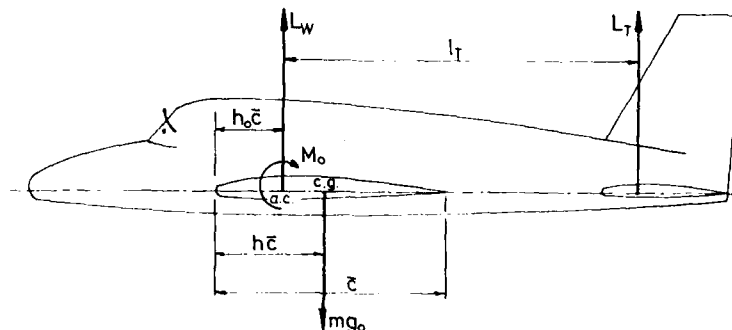


FIG 8. Static Forces and Moments Acting on the Aircraft.

In steady flight the pitching moment about the C.G. of the aircraft is zero and the aircraft is in the state of trim,

$$\Sigma F_{CG} = 0, \Sigma M_{CG} = 0$$

The elevator control is used to achieve this state and the moment balance can be written from Fig. 8 as

$$\bar{V} a_2 \bar{\eta} = C_{m_0} + C_L (h - h_0) - \bar{V} \left\{ \frac{a_1}{a} C_L (1 - \frac{d\epsilon}{d\alpha}) + a_1 \eta_T + a_3 \beta_{\eta} \right\} \quad 4)$$

where

$\bar{\eta}$ is the elevator angle to trim,

η_T is the tailplane setting angle (constant) and

h is the C.G. location with respect to the leading edge of the mean aerodynamic chord.

It is assumed that the elevator trim tab setting, β_{η} , is constant so that the only control affecting longitudinal trim is the elevator.

Differentiating eqn. 4) with respect to C_L gives the static stability criterion (dC_m/dC_L) controls fixed which can be expressed as

$$\bar{V} a_2 \frac{d\bar{\eta}}{dC_L} = h - \left\{ h_0 + \frac{\bar{V} a_1}{a} \left(1 - \frac{d\epsilon}{d\alpha} \right) \right\} = \left(\frac{dC_m}{dC_L} \right) \text{ controls fixed.} \quad 5)$$

Now since for stability (dC_m/dC_L) controls fixed must be negative the slope of the trim curve $(d\bar{\eta}/dC_L)$ must also be negative and Fig. 9 shows typical trim curves for two locations of the C.G. of the aircraft. Here it should be noted that the movement of the elevator control to achieve a state of trim throughout the speed range of the aircraft is very much less at aft centre of gravity locations than at forward centre of gravity locations. This feature can be used to extract from the static stability trim curves values of the elevator characteristic, a_2 , ref. 4.

Consider eqn. 4), at some specific value of C.G. location, h_1 , the value of elevator angle to trim, η_1 , at a given C_L can be compared with the elevator angle to trim, η_2 , at the same C_L but alternative C.G. location, h_2 . Thus from eqn. 4 it can be seen that

$$a_2 = \frac{C_L (h_1 - h_2)}{\bar{V} (\eta_1 - \eta_2)} \quad 6)$$

since all other parameters in the equation are unchanged.

A similar analysis can be performed on the static stability trim curves, controls free, to extract the elevator control heaviness parameter, b_2 .

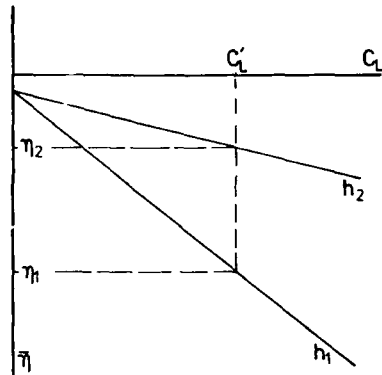


FIG 9. Static Stability Trim Curves, controls fixed.

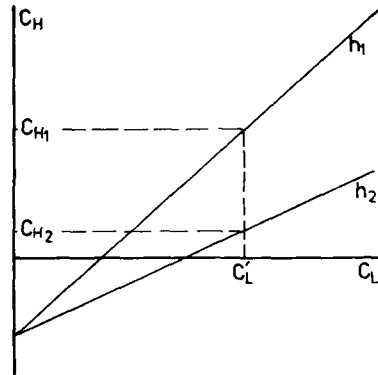


FIG 10. Static Stability Trim Curves, controls free.

From eqn. 2) the elevator control hinge movement can be written in terms of the elevator control deflection η , thus

$$\eta = \frac{-(b_1 a_2 + b_3 \delta_n) + C_{Hn}}{b_2} \quad (7)$$

which on substitution into eqn. 4) gives

$$\frac{\bar{v} a_2}{b_2} \bar{C}_{Hn} = c_{m_0} + C_L (h - h_0) - \nabla \left\{ \frac{\bar{a}_1}{a} C_L (1 - \frac{d\epsilon}{d\alpha}) + \bar{a}_1 \eta_T + \bar{a}_3 \delta_n \right\} \quad (8)$$

Where \bar{C}_{Hn} is the elevator hinge moment to trim and

$$\bar{a}_1 = a_1 \left(1 - \frac{a_2 b_1}{b_2 a_1} \right) \text{ and } \bar{a}_3 = a_3 \left(1 - \frac{a_2 b_3}{b_2 a_3} \right) \text{ are}$$

modified values of a_1 and a_3 respectively.

Differentiating eqn. 8) with respect to C_L gives the static stability criterion (dC_m/dC_L) controls free which can be expressed as

$$\frac{\bar{v} a_2}{b_2} \frac{d\bar{C}_{Hn}}{dC_L} = h - \left\{ h_0 + \frac{\bar{v} a_1}{a} (1 - \frac{d\epsilon}{d\alpha}) \right\} = \left[\frac{dC_m}{dC_L} \right]_{\text{controls free}} \quad (9)$$

In this case the slope of the trim curve of hinge moment coefficient to trim with lift coefficient must be positive for stability since the control heaviness parameter b_2 is negative, Fig. 10.

Following the same argument as in the case of the controls fixed static stability the control heaviness parameter, b_2 , can be estimated from the trim curves at two C.G. locations. In this case

$$\frac{a_2}{b_2} = \frac{C_L (h_1 - h_2)}{\nabla (C_{H1} - C_{H2})} \quad (10)$$

and, using the value of a_2 estimated from eqn. 6), at the same value of C_L , b_2 can be evaluated.

These estimations of b_2 and a_2 depend on the flight conditions which could affect the trim equation being similar in both tests, only the C.G. location must change. The simplified pitching moment equations, eqns. 4) and 8), are linearised and highly simplified. No propulsive forces or aeroelastic forces or distortions have been included and so as far as possible the engine power and propeller speeds or thrust must be matched before tests, also the possibility of increased tail loads producing structural distortion must be considered, ref. 2, 3, 5.

The control tab characteristics can be evaluated by the addition of a simple test. If the aircraft is flown in steady, level, symmetric flight then the tail lift and elevator hinge moment will be constant. At that steady speed the control tab is moved and the aircraft held into the same trim state so that from eqn. 1) C_{L_δ} remains constant then the local angle of attack α_x will not be changed and, differentiating eqn. 1) with respect to β_η gives

$$a_2 \frac{d\eta}{d\beta_\eta} + a_3 = 0$$

$$\text{or} \quad \frac{-a_3}{a_2} = \frac{d\eta}{d\beta_\eta} \quad 11)$$

Thus for several random settings of trim tab angle the corresponding elevator angles to trim are measured and plotted to evaluate $(d\eta/d\beta_\eta)$, Fig. 11.

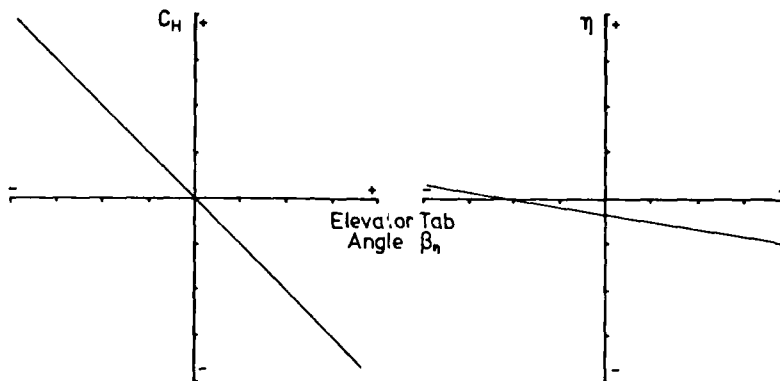


FIG 11, Elevator-Elevator Tab Characteristics.

At the same time the control forces and hence hinge moments are measured since movement of the trim tab will produce an out of trim force at the pilots hands. From eqn. 2), differentiating with respect to β_η gives

$$\frac{dC_{H_\eta}}{d\beta_\eta} = b_2 \frac{d\eta}{d\beta_\eta} + b_3 = \frac{-a_3 b_2}{a_2} + b_3$$

By plotting the control hinge moments against the tab angles the slope $(dC_{H_\eta}/d\beta_\eta)$ can be evaluated, Fig. 11.

Using eqn. 12) and the result from eqn. 6) enables the tab lift parameter a_3 to be evaluated and using eqn. 12) and the result of eqn. 10) with eqn. 11) enables the tab heaviness parameter b_3 to be found.

The measurement of a_2 , a_3 , b_2 and b_3 by this technique is relatively simple requiring basically only the instrumentation used in the static stability trials and a means of sensing elevator tab position. The flight trials are simple and do not depend on pilot technique to any extent. Provided that care is taken to match the peripheral influences for the tests then reasonable values of the control parameters can be obtained.

3.1.2. Lateral - directional static stability

The lateral static stability is based on the rolling moment equation of the aircraft and the directional static stability on the yawing moment equation; they are controlled by the aileron and rudder controls respectively although, due to aerodynamic cross-coupling and sometimes mechanical cross-coupling, the effects of these controls cannot be entirely separated.

The lateral-directional static stability is measured in terms of the rate of change of rolling moment and yawing moment with sideslip (cf. pitching moment - incidence in longitudinal static stability). Because there is no moment due to component of weight in either the lateral or directional senses of the aircraft axis system the normal balance of forces in the lateral sense is zero and the moments about the rolling and yawing axes should also be zero, this is the state of trim.

The static stability is determined by applying a control deflection to the aileron to produce a lateral disturbance (a bank angle) and a corresponding rudder control input to hold the aircraft into steady asymmetric flight, that is with the sideslip angle, β , not zero. If the aileron and rudder controls require increased deflection to increase the sideslip angle then the aircraft is producing rolling and yawing moments which would tend to restore it to equilibrium if the disturbing influence was removed; this indicates lateral-directional static stability. The form of the trim curves indicating stability are shown in Fig. 12.

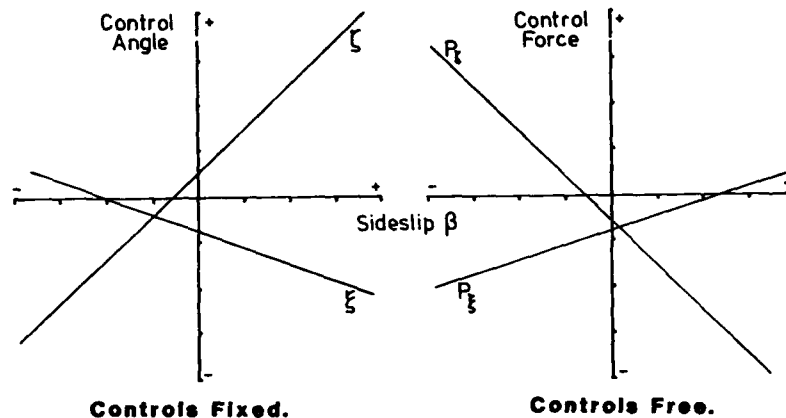


FIG 12. Lateral-Directional Static Stability Trim Curves.

The lateral-directional static stability equations are given by,
lateral

$$-l_v \beta = l_{\xi} \xi + l_{\zeta} \zeta$$

directional

$$-n_v \beta = n_{\xi} \xi + n_{\zeta} \zeta$$

13)

Now differentiating each with respect to β gives

$$-l_v = l_{\xi} \frac{d\xi}{d\beta} + l_{\zeta} \frac{d\zeta}{d\beta}$$

14)

$$-n_v = n_{\xi} \frac{d\xi}{d\beta} + n_{\zeta} \frac{d\zeta}{d\beta}$$

The slopes of the control trim curves, together with the control derivatives l_{ξ} , l_{ζ} , n_{ξ} , n_{ζ} , thus determine the lateral and directional static stability derivatives l_v , n_v respectively.

Since the C.G. of the aircraft has no effect on lateral-directional static stability (at least to the first order) the control characteristics cannot be estimated from the trim curves as they could be in the case of the elevator. The only way to assess the control characteristics by static means is to introduce some form of change in balance artificially.

Aileron Control characteristics can be estimated by applying a rolling moment by means of a fuel transfer between wing tip tanks. Initially the aircraft would be trimmed into symmetric flight with tip tanks empty and the control position and hinge moment recorded, (the latter in terms of pilot wheel or stick force). A known amount of fuel would be transferred into a tip tank and the control forces and positions noted in symmetric flight, the fuel would then be transferred into the other tank and the procedure repeated. Great care needs to be taken to ensure that during the transfer of fuel no unwanted lateral C.G. shift occurs. The known moment due to the fuel load shift can then be used to evaluate the aileron effectiveness parameter a_2 , and the out of balance hinge moment produced by the control deflection enables b_2 to be evaluated.

$$a_2 = \frac{L_{f1} - L_{f2}}{\frac{1}{2} \rho V^2 S b (\xi_1 - \xi_2)} \quad 15)$$

$$\text{and} \quad b_2 = \frac{-(C_{H1} - C_{H2})}{(\xi_1 - \xi_2)}$$

where L_{f1} , L_{f2} are the rolling moments produced by the fuel transfer.

Rudder control characteristics are more difficult to assess without recourse to special equipment to produce a pure yawing disturbance of known magnitude. Wing tip drag parachutes and load sensors would be a possibility but obviously costly to install and probably difficult to operate in a really satisfactory manner. Differential thrust from engines would be unlikely to be of sufficient accuracy for this purpose. Since the rudder is not normally called upon to produce a large yawing moment, except in the emergency case with one engine (or more) failed, the critical case is unlikely to be in steady flight and the adequacy of the rudder system will be evaluated as a special test.

The control tab characteristics of both aileron and rudder can be evaluated, as ratios of the control characteristic, in the same manner as the elevator; that is by holding steady flight and measuring the control deflections and force changes for various tab angle settings. This may provide an indication of the control characteristic and any cross-coupling which may be present.

3.2. Dynamic Stability Trials

These trials depend on the analysis of the motion of the aircraft arising from a control input. Usually the motion is oscillatory but it may take the form of an acceleration to a steady state.

Civil airworthiness requirements are basically very simple requiring fundamentally only demonstration that the short period oscillations are adequately damped (short period pitching oscillation and dutch roll) and that the time to double amplitude of any unstable long period mode is sufficiently large (phugoid and spiral mode).

Combat aircraft require a much more rigorous assessment of their handling qualities in manoeuvre. The first stage of such assessment is to lay down criteria for the handling qualities, these can be determined by an analysis of the dynamic stability characteristics of the aircraft and the combat manoeuvre in both simulated flight and real flight. Since this work will involve test pilots and service pilots, and because pilot response, ability and opinion are personal parameters, the definition of the handling criteria can never be precise. The criteria can be estimated in terms of pilot opinion ratings for certain manoeuvres, the handling qualities may be described as "good" when the aircraft's handling characteristics allow the pilot to complete the manoeuvres with little or no mental or physical effort or "bad" if the pilot can only achieve the objectives with great effort and concentration, if at all. The assessment of "goodness" or "badness" will be essentially a matter of the pilot's judgement in any given case.

The assessment of handling qualities by monitoring pilot performance in a given task, for example, tracking a target and using an error assessment to "score" the pilot's ability to carry out the task has not been a conclusive means of assessment. This is perhaps due to the curve of learning and adaptability of the pilot to the task. A better system is to use a pilot opinion rating of his own performance, and a commonly accepted rating is the Cooper-Harper scale, ref. 6, this is shown in Table I. In this system the pilot is asked to give a number to the handling qualities considered based on an answer to certain questions.

- i) Can the primary mission be accomplished ?
- ii) Could the aircraft be landed ?
- iii) What level of concentration or effort is required ?

By using several pilots to assess a particular handling quality an idea of how acceptable the aircraft is can be formed.

The acceptability of the aircraft can then be correlated to measurable dynamic stability characteristics of the aircraft, for example, frequencies of oscillation, damping factors, time constants and accelerations, and boundaries postulated to divide acceptable and unacceptable handling qualities, Figs. 13 and 14 show the sort of diagram which may result from such an investigation.

<u>Adjective Rating</u>	<u>Numerical Rating</u>	<u>Aircraft characteristic</u>	<u>Demand on Pilot in selected task or required operation</u>	<u>Can be landed?</u>
Satisfactory	1	Excellent; includes optimum	Nil	Yes
	2	Good; negligible deficiencies	Nil	Yes
	3	Satisfactory; some mildly unpleasant deficiencies	Minimal	Yes
Unsatisfactory	4	Acceptable; minor but annoying deficiencies	Moderate	Yes
	5	Unacceptable for normal operation; moderately objectionable deficiencies	Extensive	Yes
	6	Acceptable for emergency condition only - objectionable but tolerable deficiencies (e.g. Failure of Stability augmentor).	Extensive	Yes
Unacceptable	7	Major deficiencies - unacceptable even for emergencies.	Maximum tolerable	Doubtful
	8	Major deficiencies - dangerous	Considerable	No
	9	Major deficiencies - becoming uncontrollable	Intense	No
Catastrophic	10	Violent	Saturation	No

Table 1. The Cooper-Harper Handling Qualities Scale.

A further analysis and classification may be possible based on the aircraft type, phase of flight and flying qualities, the military specifications, ref. 7 classify the flying qualities under the headings.

i) Aircraft Classification:

Class I	Small light aircraft
Class II	Medium weight aircraft
Class III	Large transport aircraft
Class IV	Combat aircraft

ii) Flight Phase:

Category A	Non-terminal, fast precise manoeuvring, e.g. weapons delivery
Category B	Non-terminal, medium precision flight path control, e.g. cruise.
Category C	Terminal, precise flight path control, e.g. take-off, landing.

iii) Level of flying qualities, (approximate):

Level 1	Cooper Harper rating 1 to 3
Level 2	Cooper Harper rating 4 to 6

Level 3 Cooper Harper rating 6 to 8
 (Below level 3 Cooper Harper rating 8 +)

Levels of flying qualities can now be determined for aircraft classification and flight phases based on the measurable dynamic stability characteristics of the basic modes of motion and the response of the aircraft to control input.

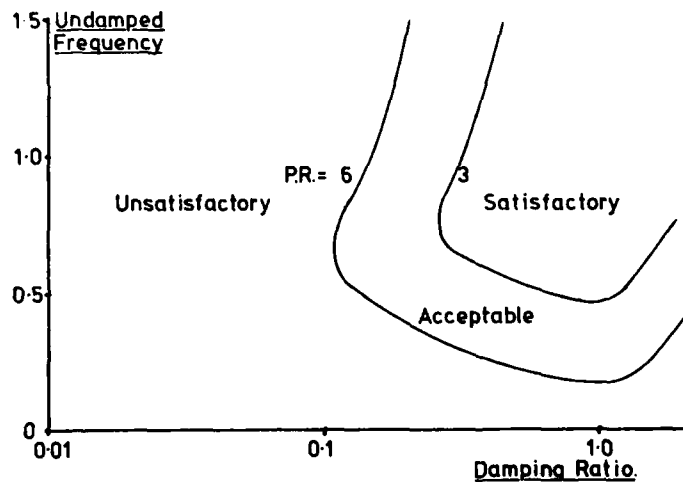


FIG 13. Short Period Criterion, large aircraft.

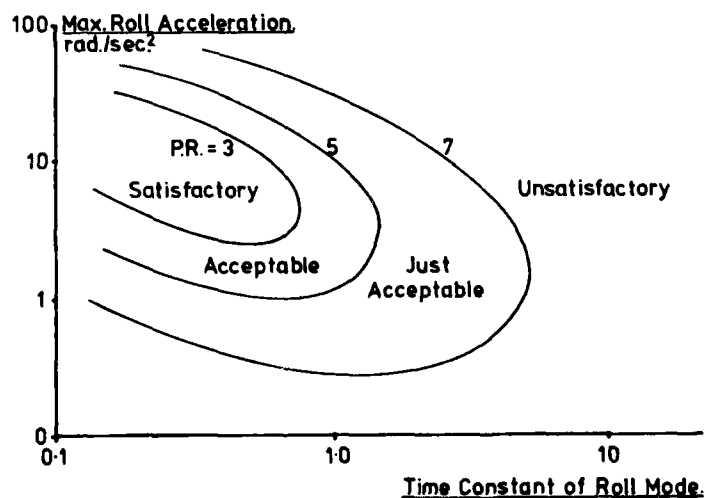


FIG 14. Roll Mode Criterion, fighter aircraft.

3.2.1. Control Characteristic Measurement

In dynamic tests the actual control characteristic in terms of the simple parameters, a_2 , b_2 etc. are not primarily considered. The characteristic is the aircraft response to control input as a measure of the control authority. The tests tend to be less formally regulated than the static stability trials since they are basically producing only a specific value of a response parameter.

An example of a relatively simple test is the roll mode; the roll rate response to aileron being considered. The rate of roll is measured during a step input of aileron control, Fig. 15. From this test the maximum acceleration in roll and time constant are measured, and the maximum steady roll rate per unit aileron input can be assessed. These parameters can then be used to compare with pilot opinion ratings to give acceptability boundaries on a "thumbprint" diagram, Fig. 14, ref. 8.

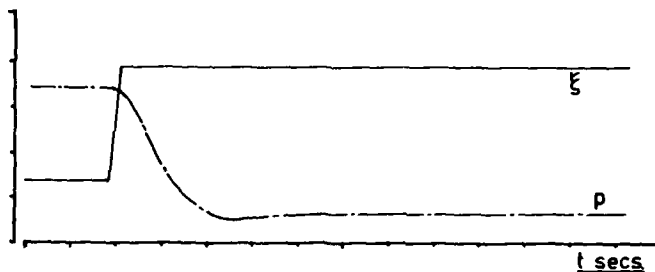


FIG 15. Roll Response to Step Input of Aileron.

Similar boundaries can be found for other handling characteristics, Fig. 13 shows a short period criterion for large aircraft, ref. 9. From such boundaries guideline values of parameters which can be measured relatively easily can be used to indicate design aims for acceptability in handling qualities. In this case the control characteristics themselves are not measured, only the aircraft response to a control input, and the adequacy of the control is based on that response.

3.2.2. Control Characteristic Research

In any systematic research into the aerodynamic properties of the aircraft and its controls methods have been adopted to extract aerodynamic derivatives from dynamic manoeuvres. In most cases at least some information must be available from other sources, such as static tests or wind tunnel tests, and the dynamic test is used to improve quality of the measured control derivative.

For example, simple rolling tests may be performed to provide information relating to roll damping and aileron power, Fig. 15. For a small (step) input of aileron deflection the aircraft builds up to a constant roll rate in which state the roll damping moment is equal to the control moment input,

$$L_p \dot{p} = L_\xi \xi \quad 16)$$

If the roll damping parameter L_p is known, measurement of steady rate of roll and aileron deflection will give a value of the aileron derivative L_ξ

The *time-vector method* is also useful for determining derivatives providing that good data is available for all other parameters. From an oscillatory motion, a dutch roll for example, the magnitudes and relative phases of the motions of the aircraft are measured, in this case the sideslip, roll rate and yaw rate from which the roll acceleration and yaw accelerations can be found. The equations of motion of the aircraft are given in eqns 17) and 18) for the rolling and yawing motions respectively in forced and damped motion.

$$\begin{array}{ccc} \text{ROLLING} & \text{Forced} & \text{Damped} \\ i_A \ddot{\phi} - i_P \dot{\phi} - v_2 i_V \delta - i_E \ddot{\psi} - i_R \dot{\psi} & = & v_2 i_\xi \xi + v_2 i_\zeta \zeta = 0 \end{array} \quad 17)$$

$$\begin{array}{ccc} \text{YAWING} & & \\ i_C \ddot{\psi} - n_R \dot{\psi} - v_2 n_V \delta - i_E \ddot{\phi} - n_P \dot{\phi} & = & v_2 n_\xi \xi + v_2 n_\zeta \zeta = 0 \end{array} \quad 18)$$

i_E is usually very small and may be neglected; aileron input is zero, $\xi = 0$, since the

rudder only is used to produce the dutch roll motion.

Using estimated (or measured) values of the moments of inertia and static derivatives l_v and n_v the rotary derivatives l_p , l_r and n_p , n_r can be determined from the damped dutch roll oscillation by drawing the polygon of forces, Figs. 16a) and 16b), for the rolling and yawing motions.

Using the values of the rotary derivatives thus obtained in the polygon of forces for the forced dutch roll will then enable the rudder control derivatives to be estimated, Fig. 16c) and 16d).

The time-vector method can produce relatively good results for control derivatives but it does depend on reliable data relating to the rolling and yawing motions and to the moments of inertia and static derivatives of the aircraft.

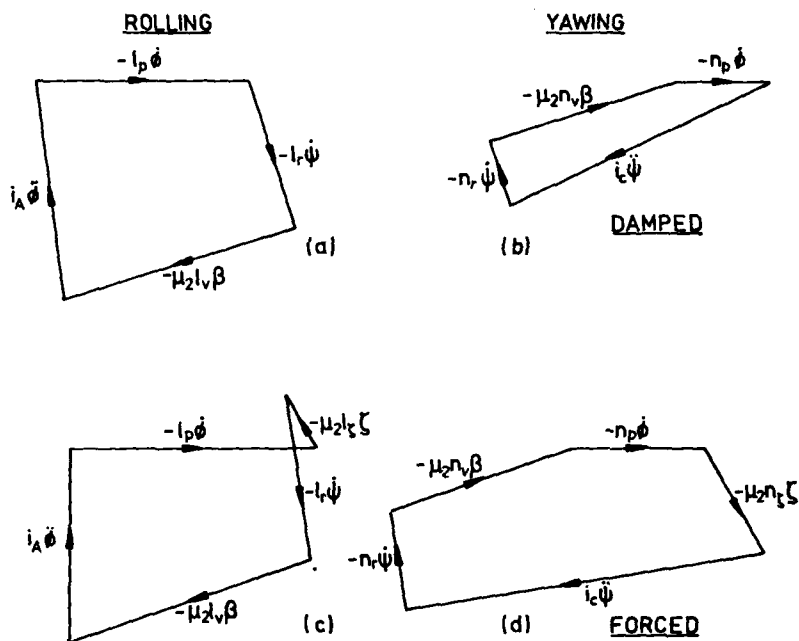


FIG 16. Force -Vector Diagrams for the Dutch Roll.

An advanced technique for determining the aerodynamic derivatives of an aircraft is System Parameter Identification. Briefly the method can be outlined as follows. If the controls of an aircraft are disturbed then the aircraft will respond by a change in the motion of the aircraft; and response is determined by the equations of motion. This can be represented by Fig. 17.

$$\begin{bmatrix} \xi \\ \zeta \end{bmatrix} \begin{bmatrix} \text{Roll} \cdots \cdots \cdots \\ \text{Yaw} \cdots \cdots \cdots \\ \text{Sideslip} \cdots \cdots \cdots \end{bmatrix} = \begin{bmatrix} p \\ r \\ v \end{bmatrix}$$

Control Input = Aircraft Eqns of Motion = Aircraft Response

FIG 17. Principle of System Parameter Identification.

Normally the control input consists of step inputs of aileron and rudder phased so that all the modes of motion are excited and therefore all the derivatives in the equations of motion will be contributing to the aircraft response. An initial step input of aileron will produce a disturbance in roll which is restricted by the roll damping mode, the resulting sideslip starts the spiral divergence. If a step input of opposite rudder is now applied the yawing motion initiates a dutch roll and all modes of motion are thus excited. The actual control input and relative phases can be chosen to suit the aircraft and the motions of particular interest.

By knowing any two parameters of the equation the third parameter can be calculated, so that by measuring the control input and the aircraft response the equations of motion can be calculated.

In practice this is not a simple process. Firstly, a reasonable guess of the equations of motion are required so that the response of the aircraft can be calculated and the calculated response compared with the measured response. The mis-match of the calculated and measured responses are then used to calculate new values of the coefficients in the equations of motion. This is a complex statistical process since a "weighting" function is required to connect particular characteristics of the mis-match of the response with particular derivatives. When successive corrections have been applied to the equations of motion and the calculated and measured responses agree then the equations of motion represent the aircraft at the test state. The aircraft derivatives thus produced will include the control derivatives and so this method enables the characteristics of the aircraft controls to be evaluated.

The Parameter Identification method is however very difficult to apply. It requires a large number of parameters to be recorded, the data digitised and an extensive computing facility for the data analysis. If however the aircraft is suitably instrumented it can produce a substantial improvement to the knowledge of the aerodynamic derivatives of the aircraft.

4. CONTROL CHARACTERISTICS IN EXTREME FLIGHT CONDITIONS

Some mention should be made of flight in attitudes not normally encountered in flight, typically flight at very high angles of attack, stalled flight and spinning.

Normally a pilot would not expect to fly the aircraft into such flight conditions but, when the aircraft is being manoeuvred in tight turns or at low speeds, the possibility of inadvertently exceeding the angle of attack for normal flight may be met. In this state it is necessary to know the likely response of the aircraft, if it is predictable, and the correct means of recovery.

Wind tunnel trials and free fall model tests are extensively used to determine the probable behaviour of the aircraft when departure from steady flight conditions occur. By these tests rates of rotation and possible flow patterns can be investigated to help determine methods of recovery to steady flight. Since extensive separation of flow may have taken place and flow directions may be grossly changed, non-standard recovery procedures may be required, for example, one high performance combat aircraft requires full aft movement of the stick to recover from the stall; such movement is contradictory to normal reactions but necessary due to the extreme attitude of the aircraft in the stall. The importance of a thorough investigation can be highlighted by the loss of the BAC 111 in early stalling trials when separated flow from the wing blanketed the tail and engine intakes and produced an irrecoverable situation; this phenomenon became known as Deep-stall or Super-stall.

Flight trials can only be approached with extreme caution following the experimental investigation on the model tests. Normally these trials will start with assessment of pre-departure warnings, both natural and artificial, and lead up to the recovery from the incipient departure case. If the recovery procedure follows the predicted pattern then departure would be allowed and the recovery actions checked in the early stages of the motion, the procedure continuing until recovery from the fully developed stall or spin was demonstrated. At all stages emergency recovery aids would be fitted to the aircraft to assist if normal control failed to achieve a recovery to normal flight, devices such as parachutes to produce a pitch-down moment are usually used for this purpose.

No particular procedures or methods can be detailed here as each aircraft has its own peculiarities and the test procedure must be tailored to suit the needs of the aircraft and its operation.

Similar comment may be made about the testing of special aerodynamic controls, e.g. airbrakes or flaps, especially when these are used in manoeuvre to enhance the performance of the aircraft. Although preliminary tunnel and steady flight trials may have indicated that no adverse handling qualities may be expected their operation under load may not be as predicted and a cautious approach to their deployment should be taken.

5. CONCLUSIONS

The in-flight measurement of aircraft control characteristics is not a straightforward process. In fact the control characteristics are measured in terms of aircraft flying and handling qualities and do not normally appear as separate coefficients. However, it is possible to extract some data relating to the controls from the handling and stability tests although this data will be indirectly measured in general.

From the longitudinal static stability tests it is possible to estimate the elevator and elevator tab characteristics. The aileron and rudder tab effectiveness relative to the parent control can also be found by a simple static test. Aileron and rudder control characteristics cannot however be found by static test unless special equipment is used, these need to be determined from dynamic manoeuvres. Other methods such as System Parameter Identification can be used but require both extensive instrumentation and computing facilities and a good basic knowledge of the parameters if the method is to be successful.

Whilst in general the control derivatives or characteristics are not considered separately from the overall handling qualities there may be cases where further knowledge may be useful to the development of the aircraft, this paper has shown some methods by which that knowledge may be obtained.

REFERENCES

1. Mabey D.G. "Experimental Methods to determine control effectiveness in wind tunnels"
AGARD Special course on Aerodynamic Characteristics of Controls.
VK1 March 1983
2. Babister A.W. "Aircraft Dynamic Stability and Response"
Pergamon 1980
3. Irving F.G. "An Introduction to the Longitudinal Static Stability of low-speed Aircraft"
Pergamon 1966
4. Eshelby M.E. "The Estimation of Tail Parameters from Static Stability Trim Curve data"
College of Aeronautics Memo. 7508
5. Klawans, B.B. & Johnson, H.I. "Some effects of fuselage flexibility on longitudinal stability and control".
NACA Tech. Note 3543 1956
6. Cooper G.E. & Harper R.P. "The use of pilot rating in the evaluation of aircraft handling qualities".
NASA TND-5153 1969
7. - "Military Specification - Flying Qualities of Piloted Airplanes"
MIL-F-8785B 1971
8. Bisgood, P.L. "A Review of Recent Research on Handling Qualities, and its Application to the Handling Problems of Large Aircraft".
R&M 3458 (Parts I and II) 1967
9. Bisgood, P.L. "A Review of Recent Research on Handling Qualities and its Application to the Handling Problems of Large Aircraft".
R&M 3606 (Part III) 1970

AERODYNAMIC CHARACTERISTICS OF MISSILE CONTROLS

Jack N. Nielsen
Nielsen Engineering & Research, Inc.
510 Clyde Avenue, Mountain View, CA 94043

SUMMARY

The present work contains material to accompany a set of lectures on the aerodynamic characteristics of controls. The first chapters cover the subjects of missile control types and terminology.

The subjects of jet spoilers and combining controls and the airframe are then considered. As the basic approach to integrating the presentation of all-movable controls, the equivalent angle-of-attack concept is next taken up followed by detailed considerations of all-movable planar and cruciform controls. These are treated from the phenomenological point of view as well as from the quantitative point of view. Methods for determining the effects of vortices on control characteristics are presented in sufficient detail to carry out calculations. The final chapter discusses control hinge moments and presents a preliminary method for their calculation at supersonic speed.

LIST OF SYMBOLS

Sections 1 through 3

M_o	free-stream Mach number
p	local static pressure in front of forward facing step
p_o	free-stream static pressure
R_L	Reynolds number based on distance up to forward facing step
δ	all-movable control deflection angle
$\delta_1, \delta_2, \delta_3, \delta_4$	all-movable control deflections for fins 1, 2, 3, and 4, respectively; see sketch in section 2

Section 4

A	downstream cross-section area of two-dimensional jet, figure 5
A_j	area of jet sonic throat
C_{m_j}	pitching-moment coefficient about lateral axis through jet center, $\frac{M_j}{\frac{\pi}{4} q_\infty D^3}$
C_N	normal-force coefficient of jet for both reaction and aerodynamic forces
C_T	$P_{o_j} A_j / q_\infty S_B$
d_j	diameter of jet sonic throat
D	diameter of circular body
K_{m_j}	C_{m_j} / C_T
K_N	C_N / C_T
ℓ	length of jet in front of body base
M	downstream Mach number of two-dimensional jet
M_j	moment induced by jet about axial position of jet spoiler
M_1, M_∞	free-stream Mach number
N_V	jet momentum, equation (3)
N_{V_i}	normal force induced on plate or body by jet
p	local static pressure
p_1, p_∞	free-stream static pressure
p_{o_j}, p_{t_j}	total pressure of jet
q_1, q_∞	free-stream dynamic pressure

S_B	body cross-sectional area
V_j	jet exit velocity
α	angle of attack of body
γ	ratio of specific heats
δ	angle of separation induced by jet, figure 5
ρ_j	mass density of jet at exit

Section 5

C_ℓ	missile rolling-moment coefficient based on S_R and ℓ_r
C_m	missile pitching-moment coefficient based on S_R and ℓ_r
C_n	missile yawing-moment coefficient
C_Y	missile side-force coefficient based on S_R
$\frac{dC_m}{d\alpha}$	moment-curve slope
C_{m_δ}	$\partial C_m / \partial \delta$ for fixed α
$C_{L_{trim}}$	lift coefficient at which $C_m = 0$
$\Delta C_{D_{trim}}$	trim drag, figure 16
d	body diameter
ℓ_r	reference length, d
L/D	lift-drag ratio
M_∞	free-stream Mach number
S_R	reference area, $\pi d^2/4$
x	axial position of missile center of pressure
x_{cg}	axial position of center of gravity measured from same zero datum as x
α	missile angle of attack
α_{trim}	value of α for $C_m = 0$
δ	canard control deflection, positive trailing edge down
δ_{roll}	value of δ for all canards deflected to produce negative rolling moment
ϕ	missile roll angle

Section 6

a	body radius
A	aspect ratio of wing alone
c	local wing chord
C_n	section normal-force coefficient
$C_{N(F)1}$	normal-force coefficient of fin 1 in the presence of a circular body
C_{N_W}	normal-force coefficient of the wing alone which is composed of two fins joined at their root chords (based on wing planform area)
$\left(\frac{C_{N_0}}{C_{N_0}}\right)_W$	slope at zero angle of attack of the normal-force coefficient curve of the wing alone
$\left(\frac{dC_N}{da}\right)_W$	normal-force curve slope of wing alone
k_W	fin deflection factor, see equation (19)
K_W	upwash factor, see equation (17)
K_ϕ	sideways factor, see equation (27)
M_L	local Mach number
M_∞	free-stream Mach number
$N_{F(B)}$	normal force of fin in presence of body
N_W	normal force of wing alone
q_L	local dynamic pressure
s	semispan of wing alone
s_m	semispan of fin as measured from the body axis
S_F	fin planform area
S_W	wing alone planform area
V_{n1}	component of average velocity acting normal to fin 1
V_{p1}	component of average velocity acting parallel to root chord of fin 1
V_∞	free-stream velocity
$\bar{x}_{F(B)}$	axial location of center of pressure for a fin in the presence of a body (measured from leading edge of root chord)
\bar{x}_W	axial location of center of pressure for wing alone
y	lateral distance from body axis measured in plane of the fin
$\bar{y}_{F(B)}$	spanwise location of center of pressure of fin in the presence of a body measured from body axis
\bar{y}_W	spanwise location of center of pressure of wing alone
α	angle of attack of fin, $\alpha_c \cos \phi$
α_c	angle between body axis and wind velocity vector
α_{eq1}	equivalent angle of attack of fin 1, i.e., angle of attack of wing alone which gives same normal-force coefficient as that of fin 1
$\hat{\alpha}_{eq1}$	equivalent angle of attack of fin 1 if all fins are undeflected
α_L	angle of attack of fin in plane normal to fin planform at given spanwise position
β	angle of sideslip of fin, $\alpha_c \sin \phi$
δ_1	deflection of fin 1, positive when the leading edge is rotated toward the leeward side of the body

$(\Delta\alpha)_{v1}$	average angle of attack induced on fin 1 by vortices
Λ_{ij}	fin deflection factor, see equations (36) and (37)
ϕ_B	bank angle of wing-body combination, see figure 32
ϕ_1	roll angle of fin 1, see figure 32

Sections 7 and 8

a	body radius
A, A_W	wing-alone aspect ratio
C_L	rolling-moment coefficient
$C_{L\delta_a}$	$\partial C_L / \partial \delta_a$, (radians) ⁻¹ ; also $C_{L\delta}$
c_r	fin root chord
c_t	fin tip chord
C_{Lp}	damping-in-roll coefficient, see equation (62)
$C_{m(B)}$	pitching moment of body due to effect of fins
$C_{m(F)}$	pitching moment of fin in presence of body
C_{mBW}	pitching moment of wing-body combination
C_{HM}	fin hinge-moment coefficient
$C_{N(B)}$	normal force of body due to presence of fin
$C_{N(F)}$	normal force on fin in presence of body
C_{RB}	root bending-moment coefficient
k_W	fin interference factor for pitch control, equation (17)
k_B	body interference factor for local carry-over from fin, equation (49)
K_B	wing-body interference factor for body, see equation (49)
K_W	wing-body interference factor for fin, see equation (17)
K_ϕ	interference factor for $\alpha\beta$ coupling, see equation (27)
L_r	reference length
$N_{B(F)}$	normal force on body due to fins
$N_{F(B)}$	normal force on fin in presence of body
N_W	normal force of wing alone
p	missile roll rate, positive clockwise looking forward
RM	missile rolling moment
s_m	semispan of body-fin combination
S_W	planform area of wing alone
S'_W	area of wing alone formed by extending the leading and trailing edges of the fin to the body centerline
x_{CG}	distance of center of gravity behind leading edge of fin root chord
x_{HL}	distance of hinge line behind leading edge of fin root chord
x, y	axes shown in figure 47
x_b, y_b	x, y coordinates of forward boundary of influence of one fin on another for planar configuration
\bar{z}	distance behind leading edge of root chord to wing (or fin) center-of-pressure position

\bar{y}	distance from body axis to center-of-pressure position of fin or distance from root chord to center of pressure of wing alone	α	angle of attack
\bar{x}_a, \bar{y}_a	values of \bar{x} or \bar{y} for $\delta = 0$	$(\Delta\alpha)_v$	change in equivalent angle of attack of fin due to vortices
\bar{y}_ϕ	distance from body axis to fin center of pressure associated with loading due to $\alpha\delta$ coupling, figure 29	Γ	strength of vortex; circulation about the core
α	$\alpha_c \cos \phi$	Γ_B	vortex strength of symmetric body in first quadrant
α_c	angle between free-stream velocity vector and missile longitudinal axis	Γ_l	vortex strength associated with potential lift on canard fin, figure 65
α_{eq}	equivalent angle of attack of fin including control deflection of two fins	Γ_t	vortex strength associated with leading-edge vortex of canard fin
$\hat{\alpha}_{eq}$	equivalent angle of attack of fin without control deflections	θ_n	nose half angle
$(\Delta\alpha)_v$	change in equivalent angle of attack of fin due to vortices	Section 10	
Λ_{ij}	fin deflection factor, equations (36) and (37)	A_1, A_2, A_3	coefficients of a truncated sine series, equation (94)
δ	fin deflection angle	R	wing-alone aspect ratio
δ_a	aileron control deflection; opposing deflections of opposite fins	b	full span of wing alone
δ_p	equal deflections of fins 2 and 4	c	chord of airfoil
δ_y	equal deflections of fins 1 and 3	c_l	section lift coefficient at local spanwise station of wing alone
$\delta_1, \delta_2, \delta_3, \delta_4$	control deflections for fins 1, 2, 3, and 4, respectively; see figure 32 for sign conventions	c_r	fin root chord
λ	fin taper ratio, c_t/c_r ; also a/s_m	C_{HM}	hinge-moment coefficient
ϕ	angle of bank, positive clockwise looking forward	$CHMC$	hinge-moment coefficient for canard fin
Section 9		$CHMC1, CHMC2, CHMC3, CHMC4$	values of CHMC for canard fins 1, 2, 3, and 4, respectively.
a	cylindrical body radius	C_N	normal-force coefficient
$ C_Y _{max}$	maximum value of sideforce coefficient due to asymmetric vortices	CNC	normal-force coefficient of canard fin
d	cylindrical body diameter, $2a$	$C_{N(F(B))}$	normal-force coefficient of fin in presence of body including vortex effects
i_T	tail interference factor, equation (83)	$C_{N(F(B)),1}$	normal-force coefficient of fin in presence of body without vortice effects
M, M_∞	free-stream Mach number	C_{N_W}	normal-force coefficient for wing alone
M_C, M_N	crossflow Mach number, $M_\infty \sin \alpha$	K_W	fin interference factor for pitch control, equation (19)
N_T	normal force on tail alone at angle of attack, α	K_W	wing-body interference factor for fin, see equation (17)
$N_{T(V)}$	normal force on tail fins due to symmetric pair of body vortices	K_ϕ	interference factor for $\alpha\delta$ coupling, see equation (27)
q_∞	free-stream dynamic pressure	ℓ_r	reference length
r_e	radial distance to external vortex	M_∞	free-stream Mach number
r_j	radial distance to image vortex	$\left(\frac{t}{c}\right)_{max}$	maximum thickness ratio for fin root section
r_t	cylindrical body radius at tail location	x_{HL}	distance of hinge line behind leading edge of wing root chord
r_N	radius of cylindrical body behind nose	\bar{x}	axial center-of-pressure distance behind leading edge of root chord for fin or wing alone
s_t	semispan of tail fin measured from body axis	$\bar{x}_{F(B)}$	value of \bar{x} for fin in presence of body
S_T	planform area of tail alone	$\bar{x}_{F(B),1}$	value of $\bar{x}_{F(B)}$ without vortex effects
V_∞	free-stream velocity	$\bar{x}_{F(B),2}$	value of $\bar{x}_{F(B)}$ for vortex loading
x_s	distance from start of nose to beginning of separation on body of revolution at angle of attack	\bar{x}_v	value of \bar{x} due to vortex component of fin loading
y_B, x_B	y, x coordinates of body vortex core in first quadrant for symmetrical body vortices	$\left(\frac{\bar{x}}{c_r}\right)_{45^\circ}$	value of (\bar{x}/c_r) for wing alone at $\alpha = 45^\circ$
		$\Delta\bar{x}$	shift in \bar{x} due to thickness or vortices
		$(\Delta\bar{x})_t$	value of $\Delta\bar{x}$ associated with airfoil or wing thickness

$(\Delta \bar{x})_V$	shift in value of $\bar{x}_{F(B)}$ due to vortices	α_{eq_2}	value of α_{eq} with vortex effect
$(\Delta \bar{x})_W$	shift in \bar{x} of the wing due to wing thickness	$(\Delta \alpha)_V$	change in equivalent angle of attack of fin in presence of body due to vortices
\bar{y}_V, \bar{z}_V	coordinates of center-of-pressure position of fin loading due to vortices	δ	fin deflection
\bar{y}	lateral position of center of pressure measured from body axis	$\delta_1, \delta_2, \delta_3, \delta_4$	values of δ for fins 1, 2, 3, and 4, respectively
α	angle of attack	Λ_{if}	fin deflection factor, equations (36) and (37)
α_W	angle of attack of wing alone	λ	fin taper ratio
α_{eq}	equivalent angle of attack	τ	see equation (95)
α_{eq_1}	value of α_{eq} without vortex effect	ϕ	roll angle

1. INTRODUCTION

This paper consists of Lecture Notes on the subject of missile controls to be presented at the AGARD Special Course on "Aerodynamic Characteristics of Control" at the von Karman Institute, Rhode-Saint-Genese, Belgium on 21-25 March 1983. The purpose of the lectures is to explain the basic aerodynamic phenomena involved in missile controls and the available calculative methods for predicting the characteristics of such controls.

A number of overall treatments of missile controls or subclasses of them exist. In reference 1, Nielsen gives a broad overview of aerodynamic controls for missiles. The AGARD 1974 Lecture Series 67 (ref. 2) covers aerodynamic controls, thrust vector controls, and spoiler controls. The AGARD 1979 Lecture Series 98 (ref. 3) contains a section on control of guided missiles. Also, an AGARD Short Course on Flight Mechanics for Tactical Missiles given at the Hellenic Air Force Research and Technology Center, Athens, Greece, March 31 to April 2, 1981, presents Chapter VI on Missile Stability and Control (ref. 4). The present treatment draws on these references for general information, but it includes considerable more information, especially in the areas of nonlinear phenomena and prediction methods.

Some general observations on missile controls are now made before embarking into technical details. First, there are many types of missile controls which generally break down into aerodynamic types, reaction types, and thrust vector types. We will only be able to treat reaction controls and all-movable controls in any depth. In many types of controls, it is possible to predict normal force with good accuracy, but predictive methodology for hinge moments of aerodynamic controls is not highly developed. In designing controls for a missile, it makes sense to use control types for which the predictive methodology is in good order. This will save much expensive wind-tunnel testing and will permit trade-off studies in preliminary design. Testing controls over the entire operating region in a wing tunnel involves extensive testing. In what follows, we will not be concerned about autopilot considerations.

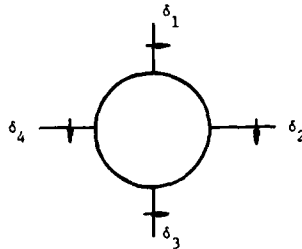
A list of the subjects to be covered in the present lectures follows:

1. definition of control terms
2. types of controls (descriptions)
3. jet spoilers
4. combining controls and airframes
5. equivalent angle of attack
6. planar all-movable controls
7. cruciform all-movable controls
8. vortex effects for circular bodies
9. hinge-moment prediction methodology at supersonic speed

2. DEFINITIONS OF CONTROL TERMS

1. All-movable controls.— All-movable controls are fins which can be rotated as a unit about a lateral hinge line for control purposes.
2. Body vortex interference.— The effects on fin loading induced by the flow field associated with separation vortices over a body at angle of attack.
3. Canard, wing, tail control.— Canard control refers to the use of canard fins for control in pitch, yaw, or roll; wing control refers to the use of the main lifting fins of a wing-body-tail combination for control; and tail control refers to the use of tail fins for control.
4. Control cross-coupling.— Interference among the pitch, yaw, and roll functions of control; for instance, the generation of a rolling moment by a pure yaw command.
5. Control effectiveness (all-movable controls).— Loosely the amount of normal force produced by a control as a result of deflection δ divided by the normal force produced by the fin if it were part of the wing alone at an angle of attack equal to δ . A more precise mathematical definition is given in the section on equivalent angle of attack.
6. Equivalent angle of attack.— The angle of attack of the wing alone at which the fin develops the same normal force as part of the wing alone that it develops when mounted on the missile.
7. Fin-body interference.— The aerodynamic effect induced on the fins by the presence of the body and the effects induced on the body by the presence of the fins.

8. Fin-fin interference.— The aerodynamic effects on a fin due to the presence of another fin.
9. Hinge line, hinge moment.— The hinge line is the axis about which a control rotates; the moment developed around this line by the forces on the fin is the hinge moment.
10. Nonlinearities.— To the extent that the forces and moments developed by a control are not linear function of α , δ , M_∞ , and ϕ , they are nonlinear.
11. Pitch, yaw, and roll control.— Consider a missile with cruciform fins as sketched.



The positive deflection directions of the trailing edges are as shown.

$$\begin{aligned}
 \text{Pitch control} \quad & \delta_2 = \delta_4 \neq 0 \\
 \text{Yaw control} \quad & \delta_1 = \delta_3 \neq 0 \\
 \text{Roll control} \quad & \delta_1 = -\delta_3 \neq 0 \\
 & \text{and/or} \\
 & \delta_2 = -\delta_4 \neq 0
 \end{aligned}$$

The definitions hold also for a planar missile for the same deflections except that δ_1 and δ_3 are zero. No yaw control exists unless a vertical fin is introduced elsewhere.

12. Trim drag.— The change in missile drag between the $\alpha \neq 0$, $\delta = 0$, and a trim condition at the same angle of attack for which $\delta \neq 0$.
13. Wing alone.— The planar lifting surface formed by joining two opposite fins at their root chords. The concept does not depend on the location of the set of fin.

3. TYPES OF MISSILE CONTROLS

3.1 Introductory Remarks

There are many different missile controls, far more than can be listed herein. There are a number of categories under which most controls can be classified. These classifications are purely aerodynamic controls, reaction controls and thrust vector controls. We will now describe some specific controls which fall within the various classifications.

3.2 Aerodynamic Controls

Probably the simplest and most broadly used type of aerodynamic control is the all-movable control. An all-movable control is a fin free to rotate in its entirety about some lateral axis. This type of control is popular because it maximizes the control force and enhances maneuverability. We will discuss it at some length.

A second type of aerodynamic control usually used on aircraft but also used for missiles is the flap-type of control. The trailing-edge flap is the common one used in missiles, and a number of examples of this class are shown in figure 1. The characteristics of flap-type controls are extensively covered in DATCOM (ref. 5).

Another type of aerodynamic control is the mechanical spoiler or forward-facing step. The spoiler causes separation of the boundary layer ahead of the step accompanied by a pressure rise. Some data in figure 2, taken from reference 6, show how boundary-layer type and Mach number affect the pressure distribution in front of the spoiler. For transitional separation, transition occurs near the end of the pressure plateau, and transition moves downstream as Mach number increases. The extent of separation is greater for the laminar and transitional cases, but the extent does not vary much with Mach number. The extent of separation is least for the turbulent case but the average pressures in the separation region are largest.

The use of a spoiler well in front of the trailing edges tends to reduce its effectiveness because of suction pressures behind the spoiler. The geometric and hinge-moment advantages of a spoiler are clear. However, spoilers increase drag and their effects are nonlinear in spoiler height.

3.3 Reaction Controls

Reaction controls develop their control force as the reaction to the momentum of a fluid being ejected from the missile usually in the form of a jet. In the case of a jet, the throat usually occurs at the

surface so that the jet is sonic at this point. A pure reaction control operates in a vacuum, outside the atmosphere. However, reaction jets are used in the atmosphere and usually induce aerodynamic effects which can amplify the reaction force. In this case, the term "jet spoiler" is applied. We will consider the case of the jet spoiler in some detail. The jet spoiler is depicted in figure 3.

Another example of a reaction control is the ram airjet spoiler (ref. 7). The ram airjet spoiler operates fundamentally through reaction but is augmented by aerodynamics.

3.4 Thrust Vector Controls

Thrust vector controls are devices used to change the direction of the line of action of a propulsive jet. The simplest embodiment of this concept is the swiveling nozzle which directs the thrust in any desired direction. A sketch of a swiveling nozzle is shown in figure 4. There are many hardware implementations of the swiveling nozzle.

Fluid injection is a useful way to produce thrust vector control for a fixed nozzle. In this concept a side wall jet is used in the expanding part of the nozzle to trigger boundary-layer separation on the wall so that the nozzle flow is no longer axisymmetric. By having such jets on different sides of the nozzle some degree of control over the thrust direction can be maintained. The power requirement for such injection devices is small.

Another type of thrust vector control is the jet vane. The jet vane is an all-movable lifting surface of heat resistant material which is immersed in the propulsive jet. It is useful when aerodynamic controls are ineffective because of low free-stream dynamic pressure.

4. AERODYNAMICS OF THE JET SPOILER

4.1 Description of the Flow

The jet spoiler is typically a sonic circular jet issuing laterally from an orifice throat in the side of a body or fin. It may issue normal to the body or not. When normal to the body, it is sometimes thought of as a solid cylinder causing pressure distributions on the adjacent surfaces. The flow at supersonic speed is depicted schematically in figure 3. The issuing jet forms a barrel shock which is capped by a Mach disk. The shock produces an upstream pressure disturbance which causes the boundary layer to separate and gives positive pressures in front of the jet. Behind the jet negative pressures are induced. The jet mixes with the free-stream air forming a trailing vortex pair which downstream has the following kidney-shaped cross section. The distance from the body surface to the center of the



Mach disc is termed the jet penetration distance.

4.2 Parameters Influencing Jet Thrust

The fluid mechanics of a circular jet in a crossflow is clearly very complicated. While a simple theory (ref. 8) to calculate the pressure for a two-dimensional jet has been advanced, its accuracy is not good. In fact, for design purposes, we must rely principally on data correlations. The rationale for the data correlation is now given.

It is important to establish the parameters which control the jet thrust and the induced aerodynamic force which can augment it. Since boundary-layer, shock-wave interaction is the driving mechanism, Mach number is an important parameter. The diameter of the jet and the total pressure of the jet are other obvious parameters. Since the jet induces positive pressures upstream, and negative downstream, its location with respect to the body base is a significant parameter. Another parameter is the angle of attack. The primary variables and their ranges in available test data are:

$$\text{Mach number: } 0.3 \leq M_\infty \leq 2.5$$

$$\text{Ratio of jet diameter to body diameter: } 0 < \frac{d_j}{D} < 0.5$$

$$\text{Ratio of jet total pressure to free-stream pressure: } 5 \leq \frac{p_{o1}}{p_\infty} \leq 500$$

$$\text{Angle of attack: } -10^\circ \leq \alpha \leq 10^\circ$$

4.3 Simplified Theory for Two-Dimensional Isentropic Jet

It is possible to give a simple theory of the amplification of a jet spoiler due to interaction with the outer flow for the two-dimensional case. This theory (ref. 8), applied to the flow model shown in figure 5, yields insight into the action of a jet spoiler. The jet is assumed to turn 90° while expanding from sonic speed at the throat to the free-stream pressure at the end of the turn. For isentropic flow, we can write for the pressure ratio and area ratio

$$\frac{p_{o1}}{p_1} = \left(1 + \frac{\gamma-1}{2} M^2 \right)^{\frac{\gamma}{\gamma-1}} \quad (1)$$

$$\frac{A}{A_j} = \left(\frac{2}{\gamma + 1} \right)^{\frac{\gamma+1}{2(\gamma-1)}} \frac{\left(\frac{p_{o_j}}{p_1} \right)^{\frac{\gamma+1}{2\gamma}}}{\sqrt{\frac{2}{\gamma-1} \left[\left(\frac{p_{o_j}}{p_1} \right)^{\frac{\gamma-1}{\gamma}} - 1 \right]}} \quad (2)$$

The total momentum of the jet at the orifice is

$$\begin{aligned} N_V &= (p_1 + \rho_j v_j^2) A_j \\ &= p_1 A_j \left[1 + \gamma M_j^2 \right] \\ &= \left(\frac{p_1}{p_{o_j}} \right) \left(p_{o_j} A_j \right) (\gamma + 1) \\ &= 2 \left(\frac{2}{\gamma + 1} \right)^{\frac{1}{\gamma-1}} p_{o_j} A_j = 1.268 p_{o_j} A_j \end{aligned} \quad (3)$$

for $\gamma = 1.4$.

The normal force induced on the plate by the jet is (neglecting A_j)

$$\begin{aligned} N_{V_i} &= \left(\delta \frac{dp}{d\delta} \right) \left(\frac{A}{\delta} \right) \\ &= A \frac{dp}{d\delta} \end{aligned} \quad (4)$$

On a nondimensional basis this augmentation is given by

$$\frac{N_{V_i}}{N_V} = \frac{(A/A_j) \frac{d(p/p_1)}{d\delta}}{2 \left(\frac{2}{\gamma + 1} \right)^{\frac{1}{\gamma-1}} \left(\frac{p_{o_j}}{p_1} \right)} \quad (5)$$

With the help of equations (1) and (2), we have

$$\frac{N_{V_i}}{N_V} = \frac{1}{2} \left(\frac{2}{\gamma + 1} \right)^{1/2} \frac{\frac{d(p/p_1)}{d\delta}}{\left(\frac{p_{o_j}}{p_1} \right)^{\frac{\gamma-1}{2\gamma}} \left\{ \frac{2}{\gamma-1} \left[\left(\frac{p_{o_j}}{p_1} \right)^{\frac{\gamma-1}{\gamma}} - 1 \right] \right\}^{1/2}} \quad (6)$$

Since supersonic two-dimensional theory gives

$$\frac{p - p_1}{q_1} = \frac{2\delta}{\sqrt{M_1^2 - 1}}$$

equation (6) yields

$$\frac{d}{d\delta} \left(\frac{p}{p_1} \right) = \frac{q_1}{p_1} \frac{d}{d\delta} \left(\frac{p - p_1}{q_1} \right) = \frac{\gamma M_1^2}{\sqrt{M_1^2 - 1}} \quad (7)$$

From equation (6) it is clear that the amplification factor N_{V_i}/N_V goes down with increase in pressure ratio. Also from equations (6) and (7), it is clear that it goes up with M_1 . Some calculated results showing the effect of these parameters and γ on the amplification ratio are shown in figure 6. Note that increases in γ reduce amplification ratio.

The preceding results have not been corrected for the imbalance force $p_1 A_j$ on the inside of the body with the jet off which cannot be ascribed to augmentation of the jet. For this reason the quantity

$$\left[2 \left(\frac{\gamma}{\gamma + 1} \right)^{\frac{1}{\gamma-1}} \left(\frac{p_{o1}}{p_1} \right)^{-1} \right] \quad (8)$$

should be subtracted from equation (6).

4.4 Data Correlation for Circular Bodies

In what follows we will present empirical results for the induced sideforce due to jets issuing laterally from an orifice on the cylindrical section of a circular body of revolution. For the purpose of the correlation we will define certain dimensionless quantities. First we define a jet thrust coefficient, C_T , as follows.

$$C_T = \frac{p_{o1} A_j}{q_\infty S_B} \quad (9)$$

with

$$\begin{aligned} p_{o1} &= \text{jet total pressure} \\ A_j &= \text{jet throat area, } \frac{\pi d_j^2}{4} \\ q_\infty &= \text{free-stream Mach number} \\ S_B &= \text{body cross-sectional area, } \frac{\pi D^2}{4} \end{aligned}$$

The thrust coefficient thus becomes

$$C_T = \frac{2}{\gamma M_\infty^2} \left(\frac{p_{o1}}{p_\infty} \right) \left(\frac{d_j}{D} \right)^2 \quad (10)$$

Note that $p_{o1} A_j$ is not the true jet momentum, N_j , as given by equation (3) but is only 21 percent lower. It is, however, a convenient reference quantity for nondimensionalizing as used in reference 9.

Let C_N be the total force coefficient due to a lateral jet (fig. 9) including both reaction and aerodynamically induced forces. Then a normal-force factor K_N is defined as follows:

$$K_N = \frac{C_N}{C_T} \quad (11)$$

Here C_N and C_T are based on the same dynamic pressure and reference area. Also establish a moment coefficient C_{m_j} due to C_N about the jet orifice center. The moment factor K_{m_j} is then taken to be

$$K_{m_j} = \frac{C_{m_j}}{C_T} ; \quad C_{m_j} = \frac{M_j}{q_\infty \left(\frac{\pi}{4} \right) D^3} \quad (12)$$

where M_j is the pitching moment of the jet induced effects about the orifice center.

It is of interest to see how the various parameters of interest influence K_N and K_{m_j} as exhibited by experiment. In figure 8 the effect of the distance ℓ from the body base is shown. As the jet position is moved upstream, the negative pressure behind the orifice reduces K_N . Included on this figure and subsequent figures are the "theory" and the 2σ bands based on correlations which will subsequently be given. In figure 9 an increase in Mach number is shown to increase K_N , a trend predicted by the two-dimensional theory. In figure 10 increments in C_N and C_m are shown versus angle of attack for various jet pressure ratios. Note that the increments in C_N and C_m due to changes in p_{o1}/p are independent of angle of attack over the range tested. Finally, the variation of K_N with C_T is shown in figure 11 for four ℓ/D values.

Figure 12 shows the variation of K_{m_j} with C_T for an ℓ/D of 3.27 for various Mach numbers. The effect of M_∞ is confined to the 2σ band about the correlation. Finally figure 13 exhibits the variation of K_{m_j} with M_∞ for various jet pressure ratios. The agreement with the prediction is fair.

In order to correlate the systematic data from references 8, 10, 12, and 13, a least-squares fit was made by Kuhn, et al. (ref. 9) of about 350 data points to the empirical curve

$$K_N = \frac{C_N}{C_T} = a_1 + a_2 \left(1 - a_3 \sqrt{\ell/D} \right) / \sqrt{C_T} + a_3 M_\infty + a_4 \left(\frac{D}{\ell} \right) \quad (13)$$

The resulting fit yielded the following result:

$$K_N = 0.6118 + 0.1358(1 - 0.485 \sqrt{L/D}) / \sqrt{C_T} + 0.0946 M_\infty + 0.004317 \left(\frac{D}{L} \right) \quad (14)$$

with a standard deviation of 0.101. This equation can be used to obtain K_N for the range of parameters given in section 4.2 above.

A similar correlation was made for K_{m_j} with the result that

$$K_{m_j} = 0.5582 - \frac{0.1884}{\sqrt{C_T}} - 1.9659 \frac{D}{L} \quad (15)$$

The moment correlation is based on 129 points with a standard deviation of 0.33. The larger standard deviation in this case may be associated with the fact that the difference of two large numbers enters in determining the pitch moment about the orifice center.

It is possible to resolve the C_N results for equation (14) in C_z and C_y components as shown in figure 7. Likewise C_{m_j} can be resolved into moments about the y and z axes.

5. COMBINING CONTROLS AND THE AIRFRAME

5.1 Introductory Remarks

In this section we will discuss the influence of controls on the airframe characteristics. Controls are added to an airframe first of all to produce trim; i.e., no resultant moments about the center of mass. Modern practice requires trimming the airframe to high lift coefficients so that the airframe can maneuver at high rates of normal acceleration. For this purpose, the control time constant, the time it takes to achieve a substantial function of the final maneuver force, should be short. Also, the amount of control deflection should not be excessive since this leads to various control nonlinearities which greatly increase the complexity and cost of the autopilot.

There are a number of desirable features for controls in addition to those mentioned above. High control effectiveness is desired so that small control deflections produce high normal or lateral accelerations or high roll rates. Application of pitch control changes the missile trim angle of attack for one value to another. It is generally desired to produce a stable trim point for a given angle of attack such that for the airframe dC_M/da is a negative quantity. However, neutral stability or slight negative stability can be handled by some autopilots and the maneuverability is usually enhanced thereby. Sometimes an airframe will trim at two or more angles of attack for one control deflection because of nonlinearities, and not all of these trim points will be stable. Multiple trim points are to be avoided.

Two characteristics which are sought are low hinge moments and low trim drag for cruise. High hinge moments require a more powerful control actuator and thereby involve a weight penalty. Proper location of the control hinge-line position can have an important effect on hinge moments. Trim drag should not have a large adverse effect on airframe lift-drag ratio and thus decrease range. In some cases the increase in lift and drag due to control deflection can actually increase airframe lift-drag ratio. A case will be subsequently shown.

One complicating factor in achieving trim with controls is the varying center-of-mass location due to fuel weight changes during flight.

5.2 Characteristics of Canard Control

By examining actual data for a canard controlled missile we can get insight into some of the characteristics of canard controls. For this purpose we examine some of the data obtained by Graves and Fournier (ref. 14). The model planform of the subject canard-controlled missile is shown in figure 14. The model is about 22.3 diameters long. The control fin has an aspect ratio of 1.73 based on two fins joined together. On the same basis the tail fins have an aspect ratio of 0.88 and a taper ratio of 0.673. Note that the trailing edge of the canard and tail fins are essentially unswept, a common all-movable control characteristic. The ratio of the span of the canard to that of the tail is 0.748. The distance between the canard wing tip and the leading edge of the tail fin root chord is 13.3 diameters. The hinge line of the canard panel is close to the middle of the root chord. For canards with $s_c < s_t$ a rule of thumb for small angles of attack is that an upload on the canard creates an equal and opposite download on the tail so that a pure couple is produced. Also for missiles with bodies of high fineness ratio, body vortices can be expected to produce nonlinearities at high angles of attack.

It is instructive to examine the pitch-control characteristics of the missile for canard control. In figure 15 the normal-force coefficients and pitching-moment coefficients are shown against angle of attack for $M_\infty = 0.2$ and 2.86 for three deflection angles. The reference area is the maximum body cross-sectional area and the reference length is the body diameter. It is noted that an angle of attack of 20° for the entire configuration produces a normal-force coefficient of about 20, whereas 20° of control deflection produces very little change in the normal-force coefficient. Yet substantial pitching-moment increments are produced by control deflection. Between -4° and 4° angle of attack at the lower Mach number there are nonlinearities in the normal-force curves. These are probably due to canard vortex interference on after-body and tail fins where canard vortices pass close to the tail. At $M_\infty = 2.86$ the nonlinearities have disappeared although they persist to about $M_\infty = 1.75$. Examining the pitching-moment curves, it is seen that at high values of α and δ , the control effectiveness in producing pitching-moment increment is small.

This is probably the result of canard stall. Both canard vortices and afterbody vortices interact with each other and influence the empennage forces and moments.

Let us now examine the ability of the canards to trim the airframe. The trim angle of attack is shown versus canard deflection angle in figure 16. As the canard deflection angle increases, the trim angle of attack does not increase proportionately. This result can be seen in figure 15 for $M_\infty = 0.2$ where the difference in α for $C_M = 0$ between $\delta = 0$ and $\delta = 10^\circ$ is much greater than between $\delta = 10^\circ$ and $\delta = 20^\circ$ due to reduced control effectiveness at high δ . At $M_\infty = 2.86$ it is seen in figure 15 that the lower trim angle of attack are due to lower control effectiveness. The trim lift coefficients corresponding to the trim angles of attack are shown in figure 17, and they exhibit similar behavior as a function of canard deflection angle and Mach number as the trim angles of attack. Despite lower trim lift coefficients at high Mach numbers the missile with 20° of canard control produces more normal acceleration the higher the Mach number at all altitudes for center-of-mass locations between 0.55 and 0.65 of the body length because of higher dynamic pressure.

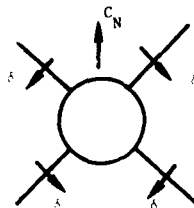
In an actual case of the center-of-mass location will vary during the trajectory as fuel is expended. The normal acceleration achievable will depend on the actual trajectory because of changes in center-of-gravity location with time and dynamic pressure with altitude and Mach number. This aspect of maneuverability cannot be separated from the specific missile flight profiles.

Often missile range is compromised because of the adverse effect of trim drag on lift-drag ratio. Figure 18 is included to define trim drag. The figure shows linear missile moment curves and quadratic missile drag curves versus α for two control deflection angles. For $\delta = \delta_1$ let the trim angle of attack be α_{trim} . The trim drag is the difference in missile drag between the $\delta = 0$ and $\delta = \delta_1$ curves at $\alpha = \alpha_{trim}$. The increment in drag due to trim for the canard-control missile of figure 14 is shown in figure 19 for three Mach numbers. The importance of this trim drag increment can be expressed by its effect on L/D. The lift-drag ratio is shown in figure 20 for four Mach numbers. Trim drag and lift have an adverse effect at the lower Mach numbers on L/D ratio, but a favorable effect at the higher Mach numbers. This is possible in this case because the basic airframe with $\delta = 0$ has such a low lift-drag ratio.

The effectiveness of canards in pitch control has been shown by the foregoing figures. However, it is well known that canards are not good as roll controls. An example of roll control for $M_\infty = 2.10$ with each of the four fins deflected 10° to produce roll is shown in figure 21. In the range $-4^\circ < \alpha \leq 8^\circ$ there is practically no roll control effectiveness because the roll torque developed by the canard is taken out by an opposite roll torque on the tail fins as the canard wake pass over them. The roll control is good up to about 18° at higher angles of attack. However at $\alpha = 20^\circ$ we see a case of *control reversal*. The developed roll torque is of the opposite sign to that called for.

Another nonlinearity, that of *control cross-coupling*, is illustrated by figure 21. The use of pure roll control has also induced side force and yawing moment. If canards are used for pitch control, alternate means of roll control are required.

The effect of roll angle on canard pitch-control effectiveness is of interest. Consider the $\phi = 45^\circ$ case where all four fins are deflected by angle δ to produce normal force in the vertical plane.



Neglecting nonlinearities and interference effects each fin will produce the same increment in normal-force coefficient. However, the forces must be multiplied by $\sin 45^\circ$ to get their components in the C_N direction. Since we now have four fins, we get a $\sqrt{2}$ increase in pitch control as compared to the planar case. The data in reference 14 for the missile of figure 14 show that a significant part of this predicted increase occurs up to Mach numbers of 2.0 but the increase is much diminished for $M = 3.0$.

5.3 Characteristics of Tail Control

Some of the distinguishing features of tail control will now be illustrated by data for a tail-controlled cruciform missile in the supersonic regime (ref. 15). It is also of interest to contrast canard and tail control by reference to the previous section. The missile configuration being considered is that shown in figure 22. The wing has an aspect ratio of 1.40 and a radius to semispan ratio of 0.31. The ratio of body radius to tail semispan is 0.685. The tail is close enough to the wing that the wing vortices are not fully rolled up at the tail.

Let us first examine some of the longitudinal aerodynamic characteristics of the missile. Figure 23 shows the normal-force and pitching-moment coefficients as functions of angle of attack for Mach numbers of 1.60 and 3.95. The reference area is the body cross-sectional area and the reference length is the body length. We first note that the tail deflection for trim is negative in this case since downward load is needed on the tail to trim just as for an airplane. At both Mach numbers the increment in tail download due to tail fin deflection is significant compared to the canard control case, where the wing-tail interference cancels out the upload on the canard fins. At $M_\infty = 1.60$ the increment in C_N due to δ is fairly constant over the angle of attack range, and the reduction in C_{M_0} with larger deflection angles is apparent. However, the data (extrapolated) tend to suggest that trim can be achieved to very high angles of attack.

The moment data at $M_\infty = 3.95$ show a definite decrease in static stability, $-dC_m/d\alpha$, as δ becomes more negative. While trim can be achieved to the highest angle of attack, the static stability is almost neutral under these conditions.

The trim angle of attack is shown versus tail-fin deflection in figure 24. The ability to trim to high angle of attack is maintained to the highest Mach number shown. There is no problem maintaining pitch control over the range M_∞ and α . The trim lift coefficients are shown in figure 25. The high trim lift coefficients attainable at high Mach numbers probably represents a pitch control capability required only at very high altitudes since the dynamic pressure is otherwise very large.

The effect of tail control on lift-drag ratio is illustrated in figure 26. The trimmed L/D is less than the trimmed L/D. However, there is a difference between the canard and tail control cases in the lift and drag increments due to trim. Since a negative fin deflection is required for trim (trailing edge up) both the trim drag and trim lift increments are negative, whereas for canard control they are both positive.

If the missile is rolled to the 45° position, the control effectiveness in pitch is increased about 40 percent.

Some results on the effect of center-of-gravity location on attainable trim lift coefficient are shown in figure 27. Results for both $\phi = 0^\circ$ and $\phi = 45^\circ$ are shown for $M_\infty = 2.86$. It is noted that the axial position of the center of pressure of the airframe with $\phi = 0$ is close to 60 percent of the missile length behind the nose. At this position the airframe is trimmed at $\delta = 0$ at nearly all angles of attack, being neutrally stable. Stability is achieved when the center-of-gravity position x_{cg} is in front of the center-of-pressure position x so that $x - x_{cg}$, the so-called static margin, is positive. As the static margin becomes larger, trim occurs at lower trim lift coefficients for a given deflection angle, and the maneuverability is thus reduced. The same basic behavior holds for $M_\infty = 1.60$ to 4.63 . The $\phi = 45^\circ$ results show more powerful pitch control than the $\phi = 0$ results.

A few remarks on the lateral-directional stability and control characteristics of the tail controlled missile are in order. The basic airframe with $\delta = 0$ shows strong induced yaw moments and rolling moments above $\alpha = 10^\circ$ for roll orientations away from the $\phi = 0$ or $\phi = 45^\circ$ positions. These phenomena are Mach number dependent since the induced moments are greatly reduced or eliminated above $M_\infty = 3.95$. However, these induced moments represent unwanted moments which must be offset by the use of yaw and roll control. The tail controls have enough power to offset these induced effects with margin for maneuvering over the entire $M_\infty - \alpha$ range tested. Thus tail control does not possess the canard control disadvantages of poor yaw and roll control.

6. EQUIVALENT ANGLE OF ATTACK

6.1 Preliminary Remarks

The following derivation of the equivalent angle of attack is being made because it unifies into one concept the separate effects on fin forces and moments of wing-body interference, fin deflection, roll angle, body or fin vortices, and fin-fin interference. A complete data set for the forces and moments on a fin at a fixed Mach number as a function of α , δ , and ϕ would be very extensive, and the equivalent angle-of-attack approach yields a method for correlating the various effects of these variables. The equivalent angle of attack method also provides a means for scaling data for one missile configuration to another. The derivation will be done allowing large angles of attack and deflections, although much simplification of the results is possible for small angles. We follow reference 16 in the derivation.

6.2 Linear Equivalent Angle-of-Attack Concept

It is instructive first to illustrate the equivalent angle-of-attack concept in a form which uses linear superposition of the components of α_{eq} . The equivalent angle of attack for a fin or a body is the angle of attack at which the wing alone has the same normal-force coefficient based on its planform area as the fin has based on its planform area. The wing alone is the lifting surface formed by joining two fins with mirror symmetry at a common root chord.

Let us assume that $\phi = 0$ and consider how the effects of angle of attack, fin deflection, and vortices are superimposed. For small angles of attack at subsonic and supersonic speeds the body exhibits an upwash field in the positions that horizontal fins would occupy. For slender-body theory the local angle of attack, α_L , is given by

$$\alpha_L = \alpha \left(1 + \frac{s^2}{y^2} \right); \quad \phi = 0 \quad (16)$$

where y is the lateral distance from body axis. At the side of the body the local angle of attack is thus 2α . If an infinitesimal fin was placed there with $\delta = 0$, it would develop twice the normal force that it would as part of the wing alone at α . This amplification of the fin normal force is expressed more generally by an interference factor K_W defined as

$$K_W = \frac{N_F(B)}{1/2 N_W} \quad (17)$$

where

$N_{F(B)}$ = normal force acting on a fin at α

N_w = normal force on wing alone at α

The equivalent angle of attack for the fin is given by

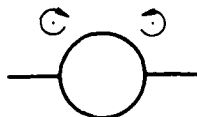
$$\alpha_{eq} = K_w \alpha \quad (18)$$

Let us now deflect the horizontal fins by angle δ positive trailing edge downward. The fins will not develop quite as much normal force as the wing alone for an angle of attack change equal to δ because the round body is not a perfect reflection plane. This slight loss of normal force is measured by an interference parameter k_w

$$k_w = \frac{N_{F(B)}(\alpha, \delta) - N_{F(B)}(\alpha, 0)}{(1/2)N_w(\delta)} \quad (19)$$

The change in equivalent angle of attack due to fin deflection is thus $k_w \delta$.

The effect of vortices of the sign shown in the following sketch of the cross flow plane of a missile at moderate to high angles of attack



is to decrease the normal force on the horizontal fins. This decrease in normal force is related to change in angle of attack of the wing alone equal to $(\Delta\alpha)_v$, a negative quantity.

Superimposing the three above components of the equivalent angle of attack, we have

$$\alpha_{eq} = K_w \alpha + k_w \delta + (\Delta\alpha)_v \quad (20)$$

and

$$C_{N_F} = C_{N_w}(\alpha_{eq}) \quad (21)$$

From a knowledge of K_w , k_w , and $(\Delta\alpha)_v$, and the normal-force curve of the wing alone (experimental or theoretical) we can thus calculate the fin normal force.

Consider now methods for determining the values of K_w and k_w . The easiest method is based on slender-body theory which gives the result that these parameters depend only on the ratio of body radius to wing-body semispan, a/s_m . The values of K_w and k_w are listed for various values of a/s_m in the table of figure 28. We note that at $a/s_m = 0$, $K_w = 1$ by definition. The value for $a/s_m = 1$ is $K_w = 2$ as previously noted. The variation of K_w with a/s_m is nearly linear.

Any method such as a panel method which will determine the loading on the fin in the presence of a body can be used to obtain K_w or k_w . Also experimental values of K_w or k_w can be determined. However, if vortices affect the fin loads, the vortex contributions must be removed from the measured fin loads before calculating K_w . To the first order the vortex contribution to fin load is the same for the fin at $\delta = 0$ or $\delta \neq 0$.

Another method of obtaining K_w or k_w is by the use of strip theory. At high Mach numbers and high angles of attack, the flow over the body alone at a position to be occupied by a fin can be nonuniform with respect to upwash angle α_ℓ , dynamic pressure q_ℓ , and Mach number M_ℓ . If these values are known from experiment or calculation, and if c_n is the section normal-force coefficient depending only on α_ℓ and M_ℓ , then the fin normal-force coefficient is

$$C_{N_{F(B)}} = \frac{\int_0^{S_F} \frac{q_\ell}{q_\infty} c_n(\alpha_\ell, M_\ell) dy}{S_F} \quad (22)$$

where S_F = fin planform area and c = local chord.

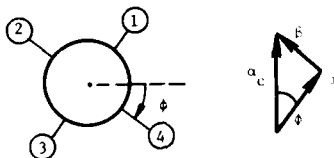
If C_{N_w} is calculated by the wing-alone analog of equation (22)

$$C_{N_W} = \frac{2 \int_0^{s_m} c_{n_n}(\alpha, M_\infty) dy}{S_W} \quad (23)$$

The value of K_W is obtained by forming the ratio $C_{NF(B)}/C_{N_W}$. Any errors due to the use of strip theory will tend to compensate since it is used in both numerator and denominator.

The determination of the average angle of attack induced on a fin by external vortices can be accomplished by several methods. The first method makes use of the Biot-Savart law to determine the flow velocities induced normal to the fin by the external vortices and their images. This induced flow component, which depends only on lateral distance, can be averaged across the external fin semispan using the local chord as a weighting factor. A more precise method based on reverse-flow methods yields better weighting factors (ref. 17). More detail treatment will be given in connection with the subsequent section on vortices.

The effect of roll angle on fin forces and moments is characterized principally by a change in angle of attack of the fin as viewed in planes normal to the fin chord plane. Consider the rear view of a cruciform fin-body arrangement in which the horizontal fin has been rotated by angle ϕ in a clockwise direction.



With regard to fin 4 and the angle of attack α is now

$$\alpha = \alpha_c \cos \phi \quad (24)$$

with a sideslip angle β of

$$\beta = \alpha_c \sin \phi \quad (25)$$

so that

$$\alpha_c^2 = \alpha^2 + \beta^2 \quad (26)$$

This value of α is to be used in equation (20).

A second effect of roll angle is that it introduces sideslip angle β and therefore a loading proportional to $\alpha\beta$. The fin on the windward side picks up load and the fin on the leeward side loses load. The change in fin equivalent angle of attack due to the $\alpha\beta$ term can be expressed through an interference factor K_ϕ .

$$\left(\Delta \alpha_{eq} \right)_{\alpha\beta} = \frac{4}{\pi} K_\phi \alpha\beta = \frac{4}{\pi} K_\phi \alpha_c^2 \sin \phi \cos \phi \quad (27)$$

The quantity $4/\pi$ is introduced into the expression to make K_ϕ independent of aspect ratio for delta wings. Slender-body values of K_ϕ for planar and cruciform delta fins are given in figure 29. The version of equation (20) for fin 4 at roll angle ϕ is

$$\alpha_{eq} = K_W \alpha_c \cos \phi + \sum_{j=1}^4 \Lambda_{ij} \delta_j + (\Delta \alpha)_V + \frac{4}{\pi} K_\phi \alpha_c^2 \sin \phi \cos \phi \quad (28)$$

The term Λ_{ij} is a factor similar to k_W which is defined by equation (36).

As an example of the power of the equivalent angle of attack concept for correlation and prediction we have included in figures 30 and 31 correlations (ref. 16) for two sets of canard cruciform fins tested with pitch control at $\phi = 0$ on a body of revolution. In figure 30 data are shown for $M_\infty = 0.8$ and 1.3 with control deflections of 0° , 5° , 10° , 15° . The linear form of the equivalent angle of attack correlates the data well at both Mach numbers. What is interesting is that the nonlinear behavior of $C_{NF(B)}$ versus α_{eq} is exhibited by the linear form of the α_{eq} formulation. This is the consequence of the known result that flow fields follow the linear superposition law to greater angles of attack than loads or pressure distribution. The wing-alone data match with the correlation shown in figure 30(a) suggests a prediction method. If the wing-alone normal-force curve is known based on experiment, it is possible to predict the pitch-control effectiveness of the fins assuming a correlation of the type shown. Results for a fin of lower aspect ratio are shown in figure 31. It is noted that fin stall occurs at a slightly lower equivalent angle of attack than for the wing alone.

6.3 Derivation of Nonlinear Equivalent Angle-of-Attack Equation

We now derive the nonlinear equivalent angle-of-attack equation following the derivation in reference 16. We want the general derivation to include the effects of angle of attack, bank angle, fin deflections, semispan-to-body radius ratio, and vortical flow field; i.e., we want to find an α_{eq1} for fin 1 such that

$$C_{N_W}(\alpha_{eq1}) = C_{N_F(B)} \left[\alpha_c, \phi_1, \delta_{1-4}, s/s_m, (\Delta\alpha)_v \right] \quad (29)$$

For large angles of attack a nonlinear definition of α_{eq} is required. Since there is no unique way to derive a nonlinear formula from the linear result, we are free to choose our approach provided that it is valid in certain limiting cases and reduces to the linear result in the limit of small angles. The method of reference 16 is based on the use of average velocity components seen by the fin of interest. Those velocity components are put together to give α_{eq} .

Consider a cruciform wing-body combination with the x-axis rearward along the body axis, the y-axis lateral along the right horizontal fin (fin 4) and the z-axis vertical (leeward) along the upper fin (fin 1). Let the combination first be pitched in a plane containing the free-stream velocity and the x-axis by an angle α_c . Let it then be rolled right wing down (windward) by angle ϕ_B . In a plane normal to the body axis we now have the picture shown in figure 32.

We determine first the flow field seen by the fins with no fin deflection and then consider the effects of rotating (deflecting) the fins in that flow field. Referring to figure 32 we see that the components of the free-stream velocity along x, y, and z are $V \cos \alpha_c$, $-V \sin \alpha_c \sin \phi_4$, and $V \sin \alpha_c \cos \phi_4$, respectively.* The component of free-stream velocity normal to the plane of fin 4, V_{n4} , is $V \sin \alpha_c \cos \phi_4$. Thus the angle of attack induced on fin 4 if it sees the free-stream only is

$$\begin{aligned} \tan \alpha_{eq4} &= \frac{V_{n4}}{V_{p4}} \\ &= \tan \alpha_c \cos \phi_4 \end{aligned} \quad (30)$$

Equation (30) does not yet represent the actual angle of attack induced on fin 4 with no fins deflected because effects of the body, sideslip and vortices have not been incorporated. We now consider these one at a time.

The presence of the body affects the flow in the crossflow plane (wing-body interference). We account for this effect by multiplying V_{n4} by the upwash factor K_W , i.e.,

$$V_{n4} \Big|_{\text{free stream+body}} = K_W V \sin \alpha_c \cos \phi_4 \quad (31)$$

For favorable interference, $K_W > 1$. With increasing α_c and M_∞ , K_W tends to decrease and become less than one (ref. 17). We will assume that K_W is independent of ϕ as predicted by slender-body theory.

Any fin for which ϕ is not zero is sideslipping. Spreiter and Sacks (ref. 20) investigated this effect and found that the increment due to sideslip in the fin normal force was proportional to the product of α and β for the fin, i.e., $\alpha_c^2 \sin \phi \cos \phi$. We use the same idea here to account for changes in V_{n4} due to sideslip, i.e.,

$$\begin{aligned} V_{n4} \Big|_{\text{sideslip}} &= \frac{4}{\pi} K_\phi V \alpha \beta \\ &= \frac{4}{\pi} K_\phi V \sin^2 \alpha_c \sin \phi_4 \cos \phi_4 \end{aligned} \quad (32)$$

The introduction of the $4/\pi$ coefficient makes the slender-body value of K_ϕ independent of aspect ratio.

To account for the effects of body vortices and vortices generated by upstream fins, we need a method for calculating the equivalent angle of attack, $(\Delta\alpha)_v$ induced on fin 1 by the vortical flow field. By definition, we have

$$\left(\frac{V_{n4}}{V_{p4}} \right)_{\text{vortices}} = \tan(\Delta\alpha)_v \quad (33)$$

If we assume that the vortices are rectilinear and parallel to the body axis, $(V_{p4})_{\text{vortices}}$ is equal to the component of the free-stream velocity which is parallel to the fin chord, $V \cos \alpha_c$, and we can write

$$V_{n4} \Big|_{\text{vortices}} = V \cos \alpha_c \tan(\Delta\alpha)_v \quad (34)$$

*Note that we are using the sine definition of the angle of attack (see pg. 5 of ref. 1).

Using relations (31-33) and noting that V_{p4} is $V_{\infty} \cos \alpha_c$ we can define an equivalent angle of attack, $\hat{\alpha}_{eq4}$, including body, sideslip, and vortex effects but with no fin deflections, i.e.,

$$\begin{aligned} \tan \hat{\alpha}_{eq4} &= \frac{V_{n4} \left| \text{free-stream+body} \right| + V_{n4} \left| \text{sideslip} \right| + V_{n4} \left| \text{vortices} \right|}{V_{p4}} \\ &= K_W \tan \alpha_c \cos \phi + \frac{4}{R} K_{\phi} \tan \alpha_c \sin \alpha_c \sin \phi_4 \cos \phi_4 \\ &\quad + \tan(\Delta \alpha)_{V_4} \end{aligned} \quad (35)$$

Note that the sideslip and vortex terms in equation (35) cannot increase $\hat{\alpha}_{eq4}$ beyond 90 degrees.

To account for the change in equivalent angle of attack due to fin deflection, we define a new quantity, Λ_{ji} , such that the effect on the angle of attack of fin i of the deflection of fin j is given by

$$(\Delta \alpha_{eq})_{ji} = \Lambda_{ji} \delta_j \quad (36)$$

where Λ_{ji} is given in figure 33 for slender-body theory for zero angle of attack. The final expression for the equivalent angle of attack of fin 4 which includes fin deflection is*

$$\alpha_{eq4} = \hat{\alpha}_{eq4} + \sum_{j=1}^4 \Lambda_{ji} \delta_j \quad (37)$$

On physical grounds we must use an angle addition theorem for fin deflection rather than a tangent addition theorem to allow for the possibility of α_{eq4} exceeding 90 degrees. In the definition of Λ_{ji} as incorporated in equations (36) and (37), we have assumed implicitly that any vortex effects on fin i are not changed by deflecting the fins.

We can generalize equations (35) and (37) by defining ϕ_4 to be the bank angle of fin i measured positive to windward from the y_0 axis. The generalized equations for fin i are

$$\tan \hat{\alpha}_{eqi} = K_W \tan \alpha_c \cos \phi_i + \frac{4}{R} K_{\phi} \tan \alpha_c \sin \alpha_c \sin \phi_i \cos \phi_i + \tan(\Delta \alpha)_{V_i} \quad (38)$$

and

$$\alpha_{eqi} = \hat{\alpha}_{eqi} + \sum_{j=1}^4 \Lambda_{ji} \delta_j \quad (39)$$

6.4 Extension of Data Bases Using α_{eq} Concept

It has already been demonstrated in a previous section that a wing-alone data base can be used to estimate the normal-force coefficients of the horizontal fins on a circular body including effects of fin deflection. In this subsection we show how normal-force data for horizontal fins together with the corresponding wing-alone curve can be extended to any bank angle. For this discussion we will not include vortex effects nor fin deflection.

For this case equation (38) reduces to

$$\tan \hat{\alpha}_{eqi} = K_W \tan \alpha_c \left(\cos \phi_i + \frac{4}{R} \frac{K_{\phi}}{K_W} \sin \alpha_c \sin \phi_i \cos \phi_i \right) \quad (40)$$

But for $\phi_i = 0$, we have

$$\tan \hat{\alpha}_{eqi} \Big|_{\phi_i=0} = K_W \tan \alpha_c \quad (41)$$

Substituting equation (41) into equation (42) gives

$$\tan \hat{\alpha}_{eqi} = \tan \hat{\alpha}_{eqi} \Big|_{\phi_i=0} \left(\cos \phi_i + \frac{4}{R} \frac{K_{\phi}}{K_W} \sin \alpha_c \sin \phi_i \cos \phi_i \right) \quad (42)$$

*The zero angle of attack assumption built into figure 33 results in no effect of sideslip on $(\Delta \alpha_{eq})_{ji}$ if those factors are used. However, in general Λ_{ji} is a function of ϕ .

To use equation (41), one obtains $C_{NF(B)}$ for $\phi_1 = 0$ and the angle of attack of interest. Then $\hat{\alpha}_{eq1}|_{\phi_1=0}$ is found from the fact that $C_{NF(B)}$ is equal to $C_{NW}(\alpha_{eq})$, and equation (42) is used to solve for $\hat{\alpha}_{eq1}$. Then we again use the fact that $C_{NF(B)}$ is equal to $C_{NW}(\alpha_{eq})$ to find $C_{NF(B)}$ for $\phi_1 \neq 0$. The procedure is illustrated in figure 34.

An example of the accuracy of the method is given in figure 35 for aspect-ratio-one clipped delta fins with exposed semispan equal to the body radius. The Mach number is two. The data came from the body-tail data base of reference 21 with the vortex effects removed (ref. 17). Slender-body theory values of K_W and K_ϕ were used. The agreement is excellent except for the leeward bank angles at the higher angles of attack. We believe that the disagreement there is due to inaccuracies in the model used to extract the body vortex effects.

Note that we have not shown high angle-of-attack comparisons for subsonic Mach numbers. For this speed regime, stall effects are not handled particularly well by the method. This is probably because sideslip has a pronounced effect on stall characteristics.

If vortex effects cannot be neglected, equation (41) becomes

$$\tan \hat{\alpha}_{eq1}|_{\phi_1=0} = K_W \tan \alpha_c + \tan(\Delta\alpha)_{v1}|_{\phi_1=0} \quad (43)$$

Hence, equation (42) becomes

$$\tan \hat{\alpha}_{eq1} = \left(\tan \hat{\alpha}_{eq1}|_{\phi_1=0} - \tan(\Delta\alpha)_{v1}|_{\phi_1=0} \right) \cdot \left(\cos \phi_1 + \frac{4}{\pi} \frac{K_\phi}{K_W} \sin \alpha_c \sin \phi_1 \cos \phi_1 \right) + \tan(\Delta\alpha)_{v1} \quad (44)$$

The values of $(\Delta\alpha)_{v1}$ must be estimated.

6.5 Correlation and Extension of Center-of-Pressure Data

The equivalent angle-of-attack concept also indicates that we can write equations for the fin center-of-pressure locations as follows:

$$\frac{\bar{x}_{F(B)}}{c_r} = \frac{\bar{x}_W(\alpha_{eq})}{c_r} \quad (45)$$

$$\frac{\bar{y}_{F(B)} - a}{s_m - a} = \frac{\bar{y}_W(\alpha_{eq})}{s} \quad (46)$$

Equations (45) and (46) suggest that it should be possible to correlate center-of-pressure data as a function of fin normal-force coefficient; i.e.,

$$\bar{x} = \bar{x}(C_N) \quad (47)$$

$$\bar{y} = \bar{y}(C_N) \quad (48)$$

This result is a consequence of the α_{eq} concept.

An extensive demonstration of the axial center-of-pressure correlation for clipped delta fins is given in reference 22. A sampling of those results for a rectangular fin is given in figure 36 for subsonic and supersonic speeds. The fin-on-body results of reference 21 for a given body angle of attack, α_c , are connected by solid lines. The wing-alone data are taken from reference 23.

The lateral center-of-pressure correlation was demonstrated in reference 17, samples of which are shown in figure 37. Note the expanded scale.

7. CHARACTERISTICS OF PLANAR ALL-MOVABLE CONTROLS

7.1 Introductory Remarks

By planar all-movable controls we mean that the controls are deployed on opposite sides of a body diameter and that there are only two controls with mirror symmetry in a vertical plane through the body axis. The planar case is representative of the cruciform case for $\phi = 0$ except to the extent that the thickness of the vertical fins influence the configuration. This influence is usually negligible. For roll control the planar and cruciform cases at zero bank differ.

In this section we will consider the effect of the control c on the body, roll control, and roll damping. The basic formulas required to calculate the forces and moments due to a control will be given. Some basic nonlinearities will be illustrated by data since they frequently represent limitations for the successful operation of the controls.

7.2 Effect of Fins on Body

In the preceding chapter, the entire emphasis is on determining the fin characteristics in the presence of the body. We now concentrate on looking at the effect of the fin on the body.

Let $N_B(F)$ be the normal force on the body due to the fins for $\delta = 0$. Then an interference factor K_B can be defined for the body similar to that for the fin.

$$K_B = \frac{N_B(F) - N_B}{N_W} \quad (49)$$

The value of K_B depends only on a/s_m according to slender-body theory. These values are given in figure 28 along with the K_W values.

With respect to the normal force carried over onto the body due to fin deflection, there is an interference factor k_B analogous to K_B . Let $N_{B(F)}$ be the normal force on the body due to the fins. Then k_B is defined as

$$k_B = \frac{N_{B(F)}(\alpha + \delta) - N_{B(F)}(\omega)}{N_W(\delta)}$$

On the basis of slender-body theory k_B depends only on a/s_m . Its values are also tabulated in figure 28.

Some aspects of this figure are worthy of notice. The ratio of the load on the body due to the fin to the load on the fin at $\delta = 0$ is given by K_B/K_W . Also the ratio of the load on the body to that on the fin due to control deflection is k_B/k_W . It is noted that these ratios are approximately equal to s/s_m . Accordingly for large values of a/s_m a substantial part of the maneuvering load due to fin deflection is generated on the body. Also the amount of load on the body, due either to fin angle of attack ($\delta = 0$) or fin deflection, is nearly the same fraction of the fin load in both cases. The span loading in the two cases are different. This leads to a rule of thumb that the load carried over onto the body by a fin is a constant fraction of the fin load regardless of how the fin load is developed. This rule of thumb has been used in predictive methods for wide ranges of angle of attack and Mach number. However, some caution with regard to its use is necessary. At hypersonic speeds with fins near the body base, the region of influence of the fins on the body can be quite small, and the amount of fin load carried over onto the body is correspondingly reduced.

The table in figure 28 suggests another rule of thumb which is used in determining the pitching moment and hinge moment of all-movable controls. First for the $\delta = 0$ case, note that wing-body interference does not displace the axial position of the center of pressure of a triangular fin more than two percent of the root chord from the position of $0.667 c_r$ for the wing alone. Note also that (\bar{x}/c_r) for the fin deflection case is within 0.003 of the value for the wing alone. This leads to the rule of thumb that the center-of-pressure position of the fin mounted on the body is close to that of the fin alone. This rule of thumb is demonstrated in figures 36 and 37.

7.3 Basic Formulas for Planar Case; $\phi = 0$

Enough theory has been presented to write equations for the fin normal force, pitching moment, root bending moment, and hinge moment for planar all-movable controls at $\phi = 0$. The body normal force due to the fin can be written as well as the body pitching moment within certain restrictions.

Fin normal force: $C_{N_{F(B)}}$

$$(a_{eq})_{F(B)} = K_W \alpha + k_W \delta + (\Delta \alpha)_V \quad (50)$$

$$C_{N_{F(B)}} = C_{N_W} \left(a_{eq_{F(B)}} \right) \quad (51)$$

Use an experimental wing alone normal-force curve if available.

Body normal force

$$C_{N_{B(F)}} = C_{N_{F(B)}} \left(\frac{K_B}{K_W} \right) \cos \delta \quad (52)$$

Fin pitching moment

$$C_{m_{F(B)}} = -C_{N_{F(B)}} \left[\left(\frac{\bar{x}}{c_r} \right)_W - \left(\frac{\bar{x}}{c_r} \right)_{c.g.} \right] \frac{c_r}{\ell_r} \cos \delta \quad (53)$$

Use an experimental value of $(\bar{x}/c_r)_W$ at $\alpha = \alpha_{eq}$ if available.

where ℓ_r = reference length

x_{cg} = distance of center of gravity behind leading edge of root chord

Root bending moment

$$C_{RB} = C_{NF(B)} \left[\frac{\bar{y}_a - a}{s_m - a} \right] \cdot \frac{(s_m - a)}{\ell_r} \quad (54)$$

The quantity $\frac{\bar{y}_a - a}{s_m - a}$ can be obtained from figure 28(a) or from a correlation such as that of figure 37.

Hinge-moment coefficient

$$C_{HM} = C_{NF(B)} \left[\left(\frac{x}{c_r} \right)_{HL} - \left(\frac{x}{c_r} \right)_W \right] \cdot \frac{c_r}{\ell_r} \quad (55)$$

Body pitching moment

$$C_{mB(F)} = -C_{NB(F)} \left[\left(\frac{\bar{x}_a}{c_r} \right)_{B(F)} - \left(\frac{x}{c_r} \right)_{c.g.} \right] \frac{c_r}{\ell_r} \quad (56)$$

Conventions

The wing-alone reference area is the wing-alone planform area. It is also the reference area for the body coefficients. The fin reference area is the fin planform area, but the reference length ℓ_r is arbitrary. The quantity $\left(\frac{x}{c_r} \right)_{HL}$ is the fin hinge-line location. All values of x are measured positive behind the leading edge of the fin root chord. Fin leading edge up corresponds to positive hinge moment. The use of experimental values of C_{N_W} , $(\bar{x}/c_r)_W$, and $(\bar{y}/s)_W$ is advised where available.

One final point should be made in connection with K_B and that is the effect of afterbody length on this quantity. It also influences $(\bar{x}_a/c_r)_{B(W)}$. At supersonic speeds the effects of the fins on the body are confined to the downstream Mach cones emanating from the leading edge of the fin root chord. Accordingly the amount of body area for load carryover from the fins depends on the length of body behind the fins. An approximate theory for this effect is included in reference 1, pp. 131-174. Also contained therein are design curves for determining K_B and $(\bar{x}_a/c_r)_{B(W)}$.

7.4 Roll Control and Roll Damping

The use of all-movable controls as ailerons to produce roll control is important for planar configurations which are not usually free to roll. Some simple results based on slender-body theory give accurate enough results for many design uses since the available roll control is usually more than adequate. Let us define the roll-control effectiveness as

$$C_{\ell_{\delta a}} = \frac{\partial C_{\ell}}{\partial \delta_a} = \frac{RM}{q_{\infty} S_W (2s_m)} \cdot \frac{1}{\delta_a} \quad (57)$$

where RM is the rolling moment for 2 fins. The slender-body result for this quantity is given in reference 1, [eq. (8) through (39)] for planar all-movable controls. The variation of $C_{\ell_{\delta a}}/R_W$ with radius-semispan ratio, a/s_m is shown in figure 38. The precise shape of the leading edge is not of importance in the theory which applies for any taper ratio provided the trailing edge is unswept.

Examination of this figure leads to more general methods for calculating roll effectiveness for non-slender configurations. Consider a model of the case for which $a/s_m = 1$. In this case each fin develops a normal force equal to half of that of the wing alone at angle of attack δ .

$$N_F = \frac{1}{2} \left(\frac{\pi R}{2} \right) \delta_a q_{\infty} S_W \quad (58)$$

where R = wing-alone aspect ratio. The lever arm is " a ." The rolling moment for two fins is

$$RM = \frac{1}{2} \left(\frac{\pi R}{2} \right) \delta_a q_{\infty} S_W (2a) \quad (59)$$

Using equation (57) we find

$$\frac{C_{\ell_{\delta a}}}{R} = \frac{\pi}{4} ; \quad \frac{a}{s_m} = 1.0 \quad (60)$$

This is the value shown in figure 38.

If we carry out the same procedure for $a/s_m = 0$, we find that the calculated result is $1/3$, twice the value given by figure 38. What this means is that interference between the two fins at $a/s_m = 0$ reduces the rolling moment to half the value which would be calculated if interference were neglected. At

$a/s_m = 1$ there is no fin-fin interference on rolling moment. Note that the value of $C_{\ell_{\delta_a}}$ is based on using the slender-body theory lift-curve slope for the wing alone. This leads to the following engineering procedure for determining the roll-control effectiveness. We will obtain $C_{\ell_{\delta_a}}$ as the product of a force and a lever arm. Obtain the force as half the force on the wing alone at angle of attack δ_a from data or the best available means. Multiply the force by a lever arm equal to

$$2 \left[a + \left(\frac{\bar{y} - a}{s_m - a} \right) (s_m - a) \right]$$

to obtain a rolling moment. Multiply the resulting rolling-moment by the following factor to allow for panel-panel interference on the lever arm.

$$\frac{C_{\ell_{\delta_a}}}{A} \frac{1}{4} \pi K_W \left[\frac{a}{s_m} + \frac{4}{3\pi} (1 - a/s_m) \right] \quad (61)$$

where $C_{\ell_{\delta_a}}/A$ is obtained from figure 38. This factor varies from 0.5 at $a/s_m = 0$ to 1 at $a/s_m = 1.0$.

Some damping-in-roll results from reference 24 are shown in figure 39 for planar wing-tail and cruciform wing-body combinations. The parameter C_{ℓ_p} is

$$C_{\ell_p} = \frac{RM}{q_\infty S_W^2 (2s_m)} \frac{\rho (2s_m)}{2V_\infty} \quad (62)$$

Note p = rolling velocity, radians per second. Also S_W^2 includes the planform area of the wing including its hypothetical extension through the body. These curves can be applied directly to slender configurations. However for improved accuracy the results should be multiplied by the ratio of the wing-alone lift-curve slope obtained from experiment to that obtained from slender-body theory.

Note that the cruciform fin arrangement does not have twice as much damping in roll as the planar fin arrangement because of adverse fin-fin interference.

7.5 Nonlinear Effects in Planar All-Movable Controls

The equivalent angle-of-attack method accounts for nonlinearities of the wing alone, and these nonlinearities would be expected to show up in the fin aerodynamic characteristics. It is of interest to know about these and other nonlinearities since they influence the control effectiveness and hinge moment of the controls. The following nonlinearities are amongst these considered.

1. Reduced transonic effectiveness
2. High M_∞ nonlinearities
3. Adverse wing-body interference at high Mach numbers
4. Field-of-influence effects
5. Vortices

Vortex effects will be considered in a separate section.

As an example of reduced pitch-control effectiveness at transonic speeds, consider the canard fins of a generalized missile shown in figure 40. This configuration was systematically tested in the 11-Foot Transonic Wind Tunnel (ref. 25) and the 6- by 6-Foot Supersonic Wind Tunnel (ref. 18) of the NASA/Ames Research Center. If only two canard fins are present and they are both deflected for pitch control, equation (39) can be written as

$$\left. \begin{aligned} \alpha_{eq_1} &= \hat{\alpha}_{eq} + (\lambda_{11} + \lambda_{12}) \delta \\ \alpha_{eq_2} &= \hat{\alpha}_{eq} + (\lambda_{22} + \lambda_{21}) \delta \end{aligned} \right\} \quad (63)$$

By the definition of k_W and the properties of the λ_{ij} factors, we have

$$k_W = \lambda_{11} + \lambda_{21} = \lambda_{22} + \lambda_{12}$$

or

$$k_W = \frac{\alpha_{eq_1} - \hat{\alpha}_{eq}}{\delta} \quad (64)$$

A different version of this equation was used with the data of references 18 and 25 to calculate k_W in reference 26.

$$k_W = \frac{\tan \alpha_{eq_1} - \tan \hat{\alpha}_{eq}}{\tan(\hat{\alpha}_{eq} + \delta) - \tan \hat{\alpha}_{eq}} \quad (65)$$

The resulting values are given in figure 41 taken from reference 26 for Mach numbers of 0.8 and 1.3. Note that for $M_\infty = 0.8$ the slender-body value of K_W is a fair approximation to the experimental values for α 's from 0 to 20°. Above 20°, there is a loss of pitch-control effectiveness until at $\alpha = 50^\circ$ it disappears. At $M_\infty = 1.3$ the nonlinearities are more striking. If equation (64) were used to extract the experimental values of K_W , somewhat different behavior might result at very high angles of attack.

Next we consider pitch-control effectiveness of a single tail fin tested in cruciform arrangement at $M_\infty = 3.0$ to high angles of attack. The body on which the fin is mounted is shown in figure 42(a) and the fin itself is shown in figure 42(b). The fin normal-force coefficient is shown in figure 43 for the angle-of-attack range $0^\circ \leq \alpha \leq 40^\circ$ and a control deflection range $-40^\circ \leq \delta \leq 40^\circ$. Only one horizontal fin is deflected. The data are unpublished NASA/Langley Research Center data. The horizontal distance between lines should be constant if 20° of control deflection is to produce equal increments in normal force. This condition is clearly not the case.

It is possible to extract the value of Λ_{11} in equation (39) using the data of figure 43. We write equation (39) in the form

$$\Lambda_{11} = \frac{\alpha_{eq_1} - \alpha_{eq_2}}{\delta_1} \quad (66)$$

All we need is a wing-alone normal-force curve to carry out the calculation. The one for a wing of $R = 2$, $\lambda = 0.5$ in reference 17 has been used. The resultant values of Λ_{11} are plotted in figure 44. It is noted since there is no interference between horizontal fins based on regions of influence for $M_\infty = 3$ that $\Lambda_{11} = K_W$ in this case. Note that the values of K_W are large for high α and negative δ . However, when α and δ add, the value of K_W goes down. At $\alpha = 20^\circ$ and $\delta = 40^\circ$ the wing has not reached maximum normal-force coefficient. However, tail control generally requires negative values of δ .

The ability of the tail controls to trim the missile to high angles of attack is not indicated by the normal-force characteristics of the fin since force normal to the body axis is the principal trimming force. Also there is lift carryover to the body which influences trim. To illustrate the ability of the fin to trim (one fin), the configuration C_m is shown versus α for various values of δ in figure 45. One fin can trim the missile to high angles of attack with negative control deflections. At high positive δ 's, the fin produces no essential change in trim between $\delta = 20^\circ$ and $\delta = 40^\circ$.

Since the K_W factor is also important in determining equivalent angle of attack for all-movable controls, the general loss of favorable wing-body interference at high M_∞ and high α is another nonlinearity of importance for such controls. It is possible to obtain K_W from normal-force data for the fin on the body and for the wing alone. However, the vortex contribution to the fin normal force must be removed before forming K_W . This was done for some data on a fin-body combination employing a delta fin of $R = 1.0$. The calculated results are shown in figure 46. If $K_W > 1$ the wing-body interference is favorable but if $K_W < 1$, it is unfavorable. The results speak for themselves.

Another nonlinearity which primarily affects fin-fin interference and fin-on-body interference is the changing field of influence of a fin with changes in Mach number. To obtain the forward boundary of the field of influence of one planar fin on another, consider the sketch of figure 47. Let a pressure pulse originate from point A, the leading edge of the root chord of the left fin. The shortest path by which this pressure pulse can reach the right fin will determine the forward boundary of the region of influence of the left fin on the right fin. To get over the top meridian, the pressure pulse must travel up the side of the body making an angle equal to the Mach angle with the parallel generators of the cylinder. Changes in the local Mach number from the free-stream Mach number are not accounted for in this derivation. The position x of the ray at any value of θ on this basis is

$$x = a\theta\sqrt{M_\infty^2 - 1} \quad (67)$$

If $\theta = \pi$, then

$$x = \pi a\sqrt{M_\infty^2 - 1} \quad (68)$$

When the root chord is less than this value of x , the right fin is not within the region of influence of the left fin. This condition is expressed as

$$\frac{c_r}{\pi a\sqrt{M_\infty^2 - 1}} < 1.0 \quad (69)$$

The forward boundary of the region of influence of one fin on another is found by considering rays which can propagate from the body in tangent planes as shown in the figure. This leads to the following parametric equations for this boundary.

$$\left. \begin{aligned} x_b &= \left[\theta + \frac{1}{(-\cot\theta)} \right] a\sqrt{M_\infty^2 - 1} \\ y_b &= -\frac{a}{\cos\theta} ; \quad \frac{\pi}{2} \leq \theta \leq \pi \end{aligned} \right\} \quad (70)$$

When viscosity is considered, some influence forward of this boundary is possible.

8.0 CHARACTERISTICS OF CRUCIFORM ALL-MOVABLE CONTROLS

8.1 Introductory Remarks

This section will discuss the characteristics of cruciform missile controls as a function of the angle of attack, roll angle, and fin deflection angle. Almost everything presented for planar all-movable controls applies equally well to cruciform all-movable controls. What must be accounted for additionally in this section are the effects of adding two more fins and the effects of roll angle.

8.2 Effect of Fins on Body; Fin-Fin Interference, Roll Effects

The purpose of this subsection is to provide the background for the formulas subsequently to be developed for the fin and body forces on the control section of the missile. In the preceding section a rule of thumb was given that the fractional part of the fin load carried over to the body does not depend on the span loading very much. The fin normal force developed at $\delta = 0$ is carried over in the ratio K_B/K_W also for cruciform fins in the first approximation. However, when the fin is deflected, it is the component of the fin normal force perpendicular to the body axis which is carried over in the ratio K_B/K_W . This can be seen in the limit of $\delta = 90^\circ$ and accounts for the term $\cos \delta$ in equation (52). Also the body center-of-pressure position, due to the load carried over onto the body by the fins, is the same as for the planar case to the first approximation.

Roll angle has the linear effect of subjecting the horizontal fins ($\delta = 0$) to angle of attack $\alpha \cos \phi$ and the vertical fins to angle of attack $\alpha \sin \phi$ neglecting interference effects. The K_B and K_W contributions to the equivalent angle of attack remain unchanged in form in going to cruciform wings. The cross-coupling contribution due to $\alpha \delta$ coupling as represented by the K_ϕ term remains unchanged in form but the value of K_ϕ is different from that for planar fins because of different fin-fin interference. On this basis equation (28) still applies to cruciform fins.

8.3 Basic Formulas for Cruciform Case, $\phi \neq 0$

In what follows, the fin coefficients are based on the fin planform area, and the wing-alone coefficients are based on the wing planform area. The body force and moment coefficients are based on the wing-alone planform area. The reference length l_r is arbitrary. The force and moment coefficients for the fin apply to the right horizontal fin rolled downward by angle ϕ . The other fins are to be obtained by adjusting ϕ . The simplified form of the equivalent angle of attack is being used. Pitching-moment coefficients are about a horizontal lateral axis and body normal force is in the vertical plane.

Fin normal force (per fin):

$$\left(a_{eq} \right)_{F(B)} = K_W \alpha + \sum_{j=1}^4 \Lambda_{jt} \delta_j + (\Delta \alpha)_V + \frac{4}{K_W} K_\phi \alpha_c^2 \sin \phi \cos \phi \quad (71)$$

$$C_{N_{F(B)}} = C_{N_W} \left(a_{eq_{F(B)}} \right) \quad (72)$$

Use an experimental wing-alone normal-force curve if available.

Body normal force in vertical plane (per fin):

$$C_{N_{B(F)}} = \frac{1}{2} C_{N_{F(B)}} \frac{K_B}{K_W} \cos \delta \cos \phi \quad (73)$$

Fin pitching moment (per fin):

$$C_{m_{F(B)}} = -C_{N_{F(B)}} \left[\left(\frac{\bar{x}}{c_r} \right)_W - \left(\frac{\bar{x}}{c_r} \right)_{cg} \right] \frac{c_r}{l_r} \cos \delta \cos \phi \quad (74)$$

Use the experimental value of $(\bar{x}/c_r)_W$ at $a_{eq_{F(B)}}$ if available.

where l_r = reference length

x_{cg} = distance of center of gravity behind leading edge of root chord

Root bending moment:

$$C_{RB} = C_{N_{F(B)}} \left(\frac{\bar{y}_a - a}{s_m - a} \right) \left(\frac{s_m - a}{l_r} \right) \quad (75)$$

with $\frac{\bar{y}_a - a}{s_m - a}$ from figure 28.

A more precise result can be obtained by obtaining $C_N(\delta = 0)$ and $\Delta C_N(\delta)$ and using the following equation:

$$C_{RB} = C_{N_{F(B)}} (\delta = 0) \left(\frac{\bar{y}_\phi - a}{s_m - a} \right) \left(\frac{s_m - a}{l_r} \right) + \Delta C_{N_{F(B)}} (\delta) \left(\frac{\bar{y}_\phi - a}{s_m - a} \right) \left(\frac{s_m - a}{l_r} \right) \quad (76)$$

with $\frac{\bar{y}_\phi - a}{s_m - a}$ from figure 29.

Hinge-moment coefficient:

$$C_{HM} = C_{N_{F(B)}} \left[\left(\frac{x}{c_r} \right)_{HL} - \left(\frac{x}{c_r} \right)_W \right] \frac{c_r}{l_r} \cos \delta \quad (77)$$

Body pitching moment (per fin):

$$C_{m_{B(F)}} = -C_{N_{B(F)}} \left[\left(\frac{x}{c_r} \right)_{B(F)} - \left(\frac{x}{c_r} \right)_{cg} \right] \frac{c_r}{l_r} \quad (78)$$

The conventions applying to these formulas are the same as those for equations (50) to (56).

8.4 Roll Control and Roll Damping

We will first consider the effect of the application of roll control to the horizontal fins of a cruciform fin arrangement at $\phi = 0$. The roll effectiveness parameter

$$C_{\ell_{\delta_a}} / R_W = \frac{RM}{q_\infty S_W^2 (2s_m)} \frac{1}{\delta_a R_W} \quad (79)$$

has been determined by Adams and Dugan (ref. 24) for the cruciform case from slender-body theory. Their results are shown in figure 48. Note that in this case the results are based on the total wing area S_W^1 formed by extending the leading edges and trailing edges to the body centerline. The horizontal surfaces contribute a positive rolling moment (clockwise looking forward) for the positive δ_a deflections pictured. However, the vertical fins are subject to a clockwise swirl of the flow as a result of the horizontal fins. They react with a reverse roll in the counterclockwise direction which at $a/s_m = 0$ is about two thirds that of the horizontal fins. This *reverse roll* effect substantially reduces the roll effectiveness of the horizontal fins.

It is possible to use these slender-body results as the basis for an approximate engineering method for the nonslender case. Since we know $C_{\ell_{\delta_a}}$ from figure (48) and can obtain the fin-normal force $C_{N_{F(B)}}$ from slender-body theory, we can determine the lever arm of the fin normal force by division. Using this fin lever arm, we can multiply it by the equivalent angle-of-attack estimate of the fin lift force to get a better approximation to the fin rolling moment. This is essentially the method described in connection with planar all-movable controls.

It is of interest to compare the roll effectiveness parameter $(C_{\ell_{\delta_a}})$ for planar and cruciform all-movable controls. This relationship is exhibited in figure 49 taken from reference 24. The planar all-movable control has greater roll effectiveness than for the cruciform case because the reverse roll of the vertical fin is not present. The values of $(C_{\ell_{\delta_a}})$ in figure 49 for the planar case are related to those in figure 38 by the factor $(1 - a/s_m)^2$ because of the difference in reference areas.

The damping-in-roll parameter C_{ℓ_p} defined by equation (62) has been discussed for cruciform wings in connection with figure 39.

8.5 Nonlinear Effects in Cruciform All-Movable Controls

While exhibiting most of the nonlinearities of planar all-movable controls at zero roll angle, cruciform all-movable controls exhibit additional nonlinearities associated with roll angle. Also fin-fin interference introduces cross-couplings between pitch, yaw, and roll control.

The first nonlinearities to be discussed are those appearing in the transonic speed range. For the configuration given in figure 40 the pitch control effectiveness is shown in figure 50 taken from reference 26. The control effectiveness referred to here is that for either the windward or leeward fin of an opposing pair equally deflected 15° to produce a force in a plane 45° from the vertical. Either fins C_1 and C_3 or C_2 and C_4 are deflected as pairs, and the values of k_W for both upper or lower fins are shown in the figure. The windward fins retain control effectiveness to high angles of attack even though there is considerable decrease in effectiveness. Both lower fins (C_3 and C_4) show the same behavior within a fairly narrow band. The upper fin shows a linear dropping off of effectiveness between 0° and 50° angle of attack. These nonlinearities for $\phi = 45^\circ$ are to be compared with those shown in figure 41(b) for pitch control of all-movable canards at $\phi = 0^\circ$. The control effectiveness of the leeward fins for $\phi = 45^\circ$ goes to zero at $\alpha = 50^\circ$, but effectiveness is maintained to higher angles by the windward fins.

Let us examine the values of k_W for pure yaw control as shown in figure 51. At $M_\infty = 0.8$ the windward fin (C_3) exhibits generally less effectiveness than the leeward fin (C_1). The reason for this is not known. However, as we will see for higher Mach numbers, this effect will be completely reversed.

It is of interest to examine control cross-coupling effects between pitch and yaw. How does the effect of 15° of pitch control at $\phi = 0$ affect the yaw control effectiveness for 15° of yaw control. This result is shown in figure 52 for the upper yaw fin and in figure 53 for the lower yaw fin for $M_\infty = 0.8$ and 1.3 . Note in figure 52 that the application of pitch control has reduced the yaw control effectiveness of the upper fin, but in this case it is not too serious. Pitch control, however, has not had any significant effect on the yaw control effectiveness of the lower fin at either Mach number. The pitch control effectiveness of the horizontal fins is not much reduced by the use of an equal amount of yaw control (15°) on the vertical panels at either $M_\infty = 0.8$ or 1.3 (ref. 26).

Let us now look at the control effectiveness question at high Mach numbers as influenced by angle of attack, angle of bank, and control deflection. The configuration under consideration is the one shown in figure 42. Figure 54 shows the normal-force coefficient on a single fin of the cruciform arrangement deflected -40° , -20° , 0° , 20° , and 40° as a function of roll angle over the entire roll range for $\alpha_c = 10^\circ$ and $M_\infty = 3.0$. The results for $\phi = 0^\circ$ have already been discussed in connection with planar all-movable controls. The vertical difference between the lines represents the control effectiveness of the fin. Note that control effectiveness is greatest with the fin on the windward meridian. This is probably due to increased dynamic pressure at this point associated with greater air density behind the body shock. The effectiveness is not sensitive to control deflection between $-40 \leq \delta \leq 40^\circ$ but is more sensitive to roll angle.

Figure 55 gives results similar to those of figure 54 for $\alpha_c = 40^\circ$. It is now clear that roll angle has a very large effect on $C_{N\delta}$ of the control. The bow wave is close to the body on the bottom surface, and the shock is strong. The density in the neighborhood of the fin on the windward meridian is quite high. By the same token, the density on the leeward meridian is very low, approaching a vacuum. As a consequence, the fin normal-force coefficient is nearly zero independent of control deflection for the leeward fin. The extensive variation in control effectiveness between the windward and leeward vertical fins means that equal deflection of these fins for yaw control will result in a large rolling moment and *yaw-roll coupling*. An estimate of the induced rolling moment by this means has been made. Taking the rolling moment for $\alpha_c = 10^\circ$ as 1, the rolling moments at the other angles of attack are estimated to be the following:

α_c	RM/RM _{10°}
10°	1.0
20°	4.3
30°	7.5
40°	9.1

A special type of nonlinearity that can occur on cruciform fins in the 45° roll position is that of fin choking. In this phenomenon, the flow between the windward fins chokes, much as the flow at the throat of a nozzle. An example configuration for which fin choking has been observed is shown in figure 56. Data taken on this configuration by Stallings, Lamb, and Watson (ref. 27) are shown in figure 57. The contours of constant ratio of local pressure to free-stream pressure are shown in the figure. Note that the flow is almost one dimensional over the finned part of the configuration, much like that in a nozzle.

As a final cruciform nonlinearity, we describe the nonlinearity caused by afterbody vortices of a wing-body-tail combination. In this case the angle-of-attack range is generally above 20° to 30° and the afterbody section between the wing and tail sheds vortices which pass over the empennage. The vortices from the wing and body nose generally pass well above the tail and the principal vortex influence on the empennage is due to the afterbody vortices.

9. VORTEX EFFECTS FOR CIRCULAR BODIES

9.1 Introductory Remarks

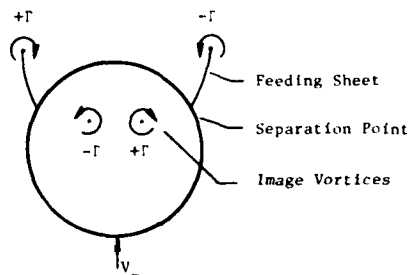
Severe nonlinearities in missile aerodynamics are due to interference of vortices on bodies and lifting surfaces. The nonlinearities arise from the fact that the vortex strengths vary with angle of attack, roll angle, and fin deflection. The vortex trajectories also depend on these parameters in a nonlinear way. To obtain an idea of general vortex interference in missiles, consider figure 58 which shows a missile divided into four sections, the nose, canard section, afterbody, and tail section. Vortices arise on the nose and interfere with the body and surfaces behind the nose. The canard fins develop vortices which influence the afterbody and tail. Also, at high angles of attack afterbody vortices impinge on the tail.

For the nose alone, two cases of body vortex formation are shown in figure 59. For the low angle-of-attack range, two symmetrical vortices form with their cores and feeding sheets. For higher angles of attack, depending on fineness ratio (typically above about 25° for fineness ratio 10) a series of asymmetric vortices form as shown in the figure. We will treat the symmetric case quantitatively, but will only consider the asymmetric case qualitatively. For supercritical cross-flow Mach numbers, shocks can form in the cross flow and cause a third type of vortex model. In this type of flow the shock waves separate the cross flow near the sides of the body, and large symmetric regions of vorticity form on the leeward side. The vorticity is smeared out, and it is difficult to characterize the vorticity by concentrated vortices with cores. Approximate vortex models for Mach numbers up to 3.0 are given in reference 17, but no model is available for higher Mach numbers.

To determine the vortex effects on a fin, we must first determine the vortex strengths and positions in the cross-flow plane of the fin. Next, we must determine the effect of the vortices on the fin forces and moments.

9.2 Model for Symmetrical Concentrated Vortices

Consider now the theoretical model for a pair of symmetrical concentrated vortices above a body of revolution. The general model is as shown in the following sketch. A vortex feeding sheet goes



from the separation line on the body to the vortex core. The vorticity in this sheet is usually ignored for simplicity in the model or lumped with the core vorticity. Also note the image vortices which are present to preserve the body tangency condition. The image vortex is located along the same radial line as the external vortex in accordance with the law of reciprocal radii.

$$r_i r_e = a^2$$

r_i = image vortex radius
 r_e = external vortex radius
 a = body radius

(80)

Let us now consider the quantitative relationship for vortex strengths and positions. The first quantity of interest is the axial position where separation exists on a body of revolution since the position will certainly influence the strength of the vortices at any lifting surface behind it. Correlations for this position, x_s , are given in figures 60 and 61 for sharp-nosed and blunt-nosed bodies as taken from reference 28. Equation (81) of figure 60 is

$$\frac{x_s}{d} = 16 \left[1 - \sqrt{\frac{\alpha - 4}{8\theta_n - 4}} \right]$$
(81)

where θ_n is the nose half angle. Both α and θ_n are in degrees. Equation (82) of figure 61 is

$$\frac{x_s}{d} = \frac{5}{\alpha - 4} + 1$$
(82)

where α is in degrees.

Correlations for the vortex core position are presented in figures 62 and 63. Note the nondimensional quantities. The coordinates y_B , Z_B are the position of the vortex core in the first quadrant. The lateral position of the vortex does not vary much with α but the vertical position is nearly linear in α . Nondimensional vortex strengths are correlated in figure 64. Separate correlations for subsonic and supersonic speeds are given. Data from references 29 to 36 are used in these correlations. These data are utilized to determine the quantity $(\Delta\alpha)_v$ used in connection with equivalent angle-of-attack concept.

For supercritical cross flow, the vorticity field can be quite spread out as mentioned previously. In reference 17, an approximate way of dealing with this effect has been developed. The different vorticity fields were calculated using vortex-cloud theory. Equivalent vortex strengths and locations were obtained by fitting the assumed model to the flow fields calculated from the vortex-cloud calculation. Empirical expressions for vortex strengths and positions based on this approximate method are given on pp. 108-110 of reference 17 for angles of attack up to 50° and Mach numbers to 3.0.

9.3 Determination of $(\Delta\alpha)_v$

It will be recalled in connection with the equivalent angle-of-attack concept, that the change in α_{eq} of the fin due to external vortices was designated as $(\Delta\alpha)_v$ in equations (20) and (35) but was left for future discussion. We now consider the method for the determination of $(\Delta\alpha)_v$. The three principal ways for doing this are the i_t method, the reverse-flow method, and strip theory.

The i_t method is based on the tail interference factor i_t defined as follows:

$$i_t = \frac{N_T(V) \left(\frac{N_T}{\alpha} \right)}{\Gamma / 2\pi V_\infty (\theta_t - r_t)}$$
(83)

where i_t = tail interference factor
 $N_{T(V)}$ = normal force on tail fins due to symmetric pair of body vortices
 $(N_T)_\alpha$ = normal force on tail alone at angle of attack α
 Γ = circulation about body vortex
 s_t = semispan of tail fin measured from body axis
 r_t = body radius at tail position

Although written in terms of tail fin variables, the method is equally valid for wing on canard fins.

The determination of i_t charts are carried out in reference 37 using strip theory and determining the upwash on the exposed fin due to the vortex pairs and their images by the Biot-Savart law. The factor i_t depends only on the vortex position y_v/a , z_v/a ; the fin taper ratio, λ ; and the radius-semispan ratio, a/s_m . With

$$(\Delta\alpha)_V \equiv \frac{N_{T(V)}}{q_\infty S_T} \quad (84)$$

$$(\Delta\alpha)_V = \frac{i_t (N_T)_\alpha \left[\Gamma / 2\pi V_\infty (s_t - r_t) \right]}{q_\infty S_T} \quad (85)$$

The value of i_t is to be obtained from the charts of reference 37. The values of $(\Delta\alpha)_V$ so obtained are valid for small value of α and δ , and contain some error due to fin-body interference that has been properly accounted for only approximately.

The second method of determining $\Delta\alpha_V$ based on reverse-flow theorems accounts for fin-body interference within the framework of linear theory. Essentially instead of using the local chord as the weighting factor in the strip theory, the reverse-flow method provides a weighting factor that accounts for fin-body interference. The derivation is too lengthy to include here, but is carried out in Appendix B of reference 17. It also derives results for obtaining the value of the lateral center-of-pressure location of the vortex-induced normal force on the fin. It does not, however, give axial position of the vortex-induced normal force which is of interest in determining hinge moments. The procedure for carrying out the calculation is contained in PROGRAM MISSILE as described in reference 17.

The third way of carrying out the calculation of $(\Delta\alpha)_V$ to account for a nonuniform flow field is the direct application of strip theory. Consider the sketch in section 9.2, and assume the vortices are infinite line vortices parallel to the body axis. Then the induced velocities normal to the fin in any position can be calculated using the Biot-Savart law. This vortex-induced flow field normal to the wing varies only with distance from the body axis and is thus usable in a strip theory. One should use airfoil section characteristics in the strip theory if available. Strip theory yields results for $(\Delta\alpha)_V$ and for the axial and lateral positions of the center of pressure due to the vortex-induced loading. The method is well-suited to hypersonic speeds where the fin-body and fin-fin interference is much decreased, and Mach cones are of small included angle. However, in this case, large local changes in dynamic pressure and Mach number can be induced by the body nose shock wave. These can be included in the strip theory. The best way to obtain these local values is by means of an Euler code as in reference 38.

9.4 Interference of Canard Fins on Tail Fins

The interference of canard fins on tail fins caused by the canard fin vortices is a complicated phenomenon. If the canard fins are used as controls, then the vortex effects are further complicated. We will not give quantitative relationships for the vortex strengths and positions at the tail, but will describe the methodology which is given in reference 17.

What is needed is the fin vortex strengths and positions at the fin trailing edge. Then the fin trajectory from its trailing edge to the tail is required. A fin may have a trailing vortex due to its span loading; which roll up at a spanwise position corresponding to the lateral centroid of vorticity. If the fin span loading peaks outboard of the root chord, it can shed several vortices. In addition, sharp subsonic leading edges can cause leading-edge vortices. The trailing vortex system of a wing or canard fin can be quite complicated. Methods for determining the shed vortex strengths and positions are given in reference 17.

It is possible to use equivalent angle-of-attack methodology to obtain a model of one vortex per fin based on experimental data. Equivalent angle-of-attack correlations gives the fin C_N and its lateral center-of-pressure position. From these two experimental quantities and the assumption that the fin span loading is a linear combination of an elliptical loading and a linear loading, expressions for the fin vortex strength and its lateral position can be derived. Such expressions are given in Appendix C of reference 39. This method gives good results if the fin sheds only one vortex. However, if the wing sheds two vortices of opposite signs as from the root chord and the tip chord, the method can give a vortex position off the fin.

In order to determine the canard fin vortex effects on the tail fins, we require a knowledge of the vortex strengths and positions at the tail fins. To obtain these we use a vortex trajectory program which takes as input the vortex strengths and positions at the canard fin trailing edge. It calculates the vortex trajectories along the afterbody to the tail using slender-body theory. A computer program to accomplish this task is described in reference 40. An example of calculated vortex trajectories taken

from reference 28 is shown in figure 65. The circulation Γ is that associated with the main span loading and Γ_L is associated with leading-edge separation. Comparison of the calculated trajectories with that determined by flow visualization shows good agreement.

9.5 Other Vortex Phenomenon

At the beginning of this section on vortices reference was made to asymmetric vortices developed by the body on which fins are mounted (fig. 59). Such asymmetric vortices are of importance for controls primarily because large yawing moments are induced even without the fins and large rolling moment with the fins. The maximum side-force coefficients (based on body cross-sectional area) induced by asymmetric vortices shed from bodies of revolution are presented in figure 66 as taken from reference 41. The maximum side-force coefficient encountered is independent of cross-flow Mach number up to 0.4, the critical Mach number for a circular cylinder. Thereafter it decreases until at a cross-flow Mach number at about 0.8 it is zero.

If we assume that up to a Mach number of about 0.5, $\alpha = 25^\circ$ angle of attack is the dividing line between asymmetric and asymmetric body vortices, then we can construct a diagram like that in figure 67. Above $M_c = 0.8$ the vorticity is smeared out in elliptical regions because of shock waves in the cross flow. We thus can avoid asymmetric vortices by operating in the subcritical region of symmetric vortices or in the supercritical region. If both regions are included in the operating range, we must pass through the cross-hatched region of reduced asymmetry.

To determine vortex effects in the supercritical region, the only method which is presently available is to use the Euler equations. The body separation lines are fed into the code as input, and special boundary conditions are used at the separation line (ref. 42).

It is possible to evaluate $(\Delta\alpha)_v$ using a panel code for cruciform wing-body combinations such as that in reference 43.

10. HINGE-MOMENT PREDICTION METHODOLOGY AT SUPERSONIC SPEED

10.1 Introductory Remarks

The prediction of hinge moments of all-movable controls is a difficult task because anything that affects fin normal force or fin axial center-of-pressure location will influence hinge moment. It is generally thought that accurate hinge-moment prediction is very difficult. However, accurate hinge-moment prediction is possible under certain circumstances as we will find.

A number of factors can influence hinge moment. First, any of the nonlinearities pointed out previously which influence fin-normal force or axial center of pressure will be relevant to hinge moment. Body vortices will affect forward fins and the forward fin vortices will affect the rearward fins. It will turn out that fin thickness and thickness distribution will have significant effects at supersonic and hypersonic speeds. Fin trailing-edge shock-wave/boundary-layer interaction can change axial center-of-pressure location. Fin choking is another factor which can influence hinge moments as well as aeroelasticity.

In a recent publication, reference 22, a general hinge-moment prediction method is advanced. It is fairly good for supersonic speeds for canard all-movable controls. However, in the transonic range many unknown nonlinearities appear which require further study. The following discussion will draw heavily on this reference.

The basic method can be described simply as follows. To obtain C_N of the fin on the body, the equivalent angle-of-attack concept is used. To obtain the center-of-pressure location, the correlations based on the equivalent angle-of-attack concept can be used. However, since fin thickness is a definite parameter in axial center-of-pressure location, \bar{x}/c_r data are not usually available for the thickness distribution of interest. Accordingly at supersonic speed the center-of-pressure location is first determined from design charts for wings alone of zero thickness as in DATCOM (ref. 5) or a paneling method such as reference 43. Then a thickness correction to \bar{x}/c_r is applied to these results by strip theory. The effect of thickness on \bar{x}/c_r for the airfoil section characteristics used in the strip theory are determined by the Busemann supersonic airfoil theory or by shock-expansion theory. Note that these thickness effects on \bar{x}/c_r are second-order effects of thickness which are present at $\alpha = 0$ and cannot be determined by linearized wing theory. Alternately we could apply thickness corrections to experimental data for the wing-alone or fin-on-body.

The above procedure works when vortex effects are not present. However any vortex-induced load acts at a center-of-pressure while depends on vortex position. The hinge moment in this case must be determined as caused in part by normal force not including vortex effects, and in part due to vortex-induced normal force. The hinge-moment contributions are added in accordance with the following equations.

The basic equations for hinge moment is

$$C_{HM} = C_{N_{F(B)}} \cos \delta \left[\frac{\bar{x}_{F(B)}}{c_r} - \left(\frac{\bar{x}}{c_r} \right)_{HL} \right] \frac{c_r}{l_r} \quad (86)$$

where \bar{x}_{HL} = distance of hinge line behind leading edge of fin root chord

Nonvortex normal force:

$$\alpha_{eq1} = K_W \alpha_c \cos \phi + \sum_{j=1}^4 A_{j1} \delta_j + \frac{4}{\pi} K_\phi \alpha_c^2 \cos \phi \sin \phi \quad (87)$$

$$C_{N_{F(B),1}} = C_{N_W}(\alpha_{eq1}) ; \quad (88)$$

Viscous normal force:

$$\alpha_{eq2} = \alpha_{eq1} + (\Delta \alpha)_V \quad (89)$$

$$C_{N_{F(B)}} = C_{N_W}(\alpha_{eq2}) ; \quad (90)$$

$$C_{N_{F(B),V}} = C_{N_{F(B)}} - C_{W_{F(B),1}}$$

Nonvortex c.p.:

$$\left(\frac{\bar{x}}{c_r} \right)_{F(B),1} = \left(\frac{\bar{x}}{c_r} \right)_W (\alpha_W = \alpha_{eq1}) \quad (91)$$

This last term may also be available from an α_{eq} correlation.

Vortex c.p.:

$$\left(\frac{\bar{x}}{c_r} \right)_{F(B),2} = \left(\frac{\bar{x}}{c_r} \right)_V^* \quad (92)$$

Total hinge moment:

$$C_{HM} = \cos \delta \left\{ C_{N_{F(B),1}} \left[\left(\frac{\bar{x}}{c_r} \right)_{F(B),1} - \left(\frac{\bar{x}}{c_r} \right)_{HL} \right] + \left(C_{N_{F(B)}} - C_{N_{F(B),1}} \right) \left[\left(\frac{\bar{x}}{c_r} \right)_V - \left(\frac{\bar{x}}{c_r} \right)_{HL} \right] \right\} \frac{c_r}{\ell_r} \quad (93)$$

Fin normal-force coefficient is based on fin planform area and wing-alone normal-force coefficient is based on wing planform area. The reference length ℓ_r is arbitrary.

10.2 Some Wing-Alone Characteristics

In order to apply the hinge-moment prediction method, it is necessary to use experimental normal-force curves and it is helpful to have experimental \bar{x}/c_r data for wings alone. For this purpose we refer to the systematic supersonic data base of Stallings and Lamb, reference 44, and its continuation to transonic and subsonic speeds in reference 45.

A systematic series of wing planforms was tested across the Mach number range up to high angles of attack, 45° or higher. The wing planforms and their thickness distributions are given in figure 68. The normal-force curves were fitted up to 50° angle of attack by least squares using a truncated sine series of the following form:

$$C_N = A_1 \sin \alpha + A_2 \sin 3\alpha + A_3 \sin 5\alpha \quad (94)$$

The coefficients A_1 , A_2 , and A_3 are functions of fin planform (M, λ) and Mach number. A tabulation of these coefficients is provided in figure 69. This information yields normal-force curves for the following ranges:

$$0.5 \leq M \leq 2.0 ; \quad 0 \leq \lambda \leq 1.0$$

and

$$M = 4 \quad \lambda = 0.5$$

for the Mach number range

$$1.6 \leq M_\infty \leq 4.6$$

Used with the equivalent angle-of-attack concept, they provide $C_{N_{F(B)}}$ for use in the hinge-moment prediction method.

*A method for obtaining $(\bar{x}/c_r)_V$ is given in the next section.

The determination of $(\bar{x}/c_r)_w$ for use in the method is not so easy as $C_{NF(B)}$ since this quality is influenced by airfoil section (thickness effects). Center-of-pressure locations for the wings of the Stallings-Lamb data base have been determined from the pressure distributions, and tables of these results are included in reference 22. Typical data tabulations for delta and rectangular wings of aspect ratio 2 are shown in figures 70 and 71, respectively. These represent data for use in the equivalent angle-of-attack method if data such as those in figure 36 are not available. It must be remembered that they apply only to the thickness distributions of the wings tested.

In case data on $(\bar{x}/c_r)_w$ are not available, they are estimated in the following steps.

1. Find $(\bar{x}/c_r)_w$ for no thickness.
2. Subtract an increment $(\Delta\bar{x}/c_r)_w$ from $(\bar{x}/c_r)_w$ to account for the thickness distribution up to the angle of attack of shock detachment.
3. Above the angle of shock detachment fair the results into the experimental value of $(\bar{x}/c_r)_w$ for $\alpha = 45^\circ$.

Let us discuss these three steps in turn.

The determination of $(\bar{x}/c_r)_w$ with no thickness can be accomplished using linear supersonic wing theory based on the wave equation. Charts of this quantity are to be found in DATCOM (ref. 5) for conventional wing planforms. For any planform the computer program of reference 43 can be used.

The increment $(\Delta\bar{x}/c_r)_w$ due to thickness is important as can be seen from some calculated airfoil section results. These airfoil sections are shown in figure 72. For zero thickness these sections all have their centers of pressure at the midchord for attached leading-edge shocks. With thickness their centers of pressure are forward of the midchord by the amounts shown in figure 73. The large values of $(\Delta\bar{x}/c_r)_w$ show the importance of thickness on centers-of-pressure location. The data points are the values calculated using shock-expansion theory. Note that $(\Delta\bar{x}/c_r)_w$ is a maximum at $\alpha = 0$ and decreases as α increases. Basemann's second-order theory is close to shock-expansion theory at $\alpha = 0^\circ$. However, significant change in $\Delta\bar{x}/c$ occur over the angle-of-attack range as calculated by shock-expansion theory which are third-order effects of thickness. All airfoils have the same thickness ratio.

For one of the airfoils, figure 73(b) shows the effect of Mach number on $(\Delta\bar{x}/c)$ as calculated from shock-expansion theory. The value of $\Delta\bar{x}/c$ increases with increase in Mach number for a fixed angle of attack.

These results suggest the obvious method for correcting $(\bar{x}/c_r)_w$ for wings of no thickness to account for thickness effects. Strip theory is used across the wing semispan to average the center-of-pressure position with respect to chord. Let c_ℓ and \bar{x} be the local section lift coefficient and center-of-pressure location as determined by shock-expansion theory. Then the shift in $\Delta\bar{x}$ for the wing based on strip theory is

$$(\Delta\bar{x})_w = \frac{\int_0^s c c_\ell (\bar{x} - c/2) dy}{\int_0^s c c_\ell dy}$$

Some examples of how predictions of this method compare with experiment are shown in figures 74 and 75. In figure 74 for an $R = 2$ delta wing, it is seen that the method is quite good for the range of attached shocks. The data are from the Stallings-Lamb data base. For the $R = 2$ rectangular wing the comparisons are equally favorable. The comparisons are favorable over the Mach number range $1.6 \leq M_\infty \leq 4.6$ and the aspect-ratio range $0.5 \leq R \leq 2$ for delta wings and also for rectangular wings when the shock is attached considering two-dimensional flow in planes parallel to the vertical plane of symmetry. Wings of taper ratio 0.5 do not show good agreement between data and predictions at $R = 0.5$ or at $R = 1.0$ for Mach numbers less than about 3.0. For $R = 2$ and $R = 4$ the agreement is good.

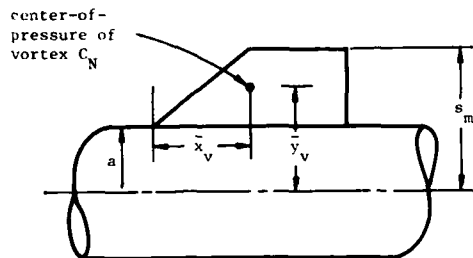
The engineering method described above does not go through above the shock-detachment angle since it is based on shock-expansion theory. The third step addresses this problem. One might imagine that the effect of wing thickness distribution will not be an important parameter in $(\bar{x}/c)_w$ at high angles of attack such as 45° . Another set of data besides the Stallings-Lamb set exists for checking this hypothesis. The data set referred to is the Fidler-Baker data base for the wings of figure 76 as given in reference 46. These wings have generally about one-half the root chord thickness ratio of the corresponding wings of the Stallings-Lamb data base. The values of $(\bar{x}/c)_w$ at $\alpha = 45^\circ$ are compared from the two data bases in figure 77. For the $R = 0.5$ and 1.0 wings the values agree within 1 to 2 percent of the root chord. For $R = 2$ in some cases they disagree as much as 3 percent of the fin root chord. We have adopted the Stallings-Lamb values in the design method and have faired lines through these values. The engineering method for angles of attack above shock detachment is then simply to fair the results below shock detachment into the value given by figure 77 for $\alpha = 45^\circ$.

10.3 Effect of External Vortices on Hinge Moments

It is noted in connection with equation (93) that account is taken of the fact that the vortex-induced load on a fin has its own center-of-pressure location $(\bar{x}/c_r)_v$. The normal force due to the vortex is given by the equivalent angle-of-attack method, but the value of $(\bar{x}/c_r)_v$ is not. This quantity depends not only on wing planform but also on the vortex positions and strengths.

The effect of vortices on the axial center-of-pressure location of a fin can be studied using panel methods, and this has been done in reference 22. A figure from this reference is reproduced in figure 78. The wing center-of-pressure location without the vortices is known from the equivalent angle-of-attack method (embodied in the computer program of reference 17) utilizing data-base correlations of the type shown in figures 36 and 37. This establishes a "lifting line" of constant percent chord through the fin center of pressure without vortex effects. The vortex download is inboard of the above center-of-pressure location but close to the line of constant percent chord. If we could determine \bar{y}_v , the lateral coordinate of the fin normal force due to the vortex and assume it is on the constant percent chord line, we pin down \bar{x}_v , the axial coordinate of the vortex center of pressure. In the example note that the fin center of pressure has moved rearward by 6.75 percent of the root chord. The change in hinge moment due to such a shift is significant.

The engineering method outlined above leads to the following procedure for determining $(\bar{x}/c_r)_v$.



1. Determine the lateral center-of-pressure position of the vortex normal force, $(\bar{y}/a)_v$, from the computer program of reference 17.
2. Determine $(\bar{x}/c_r)_{F(B)}$ by the methods discussed in the previous section for $C_{NF(B)}$ with no vortices.
3. Determine the lateral center of pressure of the fin (with or without deflection) and with no vortex effects $(\bar{y} - a)/(s_m - a)_{F(B)}$ by interpolating or extrapolating in the tables of reference 17.
4. Determine the local fractional chord τ of the fin center of pressure with no vortex effects from

$$\tau = \frac{\left(\frac{\bar{x}}{c_r}\right)_{F(B)} - (1 - \lambda) \left(\frac{\bar{y} - a}{s_m - a}\right)_{F(B)}}{1 - (1 - \lambda) \left(\frac{\bar{y} - a}{s_m - a}\right)_{F(B)}} \quad (95)$$

5. Determine the percent root chord corresponding to the axial position of the normal force induced on the fin by the vortices, $(\bar{x}/c_r)_v$.

$$\left(\frac{\bar{x}}{c_r}\right)_v = \tau + (1 - \tau)(1 - \lambda) \left(\frac{\bar{y} - a}{s_m - a}\right)_v \quad (96)$$

We know the normal force induced on the fin by the vortices and we are now in a position to determine its contribution to the hinge-moment coefficient.

10.4 Some Comparisons Between Prediction and Measurement

In reference 22 a number of comparisons are made between data and the predictions of theory. Some of these are now presented. The configuration in question is shown in figure 79 and consists of a body and cruciform canard fins with hingeline at the station MS 15.000.

The first comparison is for horizontal fins deflected at $\delta = 0^\circ$ and $\delta = 15^\circ$ at $M_\infty = 1.3$ and $M_\infty = 1.75$ for zero roll. Fairly good agreement between prediction and data is shown in figure 80 considering repeatability of the data.

The second comparison between prediction and data is for the same configuration at $\phi = 45^\circ$ and $M_\infty = 1.3$. The hinge-moment characteristics of the upper fins are shown in figure 81(a) and of the lower fins in figure 81(b). The comparisons show fair agreement.

The third comparison in figure 82 shows the effect of roll angle on the fin normal-force and hinge-moment coefficients at $M_\infty = 1.3$. The roll angle range from -90° to $+90^\circ$ has been covered by the four fins by rolling the body 45° and assuming left-right mirror symmetry. At $\phi = \pm 45^\circ$ and 0° , there are two data points which should coincide if the model and tests were perfect. The normal-force coefficient is well predicted. The hinge moments are predicted within the accuracy of the measurements.

These comparisons are shown for canard fins where body vortex effects are not significant. Further comparisons show that the accuracy of prediction is poor for leeward fins near strong vortices. The method gives fair results for inline canard and tail fins for $\phi = 0$, both with and without canard deflections.

REFERENCES

1. Nielsen, J. N.: *Missile Aerodynamics*. McGraw-Hill Book Co., 1960.
2. Von Karman Institute Lecture Series No. 67, *Missile Aerodynamics*. Apr. 22-26, 1974, Vols. 1 and 2.
3. AGARD Lecture Series No. 98, *Missile Aerodynamics*. Feb. 1979.
4. AGARD Short Course, *Flight Mechanics for Tactical Missiles*. Mar. 31 - Apr. 2, 1981.
5. McDonnell-Douglas Aircraft Co., Inc. USAF Stability and Control Handbook. Air Force Flight Dynamics Laboratory, Wright-Patterson AFB, OH, 1978.
6. Chapman, D. R., Kuehn, D. M., and Larson, H. K.: *Investigation of Separated Flows in Supersonic and Subsonic Streams with Emphasis on the Effect of Transition*. NACA TN 3869, Mar. 1957.
7. Blair, A. B., Jr.: *Wind-Tunnel Investigation at Mach Numbers from 1.90 to 2.86 of a Canard-Controlled Missile with Ram-Air-Jet Spoiler Roll Control*. NASA TP 1124, Mar. 1978.
8. Vinson, P. W., Amick, J. L., and Leipman, H. P.: *Interaction Effects Produced by Jet Exhausting Laterally Near the Base of an Ogive-Cylinder Model in a Supersonic Main Stream*. NASA Memo 12-5-58W, Feb. 1959.
9. Kuhn, G. D., Canning T. N., and Nielsen, J. N.: *The Forces and Moments on a Missile Due to a Fluid Jet Ejecting Laterally (U)*, Vol. 1 - Analysis and Correlations (U). Nielsen Engineering & Research, Inc., NEAR TR 218, Oct. 1980. (CONFIDENTIAL)
10. Spring, D. J.: *An Experimental Investigation of the Interference Effects Due to a Lateral Jet Issuing from a Body of Revolution Over the Mach Number Range 0.8 to 4.5*. U.S. Army Missile Command, Rept. No. RD-TR-68-10, Aug. 1968.
11. Coble, D. F.: *Lateral Jet-Missile Interference Data Correlation Study*. Lockheed Missiles & Space Co., Rept. No. HREC-A791585, Huntsville, AL, Jun. 1968.
12. Gilman, B. G.: *Control Jet Interaction Investigation*. J. of Spacecraft & Rockets, Vol. 8, No. 4, Apr. 1971, pp. 334-339.
13. Amick, J. L. and Hays, P. B.: *Interaction Effects of Side Jets Issuing from Flat Plates and Cylinders Aligned with a Supersonic Stream*. WADD TR-60-329, Jun. 1960.
14. Graves, E. B. and Fournier, R. H.: *Stability and Control Characteristics at Mach Numbers from 0.20 to 4.63 of a Cruciform Air-to-Air Missile with Triangular Canard Controls and a Trapezoidal Wing*. NASA TM X-3070, Jul. 1974.
15. Corlett, W. A.: *Supersonic Stability and Control Characteristics of a Cruciform Missile Model with Delta Wings and Aft Tail Fin Controls*. NASA TM 80171, Dec. 1979.
16. Hemsch, M. J. and Nielsen, J. N.: *The Equivalent Angle-of-Attack Method for Estimating the Nonlinear Aerodynamic Characteristics of Missile Wings and Control Surfaces*. AIAA-82-1338, Aug. 9-11, 1982.
17. Nielsen, J. N., Hemsch, M. J., and Smith, C. A.: *A Preliminary Method for Calculating the Aerodynamic Characteristics of Cruciform Missile to High Angles of Attack Including Effects of Roll Angle and Control Deflections*. Report ONR-CR215-226-4F, Nov. 1977.
18. Hemsch, M. J. and Nielsen, J. N.: *Test Report for Canard Missile Tests in Ames 6- by 6-Foot Supersonic Wind Tunnel*. Nielsen Engineering & Research, Inc., TR 72, Aug. 1974.
19. Emerson, H. F.: *Wind-Tunnel Investigation of the Effect of Clipping the Tips of Triangular Wings of Different Thickness, Camber, and Aspect Ratio - Transonic Bump Method*. NACA TN 3671, Jun. 1956.
20. Spreiter, J. R. and Sacks, A. H.: *A Theoretical Study of the Aerodynamics of Slender Cruciform-Wing Arrangements and Their Wakes*. NACA Rept. 1296, 1957.
21. Derrick, J., Spring, D., and Winn, G.: *Aerodynamic Characteristics of a Series of Bodies With and Without Tails at Mach Numbers from 0.8 to 3.0 and Angles of Attack from 0° to 45°*. MICOM-TR-RD-7T-3, Jul. 1976.
22. Nielsen, J. N. and Goodwin, F. K.: *Preliminary Method for Estimating Hinge Moments of All-Movable Controls*. Nielsen Engineering & Research, Inc. TR 268 (to be published).
23. Baker, W. B., Jr.: *Static Aerodynamic Characteristics of a Series of Generalized Slender Bodies With and Without Fins at Mach Numbers from 0.6 to 3.0 and Angles of Attack from 0 to 180 Degrees*. AEDC-TR-75-124, Vols. I and II, May 1976.
24. Adams, G. J. and Dugan, D. W.: *Theoretical Damping in Roll and Rolling Moment Due to Differential Wing Incidence for Slender Cruciform Wings and Wing-Body Combinations*. NACA TR 1088, 1952.
25. Schwind, R. G.: *High Angle Canard Missile Test in the Ames 11-Foot Transonic Wind Tunnel*. NASA CR 2993, 1978.

26. Smith, C. A. and Nielsen, J. N.: Nonlinear Aerodynamics of All-Movable Controls. AGARD Conference Proceedings No. C.P. 262, Aerodynamic Characteristics of Controls, 1979.
27. Stallings, R. L., Jr., Lamb, M., and Watson, C. B.: Effect of Reynolds Number on Stability Characteristics of a Cruciform Wing Body at Supersonic Speeds. NASA Tech. Paper 1683, Jul. 1980.
28. Mendenhall, M. R. and Nielsen, J. N.: Effects of Symmetrical Vortex Shedding on the Longitudinal Aerodynamic Characteristics of Wing-Body-Tail Combinations. NASA CR-2473, 1975.
29. Tinling, B. E. and Allen, C. Q.: An Investigation of the Normal-Force and Vortex-Wake Characteristics of an Ogive-Cylinder Body at Subsonic Speeds. NASA TN D-1297, Apr. 1962.
30. Mello, J. F.: Investigation of Normal Force Distributions and Wake Vortex Characteristics of Bodies of Revolution at Supersonic Speeds. J. of Aero/Space Sci., Vol. 26, No. 3, Mar. 1959, pp. 155-168.
31. Cooper, Morton, Gapcynski, J. P., and Hasel, L. E.: A Pressure Distribution Investigation of a Fineness-Ratio-12.2 Parabolic Body of Revolution (NACA RM-10) at $M = 1.59$ and Angles of Attack up to 36° . NACA RM L52G14a, Oct. 1952.
32. Chamberlain, T. E.: Aerodynamic Forces, Separation Lines, and Vortex Trajectories on Slender Bodies with Several Nose Shapes. Thesis, Mass. Inst. of Tech., Jun. 1966.
33. Hill, Jacques, A. F.: A Non-Linear Theory of the Lift on Slender Bodies of Revolution. Presented at U.S. Navy Symposium on Aeroballistics, Laurel, MD, Oct. 19-20, 1954.
34. Rodgers, E. J.: Real Flow Over a Body of Revolution at Angle of Attack. Pennsylvania State Univ. Ordnance Research Lab. Tech. Memo, File No. TM 5.2420-13, Mar. 28, 1963.
35. Jorgensen, L. H. and Perkins, Edward W.: Investigation of Some Wake Vortex Characteristics of an Inclined Ogive-Cylinder Body at Mach Number 1.98. NACA RM A55E31, Aug. 1955.
36. Jorgensen, L. H.: Inclined Bodies of Various Cross Sections at Supersonic Speeds. NASA Memo 10-3-58A, Nov. 1958.
37. Pitts, W. C., Nielsen, J. N., and Kaattari, G. E.: Lift and Center of Pressure of Wing-Body-Tail Combinations at Subsonic, Transonic, and Supersonic Speeds. NACA TR 1307, 1957.
38. Wardlaw, A. B., Jr., Baltakis, J. P., Solomon, J. M., and Hackerman, L. B.: An Inviscid Computational Method for Tactical Missile Configurations. NSWC TR 81-457, 1981.
39. Hensch, M. J., Smith, C. A., Nielsen, J. N., and Perkins, S. C., Jr.: Calculation of Component Forces and Moments of Arbitrarily Banked Cruciform Missiles with Control Deflection. Rept. ONR-CR215-226-3, Nov. 1, 1976.
40. Mendenhall, M. R., Spangler, S. B., and Perkins, S. C., Jr.: Vortex Shedding from Circular and Non-circular Bodies at High Angles of Attack. AIAA Paper 79-0026, Jan. 1979.
41. Wardlaw, A. B., Jr. and Morrison, A. M.: Induced Side Forces at High Angles of Attack. J. of Spacecraft & Rockets, Vol. 13, No. 10, Oct. 1976, pp. 589-593.
42. Klopfer, G. H. and Nielsen, J. N.: Euler Solutions of the Body Vortices of Tangent Ogive Cylinder at High Angles of Attack and Supersonic Speeds. AIAA Paper 81-0361, Jan. 1981.
43. Dillenius, M. F. E. and Nielsen, J. N.: Computer Programs for Calculating Pressure Distributions Including Vortex Effects on Supersonic Monoplane or Cruciform Wing-Body-Tail Combinations with Round or Elliptical Bodies. NASA CR 3122, Apr. 1979.
44. Stalling, R. L. and Lamb, M.: Wing Alone Aerodynamic Characteristics for High Angles of Attack at Supersonic Speeds. NASA Technical Paper 1889, Jul. 1981.
45. Briggs, M. M., Reed, R. E., and Nielsen, J. N.: Wing Alone Aerodynamic Characteristics to High Angles of Attack at Subsonic and Transonic Speeds. NEAR TR 269, Sep. 1982 (to be published).
46. No author listed: High Alpha Aerodynamics - Fin Alone (Data reported in AEDC-TR-75-1240, Vols. 1 and 2; Propulsion Wind Tunnel Facility, ARO, Inc., Jul. 1974).

ACKNOWLEDGEMENTS

I would like to acknowledge the contributions of Mr. Vernon Hoehne of AFFDL and Dr. Robert Whitehead of ONR in sponsoring most of the work on which the section of hinge-moment predictions is based. In addition, the data in figures 42-45 and 54-55 were taken in an ongoing program sponsored by all three services, contracted by ONR, and jointly carried out by NASA and NEAR, Inc.

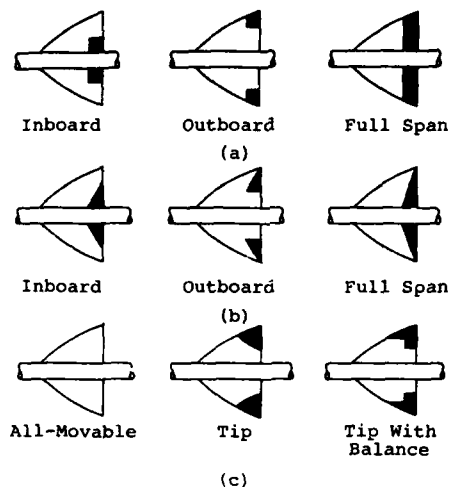


Figure 1.- Types of trailing-edge controls: (a) constant; (b) constant taper; and (c) others.

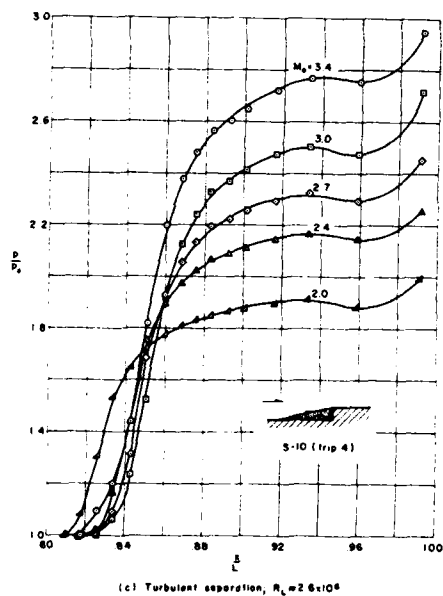


Figure 2.- (Concluded).

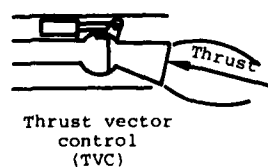


Figure 4.- Thrust vector control by swiveling nozzle.

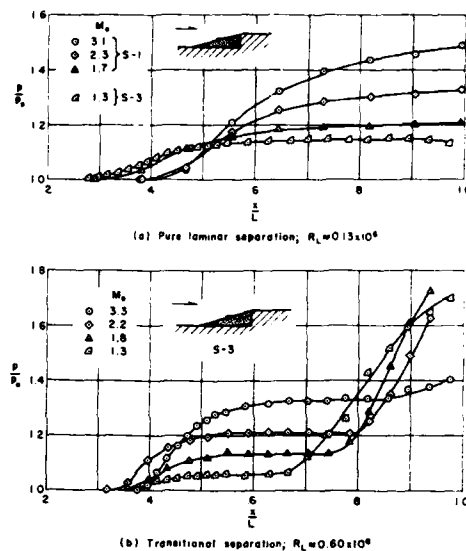


Figure 2.- Effect of Mach number on the pressure distribution on a step for the three flow regimes.

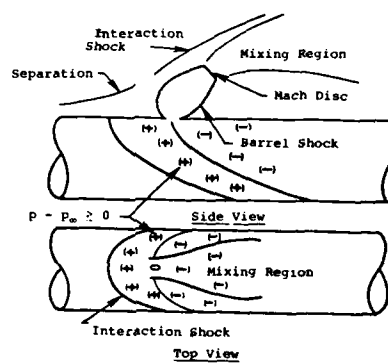


Figure 3.- Jet spoiler.

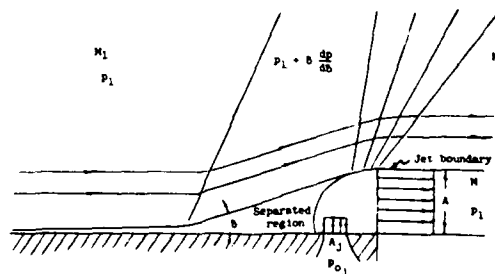


Figure 5.- Simple model for two-dimensional jet amplification.

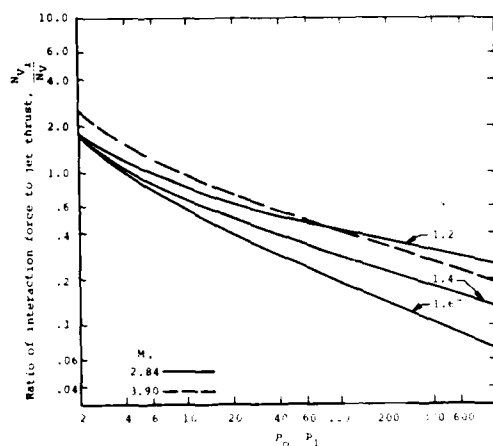


Figure 6.- Two-dimensional isentropic theory for simple jet amplification.

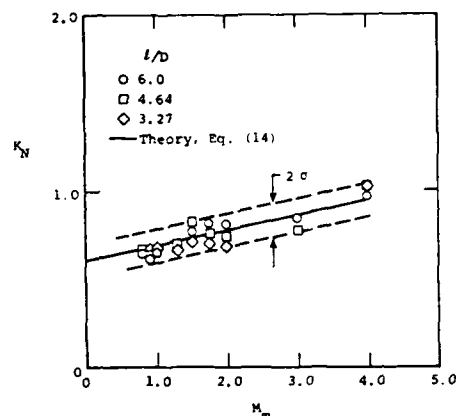


Figure 9.- Normal-force amplification as a function of M_{∞} . $d_j/D = 0.08$; $p_{tj}/p_{\infty} = 60$ (Ref. 10).

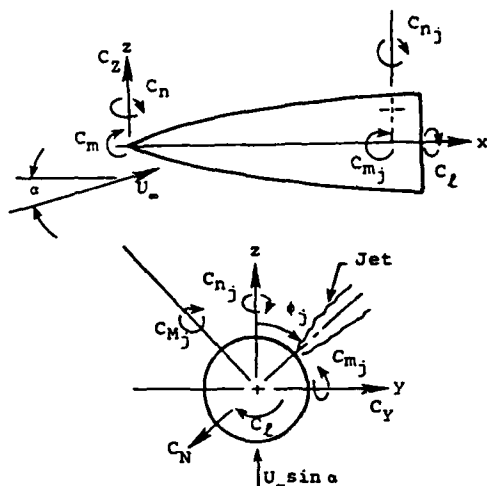
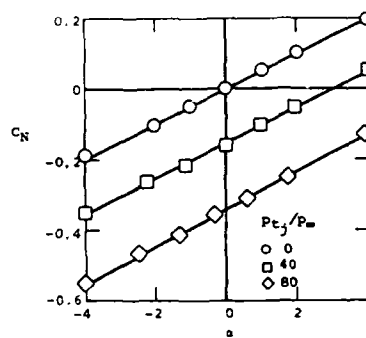


Figure 7.- Coordinates for a finless missile.



(a) Normal-force coefficient.

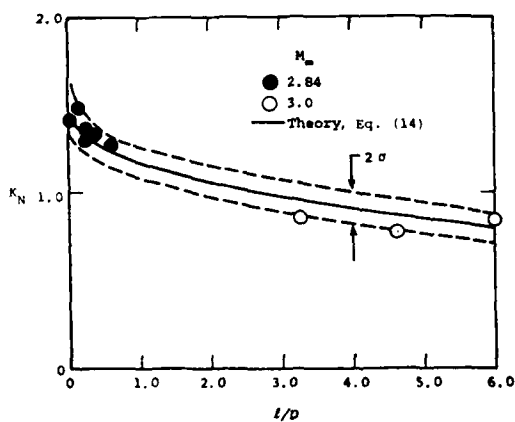
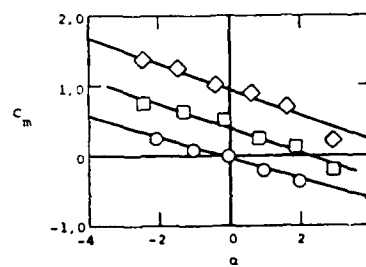


Figure 8.- Normal-force amplification as a function of distance from model base. $d_j/D = 0.08$; $p_{tj}/p_{\infty} = 60$ (Refs. 8 and 10).



(b) Pitching-moment coefficient

Figure 10.- Typical variation of normal-force and pitching-moment coefficients with angle of attack (Ref. 10) $M_{\infty} = 1.3$.

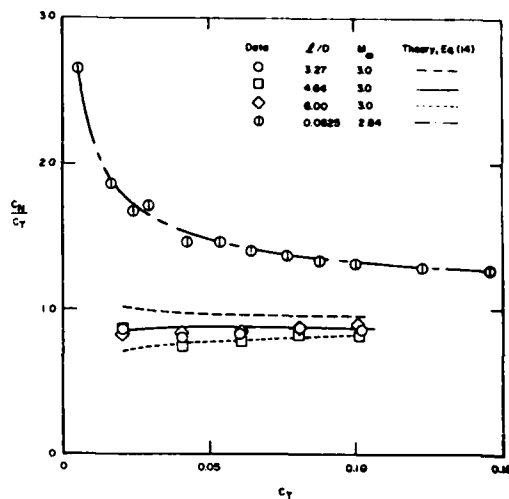


Figure 11.- Normal-force amplification as a function of jet-thrust coefficient.

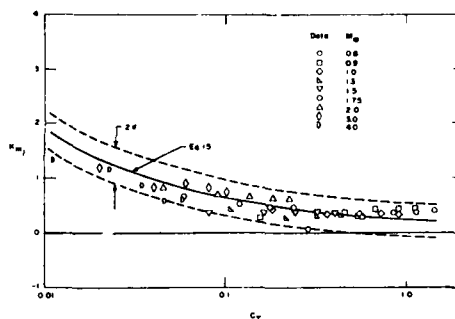


Figure 12.- Typical variation of pitching-moment factor with thrust coefficient (Ref. 10) $L/D = 3.27$.

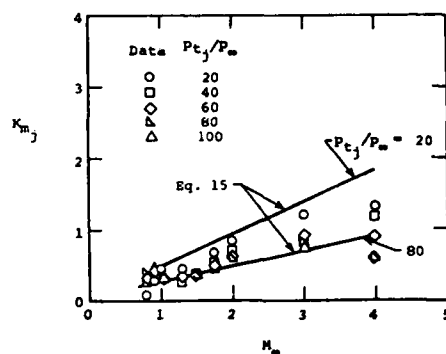


Figure 13.- Typical variation of pitching-moment factor with Mach number (Ref. 10) $L/D = 3.27$.



Figure 14.- Canard-controlled missile.

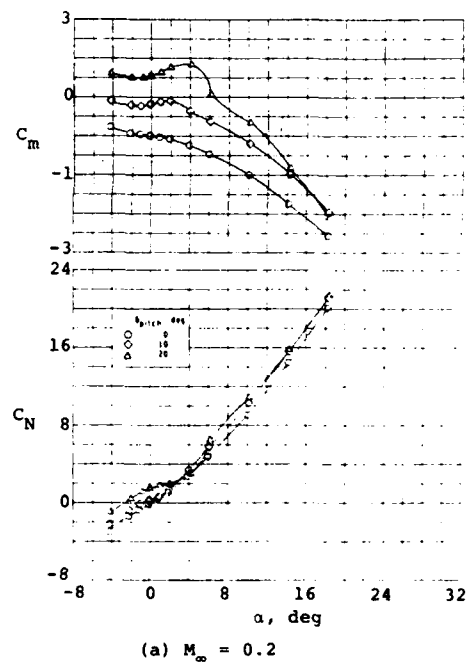


Figure 15.- Effects of pitch-control deflections on longitudinal aerodynamic characteristics of example tail-control missile; $\phi = 0$.

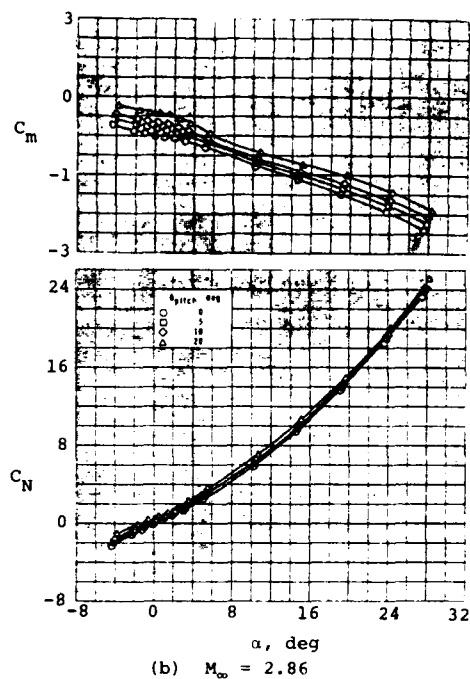


Figure 15.- (Concluded).

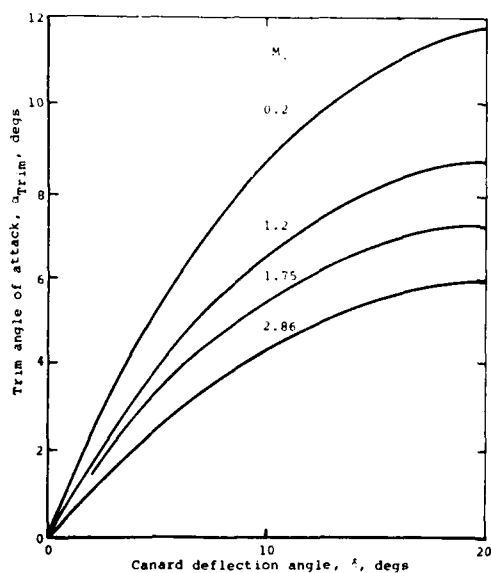


Figure 16.- Trim angle of attack for example canard missile with pitch control.

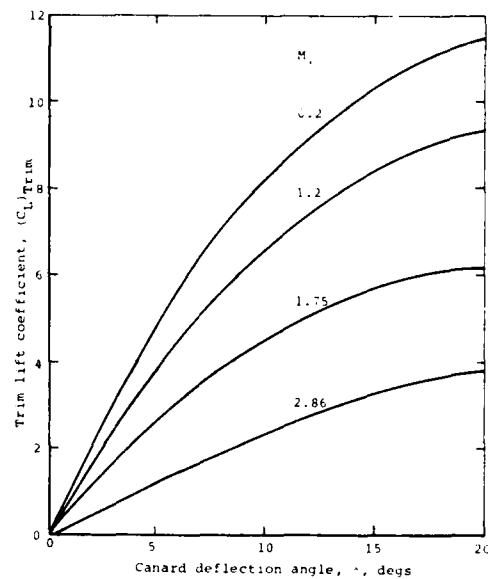


Figure 17.- Trim lift coefficients for example canard missile with pitch control.

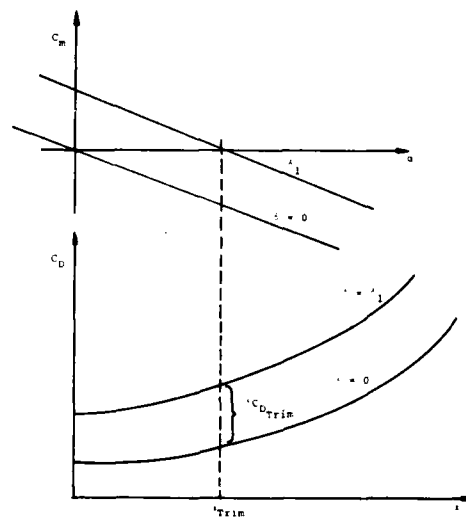


Figure 18.- Illustration of trim drag.

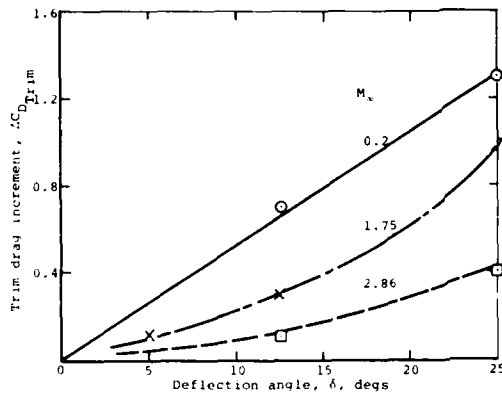


Figure 19.- Trim drag increment for example canard missile.

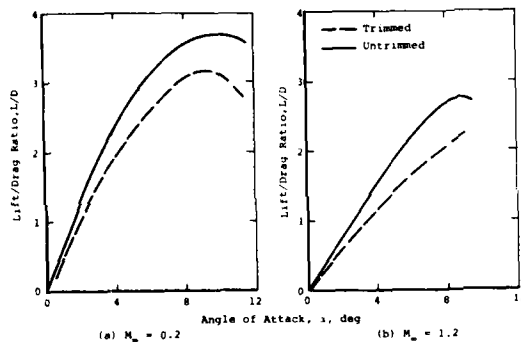


Figure 20.- Effect of trim drag and trim lift on lift-drag ratio for example canard missile.

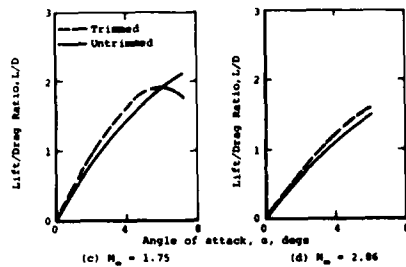


Figure 20.- (Concluded).

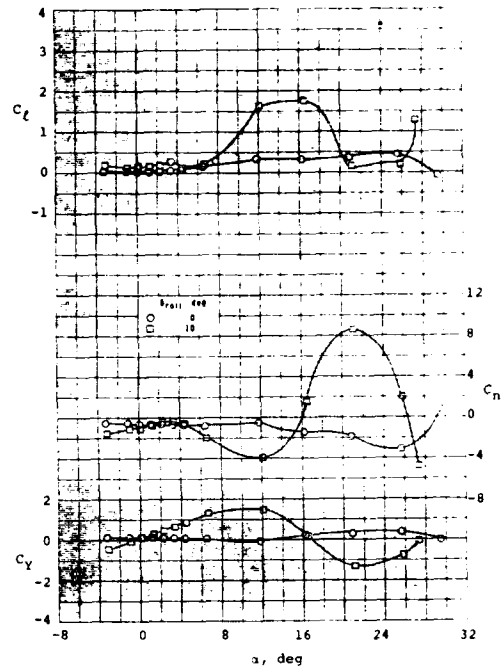


Figure 21.- Lateral control characteristics of example canard missile with roll control; $M_\infty = 2.10$.

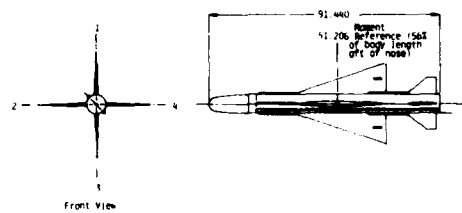


Figure 22.- Example tail-controlled missile.

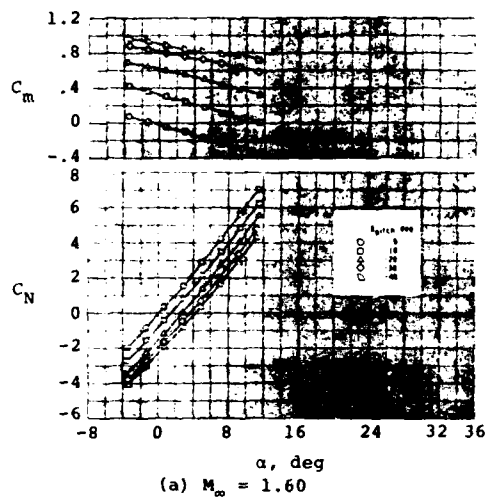


Figure 23.- Effect of pitch-control deflections on longitudinal aerodynamic characteristics of example tail-controlled missile $\phi = 0$.

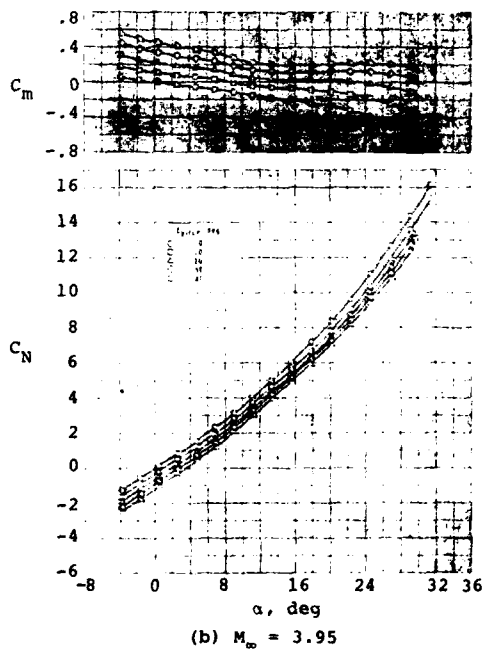


Figure 23.- (Concluded).

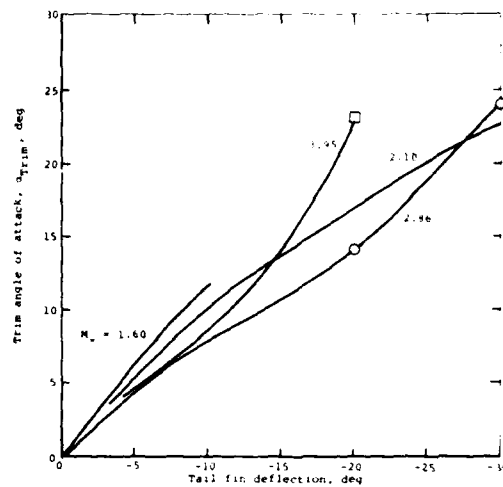


Figure 24.- Trim angle of attack due to tail pitch control; $\phi = 0$.

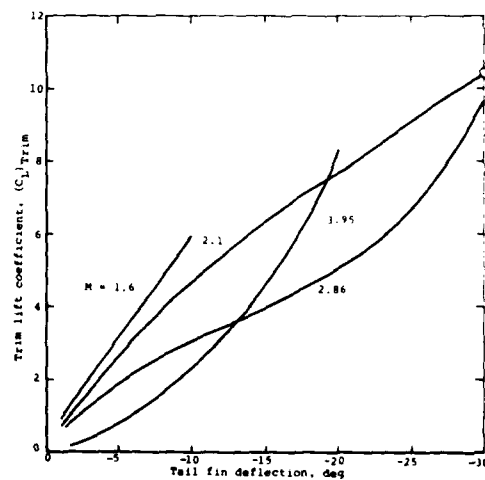


Figure 25.- Trim lift coefficient due to tail pitch control; $\phi = 0$.

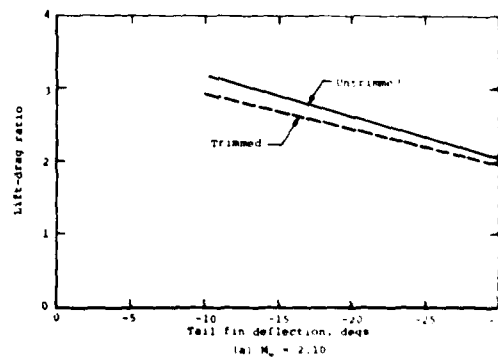


Figure 26.- Trimmed and untrimmed lift-drag ratios with tail pitch control $\phi = 0$.

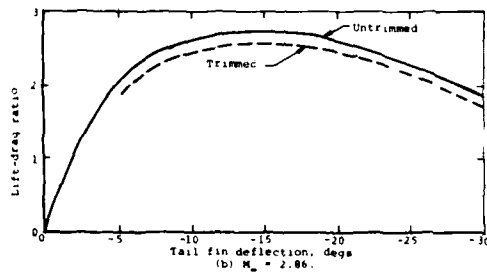


Figure 26.- (Concluded).

$\frac{a}{s_m}$	K_W	K_B	$\left(\frac{R}{C_F}\right)_{W(B)}$	$\left(\frac{R}{C_F}\right)_{B(W)}$	$\frac{\bar{y}_a - a}{s_m - a}$
0	1.000	0	0.667(2/3)	0.600(1/2)	0.424(4/3 π)
0.1	1.077	0.133	0.657	0.521	0.421
0.2	1.162	0.278	0.650	0.542	0.419
0.3	1.253	0.437	0.647	0.653	0.418
0.4	1.349	0.611	0.646	0.581	0.417
0.5	1.450	0.800	0.647	0.598	0.417
0.6	1.555	1.005	0.650	0.613	0.416
0.7	1.663	1.227	0.654	0.628	0.418
0.8	1.774	1.467	0.658	0.641	0.420
0.9	1.887	1.725	0.662	0.654	0.422
1.0	2.000	2.000	0.667(2/3)	0.667(2/3)	0.424(4/3 π)

* Triangular panel.

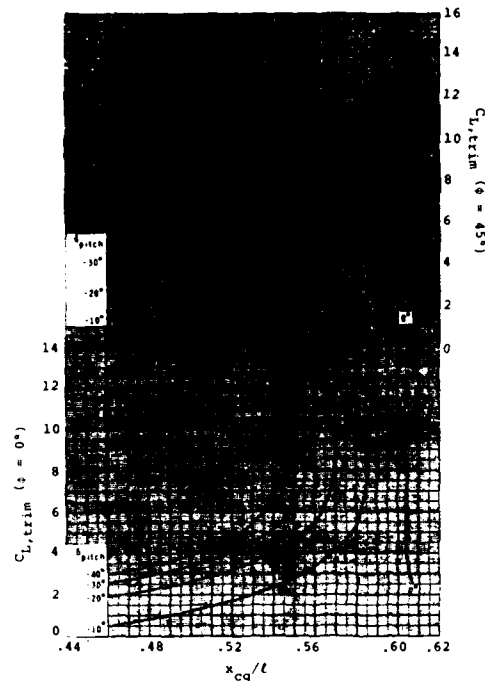
(a) Angle of attack ($\delta = 0$)

$\frac{a}{s_m}$	K_W	K_B	$\frac{K_B}{K_W}$	$\frac{K_B}{K_W}$	$\left(\frac{R}{C_F}\right)_{W(B)}$
0	1.000	0	0	0	0.667
0.1	0.963	0.114	0.118	0.123	0.669
0.2	0.944	0.218	0.231	0.239	0.668
0.3	0.936	0.317	0.338	0.349	0.666
0.4	0.935	0.414	0.442	0.454	0.665
0.5	0.940	0.510	0.542	0.551	0.664
0.6	0.948	0.607	0.641	0.646	0.663
0.7	0.958	0.705	0.736	0.737	0.664
0.8	0.971	0.803	0.827	0.827	0.666
0.9	0.985	0.902	0.916	0.915	0.667
1.0	1.000	1.000	1.000	1.000	0.667

* Triangular panel.

(b) Fin deflection

Figure 28.- Interference factors and center-of-pressure positions for all-movable fins mounted on a circular body (slender-body theory).

Figure 27.- Effect of C.G. location on trimmed lift coefficients for tail controlled missile: $M_\infty = 2.86$.

$\frac{a}{s_m}$	Planar			Cruciform		
	K_F	$\left(\frac{R}{C_F}\right)_{W(B)}$	$\frac{\bar{y}_a - a}{s_m - a}$	K_F	$\left(\frac{R}{C_F}\right)_{W(B)}$	$\frac{\bar{y}_a - a}{s_m - a}$
0	0.637(2/ π)	0.667(2/3)	0.524($\pi/6$)	0.382	0.667(2/3)	0.556
0.1	0.687	0.667	0.518	0.447	0.654	0.532
0.2	0.681	0.677	0.531	0.490	0.660	0.530
0.3	0.649	0.688	0.546	0.508	0.673	0.540
0.4	0.597	0.699	0.560	0.502	0.687	0.554
0.5	0.529	0.709	0.575	0.471	0.700	0.569
0.6	0.447	0.719	0.588	0.417	0.714	0.605
0.7	0.352	0.729	0.601	0.342	0.725	0.598
0.8	0.246	0.736	0.614	0.244	0.734	0.612
0.9	0.128	0.744	0.616	0.127	0.743	0.625
1.0	0	0.750(3/4)	0.637(2/ π)	0	0.750(3/4)	0.637(2/ π)

Figure 29.- Slender-body parameters for loading due to bank; triangular panels.

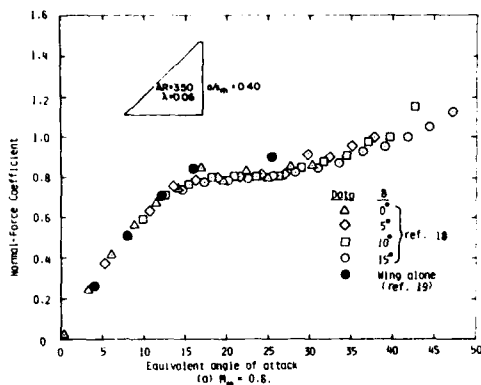


Figure 30.- Correlation of normal-force coefficient with equivalent angle of attack for moderate aspect ratio fin.

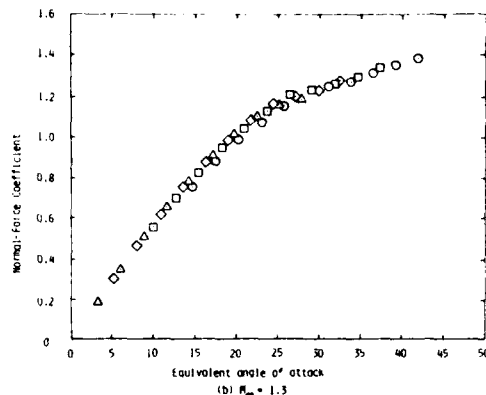


Figure 30.- (Concluded).

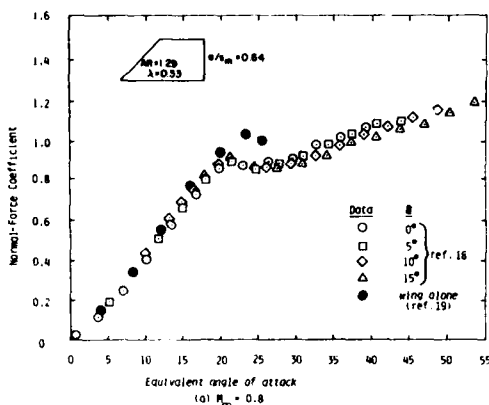


Figure 31.- Correlation of normal-force coefficient with equivalent angle of attack for low aspect ratio fin.

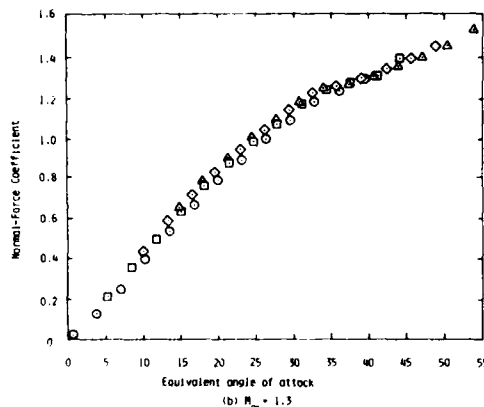


Figure 31.- (Concluded).

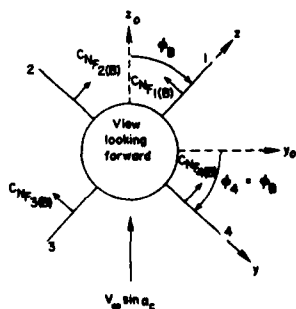


Figure 32.- Nomenclature for derivation of a_{eq} formulas. Fin deflection is positive leading edge toward leeward side of body.

a/b	A_{41}	A_{42}	A_{43}	A_{44}
0.0	-.275	.079	.275	.921
0.1	-.230	.073	.230	.890
0.2	-.188	.066	.188	.878
0.3	-.149	.057	.149	.879
0.4	-.112	.046	.112	.889
0.5	-.078	.034	.078	.905
0.6	-.050	.023	.050	.925
0.7	-.027	.013	.027	.946
0.8	-.012	.006	.012	.966
0.9	-.003	.001	.003	.984
1.0	0	0	0	1.000

Figure 33.- Slender-body fin deflection factors (Fin 4) for zero angle of attack (Ref. 17).

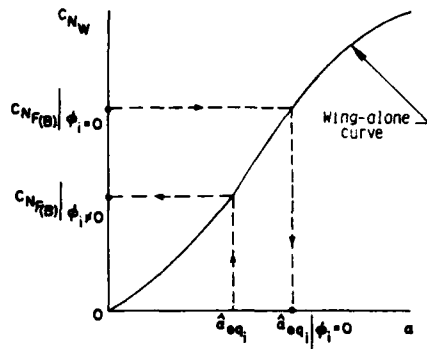


Figure 34.- Illustration of use of Eq. (42).

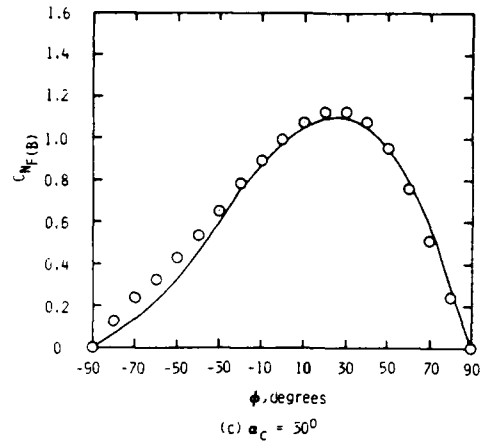


Figure 35.- (Continued).

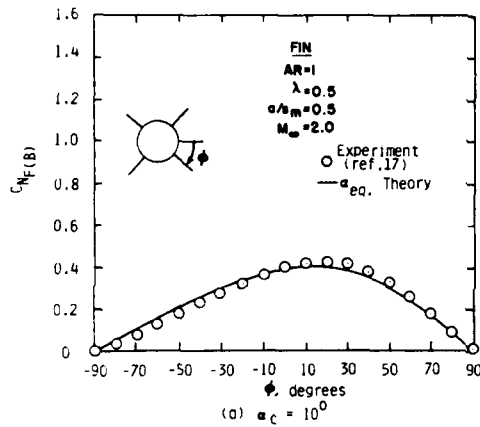
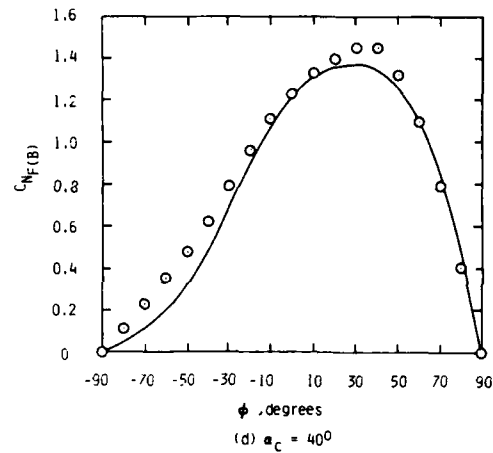
Figure 35.- Comparison of experiment with α_{eq} theory for extending low aspect ratio fin-on-body data base for $\delta = 0$ to include effects of roll.

Figure 35.- (Concluded).

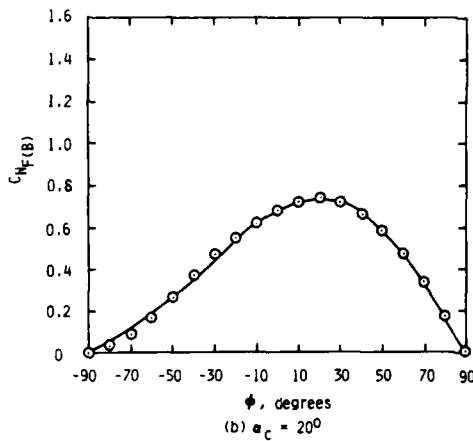
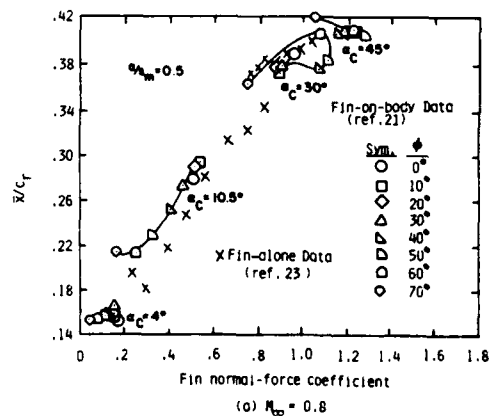


Figure 35.- (Continued).

Figure 36.- Correlation of axial center-of-pressure positions for rectangular wing alone and fin-on-body at $\delta = 0$; $M_\infty = 1.0$.

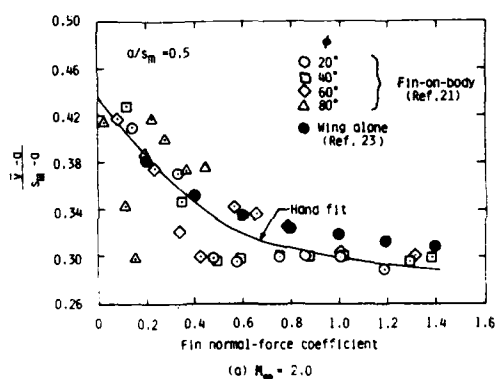
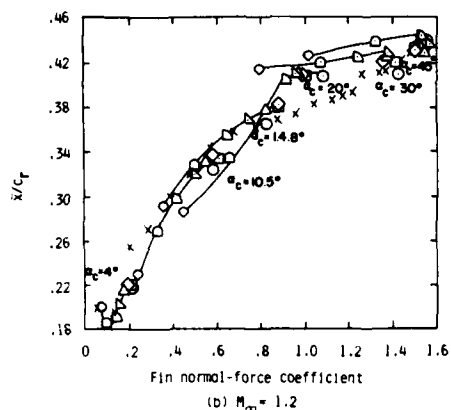


Figure 37.- Correlation of spanwise center-of-pressure positions for delta wing alone and fin-on-body at $\delta = 0$; $AR = 1.0$.

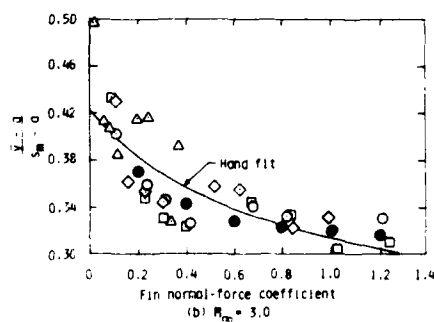


Figure 38.- (Concluded).

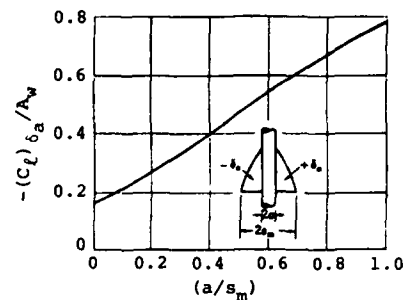


Figure 39.- Coefficient of damping in roll for cruciform and planar wing-body combinations.

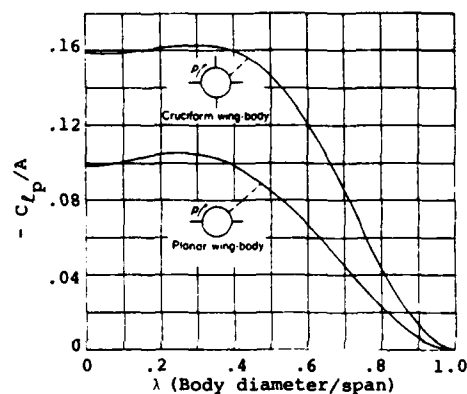


Figure 40.- Test configuration, Army generalized missile.

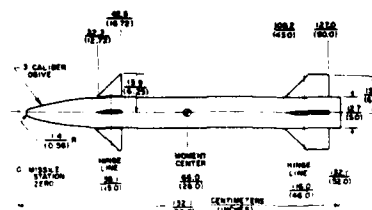


Figure 41.- (a) Body-canard-tail



Figure 42.- (b) Canard fin

Figure 43.- (c) Tail fin

Figure 40.- Test configuration, Army generalized missile.

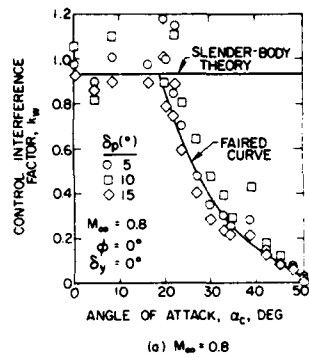


Figure 41.- Effect of angles of attack and control deflection on pitch control effectiveness of canard fins; $\phi = 0$.

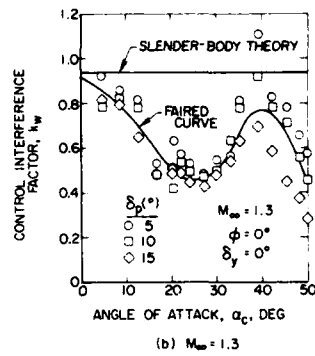


Figure 41.- (Concluded).

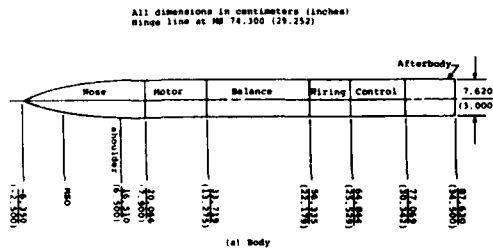


Figure 42.- Example body and cruciform fin combination.

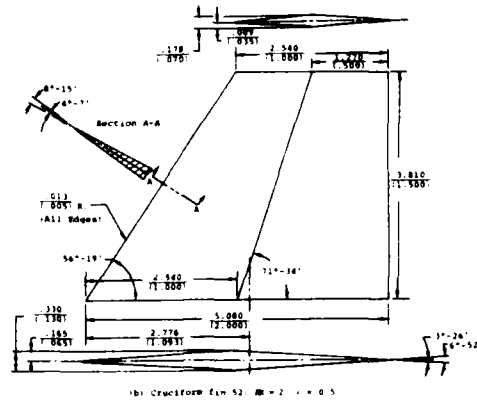


Figure 42.- (Concluded).

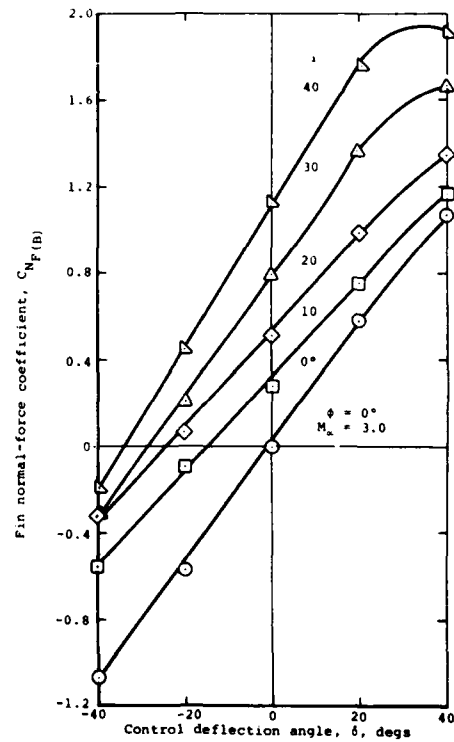


Figure 43.- Fin normal-force coefficient of horizontal fin for example wing-body combination; one fin deflection.

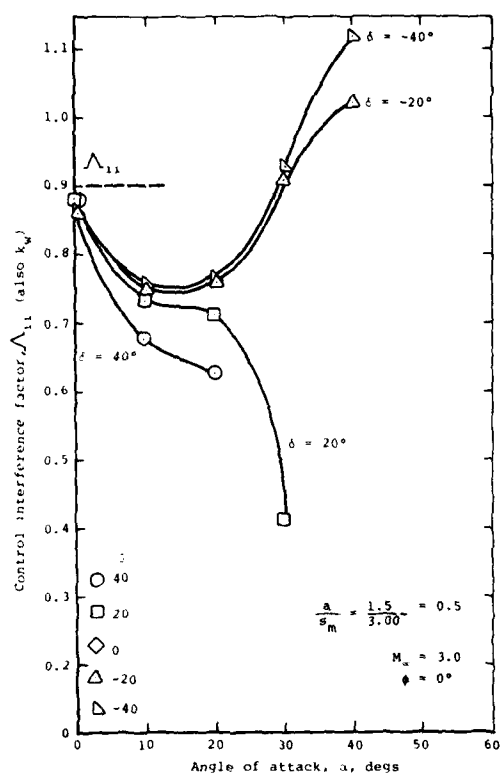


Figure 44.- Control interference factor for deflection of one horizontal fin of sample wing-body combination.

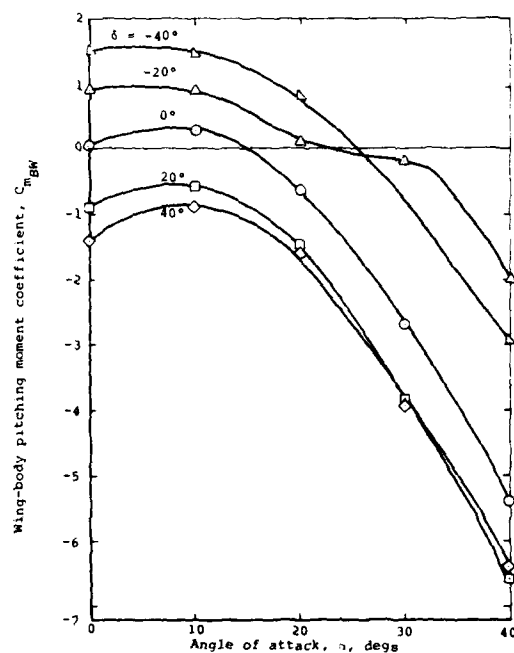


Figure 45.- Pitching-moment coefficient of subject wing-body combination with one horizontal fin deflected.

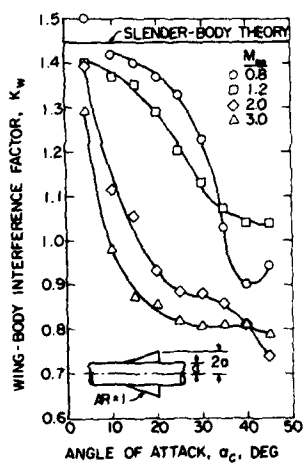


Figure 46.- Effect of angle of attack and free-stream Mach number on interference of body on wing.

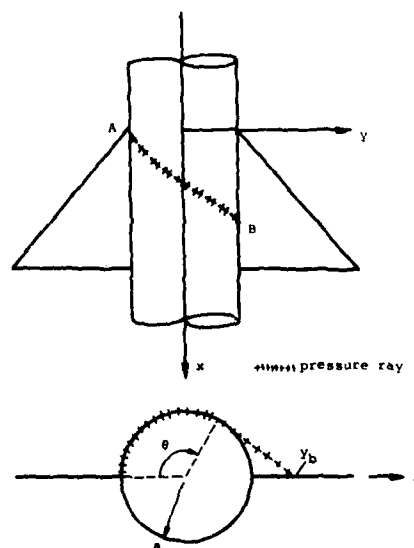


Figure 47.- Forward region of influence of one planar fin on another.

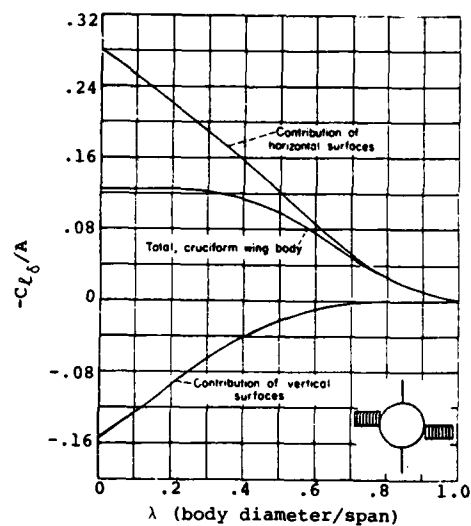


Figure 48.- Coefficient of rolling-moment effectiveness for cruciform wing-body combinations with differential incidence of the horizontal surfaces.

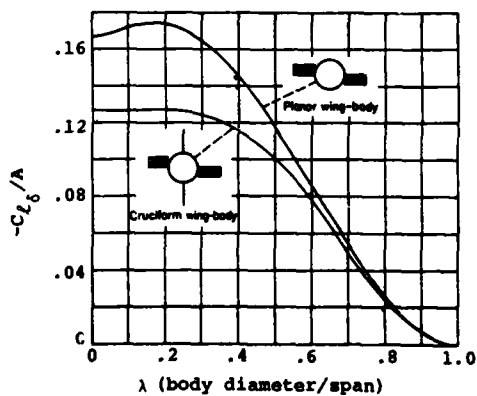


Figure 49.- Coefficient of rolling-moment effectiveness for cruciform and planar wing-body combinations with differential incidence of the horizontal surfaces.

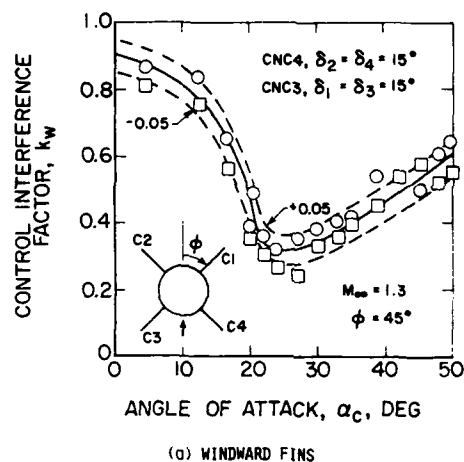


Figure 50.- Pitch control effectiveness of all-movable cruciform fins at $\phi = 45^\circ$.

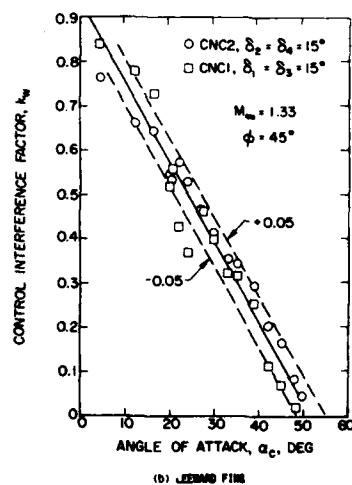


Figure 50.- (Concluded).

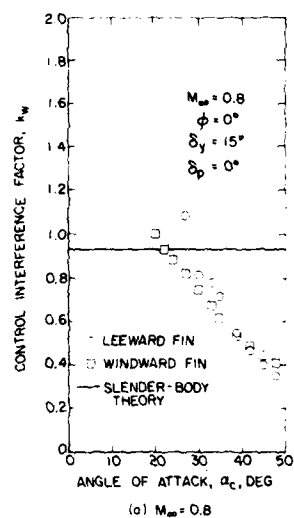


Figure 51.- Effect of angle of attack on yaw control effectiveness.

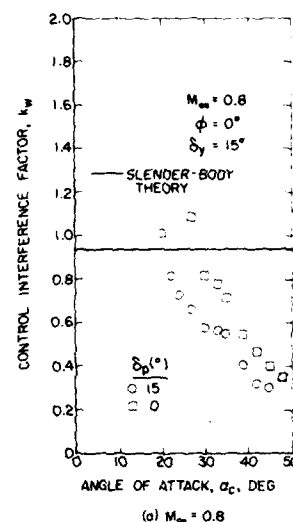


Figure 52.- Effect of pitch control on yaw control effectiveness at angle of attack (leeward fin).

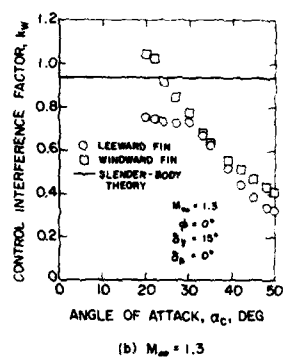


Figure 51.- (Concluded).

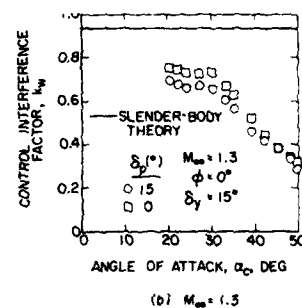


Figure 52.- (Concluded).

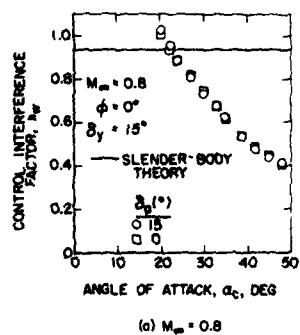


Figure 53.- Effect of pitch control on yaw control effectiveness at angle of attack (windward fin).

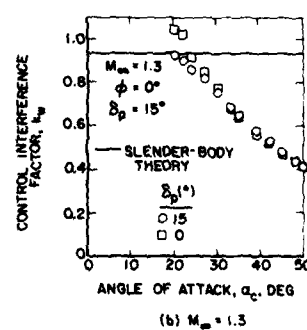


Figure 53.- (Concluded).

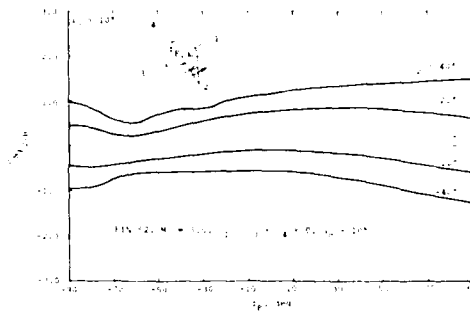


Figure 54.- Normal-force coefficient of tail fin versus angle of roll for various fin deflections; $\alpha = 10^\circ$.

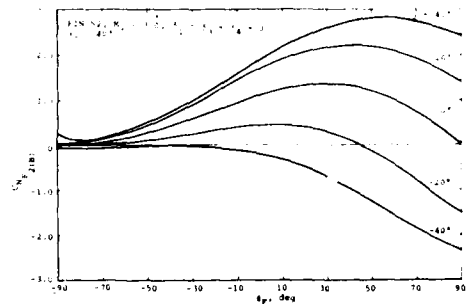


Figure 55.- Normal-force coefficient of tail fin versus angle of roll for various fin deflections; $\alpha_c = 40^\circ$.

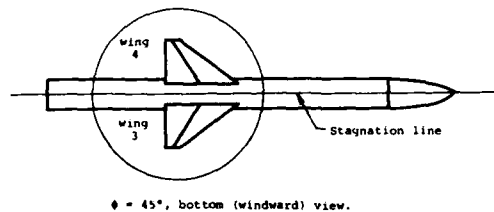


Figure 56.- Example cruciform wing-body combination for fin choking.

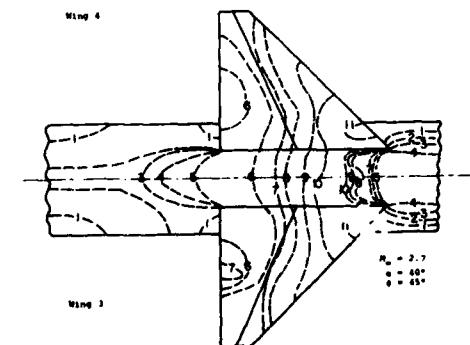


Figure 57.- Contours of P/P_∞ on windward side of wing-body combination with fin choking.

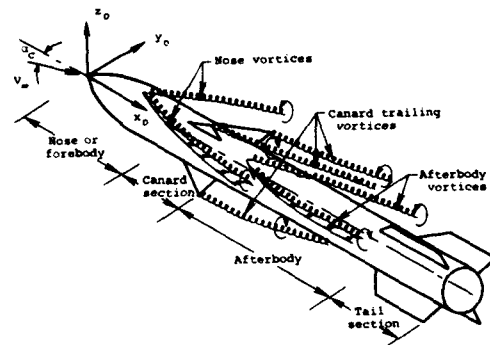


Figure 58.- Banked canard-cruciform missile at angle of attack showing typical vortex field.

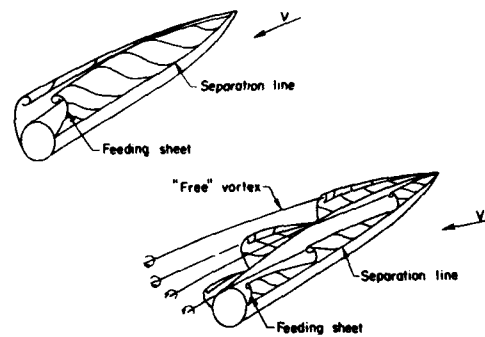


Figure 59.- Types of vortex formation on leeside of inclined body of revolution.

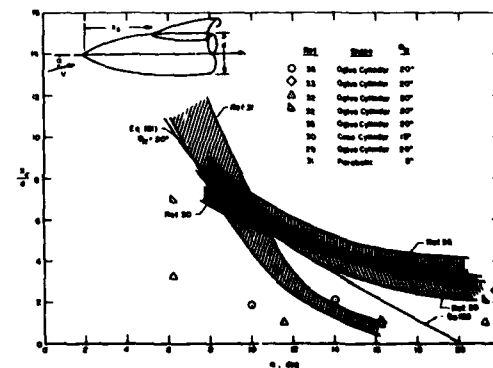


Figure 60.- Axial location of separation of bodies of revolution with sharp noses.

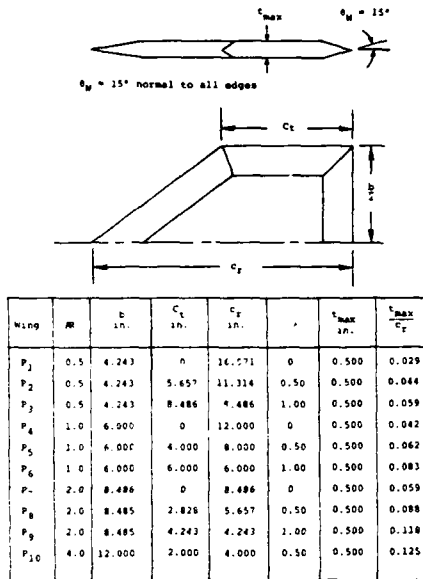


Figure 68.- Summary of characteristics of wings of Stallings-Lamb data base.

$$C_N = A_1 \sin \alpha + A_2 \sin 3\alpha + A_3 \sin 5\alpha$$

AN	LAMBDA	MACH NO.	A1	A2	A3
.400	0.000	1.000	1.63603	.201143E-01	-.10+150
.500	0.000	2.100	1.61551	-.001837E-01	-.023221E-01
.500	0.000	2.800	1.57093	-.160955	-.632184E-01
.500	0.000	3.500	1.50544	-.206444	-.675144E-01
.500	0.000	4.000	1.47765	-.206444	-.681330E-01
1.000	0.000	1.000	1.50240	-.240389	-.123300
1.000	0.000	2.100	1.46441	-.290765E-01	-.663566E-01
1.000	0.000	2.800	1.59067	-.063824E-01	-.578519E-01
1.000	0.000	3.500	1.50315	-.160054	-.505923E-01
1.000	0.000	4.000	1.54076	-.101567	-.508119E-01
2.000	0.000	1.000	1.02065	-.700054E-01	-.302322E-01
2.000	0.000	2.100	1.73063	-.279736E-01	-.256000E-01
2.000	0.000	2.800	1.62160	-.302756E-01	-.545200E-01
2.000	0.000	3.500	1.58120	-.938350E-01	-.675402E-01
2.000	0.000	4.000	1.52894	-.117949	-.784214E-01
.500	.500	1.000	1.57452	-.195191	-.102592
.500	.500	2.100	1.65113	-.170250E-01	-.605538E-01
.500	.500	2.800	1.61547	-.037858E-01	-.509234E-01
.500	.500	3.500	1.61623	-.164185	-.425366E-01
.500	.500	4.000	1.52538	-.172044	-.671843E-01
1.000	.500	1.000	1.61713	-.295073	-.648054E-01
1.000	.500	2.100	1.70531	-.623867E-01	-.659214E-01
1.000	.500	2.800	1.63332	-.162027E-01	-.609140E-01
1.000	.500	3.500	1.60389	-.793663E-01	-.776433E-01
1.000	.500	4.000	1.54452	-.128048	-.923145E-01
2.000	.500	1.000	1.90672	-.144431	-.535941E-01
2.000	.500	2.100	1.80255	-.750850E-01	-.177170E-01
2.000	.500	2.800	1.70693	-.297995E-01	-.635834E-01
2.000	.500	3.500	1.60844	-.396432E-01	-.763933E-01
2.000	.500	4.000	1.59519	-.777601E-01	-.857075E-01
4.000	.500	1.000	2.82696	-.143805	-.842506E-01
4.000	.500	2.100	1.60104	-.608000E-01	-.106451E-01
4.000	.500	2.800	1.78481	-.785871E-01	-.120508E-01
4.000	.500	3.500	1.71704	-.354300E-01	-.311420E-01
4.000	.500	4.000	1.60950	-.540661E-01	-.508402E-01
.500	1.000	1.000	1.38074	-.340902	-.102488
.500	1.000	2.100	1.68793	-.220761E-01	-.509071E-01
.500	1.000	2.800	1.62719	-.111045	-.369584E-01
.500	1.000	3.500	1.62445	-.166713	-.356810E-01
.500	1.000	4.000	1.54524	-.182116	-.528080E-01
1.000	1.000	1.000	1.60417	-.343850	-.108201
1.000	1.000	2.100	1.73067	-.623373E-01	-.345330E-01
1.000	1.000	2.800	1.64207	-.280700E-01	-.626710E-01
1.000	1.000	3.500	1.60505	-.105324	-.608927E-01
1.000	1.000	4.000	1.57580	-.113018	-.626441E-01
2.000	1.000	1.000	1.80302	-.172125	-.312901E-01
2.000	1.000	2.100	1.82154	-.642040E-01	-.124304E-01
2.000	1.000	2.800	1.71300	-.136117E-01	-.386873E-01
2.000	1.000	3.500	1.60051	-.311840E-01	-.504705E-01
2.000	1.000	4.000	1.50019	-.567040E-01	-.761404E-01

Figure 69.- Curve fits to the wing-alone normal-force curves of the Stallings-Lamb data.

1	2	3	4	5	6	7	8	9	10
$M_\infty = 1.60$									
α	C_N	$\frac{C_N}{C_D}$	$\frac{C_L}{C_D}$	$\frac{C_L}{C_D}$	$\frac{C_L}{C_D}$	$\frac{C_L}{C_D}$	$\frac{C_L}{C_D}$	$\frac{C_L}{C_D}$	$\frac{C_L}{C_D}$
-5	-.180	-	-	-.140	-	-	-.115	-	-
0	0	-	0	0	-	0	0	-	0
5	.290	.652	.385	.140	.635	.370	.115	.620	.370
10	.395	.647	.380	.220	.622	.367	.222	.615	.358
15	.500	.637	.362	.300	.612	.350	.300	.607	.345
20	.575	.632	.345	.380	.604	.340	.370	.602	.340
25	.640	.630	.332	.460	.602	.332	.460	.602	.335
30	1.080	.623	.322	.540	.600	.322	.540	.600	.330
35	1.180	.618	.315	.620	.598	.312	.620	.598	.325
40	1.280	.617	.310	.700	.597	.310	.700	.597	.320
45	1.370	.618	.310	.780	.597	.310	.780	.597	.315
50	1.500	.623	.312	1.350	.619	.312	1.280	.624	.318
55	-	-	-	1.455	.626	.312	1.350	.625	.315
60	-	-	-	1.592	.634	.312	1.455	.631	.312

$M_\infty = 3.50$									
α	C_N	$\frac{C_N}{C_D}$	$\frac{C_L}{C_D}$	$\frac{C_L}{C_D}$	$\frac{C_L}{C_D}$	$\frac{C_L}{C_D}$	$\frac{C_L}{C_D}$	$\frac{C_L}{C_D}$	$\frac{C_L}{C_D}$
-5	-.695	-	-	-.675	-	-	-	-	-
0	0	-	0	0	-	0	0	-	0
5	.090	.605	.374	.075	.600	.373	-	-	-
10	.180	.606	.360	.155	.601	.370	-	-	-
15	.282	.609	.348	.240	.603	.367	-	-	-
20	.400	.612	.340	.325	.606	.364	-	-	-
25	.520	.615	.328	.410	.610	.360	-	-	-
30	.640	.620	.320	.500	.618	.350	-	-	-
35	.810	.625	.324	.590	.622	.348	-	-	-
40	.960	.627	.324	.680	.620	.345	-	-	-
45	1.105	.630	.322	.770	.617	.342	-	-	-
50	1.250	.620	.310	1.200	.622	.338	-	-	-
55	1.385	.625	.314	1.300	.627	.335	-	-	-
60	1.430	.621	.312	1.385	.626	.335	-	-	-

Figure 70.- Stallings-Lamb data base for wing of $M = 2$, $\lambda = 0$.

1	2	3	4	5	6	7	8	9	10
$M_\infty = 1.60$									
α	C_N	$\frac{C_N}{C_D}$	$\frac{C_L}{C_D}$	$\frac{C_L}{C_D}$	$\frac{C_L}{C_D}$	$\frac{C_L}{C_D}$	$\frac{C_L}{C_D}$	$\frac{C_L}{C_D}$	$\frac{C_L}{C_D}$
-5	-.200	-	-	-.185	-	-	-.130	-	-
0	0	-	0	0	-	0	0	-	0
5	.220	.335	.442	.140	.337	.445	.130	.332	.445
10	.420	.360	.480	.250	.342	.458	.270	.349	.470
15	.620	.380	.483	.355	.358	.467	.380	.352	.469
20	.830	.392	.474	.470	.375	.472	.580	.355	.470
25	1.020	.395	.461	.600	.380	.476	.730	.375	.475
30	1.165	.398	.464	.800	.400	.479	.865	.392	.474
35	1.260	.402	.467	1.130	.403	.481	.995	.402	.480
40	1.325	.408	.466	1.220	.407	.487	1.140	.408	.484
45	1.415	.417	.488	1.325	.415	.488	1.245	.492	.485
50	1.530	.440	.485	1.400	.425	.489	1.335	.440	.487
55	-	-	-	1.520	.461	.489	1.430	.438	.488
60	-	-	-	1.580	.454	.490	1.520	.430	.481

$M_\infty = 3.50$									
α	C_N	$\frac{C_N}{C_D}$	$\frac{C_L}{C_D}$	$\frac{C_L}{C_D}$	$\frac{C_L}{C_D}$	$\frac{C_L}{C_D}$	$\frac{C_L}{C_D}$	$\frac{C_L}{C_D}$	$\frac{C_L}{C_D}$
-5	-.105	-	-	-.080	-	-	-	-	-
0	0	-	0	0	-	0	0	-	0
5	.110	.309	.467	.080	.303	.463	-	-	-
10	.220	.317	.470	.180	.300	.470	-	-	-
15	.360	.342	.470	.290	.322	.470	-	-	-
20	.520	.349	.467	.420	.340	.470	-	-	-
25	.680	.360	.470	.560	.360	.470	-	-	-
30	.870	.380	.474	.710	.370	.474	-	-	-
35	.940	.399	.480	.850	.380	.478	-	-	-
40	1.060	.408	.483	1.000	.484	.480	-	-	-
45	1.210	.413	.485	1.150	.482	.484	-	-	-
50	1.380	.417	.487	1.300	.484	.486	-	-	-
55	1.415	.427	.488	1.460	.485	.487	-	-	-
60	1.510	.445	.488	1.460	.480	.488	-	-	-

Figure 71.- Stallings-Lamb data base for wing of $M = 2$, $\lambda = 1$.

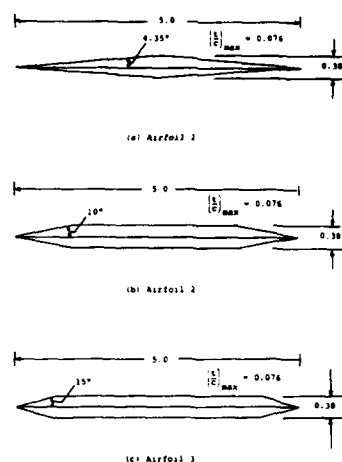


Figure 72.- Three airfoil sections with different wedge angles but the same thickness ratio.

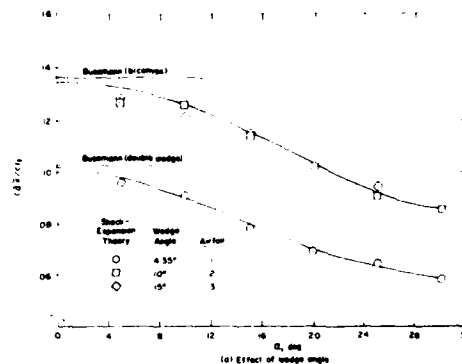


Figure 73.- Center-of-pressure position (positive forward from the 50 percent chord location) for three airfoils of the same thickness ratio, $M_{\infty} = 4.50$.

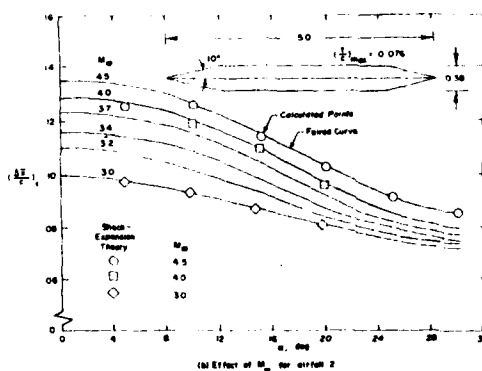


Figure 73.- (Concluded).

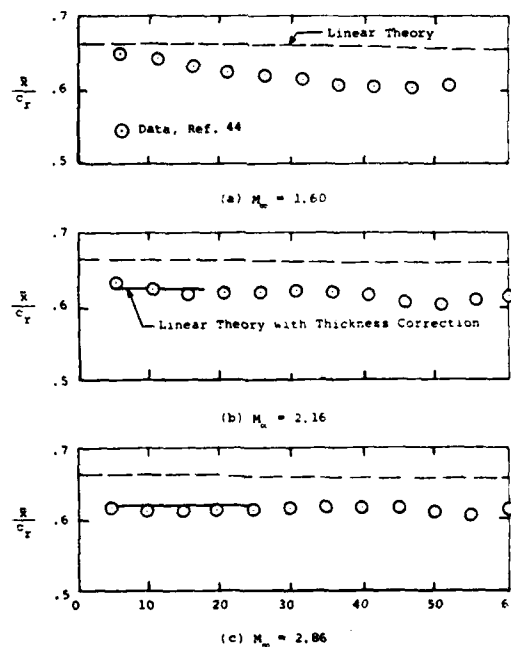


Figure 74.- Longitudinal center-of-pressure location of aspect ratio 2.0 delta wing.

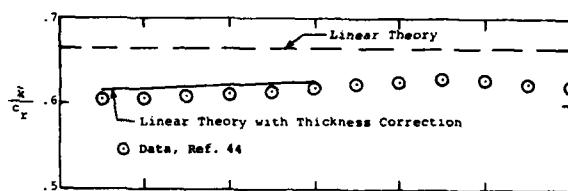
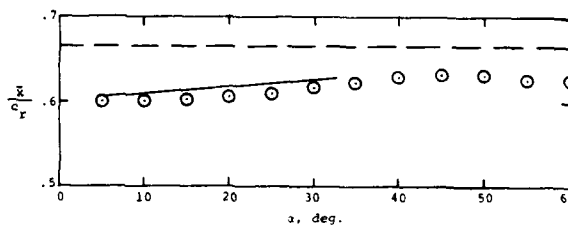
(d) $M_\infty = 3.50$ (e) $M_\infty = 4.60$

Figure 74.- (Concluded).

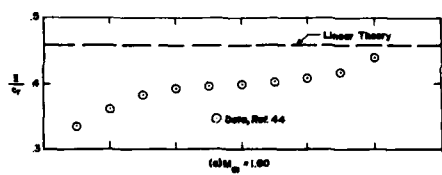
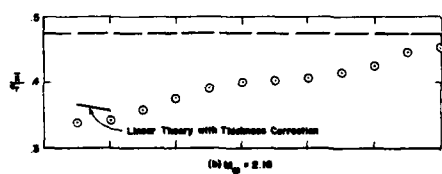
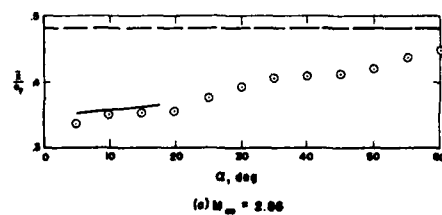
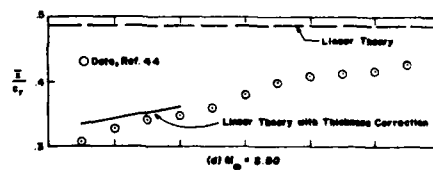
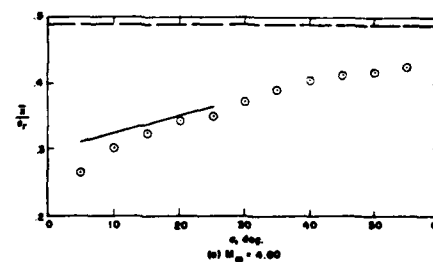
(a) $M_\infty = 1.00$ (b) $M_\infty = 2.10$ (c) $M_\infty = 3.00$ (d) $M_\infty = 3.90$ (e) $M_\infty = 4.90$

Figure 75.- Longitudinal center-of-pressure locations of an aspect ratio 2.0 rectangular wing.

Figure 75.- (Concluded).

Tabl Fin Config	S_{F1} in	AR	$H/2$ in	λ	A	A_1 in	C_{T1} in	B_1 in	C_{T1} in	H/C_R	C_{T1} in	C_{T1} in	C_{T1} in
16	7.916	2.0	7.921	1.0	90°	0.800	2.813	1.140	2.813	0.45	0.140	0.140	0.050
17	7.916	2.0	7.921	0.5	56°15'	1.158	1.873	1.140	2.749	0.55	0.187	0.187	0.050
18	7.947	2.0	7.921	0	26°34'	1.172	0	1.140	5.625	0.62	0.187	0.187	0.033
21	7.5119	2.0	1.874	1.0	90°	0.696	1.874	0.696	1.874	0.45	0.125	0.125	0.067
22	7.4046	2.0	1.875	0.5	55°30'	0.713	1.282	0.696	2.565	0.55	0.125	0.125	0.049
23	7.5156	2.0	1.875	0	26°34'	0.728	0	0.696	3.750	0.62	0.125	0.125	0.033
11	7.028	1.0	1.875	1.0	90°	0.800	2.749	0.800	2.749	0.45	0.140	0.140	0.037
15	7.024	1.0	1.875	0.5	36°54'	1.165	2.497	1.140	4.996	0.55	0.187	0.187	0.037
14	7.028	1.0	1.875	0	14°5'	1.125	0	1.140	7.499	0.62	0.187	0.187	0.025
12	34.816	0.5	1.875	1.0	90°	1.587	7.499	1.587	7.499	0.45	0.250	0.250	0.033
13	34.800	0.5	1.875	0.5	20°36'	1.626	4.990	1.587	9.980	0.55	0.250	0.250	0.025
16	34.056	0.5	1.875	0	7°8'	1.682	0	1.587	14.990	0.62	0.250	0.250	0.017

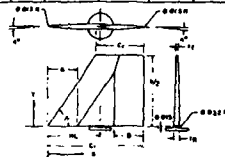


Figure 76.- Summary of characteristics of wings of Fidler-Baker data base.

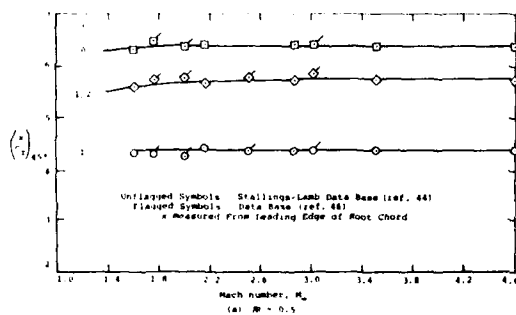
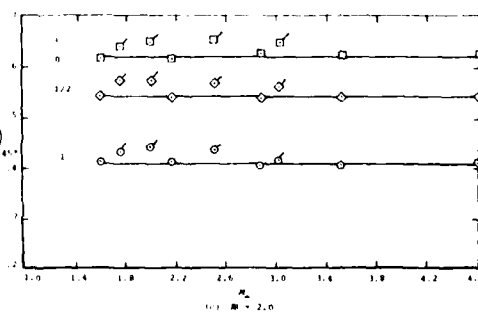
Figure 77.- Comparison of longitudinal center-of-pressure position at $\alpha = 45^\circ$ of wings of Stallings-Lamb and Fidler-Baker data bases.

Figure 77.- (Concluded).

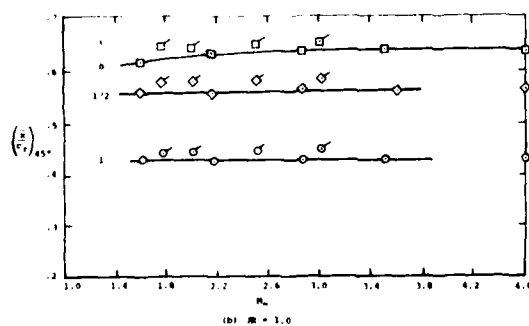


Figure 77.- (Continued).

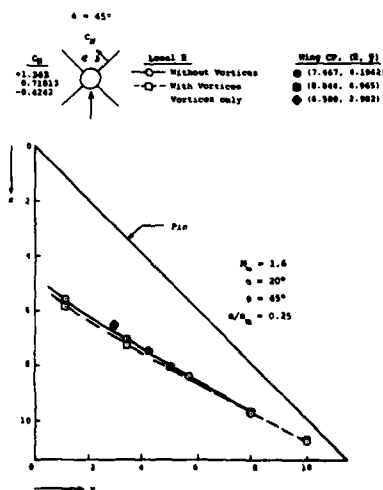


Figure 78.- Effect of body vortices of fin axial center-of-pressure position as calculated by a panel method.

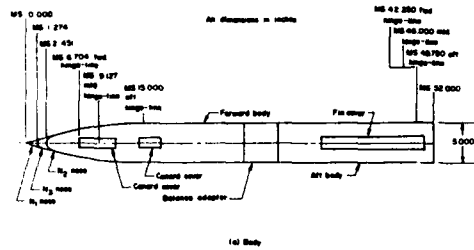
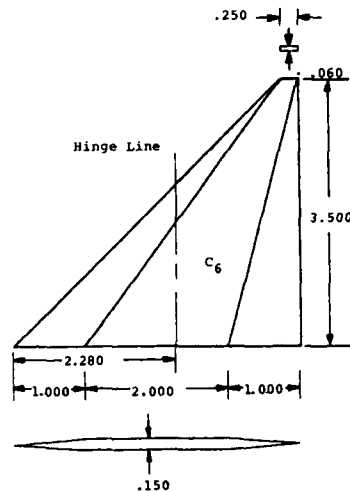


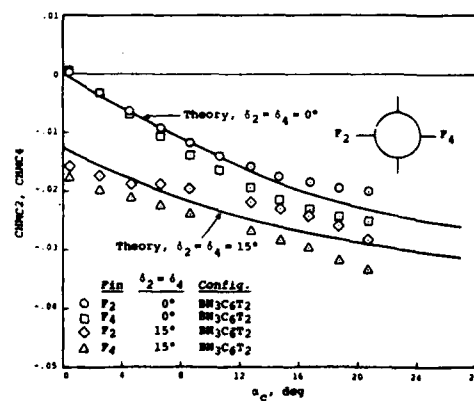
Figure 79.- Sketch of model body showing hinge-line positions for canard and tail panels.

Note 1: All dimensions are in inches.
Note 2: Leading- and trailing-edge radii are 0.020



(b) Canard fin C_6 .

Figure 79.- (Concluded).



(a) $M_\infty = 1.3$

Figure 80.- Hinge moment characteristics of canard C_6 at $\phi = 0$; $\delta_1 = \delta_2 = 0$.

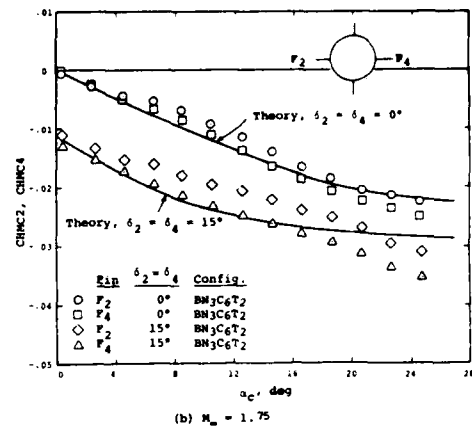
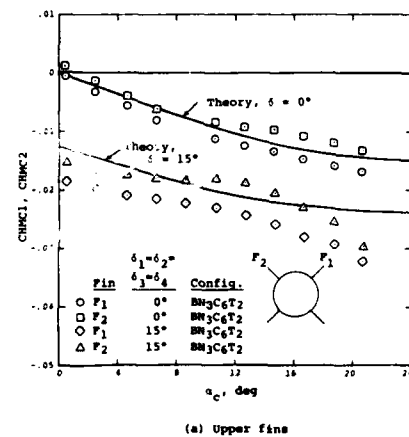
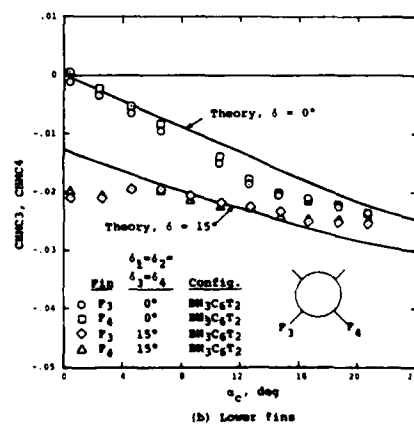


Figure 80.- (Concluded).



(a) Upper fins

Figure 81.- Hinge moment characteristics of upper and lower canard fins C_6 at $\phi = 45^\circ$ at $M_\infty = 1.3$.



(b) Lower fins

Figure 81.- (Concluded).

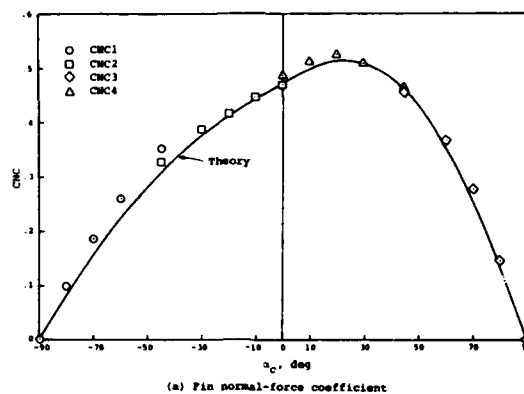


Figure 82.- Effect of roll angle on characteristics of canard fin C_0 on body BN_3 at $M_\infty = 1.3$ with no control deflection.

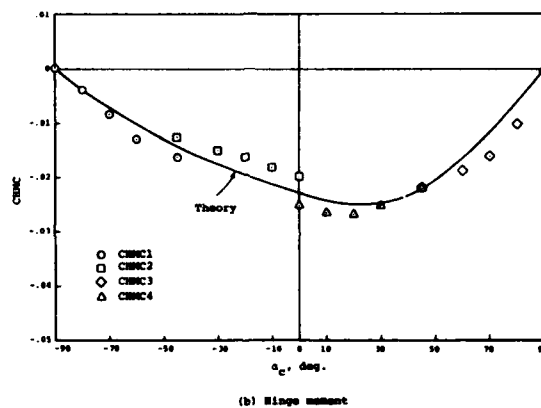


Figure 82.- (Concluded).

REPORT DOCUMENTATION PAGE			
1. Recipient's Reference AD-A133950	2. Originator's Reference AGARD-R-711	3. Further Reference ISBN 92-835-1457-2	4. Security Classification of Document UNCLASSIFIED
5. Originator	Advisory Group for Aerospace Research and Development North Atlantic Treaty Organization 7 rue Ancelle, 92200 Neuilly sur Seine, France		
6. Title	SPECIAL COURSE ON AERODYNAMIC CHARACTERISTICS OF CONTROLS		
7. Presented at	von Kármán Institute, Rhode-St-Genèse, Belgium on 21-25 March 1983.		
8. Author(s)/Editor(s) Various	9. Date July 1983		
10. Author's/Editor's Address Various	11. Pages 260		
12. Distribution Statement	This document is distributed in accordance with AGARD policies and regulations, which are outlined on the Outside Back Covers of all AGARD publications.		
13. Keywords/Descriptors <div style="display: flex; justify-content: space-between;"> <div style="width: 45%;"> Aircraft Flight control Avionics </div> <div style="width: 45%;"> Control surfaces Aerodynamic characteristics </div> </div>			
14. Abstract <p>The use of electronic aids for aircraft guidance and control has increased the importance of the aerodynamic characteristics of the various forms of aircraft control and the need to improve our understanding of them. There has also been increasing interest in Direct Force Controls where the immediate response due to the force changes produced by the control is exploited rather than the slowly developing response of the resulting moment. The performance advantages of reducing the size of stabilising surfaces by achieving artificial stability through the use of the control surfaces coupled to electronic stabilising systems are now well appreciated. Such developments also have promise for gust alleviation and flutter. They have brought to the fore the need to understand the aerodynamic behaviour of non-steady or oscillatory controls.</p> <p>A symposium on this subject was sponsored by the Fluid Dynamics Panel of AGARD in May 1979. The Course aimed to produce a review of the main points of interest from that symposium and to present expert surveys of the state of the art.</p> <p>The material assembled in this book was prepared under the combined sponsorship of the Fluid Dynamics Panel, the von Kármán Institute and the Consultant and Exchange Program of AGARD and was presented as an AGARD Special Course at the von Kármán Institute, Rhode-St-Genèse, Belgium on 21-25 March 1983.</p>			

<p>AGARD Report No.711 Advisory Group for Aerospace Research and Development, NATO SPECIAL COURSE ON AERODYNAMIC CHARACTERISTICS OF CONTROLS Published July 1983 260 pages</p> <p>The use of electronic aids for aircraft guidance and control has increased the importance of the aerodynamic characteristics of the various forms of aircraft control and the need to improve our understanding of them. There has also been increasing interest in Direct Force Controls where the immediate response due to the force changes produced by the control is exploited rather than the slowly developing response of the</p> <p>P.T.O</p>	<p>AGARD-R-711</p> <p>Aircraft Flight control Avionics Control surfaces Aerodynamic characteristics</p>	<p>AGARD Report No.711 Advisory Group for Aerospace Research and Development, NATO SPECIAL COURSE ON AERODYNAMIC CHARACTERISTICS OF CONTROLS Published July 1983 260 pages</p> <p>The use of electronic aids for aircraft guidance and control has increased the importance of the aerodynamic characteristics of the various forms of aircraft control and the need to improve our understanding of them. There has also been increasing interest in Direct Force Controls where the immediate response due to the force changes produced by the control is exploited rather than the slowly developing response of the</p> <p>P.T.O</p>	<p>AGARD-R-711</p> <p>Aircraft Flight control Avionics Control surfaces Aerodynamic characteristics</p>
<p>AGARD Report No.711 Advisory Group for Aerospace Research and Development, NATO SPECIAL COURSE ON AERODYNAMIC CHARACTERISTICS OF CONTROLS Published July 1983 260 pages</p> <p>The use of electronic aids for aircraft guidance and control has increased the importance of the aerodynamic characteristics of the various forms of aircraft control and the need to improve our understanding of them. There has also been increasing interest in Direct Force Controls where the immediate response due to the force changes produced by the control is exploited rather than the slowly developing response of the</p> <p>P.T.O</p>	<p>AGARD-R-711</p> <p>Aircraft Flight control Avionics Control surfaces Aerodynamic characteristics</p>	<p>AGARD Report No.711 Advisory Group for Aerospace Research and Development, NATO SPECIAL COURSE ON AERODYNAMIC CHARACTERISTICS OF CONTROLS Published July 1983 260 pages</p> <p>The use of electronic aids for aircraft guidance and control has increased the importance of the aerodynamic characteristics of the various forms of aircraft control and the need to improve our understanding of them. There has also been increasing interest in Direct Force Controls where the immediate response due to the force changes produced by the control is exploited rather than the slowly developing response of the</p> <p>P.T.O</p>	<p>AGARD-R-711</p> <p>Aircraft Flight control Avionics Control surfaces Aerodynamic characteristics</p>

<p>resulting moment. The performance advantages of reducing the size of stabilising surfaces by achieving artificial stability through the use of the control surfaces coupled to electronic stabilising systems are now well appreciated. Such developments also have promise for gust alleviation and flutter control. They have brought to the fore the need to understand the aerodynamic behaviour of non-steady or oscillatory controls.</p> <p>A symposium on this subject was sponsored by the Fluid Dynamics Panel of AGARD in May 1979. The Course aimed to provide a review of the main points of interest from that symposium and to present expert surveys of the state of the art.</p> <p>The material assembled in this book was prepared under the combined sponsorship of the Fluid Dynamics Panel, the von Kármán Institute and the Consultant and Exchange Program of the AGARD and was presented as an AGARD Special Course at the von Kármán Institute, Rhode-St-Genève, Belgium on 21-25 March 1983.</p> <p>ISBN 92-835-1457-2</p>	<p>resulting moment. The performance advantages of reducing the size of stabilising surfaces by achieving artificial stability through the use of the control surfaces coupled to electronic stabilising systems are now well appreciated. Such developments also have promise for gust alleviation and flutter control. They have brought to the fore the need to understand the aerodynamic behaviour of non-steady or oscillatory controls.</p> <p>A symposium on this subject was sponsored by the Fluid Dynamics Panel of AGARD in May 1979. The Course aimed to provide a review of the main points of interest from that symposium and to present expert surveys of the state of the art.</p> <p>The material assembled in this book was prepared under the combined sponsorship of the Fluid Dynamics Panel, the von Kármán Institute and the Consultant and Exchange Program of the AGARD and was presented as an AGARD Special Course at the von Kármán Institute, Rhode-St-Genève, Belgium on 21-25 March 1983.</p> <p>ISBN 92-835-1457-2</p>
<p>resulting moment. The performance advantages of reducing the size of stabilising surfaces by achieving artificial stability through the use of the control surfaces coupled to electronic stabilising systems are now well appreciated. Such developments also have promise for gust alleviation and flutter control. They have brought to the fore the need to understand the aerodynamic behaviour of non-steady or oscillatory controls.</p> <p>A symposium on this subject was sponsored by the Fluid Dynamics Panel of AGARD in May 1979. The Course aimed to provide a review of the main points of interest from that symposium and to present expert surveys of the state of the art.</p> <p>The material assembled in this book was prepared under the combined sponsorship of the Fluid Dynamics Panel, the von Kármán Institute and the Consultant and Exchange Program of the AGARD and was presented as an AGARD Special Course at the von Kármán Institute, Rhode-St-Genève, Belgium on 21-25 March 1983.</p> <p>ISBN 92-835-1457-2</p>	<p>resulting moment. The performance advantages of reducing the size of stabilising surfaces by achieving artificial stability through the use of the control surfaces coupled to electronic stabilising systems are now well appreciated. Such developments also have promise for gust alleviation and flutter control. They have brought to the fore the need to understand the aerodynamic behaviour of non-steady or oscillatory controls.</p> <p>A symposium on this subject was sponsored by the Fluid Dynamics Panel of AGARD in May 1979. The Course aimed to provide a review of the main points of interest from that symposium and to present expert surveys of the state of the art.</p> <p>The material assembled in this book was prepared under the combined sponsorship of the Fluid Dynamics Panel, the von Kármán Institute and the Consultant and Exchange Program of the AGARD and was presented as an AGARD Special Course at the von Kármán Institute, Rhode-St-Genève, Belgium on 21-25 March 1983.</p> <p>ISBN 92-835-1457-2</p>